THE FIBROBLAST GROWTH FACTOR SIGNALING PATHWAY IN METABOLIC REGULATION, DEVELOPMENT, DISEASE AND REPAIR AFTER INJURY

EDITED BY: Zhouguang Wang, Xiaokun Li, Li Lin, Saverio Bellusci and Jin-San Zhang

PUBLISHED IN: Frontiers in Pharmacology

frontiers Research Topics

ISSN 1664-8714
ISBN 978-2-88966-128-2
DOI 10.3389/978-2-88966-128-2

About Frontiers

Frontiers is more than just an open-access publisher of scholarly articles: it is a pioneering approach to the world of academia, radically improving the way scholarly research is managed. The grand vision of Frontiers is a world where all people have an equal opportunity to seek, share and generate knowledge. Frontiers provides immediate and permanent online open access to all its publications, but this alone is not enough to realize our grand goals.

Frontiers Journal Series

The Frontiers Journal Series is a multi-tier and interdisciplinary set of open-access, online journals, promising a paradigm shift from the current review, selection and dissemination processes in academic publishing. All Frontiers journals are driven by researchers for researchers; therefore, they constitute a service to the scholarly community. At the same time, the Frontiers Journal Series operates on a revolutionary invention, the tiered publishing system, initially addressing specific communities of scholars, and gradually climbing up to broader public understanding, thus serving the interests of the lay society, too.

Dedication to Quality

Each Frontiers article is a landmark of the highest quality, thanks to genuinely collaborative interactions between authors and review editors, who include some of the world's best academicians. Research must be certified by peers before entering a stream of knowledge that may eventually reach the public - and shape society; therefore, Frontiers only applies the most rigorous and unbiased reviews.
Frontiers revolutionizes research publishing by freely delivering the most outstanding research, evaluated with no bias from both the academic and social point of view. By applying the most advanced information technologies, Frontiers is catapulting scholarly publishing into a new generation.

What are Frontiers Research Topics?

Frontiers Research Topics are very popular trademarks of the Frontiers Journals Series: they are collections of at least ten articles, all centered on a particular subject. With their unique mix of varied contributions from Original Research to Review Articles, Frontiers Research Topics unify the most influential researchers, the latest key findings and historical advances in a hot research area! Find out more on how to host your own Frontiers Research Topic or contribute to one as an author by contacting the Frontiers Editorial Office: researchtopics@frontiersin.org

THE FIBROBLAST GROWTH FACTOR SIGNALING PATHWAY IN METABOLIC REGULATION, DEVELOPMENT, DISEASE AND REPAIR AFTER INJURY

Topic Editors:
Zhouguang Wang, Albert Einstein College of Medicine, United States
Xiaokun Li, Wenzhou Medical University, China
Li Lin, Wenzhou Medical University, China
Saverio Bellusci, University of Giessen, Germany
Jin-San Zhang, Mayo Clinic, United States

Citation: Wang, Z., Li, X., Lin, L., Bellusci, S., Zhang, J.-S., eds. (2020). The Fibroblast Growth Factor Signaling Pathway in Metabolic Regulation, Development, Disease and Repair After Injury. Lausanne: Frontiers Media SA. doi: 10.3389/978-2-88966-128-2

Table of Contents

frontiers in Pharmacology

EDITORIAL
published: 08 September 2020
doi: 10.3389/fphar.2020.586654

Editorial: The Fibroblast Growth Factor Signaling Pathway in Metabolic Regulation, Development, Disease, and Repair After Injury

Zhouguang Wang[1,2*], *Li Lin*[1*], *Jin-San Zhang*[1,3], *Xingxing Zhong*[2], *Saverio Bellusci*[4] *and Xiaokun Li*[1*]

[1] School of Pharmaceutical Sciences, Wenzhou Medical University, Wenzhou, China, [2] Department of Molecular Pharmacology, Albert Einstein College of Medicine, Bronx, NY, United States, [3] Division of Oncology Research, Mayo Clinic, Rochester, MN, United States, [4] Cardiopulmonary Institute, Member of the German Lung Center, Justus Liebig University, Giessen, Germany

Keywords: FGF (fibroblast growth factor), regeneration, development, metabolic regulation, ischema-reperfusion injury

Editorial on the Research Topic

The Fibroblast Growth Factor Signaling Pathway in Metabolic Regulation, Development, Disease and Repair After Injury

Fibroblast growth factors, or FGFs, are a family of structurally related proteins with diverse functions during embryonic development, tissue repair, cancer, and metabolic homeostasis. In humans, 22 members of the FGFs family have been identified, all of which are structurally related signaling molecules. They have been alternately referred to as "pluripotent" growth factors and as "promiscuous" growth factors due to their multiple actions on a wide range of cell types. Four receptor subtypes of FGFs can be activated by more than 20 different FGF ligands. Thus, the functions of FGFs in developmental processes can include mesoderm induction, anterior-posterior patterning, limb development, neural induction, and neural development.

This Research Topic gathers original research and review papers on the different roles of FGFs/FGFRs in early development, organogenesis, musculoskeletal biology, nervous system, metabolism, tumorigenesis, intracellular signaling, and emerging research areas. This collection of papers sheds light on the drug development of FGF, with a focus on the new development for FGFs treatment or mechanisms of action, ranging from basic research to clinical translational studies.

The 17 accepted articles consist of 14 Original Research articles and 3 Reviews or Mini-Reviews, which demonstrated roles of FGFs in various diseases including neural diseases, diabetes-related diseases, renal injury, lung diseases, digestive diseases, and vascular diseases.

Four research articles elucidated that FGFs are involved in alleviating neural diseases *via* different mechanisms. By using 6-OHDA–induced Parkinson's disease (PD) mice model, Zhong et al. found that acid FGF promoted autophagy by inhibiting ER stress-induced TRB3 overexpression during PD development and subsequently ameliorated 6-OHDA–induced neuronal apoptosis (Zhong et al.). Zhu S. et al. reported the anti-apoptotic effect of another FGF member FGF22 in mediating neural disease (Zhu S. et al.). FGF22 treatment was associated with reduced pro-apoptosis proteins and increased recovery of the spinal cord injury in mouse animals. Intriguingly, the number of neurons and expression of an axon regeneration related protein (growth-associated protein 43) were also increased

OPEN ACCESS

Edited and reviewed by:
Alastair Stewart,
The University of Melbourne, Australia

***Correspondence:**
Zhouguang Wang
wzhouguang@gmail.com
Li Lin
linliwz@163.com
Xiaokun Li
lixk1964@163.com

Specialty section:
This article was submitted to Translational Pharmacology, a section of the journal Frontiers in Pharmacology

Received: *23 July 2020*
Accepted: *24 August 2020*
Published: *08 September 2020*

Citation:
Wang Z, Lin L, Zhang J-S, Zhong X, Bellusci S and Li X (2020) Editorial: The Fibroblast Growth Factor Signaling Pathway in Metabolic Regulation, Development, Disease, and Repair After Injury. Front. Pharmacol. 11:586654. doi: 10.3389/fphar.2020.586654

after FGF22 administration. The beneficial effects of FGF22 in ER stress-induced spinal cord injury could be partially due to neuron regeneration (Zhu S. et al.). This hypothesis is consistent with what has been claimed by Dong et al. that FGF10 treatment promoted axonal regeneration and functional recovery in sciatic nerve injury rat (Dong et al.). FGF10 was also revealed to prevent Schwann cells from oxidative stress-induced apoptosis, which was probably related to the activation of phosphatidylinositol-3 kinase/protein kinase B (PI3K/Akt) signaling (Dong et al.). In addition to the roles of anti-apoptosis and promoting regeneration, the anti-inflammatory function of FGFs were also involved in repairing neural diseases. Wang et al. treated LPS-induced depression mouse model with recombinant human FGF2 and found that depressive-like behavior was significantly relieved (Wang et al.). The decreased microglial expression of proinflammatory cytokines suggested the involvement of FGF2 in NF-κB suppression (Wang et al.).

Four of these research articles investigated roles of FGFs in diabetes-related diseases, providing new insights into treatment of diabetes and related complications. In Xu et al.'s research, db/db mice revealed improved blood glucose level and diabetes-induced liver steatosis, fibrosis and apoptosis after intraperitoneally injected with FGF1 (Xu et al.). Mechanistic investigations suggested that these effects were the results of attenuated oxidative stress and ER stress (Xu et al.). The anti-oxidative stress function of another FGF member, basic Fibroblast Growth Factor, was shown to play vital roles in ameliorating diabetic nephropathy (Wei et al.). Studies have shown that FGF1 has a wide range of physiological functions, the application *in vivo* is limited because of the lack of an efficient and safe delivery system. Nanoliposomes and ultrasound targeted microbubble destruction techniques provided hopes into solving this problem. Zheng et al. evaluated the preventive effect of FGF1-loaded nanoliposomes (FGF1-nlip) combined with ultrasound-targeted microbubble destruction (UTMD) on diabetic cardiomyopathy using ultrasound examination and found that echocardiographic indexes were significantly higher than those in FGF1 and FGF1-nlip treatment groups (Zheng et al.). Islet transplantation is considered a potential therapy for diabetes. However, the extracellular matrix (EXM) proteins essential for islets survival are impaired in the isolation process before islet transplantation. Zhu Q. et al. elucidated the beneficial effects of recombinant human collagen with FGF2 application in islet transplantation. The system provided insights into islet transplantation with a simulated EXM microenvironment for the revascularization and attachment of islets to the transplantation region (Zhu Q. et al.).

On another hand, Tan et al. investigated the molecular pathways underlying the protective effect of FGF10 on renal ischemia-reperfusion (I/R) injury using Sprague-Dawley rat model (Tan et al.). It was shown that FGF10 attenuated I/R-induced renal epithelial apoptosis by suppressing excessive ER stress in renal I/R injury, and the function was partially mediated by the activation of the MEK–ERK1/2 signaling pathway. Accumulating evidence suggests that FGFs play important roles in renal I/R injury. As summarized in Deng et al.'s review (Deng et al.), FGFs mediate repair process of I/R injury-caused acute kidney injury and could offer a potential therapeutic option in the future. Chen Q. et al. studied the physiological role of FGF21 in cisplatin-treated AKI and it was revealed that recombinant FGF21 significantly improved renal function in cisplatin-induced damage *via* SITT1 signaling pathway (Chen Q. et al.). Non-mitogenic FGF1 was found to enhance angiogenesis following ischemic stroke by regulating the sphingosine-1-phosphate 1 pathway (Zou et al.). Two reviews summarized the progress of FGF in corneal neovascularization (Chen M. et al.) and fibroblast FGF10 in duodenal atresia (Jones et al.).

In addition to neural diseases, diabetes-related diseases and renal damage, functions of FGFs were also investigated in other diseases. It was claimed by Lin et al. that administration of engineered FGF1 mutant-FGF1$^{\Delta HBS}$ protected liver in alpha naphthylisothiocyanate (ANIT)-induced intrahepatic cholestasis mice by reducing hepatic bile acid accumulation (Lin et al.). Yuan et al. found that the temporospatial expression of FGFR1 and FGFR2 varied during lung development, homeostasis, and regeneration, indicating the involvement of FGF signaling pathways in lung development and diseases (Yuan et al.). To overcome the treatment resistance toward problem of the tyrosine kinase inhibitor (TKI) in non-small-cell lung cancer (NSCLC), Chen G. et al. evaluated the efficacy of the compound 15c, a novel dual inhibitor of EGFR$^{L858R/T790M}$ and FGFR1, which revealed that the compound 15c efficiently overcame the EGFR-TKI resistance of NSCLC (Chen G. et al.).

In summary, both the research articles and reviews in this Research Topic are an excellent source of information about the current knowledge in the fibroblast growth factor signaling pathway in metabolic regulation, development, disease, and repair after injury field.

AUTHOR CONTRIBUTIONS

ZW and XZ wrote this article. LL, J-SZ, SB and XL have made a direct and intellectual contribution to the work. All authors have approved the article for publication.

FUNDING

This work was supported by grants from Advanced Postdoctoral Programs of Zhejiang (zj2019030 to Z.W.), China Postdoctoral Science Foundation (2019M662015 to Z.W.). National Natural Science Foundation of China (No.81771284, 81971180 to L.L.), Research Unit of Research and Clinical Translation of Cell Growth Factors and Diseases, Chinese Academy of Medical Science (No.2019RU010 to X.L.).

Conflict of Interest: The authors declare that the research was conducted in the absence of any commercial or financial relationships that could be construed as a potential conflict of interest.

frontiers in Pharmacology

ORIGINAL RESEARCH
published: 16 October 2019
doi: 10.3389/fphar.2019.01224

FGF10 Enhances Peripheral Nerve Regeneration *via* the Preactivation of the PI3K/Akt Signaling-Mediated Antioxidant Response

Lvpeng Dong[1,2†], Rui Li[2,3†], Duohui Li[2], Beini Wang[2], Yingfeng Lu[1], Peifeng Li[1], Fangzheng Yu[1], Yonglong Jin[1], Xiao Ni[1], Yanqing Wu[2], Shengnan Yang[2], Guanxi Lv[2], Xiaokun Li[2], Jian Xiao[2] and Jian Wang[1]**

[1] Department of Hand Surgery and Peripheral Neurosurgery, The First Affiliated Hospital of Wenzhou Medical University, Wenzhou, China, [2] Molecular Pharmacology Research Center, School of Pharmaceutical Science, Wenzhou Medical University, Wenzhou, China, [3] School of Chemistry, Sun Yat-sen University, Guangzhou, China

OPEN ACCESS

Edited by:
Zhouguang Wang,
Albert Einstein College of Medicine,
United States

Reviewed by:
Yingnyu Gao,
Marshall University,
United States
Dinghong Zhang,
University of California,
San Diego,United States

***Correspondence:**
Jian Xiao
xfxj2000@126.com
Jian Wang
jianwang0516@126.com

†These authors have contributed equally to this work

Specialty section:
This article was submitted to Translational Pharmacology, a section of the journal Frontiers in Pharmacology

Received: 25 July 2019
Accepted: 23 September 2019
Published: 16 October 2019

Citation:
Dong L, Li R, Li D, Wang B, Lu Y, Li P, Yu F, Jin Y, Ni X, Wu Y, Yang S, Lv G, Li X, Xiao J and Wang J (2019) FGF10 Enhances Peripheral Nerve Regeneration via the Preactivation of the PI3K/Akt Signaling-Mediated Antioxidant Response. Front. Pharmacol. 10:1224. doi: 10.3389/fphar.2019.01224

The process of axonal regeneration after peripheral nerve injury (PNI) is slow and mostly incomplete. Previous studies have investigated the neuroprotective effects of fibroblast growth factor 10 (FGF10) against spinal cord injury and cerebral ischemia brain injury. However, the role of FGF10 in peripheral nerve regeneration remains unknown. In this study, we aimed to investigate the underlying therapeutic effects of FGF10 on nerve regeneration and functional recovery after PNI and to explore the associated mechanism. Our results showed that FGF10 administration promoted axonal regeneration and functional recovery after nerve damage. Moreover, exogenous FGF10 treatment also prevented SCs from excessive oxidative stress-induced apoptosis, which was probably related to the activation of phosphatidylinositol-3 kinase/protein kinase B (PI3K/Akt) signaling. The inhibition of the PI3K/Akt pathway by the specific inhibitor LY294002 partially reversed the therapeutic effects of FGF10 both *in vivo* and *in vitro*. Thus, from our perspective, FGF10 may be a promising therapeutic drug for repairing sciatic nerve damage through countering excessive oxidative stress-induced SC apoptosis.

Keywords: fibroblast growth factor 10, axonal regeneration, peripheral nerve injury, oxidative stress, apoptosis

INTRODUCTION

Unlike the central nervous system (CNS), the peripheral nervous system (PNS) retains a certain regeneration capacity, which enables the regrowth of damaged axons and impaired nerves (Chen et al., 2007). Nevertheless, the regeneration rate of peripheral nerves is slow, and proximal nerve segments rarely regrow over long distances to their target organs. As a result, it affects the quality of life of patients and is a major socioeconomic burden (Sulaiman and Gordon, 2009; Gordon, 2016).

Abbreviations: bFGF, basic fibroblast growth factor; BSA, bovine serum albumin; CCK-8, cell counting kit; CNS, central nervous system; DCFH-DA, 2′, 7′-dichlorodihydrofluorescein diacetate; DMEM, Dulbecco's modified Eagle medium; FBS, fetal bovine serum; FGFs, fibroblast growth factors; FGF10, fibroblast growth factor 10; FGF21, fibroblast growth factor 21; HE, hematoxylin and eosin; NGF, nerve growth factor; OCT, optimum cutting temperature; PNI, peripheral nerve injury; PNS, peripheral nervous system; PWT, paw withdrawal threshold; P/S, penicillin/streptomycin; ROS, reactive oxygen species; SCI, spinal cord injury; SCs, Schwann cells; SFI, sciatic function index.

Because nerve regeneration is a complex process that involves interactions among cellular elements, cytokines, extracellular matrix, and growth factors, the complete recovery of injured nerves is difficult (Caillaud et al., 2018).

Schwann cells (SCs), the myelinating cells of the PNS, are essential for nerve regeneration and for the saltatory conduction of action potentials (Scherer and Wrabetz, 2008). Following nerve injury, denervated SCs begin to dedifferentiate, migrate, proliferate, and transform into regeneration-promoting new cells, called repair SCs (Jessen and Mirsky, 2016). This type of SCs is able to generate a favorable microenvironment for axonal growth by clearing degenerated myelin debris and secreting neurotrophic factors (Jessen et al., 2015). Thus, promoting SCs survival and inhibiting apoptosis are vital for maintaining structural and functional integrity following peripheral nerve injury (PNI).

Oxidative stress, characterized by excessive reactive oxygen species (ROS), is a critical initiating factor for PNI (Yang et al., 2016; Ino and Iino, 2017; He et al., 2018). The overproduction of ROS disturbs the oxidation-antioxidant equilibrium and leads to mitochondrial dysfunction, lipid peroxidation, and cell apoptosis. Furthermore, excessive ROS production in SCs causes dysfunction in DNA synthesis, protein expression, and mitochondrial structure (Finkel and Holbrook, 2000; Wang et al., 2013). Therefore, it is essential to inhibit excessive ROS generation to maintain the SC function and the interactions between SCs and other cell types after PNI.

The nuclear factor transcription erythroid-like factor 2 (Nrf2) plays a critical role in regulating redox homoeostasis. The activation of Nrf2 results in the accumulation of some enzymes, such as heme oxygenase-1 (HO-1), NAD(P)H:quinone oxidoreductase (NQO1), and superoxide dismutase (SOD2) (Son et al., 2013). Nrf2 is also closely related to cell apoptosis through upregulating the expression of Bcl-2, an antiapoptotic protein. Low levels of Bcl-2 expression and increased expression of proapoptotic proteins, including Bax and caspase-3, are typical markers of cell apoptosis (Niture and Jaiswal, 2011; Niture and Jaiswal, 2012; Niture et al., 2014).

The phosphatidylinositol-3 kinase/protein kinase B (PI3K/Akt) pathway has been reported to play a major role in the modulation of axonal growth, myelin sheath formation, and SC function in the PNS. The activation of Akt in SCs increases the expression of myelin proteins, including myelin basic protein (MBP) and myelin basic zero (MPZ), which regulates remyelination. In contrast, inhibiting the PI3K/Akt pathway with LY294002 significantly attenuates SCs migration (Lv et al., 2015; Domenech-Estevez et al., 2016). Furthermore, the inhibition of this signaling pathway also obviously decreases the synthesis of proliferating cell nuclear antigen (PCNA; a marker of cell proliferation) in SCs (He et al., 2011). All of these findings show that the PI3K/Akt pathway modulates the multiple functions of SCs, including migration, proliferation, and remyelination.

FGF10 is a member of the fibroblast growth factors (FGFs) that plays important roles in regulating biological functions such as morphogenesis, proliferation, and the inhibition of apoptosis (Kelleher et al., 2013). FGF10, which was originally identified in rat embryos, mediates biological signaling in a paracrine manner (Itoh, 2016). Furthermore, FGF10 is widely distributed in many organs, such as adipose tissue, the lungs, the limbs, and the prostate, and plays an essential role in regulating cell mitogenesis, proliferation, differentiation, and migration (Min et al., 1998; Thomson and Cunha, 1999; Jimenez and Rampy, 1999; Sakaue et al., 2002). A recent study showed that FGF10 expression in neurons is increased after spinal cord injury (SCI) and that exogenous FGF10 administration induces functional recovery and attenuates the inflammatory response by activating PI3K/Akt signaling in an animal model of SCI (Chen et al., 2017). Another study demonstrated that FGF10 protects neurons and ameliorates cerebral ischemia injury by activating the PI3K/Akt signaling pathway and reducing NF-κB-mediated neuroinflammation (Li et al., 2015b; Li et al., 2016). However, the effects of FGF10 on functional recovery after PNI and the associated molecular mechanism have not been documented to date.

The aim of the present study was to investigate whether FGF10 plays a neuroprotective role in facilitating axonal regeneration and functional recovery after PNI and to explore the related molecular mechanisms. Our results indicate that FGF10 treatment reduces SCs apoptosis, enhances axonal growth and regeneration, and improves functional recovery following PNI. Furthermore, this beneficial effect is most likely regulated by attenuating PI3K/Akt signaling-mediated oxidative stress both *in vivo* and *in vitro*. Collectively, our results suggest that FGF10 performs a certain role and may be a potential agent for the treatment of PNI.

MATERIALS AND METHODS

Reagents and Antibodies

FGF10 was obtained from the School of Pharmacy, Wenzhou Medical University (Wenzhou, China). Antibodies against *p*-Akt (#13038), Bax (#14796), Bcl-2 (#2764), and cleaved-caspase-3 (#9664) were obtained from Cell Signaling Technology. Antibodies against MBP (ab40390), NF200 (ab4680), Nrf2 (ab62352), NQO1 (ab34173), MPZ (ab31851), and Akt (ab179463), Histone H3 (ab176842) and the PI3K/Akt inhibitor LY294002 (ab120243), were purchased from Abcam. Antibodies against GAPDH (10494-1-AP), HO-1 (10701-1-AP), SOD2 (24217-1-AP), and PCNA (10205-2-AP) were purchased from Proteintech. An antibody against S100 (sc-53438) was obtained from Santa Cruz Biotechnology.

Animals

Male SD rats (200~220 g) were purchased from the Laboratory Animal Center of Fujian Medical University (Fujian, China). A temperature of 23 ± 2 °C, a humidity of 35-60%, and a 12:12 h light-dark cycle were applied as standardized laboratory conditions for housing all rats. Meanwhile, they were provided with food and water and were habituated to these conditions for at least 7 days before the experiment. The use of animals in this study was approved by the Animal Experimentation Ethics Committee of Wenzhou Medical University, Wenzhou,

China. The living conditions and experimental procedures were conducted in accordance with the National Institutes of Health Guideline concerning the Care and Use of Laboratory Animals.

PNI Model and Drug Injection

The procedure for generating the animal model was described previously (Li et al., 2017b). In brief, each animal was anaesthetized by an intraperitoneal injection of 10% chloral hydrate (3.5 ml/kg). An incision was made in the skin to expose the right sciatic nerve. Then, this exposed nerve was crushed with two vascular clips (Oscar, China). The vascular clips clamped the sciatic nerve 7 mm proximal from the sciatic notch at the two ends with 30 g of force for 2 min. Thereafter, the incised skin was sutured with a 4-0 nonabsorbable suture.

Following surgery, all the animals were randomly allocated to four groups (n = 10 for each): the sham group, the PNI group, the FGF10 group, and the FGF10+LY294002 group. The sham group received the same surgical procedure to expose the sciatic nerve but did not undergo compression injury. For the FGF10 group, each rat was injected intramuscularly with 5 μg of FGF10 solution (25 μg/ml) once daily for 28 consecutive days. For the FGF10 + LY294002 group, after the injection of FGF10 solution, each rat was also intravenously injected with LY294002 (a PI3K inhibitor, 0.3 mg/kg/day) (Chen et al., 2017). The rats in the sham and PNI groups were only injected with the same volume of saline solution. After 28 days, all rats were sacrificed to harvest the sciatic nerve for pathology index analysis.

Von Frey Test and Walking Track Analysis

Rats were habituated to an elevated metal mesh floor for at least 1 h before their responses to mechanical stimulation were tested with von Frey filaments (NC12775; North Coast Medical Inc, CA, USA). von Frey filaments with forces ranging from 2–180 g were applied in ascending order to the third and fourth toes of the plantar surface of the hind paw until they bent. The filaments were repeated five times, and the results of paw withdrawal were recorded.

The gait of the rats along a 100 × 10 × 15 cm corridor, the bottom of which was covered with a 90 × 10 cm piece of white paper, was analyzed. Red ink was painted on the hind paws of the rats. The sciatic functional index (SFI) was calculated based on the colored footprints according to the following formula by Bain et al. (1989): SFI = −38. 3 × (EPL- NPL)/NPL + 109.5 × (ETS -NTS)/NTS + 13.3 × (EIT - NIT)/NIT-8.8, where E is the right hind limb; N is the left hind limb; PL is the longitudinal distance of the longest footprint; IT is the distance between the second and fourth toes; and TS is the distance between the first and fifth toes. An index of approximately 0 reflects normal function, whereas an index of −100 indicates complete impairment. Two observers who were unaware of the experimental procedures performed the test from day 1 to day 28 following the surgical procedures.

RSC96 Culture and Treatment

The RSC96 SC line was obtained from ScienCell Research Laboratories. The cells were cultured in Dulbecco's modified Eagle medium (DMEM) with 10% fetal bovine serum (FBS, Gibco, USA) and 1% penicillin/streptomycin solution (P/S) in a humidified incubator (37°C, 5% CO_2). After two passages, the cells were seeded in 96-well plates (5×10^3 cells/well), and various concentrations of FGF10 (0.043, 0.43, 4.3, 43 nm) were added for 2 h. Then, the medium was supplemented with 100-μm H_2O_2 for another 2 h. To further evaluate the effect of PI3K/Akt activation on oxidative injury, cells were pretreated with the PI3K inhibitor LY294002 (20 μm) (Wang et al., 2012) for 2 h before the addition of FGF10.

To evaluate cell survival, a cell counting kit (CCK-8, Beyotime Institute of Biotechnology, China) was used. The test was performed according to the manufacturer's instructions. In brief, 10 μl of CCK-8 solution were added to each well, and the cells were incubated for 2 h at 37°C. The optical density was measured at 450 nm using a microplate reader (Thermo Fisher Scientific, Waltham, MA). All experiments were repeated at least three times.

Assays of Intracellular ROS Generation

Intracellular ROS generation was measured by an ROS Assay Kit (DCFH-DA, S0033, Beyotime, China). SCs were plated in 6-well plates at a density of 1×10^5 cells/ml for 24 h. After treatment with H_2O_2 with/without FGF10 plus LY294002, 10 μm 2′, 7′-dichlorodihydrofluorescein diacetate (DCFH-DA) were added to the culture medium for 20 min. Subsequently, the fluorescence of the cells in five randomly fields for each group was imaged with a Nikon ECLIPSE 80i microscope (Nikon, Japan). ImageJ software was used for quantitative analysis.

To further analyze the change of ROS, the DCF fluorescence was detected by a fluorescence microplate reader (Genios, TECAN) at 485-nm excitation and 53-nm emission.

Hematoxylin-Eosin (He) Staining

The sciatic nerve tissues were harvested following the established methods and embedded in paraffin (Li et al., 2017b). The nerves were fixed in 4% paraformaldehyde in 0.1 M phosphate buffer overnight and embedded in paraffin the next day. The longitudinal sections were cut into 5-μm thick sections for HE staining; the sections were dyed with hematoxylin for 5 min and with eosin for 10 min. The images were captured using a Nikon ECLIPSE 80i microscope (Nikon, Japan).

Immunoblotting

Immunoblotting analysis of sciatic nerves and cell extracts were performed as described previously (Zhang et al., 2014; Li et al., 2018b). Briefly, cells and sciatic nerves were lysed using RIPA with protease (Boster, AR0101/AR0103) and phosphatase inhibitors (Applygen, P1260). The lysate was centrifuged at 12 000 g for 20 min. For PCNA detection, the sciatic nerve segments was mechanically homogenized. Then, cytosol and nuclear proteins were extracted using the nuclear and cytoplasmic protein extraction kit (Beyotime Biotechnology, Wuhan, China) and centrifuged at 5000 r.p.m. for 10 min at 4°C to extract the nuclear components (Li et al., 2015a). The protein concentration

was determined by bicinchoninic acid (BCA) reagents (Thermo Fisher Scientific, Rockford, IL, USA). Sixty micrograms of protein was separated by 8-12% SDS-PAGE and transferred onto PVDF membranes (Bio-Rad, Hercules, CA, USA). After blocking with 5% nonfat milk, the membranes were incubated with primary antibodies overnight at 4°C. The antibodies included *p*-Akt (1:1000), Akt (1:1000), Nrf2 (1:1000), NQO1 (1:1000), HO-1 (1:1000), SOD2 (1:2000), MPZ (1:1000), S100 (1:200), PCNA (1:1000), Bcl-2 (1:1000), Bax (1:1000), Histone H3 (1:1000) and GAPDH (1:10000). The next day, the membranes were incubated with horseradish peroxidase-conjugated secondary antibodies for 1 h. The visualization of signals and band intensity were analyzed by chemiluminescence using a gel imaging system (Bio-Rad Laboratories, Hercules, CA, USA). Three independent samples were analyzed.

Immunofluorescence Staining

For animal tissues, 5-μm thick longitudinal sections were washed in PBS three times after being embedded in optimum cutting temperature (OCT) compound. For cells, SCs were fixed in 4% paraformaldehyde in PBS for 20 min. Then, the tissue or cell samples were blocked in 5% bovine serum albumin (BSA) containing 0.1% Triton X-100 for 30 min. After incubation with primary antibodies overnight at 4°C, the slides were incubated with a fluorochrome-labeled secondary antibody for 1 h. The primary antibodies included NF200 (1:10000), MBP (1:1000), and Nrf2 (1:1000). The nuclei were stained with DAPI for 7 min. Image acquisition was performed with a Nikon ECLIPSE Ti microscope (Nikon, Tokyo, Japan).

Statistical Analysis

All data are expressed as the mean ± SEM. Analysis of statistical significance was performed by one-way ANOVA with Tukey's posttest with GraphPad Prism (GraphPad Software version 6.0, La Jolla, CA, USA). *P*-values less than 0.05 were considered statistically significant.

RESULTS

Fgf10 Promotes Functional Recovery

To assess whether the injection of FGF10 increase sensory and motor recovery, walking track analysis and paw withdrawal thresholds were evaluated every week for 4 weeks following surgery. The walking tracks indicated no significant difference among the three groups in the first 2 weeks after surgery. However, the SFI value of the FGF10-treated group began to increase and was significantly greater than that of the PNI group at weeks 3 and 4 (**Figures 1A**, **B**, $^{***}P < 0.001$). Nevertheless, compared with the group that received FGF10 only, the group that received FGF10 and LY294002 co-administration exhibited motor functional recovery by week 4 (**Figures 1A**, **B**, $^{***}P < 0.001$).

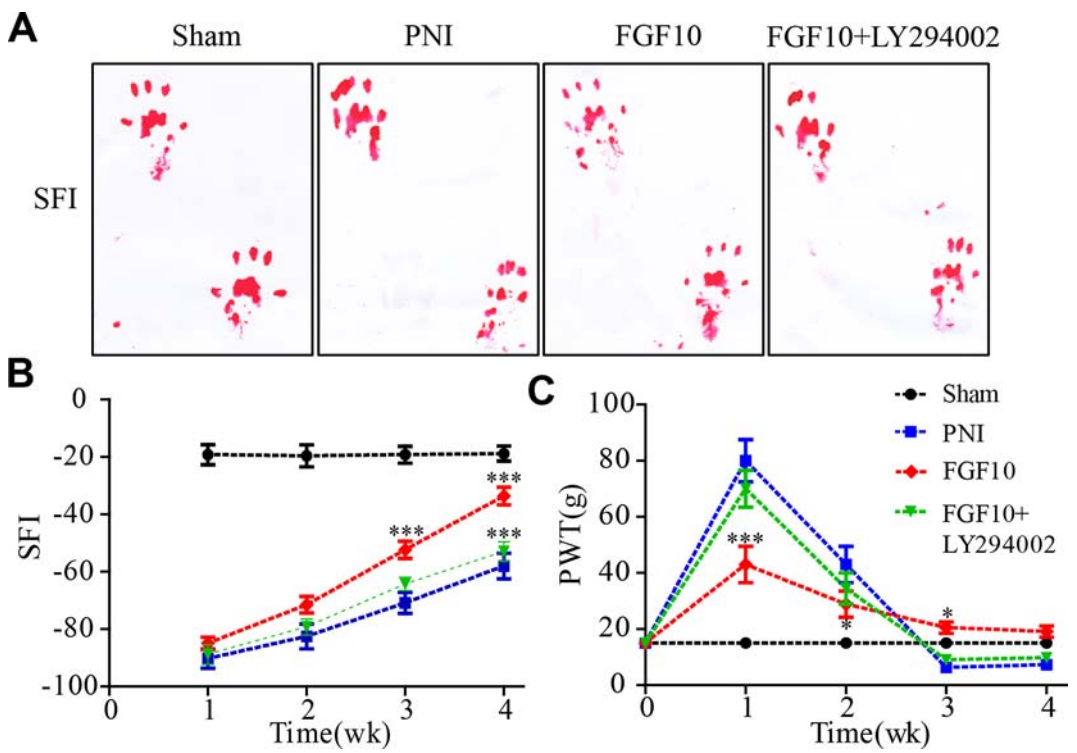

FIGURE 1 | Fibroblast growth factor 10 (FGF10) enhances motor and sensory functional recovery after peripheral nerve injury (PNI). **(A)** Photographs of rat footprints 4 weeks after sciatic nerve crush. **(B)** Statistical analysis of the sciatic functional index (SFI) at the indicated times postoperatively. **(C)** Paw mechanical withdrawal thresholds were measured at predetermined time points. FGF10 group vs PNI group: $^{*}P < 0.05$, $^{***}P < 0.001$. FGF10 group vs FGF10+ LY294002 group: $^{***}P < 0.001$. All data represent the mean values ± SEM; n = 8 in each group.

To evaluate sensory functional recovery to mechanical stimuli, all animals from the four groups were subjected to the von Frey test. As illustrated in **Figure 1C**, the sensory recovery of all groups was rather poor 1 week after crush injury, but recovery in the FGF10 group was better than that in the PNI group (***$P < 0.001$). The mechanical thresholds gradually decreased in the subsequent weeks. Although the results seemed to show that sensory recovery in the FGF10 group was inferior to that in the PNI group and FGF10 + LY294002 group, the withdrawal threshold in the two latter groups was even lower than that in the control group, suggesting that the PNI rats treated with/without FGF10+LY294002 exhibited hyperalgesia and that FGF10 treatment rescued PNI-induced hyperalgesia at a later stage of nerve recovery. Taken together, these results suggest that FGF10 continuously enhances the recovery of locomotor and sensory function in acute PNI.

Fgf10 Facilitates Nerve Regeneration

The histological recovery of the injured nerve in each group was evaluated by HE staining and coimmunostaining for neurofilament 200 (NF-200; represents axonal growth) and MBP (a marker of myelination). HE staining revealed that the axonal fibers in the PNI group were scarce and irregular, while the nerve fibers in the FGF10-treated group appeared remarkably regenerated and regular (**Figure 2A**). Double immunofluorescence staining for MBP and NF200 showed that the density of regenerated axons and myelin in the FGF10 group was significantly higher than that in the PNI group and that the degree of regeneration was enough to induce a morphology similar to that of normal nerves (**Figures 2B–D**). In contrast, the immunoreactivity of NF200 and MBP was greatly attenuated after the coadministration of LY294002 and FGF10.

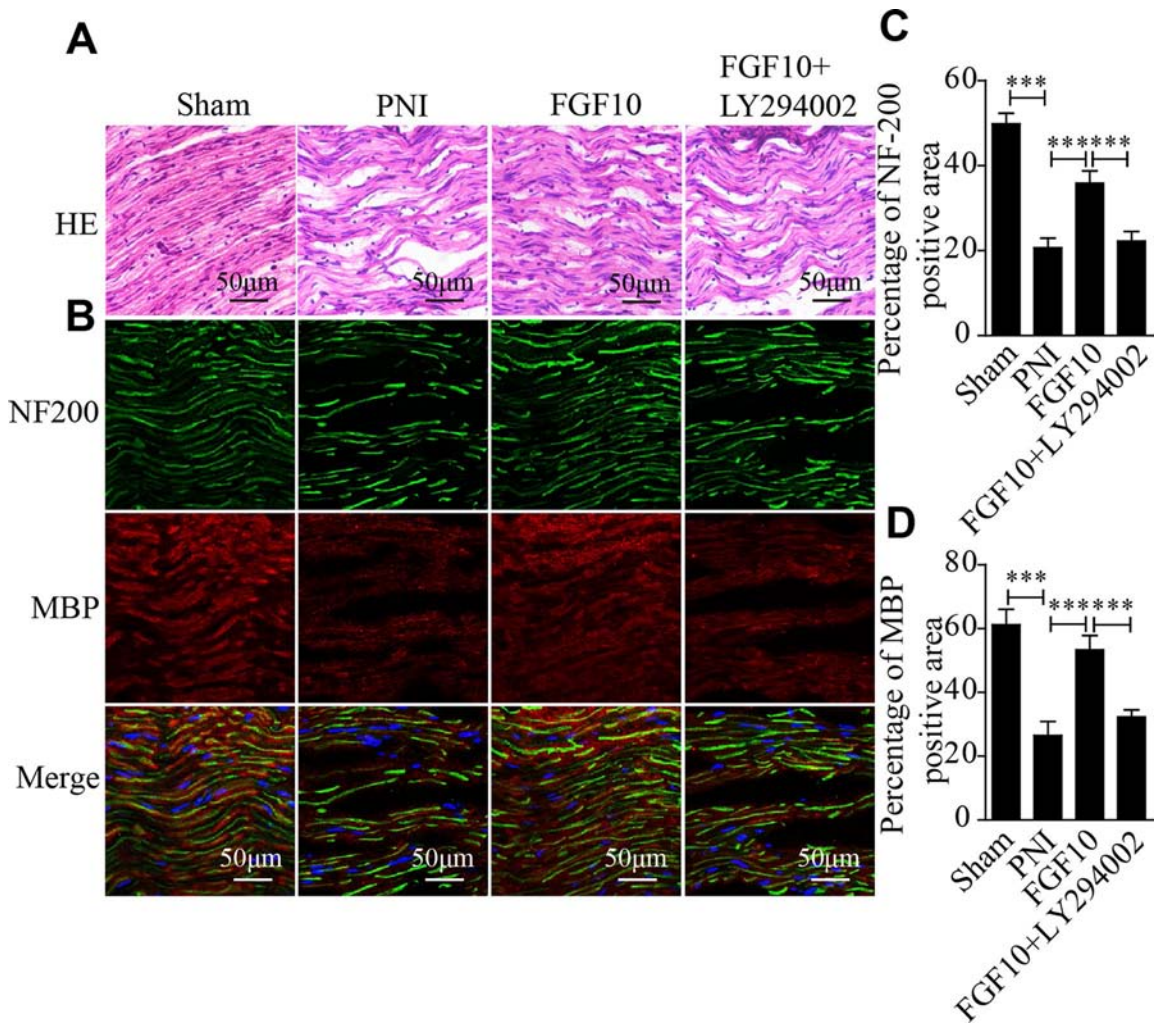

FIGURE 2 | Fibroblast growth factor 10 (FGF10) promotes axonal regeneration, as determined by histological evaluation. **(A)** Longitudinal sections of regenerated nerves from each group were stained with Hematoxylin-Eosin (HE) 28 days postinjury. Scale bars = 50 μm. **(B)** Immunofluorescence staining for myelin basic protein (MBP) (red) and NF-200 (green) in longitudinal sections. Scale bars = 50 μm. **(C, D)** Quantitative analysis of the fluorescence intensity of MBP and NF-200 28 days following injury. The data are presented as the mean ± SEM, n = 5. Sham group vs PNI group: ***$P < 0.001$. FGF10 group vs peripheral nerve injury (PNI) group: ***$P < 0.001$. FGF10 group vs FGF10+LY294002 group: ***$P < 0.001$.

Fgf10 Increases Functional Protein Secretion

S100 is a SC marker that regulates cellular metabolism, motility and proliferation. Myelin protein zero (MPZ; also called P0) is a major extrinsic membrane protein of myelin in the PNS. MPZ function includes forming myelin and maintaining compact myelin morphology. PCNA is a nucleoprotein that is a marker of cell proliferation. The expression of these proteins was quantified using western blotting analysis. As shown in **Figure 3A**, the protein expression of S100, MPZ and PCNA in the FGF10 group was significantly increased compared with that in the PNI group, while this effect was reversed by the injection of LY294002. Quantitative analysis also showed the same trend (**Figures 3B–D**). These data reveal that the beneficial effect of FGF10 is able to upregulate the functional expression of these proteins and that this effect further contributes to SC remyelination and axonal regeneration.

FGF10 Inhibits the Excessive Expression of Oxidative Stress- and Apoptosis-Related Proteins by Activating PI3k/Akt Signaling

To test whether FGF10 treatment inhibits PNI-induced oxidative stress in the sciatic nerve, the expression of oxidative stress-related proteins, including Nrf2, NQO1, SOD2 and HO-1, was detected by western blotting. The levels of these oxidative stress-associated molecules were slightly increased by PNI. FGF10 treatment further increased the production of these antioxidant proteins to a large degree (**Figures 4A–E**).

Previous studies have demonstrated that the recovery of neurological deficits is closely related to the activation of the PI3k/Akt pathway (Wu et al., 2016; Sang et al., 2018). Inspired by this fact, we measured the *p*-Akt and Akt levels using western blotting. Here, we found that the levels of Akt phosphorylation were slightly increased after PNI, and these levels were further

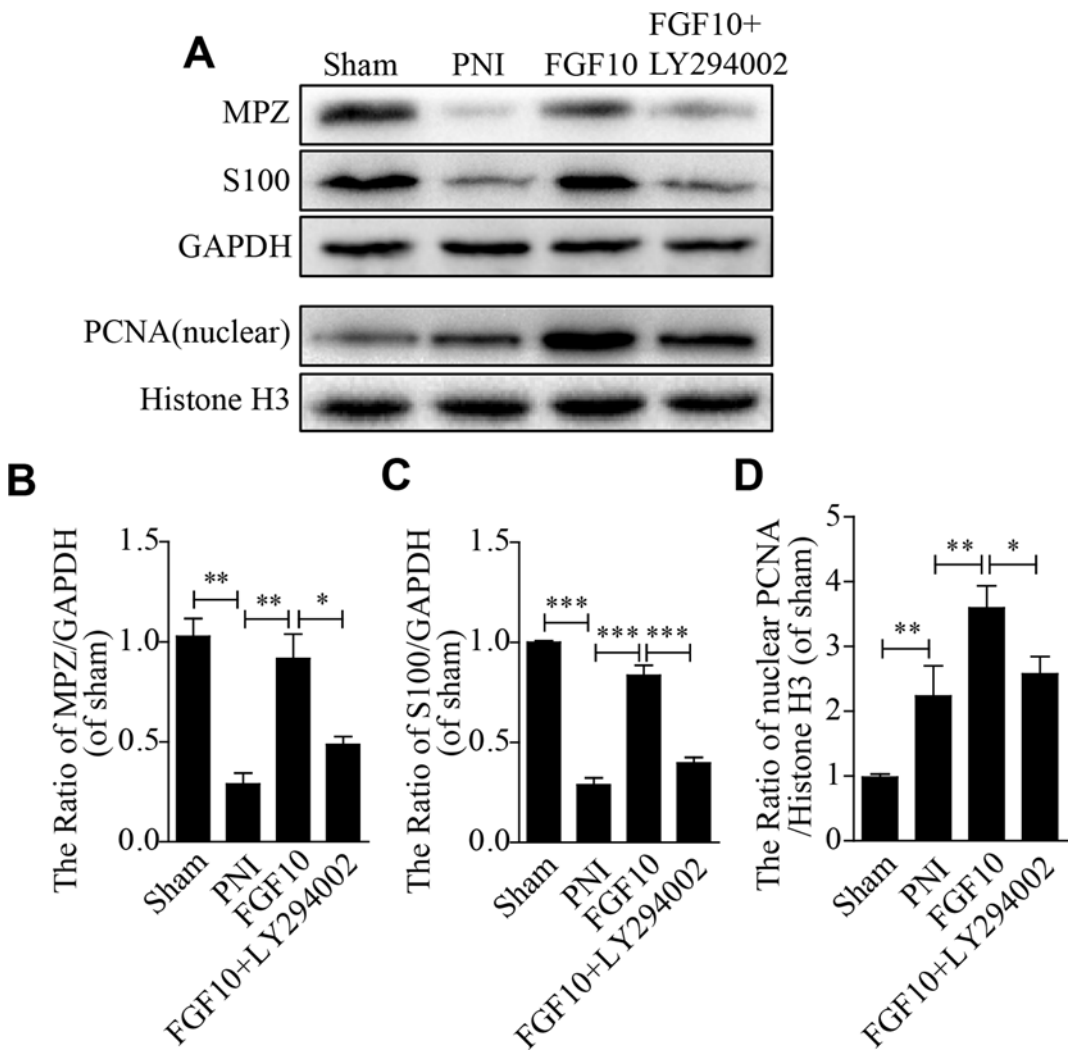

FIGURE 3 | Fibroblast growth factor 10 (FGF10) enhances the expression of functional proteins after sciatic nerve injury. **(A–D)** Representative immunoblotting images of myelin basic zero (MPZ), S100, and proliferating cell nuclear antigen (PCNA) expression and the quantification of protein levels in sciatic nerve lesions 28 days postinjury. The data are presented as the mean ± SEM, n = 3. Sham group vs peripheral nerve injury (PNI) group: $^{**}P < 0.01$, $^{***}P < 0.001$. FGF10 group vs PNI group: $^{**}P < 0.01$, $^{***}P < 0.001$. FGF10 group vs FGF10+LY294002 group: $^{*}P < 0.05$, $^{**}P < 0.01$, $^{***}P < 0.001$.

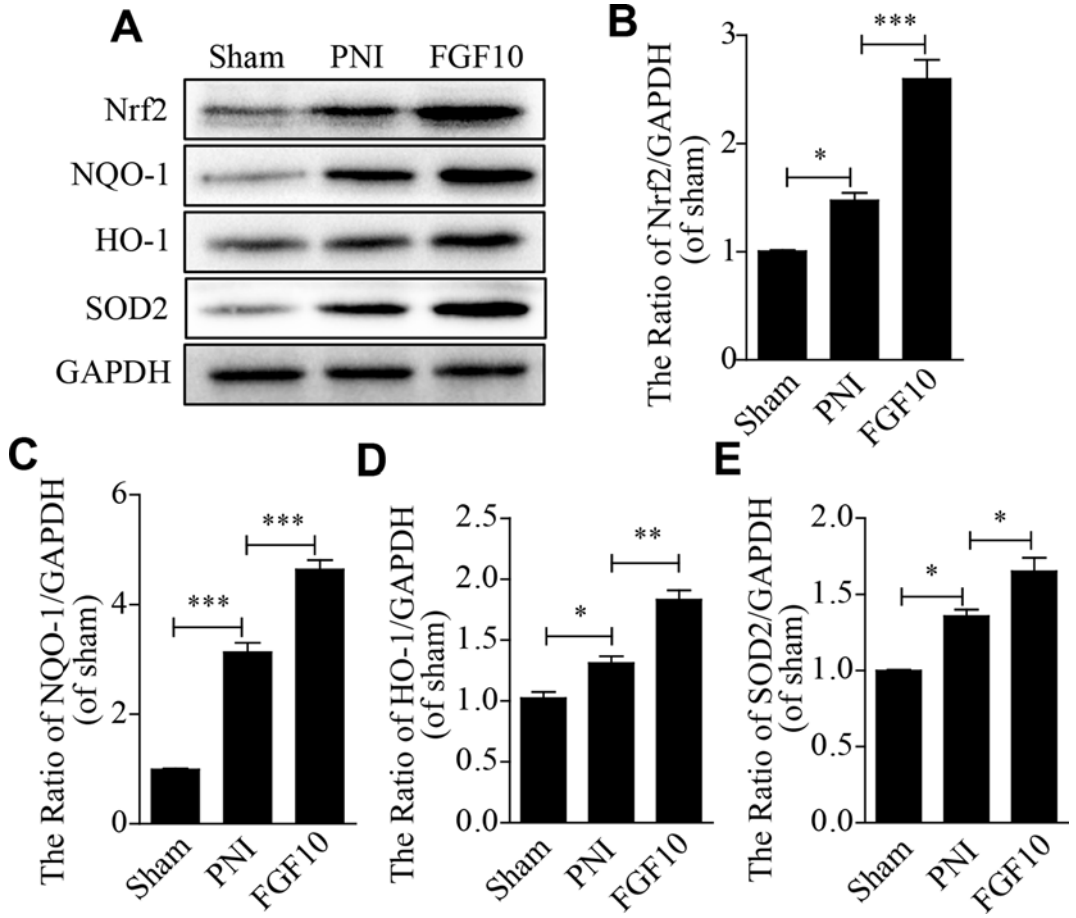

FIGURE 4 | Fibroblast growth factor 10 (FGF10) suppresses oxidative stress after peripheral nerve injury (PNI). **(A-E)** western blotting analysis showed the expression of Nrf2, NQO1, HO-1, and SOD2 after treatment with FGF10. Data are presented as the mean ± SEM, n = 3. Sham group vs PNI group: $^{*}P < 0.05$, $^{***}P < 0.001$. FGF10 group vs PNI group: $^{*}P < 0.05$, $^{**}P < 0.01$, $^{***}P < 0.001$.

upregulated after PNI rats received FGF10 treatment, which was also confirmed by the *p*-Akt/Akt ratio. However, LY294002 dramatically inhibited this effect on the expression of these proteins (**Figures 5A**, **B**). Nrf2 and HO-1 showed nearly the same trend (**Figures 5A**, **C**, **D**).

We also detected the expression of apoptosis-related proteins (including Bax and Bcl-2) to evaluate whether the anti-oxidative capability of FGF10 helps to decrease cell apoptosis following PNI. Western blotting showed that the level of the pro-apoptotic protein Bax was down-regulated and that the level of the anti-apoptotic protein Bcl-2 was up-regulated in the FGF10 group when compared to the PNI group (**Figures 5E–G**). However, the administration of LY294002 partially abolished the effects of FGF10. These results confirm that the antioxidant and anti-apoptotic properties of FGF10 may be involved in the activation of PI3k/Akt signaling.

Fgf10 Reduces Sc Apoptosis *in Vitro*

To further confirm the protective effect of FGF10, SCs were exposed to 100-μm H_2O_2 alone or in combination with various concentrations of FGF10. The CCK-8 results showed that cell viability increased as the FGF10 concentration increased and that 4.3-nm FGF10 was the most effective concentration (**Figure 6A**). Therefore, this concentration of FGF10 was chosen for subsequent experiments. Double immunostaining for cleaved-caspase-3 and S100 showed that FGF10 significantly reduced the cleaved-caspase-3 signal intensity, and LY294002 partially reversed this effect (**Figures 6B**, **D**). Consistent with the immunofluorescence, SC apoptosis in all four treatment groups was further confirmed *via* detecting Bax and Bcl-2 expression levels by western blotting (**Figures 6C**, **E**, **F**). These data suggest that FGF10 maintains SC bioactivity under H_2O_2 exposure.

Fgf10 Alleviates Oxidative Injury Through Pi3k/Akt Signaling *in Vitro*

To investigate the molecular mechanism by which FGF10 protects SCs against H_2O_2-induced apoptosis *in vitro*, we first detected the *p*-Akt and Akt levels using western blotting, the change in the *p*-Akt/Akt ratio was slightly increased in the H_2O_2 group and was further increased in the FGF10-treated

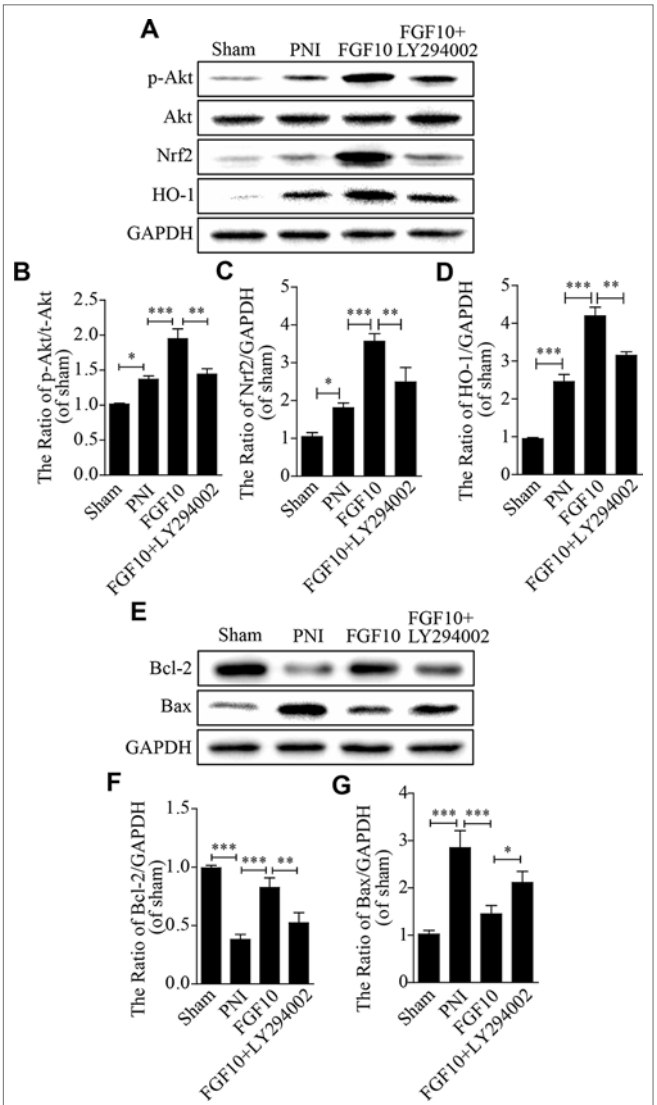

FIGURE 5 | The antioxidative and antiapoptotic functions of fibroblast growth factor 10 (FGF10) are mediated by the activation of the PI3K/Akt pathway *in vivo*. **(A–D)** Representative western blots and the quantification of *p*-Akt, Akt, Nrf2, and HO-1 expression in each group. **(E–G)** Western blotting and the quantification of Bcl-2 and Bax expression 28 days after injury. The data are presented as the mean ± SEM, n = 3. Sham group vs peripheral nerve injury (PNI) group: $^{*}P < 0.05$, $^{***}P < 0.001$. FGF10 group vs PNI group: $^{***}P < 0.001$. FGF10 group vs FGF10+LY294002 group: $^{*}P < 0.05$, $^{**}P < 0.01$.

group. This upregulation was reversed by LY294002 treatment. Nrf2 showed nearly the same trend (**Figures 7A–C**).

The change in ROS levels in each group since ROS represents the core component of the biology of oxidative stress. Compared with that in the H_2O_2-treated group, the fluorescence intensity was lower in the FGF10 group but was significantly higher in the FGF10+LY294002 group (**Figures 7D**, **F**). The intracellular ROS level was as similar change as the fluorescence intensity (**Figure 7G**). However, Nrf2 expression was slightly increased in the H_2O_2 group, which further increased in the FGF10-treated group. This upregulation was markedly reduced after the addition of LY294002 (**Figures 7E**, **H**).These results reveal that FGF10 may have the potential to enhance antioxidant ability *via* activating PI3K/Akt signaling.

DISCUSSION

Nerve recovery in the PNS is a complex process that triggers a sequence of events, including axonal regeneration, SC proliferation and migration, macrophage infiltration, and angiopoiesis, within the lesion area. During this process, the FGF family is particularly important for directing cellular activity and tissue remodeling. FGFs participate in SC dedifferentiation, proliferation, and remyelination during axonal regrowth (Chen et al., 2007; Jessen et al., 2015). FGF secretion is essential for maintaining neuronal survival after PNI. Furthermore, numerous studies have reported that FGFs, such as basic FGF (bFGF) and nerve growth factor (NGF), are essential for supporting neurite outgrowth and functional recovery during nerve regeneration (Grothe et al., 2006; Sun et al., 2009; Chen et al., 2010; Takagi et al., 2012; Li et al., 2017a). However, there is no knowledge of whether FGF10 promotes nerve regeneration after PNI.

In this article, we reported a new role for FGF10 in improving sensory and motor functional recovery, enhancing axonal regrowth and remyelination, and increasing the expression of functional proteins after traumatic PNI. Moreover, FGF10-induced neuroprotection and neuranagenesis is associated with attenuating the acute activation of oxidative stress and apoptosis in SCs, which is likely regulated by the activation of PI3K/Akt signaling. These findings indicate that FGF10 may be regarded as a potential therapeutic agent for peripheral nerve reconstruction after injury.

FGF10, a typical paracrine growth factor, is also essential for tissue development and regenerative medicine through specifically binding to the epithelial receptor FGFR2b (Zhang et al., 2006). The exogenous supplementation of FGF10 has been shown to prevent the formation and development of numerous diseases, including wound healing deficits, cardiovascular diseases, metabolism syndrome, and acute kidney injury (Konishi et al., 2006; Rochais et al., 2014; Li et al., 2017c; Tan et al., 2018). Previous studies have shown that FGF10 protects neurons against inflammation-induced apoptosis during SCI through the activation of FGFR2/PI3K/Akt signaling (Chen et al., 2017). However, the effect of FGF10 in acute PNI *in vivo* is unknown. In the present study, we reported that FGF10 is sufficient to continuously enhance motor and sensor recovery, improve nerve morphological recovery and reconstruction, and reduce SC apoptosis. These advantages suggest that FGF10 may be a potential therapeutic agent for peripheral nerve repair.

Oxidative stress is a redox-reactive imbalance in which the generation of oxygen-free radicals and ROS is far greater than the formation of antioxidative entities. During PNI, excessive oxidative stress activation is closely linked to SC apoptosis and axonal atrophy, which is unfavorable for nerve repair (Mirzakhani et al., 2018; Ullah et al., 2018; Lu et al., 2019). Numerous lines of evidence have implicated PI3K/Akt signaling in modifying oxidative stress (Pan et al., 2017; Liu et al., 2018; Li et al., 2018a; Gong et al., 2018).

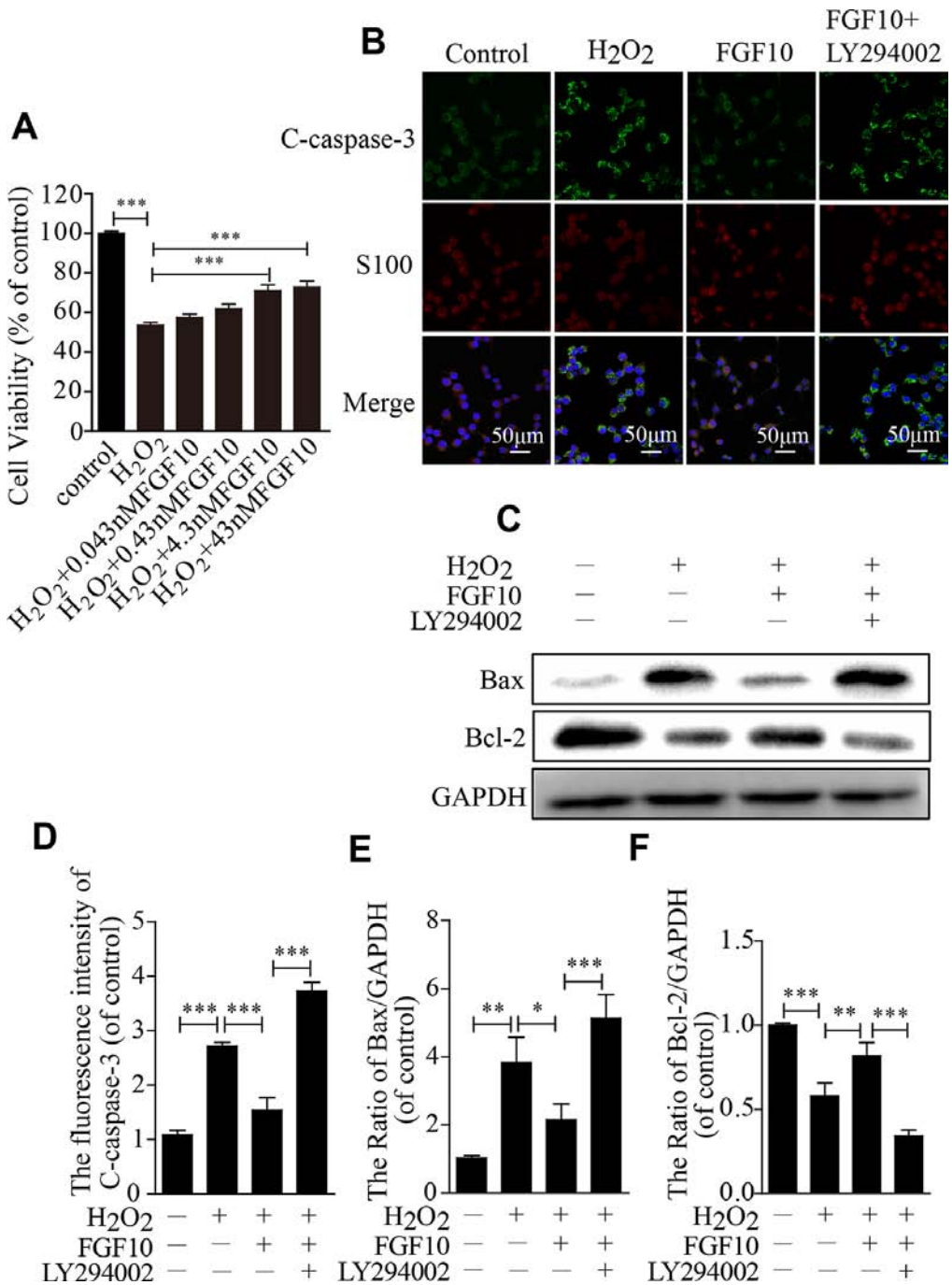

FIGURE 6 | Fibroblast growth factor 10 (FGF10) inhibits Schwann cell (SC) apoptosis *in vitro*. **(A)** H_2O_2-induced cell survival was evaluated by the CCK-8 assay. **(B)** Immunofluorescence staining results of cleaved-caspase-3 (green) and S100 (red) in each group. Scale bar = 50 μm. **(C)** The protein levels of Bax and Bcl-2 were detected by western blotting. **(D)** Statistical analysis of the cleaved-caspase-3 intensity in each group. **(E, F)** The quantification of Bax and Bcl-2 expression was assessed *via* a gel imaging system. All of these data represent the means ± SEM, n = 3. Control group vs H_2O_2 group: $^{**}P < 0.01$, $^{***}P < 0.001$. FGF10 group vs H_2O_2 group: $^{*}P < 0.05$, $^{**}P < 0.01$, $^{***}P < 0.001$. FGF10 group vs H_2O_2+LY294002 group: $^{***}P < 0.001$.

Hyperglycemia-induced oxidative stress can be negatively regulated by PI3K/Akt signaling (Pan et al., 2017). Furthermore, previous research has shown that the neuroprotective effect of fibroblast growth factor 21 (FGF21) in promoting neuronal survival and neurofunctional recovery after brain injury is mediated by the activation of PI3K/Akt signaling (Lu et al., 2019). In addition, the PI3K/Akt signaling pathway also participates in neuronal differentiation, survival and synaptic function (Li et al., 2006; Ketschek and Gallo, 2010; Fu et al., 2014). Given the important role of PI3K/Akt signaling in promoting cell survival and resisting

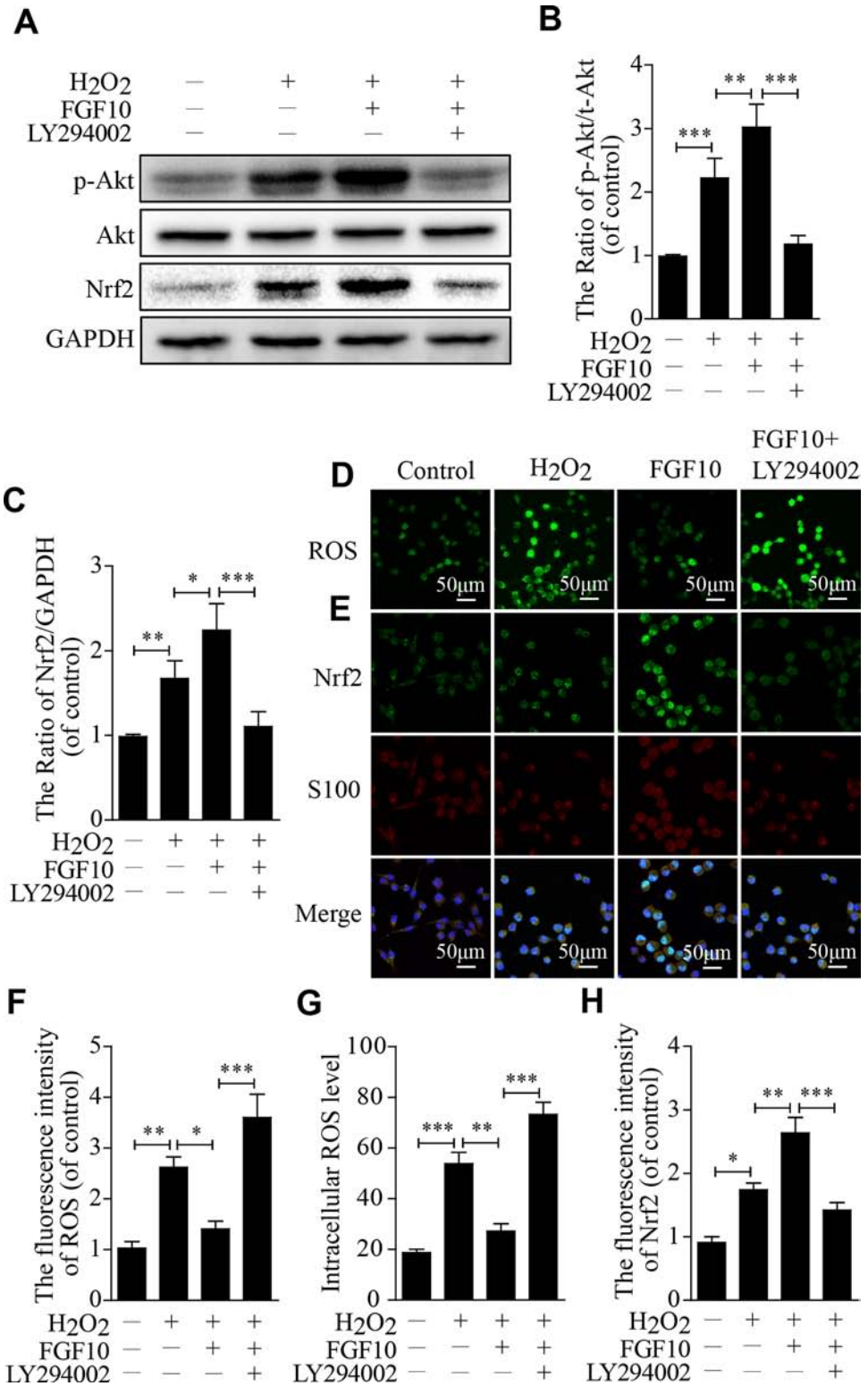

FIGURE 7 | Fibroblast growth factor 10 (FGF10) has antioxidant effects through the activation of the PI3K/Akt pathway *in vitro*. **(A–C)** Then, quantification of *p*-Akt, Akt, and Nrf2 expression was determined by western blotting in Schwann cells (SCs)**. (D)** Immunofluorescence staining of reactive oxygen species (ROS) labeled by dichlorodihydrofluorescein diacetate (DCFH-DA) in SCs. **(E)** Double immunofluorescence of Nrf2 (green) and S100 (red) in each group. Scale bar = 50 μm. **(F–H)** Statistical analysis of the ROS and Nrf2 levels in each group. These data represent the means ± SEM, n = 3. Control group vs H_2O_2 group: $^*P < 0.05$, $^{**}P < 0.01$, $^{***}P < 0.001$. FGF10 group vs H_2O_2 group: $^*P < 0.05$, $^{**}P < 0.01$. FGF10 group vs H_2O_2+LY294002 group: $^{***}P < 0.001$.

cellular stress, we hypothesize that PI3K/Akt signaling may act as an important antioxidant mechanism for regulating FGF10-induced neuroprotection and neuranagenesis following PNI.

Here, we found that the levels of stress-related proteins, including Nrf2, NQO1, SOD2, and HO-1, and the ratio of *p*-Akt/Akt increased markedly; meanwhile, ROS generation and the level of apoptosis were significantly decreased after the administration of FGF10. Suppressing Akt phosphorylation with LY294002 partially reversed these therapeutic effects. This result might be explained that the nerve tissue had the capable of synthetizing and secreting certain amounts of antioxidant enzymes to resist PNI-induced oxidative damage, although this capability was not satisfied the demand of cellular antioxidant defense (Ornitz and Itoh, 2015; Yu et al., 2017). After administration of FGF10 to the PNI rats, the interaction between FGF10-FGFR pairs activated the downstream of signal transduction pathways, such as PI3K/Akt, to dramatically stimulate the expression of antioxidant proteins which further enhanced antioxidative capability and, therefore, promoting SCs proliferation and nerve regeneration. Consequently, FGF10-induced nerve regeneration and functional recovery may occur through PI3K/Akt signaling-mediated antioxidant enhancement.

Previous studies reported that oxidative-induced SCs apoptosis is a critical mechanism of neurodegenerative diseases (Purves et al., 2001). In mammalian cells, Bax and Bcl-2 are involved in the regulation of apoptosis. Among them, Bax belongs to proapoptotic gene, whereas Bcl-2 is antiapoptotic gene. Abnormal oxidative stress activity triggers a decreased expression of Bcl-2 and an increased expression of Bax, which severely influences cell survival and induce cell apoptosis (Jezek and Plecitá-Hlavatá, 2009). Moreover, the excessive ROS-induced apoptosis after PNI is closely associated with the ratio of activity of Bax/Bcl-2 (Zhang et al., 2016). In our study, we observed that the downregulation of Bcl-2 and the upregulation of Bax after PNI were reversed after treatment of FGF10, while this effect was partially abolished when combination of FGF10 and LY294002 together. This result indicates that ROS-induced apoptosis after PNI is probably regulated by PI3K/Akt signaling.

In conclusion, our data indicate that the administration of FGF10 can be effective in facilitating SC proliferation, axonal regeneration, and functional recovery after sciatic nerve injury. In addition, the neuroprotective effect of FGF10 treatment is likely associated with suppressing excessive oxidative stress-induced cell apoptosis *via* activating PI3K/Akt signaling. Thus, our research may provide an alternative therapeutic strategy for utilizing FGF10 for treating acute traumatic PNI.

DATA AVAILABILITY STATEMENT

All datasets generated for this study are included in the manuscript/supplementary files.

ETHICS STATEMENT

The animal study was reviewed and approved by Male SD rats (200~220g) were purchased from Laboratory Animal Center of Fujian Medical University (Fujian, China). The temperature between 23 ± 2°C, humidity between 35 and 60%, and a light-dark cycles with the ratio of 12:12h were applied as the standardized laboratory conditions for housing all the rats. Meanwhile, they were provided with food and water, and adjusted to this condition for at least 7 days before experiment. The animals used in this study were approved by the Animal Experimentation Ethics Committee of Wenzhou Medical University, Wenzhou, China. The living condition and experimental procedures were conducted in accordance to the National Institutes of Health Guideline concerning the Care and Use of Laboratory Animals.

AUTHOR CONTRIBUTIONS

XJ and WJ conceived and designed the research. DL, LD, and WB performed the experiments. DL and LR performed the statistical analysis and wrote the paper. LY, LF, YF, NX, JY, WY, YS, LG, and LX provided assistance with the experiments. All authors discussed the drafting of the manuscript.

FUNDING

This work was supported by grants from the National Natural Science Foundation of China (81802238,81972150, 81722028), Zhejiang Provincial Natural Science Foundation of China (LR18H50001) and the Project of Wenzhou Science and Technology Bureau(2018Y0498,2015Y0416, 2015Y0235).

REFERENCES

Bain, J. R., Mackinnon, S. E., and Hunter, D. A. (1989). Functional evaluation of complete sciatic, peroneal, and posterior tibial nerve lesions in the rat. *Plast. Reconstr. Surg.* 83 (1), 129–138. doi: 10.1097/00006534-198901000-00024

Caillaud, M., Chantemargue, B., Richard, L., Vignaud, L., Favreau, F., Faye, P. A., et al. (2018). Local low dose curcumin treatment improves functional recovery and remyelination in a rat model of sciatic nerve crush through inhibition of oxidative stress. *Neuropharmacology* 139, 98–116. doi: 10.1016/j.neuropharm.2018.07.001

Chen, J., Chu, Y. F., Chen, J. M., and Li, B. C. (2010). Synergistic effects of NGF, CNTF and GDNF on functional recovery following sciatic nerve injury in rats. *Adv. Med. Sci.* 55 (1), 32–42. doi: 10.2478/v10039-010-0020-9

Chen, J., Wang, Z., Zheng, Z., Chen, Y., Khor, S., Shi, K., et al. (2017). Neuron and microglia/macrophage-derived FGF10 activate neuronal FGFR2/PI3K/Akt signaling and inhibit microglia/macrophages TLR4/NF-kappaB-dependent neuroinflammation to improve functional recovery after spinal cord injury. *Cell Death Dis.* 8 (10), e3090. doi: 10.1038/cddis.2017.490

Chen, Z. L., Yu, W. M., and Strickland, S. (2007). Peripheral regeneration. *Annu. Rev. Neurosci.* 30, 209–233. doi: 10.1146/annurev.neuro.30.051606.094337

Domenech-Estevez, E., Baloui, H., Meng, X., Zhang, Y., Deinhardt, K., Dupree, J. L., et al. (2016). Akt Regulates axon wrapping and myelin sheath thickness in the PNS. *J. Neurosci.* 36 (16), 4506–4521. doi: 10.1523/JNEUROSCI.3521-15.2016

Finkel, T., and Holbrook, N. J. (2000). Oxidants, oxidative stress and the biology of ageing. *Nature* 408 (6809), 239–247. doi: 10.1038/35041687

Fu, H., Xu, H., Chen, H., Li, Y., Li, W., Zhu, Q., et al. (2014). Inhibition of glycogen synthase kinase 3 ameliorates liver ischemia/reperfusion injury via an energy-dependent mitochondrial mechanism. *J. Hepatol.* 61 (4), 816–824. doi: 10.1016/j.jhep.2014.05.017

Gong, G., Yin, L., Yuan, L., Sui, D., Sun, Y., Fu, H., et al. (2018). Ganglioside GM1 protects against high altitude cerebral edema in rats by suppressing the oxidative stress and inflammatory response via the PI3K/AKT-Nrf2 pathway. *Mol. Immunol.* 95, 91–98. doi: 10.1016/j.molimm.2018.02.001

Gordon, T. (2016). Nerve regeneration: understanding biology and Its Influence on Return of Function After Nerve Transfers. *Hand Clin.* 32 (2), 103–117. doi: 10.1016/j.hcl.2015.12.001

Grothe, C., Haastert, K., and Jungnickel, J. (2006). Physiological function and putative therapeutic impact of the FGF-2 system in peripheral nerve regeneration–lessons from in vivo studies in mice and rats. *Brain. Res. Rev.* 51 (2), 293–299. doi: 10.1016/j.brainresrev.2005.12.001

He, B., Liu, S. Q., Chen, Q., Li, H. H., Ding, W. J., and Deng, M. (2011). Carboxymethylated chitosan stimulates proliferation of Schwann cells in vitro via the activation of the ERK and Akt signaling pathways. *Eur. J. Pharmacol.* 667 (1-3), 195–201. doi: 10.1016/j.ejphar.2011.06.001

He, B., Wu, F., Fan, L., Li, X. H., Liu, Y., Liu, Y. J., et al. (2018). Carboxymethylated chitosan protects Schwann cells against hydrogen peroxide-induced apoptosis by inhibiting oxidative stress and mitochondria dependent pathway. *Eur. J. Pharmacol.* 825, 48–56. doi: 10.1016/j.ejphar.2018.02.024

Ino, D., and Iino, M. (2017). Schwann cell mitochondria as key regulators in the development and maintenance of peripheral nerve axons. *Cell Mol. Life Sci.* 74 (5), 827–835. doi: 10.1007/s00018-016-2364-1

Itoh, N. (2016). FGF10: A multifunctional mesenchymal-epithelial signaling growth factor in development, health, and disease. *Cytokine Growth Factor Rev.* 28, 63–69. doi: 10.1016/j.cytogfr.2015.10.001

Jessen, K. R., and Mirsky, R. (2016). The repair Schwann cell and its function in regenerating nerves. *J. Physiol.* 594 (13), 3521–3531. doi: 10.1113/JP270874

Jessen, K. R., Mirsky, R., and Lloyd, A. C. (2015). Schwann cells: development and role in nerve repair. *Cold Spring Harb. Perspect Biol.* 7 (7), a020487. doi: 10.1101/cshperspect.a020487

Jezek, P., and Plecitá-Hlavatá, L. (2009). Mitochondrial reticulum network dynamics in relation to oxidative stress, redox regulation, and hypoxia. *Int. J. Biochem. Cell Biol.* 41 (10), 1790–1804. doi: 10.1016/j.biocel.2009.02.014

Jimenez, P. A., and Rampy, M. A. (1999). Keratinocyte growth factor-2 accelerates wound healing in incisional wounds. *J. Surg. Res.* 81 (2), 238–242. doi: 10.1006/jsre.1998.5501

Kelleher, F. C., O'Sullivan, H., Smyth, E., McDermott, R., and Viterbo, A. (2013). Fibroblast growth factor receptors, developmental corruption and malignant disease. *Carcinogenesis* 34 (10), 2198–2205. doi: 10.1093/carcin/bgt254

Ketschek, A., and Gallo, G. (2010). Nerve growth factor induces axonal filopodia through localized microdomains of phosphoinositide 3-kinase activity that drive the formation of cytoskeletal precursors to filopodia. *J. Neurosci.* 30 (36), 12185–12197. doi: 10.1523/JNEUROSCI.1740-10.2010

Konishi, M., Asaki, T., Koike, N., Miwa, H., Miyake, A., and Itoh, N. (2006). Role of Fgf10 in cell proliferation in white adipose tissue. *Mol. Cell Endocrinol.* 249 (1-2), 71–77. doi: 10.1016/j.mce.2006.01.010

Li, H., Tang, Z., Chu, P., Song, Y., Yang, Y., Sun, B., et al. (2018a). Neuroprotective effect of phosphocreatine on oxidative stress and mitochondrial dysfunction induced apoptosis in vitro and in vivo: Involvement of dual PI3K/Akt and Nrf2/HO-1 pathways. *Free Radic. Biol. Med.* 120, 228–238. doi: 10.1016/j.freeradbiomed.2018.03.014

Li, R., Li, Y., Wu, Y., Zhao, Y., Chen, H., Yuan, Y., et al. (2018b). Heparin-poloxamer thermosensitive hydrogel loaded with bFGF and NGF enhances peripheral nerve regeneration in diabetic rats. *Biomaterials* 168, 24–37. doi: 10.1016/j.biomaterials.2018.03.044

Li, R., Ma, J., Wu, Y., Nangle, M., Zou, S., Li, Y., et al. (2017a). Dual Delivery of NGF and bFGF Coacervater Ameliorates Diabetic Peripheral Neuropathy via Inhibiting Schwann Cells Apoptosis. *Int. J. Biol. Sci.* 13 (5), 640–651. doi: 10.7150/ijbs.18636

Li, R., Wu, J., Lin, Z., Nangle, M. R., Li, Y., Cai, P., et al. (2017b). Single injection of a novel nerve growth factor coacervate improves structural and functional regeneration after sciatic nerve injury in adult rats. *Exp. Neurol.* 288, 1–10. doi: 10.1016/j.expneurol.2016.10.015

Li, W., Cai, S., Cai, L., and Li, X. (2006). Anti-apoptotic effect of hepatocyte growth factor from actinomycin D in hepatocyte-derived HL7702 cells is associated with activation of PI3K/Akt signaling. *Toxicol. Lett.* 165 (2), 142–148. doi: 10.1016/j.toxlet.2006.02.006

Li, W., Yang, J., Cai, J., Wang, H., Tian, H., Huang, J., et al. (2017c). Oil body-Bound Oleosin-rhFGF-10: A Novel Drug Delivery System that Improves Skin penetration to accelerate wound healing and hair growth in mice. *Int. J. Mol. Sci.* 18 (10), 27–41. doi: 10.3390/ijms18102177

Li, Y. H., Fu, H. L., Tian, M. L., Wang, Y. Q., Chen, W., Cai, L. L., et al. (2016). Neuron-derived FGF10 ameliorates cerebral ischemia injury via inhibiting NF-kappaB-dependent neuroinflammation and activating PI3K/Akt survival signaling pathway in mice. *Sci. Rep.* 6, 19869. doi: 10.1038/srep19869

Li, L., Li, T., Zhang, Y., Pan, Z., Wu, B., Huang, X., et al. (2015a). Peroxisome proliferator-activated receptorbeta/delta activation is essential for modulating p-Alim. Pharm. Ther./Foxo1 status in functional insulin-positive cell differentiation. *Cell Death Dis.* 6, e1715. doi: 10.1038/cddis.2015.88

Li, Y. H., Yang, L. Y., Chen, W., Li, Y. K., and Yuan, H. B. (2015b). Fibroblast growth factor 10 protects neuron against oxygen-glucose deprivation injury through inducing heme oxygenase-1. *Biochem. Biophys. Res. Commun.* 456 (1), 225–231. doi: 10.1016/j.bbrc.2014.11.063

Liu, D., Xu, J., Qian, G., Hamid, M., Gan, F., Chen, X., et al. (2018). Selenizing astragalus polysaccharide attenuates PCV2 replication promotion caused by oxidative stress through autophagy inhibition via PI3K/AKT activation. *Int. J. Biol. Macromol.* 108, 350–359. doi: 10.1016/j.ijbiomac.2017.12.010

Lu, Y., Li, R., Zhu, J., Wu, Y., Li, D., Dong, L., et al. (2019). Fibroblast growth factor 21 facilitates peripheral nerve regeneration through suppressing oxidative damage and autophagic cell death. *J. Cell Mol. Med.* 23 (1), 497–511. doi: 10.1111/jcmm.13952

Lv, J., Sun, X., Ma, J., Ma, X., Zhang, Y., Li, F., et al. (2015). Netrin-1 induces the migration of Schwann cells via p38 MAPK and PI3K-Akt signaling pathway mediated by the UNC5B receptor. *Biochem. Biophys. Res. Commun.* 464 (1), 263–268. doi: 10.1016/j.bbrc.2015.06.140

Min, H., Danilenko, D. M., Scully, S. A., Bolon, B., Ring, B. D., Tarpley, J. E., et al. (1998). Fgf-10 is required for both limb and lung development and exhibits striking functional similarity to Drosophila branchless. *Genes Dev.* 12 (20), 3156–3161. doi: 10.1101/gad.12.20.3156

Mirzakhani, N., Farshid, A. A., Tamaddonfard, E., Imani, M., Erfanparast, A., and Noroozinia, F. (2018). Carnosine improves functional recovery and structural regeneration after sciatic nerve crush injury in rats. *Life Sci.* 215, 22–30. doi: 10.1016/j.lfs.2018.10.043

Niture, S. K., and Jaiswal, A. K. (2011). INrf2 (Keap1) targets Bcl-2 degradation and controls cellular apoptosis. *Cell Death Differ.* 18 (3), 439–451. doi: 10.1038/cdd.2010.114

Niture, S. K., and Jaiswal, A. K. (2012). Nrf2 protein up-regulates antiapoptotic protein Bcl-2 and prevents cellular apoptosis. *J. Biol. Chem.* 287 (13), 9873–9886. doi: 10.1074/jbc.M111.312694

Niture, S. K., Khatri, R., and Jaiswal, A. K. (2014). Regulation of Nrf2-an update. *Free Radic. Biol. Med.* 66, 36–44. doi: 10.1016/j.freeradbiomed.2013.02.008

Ornitz, D., and Itoh, N. (2015). The Fibroblast Growth Factor signaling pathway. *Wiley Interdiscip. Rev. Dev. Biol.* 4 (3), 215–266. doi: 10.1002/wdev.176

Pan, W., Miao, L., Lin, Y., Huang, X., Ge, X., Moosa, S. L., et al. (2017). Regulation mechanism of oxidative stress induced by high glucose through PI3K/Akt/Nrf2 pathway in juvenile blunt snout bream (Megalobrama amblycephala). *Fish Shellfish Immunol.* 70, 66–75. doi: 10.1016/j.fsi.2017.09.005

Purves, T., Middlemas, A., Agthong, S., Jude, E., Boulton, A., Fernyhough, P., et al. (2001). A role for mitogen-activated protein kinases in the etiology of diabetic neuropathy. *FASEB J.* 15 (13), 2508–2514. doi: 10.1096/fj.01-0253hyp

Rochais, F., Sturny, R., Chao, C. M., Mesbah, K., Bennett, M., Mohun, T. J., et al. (2014). FGF10 promotes regional foetal cardiomyocyte proliferation and adult cardiomyocyte cell-cycle re-entry. *Cardiovasc. Res.* 104 (3), 432–442. doi: 10.1093/cvr/cvu232

Sakaue, H., Konishi, M., Ogawa, W., Asaki, T., Mori, T., Yamasaki, M., et al. (2002). Requirement of fibroblast growth factor 10 in development of white adipose tissue. *Genes Dev.* 16 (8), 908–912. doi: 10.1101/gad.983202

Sang, Q., Sun, D., Chen, Z., and Zhao, W. (2018). NGF and PI3K/Akt signaling participate in the ventral motor neuronal protection of curcumin in sciatic nerve injury rat models. *Biomed. Pharmacother.* 103, 1146–1153. doi: 10.1016/j.biopha.2018.04.116

Scherer, S. S., and Wrabetz, L. (2008). Molecular mechanisms of inherited demyelinating neuropathies. *Glia* 56 (14), 1578–1589. doi: 10.1002/glia.20751

Son, T. G., Kawamoto, E. M., Yu, Q. S., Greig, N. H., Mattson, M. P., and Camandola, S. (2013). Naphthazarin protects against glutamate-induced neuronal death via activation of the Nrf2/ARE pathway. *Biochem. Biophys. Res. Commun.* 433 (4), 602–606. doi: 10.1016/j.bbrc.2013.03.041

Sulaiman, O. A., and Gordon, T. (2009). Role of chronic Schwann cell denervation in poor functional recovery after nerve injuries and experimental strategies to combat it. *Neurosurgery* 65 (4 Suppl), A105–A114. doi: 10.1227/01.NEU.0000358537.30354.63

Sun, W., Sun, C., Lin, H., Zhao, H., Wang, J., Ma, H., et al. (2009). The effect of collagen-binding NGF-beta on the promotion of sciatic nerve regeneration in a rat sciatic nerve crush injury model. *Biomaterials* 30 (27), 4649–4656. doi: 10.1016/j.biomaterials.2009.05.037

Takagi, T., Kimura, Y., Shibata, S., Saito, H., Ishii, K., Okano, H. J., et al. (2012). Sustained bFGF-release tubes for peripheral nerve regeneration: comparison with autograft. *Plast. Reconstr. Surg.* 130 (4), 866–876. doi: 10.1097/PRS.0b013e318262f36e

Tan, X., Zhu, H., Tao, Q., Guo, L., Jiang, T., Xu, L., et al. (2018). FGF10 Protects Against renal ischemia/reperfusion injury by regulating autophagy and inflammatory signaling. *Front. Genet.* 9, 556. doi: 10.3389/fgene.2018.00556

Thomson, A. A., and Cunha, G. R. (1999). Prostatic growth and development are regulated by FGF10. *Development* 126 (16), 3693–3701.

Ullah, I., Choe, Y. H., Khan, M., Bharti, D., Shivakumar, S. B., Lee, H. J., et al. (2018). Dental pulp-derived stem cells can counterbalance peripheral nerve injury-induced oxidative stress and supraspinal neuro-inflammation in rat brain. *Sci. Rep.* 8 (1), 15795. doi: 10.1038/s41598-018-34151-x

Wang, C. H., Wu, S. B., Wu, Y. T., and Wei, Y. H. (2013). Oxidative stress response elicited by mitochondrial dysfunction: implication in the pathophysiology of aging. *Exp. Biol. Med. (Maywood)* 238 (5), 450–460. doi: 10.1177/1535370213493069

Wang, Z., Zhang, H., Xu, X., Shi, H., Yu, X., Wang, X., et al. (2012). bFGF inhibits ER stress induced by ischemic oxidative injury via activation of the PI3K/Akt and ERK1/2 pathways. *Toxicol. Lett.* 212 (2), 137–146. doi: 10.1016/j.toxlet.2012.05.006

Wu, W., Liu, Y., and Wang, Y. (2016). Sam68 promotes Schwann cell proliferation by enhancing the PI3K/Akt pathway and acts on regeneration after sciatic nerve crush. *Biochem. Biophys. Res. Commun.* 473 (4), 1045–1051. doi: 10.1016/j.bbrc.2016.04.013

Yang, X., Yao, W., Shi, H., Liu, H., Li, Y., Gao, Y., et al. (2016). Paeoniflorin protects Schwann cells against high glucose induced oxidative injury by activating Nrf2/ARE pathway and inhibiting apoptosis. *J. Ethnopharmacol.* 185, 361–369. doi: 10.1016/j.jep.2016.03.031

Yu, P., Wilhelm, K., Dubrac, A., Tung, J., Alves, T., Fang, J., et al. (2017). FGF-dependent metabolic control of vascular development. *Nature* 545 (7653), 224–228. doi: 10.1038/nature22322

Zhang, Y., Dai, C., Chen, Y., Iqbal, K., Liu, F., and Gong, C. (2016). Intranasal insulin prevents anesthesia-induced spatial learning and memory deficit in mice. *Sci. Rep.* 6, 21186. doi: 10.1038/srep21186

Zhang, H., Wu, F., Kong, X., Yang, J., Chen, H., Deng, L., et al. (2014). Nerve growth factor improves functional recovery by inhibiting endoplasmic reticulum stress-induced neuronal apoptosis in rats with spinal cord injury. *J. Transl. Med.* 12, 130. doi: 10.1186/1479-5876-12-130

Zhang, X., Ibrahimi, O. A., Olsen, S. K., Umemori, H., Mohammadi, M., and Ornitz, D. M. (2006). Receptor specificity of the fibroblast growth factor family. The complete mammalian FGF family. *J. Biol. Chem.* 281 (23), 15694–15700. doi: 10.1074/jbc.M60125220

Conflict of Interest: The authors declare that the research was conducted in the absence of any commercial or financial relationships that could be construed as a potential conflict of interest.

The handling editor is currently organizing a Research Topic with one of the authors, XL, and confirms the absence of any other collaboration.

frontiers in Pharmacology

ORIGINAL RESEARCH
published: 02 December 2019
doi: 10.3389/fphar.2019.01428

Autophagy Activation Is Involved in Acidic Fibroblast Growth Factor Ameliorating Parkinson's Disease *via* Regulating Tribbles Homologue 3

Xingfeng Zhong[1,2,†], Beini Wang[3†], Guanyinsheng Zhang[1†], Yuan Yuan[3], Xiaoli Hu[1], Jun Xiong[3], Peipei Zheng[3], Yaqian Liu[3], Ke Xu[4], Jian Xiao[3], Yanqing Wu[4]* and Junming Ye[1]**

[1] Department of Anesthesia, The First Affiliated Hospital, Gannan Medical University, Ganzhou, China, [2] Department of Anesthesia, Affiliated Hospital of Guizhou Medical University, Guiyang, China, [3] Molecular Pharmacology Research Center, School of Pharmaceutical Science, Wenzhou Medical University, Wenzhou, China, [4] The Institute of Life Sciences, Wenzhou University, Wenzhou, China

OPEN ACCESS

Edited by:
Zhouguang Wang,
Albert Einstein College of Medicine,
United States

Reviewed by:
Yingnyu Gao,
Marshall University, United States
Dinghong Zhang,
University of California,
San Diego, United States

***Correspondence:**
Jian Xiao
xfxj2000@126.com
Yanqing Wu
yqwu220946@yeah.net
Junming Ye
yjm7798@sina.com

[†]These authors have contributed equally to this work

Specialty section:
This article was submitted to Translational Pharmacology, a section of the journal Frontiers in Pharmacology

Received: 03 September 2019
Accepted: 08 November 2019
Published: 02 December 2019

Citation:
Zhong X, Wang B, Zhang G, Yuan Y, Hu X, Xiong J, Zheng P, Liu Y, Xu K, Xiao J, Wu Y and Ye J (2019) Autophagy Activation Is Involved in Acidic Fibroblast Growth Factor Ameliorating Parkinson's Disease via Regulating Tribbles Homologue 3. Front. Pharmacol. 10:1428. doi: 10.3389/fphar.2019.01428

Parkinson's disease (PD) is a degenerative disorder of the central nervous system, resulting in loss of dopamine neurons. Excessive endoplasmic reticulum (ER) stress and autophagy dysfunction play a crucial role on Parkinson's disease (PD) development. It has been showed that acidic fibroblast growth factor (aFGF) alleviates the development of PD by inhibiting ER stress. But the role of autophagy and its relationship with ER stress during aFGF treatment for PD has not been elucidated. We found that both aFGF and rapamycin (Rapa) improved 6-Hydroxy Dopamine (6-OHDA)-induced PD development as shown with histomorphology results in striatum and substantia nigra (SNpc). Additionally, aFGF promoted autophagy with increasing mTOR and decreasing p62 expressions, and then exerts its neuroprotective role in 6-OHDA-treated PC12 cells, which were abolished by chloroquine (CQ) treatment. Moreover, 4-phenylbutyric acid (4-PBA) administration inhibited the expressions of autophagy markers during 6-OHDA-treated PC12 cells, which was similar with aFGF treating PC12 cells under 6-OHDA condition. Furthermore, we had detected the expressions of CHOP and its downstream factor, tribbles homologue 3 (TRB3), a pro-apoptotic protein. We found that TRB3 and CHOP expressions were significantly downregulated after treating with aFGF and 4-PBA in 6-OHDA-treated PC12 cells and PD model. Taken together, this study has demonstrated that aFGF treatment ameliorates 6-OHDA-induced elevated ER stress and subsequently suppression of autophagy *via* inhibiting TRB3 activation, and consequently ameliorates 6-OHDA-induced neurotoxicity.

Keywords: Parkinson's disease, acidic fibroblast growth factor, autophagy, endoplasmic reticulum stress, tribbles homologue 3

INTRODUCTION

Parkinson's disease (PD) is a kind of neurodegenerative disease, which is associated with the abnormally accumulated α-synuclein (α-syn) in the substantia nigra pars compacta (SNpc). In the early study of PD development, gene mutation of α-syn on the autosome caused excessive aggregation damage (Fujiwara et al., 2002; Hasegawa et al., 2002; Samuel et al., 2016; Longo et al., 2017). The cellular mechanisms, include autophagy (Magalhaes et al., 2016), endoplasmic reticulum

(ER) stress (Kuang et al., 2010; Ning et al., 2019), oxidative stress (Ding et al., 2018; Mamelak, 2018), and others, are involved in the amelioration of misfolded protein. Thus, regulation of cellular stress may be the target for treating PD.

Acidic fibroblast growth factor (aFGF or FGF1) is an important member of fibroblast growth factors, which can be synthesized and released from neuron (Walicke and Baird, 1988). aFGF exerts neuroprotective role in the peripheral and central nervous systems (Tsai et al., 2015; Wu et al., 2017; Aiki et al., 2018; Ko et al., 2018). The previous studies have showed that aFGF can attenuate 6-OHDA-induced dopaminergic neuron toxicity (Wei et al., 2014). In addition, aFGF protects human primary neurons against gp120 toxicity, and overexpression of aFGF alleviates the neurodegeneration of gp120 mice (Everall et al., 2001; Crews et al., 2009). The mechanism underlying aFGF treating for PD is through inhibiting ER stress (Wei et al., 2014). Promotion of autophagy is the mechanism during aFGF treating for spinal cord injury (Li et al., 2018). However, there is no studies to reveal on role of autophagy, and its' relationship with ER stress during aFGF treating for PD.

Autophagy is an adaptive process in body, which degrades and recycles the abnormal cytoplasmic components and organelles to provide nutrients for cells. Hyperactivation of autophagy triggers cell death program. In general, autophagy regulates cell fate depending on cell type, specific environment and predisposing factors (Jin et al., 2012). Accumulating evidences suggest that autophagy is impaired in PD (Lee et al., 2015). Under normal condition, a small amount of aggregated α-syn will be degraded by the giant autophagy pathway (Cao et al., 2017), however, the mutantion of α-syn can inhibit the degradation process of autophagy (Song et al., 2014; Winslow and Rubinsztein, 2014; Lohmann et al., 2019). Previous studies have also found that the enhancement of autophagy can alleviate the toxic effect of α-syn mutation on midbrain dopaminergic neurons (Decressac et al., 2013). These studies indicate that promotion of autophagy is very important for PD treatment.

The endoplasmic reticulum (ER) is responsible for the synthesis and assembly of protein in cell. Once the misfolded protein is accumulated, it triggers an unfolded protein response (UPR), but an excessively sustained response to decompensation leads to the appearance of ER stress, which in turn causes cell death. Recent studies have shown that inhibition of ER stress protects dopaminergic neurons (Shan et al., 2019). Neuronal apoptotic kinase, known as tribbles homologue 3 (TRB3), is a novel protein that induces cell death by ER stress, which is also related to the regulation of autophagy. Normally, the expression of TRB3 in brain is extremely low. Once stress is triggered, TRB3 is sharply increased. Moreover, the expression of TRB3 is significantly increased during development of PD (Aim et al., 2015) and AD (Saleem and Biswas, 2017). However, it is unclear whether aFGF alleviates PD development by suppressing TRB3 expression.

Multiple studies have also shown a crosstalk between ER stress and autophagy (Li et al., 2017; Yin et al., 2017; Zhou et al., 2017). When ER stress occurs, autophagy can be triggered by unfolded protein reactions (UPR) to remove excessive unfolded proteins and damaged organelles, and maintain cell homeostasis. Moreover, TRB3 plays a key bridge connection between ER stress and autophagy (Salazar et al., 2009; Aim et al., 2015; Tang et al., 2015; Ord and Ord, 2017). Therefore, we have used 6-OHDA to induce PD model or PC12 cells model *in vivo* and *in vitro*, and investigated the role of autophagy regulation during aFGF treating for PD *via* treating with aFGF, rapamycin (Rapa)-autophagy inducer and chloroquine (CQ)-autophagy inhibitor. Moreover, 4-phenylbutyrate (4-PBA)-ER stress inhibitor is administrated to investigate the relationship between ER stress and autophagy during these processes.

MATERIALS AND METHODS

Animals and Surgical Procedures

One hundred ten adult male SD rats (220–250 g) were purchased from the Animal Center of the Chinese Academy of Science (Shanghai, China). The rats were housed under a 12-h light/dark cycle at 21–23°C and provided access to food and water *ad libitum*. All procedures were approved by Laboratory Animal Ethics Committee of Wenzhou Medical University. After anesthetizing with 10% chloral hydrate, the head of animal was shaved and sterilized. Then, the rat was fixed on the rat brain stereogram (KOPF, Germany), and the 5% compound lidocaine cream was applied to the front of head. After the drug was absorbed, the longitudinal cleavage revealed the fascia, followed by 3% hydrogen peroxide exposing the front point on the skull. The 6-OHDA (10 μl, 2 μg/ul dissolved in 0.2% ascorbic acid, Sigma-Aldrich, St. Louis, MO, USA) was injected into the dental drill hole at the right side of position the striatum (coordinates: A: anterior +0.7 mm, L: 2.8 mm from the midline, H: +5.5 mm) using micro syringe. The injection speed was 10 nl/s, and the needle was left for 10 min after injection. The sham-operation model was performed same surgical procedures and injected an equal volume of 0.2% ascorbic acid.

Behavioral Test

One week after the right striatum stereotactic injection of 6-OHDA, the animals were tested for rotational behavior. Rats were intraperitoneally injected with apomorphine hydrochloride (0.5 mg/kg), as a dopamine receptor agonist, the dopamine receptor on the injured side is up-regulated, which can cause the rotation of the rats in Parkinson's disease to the healthy side. The device was used to detect the rotational behavior of the rats. The number of rotations of the rats to the opposite side of the injury was recorded within 30 min. The successful PD model rotated to the left side more than 7 turns/min. Then, 72 successful Parkinson's disease rats were randomly divided into six groups (n = 12): PBS, aFGF (80 μg/kg/day, tail vein), CQ (50 mg/kg/day, intraperitoneally), Rapa (1.5 mg/kg/day, intraperitoneally), aFGF + CQ, and 4-PBA (100 mg/kg/day, intraperitoneally). In addition, the sham-operation group (n = 12) was injected with PBS in the tail vein for 2 weeks. The rotational behavior test of rats was performed at 1, 2 and 3 weeks after surgical procedure and treatment.

Cell Culture and Treatment

PC12 cells were purchased from the Cell Storage Center of Wuhan University (Wuhan, China). PC12 cells were cultured in Dulbecco's Modified Eagle Medium (DMEM, Invitrogen, Carlsbad, CA) supplemented with 10% fetal bovine serum (FBS, Invitrogen) and 1% antibiotics (100 units/ml penicillin, 100 μg/ml streptomycin). They were incubated in a humidified atmosphere containing 5% CO_2 at 37 °C. The cells were seeded in a 96-well plate at density of 1×10^4, then treated with 6-OHDA at different doses of 25 μM, 50 μM, 75 μM, 100 μM, 125 μM, 150 μM, 175 μM and 200 μM for 24 h. Then, the cells were incubated with CCK-8 assay (Cell counting kit-8) at 37°C for 2 h, and measured the optical density at 450 nm. The experiments were divided into six groups: PBS, aFGF (20 ng/ml), CQ (75 μM), aFGF + CQ, Rapa (1 μM), and 4-PBA (1 mM).

Hematoxylin and Eosin (H&E) Staining and Nissl Staining

After anesthesia, the brain was dissected immediately and placed on the ice, then fixed 4% with paraformaldehyde (PFA) for 24 h in 4 °C. Subsequently, paraffin-embedded brain regions containing substantia nigra and striatum were sliced at 4 um thickness. For Nissl staining, after dewaxed and hydrated, tissue sections were stained with cresol violet and Nissl differentiation solutions according to the instructions (Beyotime) and acquired the image using light microscopy. For H&E staining, the sections were stained with hematoxylin and eosin reagent, and observed under light microscope.

Immunohistochemical Staining

After anesthesia, the brain was dissected immediately and placed on the ice, then fixed 4% with paraformaldehyde (PFA) for 24 h in 4°C. Subsequently, paraffin-embedded brain regions containing substantia nigra and striatum were sliced at 4 um thickness. After dewaxed and hydrated, the sections were incubated with 3% hydrogen peroxide for 15 min, and antigen retrieval at high temperature and pressure. Then, after blocking with 5% bovine serum albumin (BSA) for 30 min at 37 °C, the sections were incubated overnight at 4 °C with the following primary antibodies: TH (1:500, Abcam), α-syn (1:250, Millipore), CHOP (1:100, Proteintech), TRB3 (1:50, Santa Cruz Biotechnology), mTOR (1:250, Cell Signaling Technology), p62 (1:250, Abcam). Then, the sections were washed three times with PBST and incubated the horseradish peroxidase-conjugated secondary antibody at 37 °C for 2 h. Finally, these sections were reacted with 3,3-diaminobenzidine (DAB, 1:20 dilution) for 5–10 min. Hematoxylin was used to stain the nucleus. The sham operation group was used as a negative control. The signals were analyzed by counting the number of positive cells in region of interest at 400× of microscope of Nikon ECLPSE 80i (Nikon, Tokyo, Japan). The optical density of TH, α-syn, CHOP, TRB3, mTOR and p62 was randomly selected from five samples in each sample.

Immunofluorescence Staining

The cells were inoculated on coverslips, and then fixed with 4% PFA for 25 min at 4 °C. Subsequently, the cells were washed in PBS three times. The cells were incubated with 5% BSA in PBS containing 0.1% Triton X-100 for 30 min at room temperature. Then, the sections were incubated at 4°C overnight with the following primary antibodies: CHOP (1:50, Proteintech), TRB3 (1:50, Santa Cruz Biotechnology), mTOR (1:250, Cell Signaling Technology), and p62 (1:250, Abcam). After washing with PBS three times for 5 min, the sections were incubated with AlexaFluor-488 or AlexaFluor-647 donkey anti-rabbit/mouse secondary antibodies for 1 h at room temperature. After washed with PBS, the sections were staining the nuclei with DAPI and captured the image on a confocal fluorescence microscope (Nikon, A1 PLUS, Tokyo, Japan).

Tunel Staining

TUNEL staining was performed using the ApopTag Fluorescein Direct *In Situ* Apoptosis Detection Kit (Roche, Basel, Switzerland). According to the standard protocol, the fixed cell slides were incubated with 20 μg/ml proteinase K solution for 10 min at room temperature. The slides were then rinsed with PBS three times, which was followed by incubation with the TUNEL reaction mixture for 1 h at 37 °C. After rinsing with PBS three times for 5 min, sections were treated with 4 ', 6-diamidino-2-pheny-lindole (DAPI, Beyotime, Shanghai, China) for 5 min at room temperature and mounted with aqueous mounting medium. The results were imaged using a Nikon ECLIPSE 80i microscope (Nikon, Tokyo, Japan). Quantification was performed by counting the TUNEL-positive cells number in five random fields using ImageJ software.

Western Blot Analysis

The midbrain and PC12 cells were collected and lysed using RIPA buffer (20 mM Tris-HCl, pH7.5, 150 mM NaCl, 1 mM EDTA, 1% Triton-X100, 0.5% sodium dexoycholate, 1 mM PMSF and 10 μg/ml leupeptin). The lysate was centrifuged at 12,000*g* for 20 min at 4°C, and the supernatant was quantified with BCA reagents (Thermo, Rockford, IL, USA). Proteins (30 μg) were separated on a 12% gel and transferred onto a 0.22 μm PVDF membrane (Bio-Rad, Hercules, CA, USA). The membrane was blocked with 5% (w/v) non-fat milk (Bio-Rad) in Tris-buffered saline with 0.1% Tween-20 (TBST) for 0.5 h at room temperature, and then the membranes were incubated overnight at 4°C with the following primary antibodies: TH (1:1000, Abcam), α-syn (1:1,000, Abcam), FGFR1 (1:1,000, CST), GRP78 (1:1,000, Abcam), CHOP (1:500, Proteintech), TRB3 (1:100, Santa Cruz Biotechnology), LC3A/B (1:1,000, CST), mTOR (1:1,000, CST), p-mTOR (1:1,000, CST), and p62 (1:1,000, CST). The membranes were washed with TBST three times and incubated with horseradish peroxidase-conjugated secondary antibodies for 2 h at room temperature. Then, the signals were detected using the Chemi DocXRS + Imaging System (Bio-Rad), and the bands were quantified using densitometric measurement by the Quantity-One software. All experiments were repeated three times.

Statistical Analysis

Data were presented as mean ± SEM from three individual experiments. All cells culture experiments were conducted

in triplicate. Statistical analysis and mapping were performed using GraphPad Prism 5. Except for rat animal behavior using repeated measures analysis of variance, one-way analysis of variance (ANOVA) followed by Tukey's *post hoc* test were used for analyzing significant difference. Multiple comparisons were used to compare between groups. $P < 0.05$ was used to indicate significant differences in data.

RESULTS

aFGF Treatment Ameliorates 6-OHDA-Induced PD Disease *via* Activating Autophagy

To evaluate the effect of autophagy in aFGF ameliorating 6-OHDA-induced PD, we measured the rotational behavior of APO-induced rat at 7, 14 and 21 days after administration with PBS, aFGF, CQ, aFGF+CQ, and Rapa. The results of rotational behavior showed that from day 0 to 21, the number of turns in 6-OHDA group did not significantly decrease, which is similar with that in CQ group. Compared with that in 6-OHDA group, aFGF treatment significantly decreased the number of turns of 6-OHDA mice, indicating aFGF effectively alleviates the rotational behavior of PD rats. Additionally, the behaviors of PD rats from aFGF + CQ group and Rapa group have significant improved when compared with that in CQ group (**Figure 1A**). These results demonstrated that aFGF may ameliorate PD *via* enhancing autophagy.

We also assessed the striatum morphology and the number of Nissl bodies in nigral to confirm this hypothesis. It was found that the rats in 6-OHDA group and CQ group have showed damaged striatum, irregular hyperplasia and scar, decreased Nissl bodies, which were reversed by aFGF or Rapa treatment. Moreover, compared with CQ group, aFGF + CQ treatment significantly relieved the damage of 6-OHDA on striatum morphology and Nissl bodies (**Figure 1B**), indicating that aFGF treatment can block the inhibition of autophagy and ameliorate the striatum injury and death of SNpc neurons in PD. Furthermore, we had detected the TH and α-syn expressions in the SNpc of rats by immunohistochemical staining (**Figure 1B**). It was observed that the rats from 6-OHDA and CQ group have shown few TH-positive neurons and abundant α-syn deposition in the SNpc, and aFGF and Rapa treatment remarkably block them (**Figures 1C**, **D**). More importantly, aFGF + CQ treatment increased the TH level and reduced α-syn deposition in the substantia nigra region, but its effect was worse than that in aFGF treatment. Taken together, these indicate that aFGF may enhance TH level and decrease α-syn deposition in the substantia nigra neurons of PD rats by activating autophagy, and finally achieve its neuroprotective effect.

aFGF Treatment Attenuates 6-OHDA-induced PD *via* Inhibiting ER Stress

We have further confirmed the effect of ER stress on aFGF ameliorating 6-OHDA-induced PD. As shown in **Figure 2A**, aFGF and 4-PBA treatment significantly decreased the number

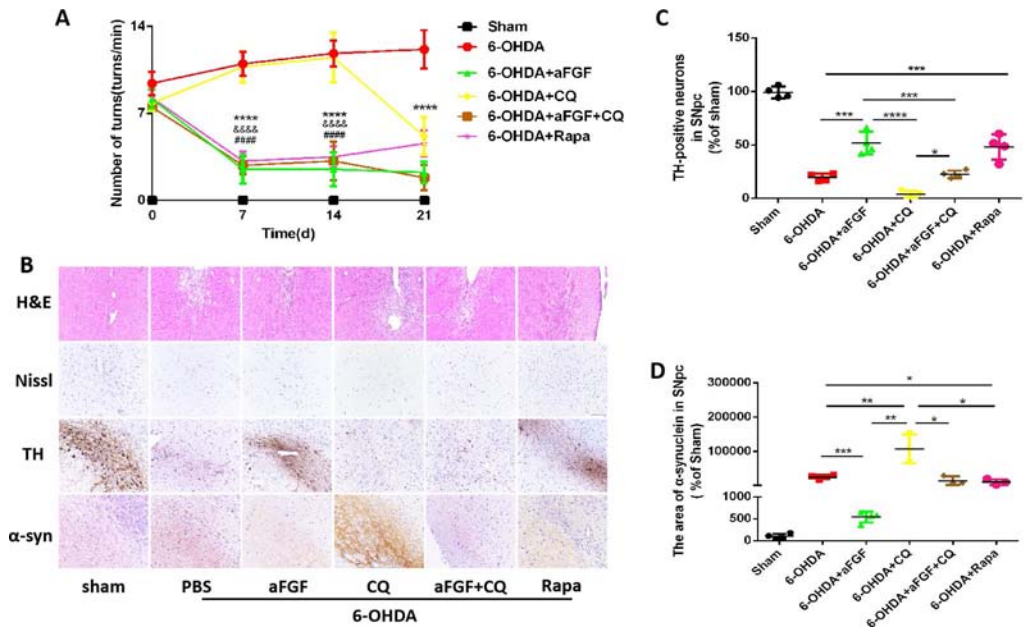

FIGURE 1 | Effect of autophagy on aFGF attenuating 6-OHDA-induced PD. **(A)** The number of rotations (turns/min) on the affected side of rats during rotational behavior test, n = 12. $^{****}P < 0.0001$: aFGF group *vs.* 6-OHDA group; $^{\#\#\#\#}P < 0.0001$: aFGF group *vs.* CQ group; $^{\&\&\&\&}P < 0.0001$: aFGF + CQ group *vs.* CQ group. **(B)** H&E staining of striatum region, Nissl staining of nigral region, and immunohistochemistry staining results of TH and α-syn expression in striatum region. Scale bar = 50 μm, n = 6. **(C**, **D)** Quantitative analysis of immunohistochemistry staining results of TH and α-syn expression in striatum region, $^{*}P < 0.05$, $^{**}P < 0.01$, $^{***}P < 0.001$, $^{****}P < 0.0001$ *vs.* the other group, n = 6.

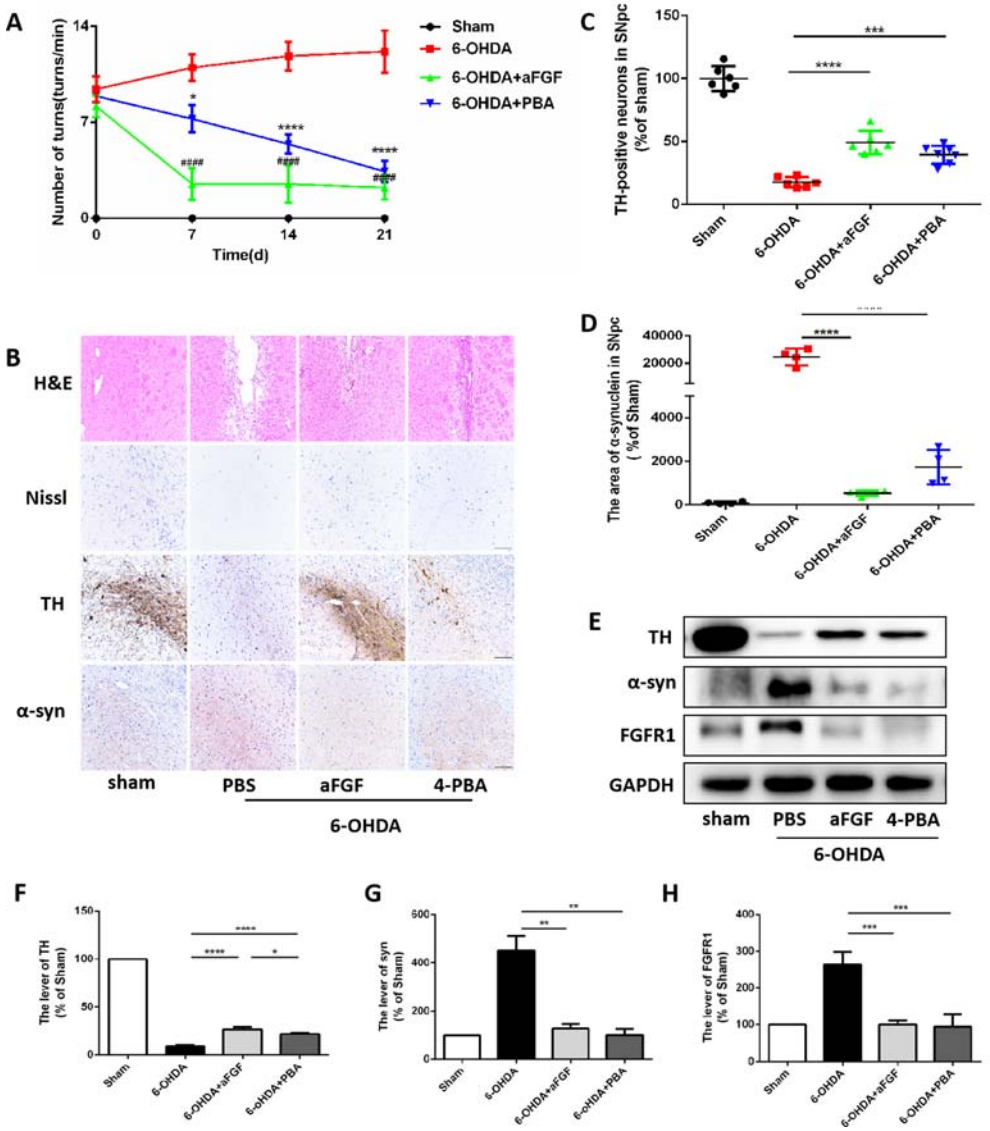

FIGURE 2 | aFGF treatment attenuates 6-OHDA-induced PD via inhibiting ER stress. **(A)** The number of rotations (turns/min) on the affected side of rats during rotational behavior test, n = 12. $^{\#\#\#\#}P < 0.0001$: aFGF group *vs.* 6-OHDA group; $^{****}P < 0.0001$: 4-PBA group *vs.* 6-OHDA group. **(B)** H&E staining of striatum region, Nissl staining of nigral region, and immunohistochemistry staining results of TH and α-syn expression in striatum region. Scale bar = 50 μm, n = 6. **(C, D)** Quantitative analysis of immunohistochemistry staining results of TH and α-syn expression in striatum region. **(E)** Western blot results of TH, α-syn and FGFR1 expressions. **(F–H)** Quantitative analysis results of TH, α-syn, and FGFR1 expressions, $^{*}P < 0.05$, $^{**}P < 0.01$, $^{***}P < 0.001$, $^{****}P < 0.0001$ *vs.* the other group, n = 6.

of turns of PD rat, indicating that aFGF may improve the symptoms of PD by inhibiting ER stress. Then, we found that the rats in 6-OHDA group have showed damaged striatum, irregular hyperplasia and scar, decreased Nissl bodies, which are reversed by aFGF or 4-PBA treatment (**Figure 2B**). Moreover, aFGF and 4-PBA treatment blocked 6-OHDA-induced loss of TH-positive neurons and α-syn deposition in the substantia nigra neurons (**Figures 2B–D**). Consistent with the results of immunohistochemical staining, western blot results showed that 4-PBA and aFGF administration increases TH expression and promotes α-syn degradation, and ameliorates 6-OHDA-induced increase FGFR1 expression (**Figures 2E–H**).

aFGF Administration Activates Autophagy Level by Inhibiting ER Stress During PD Development

Based on our prior study, it was found that ER stress and autophagy are involved in neuroprotective role of aFGF during PD treatment. Next, we have further detected the relationship of ER stress and autophaghy during aFGF treating with PD. Immunohistochemistry results showed that both 4-PBA and aFGF treatement promote autophagic flow by inhibiting mTOR activity and promoting p62 degradation (**Figures 3A–C**). Furthermore, western blot results showed that both 4-PBA and aFGF administration inhibit mTOR activity,

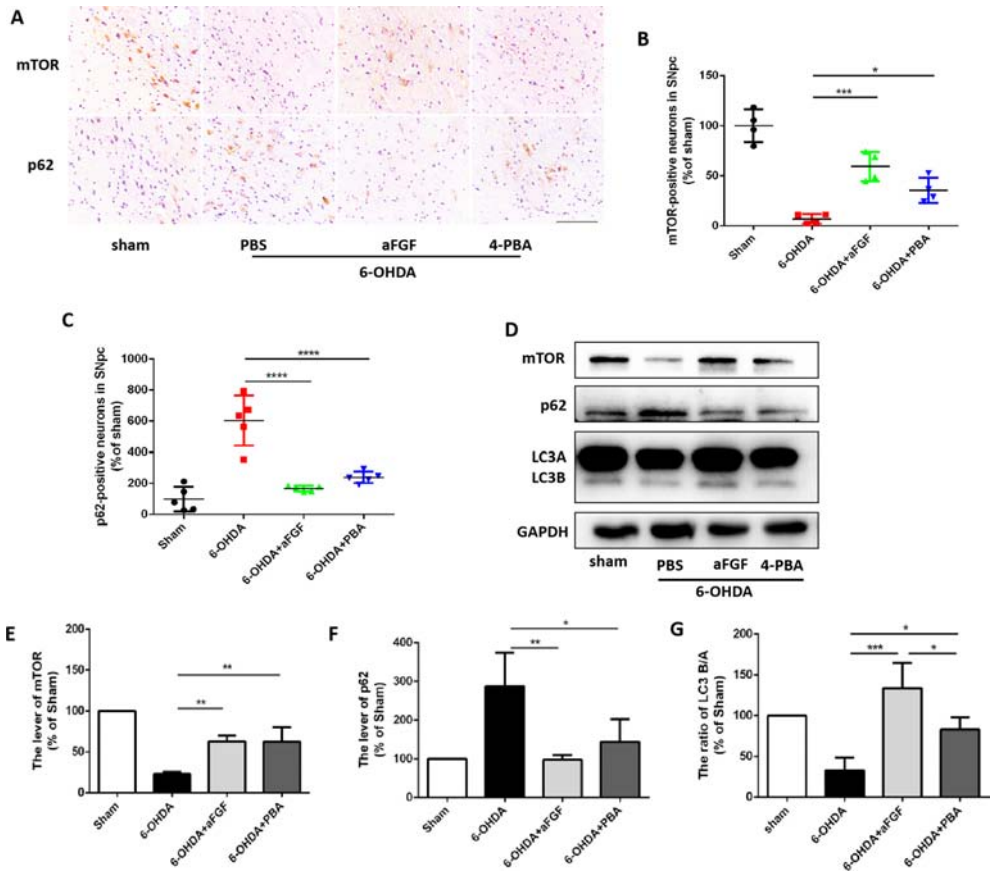

FIGURE 3 | aFGF administration activates autophagy level by inhibiting ER stress during PD treatment. **(A–C)** Immunohistochemical image and quantitative analysis of mTOR and p62 protein expressions in the substantia nigra of the affected side. Scale bar = 50 μm, n = 6. **(D)** Western blot results of mTOR, p62 and LC3 expressions. **(E–G)** Quantitative analysis of mTOR, p62 and LC3 expressions. **P < 0.05, **P < 0.01, ***P < 0.001, ****P<0.0001 vs.* the other group, n = 6.

increase LC3B expression and promote p62 degradation (**Figures 3D–G**). All of these studies suggest that aFGF promotes autophagy level and exerts its neuroprotective role during PD *via* suppressing ER stress.

aFGF Suppresses the Pro-Apoptotic Protein of TRB3 and Subsequently Activates Autophagy *via* Inhibiting CHOP Expression During PD Treatment

Progressive loss of DAergic is the main pathological manifestation of PD, and previous studies have shown that aFGF can protect neurons by inhibiting ER stress. It is reported that TRB3 is a protein that involved in ER stress-associated apoptosis and autophagic cell death. We speculated that TRB3 is critical factor for ER stress related with autophagy during aFGF treating for PD. Using immunohistochemical staining and western blot assay (**Figures 4A–F**), it was observed that 6-OHDA treatment significantly induces the expression levels of CHOP and TRB3, and both aFGF and 4-PBA treatment reduce the overexpression of these two proteins. Taken together, these studies indicate that aFGF suppresses the pro-apoptotic protein TRB3 and subsequently activates autophagy *via* inhibiting CHOP expression during PD development.

Effect of Autophagy on aFGF Attenuating 6-OHDA-Induced Apoptosis in PC12 Cells

Here, we had further investigated whether aFGF can attenuate neuronal apoptosis by regulating autophagy *in vitro*. As is shown in **Figures 5A**, **B**, aFGF and Rapa treatment significantly reduced 6-OHDA-triggered apoptotic cells. In addition, TUNEL-positive cells in CQ group was significantly increased compared with that in 6-OHDA group, while the number of apoptotic cells in aFGF + CQ group was significantly lower than that in CQ group (**Figures 5A**, **B**). These data suggest that aFGF alleviates neuronal apoptosis by regulating autophagy under 6-OHDA treatment. Then, we had further detected the expressions of autophagy related protein, and found that 6-OHDA or CQ treatment and significantly decreases the expression of mTOR and increases p62 expression, which are reversed by aFGF and Rapa treatment (**Figures 5C–F**). Moreover, there is significant difference of the expressions of mTOR and p62 between the aFGF + CQ and CQ group (**Figures 5C–F**). All of these studies indicate that aFGF

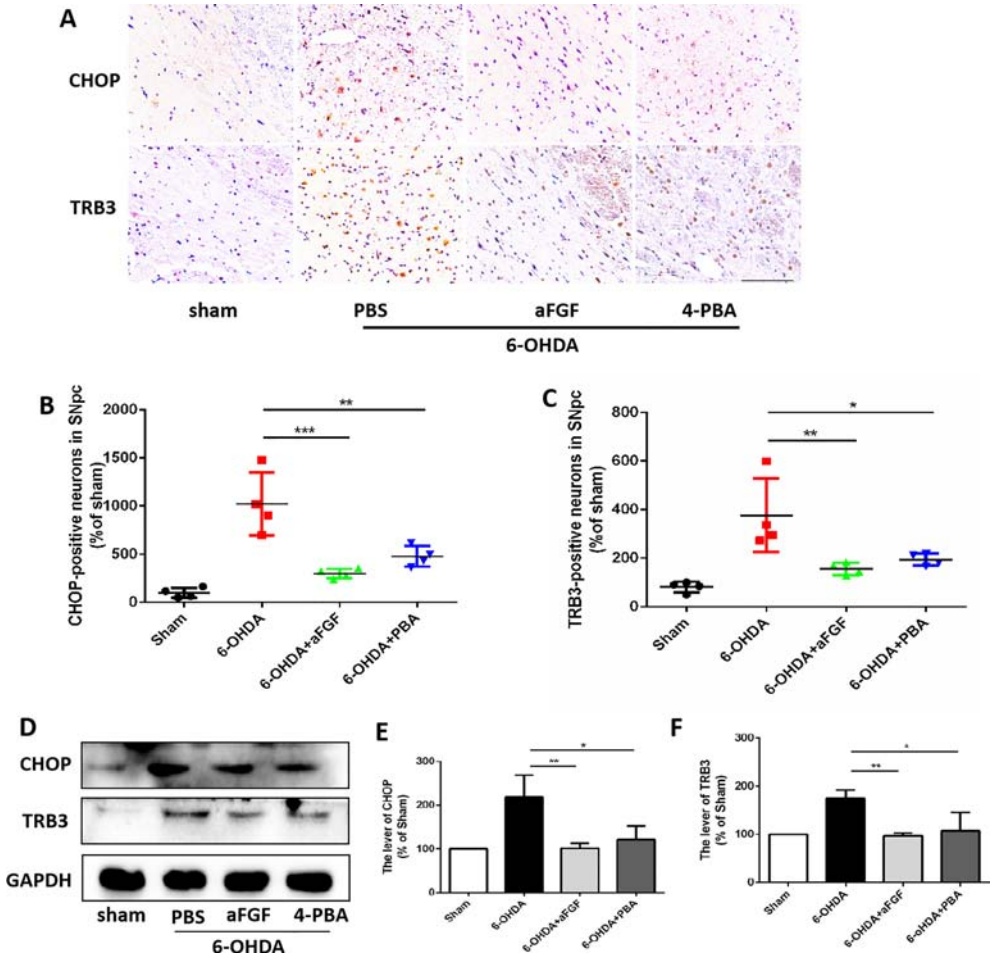

FIGURE 4 | aFGF suppresses the pro-apoptotic protein of TRB3 and subsequently activates autophagy via inhibiting CHOP expression during PD development. **(A–C)** Immunohistochemical image and quantitative analysis of CHOP and TRB3 expressions in the substantia nigra of the affected side. Scale bar = 50 μm, n = 6. **(D)** Western blot results of CHOP and TRB3 expressions. **(E, F)** Quantitative analysis of CHOP and TRB3 expressions. *$P < 0.05$, **$P < 0.01$, ***$P < 0.001$ *vs.* the other group, n = 6.

promotes autophagic circulation and ameliorates 6-OHDA-induced neuronal apoptosis *in vitro*.

aFGF Administration Activates Autophagy and Protects Neuron by Inhibiting ER Stress-TRB3 Signaling *In Vitro*

Here, we had further assessed the relationship of ER stress and autophaghy during aFGF treating PC12 cells under 6-OHDA condition. Consistent with the results *in vivo*, 6-OHDA treatment significantly decreased the expressions of mTOR and LCB, and increased p62 expression in PC12 cells, and both aFGF and 4-PBA treatment remarkably blocked them (**Figures 6A–H**), indicating that aFGF activated autophagy by inhibiting ER stress in PC12 cells

Then, we had investigated whether inhibition of ER stress-TRB3 signaling is involved in aFGF ameliorating 6-OHDA-induced neuronal apoptosis. TUNEL staining results showed that the numbers of TUNEL-positive PC12 cells in aFGF and 4-PBA treated-group are significantly reduced when compared with that in 6-OHDA group (**Figures 7A** and **B**), indicating that aFGF exerts its neuroprotective role by inhibiting ER stress. Then, using immunofluorescence staining and western blot, we detected the expressions of GRP78, CHOP and TRB3 in PC12 cells, and found that both aFGF and 4-PBA treatment decrease 6-OHDA-induced increases of GRP78, CHOP and TRB3 expressions (**Figures 7C–J**). These studies confirm that aFGF administration activates autophagy and exerts its neuroprotective role by inhibiting ER stress-TRB3 signaling *in vitro*.

DISCUSSION

With the rapid growth of the elderly population, the incidence of PD is also increasing. However, the effective treatments for PD are still limited. At present, there are many studies focused on investigating the neuroprotective drugs, and neurotrophic factors have attracted much attention in recent years. aFGF, a important

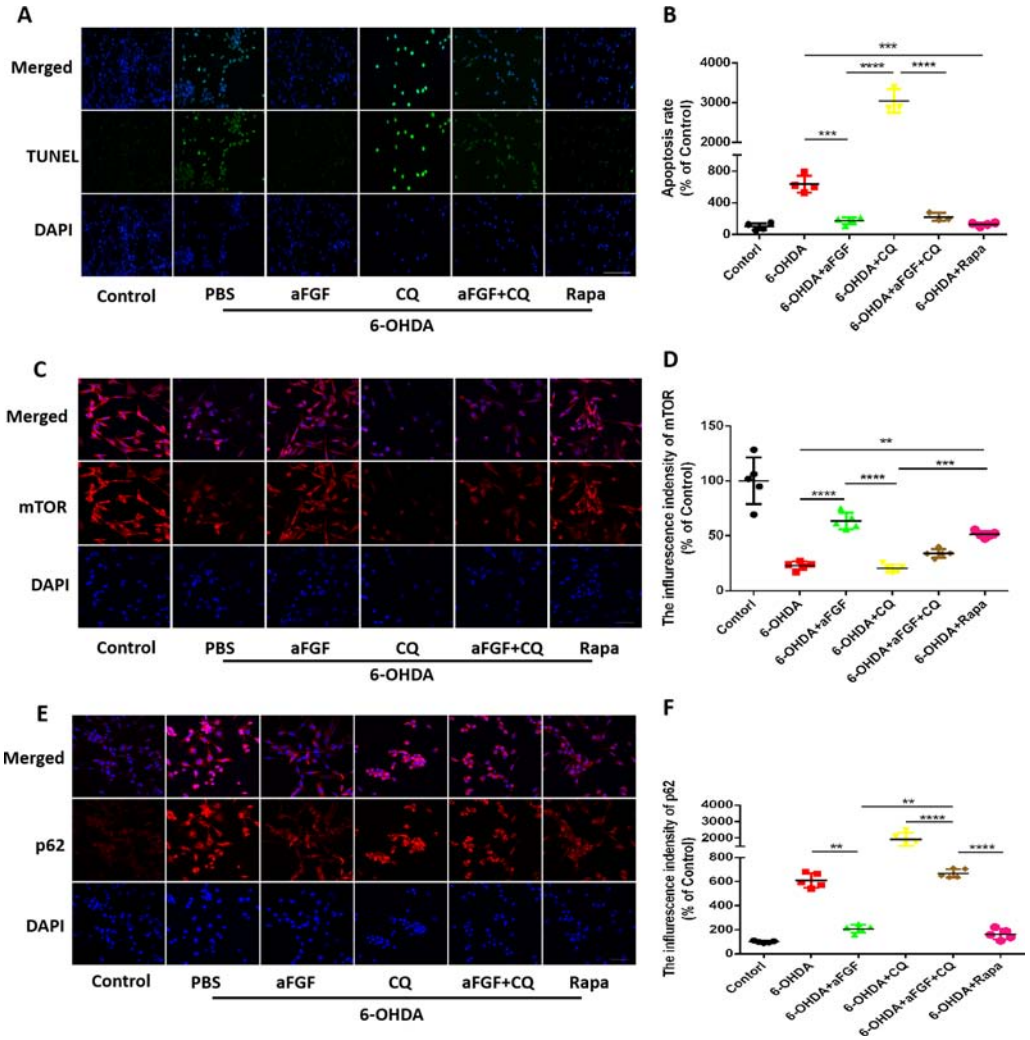

FIGURE 5 | Effect of autophagy on aFGF attenuating 6-OHDA-induced apoptosis in PC12 cells. **(A)** Representative images of TUNEL staining (green) of PC12 cells under 6-OHDA treatment; **(B)** Quantitative analysis of TUNEL-positive cells. Scale bar = 50 μm, n = 5. **(C**, **D)** Representative fluorescence images and quantitative analysis of mTOR expression in PC12 cells. Scale bar = 50 μm. **(E**, **F)** Representative fluorescence images and quantitative analysis of p62 expression in PC12 cells. Scale bar = 50 μm. ***P < 0.01, ***P < 0.001, ****P < 0.0001 vs.* the other group, n = 5.

member of FGFs, has been reported to have neuroprotective effect (Tsai et al., 2015; Wu et al., 2017). Increased expression of aFGF was observed during central neuronal injury (Walicke and Baird, 1988), which indirectly indicates that aFGF is important for neuronal survival. Previous studies have shown that aFGF has a protective effect on 6-OHDA-induced DAergic injury (Wei et al., 2014). As a disease associated with excessive accumulation of misfolded proteins, α-syn accumulation promotes PD progression. ER and autophagy are essential for the normal protein synthesis and translocation in body. Our current study has shown that aFGF ameliorates the development of PD by regulating autophagy and ER stress. The specific mechanism may be related to aFGF down-regulating TRB3 *via* inhibiting ER stress, and then activating autophagy to protect DAergic from 6-OHDA.

6-OHDA is a neurotoxin that selectively damages DAergic in SNpc. A single injection of 6-OHDA into striatum can be used to simulate the chronic progression of classical PD model. Autophagy is generally an adaptive mechanism that allows for the orderly degradation and recycling of cellular components. It has shown that the autophagy level is significantly decreased in serious of degenerative diseases (Pickford et al., 2008; Spencer et al., 2009; Menzies and Rubinsztein, 2010), indicating that promotion of autophagy may protect DAergic during PD development (Darabi et al., 2018). In our current study, a rat model of PD was established using 6-OHDA induction and behavioral evaluation indicators. According to behavioral indicators, it was found that on the 7th and 14th days after administration, the behavior of PD rat was significantly improved after treating with aFGF and Rapa, while CQ treatment not only did have no remission, but

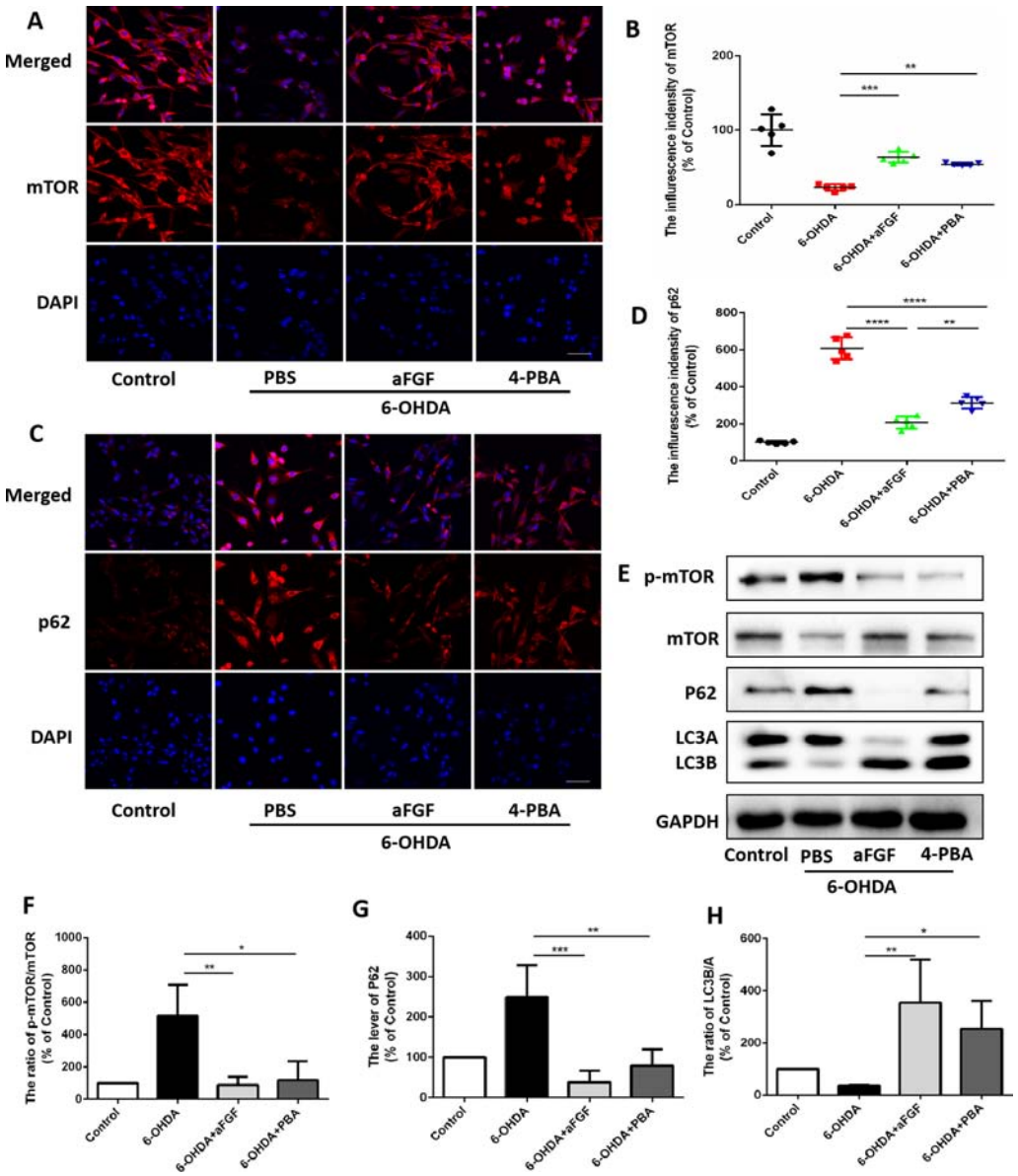

FIGURE 6 | aFGF administration activates autophagy by inhibiting ER stress in PC12 cells. **(A–D)** Representative fluorescence images and quantitative analysis of mTOR and p62 expressions in PC12 cells. Scale bar = 50 μm, n = 5. **(E)** Western blot results of p-mTOR, mTOR, p62 and LC3 expressions in PC12 cells. **(F–H)** Quantitative analysis results of p-mTOR, mTOR, p62 and LC3 expressions in PC12 cells. *$P < 0.05$, **$P < 0.01$, ***$P < 0.001$, ****$P < 0.0001$ vs.* the other group, n = 3.

also promoted the neuronal death of PD rats, which is due to the inhibition of autophagy level in PD (Michiorri et al., 2010). In addition, morphological staining results are consistent with that in behavioral test. However, the CQ group behavior was significantly improved after CQ with drawal for 1 week, which may be related to drug half-life. Tyrosine hydroxylase (TH) is a maker protein in DAergic. Immunohistochemical staining results have shown that both aFGF and autophagy activatorcould alleviate the loss of TH, while autophagy inhibitor aggravated TH loss and α-syn accumulation. aFGF and autophagy agonist alleviated the abnormal expression of protein. These results demonstrated that aFGF can alleviate PD development by regulating autophagy.

In current study, using autophagy inhibitors and agonists, it was found that aFGF can alleviate PD development by regulating autophagy. DAergic death contributes to the development of PD. *In vitro*, TUNEL staining result have further demonstrated that aFGF attenuates apoptosis of PC12 cells, which is consistent with the results that in autophagy agonist group. It has been reported that aFGF promotes autophagy level and consequently contributes to the recovery of spinal cord injury. Conversely, our and others' studies have shown that autophagy level is enhanced

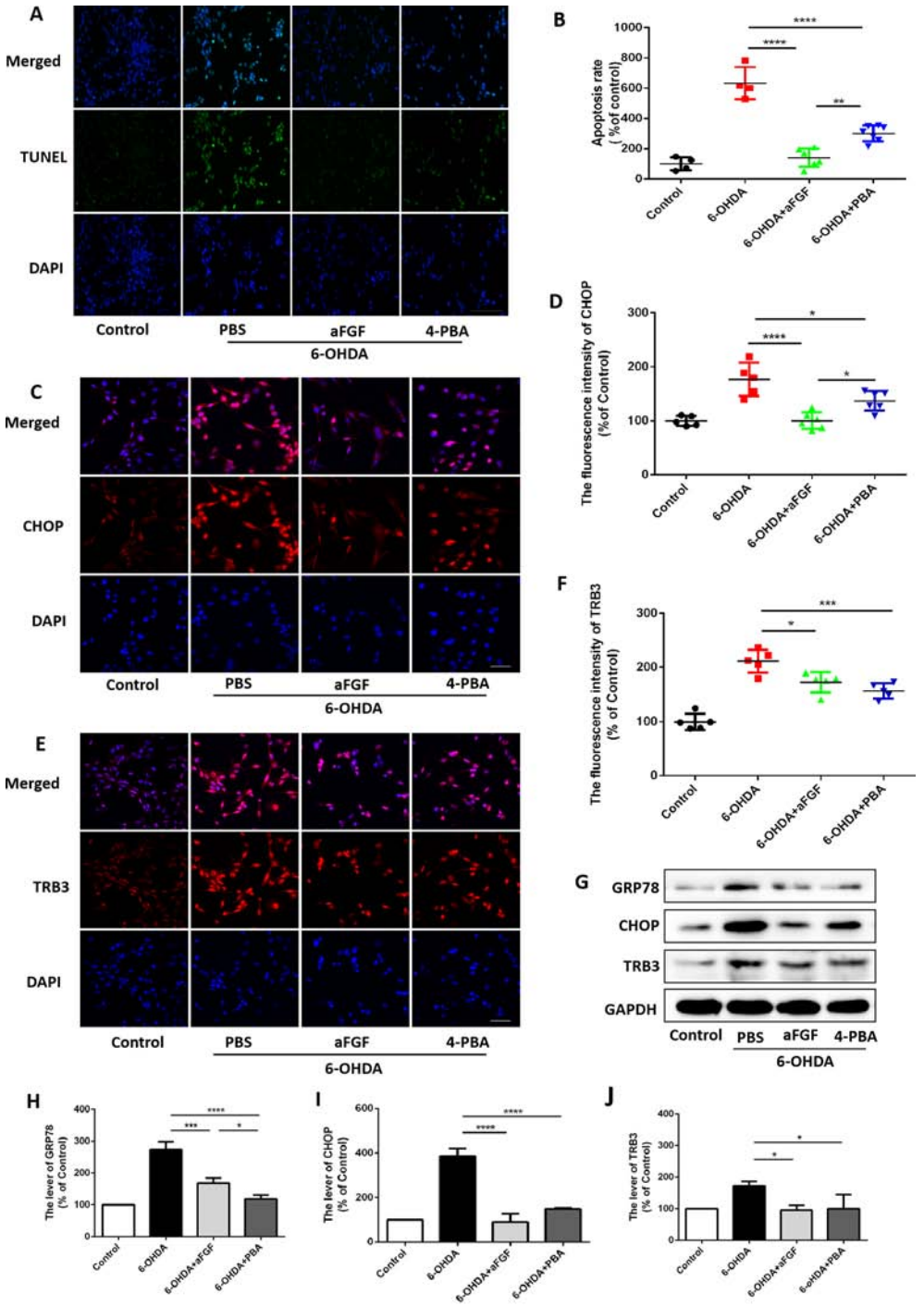

FIGURE 7 | aFGF treatment ameliorates 6-OHDA-induced neuronal death via suppressing TRB3 expression. **(A)** Representative images of TUNEL staining (green) of PC12 cells under 6-OHDA treatment. **(B)** Quantitative analysis of TUNEL-positive cells, Scale bar = 50 μm, n = 5. **(C–F)** Representative fluorescence images and quantitative analysis of CHOP and TRB3 expressions in PC12 cells. Scale bar = 50 μm, n = 5. **(G)** Western blot results of GRP78, CHOP, and TRB3 expressions in PC12 cells. **(H–J)** Quantitative analysis results of GRP78, CHOP, and TRB3 expressions in PC12 cells, n = 3. **P < 0.05, **P < 0.01, ***P < 0.001, ****P < 0.0001 vs.* the other group.

during PD, and some LC3B positive cells colocalize with TUNEL positive signals (Niu et al., 2018), which may suggest that regulatory mechanisms are different in different type of nerve injuries.

6-OHDA-induced PD rats model are considered to be a standard model, and studies have confirmed that 6-OHDA can act as an ER stress inducer (Yamamuro et al., 2006). Therefore, ER stress activators were not added in this study.

Previous studies have shown that aFGF protects DAergic by inhibiting ER stress (Wei et al., 2014). Both ER stress and autophagy are involved in the pathological process of PD. But the relationship between them is still unclear in PD. Previous studies have shown ER stress can regulate autophagy (Hetz et al., 2009; Senft and Ronai, 2015). In this study, the ER stress inhibitor was added to investigate the regulation of autophagy by ER stress. The studies *in vivo* and *in vitro* have showed that inhibition of ER stress promoted autophagy. It is indirectly shown that aFGF can protect neurons by inhibiting ER stress to promote autophagy.

Since the neuroprotective effect of aFGF is mainly through binding with FGFR1 (Li, 2019). Specifically, FGFR1 is expressed on TH-positive cells of the SNpc and terminals in striatal (Boshoff et al., 2018). Our study also showed that FGFR1 level was increased after PD (**Figure 2**), while the expression of FGFR1 was similar in the sham group and aFGF treatment group, which may suggest that FGFR1 will transfer into the nucleus due to injury. After administration, it promotes the transfer of FGFR1 to the membrane, thereby promotes the repair of neuronal damage. In contrast, studies have shown that inhibition of the FGFR1 signaling pathway in the pathogenesis of temporomandibular joint osteoarthritis activates autophagy level, thereby ameliorates disease (Wang et al., 2018), probably due to FGFR1 having the different effects on different tissue.

The PD is characterized by degenerative DAergic degeneration, which induces excessive neuronal apoptosis. CHOP is a critical protein that involved in ER stress-induced apoptosis. During prolong ER stress, CHOP expression rapidly increases and leads to apoptosis. TRB3 is an inducing factor associated with neuronal death, and it is associated with ER stress-induced apoptosis (Ohoka et al., 2005). Misfolded protein Aβ induces increases of TRB3 in neurons during PD development (Saleem and Biswas, 2017). It is shown that elevated expression of TRB3 is associated with DAergic death (Aim et al., 2015). Recently, it is unclear the relationship of ER stress and autophagy during aFGF protecting DAergic. Therefore, this study explored the role of TRB3 on this process. The results showed that the 6-OHDA treatement induces TRB3 expression and decreases the expressions of the autophagy-related indicators, mTOR and LC3B/A, which was reversed by aFGF treatment. Previous studies have shown that TRB3 blocks autophagic flow (Saleem and Biswas, 2017), and this study also confirmed that elevated TRB3 also causes increased p62 (an indicator of autophagosome clearance), indicating that autophagic flow is impaired in PD, and TRB3 binding to p62 affects the clearance of autophagosomes (Huang et al., 2015).

Our current study had showed that aFGF and autophagy inducer treatment increased the survival rate of PC12 cells. Moreover, TRB3 was significantly increased in 6-OHDA-induced PD animals and cell models, and aFGF reduced TRB3 expression. Conversely, studies have shown that TRB3 enhances autophagy (Tsai et al., 2018), leading to autophagic death of cells, which may cause excessive expression of TRB3 with varying degrees of stress, thereby aggravating cell death. Moreover, the FGF signaling pathway is involved in the activation of blastocysts by activating autophagy (Shin et al., 2017). These results indicate that aFGF ameliorates 6-OHDA-induced neuronal death *via* down-regulating the pro-apoptotic protein of TRB3 *in vivo* and *in vitro*.

CONCLUSION

This study has demonstrated that aFGF administration ameliorates 6-OHDA-induced PD development. Mechanistic study reveals that aFGF activates autophagy level by inhibiting ER stress-induced TRB3 overexpression during PD development, and subsequently ameliorates 6-OHDA-induced neuronal apoptosis. Our current study firstly elucidates the role of autophagy and its relationship with ER stress during aFGF treatment for PD, which may provide a new potential target for clinical treatment of PD.

DATA AVAILABILITY STATEMENT

All datasets generated for this study are included in the article/supplementary material.

ETHICS STATEMENT

The animal study was reviewed and approved by Laboratory Animal Ethics Committee of Wenzhou Medical University.

AUTHOR CONTRIBUTIONS

JY and YW conceived and designed the experiments. XZ, BW, and GZ performed the experiments. XZ, YW, and JiX performed statistical analysis and wrote the paper. YY, XH, JuX, PZ, YL, and KX provided assistance with experiments. All authors discussed the results and approved the final manuscript.

ACKNOWLEDGMENTS

This work was supported by research grants from the National Natural Science Foundation of China (81560375, 81760230, 81801233 and 81802251), Zhejiang Provincial Natural Science Foundation (LQ18H090011 and LQ18H150003).

REFERENCES

Aiki, H., Wada, T., Iba, K., Oki, G., Sohma, H., Yamashita, T., et al. (2018). Proteomics analysis of site- and stage-specific protein expression after peripheral nerve injury. *J. Orthop. Sci.* 23 (6), 1070–1078. doi: 10.1016/j.jos.2018.07.012

Aim, P., Sun, X., Zareen, N., Rao, A., Berman, Z., Volpicelli-Daley, L., et al. (2015). Trib3 is elevated in parkinson's disease and mediates death in parkinson's disease models. *J. Neurosci.: Off. J. Soc. Neurosci.* 35, 10731–10749. doi: 10.1523/JNEUROSCI.0614-15.2015

Boshoff, E. L., Fletcher, E. J. R., and Duty, S. (2018). Fibroblast growth factor 20 is protective towards dopaminergic neurons in vivo in a paracrine manner. *Neuropharmacology* 137, 156–163. doi: 10.1016/j.neuropharm.2018.04.017

Cao, Y. L., Yang, Y. P., Mao, C. J., Zhang, X. Q., Wang, C. T., Yang, J., et al. (2017). A role of BAG3 in regulating SNCA/alpha-synuclein clearance via selective macroautophagy. *Neurobiol. Aging* 60, 104–115. doi: 10.1016/j.neurobiolaging.2017.08.023

Crews, L., Patrick, C., Achim, C. L., Everall, I. P., and Masliah, E. (2009). Molecular pathology of neuro-AIDS (CNS-HIV). *Int. J. Mol. Sci.* 10, 1045–1063. doi: 10.3390/ijms10031045

Darabi, S., Noori-Zadeh, A., Rajaei, F., Abbaszadeh, H. A., Bakhtiyari, S., and Roozbahany, N. A. (2018). SMER28 attenuates dopaminergic toxicity mediated by 6-hydroxydopamine in the rats via modulating oxidative burdens and autophagy-related parameters. *Neurochem. Res.* 43 (12), 2313–2323. doi: 10.1007/s11064-018-2652-2

Decressac, M., Mattsson, B., Weikop, P., Lundblad, M., Jakobsson, J., and Björklund, A. (2013). TFEB-mediated autophagy rescues midbrain dopamine neurons from α-synuclein toxicity. *Proc. Natl. Acad. Sci. U.S.A.* 110, E1817–E1826. doi: 10.1073/pnas.1305623110

Ding, Y., Xin, C., Zhang, C., Lim, K., Zhang, H., Fu, Z., et al. (2018). Natural molecules from chinese herbs protecting against parkinson's disease via anti-oxidative stress. *Front. Aging Neurosci.* 10, 246. doi: 10.3389/fnagi.2018.00246

Everall, I. P., Trillo-Pazos, G., Bell, C., Mallory, M., Sanders, V., and Masliah, E. (2001). Amelioration of neurotoxic effects of HIV envelope protein gp120 by fibroblast growth factor: a strategy for neuroprotection. *J. Neuropathol. Exp. Neurol.* 60, 293. doi: 10.1093/jnen/60.3.293

Fujiwara, H., Hasegawa, M., Dohmae, N., Kawashima, A., Masliah, E., Goldberg, M. S., et al. (2002). alpha-Synuclein is phosphorylated in synucleinopathy lesions. *Nat. Cell Biol.* 4, 160–164. doi: 10.1038/ncb748

Hasegawa, M., Fujiwara, H., Nonaka, T., Wakabayashi, K., Takahashi, H., Lee, V. M., et al. (2002). Phosphorylated alpha-synuclein is ubiquitinated in alpha-synucleinopathy lesions. *J. Biol. Chem.* 277, 49071–49076. doi: 10.1074/jbc.M208046200

Hetz, C., Thielen, P., Matus, S., Nassif, M., Court, F., Kiffin, R., et al. (2009). XBP-1 deficiency in the nervous system protects against amyotrophic lateral sclerosis by increasing autophagy. *Genes Dev.* 23, 2294–2306. doi: 10.1101/gad.1830709

Huang, L. P., Deng, M. Z., He, Y. P., and Fang, Y. Q. (2015). beta-asarone and levodopa co-administration protects against 6-hydroxydopamine-induced damage in parkinsonian rat mesencephalon by regulating autophagy: down-expression Beclin-1 and light chain 3B and up-expression P62. *Clin. Exp. Pharmacol. Physiol.* 42, 269–277. doi: 10.1111/1440-1681.12344

Jin, Y., Tanaka, A., Choi, A. M., and Ryter, S. W. (2012). Autophagic proteins: new facets of the oxygen paradox. *Autophagy* 8, 426–428. doi: 10.4161/auto.19258

Ko, C. C., Tu, T. H., Wu, J. C., Huang, W. C., Tsai, Y. A., Huang, S. F., et al. (2018). Functional improvement in chronic human spinal cord injury: Four years after acidic fibroblast growth factor. *Sci. Rep.* 8, 12691. doi: 10.1038/s41598-018-31083-4

Kuang, X., Hu, W., Yan, M., and Wong, P. (2010). Phenylbutyric acid suppresses protein accumulation-mediated ER stress in retrovirus-infected astrocytes and delays onset of paralysis in infected mice. *Neurochem. Int.* 57, 738–748. doi: 10.1016/j.neuint.2010.08.010

Lee, K. I., Kim, M. J., Koh, H., Lee, J. I., Namkoong, S., Oh, W. K., et al. (2015). The anti-hypertensive drug reserpine induces neuronal cell death through inhibition of autophagic flux. *Biochem. Biophys. Res. Commun.* 462, 402–408. doi: 10.1016/j.bbrc.2015.04.145

Li, Y., Chen, Y., Huang, H., Shi, M., Yang, W., Kuang, J., et al. (2017). Autophagy mediated by endoplasmic reticulum stress enhances the caffeine-induced apoptosis of hepatic stellate cells. *Int. J. Mol. Med.* 40, 1405–1414. doi: 10.3892/ijmm.2017.3145

Li, J., Wang, Q., Cai, H., He, Z., Wang, H., Chen, J., et al. (2018). FGF1 improves functional recovery through inducing PRDX1 to regulate autophagy and anti-ROS after spinal cord injury. *J. Cell Mol. Med.* 22, 2727–2738. doi: 10.1111/jcmm.13566

Li, X. (2019). The FGF metabolic axis. *Front. Med.* 13, 511–530. doi: 10.1007/s11684-019-0711-y

Lohmann, S., Bernis, M. E., Tachu, B. J., Ziemski, A., Grigoletto, J., and Tamguney, G. (2019). Oral and intravenous transmission of alpha-synuclein fibrils to mice. *Acta Neuropathol.* 138 (4), 515–533. doi: 10.1007/s00401-019-02037-5

Longo, F., Mercatelli, D., Novello, S., Arcuri, L., Brugnoli, A., Vincenzi, F., et al. (2017). Age-dependent dopamine transporter dysfunction and Serine129 phospho-alpha-synuclein overload in G2019S LRRK2 mice. *Acta Neuropathol. Commun.* 5, 22. doi: 10.1186/s40478-017-0426-8

Magalhaes, J., Gegg, M. E., Migdalska-Richards, A., Doherty, M. K., Whitfield, P. D., and Schapira, A. H. (2016). Autophagic lysosome reformation dysfunction in glucocerebrosidase deficient cells: relevance to Parkinson disease. *Hum. Mol. Genet.* 25, 3432–3445. doi: 10.1093/hmg/ddw185

Mamelak, M. (2018). Parkinson's disease, the dopaminergic neuron and gammahydroxybutyrate. *Neurol. Ther.* 7, 5–11. doi: 10.1007/s40120-018-0091-2

Menzies, F. M., and Rubinsztein, D. C. (2010). Broadening the therapeutic scope for rapamycin treatment. *Autophagy* 6 (2), 286–287. doi: 10.4161/auto.6.2.11078

Michiorri, S., Gelmetti, V., Giarda, E., Lombardi, F., Romano, F., Marongiu, R., et al. (2010). The Parkinson-associated protein PINK1 interacts with Beclin1 and promotes autophagy. *Cell Death Differ.* 17, 962–974. doi: 10.1038/cdd.2009.200

Ning, B., Zhang, Q., Wang, N., Deng, M., and Fang, Y. (2019). beta-Asarone Regulates ER Stress and Autophagy Via Inhibition of the PERK/CHOP/Bcl-2/Beclin-1 Pathway in 6-OHDA-Induced Parkinsonian Rats. *Neurochem. Res.* 44 (5), 1159–1166. doi: 10.1007/s11064-019-02757-w

Niu, H., Shen, L., Li, T., Ren, C., Ding, S., Wang, L., et al. (2018). Alpha-synuclein overexpression in the olfactory bulb initiates prodromal symptoms and pathology of Parkinson's disease. *Transl. Neurodegener.* 7, 25. doi: 10.1186/s40035-018-0128-6

Ohoka, N., Yoshii, S., Hattori, T., Onozaki, K., and Hayashi, H. (2005). TRB3, a novel ER stress-inducible gene, is induced via ATF4-CHOP pathway and is involved in cell death. *EMBO J.* 24, 1243–1255. doi: 10.1038/sj.emboj.7600596

Ord, T., and Ord, T. (2017). Mammalian Pseudokinase TRIB3 in Normal Physiology and Disease: Charting the Progress in Old and New Avenues. *Curr. Protein Pept. Sci.* 18, 819–842. doi: 10.2174/1389203718666170406124547

Pickford, F., Masliah, E., Britschgi, M., Lucin, K., Narasimhan, R., Jaeger, P. A., et al. (2008). The autophagy-related protein beclin 1 shows reduced expression in early Alzheimer disease and regulates amyloid beta accumulation in mice. *J. Clin. Invest.* 118, 2190–2199. doi: 10.1172/JCI33585

Salazar, M., Carracedo, A., Salanueva, I., Hernández-Tiedra, S., Lorente, M., Egia, A., et al. (2009). Cannabinoid action induces autophagy-mediated cell death through stimulation of ER stress in human glioma cells. *J. Clin. Invest.* 119, 1359–1372. doi: 10.1172/JCI37948

Saleem, S., and Biswas, S. C. (2017). Tribbles Pseudokinase 3 Induces Both Apoptosis and Autophagy in Amyloid-beta-induced Neuronal Death. *J. Biol. Chem.* 292, 2571–2585. doi: 10.1074/jbc.M116.744730

Samuel, F., Flavin, W. P., Iqbal, S., Pacelli, C., Sri Renganathan, S. D., Trudeau, L. E., et al. (2016). Effects of Serine 129 Phosphorylation on alpha-Synuclein Aggregation, Membrane Association, and Internalization. *J. Biol. Chem.* 291, 4374–4385. doi: 10.1074/jbc.M115.705095

Senft, D., and Ronai, Z. A. (2015). UPR, autophagy, and mitochondria crosstalk underlies the ER stress response. *Trends Biochem. Sci.* 40, 141–148. doi: 10.1016/j.tibs.2015.01.002

Shan, S., Tian, L., and Fang, R. (2019). Chlorogenic Acid Exerts Beneficial Effects in 6-Hydroxydopamine-Induced Neurotoxicity by Inhibition of Endoplasmic Reticulum Stress. *Med. Sci. Monit.* 25, 453–459. doi: 10.12659/MSM.911166

Shin, H., Bang, S., Kim, J., Jun, J. H., Song, H., and Lim, H. J. (2017). The formation of multivesicular bodies in activated blastocysts is influenced by autophagy and FGF signaling in mice. *Sci. Rep.* 7, 41986. doi: 10.1038/srep41986

Song, J. X., Lu, J. H., Liu, L. F., Chen, L. L., Durairajan, S. S., Yue, Z., et al. (2014). HMGB1 is involved in autophagy inhibition caused by SNCA/alpha-synuclein

overexpression: a process modulated by the natural autophagy inducer corynoxine B. *Autophagy* 10, 144–154. doi: 10.4161/auto.26751

Spencer, B., Potkar, R., Trejo, M., Rockenstein, E., Patrick, C., Gindi, R., et al. (2009). Beclin 1 gene transfer activates autophagy and ameliorates the neurodegenerative pathology in alpha-synuclein models of Parkinson's and Lewy body diseases. *J. Neurosci.* 29, 13578–13588. doi: 10.1523/JNEUROSCI.4390-09.2009

Tang, B., Li, Q., Zhao, X. H., Wang, H. G., Li, N., Fang, Y., et al. (2015). Shiga toxins induce autophagic cell death in intestinal epithelial cells via the endoplasmic reticulum stress pathway. *Autophagy* 11, 344–354. doi: 10.1080/15548627.2015.1023682

Tsai, M. J., Tsai, S. K., Huang, M. C., Liou, D. Y., Huang, S. L., Hsieh, W. H., et al. (2015). Acidic FGF promotes neurite outgrowth of cortical neurons and improves neuroprotective effect in a cerebral ischemic rat model. *Neuroscience* 305, 238–247. doi: 10.1016/j.neuroscience.2015.07.074

Tsai, D. H., Chung, C. H., and Lee, K. T. (2018). Antrodia cinnamomea induces autophagic cell death via the CHOP/TRB3/Akt/mTOR pathway in colorectal cancer cells. *Sci. Rep.* 8, 17424. doi: 10.1038/s41598-018-35780-y

Walicke, P. A., and Baird, A. (1988). Neurotrophic effects of basic and acidic fibroblast growth factors are not mediated through glial cells. *Dev. Brain Res.* 40, 71–79. doi: 10.1016/0165-3806(88)90009-0

Wang, Z., Huang, J., Zhou, S., Luo, F., Tan, Q., Sun, X., et al. (2018). Loss of Fgfr1 in chondrocytes inhibits osteoarthritis by promoting autophagic activity in temporomandibular joint. *J. Biol. Chem.* 293, 8761–8774. doi: 10.1074/jbc.RA118.002293

Wei, X., He, S., Wang, Z., Wu, J., Zhang, J., Cheng, Y., et al. (2014). Fibroblast growth factor 1attenuates 6-hydroxydopamine-induced neurotoxicity: an in vitro and in vivo investigation in experimental models of parkinson's disease. *Am. J. Trans. Res.* 6, 664–677. doi: 10.1016/j.jep.2012.07.032

Winslow, A. R., and Rubinsztein, D. C. (2014). The Parkinson disease protein α-synuclein inhibits autophagy. *Autophagy* 7, 429–431. doi: 10.4161/auto.7.4.14393

Wu, F., Chen, Z., Tang, C., Zhang, J., Cheng, L., Zuo, H., et al. (2017). Acid fibroblast growth factor preserves blood-brain barrier integrity by activating the PI3K-Akt-Rac1 pathway and inhibiting RhoA following traumatic brain injury. *Am. J. Trans. Res.* 9, 910–925.

Yamamuro, A., Yoshioka, Y., Ogita, K., and Maeda, S. (2006). Involvement of endoplasmic reticulum stress on the cell death induced by 6-hydroxydopamine in human neuroblastoma SH-SY5Y cells. *Neurochem. Res.* 31, 657–664. doi: 10.1007/s11064-006-9062-6

Yin, Y., Sun, G., Li, E., Kiselyov, K., and Sun, D. (2017). ER stress and impaired autophagy flux in neuronal degeneration and brain injury. *Ageing Res. Rev.* 34, 3–14. doi: 10.1016/j.arr.2016.08.008

Zhou, Y., Wu, Y., Liu, Y., He, Z., Zou, S., Wang, Q., et al. (2017). The cross-talk between autophagy and endoplasmic reticulum stress in blood-spinal cord barrier disruption after spinal cord injury. *Oncotarget* 8, 1688–1702. doi: 10.18632/oncotarget.13777

Conflict of Interest: The authors declare that the research was conducted in the absence of any commercial or financial relationships that could be construed as a potential conflict of interest.

frontiers in Pharmacology

ORIGINAL RESEARCH
published: 20 December 2019
doi: 10.3389/fphar.2019.01515

Paracrine Fibroblast Growth Factor 1 Functions as Potent Therapeutic Agent for Intrahepatic Cholestasis by Downregulating Synthesis of Bile Acid

Huan Lin[1,2†], *Chuanren Zhou*[1†], *Yushu Hou*[1†], *Qi Li*[1], *Guanting Qiao*[1], *Yang Wang*[3], *Zhifeng Huang*[1*] and *Jianlou Niu*[1*]

[1] School of Pharmacy, Wenzhou Medical University, Wenzhou, China, [2] Engineering Laboratory of Zhejiang Province for Pharmaceutical Development of Growth Factors, Biomedical Collaborative Innovation Center of Wenzhou, Wenzhou, China, [3] School of Basic Medical Sciences, Wenzhou Medical University, Wenzhou, China

OPEN ACCESS

Edited by:
Zhouguang Wang,
Albert Einstein College of Medicine,
United States

Reviewed by:
Chen Li,
Charité Medical University of Berlin,
Germany
Yi Kou,
University of Southern California,
United States

***Correspondence:**
Zhifeng Huang
hzf@wmu.edu.com
Jianlou Niu
niujianlou@126.com

[†]These authors have contributed equally to this work

Specialty section:
This article was submitted to Translational Pharmacology, a section of the journal Frontiers in Pharmacology

Received: 22 October 2019
Accepted: 22 November 2019
Published: 20 December 2019

Citation:
Lin H, Zhou C, Hou Y, Li Q, Qiao G, Wang Y, Huang Z and Niu J (2019) Paracrine Fibroblast Growth Factor 1 Functions as Potent Therapeutic Agent for Intrahepatic Cholestasis by Downregulating Synthesis of Bile Acid. Front. Pharmacol. 10:1515. doi: 10.3389/fphar.2019.01515

Endocrine fibroblast growth factor (FGF) 19 has been shown to be capable of maintaining bile acid (BA) homeostasis and thus hold promise to be a potential therapeutic agent for cholestasis liver disease. However, whether paracrine FGFs possess this BA regulatory activity remains to be determined. In our study, we identified that paracrine fibroblast growth factor 1 (FGF1) was selectively downregulated in the liver of alpha naphthylisothiocyanate (ANIT)-induced intrahepatic cholestasis mice, suggesting a pathological relevance of this paracrine FGF with abnormal BA metabolism. Therefore, we evaluated the effects of engineered FGF1 mutant - $FGF1^{\Delta HBS}$ on the metabolism of hepatic BA and found that this protein showed a more potent inhibitory effect of BA biosynthesis than FGF19 without any hepatic mitogenic activity. Moreover, the chronic administration of $FGF1^{\Delta HBS}$ protected liver against ANIT-induced injury by reducing hepatic BA accumulation. Taken together, these data suggest that $FGF1^{\Delta HBS}$ may function as a potent therapeutic agent for intrahepatic cholestasis liver disease.

Keywords: fibroblast growth factor 1, bile acid, cholestatic liver disease, alpha naphthylisothiocyanate, negative regulator, intrahepatic cholestasis

INTRODUCTION

As synthesized from cholesterol in the liver, bile acids (BAs) are normally stored in the gallbladder. After meal, it is released into the small intestine to facilitate the digestion and absorption of dietary lipids (de Aguiar Vallim et al., 2013). However, the disturbance of this physiological homeostasis will threaten human health, due to the inherent detergent properties of BAs that are potentially cytotoxic to tissues (Kaplan and Gershwin, 2005).

Cholestasis is one of the most life-threatening liver diseases that is characterized with impaired bile flow and intrahepatic retention of toxic BAs. The occurrence and development of this disease

frequently leads to liver fibrosis, cirrhosis and even liver failure (Luo et al., 2014). To date, the main prescribed drugs to treat cholestasis are ursodeoxycholic acid (UDCA) and obelicholic acid (OCA). However, up to 40% of patients' response poorly to UDCA therapy (Lindor, 2007; Hirschfield et al., 2018). For patients with late-stage cholestasis, the only available option is liver transplantation (Lindor, 2007). Thus, there is still an unmet need for more effective therapeutic agents to relief cholestatic liver disease.

There are accumulating evidences demonstrating that endocrine fibroblast growth factor 15 (FGF15)/FGF19 signals from the intestine to the liver to suppress the expression of cholesterol 7α-hydroxylase (Cyp7A1) (the first rate-limiting enzyme in the classical BA synthetic pathway) as a negative feedback loop on BA synthesis (Inagaki et al., 2005; Goetz et al., 2007; Degirolamo et al., 2016). The discovery of these gut-liver hormonal axes raises the prospect that modulating BA metabolism by FGF1 (Nicholes et al., 2002) may be a novel approach for treating cholestasis. However, the development of a FGF19-based therapy is challenged with regard to its unwanted mitogenic activity and tumorgenicity (Nicholes et al., 2002; Wu et al., 2010). It has been attempted by several groups to uncouple the BA regulatory capacity and tumorigenic activity of FGF19 by engineering a M70 mutant (a FGF19 variant) that retains BA regulatory activity without causing hepatocellular carcinoma (HCC) (Zhou et al., 2014). This nontumorigenic FGF19 variant is shown to reduce hepatic BA accumulation and protect mice from liver injury caused by either intrahepatic or extrahepatic cholestasis, which suggests that it is an applicable approach for the treatment of cholestatic liver disease (Luo et al., 2014; Zhou et al., 2016).

More recently, serum level of FGF21 (another member of FGF endocrine subfamily besides FGF19) is found to be highly upregulated in patients with biliary atresia, suggesting a compensatory response may be initiated (Li et al., 2016). However, the therapeutic effect of this endocrine hormone on cholestasis is still controversial; both its positive and negative regulations on BA synthesis have been reported (Zhang et al., 2017; Chen et al., 2018).

The mammalian FGFs are grouped into five paracrine subfamilies and one endocrine subfamily (Beenken and Mohammadi, 2009; Degirolamo et al., 2016). These FGFs trigger a few common sets of downstream signaling pathways, including PLCγ/PKC, FRS2α/RAS-MAPK, Gab1/PI3 kinase/Akt, and CrkL/Cdc42-Rac (Kouhara et al., 1997; Larsson et al., 1999; Dailey et al., 2005; Eswarakumar et al., 2005; Seo et al., 2009; Chau et al., 2010), *via* activations of FGF receptors (FGFRs) in either an HS-dependent (in the case of paracrine FGFs) or a Klotho coreceptor dependent (in the case of endocrine FGFs) manner (Yayon et al., 1991; Kurosu et al., 2007; Goetz and Mohammadi, 2013). Due to the fact that both endocrine FGF19 and FGF21 are capable of controlling BA metabolism (Inagaki et al., 2005; Zhang et al., 2017; Chen et al., 2018), it is logical to postulate that paracrine FGFs may also possess this ability. Thus, we systematically screened expressions of all paracrine FGFs in alpha naphthylisothiocyanate (ANIT)-induced cholestasis mice and found that only FGF1 was downregulated compared to others, indicating that this paracrine FGF may be associated with the pathogenesis of BA disorders. We further confirmed that FGF1 could suppress BA synthesis both *in vitro* and *in vivo*. Moreover, the chronic administration of $FGF1^{\Delta HBS}$ protected liver against ANIT-induced injury by reducing hepatic BA accumulation. Taken together, all the data suggest that FGF1-based therapy may be an effective way to treat cholestatic liver disease.

MATERIALS AND METHODS

Materials

Full-length wide type recombinant human FGF19 ($FGF19^{WT}$) and the FGF1 variant ($FGF1^{\Delta HBS}$) carrying triple mutations (Lys127Asp, Lys128Gln, and Lys133Val) were expressed in *E.coli* (BL21) and purified as described in the previous studies (Goetz et al., 2007; Huang et al., 2017). Mouse Total BA Assay Kit was purchased from Crystal Chem INC. Alpha-naphthylisothiocyanate (ANIT) was purchased from Sigma Aldrich (St. Louis, MO, USA). Alanine transaminase (ALT) and aspartate transaminase (AST) Assay Kits were purchased from Sigma Aldrich (St. Louis, MO, USA) and performed in accordance with the protocols provided with manufacturers. All other reagents were of analytical grade.

Identification of Differential Paracrine FGFs Between ANIT-Induced Cholestasis Model and Vehicle Group

Male C57BL/6J mice (20–25 g) were acquired from the Chinese Academy of Science-Shanghai Laboratory Animal Center. All animals were maintained on a 12-h light/dark cycle and a temperature of 25°C ± 2°C. Animal care and all animal experiments conformed to the Guide for the Care and Use of Laboratory Animals provided by U.S. National Institutes of Health and were approved by the Animal Care and Use Committee of Wenzhou Medical University, China.

ANIT-induced intrahepatic cholestasis was established according to previous reports (Dai et al., 2017). Briefly, mice were randomized into two groups based on body weight. One group was orally administered with a single dose of ANIT (75 mg/kg, dissolved in olive oil), termed as ANIT-induced cholestasis model group; another group was treated with the same volume of olive oil, serving as the vehicle group. Mice were euthanized 48 h after administration. Blood of mice was collected to determine serum levels of liver enzymes (ALT and AST). Liver tissues of both groups were collected and total RNA was isolated using Trizol reagent (Invitrogen) according to the manufacturer's instructions. The differential mRNA levels of all paracrine FGFs between ANIT-induced cholestasis model and the vehicle group were determined by RT-PCR and relative mRNA levels were calculated by comparative threshold cycle method using β-actin as the internal standard. The primers of all paracrine FGFs were listed in the (**Table S1**).

Primary Hepatocyte Experiments

Primary mouse hepatocytes were isolated and cultured according to the methods described previously (Zhou et al., 2017). Primary mouse hepatocytes were plated on rat tail collagen-coated dishes at a density of 1.5×10^5 cells/cm^2 and were allowed to attach for 24 h in a 37°C incubator with 5% CO_2. Culture medium was consisted of 2% fetal bovine serum Williams' E medium supplemented with 10 nM dexamethasone, 1% penicillin/streptomycin, L-glutamine. Twenty-four hours after isolation, cells were treated with the indicated concentration of FGF1$^{\Delta HBS}$ or FGF19^{WT} (0.2, 2.0, or 20 nM) for 6 h. Total RNA was isolated using Trizol reagent (Invitrogen) according to the manufacturer's instructions. The relative mRNA levels of Cyp7A1, Cyp8B1, Cyp27A1, and Cyp7B1 were determined by real-time polymerase chain reaction (RT-PCR).

For knockdown of FGF receptor 4 (FGFR4) expression by siRNA, cells were seeded in 6-well plates for 24 h. Transient transfections were performed using Lipofectamine RNAiMAX (Thermo Fisher Scientific, Waltham, MA) according to manufacturer's protocol. After transfection with either siRNA (control or FGFR4 siRNA) (all from Santa Cruz Biotechnology, Dallas, Texas, USA) for 24 h, cells were treated with FGF1$^{\Delta HBS}$ (20 nM) for 6 h. Then, cells were extracted and analyzed the Cyp7A1 mRNA levels by RT-PCR.

Acute Effects of FGF1$^{\Delta HBS}$ on the Genes That Involved in the BA Metabolism

To directly and comprehensively evaluate the effects of FGF1$^{\Delta HBS}$ on BA metabolism, 6–8 weeks' C57BL/6J mice were administered with a single intraperitoneal injection of PBS, FGF1$^{\Delta HBS}$, or FGF19^{WT} at increasing doses (0.01, 0.1, and 1.0 mg/kg) respectively. After 4 h of administration, liver tissues were collected and snap-frozen in liquid nitrogen for analysis of the key genes involved in BA metabolism including BA biosynthesis and transport.

Effects of Subchronic Administration of FGF1$^{\Delta HBS}$ on the BA Homeostasis

A 6-day subchronic study was performed in 6–8-week-old C57BL/6J mice. Male mice were administered with vehicle, FGF1$^{\Delta HBS}$ (0.1 and 1.0 mg/kg, once daily) or FGF19^{WT} (0.1 and 1.0 mg/kg, twice daily BID), PBS and FGF19^{WT}-treated mice served as negative and positive control respectively. On the sixth day, the mice received the last dose and were placed in a new cage without food. Tissue samples including liver, gallbladder, and small intestine were collected 4 h after the last administration for genes and BA content analysis. Collect the small intestine and retain the complete contents.

Total BAs of liver, gallbladder, and small intestine were determined using Mouse Total BA Assay Kit (Crystal Chem INC). The extraction method from tissues was according to methods described previously (Chen et al., 2018). Briefly, the froze liver, gallbladder, and small intestine from subchronic treated mice were individually homogenized with 75% ethanol and total BAs were extracted by incubating the tissue homogenate in a 50°C shaker for 2 h. Supernatants from the extraction were collected after centrifugation and diluted in PBS for analysis. The dilution factors for each tissue extract were estimated to ensure that BA measurements fell in the linear range of the standard curve using mouse BA kit. The BA pool size was determined as sum of the amount of total BAs in the liver, gallbladder, and small intestine and its contents.

Real-Time Polymerase Chain Reaction (RT-PCR)

Total RNA was isolated from treated primary hepatocytes or frozen tissues, such as the liver, intestine, and gallbladder using TransZol Up Kit (TransGen Biotech). The total RNA was reverse-transcribed into complementary DNA with One-Step gDNA Removal Kit (TransGen Biotech). Quantitative real-time polymerase chain reaction (RT-PCR) was done using ChamQ Universal SYBR qPCR Master Mix (Vazyme) with specific primers (listed in the **Table S1**) on a Step One Plus Real-Time PCR system (Applied Biosystems® Quant Studio® 3). β-actin was used as an endogenous control to normalize for differences in the amount of total RNA added to each reaction. For mRNAs levels of paracrine FGFs with the cycle threshold (CT) value equal to or greater than 35 are considered undetectable.

Western Blot Analysis of Protein Expression

Liver tissues were then homogenized in protein extraction buffer (Sigma-Aldrich, St. Louis, MO) with protease and phosphatase inhibitors, and collected by centrifuging. The protein concentration was determined using a bicinchoninic acid (BCA) Protein Assay Kit (Thermo Scientific, Waltham, MA), and equal amounts of samples were mixed with loading buffer, subjected to SDS-polyacrylamide gels at 110 V for 100 min, and then the protein was transferred onto polyvinylidine fluoride membranes (PVDF) (Millipore-Billerica, MA, USA). After blocking with 5% nonfat milk for 2 h at room temperature, the PVDF membranes were washed three times with Tris-buffered saline (pH 7.6) containing 0.1% Tween-20 (TBST) and then incubated at 4°C overnight with primary antibody to mouse FGF1 (1:1000) or glyceraldehyde-3-phosphate dehydrogenase (GAPDH) (1:2000), all the antibodies were obtained from Abcam (Cambridge, MA). The membranes were washed and later incubated with HRP-conjugated secondary antibody. Immuno-reactive protein bands were visualized using the ChemiDocTM XRS with Imaging LabTM Software (Bio-Rad, Hercules, CA) and quantified by optical densitometry using Image J software (National Institutes of Health, Bethesda, MD, USA).

Therapeutic Effects of FGF1$^{\Delta HBS}$ on the ANIT-Induced Interhepatic Cholestasis

Male C57BL/6J mice (6–8 weeks old; n = 10 mice per group) were injected intraperitoneally with PBS, FGF1$^{\Delta HBS}$ (0.1 mg/kg) or FGF1$^{\Delta HBS}$ (1.0 mg/kg) once daily for 6 days. On the fourth day, a single dose of ANIT (75 mg/kg, dissolved in olive oil) was administered *via* oral gavage. Mice were euthanized on the sixth day, 4 h after the final dosage. Serum, liver, gallbladder, and

intestine samples were collected for analysis. Perform the analysis of serum liver function index (ALT and AST). Detect the BA content in serum, liver, gallbladder, and small intestine.

Histological Analysis

Hematoxylin and Eosin (H&E) staining was performed to detect the protection of $FGF1^{\Delta HBS}$ for liver injury in the ANIT-induced intrahepatic cholestasis. Briefly, liver tissues of each group were collected and kept in 4% paraformaldehyde for a post-fix overnight, and the paraffin-embedded liver tissues were then sectioned into 5 μm thickness sections by LEICA RM2235 (LEICA, Germany). The sections were dried at 40°C, deparaffinized, and then rehydrated using a series of ethanol solutions. The rehydrated sections were subjected to H&E solution based on the manufacture's protocol. After the slides were gently washed with tap water and subsequently rinsed in distilled water, the slides were mounted with mounting medium. Finally, the sections were observed and imaged using a Nikon ECLIPSE NI fluorescence microscope (Nikon, Japan).

Statistical Analysis

All results are expressed as means ± SEM. One-way ANOVA followed by Dunnett's posttest was used to compare data from multiple groups (GraphPad Prism). When indicated, Student's t test or Mann-Whitney test was used to compare two treatment groups. A P-value of 0.05 or less was considered statistically significant.

RESULTS

FGF1 Is Selectively Downregulated in the Liver of ANIT-Induced Intrahepatic Cholestasis Mice

To explore the pathological relevance of paracrine FGFs with cholestatic liver disease, C57BL/6J mice were orally challenged with a single dose of anaphthylisothiocyanate (ANIT - a xenobiotic compound) (75 mg/kg of body weight) for 48 h to induce intrahepatic cholestasis with olive oil as (Yu et al., 2017). We found that serum levels of ALT, AST, and total BA were markedly upregulated with concomitant increases of hepatic BAs in these mice (**Figures 1A**, **D**). To our surprise, we found that only mRNA level of FGF1 in the liver was selectively downregulated (51% reduction relative to vehicle group) compared to other paracrine FGFs (**Figure 1E**; **Table S2**). This was further confirmed by the fact that the protein expression of hepatic FGF1 was also significantly abrogated (**Figure 1F**). Taken together, these results suggest that FGF1 may be involved in the control of BA metabolism.

$FGF1^{\Delta HBS}$ Suppresses Biosynthesis Pathways of BA in Primary Mouse Hepatocyte

Considering the potential safety of wild type FGF1 ($FGF1^{WT}$), we used an FGF1 variant ($FGF1^{\Delta HBS}$) in the following study. As reported in our previous study, this mutant exhibits a markedly reduced proliferative potential while preserving the full metabolic activity of $FGF1^{WT}$ (Huang et al., 2017).

The synthesis of BAs in the liver are tightly controlled by two pathways to match the physiological needs, which are comprised of one classic pathway catalyzed by Cyp7A1 and an alternative pathway regulated by two key enzymes (Cyp27A1 and Cyp7B1) (Russell, 2009).

To assess the capability of $FGF1^{\Delta HBS}$ to regulate the biosynthesis of BA, primary mouse hepatocytes were stimulated with increasing concentrations of $FGF1^{\Delta HBS}$ with vehicle and $FGF19^{WT}$ as controls. Consistent with previous reports (Holt et al., 2003; Luo et al., 2014), FGF19 selectively inhibited the mRNA levels of Cyp7A1 (52% reduction verse vehicle group) in the primary mouse hepatocytes without affecting those of Cyp8B1, Cyp27A1, and Cyp7B1 (**Figures 2A–D**). Notably, $FGF1^{\Delta HBS}$ could inhibited the mRNA levels of Cyp7A1, Cyp8B1, Cyp27A1, and Cyp7B1, showing a greater potency on the inhibition of Cyp7A1 mRNA levels compared to that $FGF19^{WT}$ (**Figures 2E–H**) and these inhibitory effects were compromised by the knockdown of FGF receptor 4 (FGFR4) expression by siRNA transfection (**Figures 2I–L**). Taken together, these data indicate that $FGF1^{\Delta HBS}$ directly downregulates BA biosynthesis by FGFR4-mediated inhibiting of the classical and alternative pathways.

$FGF1^{\Delta HBS}$ Acutely Inhibits BA Synthesis Pathways *In Vivo*

To evaluate the inhibitory effect of $FGF1^{\Delta HBS}$ on hepatic BA synthesis *in vivo*, C57BL/6J mice were received with a single intraperitoneal (i.p.) injection of $FGF1^{\Delta HBS}$ at the dose of 0.01, 0.1 or 1.0 mg/kg of body weight. As previous reported (Luo et al., 2014), $FGF19^{WT}$ remarkedly suppressed the expression of Cyp7A1 mRNA levels 4 h after injection (1.0 mg/kg, 39% reduction relative to vehicle group) (**Figure 3A**). In the case of $FGF1^{\Delta HBS}$, its acute administration dose-dependently inhibited hepatic mRNA expressions of Cyp7A1, Cyp8B1, Cyp27A1, and Cyp7B1 (**Figures 3B–E**), suggesting that $FGF1^{\Delta HBS}$ might reduce BA biosynthesis through both the classic and alternative pathways, which was consistent with the *in vitro* data. Notably, $FGF1^{\Delta HBS}$ more potently inhibited the mRNA level of Cyp7A1 than $FGF19^{WT}$ (99% reduction relative to vehicle group at 1.0 mg/kg dose), probably due to that FGFR4-binding affinity of $FGF1^{\Delta HBS}$ is much higher than that of $FGF19^{WT}$ (**Figure 4B**).

In addition to BA synthesis, the maintenance of BA homeostasis relies on various hepatic membrane transporters (Zollner et al., 2006; Halilbasic et al., 2013). In the liver, the uptake of BA from hepatic portal vein is mainly mediated by basolateral uptake transporters (Ntcp, Oatp1, and Oatp2), while its excretion through microbilliary ducts is regulated by BA canalicular efflux transporters (canalicular bile salt export pump Bsep, Mrp2, and Mdr2) (Zollner et al., 2006; Halilbasic et al., 2013). To comprehensively investigate the effects of $FGF1^{\Delta HBS}$ on BA intracellular and extracellular transports, mRNA levels of both basolateral uptake transporters and BA canalicular efflux transporters in the liver were determined. As

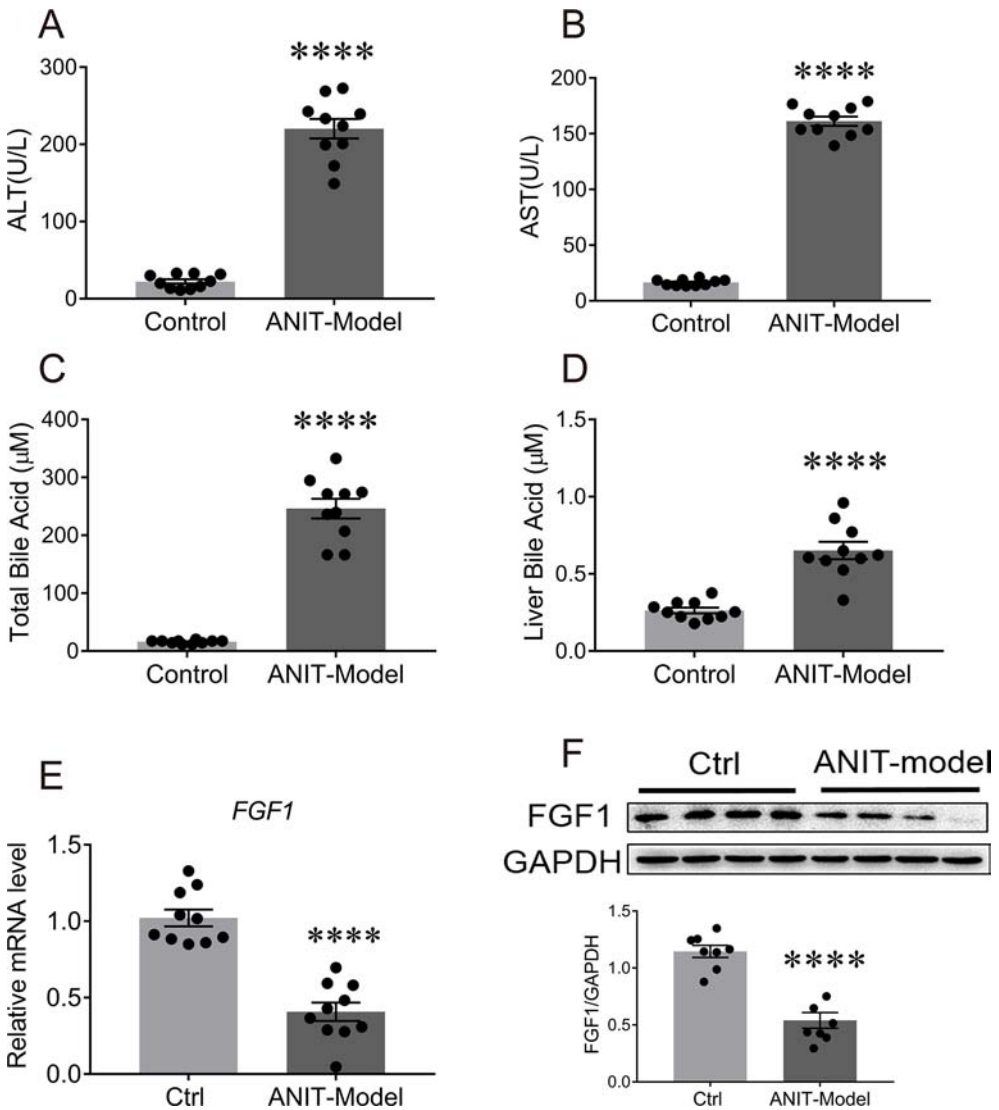

FIGURE 1 | The mRNA and protein levels of FGF1 in liver were downregulated in the ANIT-induced intrahepatic cholestasis mouse model. Eight-week-old C57BL/6J mice were orally administrated with olive oil (control group) or 75 mg/kg ANIT (cholestasis mouse model) for once and then liver tissues were collected and analyzed after 48 h. **(A**, **B)** Evaluation of liver function as determined by serum levels of ALT and AST. **(C**, **D)** Serum BA concentrations **(C)** and hepatic BA pool **(D)** of each group were measured. **(E)** The levels of hepatic FGF1 gene expression of each group were examined by real-time polymerase chain reaction (RT-PCR); **(F)** Representative western blot analysis (up panel) and densitometric quantification (down panel) of FGF1 protein expression in liver tissues from ANIT-induce intrahepatic cholestasis mouse model and control group; data are normalized to GAPDH. Data are presented as mean ± SEM; ****$p < 0.0001$ versus control group; n = 8-12. ANIT-model, ANIT-induced intrahepatic cholestasis mouse model; Ctrl, control group; FGF1, fibroblast growth factor 1; GAPDH, glyceraldehyde-3-phosphate dehydrogenase.

shown in **Figures 3F–H**, expressions of Bsep and Mrp2 were only modestly suppressed by $FGF1^{\Delta HBS}$ treatment without affecting that of Mdr2. For basolateral uptake transporters, $FGF1^{\Delta HBS}$ significantly reduced mRNA levels of Ntcp, Oatp1, Oacp2, and especially Ntcp (89% reduction verse vehicle group), indicating that $FGF1^{\Delta HBS}$ may prevent the uptake of BA from hepatic portal vein (**Figures 3I–K**). Moreover, the measurement of hepatic BA pool showed that there was no remarkable difference between $FGF1^{\Delta HBS}$-treated mice with control group (**Figure 3L**). Taken together, these data suggest that $FGF1^{\Delta HBS}$ is a more potent inhibitor on BA biosynthesis than FGF19 *in vivo* and prevent the uptake of BA from hepatic portal vein.

Chronic Administration of $FGF1^{\Delta HBS}$ Inhibits Biosynthesis of BA Without Inducing Hepatic Proliferation

A 6-day study was conducted to evaluate the long-term effect of $FGF1^{\Delta HBS}$ on BA biosynthesis. The dosage and frequency used

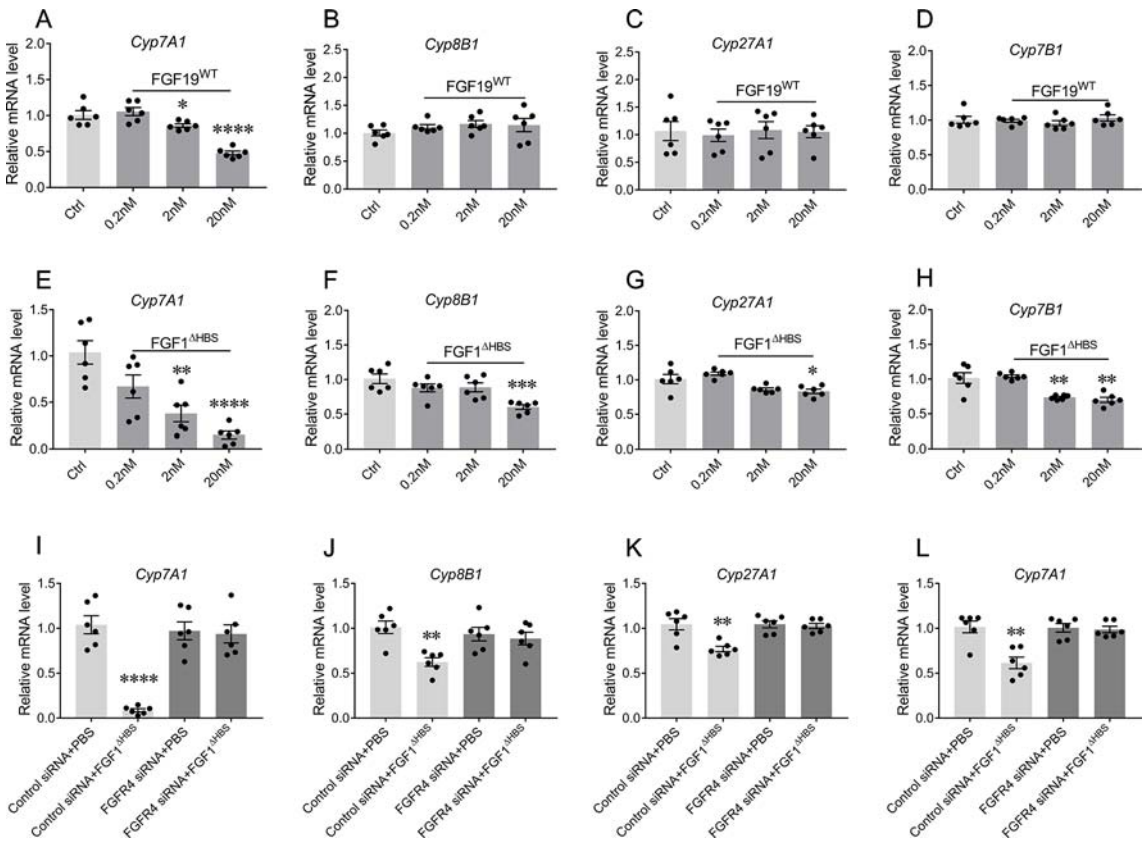

FIGURE 2 | The bile acid (BA) regulatory activity of FGF1 in primary mouse hepatocytes. **(A-H)** Primary mouse hepatocytes were stimulated by different concentrations of $FGF19^{WT}$ **(A-D)** or $FGF1^{\Delta HBS}$ **(E-H)**, relative mRNA levels of Cyp7A1, Cyp8B1, Cyp27A1, and Cyp7B1 were determined by real-time polymerase chain reaction (RT-PCR) (n = 6) and normalized to actin mRNA levels. **(I-L)** Primary mouse hepatocytes with and without knockdown FGFR4 were stimulated by PBS or 20 nM $FGF1^{\Delta HBS}$, relative mRNA levels of Cyp7A1, Cyp8B1, Cyp27A1, and Cyp7B1 were determined by RT-PCR and normalized to actin mRNA levels. Data are expressed as fold change relative to control group (PBS-treated primary mouse hepatocytes). Data are presented as mean ± SEM; ****p < 0.0001 versus control group. *P < 0.05; **P < 0.01; ***P < 0.001.

was according to previous report (Chen et al., 2018), mice were i.p. administered with $FGF19^{WT}$ (twice daily) or $FGF1^{\Delta HBS}$ (once daily) at 0.1 or 1.0 mg/kg of body weight (**Figure 4A**). Consistent with its acute effects, $FGF1^{\Delta HBS}$ at 1.0 mg/kg significantly inhibited hepatic expressions of Cyp7A1, Cyp8B1, Cyp27A1, and Cyp7B1 (**Figures 4B–E**) with a remarkable reduction of BA content in the liver and gallbladder (**Figures 4F–H**). Besides, total BA pool was also largely reduced (**Figure 4I**). These data further demonstrate that $FGF1^{\Delta HBS}$ can inhibit BA biosynthesis and reduce BA pool by downregulating BA synthetic pathways. Thus, we speculate that $FGF1^{\Delta HBS}$ may be a potential therapeutic agent for treating cholestasis.

In addition, we evaluated the safety of chronic $FGF1^{\Delta HBS}$ treatment. Serum levels of ALT and AST were not altered by $FGF1^{\Delta HBS}$, suggesting that liver was not injured (**Figures 5A, B**). We further assessed the mitogenic activity of $FGF1^{\Delta HBS}$ and $FGF19^{WT}$ in the 6-day study by determining the hepatic mRNA levels of proliferation markers including Ki67, alpha fetaprotein (AFP), and proliferating cell nuclear antigen (PCNA). Consistent with previous studies (Wu et al., 2010), $FGF19^{WT}$ significantly upregulates these proliferating signals in the liver (**Figures 5C–E**). However, mice treated with $FGF1^{\Delta HBS}$ did not exhibit any hepatic proliferation activity (**Figures 5C–E**). Moreover, signs of hyperplasia by immune-histochemical staining using PCNA showed that $FGF19^{WT}$ caused a clear increase in the number of hyperproliferating cells in the liver of mice. As expected, there was no increase in the number of hyperproliferating cells in the livers of $FGF1^{\Delta HBS}$-treated mice over that of the PBS-treated control (**Figure 5F**). This consistence with our previous study further confirms the safety of chronic $FGF1^{\Delta HBS}$ treatment.

$FGF1^{\Delta HBS}$ Ameliorates ANIT-Induced Intrahepatic Cholestasis

We further assessed the potential therapeutic efficacy of $FGF1^{\Delta HBS}$ on ANIT-induced intrahepatic cholestasis. Consistent with previous studies, increased intrahepatic BA content and reduced the intestine BA pool were observed in the mice treated by ANIT, compared with that of the vehicle group, confirming the establishment of intrahepatic cholestasis

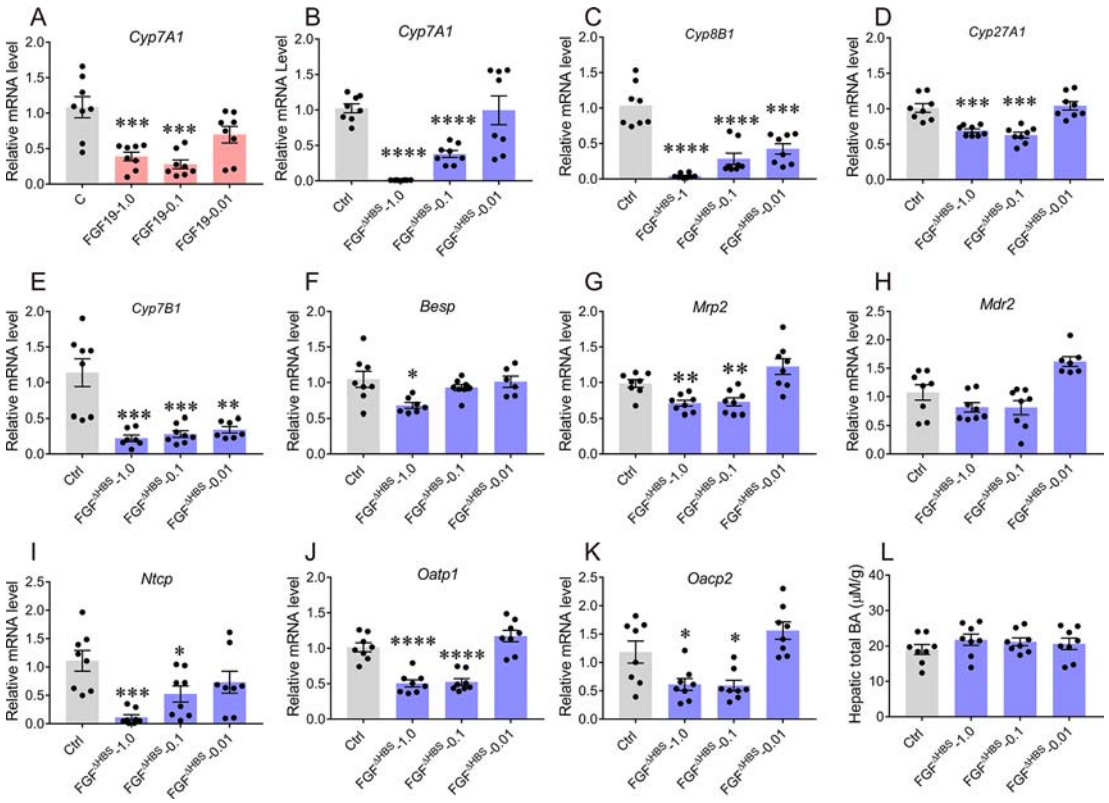

FIGURE 3 | Acute effects of FGF1$^{\Delta HBS}$ on the expression of hepatic genes involved in bile acid (BA) homeostasis. Eight-week male C57BL/6J mice were injected intraperitoneally with FGF1$^{\Delta HBS}$ or FGF19^{WT} at dose of 0.01, 0.1 and 1.0 mg/kg, FGF19^{WT}-treated mice served as a positive control. Liver tissues were collected 4 h after dosing and the hepatic genes involved in BA biosynthesis and transporter were evaluated by real-time polymerase chain reaction (RT-PCR). **(A)** Effect of FGF19^{WT} on Cyp7A1 mRNA; **(B–E)** Hepatic mRNA levels of Cyp7A1 **(B)**, Cyp8B1 **(C)**, Cyp27A1 **(D)**, and Cyp7B1 **(E)** were determined by RT-PCR. **(F–H)** RT-PCR analysis of canalicular efflux transporters (Bsep, Mrp2 and Mdr2). **(I–K)** RT-PCR analysis of basolateral uptake transporters (Ntcp, Oatp1, and Oatp2). **(L)** Hepatic BA pool after acute administration of FGF1$^{\Delta HBS}$. Data was normalized to actin mRNA levels and expressed as fold change relative to control group (PBS-treated mice). Data are presented as mean ± SEM; *P < 0.05; **P < 0.01; ***P < 0.001; **** p < 0.0001 versus control group; n = 8.

model (**Figures 6A–D**). Notably, we observed that FGF1$^{\Delta HBS}$ (1.0 mg/kg of body weight) treatment significantly reduced BA contents in the liver, gallbladder, and small intestine and thus lowered the total BA pool (**Figures 6A–D**).

The elevated hepatic BA accumulation in ANIT-induced intrahepatic cholestasis mice induced a remarkable liver damage as revealed by increasing serum levels of ALT and AST (**Figures 6E–G**). We found that the chronic treatment of FGF1$^{\Delta HBS}$ (1.0 mg/kg of body weight) significantly lowered serum levels of total BA, ALT, and AST, indicating a protective effect of FGF1$^{\Delta HBS}$ on ANIT-induced liver damage. The histological analysis suggested that FGF1$^{\Delta HBS}$ treatment reduced cholestasis associated necrotic lesions in the liver, compared to the vehicle treatment (**Figure 6H**). Taken together, all the data demonstrate that FGF1$^{\Delta HBS}$ protects against liver damage in ANIT-induced intrahepatic cholestasis by reducing hepatic BA accumulation through the inhibition of both the classic and alternative pathways.

DISCUSSION

The homeostasis of BA metabolism is tightly regulated by numerous enzymes, transporters, and nuclear receptors (Halilbasic et al., 2013). Previous studies have shown that both FGF19 and FGF21 are capable of controlling its metabolism (Schaap et al., 2009; Luo et al., 2014; Wunsch et al., 2015; Zhang et al., 2017; Chen et al., 2018). Here, we firstly identified that paracrine FGF1 was selectively downregulated in the liver of ANIT-induced intrahepatic cholestasis mice (**Figures 1E–G**). Then, we confirmed that the engineered FGF1$^{\Delta HBS}$ could suppress BA biosynthesis by downregulating both of the classical and alternative pathway *in vitro* and *in vivo* (**Figures 2** and **3**). We further demonstrate that exogenous administration of FGF1 could protect ANIT-induced cholestasis liver injury by inhibiting biosynthesis of BA (**Figures 2–4**).

FGF1 is a prototype of FGF family that has been implicated in various physiological processes including wound healing, neuroprotection and adipogenesis (Beenken and Mohammadi, 2009). Recently, Johan W. Jonker et al. identified that PPARγ-

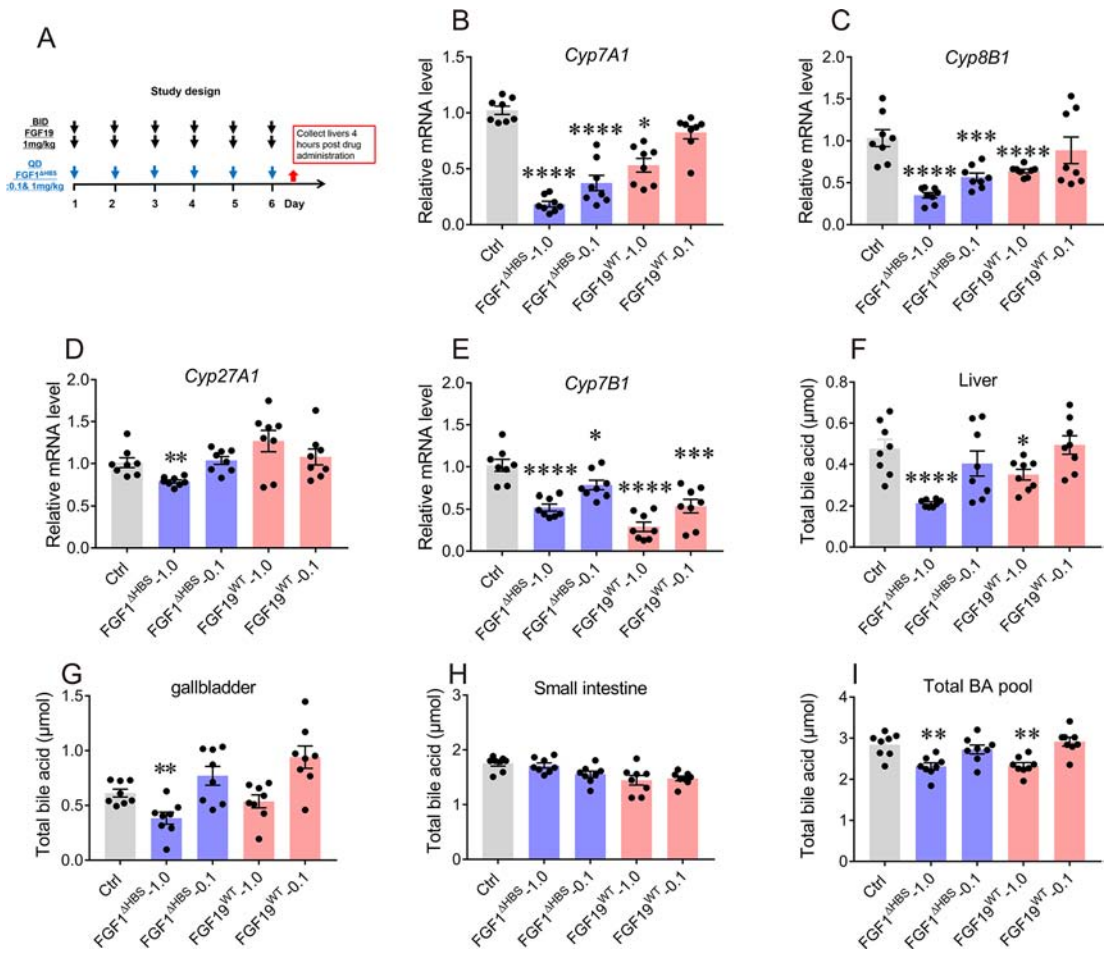

FIGURE 4 | Effects of chronic $FGF1^{\Delta HBS}$ and $FGF19^{WT}$ administration on hepatic bile acid (BA) synthetic enzyme and BA pool of liver, small intestine, and gallbladder in normal mice. **(A)** Male C57BL/6J mice were treated at indicated doses for 6 days and tissues were collected for analysis 4 h after administration. **(B-E)** The effect of chronic $FGF1^{\Delta HBS}$ and $FGF19^{WT}$ treatment on the mRNA levels of Cyp7A1 **(B)**, Cyp8B1 **(C)**, Cyp27A1 **(D),** and Cyp7B1 **(E)** in the liver of C57BL/6J mice. **(F-I)** BA pool of liver (F), small intestine (G), and gallbladder (H). Total BA pool size (I) were calculated. Data are presented as mean ± SEM; *P < 0.05; **P < 0.01; ***P < 0.001; ****p < 0.0001 versus Control group; n = 8.

FGF1 axis is critical for maintaining metabolic homeostasis and insulin sensitization (Jonker et al., 2012). Although known as a mitogenic factor, exogenous administration of FGF1 results in potent and insulin-dependent glucose lowering effect in insulin resistance mice. This discovery uncovers an unexpected, neomorphic insulin-sensitizing effect of FGF1 to treat type 2 diabetes (Suh et al., 2014) and expands the functions of this classically known mitogen. In our study, we firstly show another novel function of FGF1 to protect cholestasis liver disease by regulating BA biosynthesis.

The signaling and functions of FGFs are tightly regulated by spatial and temporal expressions of FGFs, FGFRs, and coreceptors (heparin sulfate and klotho) and most importantly by binding specificity of FGF-FGFRs (Beenken and Mohammadi, 2009). As a unique member of FGFs, FGF1 is termed as "the universal FGFR ligand" because it overrides the barrier of FGF-FGFRs binding specificity (Beenken et al., 2012), which makes it binding with liver-enriched FGFR4 and forming the structural basis for BA regulatory activity (**Figure 2**). Notably, the engineered FGF1 partial agonist ($FGF1^{\Delta HBS}$) carrying triple mutations located on the heparin sulfate binding regions, which diminishes the ability of $FGF1^{\Delta HBS}$ to induce heparin sulfate-assisted FGFR dimerization (Huang et al., 2017) but did not affect its binding specificity with FGFRs. This may be the reason that $FGF1^{\Delta HBS}$ still exhibits BA regulatory activity (**Figures 2** and **3**).

One plausible explanation for $FGF1^{\Delta HBS}$ not inducing hepatic proliferation may rely on the "threshold model" published in our previous study; as the dimerization strength of FGFR decreases, the mitogenic potential of FGF1 is dissipated much earlier before the decrease of its glucose-regulatory activity. Thus, the mitogenic and glucose-lowering activity of FGF1 could be uncoupled by dampening FGF-FGFR dimerization through triple mutations that diminish FGF1-heparin binding affinity

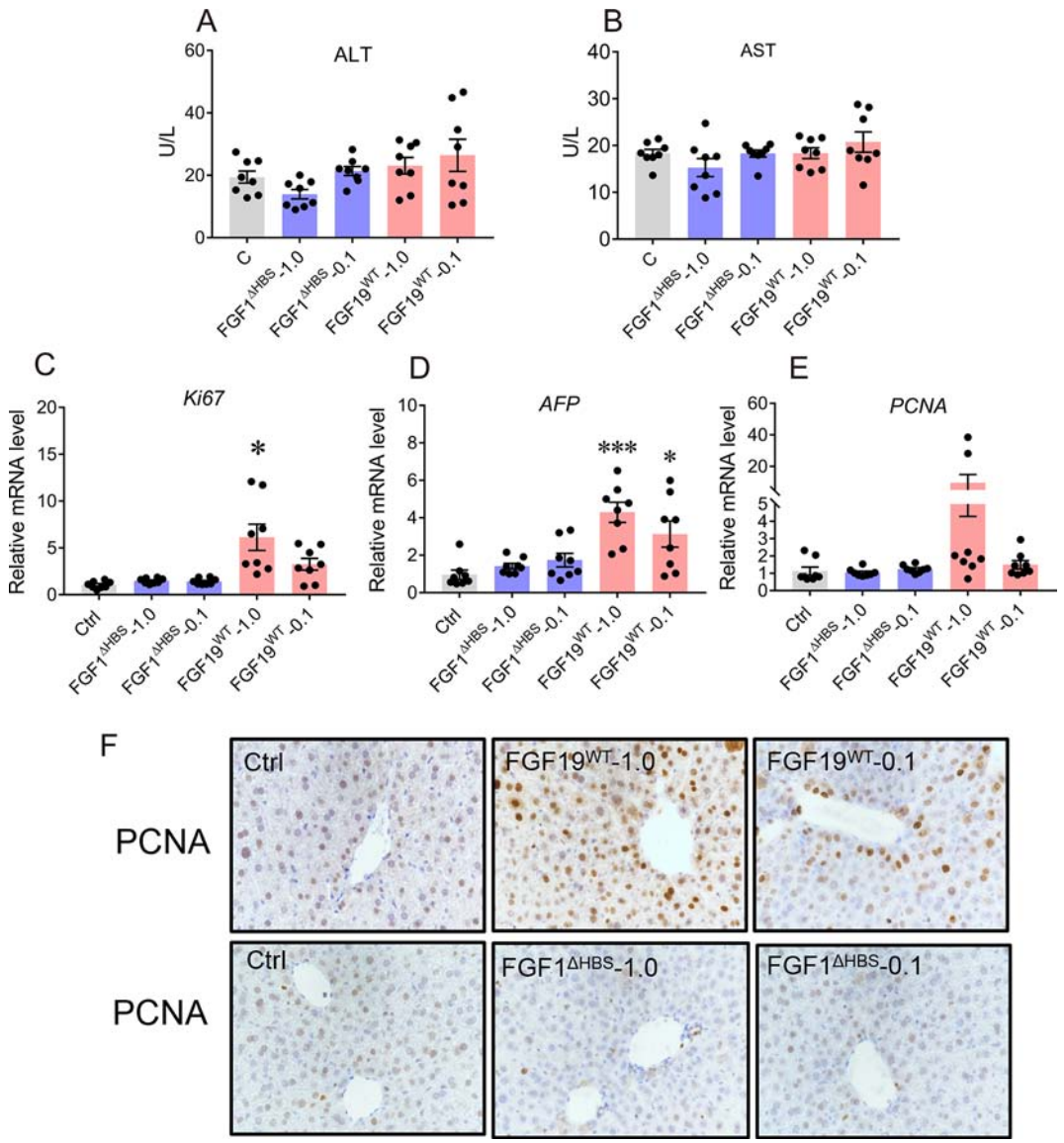

FIGURE 5 | Safety evaluation of chronic FGF1 administration. **(A, B)** Evidence of liver injury as determined by serum activities of liver enzymes Alanine transaminase and aspartate transaminase (ALT and AST). **(C–E)** Real-time polymerase chain reaction (RT-PCR) analysis of hepatic mRNA levels of the proliferation markers including Ki-67, AFP, and PCNA in C57BL/6J mice after chronic treatment, data was normalized to actin mRNA levels and expressed as fold change relative to control group (PBS-treated mice) **(F)** immune-histochemical staining using PCNA. Data are presented as mean ± SEM; *P < 0.05; ***P < 0.001; versus control group; n = 8.

(Huang et al., 2017). In the study, we found that FGF1$^{\Delta HBS}$ could regulate BA metabolism without exhibiting any hepatic proliferation activity, suggesting that the BA regulatory activity and mitogenic activity of FGF1 could be also separated in this condition.

Interestingly, acute administration of FGF1$^{\Delta HBS}$ not only reduced the BA biosynthesis by downregulating Cyp7A1 expression, but also suppressed the uptake of BA from hepatic portal vein by reducing the expression of basolateral uptake transporters (Ntcp, Oatp1, and Oatp2) (**Figure 3**). These dual effects can limit the accumulation of BA in the liver and facilitate the protective effects of FGF1 on ANIT-induced cholestasis. To further determine whether the changes of these genes are due to the direct effect of drug stimulation or the negative feedback upon changes in BA content, we measured the content of total BA in mouse liver after single injection. The results showed that synthesis of BA genes was inhibited whereas the hepatic BA content did not change, suggesting that changed expressions of these enzyme and transporters may be directly associated with drug stimulation but not negative feedback.

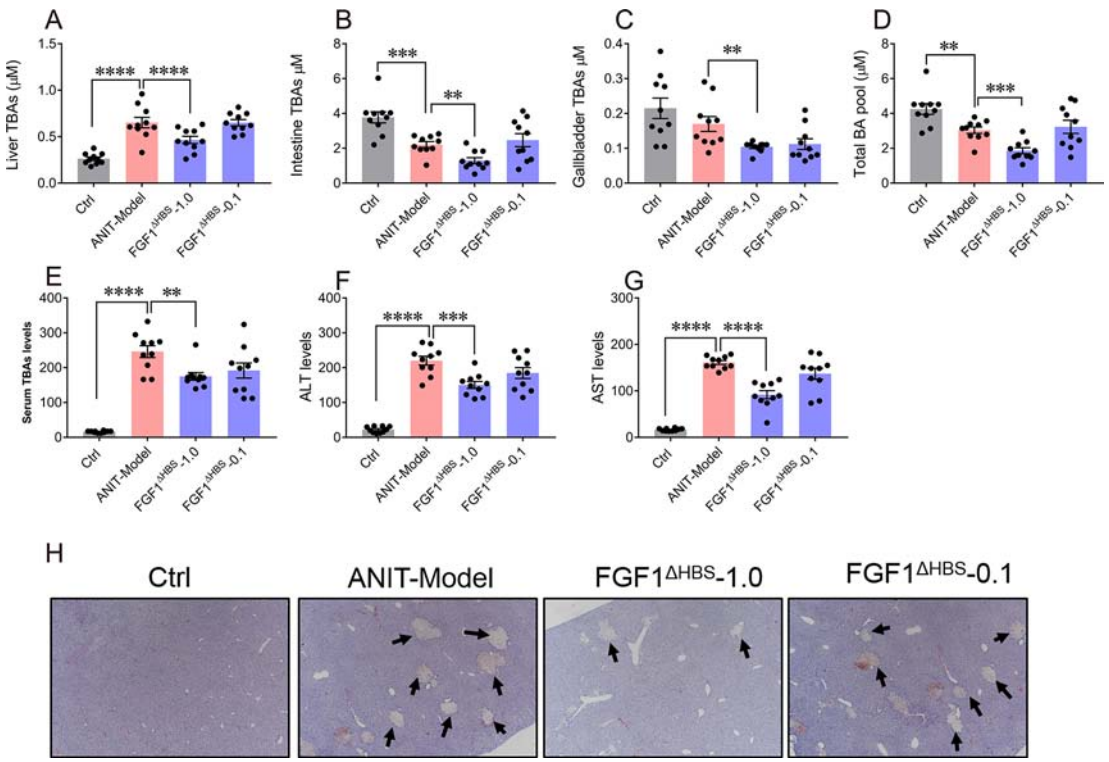

FIGURE 6 | $FGF1^{\Delta HBS}$ protects mice from ANIT-induced intrahepatic cholestasis. Male C57BL/6J mice were intraperitoneally injected by PBS or $FGF1^{\Delta HBS}$ (n = 10), for 4 days. ANIT in olive oil (75 mg/kg) was administered orally on the fourth day, and protein dosing was continued for another 2 days. **(A-D)** Size of BA pools from the liver **(A)**, intestine **(B)**, and gallbladder **(C)**. Total BA pool sizes **(D)** were calculated. **(E-G)** Analysis of biochemical parameters indicative of liver damage including serum total BA **(E)**, Alanine transaminase (ALT)_ **(F)**, and aspartate transaminase (AST) **(G)** levels. **(H)** Representative H&E-stained liver sections of each group. **P < 0.01; ***P < 0.001; ****P < 0.0001.

Although the results presented in the study demonstrate that $FGF1^{\Delta HBS}$ suppresses hepatic BA accumulation and protect liver against ANIT-induced injury, several limitations need to be addressed. Firstly, the promiscuity of FGF1 with all FGFRs and its mitogenic activity representing safety concerns hurdles the development of FGF1-based therapy. Although no significant proliferation activity and tumorgenicity in the liver were observed after chronic treatment of $FGF1^{\Delta HBS}$, further investigations are needed to comprehensively assess of safety of long-term administration of $FGF1^{\Delta HBS}$ or engineer FGF1 variants specifically binding with FGFR4. Secondly, the ANIT-induced intrahepatic cholestaisis mouse model used in the present study only depicts certain aspects of cholestatic liver disease, extra experimental models are also required to evaluate the potentially therapeutic value of FGF1 mutants.

CONCLUSION

In conclusion, our study uncovers the association of paracrine FGF1 with BA metabolism and demonstrated that FGF1 functions as a negative regulator of BA synthesis through FGFR4-mediated inhibition of the classical and alternative pathway. Thus, FGF1 can function as a protector against ANIT-induced liver injury under cholestasis. Moreover, the study from engineered $FGF1^{\Delta HBS}$ holds a promise of FGF1 to be a therapeutic candidate for cholestatic liver disease or other BA metabolism syndromes.

DATA AVAILABILITY STATEMENT

All datasets generated for this study are included in the article/ **Supplementary Material**.

ETHICS STATEMENT

The animal study was reviewed and approved by the Animal Care and Use Committee of Wenzhou Medical University.

AUTHOR CONTRIBUTIONS

HL, CZ, YH, QL, GQ, YW, ZH, and JN researched the data. ZH and JN contributed to the initial discussion and design of the

project. HL and JN wrote the manuscript. JN is the guarantor of this work and, as such, had full access to all the data in the study and takes responsibility for the integrity of the data and the accuracy of the data analysis.

FUNDING

This work was supported by grants from the Natural Science Foundation of China (81803415, to JN) and the Natural Science Foundation of Zhejiang (LY18H070002 and LQ19H300002, to YW and JW), and the Science and Technology Project of Wenzhou (Y20180176, to JW).

SUPPLEMENTARY MATERIAL

The Supplementary Material for this article can be found online at: https://www.frontiersin.org/articles/10.3389/fphar.2019.01515/full#supplementary-material

REFERENCES

Beenken, A., and Mohammadi, M. (2009). The FGF family: biology, pathophysiology and therapy. *Nat. Rev. Drug Discovery* 8 (3), 235–253. doi: 10.1038/nrd2792

Beenken, A., Eliseenkova, A. V., Ibrahimi, O. A., Olsen, S. K., and Mohammadi, M. (2012). Plasticity in interactions of fibroblast growth factor 1 (FGF1) N terminus with FGF receptors underlies promiscuity of FGF1. *J. Biol. Chem.* 287 (5), 3067–3078. doi: 10.1074/jbc.M111.275891

Chau, M. D., Gao, J., Yang, Q., Wu, Z., and Gromada, J. (2010). Fibroblast growth factor 21 regulates energy metabolism by activating the AMPK-SIRT1-PGC-1alpha pathway. *Proc. Natl. Acad. Sci. U.S.A.* 107 (28), 12553–12558. doi: 10.1073/pnas.1006962107

Chen, M. M., Hale, C., Stanislaus, S., Xu, J., and Veniant, M. M. (2018). FGF21 acts as a negative regulator of bile acid synthesis. *J. Endocrinol.* 237 (2), 139–152. doi: 10.1530/JOE-17-0727

Dai, M., Yang, J., Xie, M., Lin, J., Luo, M., Hua, H., et al. (2017). Inhibition of JNK signalling mediates PPARalpha-dependent protection against intrahepatic cholestasis by fenofibrate. *Br. J. Pharmacol.* 174 (18), 3000–3017. doi: 10.1111/bph.13928

Dailey, L., Ambrosetti, D., Mansukhani, A., and Basilico, C. (2005). Mechanisms underlying differential responses to FGF signaling. *Cytokine Growth F R* 16 (2), 233–247. doi: 10.1016/j.cytogfr.2005.01.007

de Aguiar Vallim, T. Q., Tarling, E. J., and Edwards, P. A. (2013). Pleiotropic roles of bile acids in metabolism. *Cell Metab.* 17 (5), 657–669. doi: 10.1016/j.cmet.2013.03.013

Degirolamo, C., Sabba, C., and Moschetta, A. (2016). Therapeutic potential of the endocrine fibroblast growth factors FGF19, FGF21 and FGF23. *Nat. Rev. Drug Discovery* 15 (1), 51–69. doi: 10.1038/nrd.2015.9

Eswarakumar, V. P., Lax, I., and Schlessinger, J. (2005). Cellular signaling by fibroblast growth factor receptors. *Cytokine Growth F R* 16 (2), 139–149. doi: 10.1016/j.cytogfr.2005.01.001

Goetz, R., and Mohammadi, M. (2013). Exploring mechanisms of FGF signalling through the lens of structural biology. *Nat. Rev. Mol. Cell Bio* 14 (3), 166–180. doi: 10.1038/nrm3528

Goetz, R., Beenken, A., Ibrahimi, O. A., Kalinina, J., Olsen, S. K., Eliseenkova, A. V., et al. (2007). Molecular insights into the klotho-dependent, endocrine mode of action of fibroblast growth factor 19 subfamily members. *Mol. Cell Biol.* 27 (9), 3417–3428. doi: 10.1128/MCB.02249-06

Halilbasic, E., Claudel, T., and Trauner, M. (2013). Bile acid transporters and regulatory nuclear receptors in the liver and beyond. *J. Hepatol* 58 (1), 155–168. doi: 10.1016/j.jhep.2012.08.002

Hirschfield, G. M., Dyson, J. K., Alexander, G. J. M., Chapman, M. H., Collier, J., Hübscher, S., et al. (2018). The British Society of Gastroenterology/UK-PBC primary biliary cholangitis treatment and management guidelines. *Gut* 67 (9), 1568–1594. doi: 10.1136/gutjnl-2017-315259

Holt, J. A., Luo, G., Billin, A. N., Bisi, J., McNeill, Y. Y., Kozarsky, K. F., et al. (2003). Definition of a novel growth factor-dependent signal cascade for the suppression of bile acid biosynthesis. *Genes Dev.* 17 (13), 1581–1591. doi: 10.1101/gad.1083503

Huang, Z., Tan, Y., Gu, J., Liu, Y., Song, L., Niu, J., et al. (2017). Uncoupling the mitogenic and metabolic functions of FGF1 by tuning FGF1-FGF receptor dimer stability. *Cell Rep.* 20 (7), 1717–1728. doi: 10.1016/j.celrep.2017.06.063

Inagaki, T., Choi, M., Moschetta, A., Peng, L., Cummins, C. L., McDonald, J. G., et al. (2005). Fibroblast growth factor 15 functions as an enterohepatic signal to regulate bile acid homeostasis. *Cell Metab.* 2 (4), 217–225. doi: 10.1038/nature10998

Jonker, J. W., Suh, J. M., Atkins, A. R., Ahmadian, M., Li, P., Whyte, J., et al. (2012). A PPARgamma-FGF1 axis is required for adaptive adipose remodelling and metabolic homeostasis. *Nature* 485 (7398), 391–394. doi: 10.1038/nature10998

Kaplan, M. M., and Gershwin, M. E. (2005). Primary biliary cirrhosis. *N Engl. J. Med.* 353 (12), 1261–1273. doi: 10.1056/NEJMra043898

Kouhara, H., Hadari, Y. R., Spivak-Kroizman, T., Schilling, J., Bar-Sagi, D., Lax, I., et al. (1997). A lipid-anchored Grb2-binding protein that links FGF-receptor activation to the Ras/MAPK signaling pathway. *Cell* 89 (5), 693–702. doi: 10.1016/S0092-8674(00)80252-4

Kurosu, H., Choi, M., Ogawa, Y., Dickson, A. S., Goetz, R., Eliseenkova, A. V., et al. (2007). Tissue-specific expression of betaKlotho and fibroblast growth factor (FGF) receptor isoforms determines metabolic activity of FGF19 and FGF21. *J. Biol. Chem.* 282 (37), 26687–26695. doi: 10.1074/jbc.M704165200

Larsson, H., Klint, P., Landgren, E., and Claesson-Welsh, L. (1999). Fibroblast growth factor receptor-1-mediated endothelial cell proliferation is dependent on the Src homology (SH) 2/SH3 domain-containing adaptor protein Crk. *J. Biol. Chem.* 274 (36), 25726–25734. doi: 10.1074/jbc.274.36.25726

Li, D., Lu, T., Shen, C., Shen, C., Liu, Y., Zhang, J., et al. (2016). Expression of fibroblast growth factor 21 in patients with biliary atresia. *Cytokine* 83, 13–18. doi: 10.1016/j.cyto.2016.03.003

Lindor, K. (2007). Ursodeoxycholic acid for the treatment of primary biliary cirrhosis. *N Engl. J. Med.* 357 (15), 1524–1529. doi: 10.1056/NEJMct074694

Luo, J., Ko, B., Elliott, M., Zhou, M., Lindhout, D. A., Phung, V., et al. (2014). A nontumorigenic variant of FGF19 treats cholestatic liver diseases. *Sci. Transl. Med.* 6 (247), 247ra100. doi: 10.1126/scitranslmed.3009098

Nicholes, K., Guillet, S., Tomlinson, E., Hilan, K., Wright, B., and Frantz, G. D. (2002). A mouse model of hepatocellular carcinoma: ectopic expression of fibroblast growth factor 19 in skeletal muscle of transgenic mice. *Am. J. Pathol.* 160 (6), 2295–2307. doi: 10.1016/S0002-9440(10)61177-7

Russell, D. W. (2009). Fifty years of advances in bile acid synthesis and metabolism. *J. Lipid Res.* 50, S120–S125. doi: 10.1194/jlr.R800026-JLR200

Schaap, F. G., van der Gaag, N. A., Gouma, D. J., and Jansen, P. L. (2009). High expression of the bile salt-homeostatic hormone fibroblast growth factor 19 in the liver of patients with extrahepatic cholestasis. *Hepatology* 49 (4), 1228–1235. doi: 10.1002/hep.22771

Seo, J. H., Suenaga, A., Hatakeyama, M., Taiji, M., and Imamoto, A. (2009). Structural and functional basis of a role for CRKL in a fibroblast growth factor 8-induced feed-forward loop. *Mol. Cell Biol.* 29 (11), 3076–3087. doi: 10.1128/MCB.01686-08

Suh, J. M., Jonker, J. W., Ahmadian, M., Goetz, R., Lackey, D., Osborn, O., et al. (2014). Endocrinization of FGF1 produces a neomorphic and potent insulin sensitizer. *Nature* 513 (7518), 436–439. doi: 10.1038/nature13540

Wu, X., Ge, H., Lemon, B., Vonderfecht, S., Weiszmann, J., Hecht, R., et al. (2010). FGF19-induced hepatocyte proliferation is mediated through FGFR4 activation. *J. Biol. Chem.* 285 (8), 5165–5170. doi: 10.1074/jbc.M109.068783

Wunsch, E., Milkiewicz, M., Wasik, U., Trottier, J., Kempińska-Podhorodecka, A., Elias, E., et al. (2015). Expression of hepatic Fibroblast Growth Factor 19 is enhanced in Primary Biliary Cirrhosis and correlates with severity of the disease. *Sci. Rep.* 5, 13462. doi: 10.1038/srep13462

Yayon, A., Klagsbrun, M., Esko, J. D., Leder, P., and Ornitz, D. M. (1991). Cell surface, heparin-like molecules are required for binding of basic fibroblast growth factor to its high affinity receptor. *Cell* 64 (4), 841–848. doi: 10.1016/0092-8674(91)90512-W

Yu, L., Liu, X., Yuan, Z., Yi, X., Yang, H., Yuan, Z., et al. (2017). SRT1720 Alleviates ANIT-induced cholestasis in a mouse model. *Front. Pharmacol.* 8, 256. doi: 10.3389/fphar.2017.00256

Zhang, J., Gupte, J., Gong, Y., Weiszmann, J., Zhang, Y., Lee, K. J., et al. (2017). Chronic over-expression of fibroblast growth factor 21 increases bile acid biosynthesis by opposing FGF15/19 action. *EBioMedicine* 15, 173–183. doi: 10.1016/j.ebiom.2016.12.016

Zhou, M., Wang, X., Phung, V., Lindhout, D. A., Mondal, K., Hsu, J. A., et al. (2014). Separating tumorigenicity from bile acid regulatory activity for endocrine hormone FGF19. *Cancer Res.* 74 (12), 3306–3316. doi: 10.1158/0008-5472.CAN-14-0208

Zhou, M., Learned, R. M., Rossi, S. J., DePaoli, A. M., Tian, H., and Ling, L. (2016). Engineered fibroblast growth factor 19 reduces liver injury and resolves sclerosing cholangitis in Mdr2-deficient mice. *Hepatology* 63 (3), 914–929. doi: 10.1002/hep.28257

Zhou, M., Yang, H., Learned, R. M., Tian, H., and Ling, L. (2017). Non-cell-autonomous activation of IL-6/STAT3 signaling mediates FGF19-driven hepatocarcinogenesis. *Nat. Commun.* 8, 15433. doi: 10.1038/ncomms15433

Zollner, G., Marschall, H. U., Wagner, M., and Trauner, M. (2006). Role of nuclear receptors in the adaptive response to bile acids and cholestasis: pathogenetic and therapeutic considerations. *Mol. Pharm.* 3 (3), 231–251. doi: 10.1021/mp060010s

Conflict of Interest: The authors declare that the research was conducted in the absence of any commercial or financial relationships that could be construed as a potential conflict of interest.

frontiers in Pharmacology

ORIGINAL RESEARCH
published: 10 January 2020
doi: 10.3389/fphar.2019.01536

Using Recombinant Human Collagen With Basic Fibroblast Growth Factor to Provide a Simulated Extracellular Matrix Microenvironment for the Revascularization and Attachment of Islets to the Transplantation Region

Qunyan Zhu[1,2,3†], Cuitao Lu[1†], Xuan Jiang[1], Qing Yao[1], Xue Jiang[1], Zhiwei Huang[1], Yina Jiang[1], Lei Peng[1], Hongxing Fu[1*] and Yingzheng Zhao[1,2,3*]*

[1] College of Pharmaceutical Sciences, Wenzhou Medical University, Wenzhou, China, [2] Engineering Laboratory of Zhejiang Province for Pharmaceutical Development of Growth Factors, Biomedical Collaborative Innovation Center of Wenzhou, Wenzhou, China, [3] Trauma Center, The First Affiliated Hospital of Hainan Medical College, Haikou, China

Islet transplantation is considered a potential therapeutic option to reverse diabetes. The pancreatic basement membrane contains a variety of extracellular matrix (ECM) proteins. The abundant ECM is essential for the survival of transplanted islets. However, the ECM proteins necessary for maintaining islet vascularization and innervation are impaired by enzymatic digestion in the isolation process before islet transplantation, leading to destruction of islet microvessels. These are the primary concern and major barrier for long-term islet survival and function. Thus, it is crucial to create an appropriate microenvironment for improving revascularization and islet function to achieve better transplantation outcome. Given the importance of the presence of ECM proteins for islets, we introduce recombinant human collagen (RHC) to construct a simulated ECM microenvironment. To accelerate revascularization and reduce islet injury, we add basic fibroblast growth factor (bFGF) to RHC, a growth factor that has been shown to promote angiogenesis. In order to verify the outcome, islets were treated with RHC combination containing bFGF and then implanted into kidney capsule in type 1 diabetic mouse models. After transplantation, 30-day-long monitoring displayed that 16 mg–60 ng RHC-bFGF group could serve as superior transplantation outcome. It reversed the hyperglycemia condition in host rapidly, and the OGTT (oral glucose tolerance test) showed a similar pattern with the control group. Histological assessment showed that 16 mg–60 ng RHC-bFGF group attenuated apoptosis, promoted cellular proliferation, triggered vascularization, and inhibited inflammation reaction. In summary, this work demonstrates that application of 16 mg–60 ng RHC-bFGF and islets composite enhance the islet survival, function, and long-term transplantation efficiency.

Keywords: diabetes, recombinant human collagen (RHC), basic fibroblast growth factor (bFGF), islet–matrix attachments, islet transplantation

OPEN ACCESS

Edited by:
Zhouguang Wang,
Albert Einstein College of Medicine,
United States

Reviewed by:
Yang Mei,
Northwestern University,
United States
Yu Kang,
University of Pennsylvania,
United States

***Correspondence:**
Lei Peng
15607662705@163.com
Hongxing Fu
hx_fu79@163.com
Yingzheng Zhao
pharmtds@163.com

†These authors have contributed equally to this work

Specialty section:
This article was submitted to Translational Pharmacology, a section of the journal Frontiers in Pharmacology

Received: *09 October 2019*
Accepted: *27 November 2019*
Published: *10 January 2020*

Citation:
Zhu Q, Lu C, Jiang X, Yao Q, Jiang X, Huang Z, Jiang Y, Peng L, Fu H and Zhao Y (2020) Using Recombinant Human Collagen With Basic Fibroblast Growth Factor to Provide a Simulated Extracellular Matrix Microenvironment for the Revascularization and Attachment of Islets to the Transplantation Region. Front. Pharmacol. 10:1536. doi: 10.3389/fphar.2019.01536

INTRODUCTION

Diabetes is one of the most common serious chronic diseases and is associated with several serious complications, including cardiovascular, kidney, eye, nerve, cerebrovascular, and peripheral vascular diseases (Nathan, 1993; Bader et al., 2016; Wang et al., 2017). Type 1 diabetes (T1D) is an autoimmune-mediated metabolic disease that is characterized by permanent destruction of insulin-producing beta cells, which results in absolute insulin deficiency (Davis et al., 2012). The main therapies for controlling glycemic levels are exogenous insulin administration and oral hypoglycemic agents. Unfortunately, most of the time, these treatments fail to control the blood glucose level, which results in severe hypoglycemia and complications (Bogdani et al., 2014). Islet transplantation offers therapeutic potential for patients with T1D to normalize glucose metabolism and prevent the complications of the disease (Davis et al., 2012). Despite the rapid progress that has been made in islet transplantation after the disclosure of the "Edmonton protocol," multiple donors are needed to achieve long-term insulin independence, which limits the large-scale application of this protocol. The disruption of islet–matrix attachments or the extracellular matrix (ECM) components between endocrine and exocrine cells during isolation decreases islet function and viability before and after transplantation, which severely hinders the efficiency of transplantation (Barrett-Connor and Orchard, 1985). Furthermore, numerous studies demonstrated that 20~40% of islets undergo apoptosis during the culture. However, pre-conditioning in culture prior to islet transplantation, such as the supplementation of angiogenic agents (Uzunalli et al., 2015; Qiu et al., 2017), antioxidant agents, or oxygen carriers in the culture medium, has enabled islets to obtain longer (Emamaullee et al., 2008; Maillard et al., 2011; Brandhorst et al., 2013; Schaschkow et al., 2015), better graft function and greater efficiency (Kin et al., 2008; Schaschkow et al., 2015).

ECMs, such as collagen, have been developed to address apoptosis during islet culture, to preserve islet morphology, to promote cell survival, and to provide essential physical scaffolding for cellular constituents, which can enhance islet insulin secretion and reinforce islet structure to resist mechanical stress during transplantation (Salvay et al., 2008; Schaschkow et al., 2015). Collagen type III also has been demonstrated to enhance microvascular strength and elasticity, provide adequate nutrients in cells, and directly bind to hemangioblasts, thereby promoting the formation of new blood vessels (Sailakshmi et al., 2011). In this study, recombinant human collagen (RHC), collagen type III, was obtained from a high-density fermented supernatant of GS115/Ppic9KG6 fermentation, which solved the problems of conventional extraction methods, such as poor hydrophilicity and immune rejection. Growth factors, such as basic fibroblast growth factor (bFGF), are natural substances that are capable of stimulating cellular growth, proliferation, healing, and cellular differentiation (Barrientos et al., 2008; Xiang et al., 2011). Our previous study demonstrated that bFGF had potent angiogenetic capabilities in fibroblasts and epithelial cells, which thus promote angiogenesis and are beneficial to islet revascularization (Zhao et al., 2014).

In this study, we investigated a co-culture system of combined bFGF and RHC to provide a simulated ECM microenvironment for islets. We hypothesize that such a microenvironment can rebuild the islet–matrix attachments and, thus, promote the revascularization of islets, which will benefit islet culture both *in vitro* and *in vivo* (as illustrated in **Figure 1**).

MATERIALS AND METHODS

Animals and Reagents

BALB/C male mice that were 8–10 weeks old were obtained from Shanghai, China. All the mice were housed with a 12 h light/dark cycle at 24 ± 1°C and provided with food ad libitum for a week before initiation of the study. All experimental procedures were approved by the Institutional Animal Care and Use Committee of Wenzhou Medical University. Collagenase type V, streptozotocin (STZ), fluorescein diacetate (FDA), and propidium iodide (PI) were purchased from Sigma Inc., St. Louis, MO, USA. bFGF was ordered from Gelusite Biology Technology Company, Zhejiang, China. RHC was kindly provided by Nanjing University of Science and Technology, Jiangsu JL, and Biotech Co., Ltd. Ficoll-1077, Ficoll-1119, Hanks' solution, and CMRL-1066 were purchased from Wenzhou Icelltrans Technologies Co., Ltd., Wenzhou, China.

Islet Isolation

Islets were isolated from the pancreas of mice according to methods that were modified from other studies (Zmuda et al., 2011). Briefly, the mice were anesthetized by inhaling isoflurane and were placed in the supine position on the dissecting table. The abdomen was sprayed with 75% ethanol, followed by opening it as a U-incision; the entrance of the common bile duct into the duodenum was located and ligated; and 2.5 ml collagenase type V (1 mg/ml, dissolved in cold Hank's solution) was injected into the common bile duct by retrograde intubation. Once the pancreas was perfused, it was removed from the mouse by pulling it free from the points of contact with the intestines, stomach, and spleen. The pancreas was transferred in a 50 ml centrifuge tube. Then, the appropriate amount of collagenase type V was added and subjected to digestion in a 37 ± 0.5°C water bath for 3–5 min with gentle shaking. The digested tissue was washed three times with cold Hank's solution. Subsequently, the islets were purified with a discontinuous density gradient (Ficoll-1119, Ficoll-1077, and Hanks' solution) by centrifuging at 2,000 rpm for 5 min with the brake off. The supernatant containing purified islets was washed three times with cold Hank's solution. If necessary, the islets were further purified by handpicking.

Islet Counting and Equivalent Calculation

The cultured islets were transferred into a culture dish with 0.5 mm lattices for their quantification under the microscope. The number of islets were counted and calculated to the islet

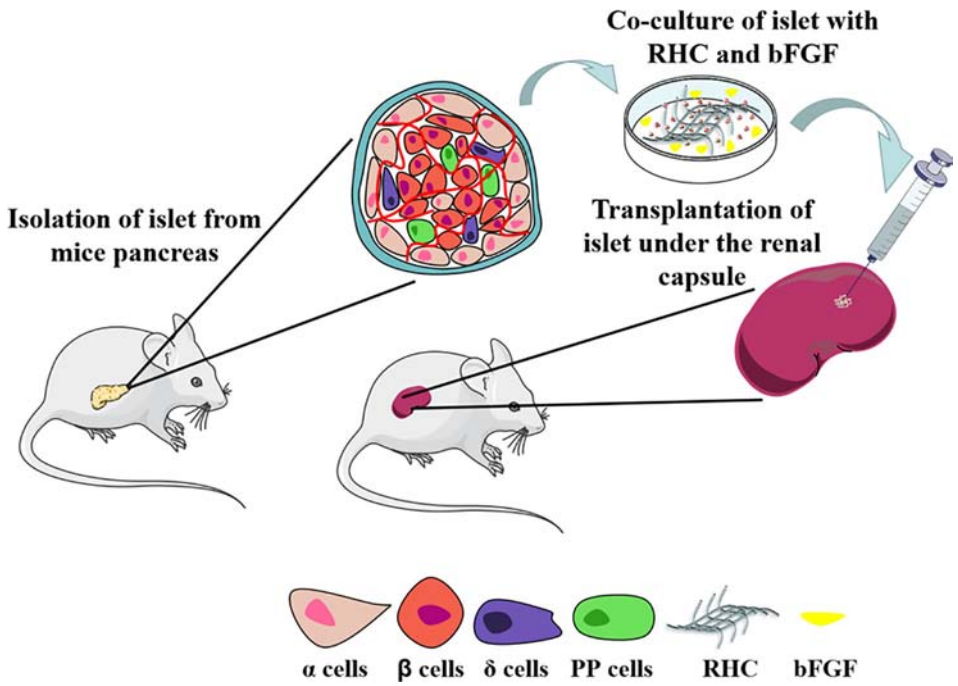

FIGURE 1 | Scheme of RHC-bFGF islet transplantation for reversal type 1 diabetes.

equivalents (IEQs; diameter standardizing to 150 mm) (Lembert et al., 2003).

Islet Culture

The purified islets were divided into six groups according to different culture conditions: 1) FREE; 2) 60 ng bFGF; 3) 1 mg RHC; 4) 16 mg RHC; 5) 1 mg–60 ng RHC-bFGF; and 6) 16 mg–60 ng RHC-bFGF. Each group contained approximately 200–300 purified islets. In the "FREE" group, the islets were cultured in CMRL-1066 medium supplemented with 10% fetal bovine serum (FBS; Gibco, Invitrogen, Inc., USA) and 1% antibiotics (100 U/ml penicillin, 100 ng/ml streptomycin). In the "60 ng bFGF" group, the islets were cultured in CMRL-1066 medium containing bFGF (60 ng/ml). In the "1 mg RHC" group, the islets were cultured in CMRL-1066 medium containing RHC (1 mg/ml). In the "16 mg RHC" group, the islets were cultured in CMRL-1066 medium containing RHC (16 mg/ml). In the "1 mg–60 ng RHC-bFGF" group, the islets were cultured in CMRL-1066 medium containing RHC (1 mg/ml) and bFGF (60 ng/ml). In the "16 mg–60 ng RHC-bFGF" group, the islets were cultured in CMRL-1066 medium containing RHC (16 mg/ml) and bFGF (60 ng/ml). The concentration of bFGF 60 ng/ml was chosen according to our previous study (Qiu et al., 2017).

Islet Viability and Reactive Oxygen Species *In Vitro*

After being cultured with the different concentration of RHC (0, 1, 16, and 25 mg/ml) and bFGF (60 ng/ml) in six groups for 24 h at 37°C in a humidified 5% CO_2, the viability of the islets was analyzed by FDA/PI staining. The ratio of green to green plus red cells provided the percentage of viability. Images were examined and recorded with an inverted microscope (Nikon ECLIPSE Ti-S; Ruikezhongyi, Beijing, China).

To visualize the reactive oxygen species, cultured islets were harvested and washed, followed by incubating with dihydroethidium (DHE, Sigma) for 30 min at 37°C, washing with phosphate-buffered saline (PBS, Gibco), and monitoring by an inverted fluorescence microscope.

Transmission Electron Microscopy Examination

To determine whether the endocrine granules in the beta cells were preserved or released, the ultrastructure of islets was observed by transmission electron microscopy (TEM) (Daoud et al., 2010). The islets in different groups were collected after culturing for 24 h and were fixed immediately in 2.5% (w/v) glutaraldehyde at 4°C overnight. After dehydration in a series of acetone–water solutions, the islets were embedded in Epon. Semi-thin section and toluidine blue staining were performed to observe the islets locations. Finally, ultra-thin sections of at least six blocks per sample were cut and examined with the electron microscope (H-7500, Hitachi, Ibaraki, Japan).

The Stability of bFGF in the Culture System

To investigate the stability of bFGF in RHC, the degradation of bFGF *in vitro* was conducted. Three bFGF formulations (60 ng/ml bFGF alone, 60 ng/ml bFGF with 1 mg/ml RHC, and 60 ng/

ml bFGF with 16 mg/ml RHC) were prepared and incubated at 37°C. At 0, 12, 24, 48, 72, 120, and 168 h, 100 μl of aliquot was extracted and stored at −80°C before detection. The concentration of bFGF was detected by an ELISA kit.

Induction of Diabetic Mellitus

Irreversible diabetes was chemically induced in mice by single intraperitoneal injections (IP) of 150 mg/kg STZ. Non-fasting blood glucose levels were measured by using a glucometer (Pro doctor®, Tai Doc Technology Corp, Beijing, China) from whole blood samples that were obtained by tail snipping. Mice with two consecutive non-fasting blood glucose levels higher than 22.2 mmol/L were used for transplantation. The diabetic mice were randomly divided into six groups of six. The blood glucose levels of donor mice were also confirmed before islet isolation to verify that they were metabolically normal.

Islet Transplantation

After 6 h culture, the islets in the six groups were collected and prepared for transplantation. The number of transplanted islets was 200 IEQ for each group. Transplantation was performed as reported (Zmuda et al., 2011; Fu et al., 2016). Mice were anesthetized with isoflurane, and the right back was shaved and sterilized with 75% ethyl alcohol. A small incision was made, and the kidney was exposed. The islets in the syringe were injected slowly and scattered under the kidney capsule. Then, the skin was sutured carefully. It is good to ensure that the kidney is kept moist with saline during the entire process. After transplantation, antibiotics were administered every day for a week to reduce the inflammatory response.

Function Assessment *In Vivo*

After transplantation, non-fasting blood glucose levels and the weights of animals were measured regularly until the end of the study. The graft was considered to be functional only if the non-fasting blood glucose levels were stably maintained at less than 11.1 mmol/L, with no reoccurrence of hyperglycinemia. An oral glucose tolerance test (OGTT) was conducted on day 30 post–islet transplantation to assess metabolic capacity. Mice were placed in fresh cages with access to water but no food for 12 h. Then, 2 mg/ml glucose in 200 mg/ml solution was administered to the mice orally. Blood glucose was evaluated at time 0 (prior to glucose administration) and then at 20, 40, 60, 90, and 120 min after glucose administration. The area under the curve (AUC) of blood glucose was also calculated.

Histologic and Immunohistochemical Analyses

At 30 days after transplantation, mice were anesthetized and were transcranially perfused with saline. Kidney with islets were resected and fixed in 4% paraformaldehyde overnight, followed by embedding in paraffin and sectioning at 5 μm thickness. The tissue was dewaxed and rehydrated in xylene and gradient alcohol for hematoxylin and eosin (H&E) staining for the evaluation of general morphology and Masson's trichrome staining for the evaluation of fibrosis. To identify proteins in grafts, immunohistochemistry staining was performed, primary anti-insulin (15848-1-AP, 1:400, Proteintech), anti-HIF-1α (ab1, 1:200, Abcam), anti-Caspase-3 (ab13847, 1:200, Abcam), anti-Ki67 (ab15580, 1:400, Abcam), anti-CD31 (ab182981, 1:200, Abcam), and anti-IL-6 (DF6087, 1:300, Affinity) staining. Digital images were acquired by using a light microscope or confocal microscope.

Statistics Analysis

All analyses were performed using Graph Pad Prism 7 software (Graph Pad Software, Inc., La Jolla, CA, USA). All results are expressed as the mean ± SD for each group. The one-way ANOVA followed by Tukey's test was for comparing the multi-group data. P-values less than 0.05 were considered statistically significant.

RESULTS

Islet Viability *In Vitro*

To calculate the viability of islets under the different conditions, FDA/PI staining was performed at 0, 7, and 24 h after culturing. The results are shown in **Figure 2**.

From the results (**Figure 2**), it can be seen that after 7 h co-culture, the viability of the 1 mg RHC group, the 1 mg–60 ng RHC-bFGF group, and the 16 mg–60 ng RHC-bFGF group increased, while the 16 mg RHC group had the opposite tendency. After culturing for 24 h, the viability of both the 1 mg–60 ng RHC-bFGF group and the 16 mg–60 ng RHC-bFGF group were over 90%, which was better than the viability of the bFGF-alone or RHC-alone groups. We suspected that simultaneous application bFGF and RHC can improve the viability of islets. However, we also found that the viability of the "25 mg RHC" and "25 mg to 60 ng RHC-bFGF" groups was inferior, at either 7 h or 24 h (**Figure 1S**).

The ultrastructure of the islets was observed by TEM (**Figure 2E**). It can be seen that the endocrine granules in the beta cells were preserved, which means that the islets did not degranulate in different culture groups. The mitochondria also did not swell, and the cristae were clear. There was no evidence of membrane disruption in the islets after cultivation for 24 h.

Islet Hypoxia *In Vitro*

After co-culturing the islets in each group for 24 h, the fluorescence staining of DHE of the 1 mg RHC group, the 1 mg–60 ng RHC-bFGF group, and the 16 mg–60 ng RHC-bFGF group significantly decreased compared to that of the FREE group, 60 ng group, and 16 mg RHC group (**Figure 3A**), which suggested that the ROS levels significantly decreased when the islets were co-cultured with RHC and/or bFGF, compared with those of the bFGF-alone or FREE islets groups.

HIF-1α was a crucial marker for cellular proliferation in a hypoxic condition (Tsuchiya et al., 2015). After islet transplantation for 30 days, the grafts were removed, and the HIF-1α immunohistochemical staining results are shown in **Figure 3B**. As shown in **Figure 3B**, there was almost no HIF-

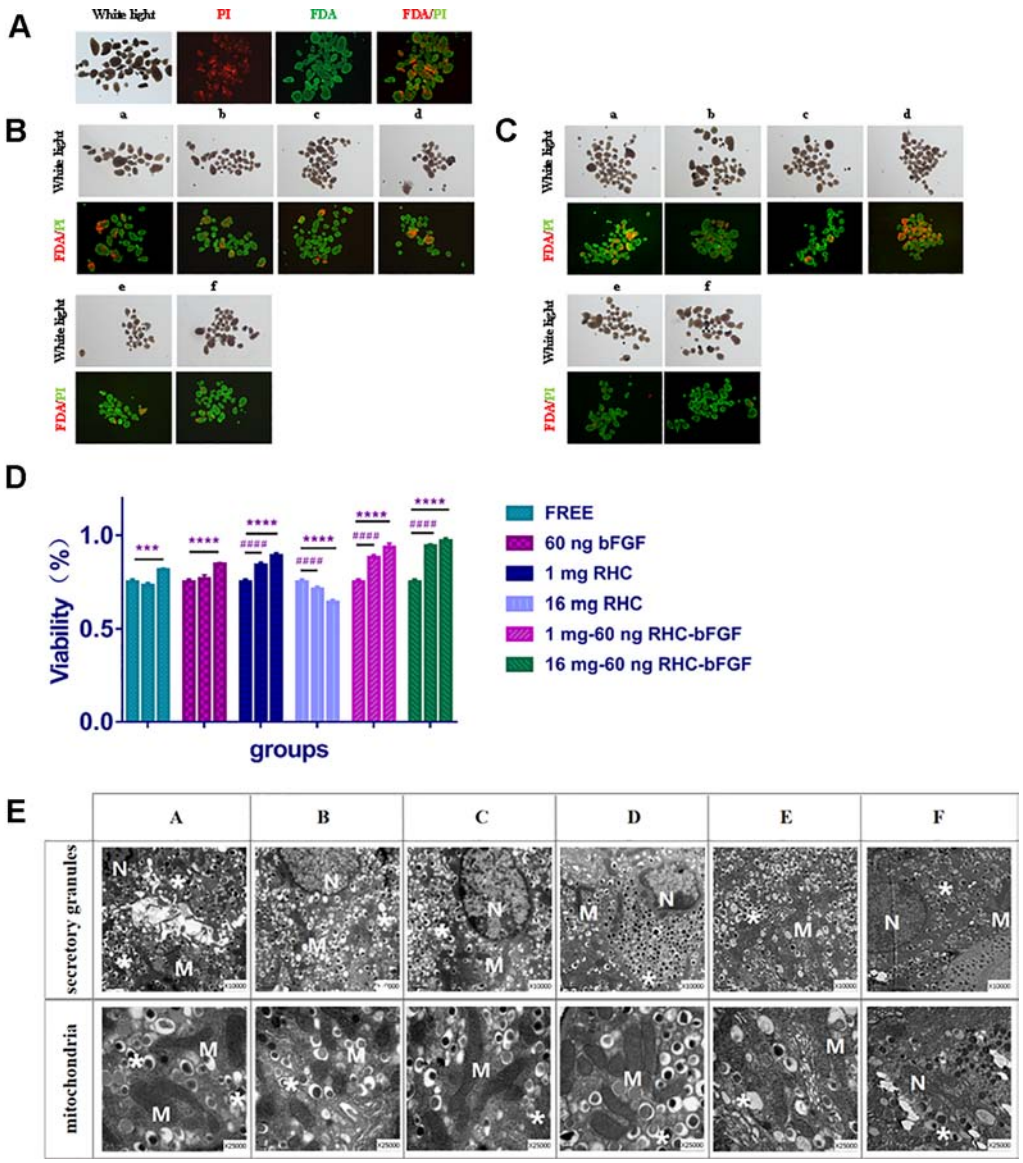

FIGURE 2 | Islet viability and transmission electron microscopy (TEM) results *in vitro*. **(A)** Islet viability at 0 h. **(B)** Islet viability of each group after cultured for 7 h. **(C)** Islet viability of each group after culturing for 24 h. **(D)** Viability statistics after cultivation. The ratio of green to green plus red cells provided the percentage of viability. The three columns of each group represent 0, 7, and 24 h from left to right (*****P* < 0.0001, ****P* < 0.001, 0 vs 24 h; ####*P* < 0.0001, 0 vs 7 h). **(E)** TEM of each group after 24 h culturing.a and A: FREE group; b and B: 60 ng bFGF group; c and C: 1 mg RHC group; d and D: 16 mg RHC group; e and E: 1 mg–60 ng RHC-bFGF group; f and F: 16 mg–60 ng RHC-bFGF group; N: nucleus; M: mitochondria; *: secretory granules.

1α expression in the islets in FREE, and HIF-1α was subtly expressed in the 60 ng bFGF and 16 mg RHC groups. For the 1 mg–60 ng RHC-bFGF group and the 16 mg–60 ng RHC-bFGF group, the expression of HIF-1α had strikingly increased. The previous reports indicated that HIF-1α expression was strongly expressed when the islets were cultured with ECM in a hypoxic condition (Maillard et al., 2011). Based on the results, RHC combined with bFGF would promote cellular proliferation and survival, whereas RHC or bFGF alone would not.

The Degradation Curve of bFGF

The impact of RHC on bFGF stability *in vitro* was assessed. The results (**Figure 4**) showed that free bFGF degraded the fastest and decreased to 40% within 12 h. In contrast, the bFGF with the 16 mg RHC group was maintained at approximately 60% bFGF within 12 h. After 72 h, the residual bFGF in the free bFGF group was lower than 5%, while the bFGF concentrations in the 1 mg RHC and 16 mg RHC groups were 10% and 25%, respectively. Even at 168 h, there was still residual bFGF in the 16 mg/ml RHC

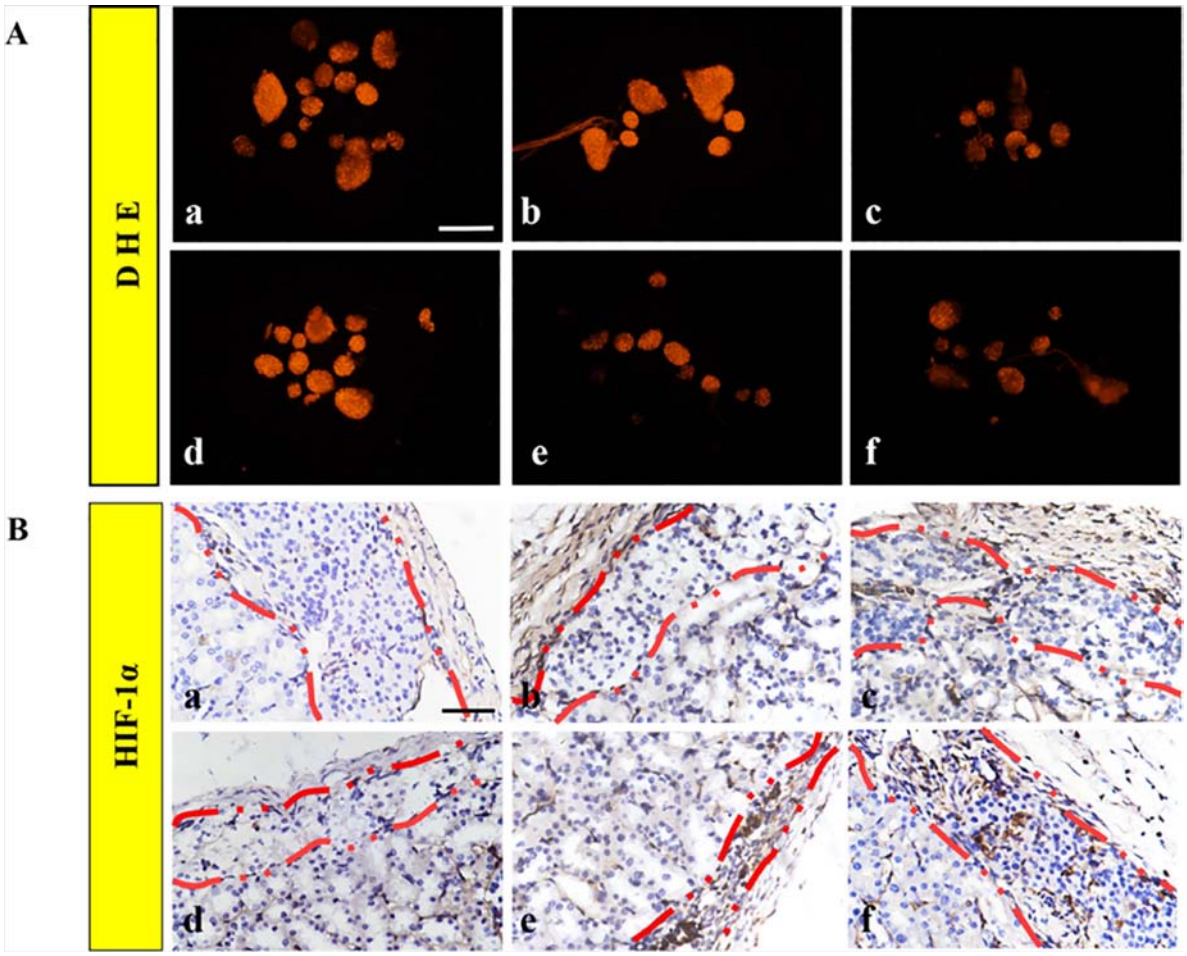

FIGURE 3 | Hypoxia. **(A)** Dihydroethidium (DHE) staining was performed on the islets after 24 h cultivation for all groups. **(B)** Representatives of HIF-1α immunohistochemical staining of the islet graft in each group. a: FREE group; b: 60 ng bFGF group; c: 1 mg RHC group; d: 16 mg RHC group; e: 1 mg–60 ng RHC-bFGF group; f: 16 mg–60 ng RHC-bFGF group.

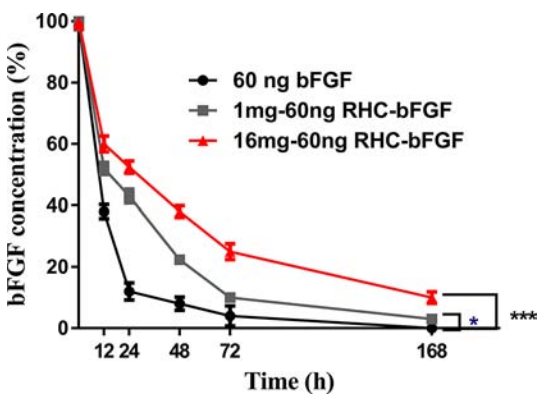

FIGURE 4 | The stability of bFGF with RHC *in vitro* (***P < 0.001, *P < 0.05, compared to 60 ng bFGF).

group. Above all, RHC could increase the stability of bFGF and prolong the action time of bFGF in the islets.

bFGF With RHC Improved Islet Function *In Vivo*

As shown in **Figure 5A**, the mice transplanted with 200 IEQ 16 mg–60 ng RHC-bFGF islets achieved euglycemia the fastest. Meanwhile, the body weight of the group increased (**Figure 5B**). The body weight of the other two groups (transplanted with 200 IEQ 1 mg RHC islets or 200 IEQ 1 mg–60 ng RHC-bFGF islets) also achieved euglycemia by the end of the experiment (**Figures 5A, B**). However, the other three groups (transplanted with 200 IEQ islets, 200 IEQ 60 ng bFGF islets, or 200 IEQ 16 mg RHC islets) maintained the hyperglycemic condition and exhibited weight loss. Above all, 200 IEQ islets transplanted after culture with 16 mg–60 ng RHC-bFGF achieved the best efficiency, while a previous report demonstrated that 400 IEQ were normally required to achieve the same outcome (Qiu et al., 2017).

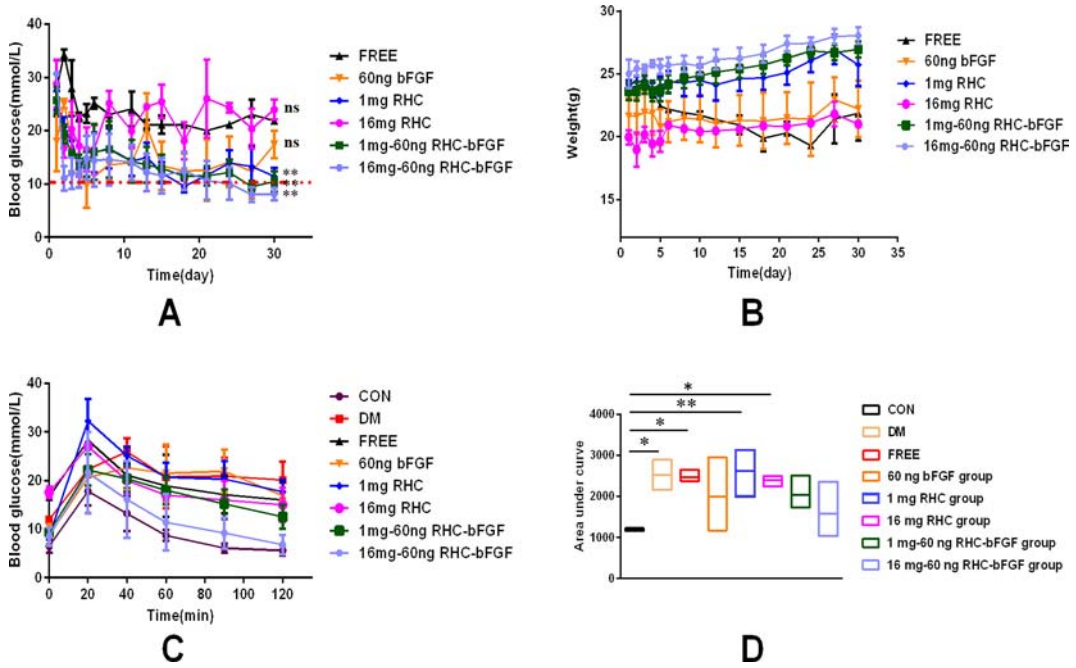

FIGURE 5 | Glucose regulation, body weight, and oral glucose tolerance test (OGTT) after islet transplantation. **(A)** No fasting blood glucose levels from day 0 (day of transplantation) to day 30 post-transplantation. (**P < 0.01, ^{ns}P > 0.05, compared to FREE.) **(B)** Change in body weight from day 0 (day of transplantation) to day 30 post-transplantation. **(C)** OGTT of all groups on day 30 post-transplantation. **(D)** Area under the curve (AUC) of corresponding OGTT values for all groups on day 30 post-transplantation. (**P < 0.01, *P < 0.05, compared to CON.)

To further investigate islet function *in vivo*, an OGTT were performed at 30 days after islet transplantation. As shown in **Figure 5C**, the 16 mg–60 ng RHC-bFGF group shared a similar blood glucose level pattern with that of the normal CON group (**Figure 5C**). Glucose levels in the 1 mg RHC group were significantly higher than those of the 1 mg–60 ng RHC-bFGF group and did not return to the baseline at 120 min. However, the blood glucose levels of the 60 ng bFGF group and the DM group remained at high levels at 120 min after glucose administration. The AUCs of the 1 mg RHC and FREE groups were similar to that of the DM group, while that of the 16 mg–60 ng RHC-bFGF group was similar to that of the CON group (**Figure 5D**). These results suggest that RHC containing bFGF contributed to better islet function.

bFGF With RHC Maintained Islet Morphology, Enhanced the Reestablishment of the Islet–ECM and Attenuated Apoptosis

The islets had a tendency to form clusters, which can lead to hypoxia and necrosis of the islets and affect the function of the islets (Uzunalli et al., 2015). To monitor the morphology of transplanted islets 30 days after transplantation, (H&E staining (**Figure 6A**), insulin-immunofluorescence staining (**Figure 6B**), and Masson's trichrome staining (**Figure 6C**) were performed on the paraffin section. H&E and positive insulin-immunofluorescence staining showed that the islets were alive, which indicated that the islets remained functional on day 30 post-transplantation. However, as shown in **Figure 6B**, the islets of the FREE and 60 ng bFGF groups gathered and fused into a large cell cluster. There was also a slight aggregation of the islets in group 16 mg RHC, and the islets boundary was blurred. While in the 1 mg RHC, 1 mg–60 ng RHC-bFGF, and 16 mg–60 ng RHC-bFGF groups, the islets had a clear boundary and were single and not clustered, and in the 16 mg–60 ng RHC-bFGF group, the islets were the most intact.

Moreover, collagen is a major component of the ECM, which indicated early attenuation of apoptosis of implanted islets in preliminary studies (Salvay et al., 2008; Davis et al., 2012). Masson's trichrome staining showed collagen existed in the region of transplanted islets of all the groups and collagen was most abundant in the 16 mg–60 ng RHC-bFGF group (**Figure 6C**). Thus, it was speculated that the successful reestablishment of the islet–ECM was crucial for minimizing islet apoptosis and preserving islet survival and function, and in turn, accounted for the better transplantation outcome (Wang and Rosenberg, 1999; Kim et al., 2012; Mao et al., 2017). Hence, it was speculated that bFGF-RHC was crucial in facilitating transplantation efficiency.

In addition, **Figure 6D** shows the caspase-3 immunohistochemistry staining of the graft on day 30 post-transplantation. The FREE group had an obvious positive staining compared with that of the other groups, especially in the central region of the islet clusters, and apoptosis was

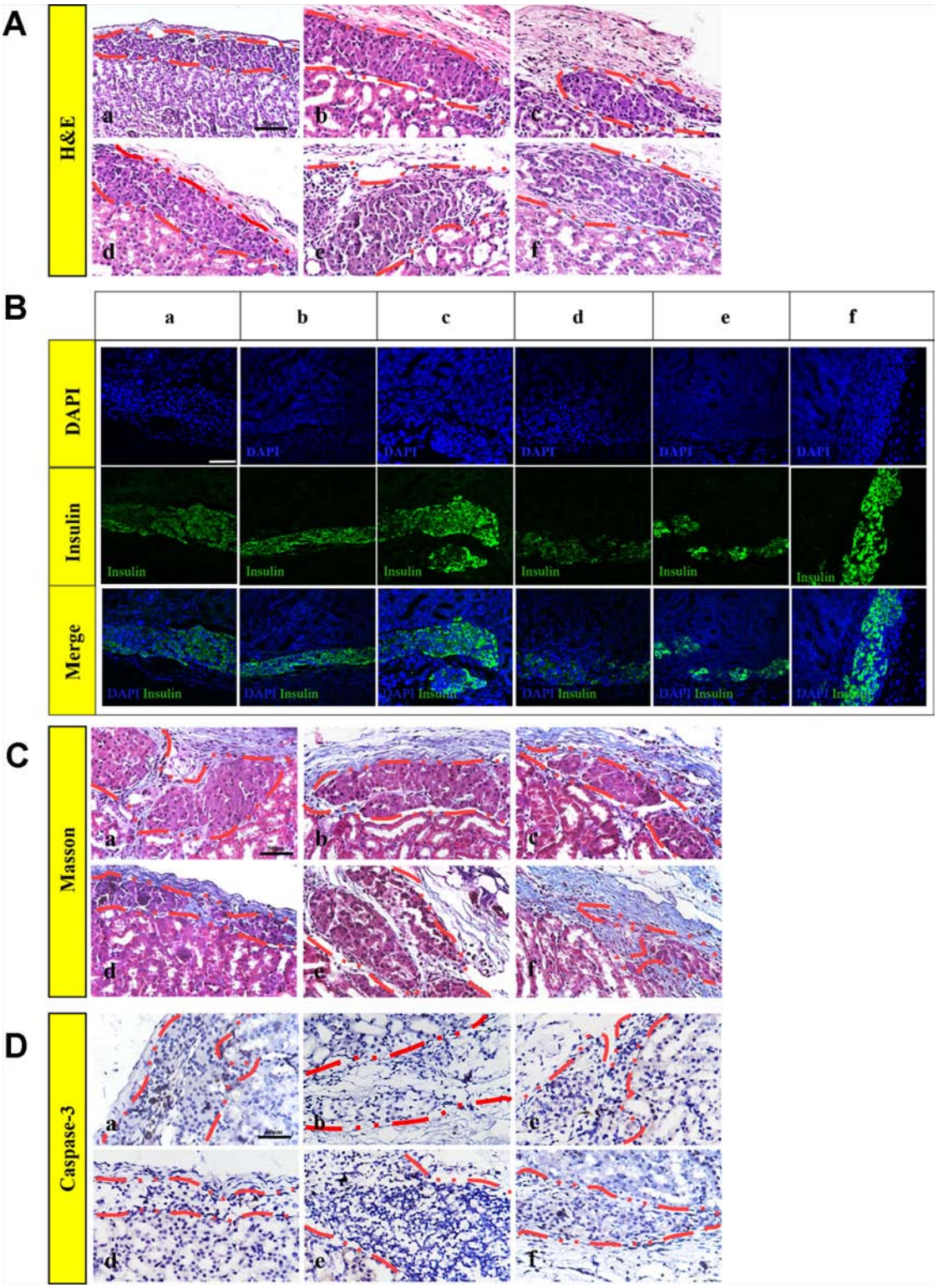

FIGURE 6 | Islet morphology. **(A)** Hematoxylin and eosin (H&E), islets conserved their morphology and integrity on post-transplantation day 30. **(B)** Insulin immunofluorescence, islets secrete insulin after transplantation, particularly 1 mg RHC and 16 mg–60 ng RHC-bFGF groups. **(C)** Masson's trichrome staining of explanted islet grafts on post-transplantation day 30. Masson's trichrome staining showed collagen expression around the transplantation site on day 30 post-transplantation. **(D)** Representative immunohistochemical staining of caspase-3 on post-transplantation day 30. a: FREE group; b: 60 ng bFGF group; c: 1 mg RHC group; d: 16 mg RHC group; e: 1 mg–60 ng RHC-bFGF group; f: 16 mg–60 ng RHC-bFGF group.

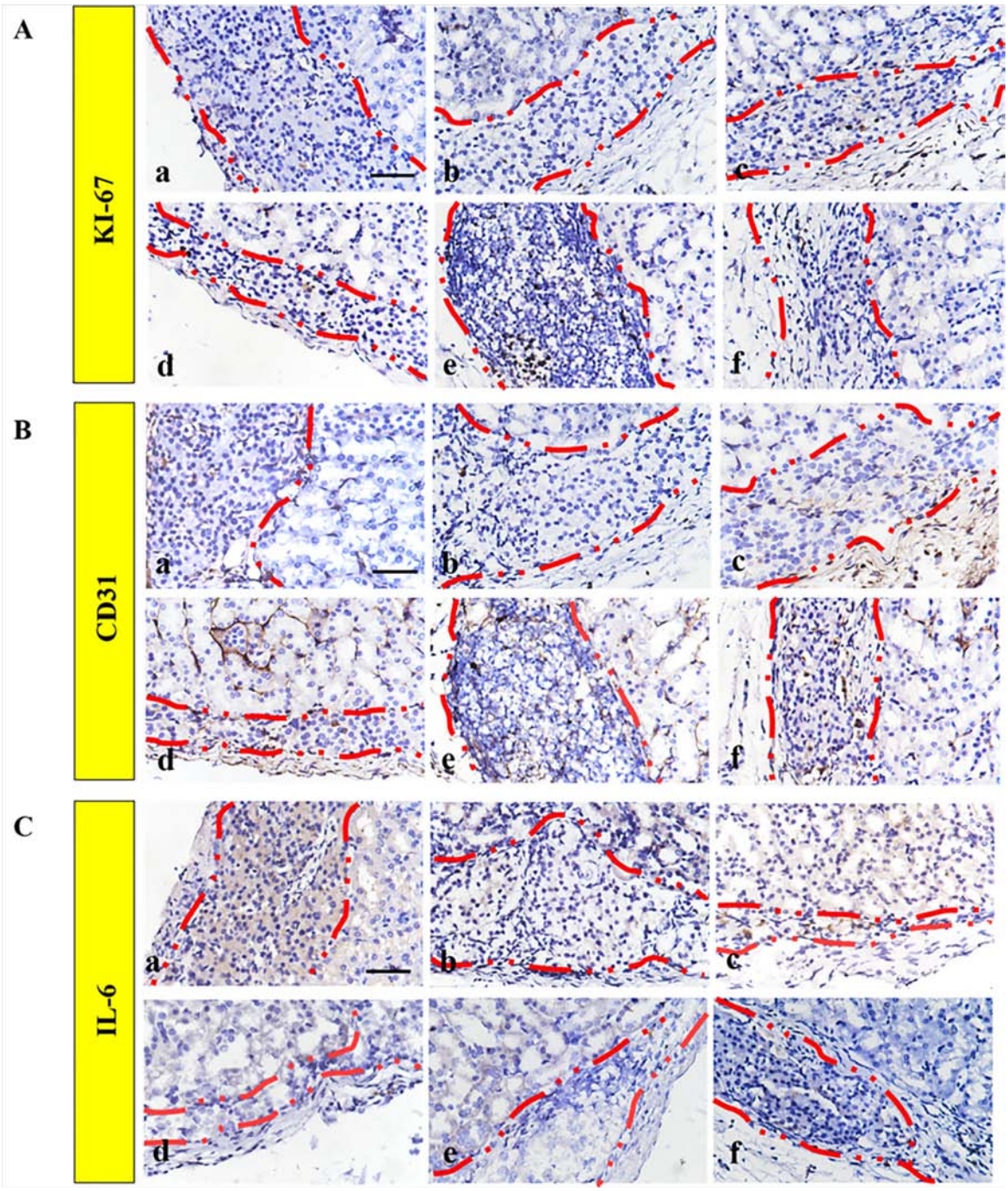

FIGURE 7 | Improved engraftment of transplanted islets by promoting proliferation and angiogenesis. Representative immunohistochemical staining of **(A)** Ki67 and **(B)** CD31 expression. **(C)** IL-6 immunohistochemistry staining was performed to monitor the inflammatory response. a: FREE group; b: 60 ng bFGF group; c: 1 mg RHC group; d: 16 mg RHC group; e: 1 mg–60 ng RHC-bFGF group; f: 16 mg–60 ng RHC-bFGF group.

obvious, which was related to the tendency of the islets to form clusters causing the central region to be susceptible to hypoxia and necrosis (**Figure 6D**). The lack of islet–matrix attachments led to rapid cell death, suggesting that the new contact attenuated apoptosis and the islets mass (Schaschkow et al., 2015). In this work, we utilized RHC and bFGF to achieve this purpose. It was proven that bFGF can promote angiogenesis, which was beneficial to the engraftment of islets (Zhao et al., 2014; Qiu et al., 2017), and ECM was shown to be capable of creating contacts.

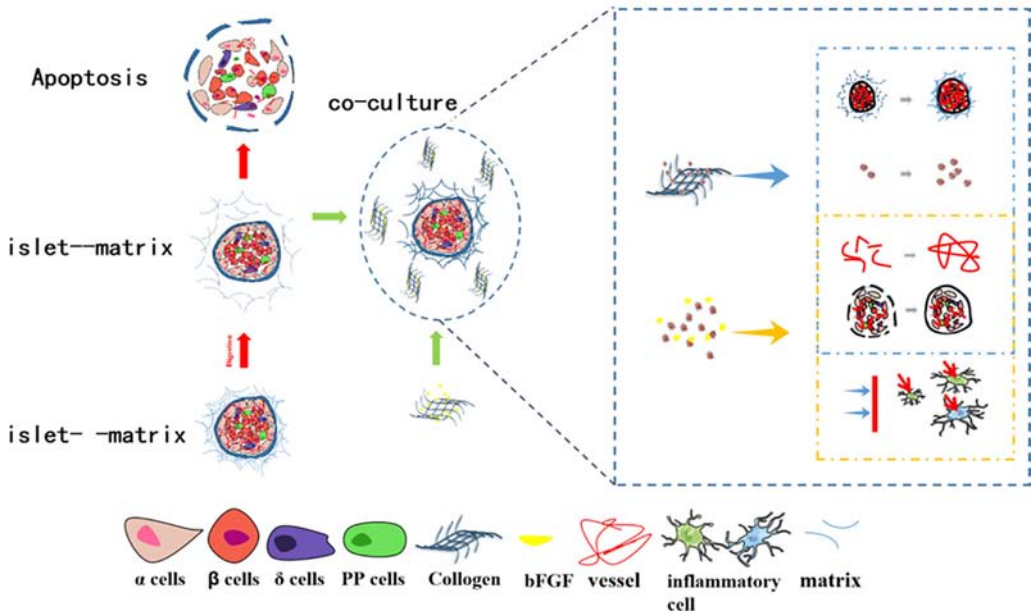

FIGURE 8 | The mechanisms of RHC-bFGF enhanced the post-transplantation outcome to reverse diabetes.

RHC Supplemented With bFGF Facilitated Graft Function by Minimizing the Post-Transplantation Inflammatory Reaction, Enhancing the Vascular Density and Increasing the Proliferation

The ECM proteins could promote cell survival and proliferation, which resulted in the functionality of β-cells (Lai et al., 2005). In addition, Ki67 is a biomarker for evaluating cell proliferation around the graft. **Figure 7A** shows that a low level of Ki67 was found in the FREE group and the 60 ng bFGF group, while significantly higher expression was found in other groups. Moreover, the level of Ki67-positive cells was significantly higher in the 1 mg–60 ng RHC-bFGF group compared with the 1 mg RHC group. These data suggest that RHC alone or RHC supplemented with bFGF facilitated islet proliferation.

The engraftment efficiency was greatly hindered by the destruction of the intra-islet blood vessel network and poor diffusion of nutrients. Therefore, it is critical to address the revascularization issue, which will improve the islet survival and functionality, and ultimately the transplantation outcome (Mao et al., 2017). To investigate the effect of pre-treated islets on islet revascularization, immunohistochemistry staining of CD31 was performed (**Figure 7B**). Based on the results, the density of the CD31 hot point was significantly higher in the high-RHC group than in the low-RHC group in the RHC-alone groups. By adding bFGF, the density of the CD31 hot point of the high concentration group was still higher than that of the low concentration group, and the expression was higher than that of the RHC-alone group, and there was a remarkable difference compared with the levels observed in the bFGF group alone. These data indicate that RHC supplemented with bFGF specifically increased the revascularization after transplantation.

We examined the inflammatory reaction to the implanted islets. IL-6 immunohistochemistry staining revealed that bFGF could inhibit the inflammatory reaction surrounding the implanted islets compared with the staining observed in the FREE group (**Figure 7C**). The RHC-alone group exhibited subtle expression of IL-6. However, IL-6 was almost not observed when RHC was combined with bFGF compared with the expression in the RHC-alone and FREE groups. As previously reported, the 60% of islets that underwent apoptosis during early transplantation was due to the inflammatory reaction (Barshes et al., 2005). In this work, RHC combined with bFGF could minimize the inflammatory reaction to improve islet survival and viability in early transplantation. Eventually, this treatment enhanced the islet transplantation outcome.

CONCLUSION

Islet transplantation is the most promising potential therapeutic option for reversing diabetes. However, despite the remarkable progress that has been made to improve the post-transplantation outcome, due to the destruction of islet–matrix attachments and the intra-islet vessel network during the isolation, the reestablishment of islet–matrix attachments and revascularization must be solved to achieve long-term graft function. Herein, we introduce RHC and bFGF into study. RHC is one of the components of the ECM. A previous study showed that the ECM that surrounded the transplanted islet *in vitro* and *in vivo* is a key factor in maintaining vascularization,

cell interaction, and the innervations of islets, and further enhances islet survival and function (Salvay et al., 2008; Pepper et al., 2015; Mao et al., 2017). Growth factors are naturally occurring substances that can stimulate cellular growth, proliferation, healing, and cellular differentiation. Our previous study demonstrated that bFGF had potent angiogenetic capabilities in fibroblasts and epithelial cells, thus promoting angiogenesis, which was beneficial in strengthening the graft revascularization (Barrientos et al., 2008; Xiang et al., 2011).

Our study (**Figure 8**) showed that RHC surrounding the islets reconstitutes islet–matrix attachments, promotes islet proliferation, and slows the degradation of bFGF. Meanwhile, bFGF eliminates inflammatory cells around the islet transplanted site. Together, these factors provide a simulated ECM microenvironment for islet survival and act on intra-islet, thereby reconstructing the damaged microvessel. Through a combination of RHC and bFGF, the supply of oxygen and nutrients inside the islets was restored, and apoptosis of the intra-islet was inhibited. The dual effects of RHC and bFGF on the inter-islet and external microenvironment of islets can decrease the quantity of islets needed to reverse diabetes compared with that indicated by the previous study, which, to a certain extent, alleviates the problem of insufficient donors.

Superior transplantation efficiency is evident from the 16 mg–60 ng RHC-bFGF group, which proved to have remarkably better blood glucose responsiveness and blood glucose control. These results suggest that the RHC-bFGF combination enables a simulated ECM microenvironment that facilitates better transplantation efficiency.

DATA AVAILABILITY STATEMENT

The raw data supporting the conclusions of this article will be made available by the authors, without undue reservation, to any qualified researcher.

ETHICS STATEMENT

The animal study was reviewed and approved by the Institutional Animal Care and Use Committee of Wenzhou Medical University.

AUTHOR CONTRIBUTIONS

QZ, CL, YZ, and HF participated in research design. QZ, XuaJ, XueJ, ZH, and YJ were responsible for performing the experiments. QZ, QY, YZ, LP, and HF contributed to the writing and editing of the manuscript. All authors have read and approved this article.

FUNDING

This research was supported by the National Natural Science Foundation of China (grant no. 81772316, 81603036, and 81903551), Key Research and Development Program of Zhejiang Province (grant no. 2018C03013), Zhejiang Provincial Natural Science Foundation (grant no. LY19H180001, LQ19H300001, LY17H180008), Zhejiang Provincial Program for the Cultivation of High-Level Innovative Health Talents (Y-ZZ), 151 Talent Project of Zhejiang Province, Zhejiang Provincial Foundation for Health Department (grant no. 2019322086), Wenzhou Municipal Science and Technology Bureau (grant no. Y20190177), and School Talent Start Fund of Wenzhou Medical University (grant no. QTJ15020).

SUPPLEMENTARY MATERIAL

The Supplementary Material for this article can be found online at: https://www.frontiersin.org/articles/10.3389/fphar.2019.01536/full#supplementary-material

FIGURE 1S | Islet viability *in vitro*. Islets were cultured for 7 **(A**, **B)** and 24 h **(C**, **D)**.

REFERENCES

Bader, E., Migliorini, A., Gegg, M., Moruzzi, N., Gerdes, J., Roscioni, S. S., et al. (2016). Identification of proliferative and mature β-cells in the islets of Langerhans. *Nature* 535, 430. doi: 10.1038/nature18624

Barrett-Connor, E., and Orchard, T. J. (1985). Insulin-dependent diabetes mellitus and ischemic heart disease. *Diabetes Care* 8 Suppl 1, 65–70. doi: 10.2337/diacare.8.1.S65

Barrientos, S., Stojadinovic, O., Golinko, M. S., Brem, H., and Tomic-Canic, M. (2008). Growth factors and cytokines in wound healing. *Wound Repair Regener.* 16 (5), 585–601. doi: 10.1111/j.1524-475X.2008.00410.x

Barshes, N. R., Wyllie, S., and Goss, J. A. (2005). Inflammation-mediated dysfunction and apoptosis in pancreatic islet transplantation: implications for intrahepatic grafts. *J. Leukocyte Biol.* 77 (5), 587–597. doi: 10.1189/jlb.1104649

Bogdani, M., Korpos, E., Simeonovic, C. J., Parish, C. R., Sorokin, L., and Wight, T. N. (2014). Extracellular matrix components in the pathogenesis of type 1 diabetes. *Curr. Diabetes Rep.* 14 (12), 552. doi: 10.1007/s11892-014-0552-7

Brandhorst, D., Brandhorst, H., Maataoui, V., Maataoui, A., and Johnson, P. R. (2013). Anti-caspase-3 preconditioning increases proinsulin secretion and deteriorates posttransplant function of isolated human islets. *Apoptosis* 18 (6), 681–688. doi: 10.1007/s10495-013-0834-6

Daoud, J., Rosenberg, L., and Tabrizian, M. (2010). Pancreatic islet culture and preservation strategies: advances, challenges, and future outlook. *Cell Transplant.* 19 (12), 1523–1535. doi: 10.3727/096368910x515872

Davis, N. E., Beenken-Rothkopf, L. N., Mirsoian, A., Kojic, N., Kaplan, D. L., Barron, A. E., et al. (2012). Enhanced function of pancreatic islets co-encapsulated with ECM proteins and mesenchymal stromal cells in a silk hydrogel. *Biomaterials* 33 (28), 6691–6697. doi: 10.1016/j.biomaterials.2012.06.015

Emamaullee, J. A., Davis, J., Pawlick, R., Toso, C., Merani, S., Cai, S. X., et al. (2008). The caspase selective inhibitor EP1013 augments human islet graft function and longevity in marginal mass islet transplantation in mice. *Diabetes* 57 (6), 1556–1566. doi: 10.2337/db07-1452

Fu, H. X., Wu, L. L., Qiu, K. Y., Zhao, Y. Z., Xu, Y. Y., Jiang, X., et al. (2016). Construction and Evaluation of Islet Transplantation Under the Kidney Capsule in Mice. *J. Biomater Tissue Eng.* 6 (3), 208–215. doi: 10.1166/jbt.2016.1431

Kim, J. S., Lim, J. H., Nam, H. Y., Lim, H. J., Shin, J. S., Shin, J. Y., et al. (2012). In situ application of hydrogel-type fibrin-islet composite optimized for rapid glycemic control by subcutaneous xenogeneic porcine islet transplantation. *J. Control Release* 162 (2), 382–390. doi: 10.1016/j.jconrel.2012.07.018

Kin, T., Senior, P., O'Gorman, D., Richer, B., Salam, A., and Shapiro, A. M. (2008). Risk factors for islet loss during culture prior to transplantation. *Transpl Int.* 21 (11), 1029–1035. doi: 10.1111/j.1432-2277.2008.00719.x

Lai, Y., Schneider, D., Kidszun, A., Hauck-Schmalenberger, I., Breier, G., Brandhorst, D., et al. (2005). Vascular endothelial growth factor increases functional beta-cell mass by improvement of angiogenesis of isolated human and murine pancreatic islets. *Transplantation* 79 (11), 1530–1536. doi: 10.1097/01.TP.0000163506.40189.65

Lembert, N., Wesche, J., Petersen, P., Doser, M., Becker, H. D., and Ammon, H. P. (2003). Areal density measurement is a convenient method for the determination of porcine islet equivalents without counting and sizing individual islets. *Cell Transplant.* 12 (1), 33–41. doi: 10.3727/000000003783985214

Maillard, E., Juszczak, M. T., Clark, A., Hughes, S. J., Gray, D. R., and Johnson, P. R. (2011). Perfluorodecalin-enriched fibrin matrix for human islet culture. *Biomaterials* 32 (35), 9282–9289. doi: 10.1016/j.biomaterials.2011.08.044

Mao, D., Zhu, M., Zhang, X., Ma, R., Yang, X., Ke, T., et al. (2017). A macroporous heparin-releasing silk fibroin scaffold improves islet transplantation outcome by promoting islet revascularisation and survival. *Acta Biomater* 59, 210–220. doi: 10.1016/j.actbio.2017.06.039

Nathan, D. M. (1993). Long-term complications of diabetes mellitus. *N Engl. J. Med.* 328 (23), 1676–1685. doi: 10.1056/nejm199306103282306

Pepper, A. R., Gala-Lopez, B., Pawlick, R., Merani, S., Kin, T., and Shapiro, A. M. (2015). A prevascularized subcutaneous device-less site for islet and cellular transplantation. *Nat. Biotechnol.* 33 (5), 518–523. doi: 10.1038/nbt.3211

Qiu, K. Y., Fu, H. X., Jiang, X., Xu, F. Y., Chen, X. S., Lin, Q., et al. (2017). Sodium Hyaluronate Gel Containing bFGF Co-Transplanted with Islets Leading to the Promotion of Angiogenesis and the Reduction of the Required Grafted Islets in Diabetic Mice. *J. Biomater Tissue Eng.* 7, 291–301. doi: 10.1166/jbt.2017.1575

Sailakshmi, G., Mitra, T., Gnanamani, A., Kumara Raja, S. T., Thiruselvi, T., Selvaraj, N. V., et al. (2011). Bonding interactions and stability assessment of biopolymer material prepared using type III collagen of avian intestine and anionic polysaccharides. *J. Mater Sci. Mater Med.* 22 (6), 1419–1429. doi: 10.1007/s10856-011-4337-0

Salvay, D. M., Rives, C. B., Zhang, X., Chen, F., Kaufman, D. B., Lowe, W. L. Jr., et al. (2008). Extracellular matrix protein-coated scaffolds promote the reversal of diabetes after extrahepatic islet transplantation. *Transplantation* 85 (10), 1456–1464. doi: 10.1097/TP.0b013e31816fc0ea

Schaschkow, A., Mura, C., Bietiger, W., Peronet, C., Langlois, A., Bodin, F., et al. (2015). Impact of an autologous oxygenating matrix culture system on rat islet transplantation outcome. *Biomaterials* 52, 180–188. doi: 10.1016/j.biomaterials.2015.02.031

Tsuchiya, H., Sakata, N., Yoshimatsu, G., Fukase, M., Aoki, T., Ishida, M., et al. (2015). Extracellular Matrix and Growth Factors Improve the Efficacy of Intramuscular Islet Transplantation. *PloS One* 10 (10), e0140910. doi: 10.1371/journal.pone.0140910

Uzunalli, G., Tumtas, Y., Delibasi, T., Yasa, O., Mercan, S., Guler, M. O., et al. (2015). Improving pancreatic islet *in vitro* functionality and transplantation efficiency by using heparin mimetic peptide nanofiber gels. *Acta Biomater* 22, 8–18. doi: 10.1016/j.actbio.2015.04.032

Wang, R. N., and Rosenberg, L. (1999). Maintenance of beta-cell function and survival following islet isolation requires re-establishment of the islet-matrix relationship. *J. Endocrinol.* 163 (2), 181–190. doi: 10.1677/joe.0.1630181

Wang, L., Gao, P., Zhang, M., Huang, Z., Zhang, D., Deng, Q., et al. (2017). Prevalence and Ethnic Pattern of Diabetes and Prediabetes in China in 2013. *Jama* 317 (24), 2515–2523. doi: 10.1001/jama.2017.7596

Xiang, Q., Xiao, J., Zhang, H., Zhang, X., Lu, M., Zhang, H., et al. (2011). Preparation and characterisation of bFGF-encapsulated liposomes and evaluation of wound-healing activities in the rat. *Burns* 37 (5), 886–895. doi: 10.1016/j.burns.2011.01.018

Zhao, Y. Z., Tian, X. Q., Zhang, M., Cai, L., Ru, A., Shen, X. T., et al. (2014). Functional and pathological improvements of the hearts in diabetes model by the combined therapy of bFGF-loaded nanoparticles with ultrasound-targeted microbubble destruction. *J. Control Release* 186, 22–31. doi: 10.1016/j.jconrel.2014.04.054

Zmuda, E. J., Powell, C. A., and Hai, T. (2011). A method for murine islet isolation and subcapsular kidney transplantation. *J. Vis Exp.* (50). doi: 10.3791/2096

Conflict of Interest: The authors declare that the research was conducted in the absence of any commercial or financial relationships that could be construed as a potential conflict of interest.

frontiers in Pharmacology

ORIGINAL RESEARCH
published: 10 January 2020
doi: 10.3389/fphar.2019.01535

Assessment of the Preventive Effect Against Diabetic Cardiomyopathy of FGF1-Loaded Nanoliposomes Combined With Microbubble Cavitation by Ultrasound

Lei Zheng[1,2], *Chuan-Li Shen*[2], *Jian-Min Li*[3], *Yu-Lei Ma*[1], *Ning Yan*[1], *Xin-Qiao Tian*[1*] *and Ying-Zheng Zhao*[4,5*]

[1] Department of Ultrasonography, Henan Provincial People's Hospital, Zhengzhou University People's Hospital, Department of Ultrasonography of Central China Fuwai Hospital, Central China Fuwai Hospital of Zhengzhou University, Zhengzhou, China, [2] Department of Ultrasonography, the First Affiliated Hospital of Wenzhou Medical University, Wenzhou, China, [3] Department of Pathology, the First Affiliated Hospital of Wenzhou Medical University, Wenzhou, China, [4] School of Pharmaceutical Sciences, Wenzhou Medical University, Wenzhou, China, [5] Engineering Laboratory of Zhejiang Province for Pharmaceutical Development of 6 Growth Factors, Biomedical Collaborative Innovation Center of Wenzhou, Wenzhou, China

OPEN ACCESS

Edited by:
Zhouguang Wang,
Albert Einstein College of Medicine, United States

Reviewed by:
Cheng-Hai Zhang,
Harvard Medical School, United States
Shuhui Liu,
Icahn School of Medicine at Mount Sinai, United States

***Correspondence:**
Xin-Qiao Tian
tianxq2005@163.com
Ying-Zheng Zhao
pharmtds@163.com

Specialty section:
This article was submitted to Translational Pharmacology, a section of the journal Frontiers in Pharmacology

Received: *09 October 2019*
Accepted: *27 November 2019*
Published: *10 January 2020*

Citation:
Zheng L, Shen C-L, Li J-M, Ma Y-L, Yan N, Tian X-Q and Zhao Y-Z (2020) Assessment of the Preventive Effect Against Diabetic Cardiomyopathy of FGF1-Loaded Nanoliposomes Combined With Microbubble Cavitation by Ultrasound. Front. Pharmacol. 10:1535. doi: 10.3389/fphar.2019.01535

Acidic fibroblast growth factor (FGF1) has great potential in preventing diabetic cardiomyopathy. This study aimed to evaluate the preventive effect of FGF1-loaded nanoliposomes (FGF1-nlip) combined with ultrasound-targeted microbubble destruction (UTMD) on diabetic cardiomyopathy (DCM) using ultrasound examination. Nanoliposomes encapsulating FGF1 were prepared by reverse phase evaporation. DM model rats were established by intraperitoneal injection of streptozotocin (STZ), and different forms of FGF1 (FGF1 solution, FGF1-nlip, and FGF1-nlip+UTMD) were used for a 12-week intervention. According to the transthoracic echocardiography and velocity vector imaging (VVI) indexes, the LVEF, LVFS, and VVI indexes (Vs, Sr, SRr) in the FGF1-nlip+UTMD group were significantly higher than those in the DM model group and other FGF1 intervention groups. From the real-time myocardial contrast echocardiography (RT-MCE) indexes, the FGF1-nlip+UTMD group A and A×β showed significant differences from the DM model group and other FGF1 intervention groups. Cardiac catheter hemodynamic testing, CD31 immunohistochemical staining, and electron microscopy also confirmed the same conclusion. These results confirmed that the abnormalities, including myocardial dysfunction and perfusion impairment, could be suppressed to different extents by the twice weekly FGF1 treatments for 12 consecutive weeks (free FGF1, FGF1-nlip, and FGF1-nlip+UTMD), with the strongest improvements observed in the FGF1-nlip+UTMD group. In conclusion, the VVI and RT-MCE techniques can detect left ventricular systolic function and perfusion changes in DM rats, providing a more effective experimental basis for the early detection and treatment evaluation of DCM, which is of great significance for the prevention of DCM.

Keywords: diabetic cardiomyopathy, acidic fibroblast growth factor, ultrasound-targeted microbubble destruction, liposomes, preventive effect

INTRODUCTION

With the development of the economy and society, as well as changes in people's dietary habits and lifestyles, the incidence of diabetes mellitus (DM) is increasing annually, and the age of onset has become younger. According to statistics, there are approximately 425 million DM patients worldwide in 2017, and the number is expected to reach 700 million by 2045 (Cho et al., 2018). The acute and chronic complications caused by DM not only endanger the physical and mental health of patients but also bring a huge economic burden to patients' families and the health industry. Diabetes cardiomyopathy (DCM) is a series of changes in the myocardial structure and function caused by DM (Borghetti et al., 2018; Parim et al., 2019) that are not related to coronary atherosclerosis, hypertension, and valvular heart disease (Rubler et al., 1972). At present, DCM has been identified as the main cause of heart failure and death in patients with DM (Evangelista et al., 2019; Gulsin et al., 2019; Zamora and Villena, 2019). Therefore, early detection and timely intervention therapy are of great significance for the prognosis of DM patients.

Fibroblast growth factors (FGFs) have at least 23 members and are widely distributed in the body. Each member has a certain structural similarity (Beenken and Mohammadi, 2009; Itoh and Ornitz, 2011; Zhang et al., 2013; Li, 2019). Among them, acidic fibroblast growth factor (FGF1) is one of the earlier founded members of the fibroblast growth factor family. Studies have shown that FGF1 has a wide range of physiological functions, such as antioxidant damage (Pena et al., 2017), induction of endothelial and smooth muscle cell proliferation and angiogenesis (Zhao et al., 2016), promotion of tissue wound repair (Xu et al., 2018), neurotrophic regeneration (Tsai et al., 2015), etc. Therefore, FGF1 has a great potential in the prevention and treatment of DCM. However, the lack of an efficient and safe delivery system limits FGF1 application *in vivo*.

Nanoliposomes are double-layer vesicle structures composed of hydrated lipids (Abu and Ishida, 2017; Kapoor et al., 2017). The particle sizes range from 10 to 1000 nm. Nanoliposomes have the characteristics of high drug loading, sustained-release drugs, high stability *in vivo*, non-toxicity, non-immunogenicity, and biodegradability (Chen and Stephen, 2019). Therefore, using nanoliposomes as drug carriers can not only effectively protect the drug from the influence of environmental conditions *in vivo* but also can penetrate the endothelial gap and complete capillaries to reach the target tissue to be absorbed by most cells, thus playing a corresponding biological effect. However, it is difficult for nanoliposomes to locally aggregate at high concentrations *in vivo* to achieve highly effective targeted therapy.

Ultrasound targeted microbubble destruction (UTMD) provides a new method for myocardial targeted delivery of FGF1. Under the energy of diagnostic or therapeutic ultrasound, ultrasound microbubbles can explode in the region of interest or target tissues. Cavitation and mechanical effects of blasting can increase the permeability of local vascular walls or cell membranes, thereby increasing the dose of drugs/genes in target organs or target tissues and their corresponding biological effects (Frenkel, 2008; Chen et al., 2018; Liang et al., 2018; Lin et al., 2018; Yang et al., 2019).

Echocardiography, as a practical tool for the non-invasive evaluation of cardiac function, has been widely applied in clinical and animal experiments. Velocity vector imaging (VVI) is based on two-dimensional gray-scale ultrasound images with a high frame rate. It uses spatial coherence, speckle and boundary tracking techniques of ultrasound pixels to automatically track and recognize the motion of echo spots in the region of interest in each frame image and quantitatively analyzes the structural mechanics of myocardial tissue motion to obtain a reflection of the myocardium. Compared with traditional techniques, VVI has no angle dependence, and its strain and strain rate measurements are relatively unaffected by respiration (Azam et al., 2012; Li et al., 2012; Zhou et al., 2015). Therefore, it is superior to conventional ultrasound and tissue imaging and its derivative technology in cardiac function abnormalities and heart disease treatment effect evaluation. Real-time myocardial contrast echocardiography (RT-MCE) technology is used to inject ultrasound contrast agents containing microbubbles into the body through peripheral veins. Because the size of microbubbles is the same as that of red blood cells, the hemodynamics is similar to that of red blood cells. Microbubbles can freely distribute in myocardial tissue through cardiac capillaries. Microbubbles produce a large number of liquid-gas interfaces in the blood, thus reflecting a large number of ultrasound signals and increasing the video density of myocardial microcirculation. By observing the contrast enhancement of the myocardium with echocardiography, the tissue perfusion information can be evaluated at the microvascular level. The whole and local perfusion of myocardium can be observed and analyzed non-invasively. The volume, velocity, and flow of myocardium can be measured quantitatively (Wei et al., 2012; Jiang et al., 2017; Danijela et al., 2018; Geng et al., 2018). Although the application of VVI and RT-MCE technology is increasing, few studies have evaluated the efficacy of DCM in prevention and treatment.

Therefore, FGF1 loaded nanoliposomes (FGF1-nlip) combined with UTMD technology were used in this study to intervene in early DM rats. The effects of this method on left ventricular function and blood flow perfusion in DM rats were evaluated by conventional echocardiography, velocity vector imaging (VVI), real-time myocardial contrast echocardiography (RT-MCE), and histomorphology.

MATERIALS AND METHODS

Preparation and Properties of FGF1-nlip

FGF1-nlip were prepared by reverse phase evaporation. The specific preparation process was as follows: FGF1 lyophilized powder (Guangzhou Jinan University Medical Biotechnology Research and Development Center) was dissolved in physiological saline to form FGF1 (1 mg/ml) solution. Next, 90 mg of natural phospholipids (Shanghai AVT) and 10 mg of cholesterol (Shanghai AVT) were weighed and dissolved in 4 ml of dichloromethane (Guangdong Guanghua Technology Co., Ltd.) for use. The FGF1 solution was slowly added dropwise to the phospholipid-dissolved methylene chloride and rapidly sonicated (100 W, 15 s) to form a stable w/o emulsion. The

methylene chloride was removed by rotary evaporation under reduced pressure. After the dichloromethane was completely removed, the mixture was hydrated with an appropriate amount of physiological saline and ultrasonically dispersed (100 W, 10 min) in an ice bath to give a final FGF1 concentration of 10 μg/ml. Blank nanoliposomes were prepared by replacing the FGF1 solution with an equal volume of distilled water. The characterization of FGF1-nlip mainly includes morphological characteristics, zeta potential, particle size, and the encapsulation efficiency of the particles. In this study, the particle size and morphological characteristics of FGF1-nlip were determined by transmission electron microscopy. The hydration particle size and zeta potential of FGF1-nlip were determined by dynamic light scattering. The determination method of the encapsulation efficiency of FGF1-nlip was as follows: 1.0 ml of liposome suspension containing FGF1 was accurately measured in an ultrafiltration tube, centrifuged at 10,000 r/min for 30 min, the filtrate was removed and diluted properly, and the FGF1 ELISA reagent was used. The cassette was assayed for FGF1 protein concentration. Encapsulation ratio (%) = (total protein amount – amount of protein in the filtrate)/total protein amount × 100%.

Experimental Animals

Seventy male Sprague-Dawley (SD) rats, aged 40 to 50 days, with body weight 180–220 g, were provided by the Experimental Animal Center of Wenzhou Medical University (Experimental Animal License No.: SYXK (Zhejiang] 2015-0009). All animal experiments were performed with the permission of the Animal Ethics Committee of Wenzhou Medical University (approval number: wydw2016-0025).

Experimental Animal Groups

After 7 days of adaptive feeding, all rats were fasted for 12 hours overnight. On the second day, 56 rats were randomly selected, and each rat was intraperitoneally injected with a 1% solution of streptozotocin 70 mg/kg. The blood glucose concentration was measured by tail vein sampling on the 1st, 3rd, and 7th days after injection. The rats with blood glucose levels exceeding 16.7 mmol/L and with higher food intake, polydipsia, and polyuria were selected as DM rats (52 rats were modeled, 4 were excluded without being modeled). Subsequently, DM rats were randomized into 4 groups with 13 rats in each group: DM model group, FGF1 solution group, FGF1-nlip group, and FGF1-nlip+UTMD group. The remaining 14 were used as the normal control group, and the same amount of citrate buffer was intraperitoneally injected and they were fed under the same conditions.

All experimental rats were housed in the SPF animal room (the average indoor temperature was approximately 20–24°C, the average humidity was approximately 50–60%), and the on-time changes were simulated by turning on and off the lights regularly. All rats were freely supplied with sterile water during the feeding process.

Experimental Animal Intervention

After intraperitoneal anesthesia with 10% chloral hydrate solution, rats in the DM model group were injected with saline *via* the caudal vein; rats in the FGF1 solution group were injected with FGF1 solution *via* the caudal vein; and rats in the FGF1-nlip group were injected with FGF1-nlip solution *via* the caudal vein. After anesthesia, rats in the FGF1-nlip+UTMD group were shaved in the anterior cardiac region and fixed in the left lateral decubitus position. FGF1-nlip solution was well mixed with SonoVue microbubbles (Bracco, Italy) before administration. The Acuson Sequoia 512C system (Siemens, Germany) was used, and the RT-MCE imaging mode was set up. The probe frequency was set to 12 to 14 MHz (15L8-w linear array probe). The probe was placed in the precordial area of the rats, and the probe and skin were filled with coupling agents. The ultrasound instrument was converted into contrast mode. Left ventricular short axis view at the papillary muscle level was taken, and the focusing depth was 3.5–4.0 cm. The mixture of FGF1-nlip and SonoVue microbubbles was slowly injected into rats. When the image showed that a large number of contrast agents were filling the myocardium, MBD function (mechanical index MI = 1.9) was used to blast the microbubbles repeatedly until the microbubbles completely disappeared. The dose of fibroblast growth factor 1 in each intervention group was 15 μg/kg (Zhao et al., 2016). Drug intervention lasted 12 weeks, twice a week, for a total of 24 times.

Ultrasound Image Acquisition

Before and 12 weeks after the intervention (De Blasio et al., 2015; Atta et al., 2018), rats in each group were anesthetized with 10% chloral hydrate intraperitoneally and shaved in the anterior cardiac region. The probe was placed in the anterior cardiac region of rats, and the coupling agent was filled between the probe and the skin. The left ventricular ejection fraction (LVEF) and left ventricular fraction shortening (LVFS) were measured by conventional M-mode echocardiography in all rats.

VVI imaging mode was started, and the RES button on the machine was pressed to enlarge the image while reducing the spatial resolution appropriately to obtain the highest frame rate possible. The frame rate of this study was adjusted to between 60 and 90 Hz. Acoustic acquisition of two-dimensional gray-scale dynamic images of the papillary muscle horizontal left ventricular short axis view for three or more cardiac cycles was used. All dynamic images were stored on MO discs and imported into Siemens Sygno US Workplace 3.01 analysis software for offline analysis.

The cadence key was pressed to enter the contrast mode. The depth of the image was 3–4 cm. The RES key was pressed to enlarge the region of interest locally. The mechanical index was 0.35. The gain was adjusted so that there was no obvious acoustic signal in the myocardial tissue and remained constant throughout the process. Contrast medium was infused slowly through the caudal vein. Left ventricular short axis myocardiography at the papillary muscle level was performed at rest to observe the filling of contrast media in the cardiac cavity and myocardium. After the filling of contrast media in the myocardium was sufficient, the contrast media in the myocardium were destroyed by high energy pulse, and then the instrument was automatically converted to low energy imaging to obtain real-time dynamic imaging. All real-time dynamic images were stored on MO discs and then imported into Siemens Sygno US Workplace 3.01 analysis software for off-line auto-tracing contrast quantitative technique (ACQ) analysis.

VVI Analysis

In the VVI analysis software, a frame image of the clearest endocardium was selected, and the boundary of the left ventricular endocardium and epicardium was drawn clockwise. According to the standard 16-segment method developed by the American Academy of Echocardiography, the left ventricular wall was automatically divided into six segments: anterior wall (AW), lateral wall (LW), posterior wall (PW), inferior wall (IW), posterior septum (PS), and anterior septum (AS). The position of each segment was monitored, and the myocardial velocity, radial strain, and strain rate curves of 6 segments were obtained automatically by software. The mean systolic peak velocity (Vs), radial peak strain (Sr), and radial peak strain rate (SRr) were measured in 6 segments of the left ventricle.

MCE Analysis

In the analysis software, the left ventricular short-axis view of the anterior wall myocardial tissue was selected to outline the region of interest (in the process of delineation, the interference of factors such as endometrial, epicardial, and papillary muscles was avoided). The software automatically tracks the region of interest in each frame of the image and allows the operator to adjust the location of the region of interest at any frame so that it is always within the corresponding myocardial tissue. The analysis software measures the average acoustic intensity of the region of interest of each frame of image and fits it to the acoustic intensity-time curve $y = A \times (1 - e^{-\beta t})$, where A is the peak acoustic intensity of the region of interest, reflecting the blood volume of the local myocardium, β is the contrast agent perfusion rate, reflecting the blood flow velocity of the myocardium, the product of the two (A×β) represents the regional myocardial blood flow, and each rat is analyzed 2~3 times and the average taken to reduce the error. All of the analysis curves with a goodness of fit (GOF) < 0.9 were excluded.

Hemodynamic Evaluation

All the experimental rats were anesthetized with 10% chloral hydrate after intraperitoneal injection, and then they were routinely disinfected. The skin of the anterior cervical region was cut, the trachea was separated, the animal ventilator was opened, the thoracic cavity was opened, and the cardiac catheter was penetrated into the left ventricle of the rat with heparin saline after filling the heart catheter with heparin saline. After the biological signal was transformed, Chart5 for Windows analysis software was synchronized. Left ventricular end-systolic pressure (LVESP), left ventricular end-diastolic pressure (LVEDP), and the maximum rise and fall rate of left ventricular internal pressure (LV ± dp/dtmax) were recorded.

CD31 Immunohistochemical Staining and Cardiac Capillary Density Measurement

The rats were sacrificed, the heart was removed, and the left ventricular myocardium was taken from the papillary muscles, fixed with 10% formaldehyde, and embedded in paraffin. The paraffin sections of myocardial tissue were stained with CD31 (Abcam, ab28364, USA) for immunohistochemistry and observed under an optical microscope. Eight slices were taken from each group, and 10 high-power fields (hpf) (400×) were randomly selected from each slice. The number of microvascular sections was calculated and averaged as the microvascular density (MVD) in the myocardial tissue.

Transmission Electron Microscopy

A portion of the left ventricle was cut into 1-mm tissue blocks and fixed in 2.5% glutaraldehyde for more than 4 h for electron microscopy. Myocardial tissue was then immobilized with 1% osmium acid for 1 h and then rinsed and stained with 1% uranium acetate for 1 h. After dehydration with acetone and embedding with epoxy resin, myocardial tissue was cut into 1-μm sections and stained with toluidine blue. The ultrathin sections were cut from the block and studied under a JEM-1230 transmission electron microscope (JEOL of Japan).

Statistical Analysis

Data analysis was performed using IBM SPSS Statistics 25.0 statistical software. The normal distribution of the measurement indicators was expressed as the mean ± SD. The multivariate sample means were compared for variance homogeneity test. The mean comparison between groups was analyzed by one-way ANOVA. The LSD-t test was used to compare the two groups. Dunnett's T3 test was performed on the variance, and the difference was statistically significant at $P < 0.05$.

RESULT

Characterization of FGF1-nlip

Observation of blank nanoliposomes and FGF1-nlip by transmission electron microscopy showed that the particle size distribution of the two was uniform, some adhesions existed, and the lipid bilayers were visible in the spherical shape (**Figure 1**). The average particle size of liposomes and FGF1-loaded liposomes was determined by the dynamic light scattering method to be 68.24 ± 1.61 nm and 96.23 ± 6.56 nm, respectively. The polydispersity index of the particle size was 0.092 ± 0.04 and 0.143 ± 0.02, respectively. Zeta potential measurements showed that the zeta potentials of the blank and drug-loaded liposomes were −1.885 ± 0.075 and −3.06 ± 0.01 mV, respectively. Further, the encapsulation efficiency measurement showed that the encapsulation efficiency of the FGF1 liposome was 73.52 ± 3.25%.

General Condition of Experimental Rats

After 12 weeks of intervention, 4 rats in the DM model group and in the FGF1-nlip group died, 3 rats in the FGF1 solution group and the FGF1-nlip+UTMD group died, and no rats in the normal control group died. The number of rats in each group was 9 in the DM model group, 10 in the FGF1 solution group, 9 in the FGF1-nlip group, 10 in the FGF1-nlip+UTMD group, and 14 in the normal control group.

Echocardiography Evaluation

Before intervention, there was no significant difference in LVEF and LVFS between the rats in each group ($P > 0.05$). After 12 weeks of intervention, the LVEF and LVFS in the DM model group were significantly lower than those in the normal control group ($P < 0.05$). Compared with the DM model group, the LVEF and LVFS of the FGF1 intervention group were significantly increased; compared

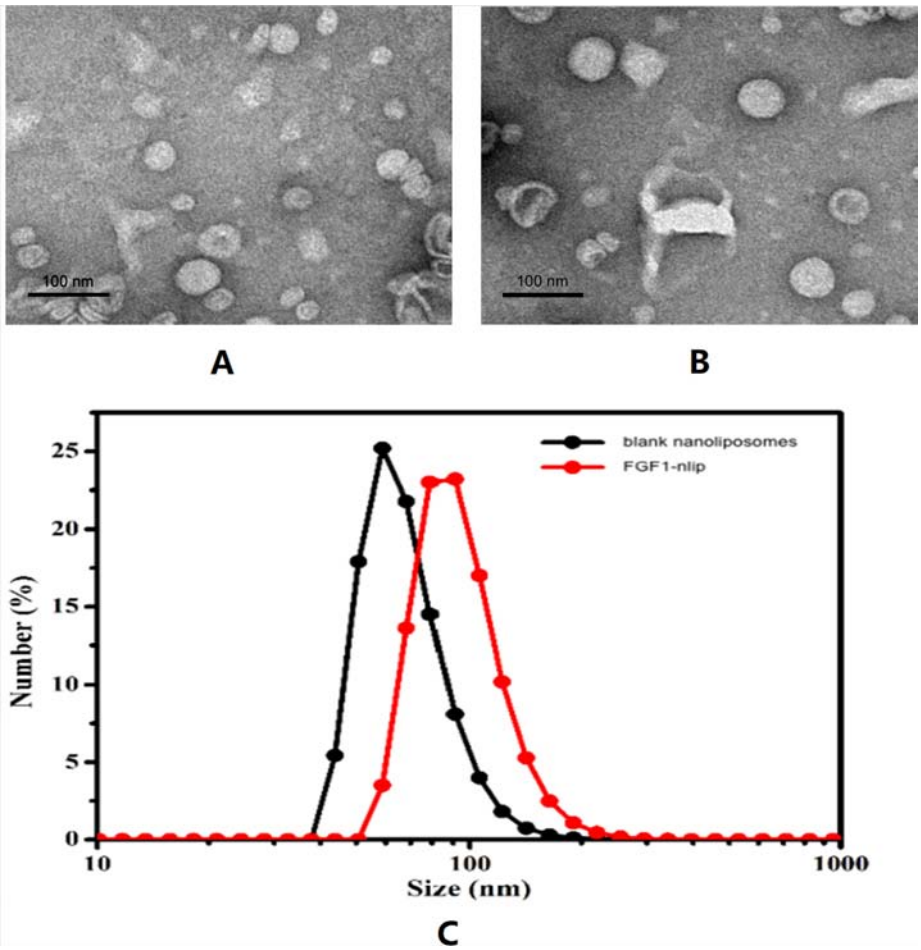

FIGURE 1 | Transmission electron micrographs of blank nanoliposomes **(A)**, FGF1-nlip **(B)**, and the size distribution of blank nanoliposomes and FGF1-nlip **(C)**.

with the other intervention groups, the rats in the FGF1-nlip +UTMD group were significantly increased ($P < 0.05$) (**Table 1**).

VVI Evaluation

As shown in **Figure 2**, the myocardial velocity, radial strain, and strain rate curves of 6 segments were obtained automatically by software. Before the intervention, there was no significant difference in Vs, Sr, and SRr among the groups ($P > 0.05$). After 12 weeks of intervention, Vs, Sr, and SRr in the DM model group were significantly lower than those in the normal control group ($P < 0.05$); Vs, Sr, and Sr in the FGF1 solution group, FGF1-nlip group, and FGF1-nlip+UTMD group were significantly higher than those in the model group ($P < 0.05$); those in the FGF1-nlip+UTMD group were higher than those in the other intervention groups ($P < 0.05$) (**Table 2**).

MCE Evaluation

Figure 3 shows the average acoustic intensity of the region of interest of each image frame. Before the experimental intervention, there was no significant difference in A, β, and A × β between the groups ($P > 0.05$). After 12 weeks of intervention, A, β, and A × β in the DM model group were significantly lower than those in the normal control group ($P < 0.05$). Compared with the DM model group, the FGF1 solution group and the FGF1-nlip group A and A × β were significantly increased ($P < 0.05$). Although there was an increasing trend of β, the difference was not statistically significant ($P > 0.05$), while the FGF1-nlip+UTMD group A, β, and A×β were significantly increased ($P < 0.05$); compared with the FGF1 solution group and FGF1-nlip group, the FGF1-nlip+UTMD group A and A × β were significantly increased ($P < 0.05$), and β increased slightly ($P > 0.05$) (**Table 3**).

Hemodynamic Analysis

After 12 weeks of intervention, the LVESP, +dp/dtmax, and −dp/dtmax in the DM model group were significantly lower than those in the normal control group ($P < 0.05$), and LVEDP was significantly higher than that in the normal control group ($P < 0.05$). LVESP, +dp/dtmax, and −dp/dtmax in the FGF1 intervention groups were significantly higher than those in the DM model group ($P < 0.05$), and the levels were significantly lower than those in the model group ($P < 0.05$). The LVESP, +dp/dtmax, and −dp/dtmax in the FGF1-nlip +UTMD group were significantly higher than those in other FGF1 intervention groups ($P < 0.05$), and the LVEDP in the FGF1-nlip

TABLE 1 | Results of LVEF and LVFS (mean ± SD).

Group	n		LVEF(%)		LVFS(%)	
	Before intervention	After intervention	Before intervention	After intervention	Before intervention	After intervention
Normal control	14	14	82.87 ± 3.88	84.27 ± 2.80	46.19 ± 4.40	48.16 ± 3.18
DM model	13	9	83.51 ± 3.15	71.85 ± 2.78[a]	46.98 ± 3.72	36.21 ± 2.19[a]
FGF1 solution	13	10	83.87 ± 3.66	76.56 ± 3.95[bc]	47.31 ± 4.26	40.32 ± 3.41[bc]
FGF1-nlip	13	9	82.69 ± 4.24	77.09 ± 2.86[bc]	46.09 ± 4.87	40.80 ± 2.54[bc]
FGF1-nlip+UTMD	13	10	84.07 ± 3.41	80.87 ± 2.97[b]	47.51 ± 4.07	44.35 ± 3.05[b]

LVEF, left ventricular ejection fraction; LVFS, left ventricular fraction shortening. Data are Mean ± SD.
[a]*P < 0.05 vs the normal control group.*
[b]*P < 0.05 vs DM model group.*
[c]*P < 0.05 vs FGF1-nlip+UTMD group.*

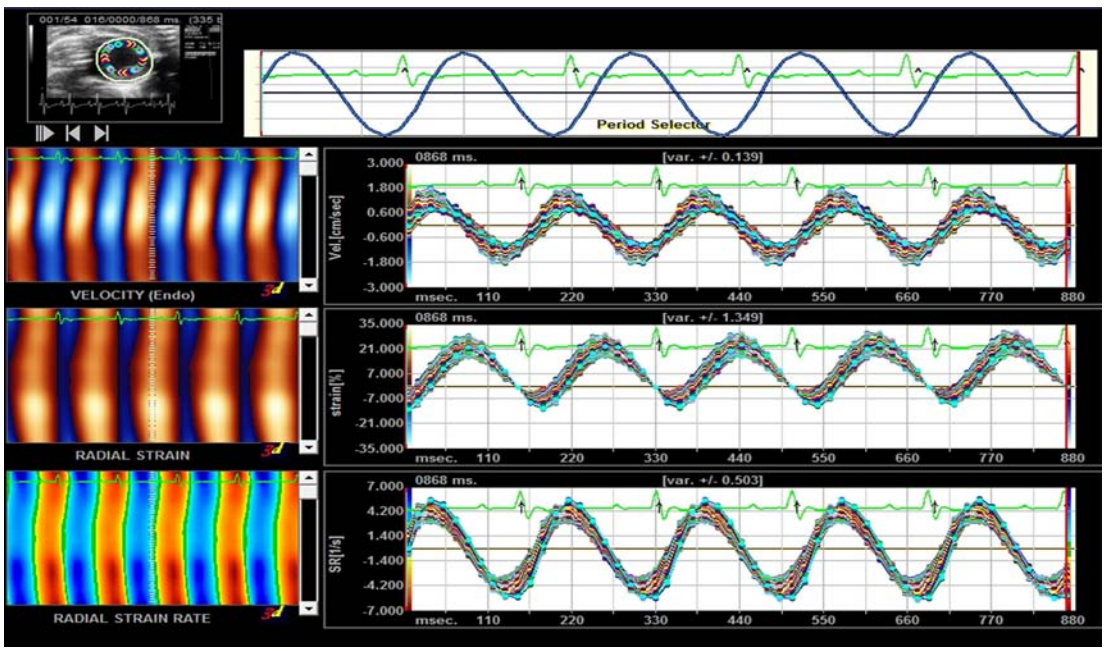

FIGURE 2 | Representative picture of the myocardial velocity, radical strain, and radical strain rate curve provided by Sygno VVI.

TABLE 2 | Results of peak velocity, radical strain, and radical strain rate in the control and study groups (mean ± SD).

Group	n		Vs(cm/s)		Sr(%)		SRr(1/s)	
	Before intervention	After intervention	Before intervention	After intervention	Before intervention	After intervention	Before intervention	After intervention
Normal control	14	14	1.082 ± 0.081	1.106 ± 0.061	21.77 ± 1.72	22.43 ± 1.67	3.41 ± 0.24	3.37 ± 0.22
DM model	13	9	1.107 ± 0.063	0.751 ± 0.060[a]	21.49 ± 1.98	12.18 ± 1.32[a]	3.36 ± 0.27	1.73 ± 0.09[a]
FGF1 solution	13	10	1.111 ± 0.069	0.843 ± 0.052[bc]	22.08 ± 1.82	14.17 ± 1.01[bc]	3.31 ± 0.25	2.16 ± 0.19[bc]
FGF1-nlip	13	9	1.093 ± 0.058	0.858 ± 0.059[bc]	21.99 ± 1.71	14.66 ± 1.23[bc]	3.34 ± 0.29	2.23 ± 0.23[bc]
FGF1-nlip +UTMD	13	10	1.079 ± 0.082	0.968 ± 0.054[b]	22.55 ± 2.19	17.56 ± 1.06[b]	3.30 ± 0.24	2.80 ± 0.15[b]

Vs = systolic peak velocity; Sr = radial peak strain; SRr = radial peak strain rate.
[a]*P < 0.05 vs the normal control group.*
[b]*P < 0.05 vs DM model group.*
[c]*P < 0.05 vs FGF1-nlip+UTMD group.*

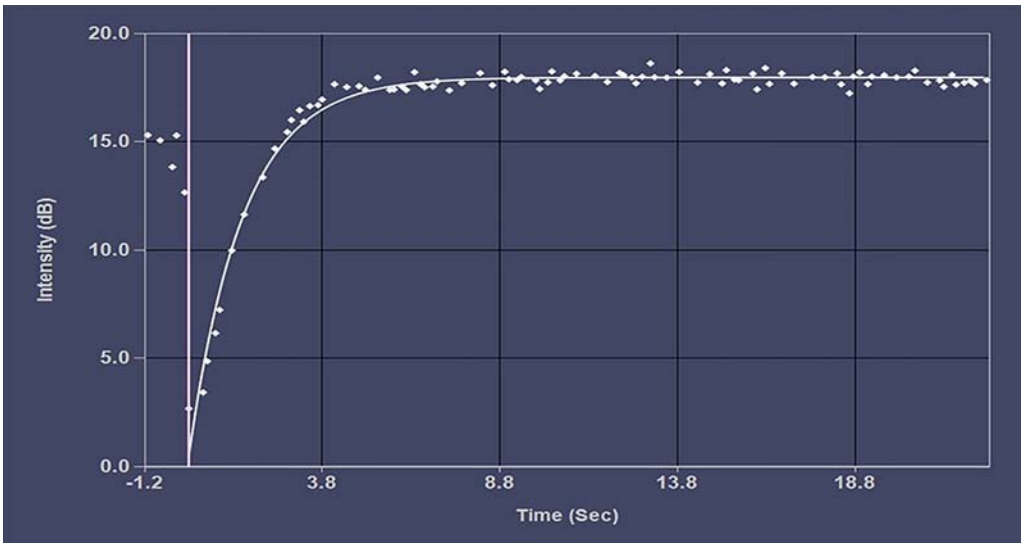

FIGURE 3 | Representative picture of the time-intensity curve.

+UTMD group was significantly lower than that in the other FGF1 intervention groups ($P < 0.05$) (**Table 4**).

Myocardial Capillary Density

CD31 immunohistochemical staining showed that the vascular endothelial cells were brown. The MVD of myocardial tissue in the DM model group was significantly lower than that in the normal control group ($P < 0.05$). The MVD in each FGF1 intervention group was significantly higher than that in the DM model group ($P < 0.05$). The MVD in the FGF1-nlip +UTMD group was significantly higher than that in the other FGF1 intervention groups ($P < 0.05$) (**Figure 4**).

Electron Microscopic Findings

As shown in **Figure 5**, compared with the normal group, in the DM model group after 12 weeks, the Z line of cardiac muscle and myocutaneous fibers was arranged in a disordered manner, partly ruptured, with swollen aggregated mitochondria, and some vacuoles appeared. However, after 12 weeks of various forms of FGF1 prevention, the ultrastructure of the heart improved, especially in the fibrous filamentts and muscle fibers of the heart of rats in the FGF1-nlip+UTMD group, which were arranged neatly, and most of the mitochondria were normal. The results showed that the myocardial ultrastructure of DM rats was improved after different forms of FGF1 prevention, but compared with other forms of prevention, FGF1-nlip combined with UTMD technology had the most obvious preventive effect.

DISCUSSION

In this study, the rat model of DM was established by intraperitoneal injection of STZ. Routine echocardiography, the VVI technique, and RT-MCE were performed before drug intervention. No significant difference was found in cardiac function and the blood perfusion index among each group. After 12 weeks of feeding, DM rats underwent routine echocardiography, VVI, and cardiac catheterization techniques. The results showed that the LVEF, LVFS, and VVI indexes (Vs, Sr, and SRr), LVESP, and ± dp/

TABLE 3 | Results of A, β and A×β in the control and study groups (mean ± SD).

Group	n		A(dB)		β(s^{-1})		A×β(dB/s)	
	Before intervention	After intervention	Before intervention	After intervention	Before intervention	After intervention	Before intervention	After intervention
Normal control	14	14	25.24 ± 2.15	25.81 ± 2.80	0.81 ± 0.07	0.82 ± 0.07	20.42 ± 2.49	21.05 ± 3.16
DM model	13	9	24.96 ± 2.55	17.49 ± 1.68[a]	0.80 ± 0.05	0.71 ± 0.05[a]	20.07 ± 2.65	12.33 ± 1.73[a]
FGF1 solution	13	10	24.26 ± 2.37	19.81 ± 2.26[bc]	0.79 ± 0.05	0.74 ± 0.06	19.28 ± 2.27	14.63 ± 1.67[bc]
FGF1-nlip	13	9	25.52 ± 2.08	20.23 ± 1.87[bc]	0.81 ± 0.06	0.75 ± 0.05	20.60 ± 2.37	15.14 ± 2.07[bc]
FGF1-nlip +UTMD	13	10	24.67 ± 3.01	23.07 ± 2.31[b]	0.82 ± 0.07	0.78 ± 0.04[b]	20.35 ± 3.31	17.94 ± 1.53[b]

A = peak acoustic intensity; β = contrast agent perfusion rate; A×β = myocardial blood flow

[a]$P < 0.05$ *vs the normal control group.*

[b]$P < 0.05$ *vs DM model group.*

[c]$P < 0.05$ *vs FGF1-nlip+UTMD group.*

TABLE 4 | The hemodynamic data in the *in vivo* experiment (mean ± SD).

Group	n	LVESP(mmHg)	LVEDP(mmHg)	+dp/dtmax(mmHg)	-dp/dtmax(mmHg)
Normal control	14	99.36 ± 7.46	3.17 ± 0.34	4926.79 ± 397.06	4438.64 ± 217.22
DM model	9	70.22 ± 5.29[a]	7.28 ± 0.51[a]	2967.33 ± 236.10[a]	2900.67 ± 151.77[a]
FGF1 solution	10	77.90 ± 5.08[bc]	6.03 ± 0.46[bc]	3682.90 ± 225.39[bc]	3373.90 ± 314.15[bc]
FGF1-nlip	9	79.67 ± 4.48[bc]	6.01 ± 0.67[bc]	3726.22 ± 251.26[bc]	3404.11 ± 226.63[bc]
FGF1-nlip+UTMD	10	88.70 ± 6.27[b]	4.83 ± 0.53[b]	4126.5 ± 340.45[b]	3835.30 ± 275.59[b]

Note : LVESP = left ventricular systolic pressure; LVEDP = left ventricular end diastolic pressure; ± dp/dt max = maximum rate of the rise and fall of left ventricular pressure.
[a]P< *0.05 vs the normal control group.*
[b]P< *0.05 vs DM model group.*
[c]P< *0.05 vs FGF1-nlip+UTMD group.*

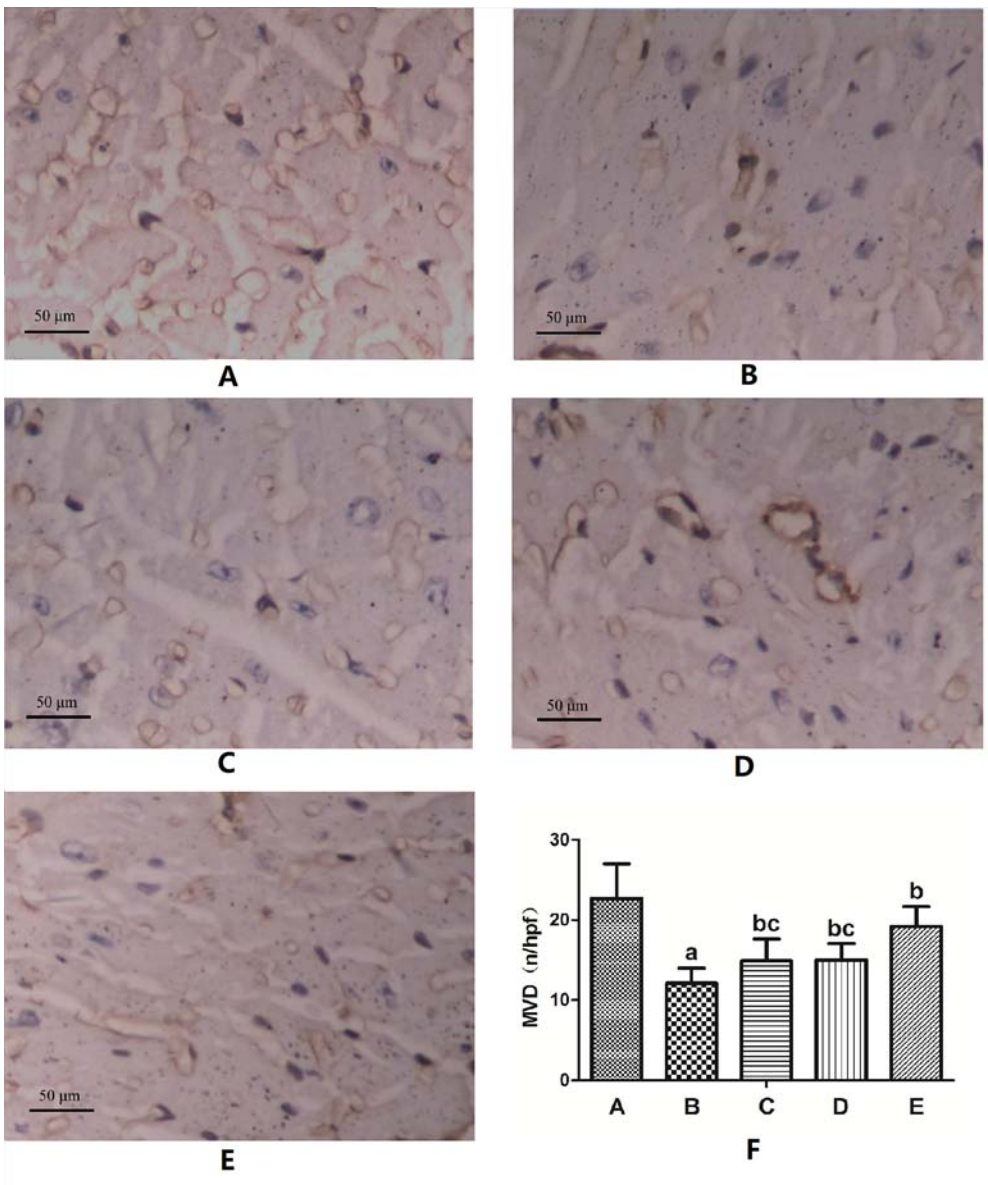

FIGURE 4 | Representative images of CD31 immunohistochemical staining of MVD and the semi-quantitative analysis for all groups (400×) **(A)** Normal control group; **(B)** DM model group; **(C)** FGF1 solution group; **(D)** FGF1-nlip group; **(E)** FGF1-nlip+UTMD group; **(F)** Statistical histogram. [a]P < 0.05 vs the normal control group, [b]P < 0.05 vs the DM model group, [c]P < 0.05 vs the FGF1-nlip+UTMD group).

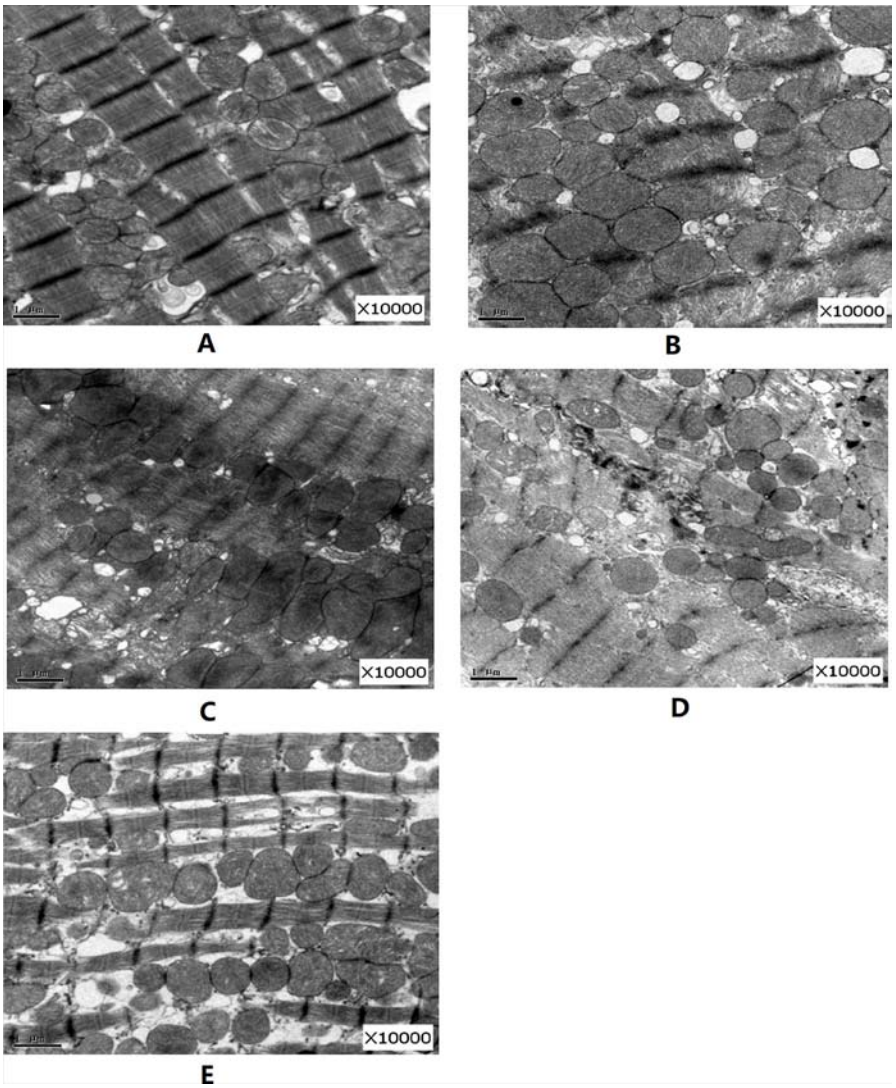

FIGURE 5 | Representative pictures of electron micrographs (magnification 10000×) of left ventricular heart muscle sections from the rats of each group **(A)** normal control group; **(B)** DM model group; **(C)** FGF1 solution; **(D)** FGF1-nlip group; **(E)** FGF1-nlip+UTMD group)].

dtmax in the DM model group were significantly lower than those in the normal control group ($P < 0.05$), while LVESP in the DM model group was higher than those in the normal control group ($P < 0.05$). RT-MCE showed that A, β, and A × β in the DM model group were significantly lower than those in the control group. This indicated that obvious abnormalities in left ventricular systolic function and blood flow perfusion appeared in DM rats at the end of 12 weeks. Histological observation also confirmed that the MVD value of myocardial tissue in DM rats was significantly lower than that in the control group, and there were pathological changes such as disordered filament arrangement, mitochondrial swelling and degeneration. Therefore, it is very important to prevent the occurrence of DCM by intervening before the obvious pathological changes in myocardium in DM rats.

FGF1 is a type of cell growth factor with many biological activities. It has a high affinity for heparin. FGF1 can promote the proliferation of vascular endothelial cells and smooth muscle cells, thereby promoting angiogenesis, alleviating myocardial ischemia, and improving cardiac function (Cochain et al., 2013; Zhang et al., 2016). In previous studies, in various animal models of myocardial ischemia or infarction, FGF1 increased the regional myocardial blood flow and the density of capillaries and arterioles and improved ventricular function (Zhao et al., 2012). Other studies have shown that non-mitotic FGF1 can prevent DCM (Zhang et al., 2013) by inhibiting oxidative stress and injury. Therefore, FGF1 is a potentially valuable therapeutic agent for the prevention and treatment of DCM.

In order to increase the stability of the drug, the reverse phase evaporation method (Yue et al., 2014; Mehrabi et al., 2016) was used to prepare nanoliposomes encapsulated with FGF1. Through the analysis of its characteristics, it was confirmed that the drug-loaded lipids had a round appearance, small particle size (<100 nm), good

dispersion (polydispersity index < 0.15), and a certain Zeta potential, which could maintain good stability (**Figure 1**). Compared with traditional liposome preparation technology, the method adopted in this study has a shorter preparation time, and the average temperature of the whole preparation process is controlled below 25°C, which can maintain the biological activity of protein drugs to a great extent. This shows that the preparation method can efficiently achieve the inclusion of FGF1 and is suitable for *in vivo* application. In order to increase the local concentration of FGF1 in the heart, exert the therapeutic effects to a greater extent, and reduce the influence on the whole body (e.g., liver, spleen, and kidney), this study injected FGF1-nlip mixed with SonoVue microbubbles into DM rats *via* the caudal vein. After myocardial development, UTMD was used to explode microbubbles to increase the dose of FGF1-nlip released into the myocardium and exert its corresponding biological effects.

After 12 weeks of intervention, routine echocardiography and VVI (**Tables 1**–**2**) showed that LVEF, LVFS, and VVI (Vs, Sr, and SRr) in the FGF1 intervention group were significantly higher than those in the DM model group ($P < 0.05$), while LVEF, LVFS, and VVI (Vs, Sr, and SRr) in the FGF1-nlip +UTMD group were significantly higher than those in the other FGF1 intervention groups ($P < 0.05$), which was confirmed by hemodynamic studies (**Table 4**). The results showed that the FGF1-nlip+UTMD group had the least damage to left ventricular systolic function in DM rats. In addition, the ultrastructural changes of the FGF1-nlip+UTMD group were the least. Therefore, this method can be used as an effective strategy to prevent the deterioration of cardiac function in DM rats.

The results of RT-MCE in this study (**Table 3**) showed that after 12 weeks of intervention, the levels of A and $A \times \beta$ in the FGF1 solution group and FGF1-nlip group were significantly higher than those in the DM model group ($P < 0.05$), while the levels of A, β, and $A \times \beta$ in the FGF1-nlip+UTMD group were significantly higher than those in the DM model group ($P < 0.05$), and A and $A \times \beta$ were significantly higher than those in the other FGF1 intervention groups. To improve myocardial microcirculation, the application of FGF1-nlip combined with UTMD has the best preventive effect. This was confirmed by CD31 immunohistochemical assay (**Figure 4**).

In addition, there was no significant difference in left ventricular function and blood perfusion between the FGF1 solution group and the FGF1-nlip group. The reason is that the drug encapsulated by liposomes alone lacks targeting ability and is easily captured by the reticuloendothelial system *in vivo* (Ishihara et al., 2012; Hsu et al., 2014). It is difficult to maximize the efficacy of the drug in cardiac aggregation. Combined with UTMD, the cavitation effect and mechanical action produced by the instantaneous blasting of ultrasound microbubbles can cause temporary open pores (Chen et al., 2013; Qian et al., 2018; Zhao et al., 2018) on the endothelial cell membrane and capillaries of the myocardium. The target delivery of FGF1-nlip to the myocardium can realize the rapid release of the target and rapid penetration, thus realizing the myocardial transmission of FGF1 and exerting its biological function.

In the present study, although each intervention group had a significant improvement in cardiac function, the survival rate was lower than that in the normal control group. The cause of death in rats is related to the deterioration of the physical condition of rats caused by diabetes injury, and may be related to the influence of anesthetic drugs. Because the animals could not cooperate effectively, the rats in the intervention group had higher requirements for anesthesia depth to ensure the stability and effectiveness of the intervention. The normal control group did not undergo relevant intervention, so there was no death.

In conclusion, the application of FGF1-nlip combined with UTMD technology can efficiently deliver FGF1 to the heart of DM rats and prevent abnormal left ventricular systolic function and myocardial perfusion in DM rats. The changes in left ventricular systolic function and blood perfusion in DM rats can be detected by VVI and RT-MCE technology, which provides a more effective basis for the evaluation of DCM therapeutic effects.

The limitations of this study are as follows: First, UTMD technology is used to promote the entry of FGF1-nlip into cells, thus causing a certain degree of damage to cells. It is necessary to further optimize the parameters of ultrasound irradiation for local release of the highest drug concentration in the case of minimal tissue damage. Second, because the pathogenesis of DCM is complex and the effect of FGF1 alone is limited, whether it is necessary to combine other drugs to improve the efficacy needs further study.

DATA AVAILABILITY STATEMENT

All datasets generated for this study are included in the article/ supplementary material.

ETHICS STATEMENT

The animal study was reviewed and approved by the Animal Ethics Committee of Wenzhou Medical University.

AUTHOR CONTRIBUTIONS

LZ: Overall experimental design, data analysis, paper writing. C-LS: Acquisition and analysis of ultrasound Image of animals. J-ML: Histopathological detection and analysis, wzyxyljmin@163.com. Y-LM: Feeding of experimental animals, imayulei@163.com. NY: Pharmaceutical intervention in laboratory animals. X-QT: Research overall guidance, paper revision, funding support. Y-ZZ: Preparation of nanoliposomes, revision of papers, financial support.

FUNDING

This research was supported by the Chinese National Natural Science Funds (Grant No. 81571696, U1704175), Medicine Grant from Wenzhou Bureau of Science and Technology (Y20170049), Key Research and Development Program of Zhejiang province (Grant No. 2018C03013).

REFERENCES

Abu, L. A. S., and Ishida, T. (2017). Liposomal delivery systems: design optimization and current applications. *Biol. Pharm. Bull.* 40 (1), 1–10.. doi: 10.1248/bpb.b16-00624

Atta, M. S., El-Far, A. H., Farrag, F. A., Abdel-Daim, M. M., Al, J. S. K., and Mousa, S. A. (2018). Thymoquinone attenuates cardiomyopathy in streptozotocin-treated diabetic rats. *Oxid. Med. Cell Longev.* 2018, 7845681. doi: 10.1155/2018/7845681

Azam, S., Desjardins, C. L., Schluchter, M., Liner, A., Stelzer, J. E., Yu, X., et al. (2012). Comparison of velocity vector imaging echocardiography with magnetic resonance imaging in mouse models of cardiomyopathy. *Circ. Cardiovasc. Imaging* 5 (6), 776–781. doi: 10.1161/CIRCIMAGING.111.972406

Beenken, A., and Mohammadi, M. (2009). The FGF family: biology, pathophysiology and therapy. *Nat. Rev. Drug Discovery* 8 (3), 235–253. doi: 10.1038/nrd2792

Borghetti, G., von, L. D., Eaton, D. M., Sourij, H., Houser, S. R., and Wallner, M. (2018). Diabetic cardiomyopathy: current and future therapies. beyond glycemic control. *Front. Physiol.* 9, 1514. doi: 10.3389/fphys.2018.01514

Chen, B. H., and Stephen, I. B. (2019). Nanoemulsion and Nanoliposome Based Strategies for Improving Anthocyanin Stability and Bioavailability. *Nutrients* 11 (5), E1052. doi: 10.3390/nu11051052

Chen, Z. Y., Yang, F., Lin, Y., Zhang, J. S., Qiu, R. X., Jiang, L., et al. (2013). New development and application of ultrasound targeted microbubble destruction in gene therapy and drug delivery. *Curr. Gene Ther.* 13 (4), 250–274. doi: 10.2174/15665232113139990003

Chen, P. P., Xu, H. L., Ting-Yue, Y, ZhuGe, D L., Jin, B. H., Zhu, Q. Y., et al. (2018). CoQ10-loaded liposomes combined with UTMD prevented early nephropathy of diabetic rats. *Oncotarget* 9 (14), 11767–11782. doi: 10.18632/oncotarget.24363

Cho, N. H., Shaw, J. E., Karuranga, S., Huang, Y., da, R. F. J. D., Ohlrogge, A. W., et al. (2018). IDF Diabetes Atlas: Global estimates of diabetes prevalence for 2017 and projections for 2045. *Diabetes Res. Clin. Pract.* 138, 271–281. doi: 10.1016/j.diabres.2018.02.023

Cochain, C., Channon, K. M., and Silvestre, J. S. (2013). Angiogenesis in the infarcted myocardium[J]. *Antioxid. Redox Signal* 18 (9), 1100–1113. doi: 10.1089/ars.2012.4849

Danijela, T., Jelena, D., Olga, P., and Zorana, V. P. (2018). Assessment of coronary microcirculation with myocardial contrast echocardiography. *Curr. Pharm. Des.* 24 (25), 2943–2949. doi: 10.2174/1381612824666180702115432

De Blasio, M. J., Huynh, K., Qin, C., Rosli, S., Kiriazis, H., Ayer, A., et al. (2015). Therapeutic targeting of oxidative stress with coenzyme Q10 counteracts exaggerated diabetic cardiomyopathy in a mouse model of diabetes with diminished PI3K(p110α) signaling. *Free Radic. Biol. Med.* 87, 137–147. doi: 10.1016/j.freeradbiomed.2015.04.028

Evangelista, I., Nuti, R., Picchioni, T., Dotta, F., and Palazzuoli, A. (2019). Molecular dysfunction and phenotypic derangement in diabetic cardiomyopathy. *Int. J. Mol. Sci.* 20 (13), E3264. doi: 10.3390/ijms20133264

Frenkel, V. (2008). Ultrasound mediated delivery of drugs and genes to solid tumors. *Adv. Drug Delivery Rev.* 60 (10), 1193–1208. doi: 10.1016/j.addr.2008.03.007

Geng, W., Zhang, Q., Liu, J., Tian, X., Zhen, L., Song, D., et al. (2018). A randomized study of prourokinase during primary percutaneous coronary intervention in acute ST-segment elevation myocardial infarction. *J. Interv. Cardiol.* 31 (2), 136–143. doi: 10.1111/joic.12461

Gulsin, G. S., Athithan, L., and McCann, G. P. (2019). Diabetic cardiomyopathy: prevalence, determinants and potential treatments. *Ther. Adv. Endocrinol. Metab.* 10, 2042018819834869. doi: 10.1177/2042018819834869

Hsu, W. H., Liu, S. Y., Chang, Y. J., Chang, C. H., Ting, G., and Lee, T. W. (2014). The PEGylated liposomal doxorubicin improves the delivery and therapeutic efficiency of 188Re-Liposome by modulating phagocytosis in C26 murine colon carcinoma tumor model[J]. *Nucl. Med. Biol.* 41 (9), 765–771. doi: 10.1016/j.nucmedbio.2014.05.142

Ishihara, A., Yamauchi, M., Tsuchiya, T., Mimura, Y., Tomoda, Y., Katagiri, A., et al. (2012). A novel liposome surface modification agent that prolongs blood circulation and retains surface ligand reactivity[J]. *J. Biomater Sci. Polym. Ed.* 23 (16), 2055–2068. doi: 10.1163/092050611X605933

Itoh, N., and Ornitz, D. M. (2011). Fibroblast growth factors: from molecular evolution to roles in development, metabolism and disease. *J. Biochem.* 149 (2), 121–130. doi: 10.1093/jb/mvq121

Jiang, L., Yao, H., and Liang, Z. G. (2017). Postoperative assessment of myocardial function and microcirculation in patients with acute coronary syndrome by myocardial contrast echocardiography. *Med. Sci. Monit.* 23, 2324–2332. doi: 10.12659/msm.901233

Kapoor, M., Lee, SL, and Tyner, K. M. (2017). Liposomal drug product development and quality: current US experience and perspective. *AAPS J.* 19 (3), 632–641. doi: 10.1208/s12248-017-0049-9

Li, P., Meng, H., Liu, S. Z., and Vannan, M. A. (2012). Quantification of left ventricular mechanics using vector-velocity imaging, a novel feature tracking algorithm, applied to echocardiography and cardiac magnetic resonance imaging. *Chin Med. J. (Engl)* 125 (15), 2719–2727.

Li, X. (2019). The FGF metabolic axis[J]. *Front. Med.* 13 (5), 511–530. doi: 10.1007/s11684-019-0711-y

Liang, X., Wu, B., Shang, H., Han, X., Jing, H., Sun, Y., et al. (2018). VTIQ evaluates antitumor effects of NET-1 siRNA by UTMD in HCC xenograft models. *Oncol. Lett.* 16 (3), 2893–2902. doi: 10.3892/ol.2018.8994

Lin, L., Fan, Y., Gao, F., Jin, L., Li, D., Sun, W., et al. (2018). UTMD-Promoted Co-Delivery of Gemcitabine and miR-21 Inhibitor by Dendrimer-Entrapped Gold Nanoparticles for Pancreatic Cancer Therapy. *Theranostics* 8 (7), 1923–1939. doi: 10.7150/thno.22834

Mehrabi, M., Esmaeilpour, P., Akbarzadeh, A., Saffari, Z., Farahnak, M., Farhangi, A., et al. (2016). Efficacy of pegylated liposomal etoposide nanoparticles on breast cancer cell lines. *Turk J. Med. Sci.* 46 (2), 567–571. doi: 10.3906/sag-1412-67

Parim, B., Sathibabu, U. V. V., and Saravanan, G. (2019). Diabetic cardiomyopathy: molecular mechanisms, detrimental effects of conventional treatment, and beneficial effects of natural therapy. *Heart Fail Rev.* 24 (2), 279–299. doi: 10.1007/s10741-018-9749-1

Pena, A. M., Chen, S., Feng, B., Cai, L., Li, X., Liang, G., et al. (2017). Prevention of diabetic nephropathy by modified acidic fibroblast growth factor[J]. *Nephron* 137 (3), 221–236. doi: 10.1159/000478745

Qian, L., Thapa, B., Hong, J., Zhang, Y., Zhu, M., Chu, M., et al. (2018). The present and future role of ultrasound targeted microbubble destruction in preclinical studies of cardiac gene therapy. *J. Thorac. Dis.* 10 (2), 1099–1111. doi: 10.21037/jtd.2018.01.101

Rubler, S., Dlugash, J., Yuceoglu, Y. Z., Kumral, T., Branwood, A. W., and Grishman, A.. (1972). New type of cardiomyopathy associated with diabetic glomerulosclerosis. *Am. J. Cardiol.* 30 (6), 595–602. doi: 10.1016/0002-9149(72)90595-4

Tsai, M. J., Tsai, S. K., Huang, M. C., Liou, D. Y., Huang, S. L., Hsieh, W. H., et al. (2015). Acidic FGF promotes neurite outgrowth of cortical neurons and improves neuroprotective effect in a cerebral ischemic rat model[J]. *Neuroscience* 305, 238–247. doi: 10.1016/j.neuroscience.2015.07.074

Wei, Z., Zhang, H., Su, H., Zhu, T., Zhu, Y., and Zhang, J. (2012). Correlation between myocardial dysfunction and perfusion impairment in diabetic rats with velocity vector imaging and myocardial contrast echocardiography. *Echocardiography* 29 (10), 1247–1255. doi: 10.1111/j.1540-8175.2012.01796.x

Xu, J., Min, D., Guo, G., Liao, X., and Fu, Z.. (2018). Experimental study of epidermal growth factor and acidic fibroblast growth factor in the treatment of diabetic foot wounds[J]. *Exp. Ther. Med.* 15 (6), 5365–5370. doi: 10.3892/etm.2018.6131

Yang, H., Sun, Y., Wei, J., Xu, L., Tang, Y., Yang, Y., et al. (2019). The effects of ultrasound-targeted microbubble destruction (UTMD) carrying IL-8 monoclonal antibody on the inflammatory responses and stability of atherosclerotic plaques. *BioMed. Pharmacother.* 118, 109161. doi: 10.1016/j.biopha.2019.109161

Yue, P. J., He, L., Qiu, S. W., Li, Y., Liao, Y. J., Li, X. P., et al. (2014). OX26/CTX-conjugated PEGylated liposome as a dual-targeting gene delivery system for brain glioma[J]. *Mol. Cancer* 13, 191. doi: 10.1186/1476-4598-13-191

Zamora, M., and Villena, J. A. (2019). Contribution of impaired insulin signaling to the pathogenesis of diabetic cardiomyopathy. *Int. J. Mol. Sci.* 20 (11), E2833. doi: 10.3390/ijms20112833

Zhang, C., Zhang, L., Chen, S., Feng, B., Lu, X., Bai, Y., et al. (2013). The prevention of diabetic cardiomyopathy by non-mitogenic acidic fibroblast

growth factor is probably mediated by the suppression of oxidative stress and damage. *PloS One* 8 (12), e82287. doi: 10.1371/journal.pone.0082287

Zhang, M., Yu, W. Z., Shen, X. T., Xiang, Q., Xu, J, Yang, J. J., et al. (2016). Advanced interfere treatment of diabetic cardiomyopathy rats by aFGF-loaded heparin-modified microbubbles and UTMD technique[J]. *Cardiovasc. Drugs Ther.* 30 (3), 247–261. doi: 10.1007/s10557-016-6639-4

Zhao, Y. Z., Lu, C. T., Li, X. K., Tang, Q. Q., Tian, X. Q., Zhao, Y. P., et al. (2012). Improving the cardio protective effect of aFGF in ischemic myocardium with ultrasound-mediated cavitation of heparin modified microbubbles: preliminary experiment[J]. *J. Drug Target* 20 (7), 623–631. doi: 10.3109/1061186X.2012.702771

Zhao, Y. Z., Zhang, M., Wong, H. L., Tian, X. Q., Zheng, L., Yu, X. C., et al. (2016). Prevent diabetic cardiomyopathy in diabetic rats by combined therapy of FGF1-loaded nanoparticles and ultrasound-targeted microbubble destruction technique. *J. Control Release* 223, 11–21. doi: 10.1016/j.jconrel.2015.12.030

Zhao, R., Jiang, J., Li, H., Chen, M., Liu, R., Sun, S., et al. (2018). Phosphatidylserine-microbubble targeting-activated microglia/macrophage in inflammation combined with ultrasound for breaking through the blood-brain barrier. *J. Neuroinflamm.* 15 (1), 334. doi: 10.1186/s12974-018-1368-1

Zhou, J., Pu, D. R., Tian, L. Q., Tong, H., Liu, H. Y., Tan, Y., et al. (2015). Noninvasive assessment of myocardial mechanics of the left ventricle in rabbits using velocity vector imaging. *Med. Sci. Monit. Basic Res.* 21, 109–115. doi: 10.12659/MSMBR.894053

Conflict of Interest: The authors declare that the research was conducted in the absence of any commercial or financial relationships that could be construed as a potential conflict of interest.

frontiers in Pharmacology

ORIGINAL RESEARCH
published: 10 January 2020
doi: 10.3389/fphar.2019.01533

Compound 15c, a Novel Dual Inhibitor of EGFR$^{L858R/T790M}$ and FGFR1, Efficiently Overcomes Epidermal Growth Factor Receptor-Tyrosine Kinase Inhibitor Resistance of Non-Small-Cell Lung Cancers

Gaozhi Chen[1,2†], Yuyan Bao[3†], Qiaoyou Weng[4], Yingxin Zhao[1], Xiaoyao Lu[1], Lili Fu[1], Lingfeng Chen[1], Zhiguo Liu[1], Xiaomin Zhang[3] and Guang Liang[1]*

[1] Chemical Biology Research Center, School of Pharmaceutical Sciences, Wenzhou Medical University, Wenzhou, China, [2] Engineering Laboratory of Zhejiang Province for Pharmaceutical Development of Growth Factors, Biomedical Collaborative Innovation Center of Wenzhou, Wenzhou, China, [3] Department of Pharmacy, Sanmen People's Hospital of Zhejiang, Sanmen, China, [4] Key Laboratory of Imaging Diagnosis and Minimally Invasive Intervention, The Fifth Affiliated Hospital of Wenzhou Medical University, Lishui, China

In the past decades, epidermal growth factor receptor-tyrosine kinase inhibitors (EGFR-TKIs) had been proved as an effective treatment strategy for the patients with EGFR-mutated non-small-cell lung cancer (NSCLC). However, the tolerance for the EGFR-TKI always occurred after continuous administration for a period of time and limiting the application of these drugs. Activation of FGFR1 signaling pathway was one of the important escape mechanisms for EGFR-TKI resistant in NSCLC. Here, a novel dual inhibitor of EGFR$^{L858R/T790M}$ and FGFR1, compound15c, was found and can efficiently overcame the EGFR-TKI resistance *via* its simultaneous inhibition of their kinase activities. Comparison with EGFR$^{L858R/T790M}$ and FGFR1 inhibitor treatment alone or combined revealed that the inhibition of EGFR$^{L858R/T790M}$ and FGFR1 activity by 15c was responsible for surmounting the intrinsic EGFR-TKI resistance in EGFR$^{L858R/T790M}$-mutated H1975 cells and the acquired resistance in Afatinib-tolerant PC9 cells (AFA-PC9). Flow Cytometry and Caspase3 activity analysis assay showed that 15c induced significant the early apoptosis of H1975 cells. Xenograft tumor formation in BALB/c mice induced by a H1975 cells was suppressed by 15c treatment, with no changes in animal body weight. Generally, 15c may act as a new-generation EGFR-TKI for the therapy of NSCLC patients suffering a resistance to current TKI.

Keywords: NSCLC, EGFR, FGFR1, drug resistance, kinase inhibitor

OPEN ACCESS

Edited by:
Zhouguang Wang,
Albert Einstein College of Medicine,
United States

Reviewed by:
Aiping Jiang,
Harvard University,
United States
Shuai Wu,
Wistar Institute,
United States

****Correspondence:***
Guang Liang
wzmcliangguang@163.com

[†]These authors have contributed equally to this work

Specialty section:
This article was submitted to Translational Pharmacology, a section of the journal Frontiers in Pharmacology

Received: *22 October 2019*
Accepted: *27 November 2019*
Published: *10 January 2020*

Citation:
Chen G, Bao Y, Weng Q, Zhao Y, Lu X, Fu L, Chen L, Liu Z, Zhang X and Liang G (2020) Compound 15c, a Novel Dual Inhibitor of EGFR$^{L858R/T790M}$ and FGFR1, Efficiently Overcomes Epidermal Growth Factor Receptor-Tyrosine Kinase Inhibitor Resistance of Non-Small-Cell Lung Cancers. Front. Pharmacol. 10:1533. doi: 10.3389/fphar.2019.01533

INTRODUCTION

In the past few decades, to improve therapeutic activity and selectivity while developing antitumor drugs is always a great challenge. By targeting the genetic differences of cancer cells, several molecule-targeting drugs, such as Afatinib and Gefitinib, had been approved by U.S. FDA and shown their promising therapeutic activity against various cancers (Cataldo et al., 2011; Hirsch and Bunn, 2012). However, the therapeutic strategies of "one drug-hits-one target-treats-one disease" still face significant challenges as the drug resistance (To et al., 2019; Wojtaszek et al., 2019). Recent studies suggested that targeting the multiple targets might be a practicable approach to ameliorate the therapeutic activity and selectivity, meanwhile preventing the drug resistance (To et al., 2019).

Among cancer-related deaths, lung cancer is the leading cause that contributed to 27% of cancer-related mortality (Quintanal-Villalonga et al., 2019) and almost 85% of lung cancers were identified as non-small cell lung cancer (NSCLC) (Chang, 2011). The high dynamic of epidermal growth factor receptor (EGFR), one of the classic receptor tyrosine kinase (RTK), in NSCLC (Hirsch et al., 2003) recommended it as an attractive target for the development of small-molecule tyrosine kinase inhibitors (TKIs) to treat with NSCLC. At the beginning, several first-generation EGFR-targeted TKIs, such as Erlotinib and Gefitinib, had been approved by U.S. FDA for the treatment of NSCLC patients that harbor activating mutations in the EGFR (L858R or delE746-A750) (Cohen et al., 2003; Cohen et al., 2005; Cataldo et al., 2011). However, resistance to those inhibitors can be acquired due to secondary mutations (Bean et al., 2007; Kuang et al., 2009). The most common secondary mutations in the EGFR is T790M at exon 20, which is named as "gatekeeper" mutation (Zhou et al., 2009). Subsequently, a series of second-generation and third-generation EGFR-TKIs had being developed to overcome the resistance, especially T790M-associated resistance (Riely, 2008; Niederst et al., 2015; Chen et al., 2017b). Unfortunately, tolerance still occurred as a second mechanism that activation of alternative pathways, such as cMet, IGF-1R, and FGFR (Kono et al., 2009). Unlike the widely reported cMet and IGF-1R, the FGFR-dependent signaling act as an escape mechanism for EGFR-TKI resistance still have long way to go (Kono et al., 2009).

Fibroblast growth factor receptors (FGFRs) are a family of RTKs with four different members (FGFR1–4), and each of the FGFR contain an extracellular immunoglobulin domains, a single transmembrane domain and an intercellular kinase domain (Li, 2019). Moreover, genetic abnormalities or aberrant activation of the FGFR signal transduction have been implicated with the pathogenesis of the various disease and disorders including cancer, Alzheimer's disease, diabetes and its complications (Ferrer and Marti, 1998; Gozgit et al., 2012; Harrison, 2012; Gallagher and LeRoith, 2013; Touat et al., 2015; Li, 2019). Among these receptors, FGFR1 amplification is identified in about 20% of NSCLC. In addition, Azuma et al., reported that the enhanced expression of FGFR1 conducted as an escape mechanism for cell survival of Afatinib-resistant cancer cells and may compensate the loss of EGFR-driven signaling pathway (Azuma et al., 2014). Further, Quintanal-Villalonga and his colleagues found that highly-expressed FGFR1 may result in a higher resistance to EGFR-TKI in the patients with EGFR-mutated lung cancer and those patients may benefit from combined EGFR/FGFR inhibition (Quintanal-Villalonga et al., 2019). Raoof and her colleagues performed whole-genome CRISPR screening and identified FGFR3 as the top target facilitating the survival of mesenchymal EGFR mutant cancers (Raoof et al., 2019). Therefore, dual EGFR-FGFR1 blockade may be a promising clinical strategy to overcome EGFR-mutated NSCLC.

Nowadays, drugs with polypharmacological activities are shown to be advantageous over combination therapy as their lower incidences of side effects and more resilient therapies (Anighoro et al., 2014). Thus, in the current study, we find that compound 15c, an $EGFR^{L858R/T790M}$ selective inhibitor in our previous study (Chen et al., 2017a), exhibited a dual inhibitory activity against $EGFR^{L858R/T790M}$ and FGFR1 and efficiently overcame the EGFR-TKI tolerance in EGFR-mutated NSCLC cells *via* concurrently inhibiting these two kinases activity. We suggest that 15c may act as a new-generation EGFR-TKI for the therapy of NSCLC patients suffering a resistance to current TKI.

MATERIALS AND METHODS

Cell Culture and Reagents

WZ4002 (#S1173) and AZD4547 (#S2801) were purchased from Selleck Chemicals. Human bronchial epithelial cell line BEAS-2B, human lung squamous cancer cell line H520, and human NSCLC cell lines H1975 and PC9 were procured from the Institute of Biochemistry and Cell Biology, Chinese Academy of Sciences and tested for mycoplasma contamination by DAPI staining before experiment. All the cells were maintained in RPMI-1640 medium (#C11875500BT, Gibco) with 10% FBS (#10270-106, Gibco), 100 μg/ml streptomycin, and 100 U/ml penicillin (#15140122, Gibco) and placed in a humidified cell incubator (5% CO_2, 37°C). Antibodies including anti-p-EGFR (#3777S), anti-p-FGFR1 (#2544S), anti-EGFR (#2646S), anti-FGFR (#9740S), anti-GAPDH (#5174S), and HRP-linked anti-rabbit IgG (#7074S) were purchased from Cell Signaling Technology (Danvers, MA, USA).

Kinase Inhibition Assay

The kinase inhibitory activities of candidate and positive inhibitors were tested *via* a Caliper Mobility Shift Assay. The difference between substrate and its phosphorylated product was detected to characterize the activity. Shortly, the reaction solution containing compounds, substrates, ATP, and enzymes was mixed well and transferred to a 384-well plate for the experiment. EDTA was introduced to terminate the process after incubate for 1h at room temperature. The data was collected on an EZ Reader II (Caliper Life Sciences, MA). The inhibitory rates of tested compounds were calculated depending on the negative control wells (without ATP) and positive control wells (without compounds). The recombinant kinases, including $EGFR^{WT}$ (#08-115), $EGFR^{L858R/T790M}$ (#08-510), and $FGFR1^{WT}$

(#08-133) were acquired from Carna Biosciences (Kobe, Japan). All the independent experiments were executed in duplicate and three times at six concentrations (0.001, 0.01, 0.1, 1, 10, and 100 μM) and IC_{50} value was calculated.

Anti-Proliferation Assay (MTS Assay)

All kinds of cells (4×10^3) were planted in 96-well plate and cultured overnight before examination. The protocol was formulated according to CellTiter 96® AQ_{ueous} One Solution Cell Proliferation Assay (MTS) Technical Bulletin. Briefly, after treated the cells with different compounds for 72 h, 20 μl CellTiter 96® AQ_{ueous} One Solution Reagent (MTS, #G3580, Promega, San Luis Obispo, CA) was added and the system was incubated for another 4 h at 37°C. The absorbance at 490 nm was recorded by using a microplate reader (SpectraMax M2, Molecular Devices, Sunnyvale, CA). The results of three independent assays were exhibited as IC_{50} value (mean ± SEM).

Western Blot Analysis

After treated with compounds, cells or tumor tissues were harvested and lysed in protein lysate buffer followed by centrifugation (12,000 rpm, 10 min, 4°C), supernatants were collected. The protein concentrations were measured using the Quick Start™ Bradford Protein Assay Kit (#5000201, Bio-Rad, Hercules, CA). Equivalent amount of protein samples were separated by 12% SDS-polyacrylamide gel (SDS-PAGE) and then transferred to PVDF membrane. The blotting was blocked with 5% nonfat milk at room temperature for 2 h and then incubated with primary antibody at 4°C for overnight. At last, anti-rabbit HRP-conjugated secondary antibody was added and incubated with membrane for 1 h. Between every two steps, the membrane will be washed with TBST for three times. The immune-reactive bands were detected *via* Clarity Max Western ECL Substrate Kit (#1705062, Bio-Rad, Hercules, CA). The density of the immune-reactive bands was analyzed by Image J (National Institute of Health, MD).

Cell Apoptosis Analysis

H1975 cells were seeded on 60-mm dishes for 12 h, and then treated with DMSO (vehicle), 15c (0.5, 2.5, 5, or 10 μM), WZ4002 (10μM), AZD4547 (10μM), or WZ4002 (10 μM) combined with AZD4547 (10 μM) for 24 h. After harvested and washed with PBS, cells were double stained with FITC Annexin V Apoptosis Detection Kit I (#556547, BD Biosciences, CA). The apoptosis were evaluated by using a FACSCalibur flow cytometer (BD Biosciences, CA).

Analysis of Caspase-3 Activity

The activity of Caspase-3 in H1975 cell lysates was detected by using a Caspase-3 Activity Kit (C1115, Beyotime Institute of Biotechnology, Nantong, China). The caspase-3 activity was normalized and calculated as percentage of control group.

Establishment of Afatinib-Resistant PC9 Cells

PC9 cells cultured in RPMI 1640 with 10% FBS were continuously exposed to Afatinib at the stepwise increased concentrations up to 1 μM over the following 3 months. After that, cells remained were cultured in Afatinib-free growth medium until the stable growth was restored. The isolated Afatinib-resistant cell line was named as AFA-PC9.

In Vivo Antitumor Study

Protocols for animal studies were approved by the Wenzhou Medical University Animal Policy and Welfare Committee. Male BALB/c nu/nu mice (6 weeks old, 18–22 g) were acquired from Vital River Laboratory Animal Technology Co., Ltd. (Beijing, China). Animals were housed at a constant room temperature with a 12 h: 12 h light/dark cycle and fed with a standard rodent diet and water. H1975 cells were injected subcutaneously into the right flank (1×10^7 cells in 200 μl of PBS). 40 mice were divided into five groups (n = 8/group): control (vehicle), 15c (10 mg/kg/day), WZ4002 (10 mg/kg/day), AZD4547 (10 mg/kg/day), and WZ4002 (10 mg/kg/day) combined with AZD4547 (10 mg/kg/day). The compounds were given by intraperitoneal (i.p.) injection. The tumor volumes were determined at the indicated time points ($V = 0.5 \times L \times W^2$; L: length, W: width, V: volume). After sacrificed, the tumors were weighed and collected for studies on the protein expression.

Statistical Analysis

At least three independent experiments were performed for each assay (n≥3). Data were shown as mean ± SEM. GraphPad Prism 5.0 (GraphPad, San Diego, CA) was used for the statistical analyses. Student's *t*-test and two-way ANOVA were employed to analyze the differences between different sets of data. $P < 0.05$ was considered statistically significant and exhibited by * or # characters.

RESULTS

Compound 15c Acted as an $EGFR^{L858R/T790M}$/FGFR1 Dual Inhibitor and Selectively Kills Human Lung Cancer Cells

In our previous work (Chen et al., 2017a), we designed and optimized a series analogue of WZ4002 and evaluated their inhibition activity against $EGFR^{L858R/T790M}$, and found that several derivatives exhibited a high potency and selectivity between $EGFR^{L858R/T790M}$ and $EGFR^{WT}$. In order to explore whether those compounds can inhibit the FGFR1 kinase activity, all the compounds were measured the kinase inhibitory effect against $EGFR^{WT}$, $EGFR^{L858R/T790M}$, and $FGFR1^{WT}$ in a cell-free system called Caliper Mobility Shift Assay. As shown in **Figures 1A, B**, 15c exhibited the high inhibition towards $EGFR^{L858R/T790M}$ and $FGFR1^{WT}$, and relatively lower inhibition against $EGFR^{WT}$. Thus, 15c can act as an $EGFR^{L858R/T790M}$ and $FGFR1^{WT}$ dual inhibitor.

Kinases such as EGFR and FGFR play a critical role in the proliferation of cancer cells. Thus, we next detected the anti-proliferation effects of 15c on cultured human lung cancer cells and normal cells. Four cell lines, lung cancer PC9 cells ($EGFR^{L858R+}$ and $FGFR1^{-}$), lung cancer H520 cells ($EGFR^{-}$

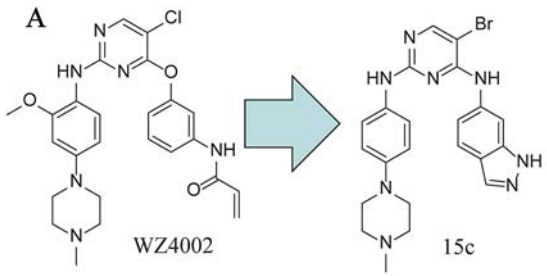

FIGURE 1 | Compound 15c acted as an $EGFR^{L858R/T790M}$/FGFR1 dual inhibitor and selectively kills human lung cancer cells. **(A)** The chemical structure of WZ4002 and 15c. **(B)** The kinase inhibitory activity against $EGFR^{WT}$, $EGFR^{L858R/T790M}$, and $FGFR1^{WT}$ of 15c. **(C)** Immunoblots of the expression levels of EGFR and FGFR1 protein in H1975, PC9, H520, and Beas-2B cell lines. **(D)** Anti-proliferation effect of 15c against H1975, PC9, H520, and Beas-2B cell lines. The IC_{50} values were reported as μM values (n = 3 independent experiments).

and $FGFR1^{+}$), lung cancer H1975 cells ($EGFR^{L858R/T790M+}$ and $FGFR1^{+}$), and normal lung epithelial cells Beas-2B cells ($EGFR^{+}$ and $FGFR1^{+}$), were chosen for the cytotoxic assay (**Figure 1C**). 15c exhibited high anti-proliferation activity against lung cancer cells rather than normal Beas-2B cells (highest concentration at 30 μM) (**Figure 1D**). Those findings indicated that 15c acted as an $EGFR^{L858R/T790M}$/FGFR1 dual inhibitor in cell-free system and selectively inhibited the proliferation of human lung cancer cells.

Compound 15c Inhibited the Phosphorylation of EGFR and FGFR1 in the Cell System

In order to further confirm whether compound 15c can impede the phosphorylation of EGFR and FGFR1 in cells, the kinase inhibitory activity of 15c was detected in various ligand stimulated cancer cells. As mentioned before, PC9 is a human lung adenocarcinoma cell line with $EGFR^{L858R}$ mutation without FGFR1 expression, while H520 is a human lung squamous cell carcinoma cell line with the high expression of FGFR1 but without EGFR expression. Thus, the p-EGFR levels in EGF-induced PC9 cells and the p-FGFR1 levels in FGF-stimulated H520 cells were determined, respectively. The third-generation EGFR-TKI WZ4002 and the FGFR1-TKI AZD4547 were selected for comparison. The results were summarized in **Figures 2A, B**. Compound 15c, similar to the positive control, can inhibit the phosphorylation of FGFR1 and EGFR in a dose-dependent manner in different cell lines.

In addition, H1975 is a human adenocarcinoma cell line with $EGFR^{L858R/T790M}$ mutation and FGFR1 expression, which can be used as an EGFR-TKI acquired resistant cell line. In this part, we treated the H1975 cells with 1 μM 15c, WZ4002, AZD4547, or WZ4002 and AZD4547 combination followed by bFGF or EGF stimulated. The p-FGFR1 and p-EGFR levels were determined by Western blot. In the EGF-stimulated H1975 cells (**Figure 2C**), 15c and WZ4002 exhibited the similar inhibitory activity against the phosphorylation of EGFR and AZD4547, a FGFR1 inhibitor, showed no effect on the phosphorylation of EGFR. The inhibitory effect of WZ4002 and AZD4547 combination was slightly better than 15c or WZ4002 alone, but no significant difference was noted. Similarly, in the bFGF-induced H1975 cells (**Figure 2D**), 15c and AZD4547 exhibited the comparable inhibitory activity against the phosphorylation of FGFR1 and WZ4002 showed no effect. The inhibitory impact of WZ4002 and AZD4547 combination was almost the same to 15c or WZ4002 alone. Those results revealed that 15c was a potential $EGFR^{L858R/T790M}$/FGFR1 dual inhibitor in the cell system.

Compound 15c Induced Caspase-Dependent Apoptosis in H1975 Cells

To explore whether 15c can accelerate H1975 cells apoptosis, a series apoptosis related experiments were introduced. H1975 cells that starved for 12 h were treated with variable level of test compounds, positive inhibitors, or vehicle for 24 h. After harvested and washed with PBS, cells were double stained with FITC Annexin V Apoptosis Detection Kit I. The apoptotic cells were detected by flow cytometry analysis and the results were also illustrated in the column chart (**Figures 3A, B**). Significant apoptosis was observed in 15c treated H1975 cells in a dose-dependent manner compared with the vehicle group. Moreover, the apoptosis rates of 15c at 5 μM and 10 μM were much higher than that WZ4002 or AZD4547 treated alone or combined at 10 μM. In addition, caspase 3 activity assay were further applied to verify the effect of 15c on inducing H1975 apoptosis (**Figure 3C**). The results

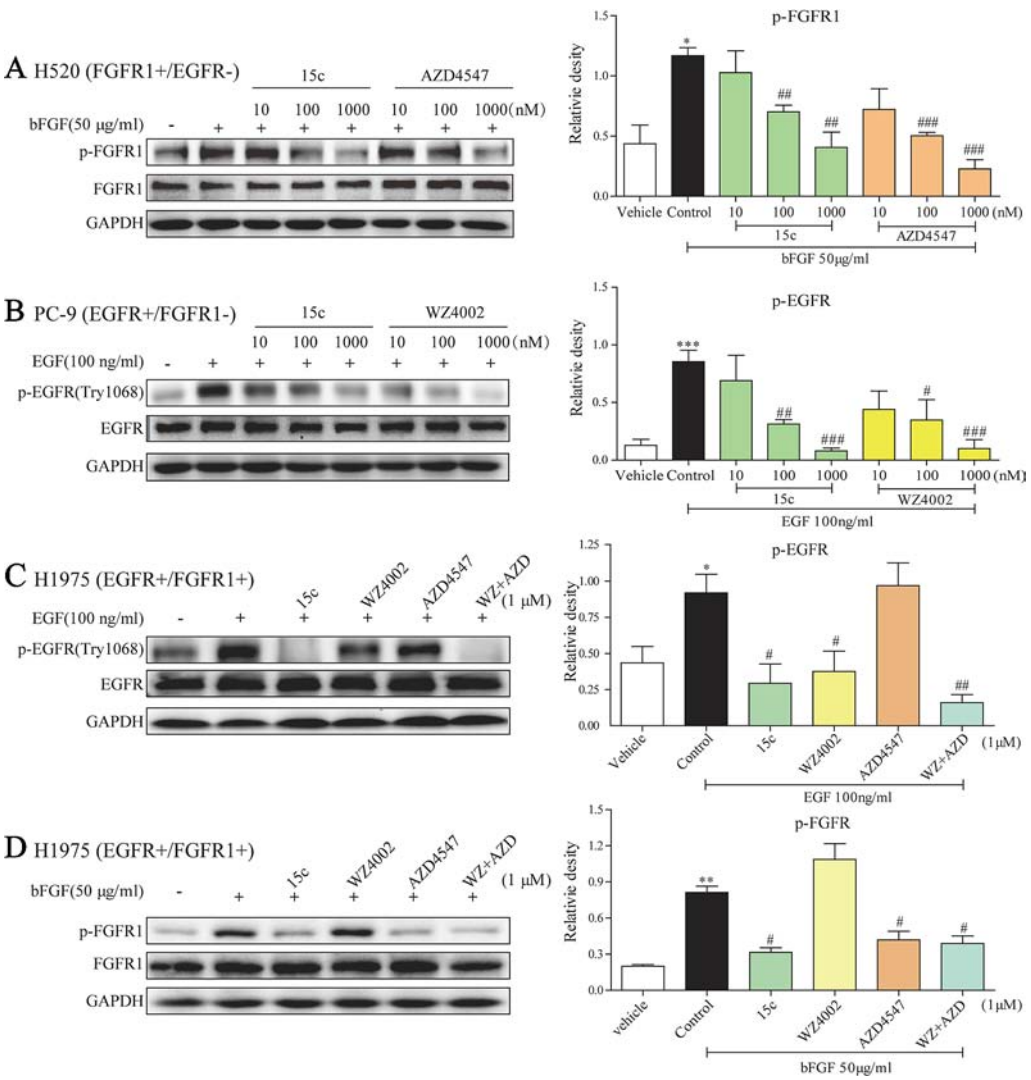

FIGURE 2 | Compound 15c inhibited the phosphorylation of EGFR and FGFR1 in the cell system. **(A–D)** Representative immunoblots of phosphorylated FGFR1/EGFR, total FGFR1/EGFR, and GAPDH (sample loading controls) in three different cell lines that treated with inhibitors (n = 3 independent experiments for each panel). **(A)** Analysis of the p-FGFR1 level in bFGF-stimulated H520 cells. **(B)** Analysis of the p-EGFR level in EGF-stimulated PC9 cells. **(C)** Analysis of the p-EGFR level in EGF-stimulated H1975 cells. **(D)** Analysis of the p-FGFR1 level in bFGF-stimulated H1975 cells. The statistical results were shown as means ± SD (n = 3) on the right of each panels. Significant difference was indicated as * or # character (*$p < 0.05$, **$p < 0.01$, and ***$p < 0.001$ versus vehicle group, $^{\#}p < 0.05$, $^{\#\#}p < 0.01$, and $^{\#\#\#}p < 0.001$ versus control group).

suggested that 15c could induced the apoptosis of H1975 cells *via* activating caspase-dependent apoptosis.

Compound 15c Overcame Afatinib-Tolerant in Established Acquired Resistant PC9 Cell Line

The effect of 15c on reversing drug resistant in lung cancer cells was further studied by domesticated a cell line resistant to Afatinib. The PC9 cells were continuously exposed to Afatinib at the stepwise increased concentrations from 0.025 to 1 μM over the following 3 months to construct the Afatinib-resistant cell lines AFA-PC9. Western blot analyses of PC9 and AFA-PC9 were shown in **Figure 4A**, and the FGFR1 expression was significantly amplified in AFA-PC9 and the EGFR expression was not affected. The morphology change of the AFA-PC9 was demonstrated in **Figure 4B**. Compared to PC9, AFA-PC9 cells started to grow in clusters, which was completely consistent with the conclusions in previous studies. MTS analysis was also carried out on the drug-resistant AFA-PC9 (**Figure 4C**). Compared with the PC9 cells, the sensitivity of AFA-PC9 cells to Afatinib was reduced by more than 1000 times. Then, we compared the anti-proliferative effects of compound 15c and WZ4002 on AFA-PC9 and PC9 cells. It turned out that the sensitivity of AFA-PC9 to WZ4002 decreased more than 100

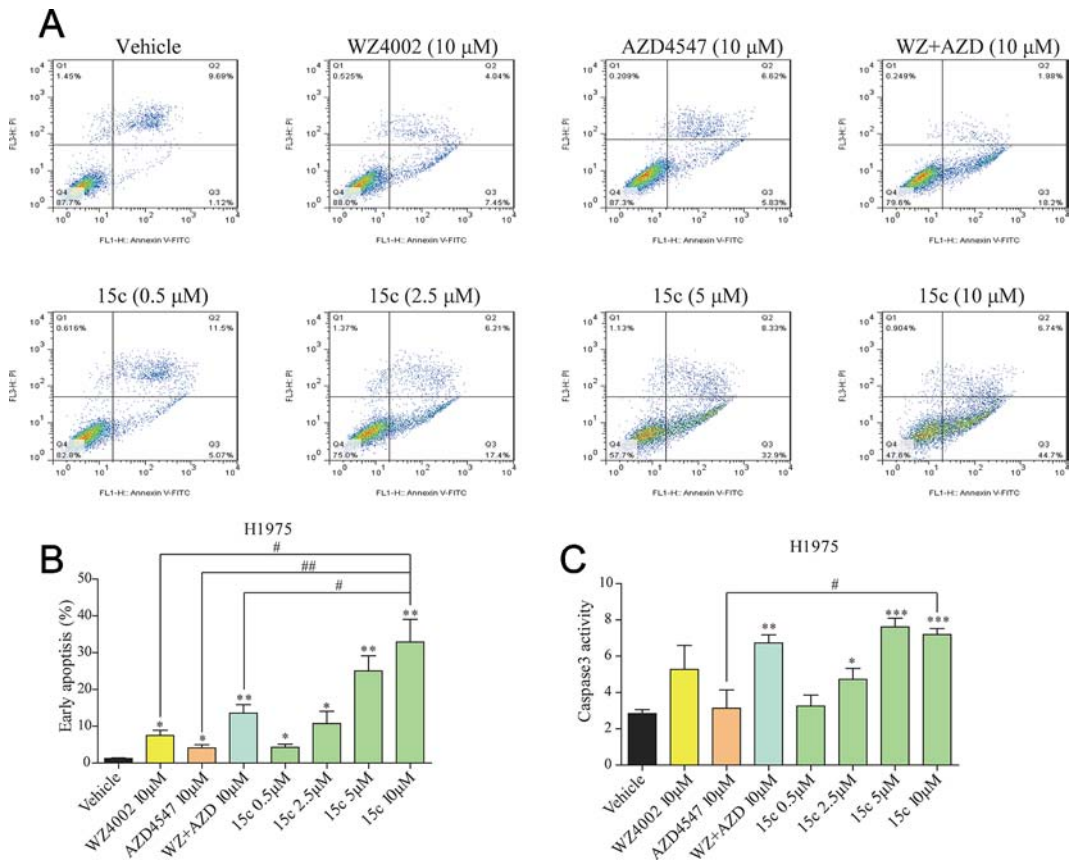

FIGURE 3 | Compound 15c induced caspase-dependent apoptosis in H1975 cells. **(A)** Apoptosis induced by inhibitors treatment in H1975 cells. Cells were incubated with the indicated doses of 15c, WZ4002, AZD4547, and WZ4002 + AZD4547 for 24 h, and then harvested and analyzed by flow cytometry. Representative data from one experiment are shown. **(B)** The percentage of apoptotic cells in the treatment groups was calculated. **(C)** Caspase-3 activity of H1975 cells treated with 15c (0.5, 2.5, 5, 10 μM), AZD4547 (10 μM), WZ4002 (10 μM), or AZD4547 (10 μM) + WZ4002 (10 μM) for 24 h. All the statistical results are shown as means ± SD (n = 3). *$p < 0.05$, **$p < 0.01$, and ***$p < 0.001$ versus vehicle group, $^{\#}p < 0.05$ and $^{\#\#}p < 0.01$ versus 10 μM 15c group.

times (IC_{50} was changed from 0.025 to 3.2 μM) while only decreased two times against 15c (IC_{50} was changed from 0.32 to 0.66 μM), indicating that 15c can overcame the acquired resistant to Afatinib in PC9 cell line.

Compound 15c Attenuated H1975 Xenograft Tumor Growth *In Vivo* by Suppressing p-EGFR and p-FGFR1 Levels

Subcutaneous xenograft model of H1975 cells in immunodeficient mice was applied to evaluate the *in vivo* anti-tumor activity of 15c. Male BALB/c nu/nu mice (6 weeks old, 18–22 g) were subcutaneously injected with H1975 cells (1×10^7 cells in 200 μl of PBS). When the tumor volume was around 80–100 mm^3, the mice were randomly divided into five groups (eight in each) including negative control group (Vehicle group), 15c group (10 mg/kg/day, ip), WZ4002 group (10 mg/kg/day, ip), AZD4547 group (10 mg/kg/day, ip), and WZ4002 combined with AZD4547 group (10 mg/kg/day, ip). After intraperitoneal administration of compound for 20 days, the tumor volume and weight of each group were measured and shown in **Figures 5A–C**. 15c significantly reduced H1975 tumor volume and weight versus vehicle control. Even compared with the positive inhibitor alone, 15c still exhibited a better tumor-inhibition effect. Only WZ4002 and AZD4547 combination administration can restrain the H1975 tumor to the same size of the tumor treated by 15c. Importantly, these is no significant weight loss of mice even treated 15c for 20 days (**Figure 5D**). Mechanistically, western blot analysis of tumor tissues revealed that 15c attenuated H1975 xenograft tumor growth *in vivo* by suppressing the phosphorylation of FGFR1 and EGFR (**Figures 5E, F**).

DISCUSSION

Lung cancer is the leading cause of cancer-related death worldwide with NSCLC accounting for 85% of cases. Therefore, it is of great theoretical and practical significance to study the pathogenesis of lung cancer and develop the corresponding therapeutic drugs. In the past few decades, it has been determined that the activation of EGFR is closely

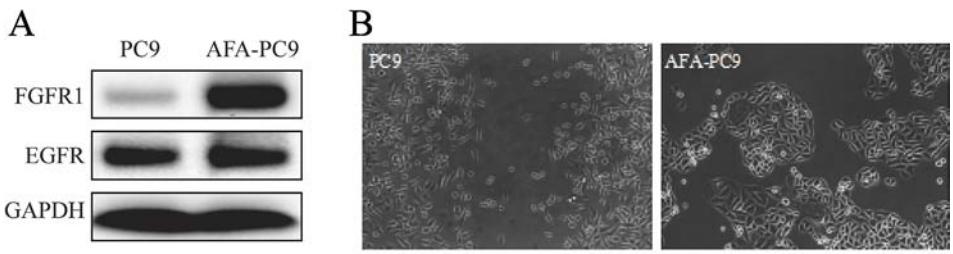

C

	IC_{50} (μM)		
Cell line	Afatinib	15c	WZ4002
PC9	<0.003	0.3208 ± 0.06491	0.02511 ± 0.001718
AFA-PC9	3.009 ± 0.1835	0.6682 ± 0.03235	3.216 ± 0.4874

FIGURE 4 | Compound 15c overcame Afatinib-tolerant in established acquired resistant PC9 cell (AFA-PC9). Cancer cell line PC9 was continuously exposed to Afatinib at stepwise increased concentrations up to 1 μM over the following 3 months to establish an Afatinib-resistant PC9 cell line named ADA-PC9. **(A)** Western Blot analysis of the EGFR and FGFR1 expression in PC9 cells and AFA-PC9 cells. **(B)** Morphological changes of AFA-PC9 cells compared to PC9 cells; **(C)** Anti-proliferation effect of 15c, WZ4002, and Afatinib against PC9 and AFA-PC9 cell lines. The IC_{50} values were reported as μM values.

related to the genesis and progress of lung cancer (Lynch et al., 2004; Paez et al., 2004; Pao et al., 2004; Sharma et al., 2007). Thus, EGFR has attracted great attentions as it is an ideal target for the cancer therapy. There are a series of small molecular inhibitors that can inhibit the kinase activity of EGFR had been found and named as EGFR-TKIs (Sequist et al., 2007; Pao and Chmielecki, 2010). Gefitinib and Erotinib are the first-generation EGFR-TKIs that have been studied clinically with a great advance. However, patients generally develop secondary mutations, such as T790M gatekeeper, and lead to drug resistance after EGFR-TKIs treated for 12 months (Chen et al., 2017b). As a result, second and third-generation EGFR-TKIs, e.g. Afatinib, WZ4002, and Osimertinib, are developed to overcome the T790M mutation-associated resistance (Zhou et al., 2009; Mok et al., 2017). The poor therapeutic window of Afatinib limited its clinical application (Chen et al., 2017b). Osimertinib exhibits an excellent treatment effect for NSCLC patients with EGFR T790M-mutated, but acquired resistance is still inevitable (Oxnard et al., 2018). Thus, there is still an urgent demand to establish an effective antitumor strategy for those NSCLC patients with acquired resistance to second or third-generation EGFR-TKIs.

Müller-Tidow and his colleagues identified the expression of 56 RTKs in primary NSCLC tumors and found that 33 RTKs are expressed at the mRNA level in 25% samples (Müller-Tidow et al., 2005), indicating that those RTKs may function as an alternatives to EGFR signal pathway in NSCLC, such as cMet, Axl, IGF-1R, and PDGFR. The amplification of cMet is a major factor of acquired resistance in lung cancer and the combination of Gefitinib and cMet antibody can significantly enhance the growth inhibition in cMet over-expressing cell lines (Bean et al., 2007; Zucali et al., 2008). Similarly, the IGF-1R survival pathway contribute to Gefitinib resistance and synergistically inhibition of IGF-1R could strengthen the anti-tumor effect of Gefinitib (Desbois-Mouthon et al., 2006). In addition, Axl lead to EGFR-TKIs resistant by increasing expression and forming a hetero-dimerization with EGFR and inhibition of Axl could prevent or overcome acquired resistance to EGFR-TKIs in EGFR-mutated lung cancer (Zhang et al., 2012; Vouri et al., 2016). Recently, several researches mentioned that the activation of the autocrine ring of FGF/FGFR, one of the typical RTKs, could act as a compensatory mechanism to promote the survival and growth of EGFR-TKIs resistant lung cancer cells. These findings declared that simultaneous inhibition of EGFR and FGFR1 activity may be a novel and effective strategy to overcome FGFR1-related EGFR-TKIs resistant in NSCLC.

Nowadays, combination therapy of various drugs with different targets has become an important strategy for cancer treatment (Bell, 2013). Combined drugs can improve the curative effect as the synergism of different activity. However, increased off-target effect and metabolic pressure restricted the application of combined administration. Moreover, drugs with polypharmacological activities are shown to be advantageous over combination therapy as their lower incidences of side effects and more resilient therapies. Thus, developing dual-inhibitors that target FGFR1 and EGFR will be an efficient way to reverse FGFR1-related EGFR-TKIs resistant in NSCLC.

Here, we presented an $EGFR^{L858R/T790M}$/FGFR1 dual-inhibitor 15c, which can simultaneous inhibited the kinase activity of $EGFR^{L858R/T790M}$ and FGFR1 both in kinase assay and cell study, for the treatment of FGFR1-amplified EGFR-TKIs resistant lung cancers. The anti-proliferation effects of 15c on NSCLC cell lines and normal BEAS-2B cell line showed that 15c could effectively hold back the proliferation of NSCLC cells rather

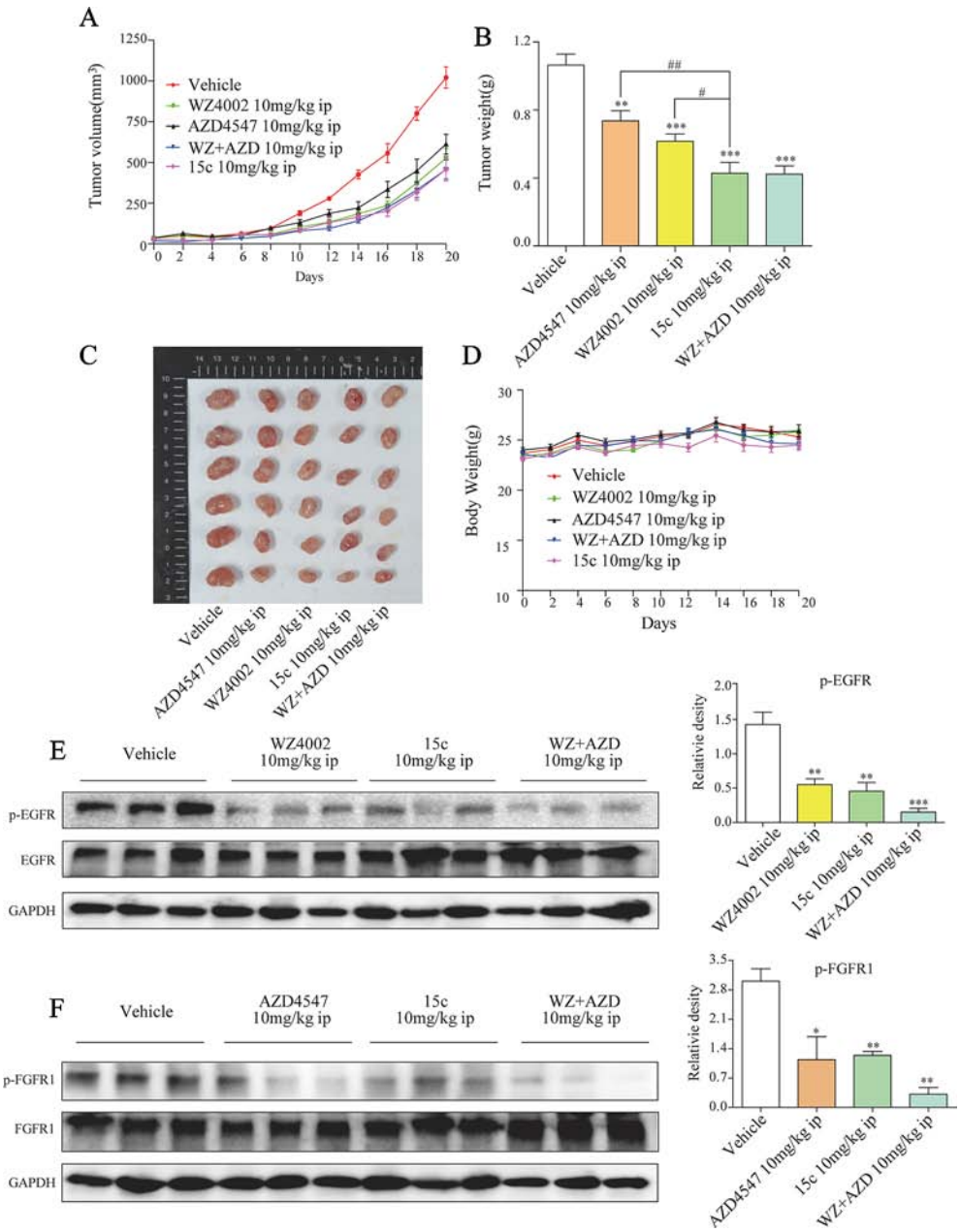

FIGURE 5 | Compound 15c inhibited H1975 xenograft tumor growth *in vivo*, accompanied with decreased p-EGFR and p-FGFR1 levels. Tumor-bearing mice were intraperitoneally injected with 15c (10 mg/kg), WZ4002 (10 mg/kg), AZD4547 (10 mg/kg), or WZ4002 (10 mg/kg) + AZD4547 (10 mg/kg). **(A–C)** Tumor volume and tumor weight of H1975 human lung cancer xenografts in nude mice. **(D)** Body weight was measured every 2 days. Points, means of seven mice; bars, SEM. **(E, F)** Analysis of pFGFR1 and p-EGFR levels in tumor tissues. *p < 0.05, **p < 0.01, and ***p < 0.001 versus vehicle group, #p < 0.05 and ##p < 0.01 versus 10 mg/kg 15c group. ip, intraperitoneally injected.

than normal cells. Particularly, 15c exhibited a better inhibitory effect to H1975 cells and AFA-PC9 cells, which contained EGFR mutation and FGFR1 overexpression, than WZ4002 and AZD4547. Further flow cytometry and Caspase 3 activity analysis demonstrated that 15c could induce the apoptosis in a dose-dependent manner and the effect was better than WZ4002 combined AZD4547 treatment. Finally, the *in vivo* study as well revealed that the anti-tumor ability of 15c was comparable to the combination administration of WZ4002 and AZD4547 but better than the separate administration.

In summary, acquired resistant is the major reason for EGFR-TKI tolerant NSCLCs and FGFR1 amplification has been proved

that contribute to the EGFR-TKI resistant. Thus, $EGFR^{L858R/T790M}$/FGFR1 dual inhibitor 15c can be developed as an ideal candidate drug for FGFR1-amplified EGFR-TKIs resistant lung cancers.

DATA AVAILABILITY STATEMENT

The raw data supporting the conclusions of this article will be made available by the authors, without undue reservation, to any qualified researcher.

ETHICS STATEMENT

The animal study was reviewed and approved by the Wenzhou Medical University Animal Policy and Welfare Committee.

AUTHOR CONTRIBUTIONS

Participated in research design: GC, QW, GL. Cell and animal study: GC, YB, QW, YZ, and XL. Kinase study: LF. Performed chemical synthesis of 15c: LC and ZL. Contributed to the writing of the manuscript: GC, XZ, GL.

FUNDING

This work was supported by the National Key R&D Program of China (2017YFA0506000), the National Natural Science Foundation of China (Grants No. 81703352 and 81773579), the Zhejiang Province Natural Science Foundation (LY17B020008), the Zhejiang Medical Health Technology Platform Project (2018KY183) and the Zhejiang Natural Science Foundation Pharmaceutical Society Joint Fund Project (LYY19H310004).

REFERENCES

Anighoro, A., Bajorath, J., and Rastelli, G. (2014). Polypharmacology: challenges and opportunities in drug discovery: miniperspective. *J. Med. Chem.* 57 (19), 7874–7887. doi: 10.1021/jm5006463

Azuma, K., Kawahara, A., Sonoda, K., Nakashima, K., Tashiro, K., Watari, K., et al. (2014). FGFR1 activation is an escape mechanism in human lung cancer cells resistant to afatinib, a pan-EGFR family kinase inhibitor. *Oncotarget* 5 (15), 5908. doi: 10.18632/oncotarget.1866

Bean, J., Brennan, C., Shih, J.-Y., Riely, G., Viale, A., Wang, L., et al. (2007). MET amplification occurs with or without T790M mutations in EGFR mutant lung tumors with acquired resistance to gefitinib or erlotinib. *Proc. Nat. Acad. Sci.* 104 (52), 20932–20937. doi: 10.1073/pnas.0710370104

Bell, D. (2013). Combine and conquer: advantages and disadvantages of fixed-dose combination therapy. *Diabetes Obesity Metab.* 15 (4), 291–300. doi: 10.1111/dom.12015

Cataldo, V. D., Gibbons, D. L., Pérez-Soler, R., and Quintás-Cardama, A. (2011). Treatment of non–small-cell lung cancer with erlotinib or gefitinib. *N. Engl. J. Med.* 364 (10), 947–955. doi: 10.1056/NEJMct0807960

Chang, A. (2011). Chemotherapy, chemoresistance and the changing treatment landscape for NSCLC. *Lung Cancer* 71 (1), 3–10. doi: 10.1016/j.lungcan.2010.08.022

Chen, L., Fu, W., Feng, C., Qu, R., Tong, L., Zheng, L., et al. (2017a). Structure-based design and synthesis of 2, 4-diaminopyrimidines as EGFR L858R/T790M selective inhibitors for NSCLC. *Eur. J. Med. Chem.* 140, 510–527. doi: 10.1016/j.ejmech.2017.08.061

Chen, L., Fu, W., Zheng, L., Liu, Z., and Liang, G. (2017b). Recent progress of small-molecule epidermal growth factor receptor (EGFR) inhibitors against C797S resistance in non-small-cell lung cancer: miniperspective. *J. Med. Chem.* 61 (10), 4290–4300. doi: 10.1021/acs.jmedchem.7b01310

Cohen, M. H., Williams, G. A., Sridhara, R., Chen, G., and Pazdur, R. (2003). FDA drug approval summary: gefitinib (ZD1839) (Iressa®) tablets. *Oncologist* 8 (4), 303–306. doi: 10.1634/theoncologist.8-4-303

Cohen, M. H., Johnson, J. R., Chen, Y.-F., Sridhara, R., and Pazdur, R. (2005). FDA drug approval summary: erlotinib (Tarceva®) tablets. *Oncologist* 10 (7), 461–466. doi: 10.1634/theoncologist.10-7-461

Desbois-Mouthon, C., Cacheux, W., Blivet-Van Eggelpoël, M. J., Barbu, V., Fartoux, L., Poupon, R., et al. (2006). Impact of IGF-1R/EGFR cross-talks on hepatoma cell sensitivity to gefitinib. *Int. J. Cancer* 119 (11), 2557–2566. doi: 10.1002/ijc.22221

Ferrer, I., and Marti, E. (1998). Distribution of fibroblast growth factor receptor-1 (FGFR-1) and FGFR-3 in the hippocampus of patients with Alzheimer's disease. *Neurosci. Lett.* 240 (3), 139–142. doi: 10.1016/s0304-3940(97)00948-8

Gallagher, E. J., and LeRoith, D. (2013). Does a single nucleotide polymorphism in the FGFR explain the connection between diabetes and cancer? *Cell Metab.* 17 (6), 808–809. doi: 10.1016/j.cmet.2013.05.006

Gozgit, J. M., Wong, M. J., Moran, L., Wardwell, S., Mohemmad, Q. K., Narasimhan, N. I., et al. (2012). Ponatinib (AP24534), a multitargeted pan-FGFR inhibitor with activity in multiple FGFR-amplified or mutated cancer models. *Mol. Cancer Ther.* 11 (3), 690–699. doi: 10.1158/1535-7163.MCT-11-0450

Harrison, C. (2012). Obesity and diabetes: an FGFR antibody with long-lasting effects. *Nat. Rev. Drug Discovery* 11 (2), 106. doi: 10.1038/nrd3660

Hirsch, F. R., and Bunn, P. A. (2012). A new generation of EGFR tyrosine-kinase inhibitors in NSCLC. *Lancet Oncol.* 13 (5), 442–443. doi: 10.1016/S1470-2045(12)70124-9

Hirsch, F. R., Varella-Garcia, M., Bunn, P. A.Jr., Di Maria, M. V., Veve, R., Bremnes, R. M., et al. (2003). Epidermal growth factor receptor in non–small-cell lung carcinomas: correlation between gene copy number and protein expression and impact on prognosis. *J. Clin. Oncol.* 21 (20), 3798–3807. doi: 10.1200/JCO.2003.11.069

Kono, S. A., Marshall, M. E., Ware, K. E., and Heasley, L. E. (2009). The fibroblast growth factor receptor signaling pathway as a mediator of intrinsic resistance to EGFR-specific tyrosine kinase inhibitors in non-small cell lung cancer. *Drug Resist. Updates* 12 (4–5), 95–102. doi: 10.1016/j.drup.2009.05.001

Kuang, Y., Rogers, A., Yeap, B. Y., Wang, L., Makrigiorgos, M., Vetrand, K., et al. (2009). Noninvasive detection of EGFR T790M in gefitinib or erlotinib resistant non–small cell lung cancer. *Clin. Cancer Res.* 15 (8), 2630–2636. doi: 10.1158/1078-0432.CCR-08-2592

Li, X. (2019). The FGF metabolic axis. *Front. Med.* 13 (5), 511–530. doi: 10.1007/s11684-019-0711-y

Lynch, T. J., Bell, D. W., Sordella, R., Gurubhagavatula, S., Okimoto, R. A., Brannigan, B. W., et al. (2004). Activating mutations in the epidermal growth factor receptor underlying responsiveness of non–small-cell lung cancer to gefitinib. *N. Engl. J. Med.* 350 (21), 2129–2139. doi: 10.1056/NEJMoa040938

Müller-Tidow, C., Diederichs, S., Bulk, E., Pohle, T., Steffen, B., Schwäble, J., et al. (2005). Identification of metastasis-associated receptor tyrosine kinases in non–small cell lung cancer. *Cancer Res.* 65 (5), 1778–1782. doi: 10.1158/0008-5472.CAN-04-3388

Mok, T. S., Wu, Y.-L., Ahn, M.-J., Garassino, M. C., Kim, H. R., Ramalingam, S. S., et al. (2017). Osimertinib or platinum–pemetrexed in EGFR T790M-positive lung cancer. *N. Engl. J. Med.* 376 (7), 629–640. doi: 10.1056/NEJMoa1612674

Niederst, M. J., Hu, H., Mulvey, H. E., Lockerman, E. L., Garcia, A. R., Piotrowska, Z., et al. (2015). The allelic context of the C797S mutation acquired upon treatment with third-generation EGFR inhibitors impacts sensitivity to subsequent treatment strategies. *Clin. Cancer Res.* 21 (17), 3924–3933. doi: 10.1158/1078-0432.CCR-15-0560

Oxnard, G. R., Hu, Y., Mileham, K. F., Husain, H., Costa, D. B., Tracy, P., et al. (2018). Assessment of resistance mechanisms and clinical implications in patients with EGFR T790M-positive lung cancer and acquired resistance to osimertinib. *JAMA Oncol.* 4 (11), 1527–1534. doi: 10.1001/jamaoncol.2018.2969

Paez, J. G., Jänne, P. A., Lee, J. C., Tracy, S., Greulich, H., Gabriel, S., et al. (2004). EGFR mutations in lung cancer: correlation with clinical response to gefitinib therapy. *Science* 304 (5676), 1497–1500. doi: 10.1126/science.1099314

Pao, W., and Chmielecki, J. (2010). Rational, biologically based treatment of EGFR-mutant non-small-cell lung cancer. *Nat. Rev. Cancer* 10 (11), 760. doi: 10.1038/nrc2947

Pao, W., Miller, V., Zakowski, M., Doherty, J., Politi, K., Sarkaria, I., et al. (2004). EGF receptor gene mutations are common in lung cancers from "never smokers" and are associated with sensitivity of tumors to gefitinib and erlotinib. *Proc. Nat. Acad. Sci.* 101 (36), 13306–13311. doi: 10.1073/pnas.0405220101

Quintanal-Villalonga, A., Molina-Pinelo, S., Cirauqui, C., Ojeda-Márquez, L., Marrugal, Á., Suarez, R., et al. (2019). FGFR1 cooperates with EGFR in lung cancer oncogenesis, and their combined inhibition shows improved efficacy. *J. Thorac. Oncol.* 14 (4), 641–655. doi: 10.1016/j.jtho.2018.12.021

Raoof, S., Mulford, I. J., Frisco-Cabanos, H., Nangia, V., Timonina, D., Labrot, E., et al. (2019). Targeting FGFR overcomes EMT-mediated resistance in EGFR mutant non-small cell lung cancer. *Oncogene* 38 (37), 6399–6413. doi: 10.1038/s41388-019-0887-2

Riely, G. J. (2008). Second-generation epidermal growth factor receptor tyrosine kinase inhibitors in non-small cell lung cancer. *J. Thorac. Oncol.* 3 (6), S146–S149. doi: 10.1097/JTO.0b013e318174e96e

Sequist, L. V., Joshi, V. A., Jänne, P. A., Muzikansky, A., Fidias, P., Meyerson, M., et al. (2007). Response to treatment and survival of patients with non-small cell lung cancer undergoing somatic EGFR mutation testing. *Oncologist* 12 (1), 90–98. doi: 10.1634/theoncologist.12-1-90

Sharma, S. V., Bell, D. W., Settleman, J., and Haber, D. A. (2007). Epidermal growth factor receptor mutations in lung cancer. *Nat. Rev. Cancer* 7 (3), 169. doi: 10.1038/nrc2088

To, C., Jang, J., Chen, T., Park, E., Mushajiang, M., De Clercq, D. J., et al. (2019). Single and dual targeting of mutant EGFR with an allosteric inhibitor. *Cancer Discov.* 9 (7), 926–943. doi: 10.1158/2159-8290.CD-18-0903.

Touat, M., Ileana, E., Postel-Vinay, S., André, F., and Soria, J.-C. (2015). Targeting FGFR signaling in cancer. *Clin. Cancer Res.* 21 (12), 2684–2694. doi: 10.1158/1078-0432.CCR-14-2329

Vouri, M., Croucher, D., Kennedy, S., An, Q., Pilkington, G., and Hafizi, S. (2016). Axl-EGFR receptor tyrosine kinase hetero-interaction provides EGFR with access to pro-invasive signalling in cancer cells. *Oncogenesis* 5 (10), e266. doi: 10.1038/oncsis.2016.66

Wojtaszek, J. L., Chatterjee, N., Najeeb, J., Ramos, A., Lee, M., Bian, K., et al. (2019). A small molecule targeting mutagenic translesion synthesis improves chemotherapy. *Cell* 178 (1), 152–159.e11. doi: 10.1016/j.cell.2019.05.028

Zhang, Z., Lee, J. C., Lin, L., Olivas, V., Au, V., LaFramboise, T., et al. (2012). Activation of the AXL kinase causes resistance to EGFR-targeted therapy in lung cancer. *Nat. Genet.* 44 (8), 852. doi: 10.1038/ng.2330

Zhou, W., Ercan, D., Chen, L., Yun, C.-H., Li, D., Capelletti, M., et al. (2009). Novel mutant-selective EGFR kinase inhibitors against EGFR T790M. *Nature* 462 (7276), 1070. doi: 10.1038/nature08622

Zucali, P., Ruiz, M. G., Giovannetti, E., Destro, A., Varella-Garcia, M., Floor, K., et al. (2008). Role of cMET expression in non-small-cell lung cancer patients treated with EGFR tyrosine kinase inhibitors. *Ann. Oncol.* 19 (9), 1605–1612. doi: 10.1093/annonc/mdn240

Conflict of Interest: The authors declare that the research was conducted in the absence of any commercial or financial relationships that could be construed as a potential conflict of interest.

frontiers in Pharmacology

ORIGINAL RESEARCH
published: 07 February 2020
doi: 10.3389/fphar.2020.00039

Fibroblast Growth Factor 10 Attenuates Renal Damage by Regulating Endoplasmic Reticulum Stress After Ischemia–Reperfusion Injury

Xiaohua Tan[1,2], Lixia Yu[3], Ruo Yang[2], Qianyu Tao[2], Lijun Xiang[2], Jian Xiao[2] and Jin-San Zhang[2,4]**

[1] Department of Pathology, School of Basic Medicine, Qingdao University, Qingdao, China, [2] School of Pharmaceutical Sciences, Wenzhou Medical University, Wenzhou, China, [3] Department of Pharmacy, Xixi Hospital of Hangzhou, Hangzhou, China, [4] Institute of Life Sciences, Wenzhou University, Wenzhou, China

OPEN ACCESS

Edited by:
Zhouguang Wang,
Albert Einstein College of Medicine,
United States

Reviewed by:
Yan Cui,
UCLA Brain Research Institute,
United States
Yue Zhang,
University of Southern California,
United States

***Correspondence:**
Jian Xiao
xfxj2000@126.com
Jin-San Zhang
Zhang_JinSan@wmu.edu.cn

Specialty section:
This article was submitted to Translational Pharmacology, a section of the journal Frontiers in Pharmacology

Received: 17 October 2019
Accepted: 14 January 2020
Published: 07 February 2020

Citation:
Tan X, Yu L, Yang R, Tao Q, Xiang L, Xiao J and Zhang J-S (2020) Fibroblast Growth Factor 10 Attenuates Renal Damage by Regulating Endoplasmic Reticulum Stress After Ischemia–Reperfusion Injury. Front. Pharmacol. 11:39. doi: 10.3389/fphar.2020.00039

Renal ischemia–reperfusion (I/R) injury is a predominant cause of acute kidney injury (AKI), the pathologic mechanism of which is highly complex involving reactive oxygen species (ROS) accumulation, inflammatory response, autophagy, apoptosis as well as endoplasmic reticulum (ER) stress. Fibroblast growth factor 10 (FGF10), as a multifunctional growth factor, plays crucial roles in embryonic development, adult homeostasis, and regenerative medicine. Herein, we investigated the molecular pathways underlying the protective effect of FGF10 on renal I/R injury using Sprague–Dawley rats. Results showed that administration of FGF10 not only effectively inhibited I/R-induced activation of Caspase-3 and expression of Bax, but also alleviated I/R evoked expression of ER stress-related proteins in the kidney including CHOP, GRP78, XBP-1, and ATF-4 and ATF-6. The protective effect of FGF10 against apoptosis and ER stress was recapitulated by *in vitro* experiments using oxidative damaged NRK-52E cells induced by tert-Butyl hydroperoxide (TBHP). Significantly, U0126, a selective noncompetitive inhibitor of MAP kinase kinases (MKK), largely abolished the protective role of FGF10. Taken together, both *in vivo* and *in vitro* experiments indicated that FGF10 attenuates I/R-induced renal epithelial apoptosis by suppressing excessive ER stress, which is, at least partially, mediated by the activation of the MEK–ERK1/2 signaling pathway. Therefore, our present study revealed the therapeutic potential of FGF10 on renal I/R injury.

Keywords: fibroblast growth factor 10, acute kidney injury, endoplasmic reticulum stress, ischemia–reperfusion, ERK1/2

INTRODUCTION

Acute kidney injury (AKI), characterized by rapidly declining glomerular filtration rate (GFR), is a clinical lethal symptom mainly caused by renal ischemia–reperfusion (I/R) injury, sepsis, and nephrotoxic drugs (Mehta et al., 2007; Bonventre and Yang, 2011). AKI is considered as a nosocomial disease with an incidence of 2–7% in hospitalized patients. Despite advances of therapeutic strategies in the past decades, the morbidity and mortality of AKI remain very high (Chertow et al., 2005; Uchino et al., 2005; Bonventre and Yang, 2011; Basile et al., 2012). Renal I/R injury, commonly caused by shock, surgery interventions, kidney transplantation, and toxic insults, accounts for the majority of AKI (Chertow et al., 2005; Ishani et al., 2009). Many previous studies have shown that the pathological mechanism of renal I/R injury is often associated with excessive reactive oxygen species (ROS), oxidative stress, autophagy, inflammation, apoptosis as well as ER stress (Paller et al., 1984; Thadhani et al., 1996; Inagi, 2009; Hotamisligil, 2010; Tan et al., 2017). Although several drugs and therapeutic treatments that could ameliorate renal ischemia injury in animal models have been reported, few of them have been successfully utilized in clinical therapies (Tsuda et al., 2012; Tan et al., 2013). Rapid restoration of renal blood flow after ischemia remains the quickest way to lessen renal tissue damage and functional deterioration caused by ischemia (Paller et al., 1984). However, reperfusion itself also has the potential to elicit additional damage, mainly caused by over-production of ROS, mitochondrial dysfunction, and inflammatory response, which further leads to apoptosis or necrosis (Tsuda et al., 2012; Tan et al., 2013; Inoue et al., 2019). Therefore, effective treatment for AKI is desperately needed.

Endoplasmic reticulum (ER) is a specialized organelle for the synthesis, folding, and trafficking of proteins (Cao and Kaufman, 2012). Many studies have shown that ER is highly sensitive to the changes of the intracellular microenvironment (Cao and Kaufman, 2014; Walter and Ron, 2011). Hypoxia and oxidative stress intrinsic to I/R injury could impair the protein folding of ER. Overaccumulation of unfolded and misfolded proteins triggers the Unfolded Protein Response (UPR) to resolve the excessive ER stress. It has been demonstrated that UPR could expand the ER membrane and thus improve the efficiency of ER for protein folding. UPR could also decrease mRNA translation and reduce protein expression (Schuck et al., 2009). It has been reported that ER stress plays an important role in cell growth, differentiation, and apoptosis. However, excessive activation of ER stress and UPR could activate apoptotic signaling pathways (Hetz et al,. 2012; Tabas and Ron, 2011). Studies have revealed that C/EBP homologous proteins (CHOP), also known as DNA damage inducible transcript 3 (DDIT3), is a master regulator of maladaptive ER stress-induced apoptosis (Rutkowski et al., 2006). Therefore, a strategy focusing on the inhibition of maladaptive ER stress may facilitate the treatment of renal I/R injury.

Fibroblast growth factor 10 (FGF10) is an important member of the FGF family, which mediates mesenchymal to epithelial signaling in a paracrine manner. FGF10 plays a crucial role in embryonic development, wound healing, and tissue regeneration with binding and activating FGF receptor (FGFR) on the cell surface (Itoh and Ohta, 2014). FGF10 highly specifically binds to FGFR2b and initiates the activation of intracellular signaling cascades, including the extracellular signal-regulated kinase (ERK) 1/2 signaling pathway (Zhang et al., 2006; Cho et al., 2009; Wang et al., 2009; Itoh, 2015). Many experimental studies using Fgf10 gene knockout mice have confirmed the crucial role of FGF10 in the development and homeostasis of multiple organs such as the kidney, lung, limb, and pancreatic gland (De Moerlooze et al., 2000; Ohuchi et al., 2000; Beenken and Mohammadi, 2009; Michos et al., 2010; El Agha et al., 2012; Itoh, 2015). It has been reported that FGF10 could accelerate the regeneration of myocardium after myocardial I/R injury (Rochais et al., 2014). Recombinant FGF10 has also been utilized for the treatment of ulcerative colitis and mucositis (Sandborn et al., 2003; Freytes et al., 2004). However, the protective mechanism of FGF10 on renal I/R injury has not yet been fully confirmed. In the present study, we hypothesized that FGF10 could attenuate renal I/R injury by suppressing excessive ER stress and inhibiting renal tubular epithelial cell apoptosis. The protective effect of FGF10 on AKI may be related to the activation of MEK–ERK1/2 signaling pathway. We verified our hypothesis with Sprague–Dawley (SD) rats subjected to renal I/R injury. Rat renal tubular epithelial cell line NRK-52E was also utilized to clarify the protective mechanism of FGF10 in the present study. Results demonstrated that the protective effect of FGF10 on AKI is intimately connected to ER stress which is, at least partially, mediated by the MEK–ERK1/2 signaling pathway.

MATERIALS AND METHODS

Reagents and Antibodies

Bovine serum albumin (BSA), recombinant human FGF10, Tert-Butyl hydroperoxide (TBHP), and U0126 (selective MKK1/2 inhibitor) were purchased from Sigma-Aldrich (St. Louis, MO, USA). Dulbecco's Modified Eagle Medium (DMEM), fetal bovine serum (FBS), Trypsin-EDTA (0.25%), and 4′, 6-Diamidino-2-phenylindole (DAPI) were purchased from Invitrogen (Carlsbad, CA, USA). Antibodies against cleaved Caspase-3 (catalog number: 9661), cleaved Caspase-9 (catalog number: 9507), and phospho-ERK1/2 (catalog number: 9101) were purchased from Cell Signaling Technology, Inc. (Danvers, MA, USA). Anti-ERK1/2 antibody (catalog number: 82380) was purchased from Thermo Fisher Scientific (Sunnyvale, CA, USA). Antibodies against GRP78 (catalog number: ab21685), ATF-6 (catalog number: ab203119), ATF-4 (catalog number: ab23760), PDI (catalog number: ab154820), CHOP (catalog number: ab11419), XBP1 (catalog number: ab37152), and GAPDH (catalog number: ab9485) were purchased from Abcam, Inc. (Cambridge, MA, USA). The secondary antibodies were purchased from Abcam, Inc. (Cambridge, MA, USA) or Santa Cruz Biotechnology, Inc. (Santa Cruz, CA, USA). Annexin V-FITC-PI Apoptosis Detection Kit was purchased from Becton Dickinson, Inc. (San Jose, CA, USA). High sensitivity ECL substrate kit, Hematoxylin and Eosin (H&E) staining kit, and

Periodic Acid Schiff (PAS) staining kit were purchased from Abcam, Inc. (Cambridge, MA, USA). The terminal deoxynucleotidyl transferase mediated dUTP nick-end labeling (TUNEL) Assay Kit was purchased form Abcam, Inc. (Cambridge, MA, USA).

Renal I/R Injury Model and Assessment of Renal Function

To confirm the protective effect of FGF10 treatment on kidney after reperfusion, rat renal I/R injury model was established by surgical operation. Male Sprague–Dawley (SD) rats, eight weeks old, were purchased from Beijing Vital River Laboratory Animal Technology Co., Ltd. and were housed in a Specific-pathogen-free (SPF) facility. The experimental protocol was approved by the Institutional Animal Ethical and Use Committee of Wenzhou Medical University. The rat model of renal I/R injury was established as we described in our previous study (Tan et al., 2017). Briefly, SD rats were anesthetized with intraperitoneal (ip) injection of pentobarbital sodium (25 mg/kg) and placed on a thermostatic surgical table. A small incision was made through the medioventral line and exposed the right kidney. The right kidney was carefully liberated from the surrounding tissue, and nephrectomy was performed. The left kidney was exposed, and the renal artery was clamped using a nontraumatic vascular clamp. Renal blood flow was re-established after 45 min ischemia, and the muscle layer and skin layer were closed using a medical suture. For measurement of renal function, serum creatinine (Cr) was measured 1 day following renal ischemia by the hospital medicine biochemical laboratory (at The First Affiliated Hospital of Wenzhou Medical University). Kidneys were harvested and stored in cryogenic refrigerator for further experiments. Rats were randomly divided into three groups: (a) Sham group: Sham-operated rats with unconstricted renal artery; (b) I/R group: rats were subjected to 45 min of ischemia *via* renal artery followed by reperfusion; (c) I/R–FGF10 group: rats were treated with 0.5 mg/kg FGF10 (ip) 1 h before ischemia. FGF10 was dissolved in sterile saline.

Cell Culture

The results of *in vivo* experiments in the present study have demonstrated that FGF10 could increase the phosphorylation of ERK1/2 in kidney tissues after reperfusion. To further clarify the role of MEK–ERK1/2 signaling pathway in the protective effect of FGF10, NRK-52E, a rat renal tubular epithelial cell line, was utilized in our present study. We verified the protective effect of FGF10 on damaged NRK-52E induced by TBHP. Furthermore, the participation role of MEK–ERK1/2 signaling pathway in the protective effect of FGF10 was clarified in the *in vitro* experiment. NRK-52E was purchased from the American Type Culture Collection (Manassas, USA) and cultured in DMEM supplemented with 10% FBS, antibiotics (100 units/ml penicillin, 100 μg/ml streptomycin) and incubated under 37°C, 95% air, and 5%CO2. To detect the effect of FGF10 on ER stress induced by TBHP, NRK-52E was cultured on 6-well plates with 2×10^5 cells per well and randomly divided into four groups: (a) Control group: NRK-52E was cultured in complete medium without any supplement; (b) TBHP group: NRK52E was cultured in complete medium, and then TBHP (200 μmol/L) was added for an additional 12 h; (c) TBHP + FGF10 group: NRK-52Ewas pretreated with recombinant FGF10 (100 ng/ml) for 2 h, and then TBHP (200 μmol/L) was added for an additional 12 h; (d) TBHP + FGF10 + U0126: NRK-52E was pretreated for 2 h with U0126 (20 μmol/L), and then cells were treated the same as TBHP + FGF10 group. The pretreatment compounds in the culture medium were not removed before successive treatment conditions. All experiments with NRK-52E were performed in triplicates.

Western Blot Analysis

To assess the regulatory role of FGF10 on ER stress and apoptosis, the expression of relevant proteins was analyzed by western blot. For protein analysis of *in vivo* samples, total kidney tissues (contain both of cortex and medulla, but don't contain the renal fibrous capsule) were homogenized and total proteins were extracted using tissue lysis buffer. For protein analysis of *in vitro* samples, NRK-52E cultured in a petri dish was rinsed with PBS buffer three times; total proteins were extracted using cell lysis buffer. An equivalent of 100 μg protein of the *in vivo* sample (30 μg protein of the *in vitro* sample) was separated by Sodium Dodecyl Sulfate PolyAcrylamide and then transferred to a polyvinylidene fluoride (PVDF) membrane for immunoblot analysis. Primary antibodies against cleaved Caspase-3 (1:1,000), cleaved Caspase-9 (1:1,000), Bax (1:3,000), Bcl-2 (1:1,000), GRP78 (1:1,000), CHOP (1:5,000), XBP-1 (1:1,000), ATF-4 (1:1,000), ATF-6 (1:2,000), PDI (1:2,000), ERK1/2 (1:1,000), and phosphor-ERK1/2 (1:1,000) were used in the present study. GAPDH (1:2,500) was used as loading control. The signals were visualized with the ChemiDic™ XRS + Imaging System (Bio-Rad Laboratories). The band densities were quantified with Multi Gauge Software of Science Lab 2006 (FUJIFILM Corporation, Tokyo, Japan).

Fluorescence Activated Cell Sorting Analysis

To assess the protective effect of FGF10 on NRK-52E against apoptosis induced by TBHP, apoptosis of NRK-52E in each group was quantified with Annexin V-FITC-PI Apoptosis Detection Kit following the manufacturing process instructions. Briefly, NRK-52E was cultured and randomly divided into four groups as described above. Cells were collected and washed twice with PBS and resuspended in binding buffer before the addition of Annexin V-FITC-PI. Cells were then gently vortex mixed and incubated for 15 min in the dark at room temperature before analysis using a BD FACSCalibur™ flow cytometer (BD Biosciences, San Jose, CA, USA) and FlowJo software (Tree Star, San Carlos, CA, USA).

Immunohistochemistry and Immunofluorescence Staining

To observe the expression and location of ER stress and apoptosis relevant proteins in kidney tissues, immunohistochemistry and immunofluorescence staining were performed. The renal morphology was detected as we described in a previous study (Tan et al., 2017). Briefly, kidneys (both of cortex and medulla)

were excised and harvested 1 day after I/R injury. After being dehydrated in gradient ethanol, renal tissue was embedded in paraffin and cut into 5 μm sections. For immunohistochemistry staining, slides were incubated with antibodies against cleaved Capase-3 (1:300), CHOP (1:300), GRP-78 (1:500), and ATF6 (1:300) separately, and then incubated at 4°C overnight. After being incubated with primary antibodies and washed with PBS solution for three times, the slides were incubated with secondary antibodies for 1 h at room temperature, washed with PBS solution for three times, stained with Diaminobenzidine (DAB), and counterstained with hematoxylin. The slides were then subjected to gradient ethanol dehydration, dimethyl benzene transparent, and mounted with neutral resin cover slides. Images were captured using a Nikon ECLPSE 80i. For immunofluorescence staining, slides were incubated with primary antibodies against CHOP (1:300) and GRP-78 (1:500) incubated at 4°C overnight. After reacting with the primary antibodies, the slides were washed 3 times with PBS and then incubated with secondary antibodies (AlexaFluor 488, Abcam) for 1 h at room temperature. Images were captured using a laser confocal microscope (Nikon, Ti-E&A1 plus).

Renal Histopathology Damage Assessment

To evaluate the renal histopathology damages, slides were stained with hematoxylin and eosin (H&E) and Periodic acid Schiff (PAS), respectively. Each image of the sections was examined under light microscope (Nikon ECLPSE 80i, Japan). Renal histopathology damage degree was evaluated based on intraluminal necrotic cells, cell swelling, interstitial congestion, edema, and protein casts. The following 5 point scoring system was utilized to assess renal damage: 0 point (normal renal morphology), 1 point (damage of kidney tissue ≤10%), 2 points (damage of kidney tissue 11–25%), 3 points (damage of kidney tissue 26–45%), 4 points (damage of kidney tissue 46–75%), 5 points (damage of kidney tissue ≥76%). The pathologists who assessed the images were blinded to the allocation group.

TUNEL Assay

The Terminal deoxynucleotidyl transferase dUTP nick end labeling (TUNEL) assay is a method for detecting DNA fragmentation. TUNEL has been widely used to identify and quantify cell death in tissues within the last two decades. To assess the protective effect of FGF10 against apoptosis, TUNEL staining and immunohistochemistry staining of cleaved Caspase-3 were used to detect the apoptosis in the kidney tissue after reperfusion. The experimental protocol was exactly the same as we described in our previous study. Kidneys were excised and harvested 1 day after I/R injury. After being dehydrated in gradient ethanol, renal tissue was embedded in paraffin and cut into 5 μm sections. For TUNEL assay, slides were handled with the TUNEL Apoptosis Assay KIT following manufacturing process instructions. The images were captured under a Laser confocal microscope (Nikon, Ti-E&A1 plus). The apoptosis index was analyzed based on five randomly selected images from each group.

Statistical Analysis

SPSS 19.0 statistical software (Cary, NC, USA) was used for the analysis of rat survival rate after reperfusion. The statistical evaluation of the data was performed using one-way Analysis of Variance (ANOVA) when two groups were compared in this study. Data are expressed as the mean ± SEM of n independent experiments ($n \geq 5$). $^{*}P < 0.05$, $^{**}P < 0.01$, and $^{***}P < 0.001$ were considered statistically significant.

RESULTS

FGF10 Protects Renal Function and Histological Integrity

We utilized a rat model of I/R injury to investigate the protective effect of FGF10 on AKI as depicted in **Figure 1A**. To evaluate the protective effect of FGF10, survival rate was analyzed for 30 days after reperfusion. As shown in **Figure 1B**, the 30-days survival rate was significantly improved in the I/R–FGF10 group (91.7%) compared with the I/R group (66.7%). Serum creatinine (Cr) levels were measured at 24 h post reperfusion to assess renal function. As expected, the level of serum Cr was increased nearly five folds in I/R rats (n = 5) compared to the Sham group (**Figure 1C**). However, the level of serum Cr in the I/R–FGF10 group was significantly decreased compared to the I/R rats ($P < 0.05$). Renal morphological changes were assessed by H&E staining; no obvious damage in the kidney of the Sham group was detected (**Figure 1D-a**), whereas the kidney of the I/R group showed typical pathological features of AKI. The arrows represent intraluminal necrotic cells, swelling of renal tubular cells, interstitial congestion, and edema. The asterisks represent protein casts in delated tubulars (**Figure 1D-b**). Administration of FGF10 significantly attenuated the extent of renal damages (**Figure 1D-c**) and largely preserved the integrity of renal morphology. Tubular injury score was analyzed based on H&E staining. As shown in **Figure 1E**, FGF10 treatment strikingly ameliorated the damage of the kidney tissue after I/R injury. There is no significant difference of the tubular injury between the I/R–FGF10 group and Sham group. PAS staining for glycogen deposition (purple plaques) further indicated that the integrity of brush border on the surface of the renal proximal epithelial cell was damaged in I/R rats. As shown in **Figure 1F-b**, the arrows point to the detachment of brush border from epithelial cell, and the asterisks represent tubular lumen narrowing caused by swelling of epithelial cells. The integrity of the brush border in the I/R–FGF10 group was significantly improved compared with the I/R group (**Figure 1F-c**). In addition, I/R rats displayed significantly increased glycogen accumulation in the glomerulus compared with that of the Sham rats, whereas FGF10 preadministration effectively reduced the deposition of glycogen in glomerulus after reperfusion (**Figure 1F**).

FGF10 Prevents I/R-Induced Apoptosis of Renal Tubular Epithelial Cells

TUNEL staining was used to assess the apoptosis of renal tubular cells caused by I/R injury. As shown in **Figure 2A**, few TUNEL-positive cells were observed in the kidney of the Sham group,

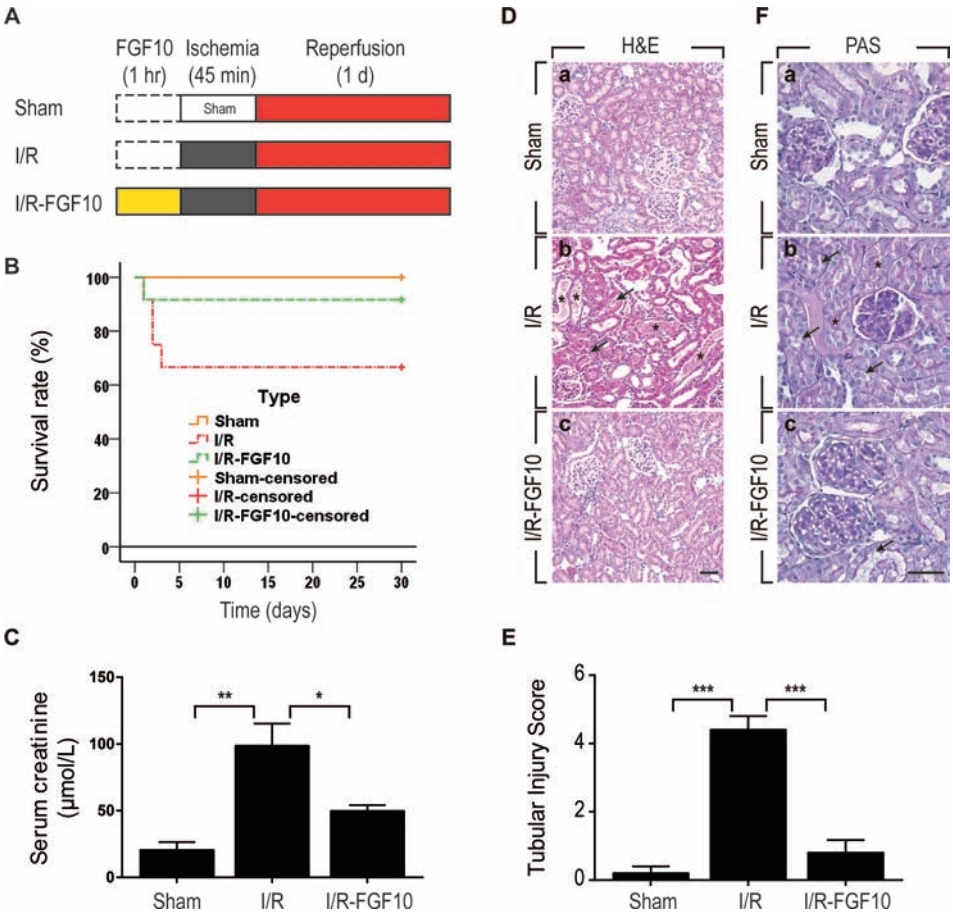

FIGURE 1 | FGF10 attenuates renal I/R injury. **(A)** Flow chart for animal procedures. **(B)** Survival rate. The survival rate of I/R–FGF10 group was significantly improved compared with the I/R group (n = 12). *$P < 0.05$. **(C)** Serum creatinine levels of animals from Sham group, I/R group and I/R-FGF10 group. *$P < 0.05$, **$P < 0.01$. n = 5. **(D)** Histological evaluations of renal tissue stained with H&E staining. Panels are representative of five animals in each group. The arrows point to renal tubular swelling, interstitial congestion and glomerular basement membrane thickening. Asterisks represent protein casts in delated tubulars. Scale bars represent 50 μm. **(E)** Tubular injury score was analyzed based on H&E staining. ***$P < 0.001$. Results are representative of five rats in each group. **(F)** Brush border of renal proximal epithelial cell was evaluated with PAS staining (purple red). The arrows represent the abscission of brush border in proximal tubulars. Asterisks represent tubular lumen narrowing caused by swelling of epithelial cells. Panels are representative of five rats in each group. Scale bars represent 50 μm.

whereas the number of TUNEL-positive cells in the kidney of the I/R–FGF10 was dramatically increased. Importantly, the number of TUNEL-positive cells in the kidney of the I/R–FGF10 group was markedly reduced compared to the I/R group. Quantification analysis of the number of TUNEL-positive cells revealed that the average percentage of dead cells was 1.19% in the Sham group, 32% in the I/R group, and 4% in the I/R–FGF10 group, respectively (**Figure 2B**).

Caspase-3, also known as CPP32, is synthesized as an inactive proenzyme that is processed to an active form (cleaved Caspase-3) in cells undergoing apoptosis (Fernandes-Alnemri et al., 1994). Previous studies have demonstrated that Caspase-3 is the most important regulatory factor in the apoptotic cell both by death ligand (extrinsic) and mitochondrial (intrinsic) pathways (Salvesen, 2002). The Bcl-2 family, including Bax and Bcl-2, plays a crucial role in the mitochondrial apoptotic pathway (Havasi and Borkan, 2011). To further clarify the mechanism under the protective effect of FGF10 against renal I/R injury, we examined the activation of cleaved Caspase-3 by immunohistochemistry staining. As shown in **Figure 3A**, I/R injury increased the production of cleaved Caspase-3 as demonstrated by strong staining in the cytoplasm of renal tubular cells. The production of cleaved Caspase-3 was markedly decreased in the kidney tissue of the I/R–FGF10 group. Furthermore, several key proteins involved in the regulation of tubular cell apoptosis including cleaved Caspase-3, Bax, and Bcl2 were determined by western blot (**Figure 3B**). As shown in **Figures 3C, D**, the production of cleaved Caspase-3 and Bax in the kidney tissue was markedly increased after reperfusion, whereas administration of FGF10 inhibited the production of cleaved Caspase-3 and Bax. Together, these results indicated that FGF10 preadministration protects the kidneys *via* alleviating apoptosis of the renal tubular epithelial cells after reperfusion.

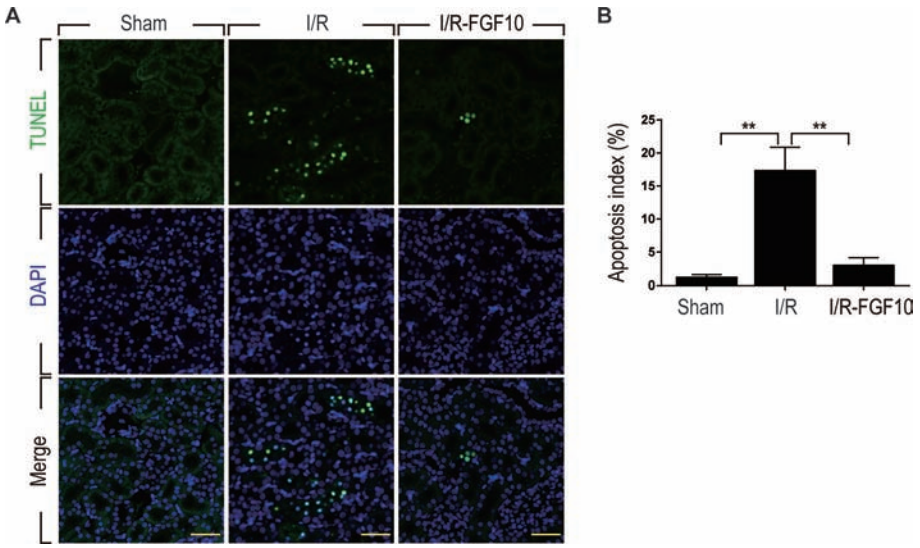

FIGURE 2 | FGF10 reduced cell death in ischemic kidneys. **(A)** Representative sections from kidney tissues 1 day after reperfusion for the detection of nuclear DNA fragmentation performed by terminal deoxynucleotidyltransferase-mediated dUTP nick end labeling (TUNEL) staining. Panels are representative of five rats in each group. Scale bars represent 50 μm. **(B)** Quantitative analysis of the proportion of TUNEL-positive renal tubular epithelial cells in kidney tissues of each group.1.19% in Sham group, 17.3% in I/R group, 1.5% in I/R–FGF10 group. FGF10 significantly reduced the apoptosis of renal tubular epithelial cells after reperfusion. Representative data of five individual samples for each group. $^{**}P < 0.001$.

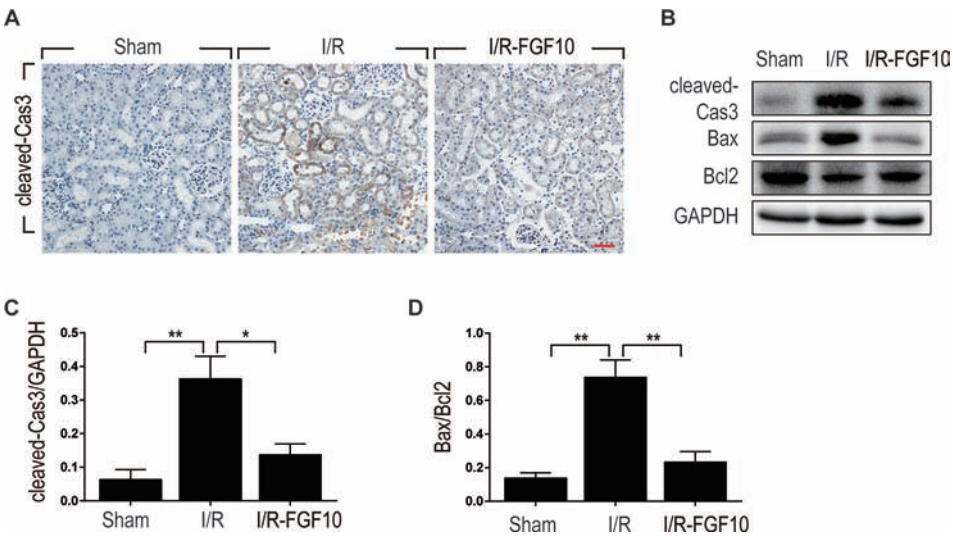

FIGURE 3 | FGF10 reduced the expression of proapoptotic proteins. **(A)** Immunohistochemistry staining of kidney tissues 1 day after reperfusion for the activation of Caspase-3. The expression of cleaved Caspase-3 was significantly increased in the cytoplasm of renal tubular cells after reperfusion, whereas FGF10 treatment reduced the expression of cleaved Caspase-3. Panels are representative of five rats in each group. Scale bars represent 50 μm. **(B)** Western blot analysis of apoptosis index expression. Total kidney tissues (contain both cortex and medulla, but don't contain renal fibrous capsule) were used for the analysis of protein expression in kidney. The expression levels of cleaved Caspase-3, Bax, and Bcl2 were detected. GAPDH was used as a loading control. **(C, D)** The column panels show the normalized optical density analysis. FGF10 significantly reduced the expression of cleaved Caspae-3 and Bax compared with I/R group. $^{*}P < 0.05$, $^{**}P < 0.01$.

The Protective Effect of FGF10 Against Renal I/R Injury Is Associated With ER Stress

ER stress is a common feature of I/R injury and known to impact renal tubular cell survival. To investigate whether the protective effect of FGF10 on renal tubular cells is associated with the inhibition of excessive ER stress, we examined the expression of ER stress related proteins by immunohistochemistry staining. As shown in **Figures 4A–C**, the expression of CHOP was dramatically increased in the nucleus and cytoplasm of renal

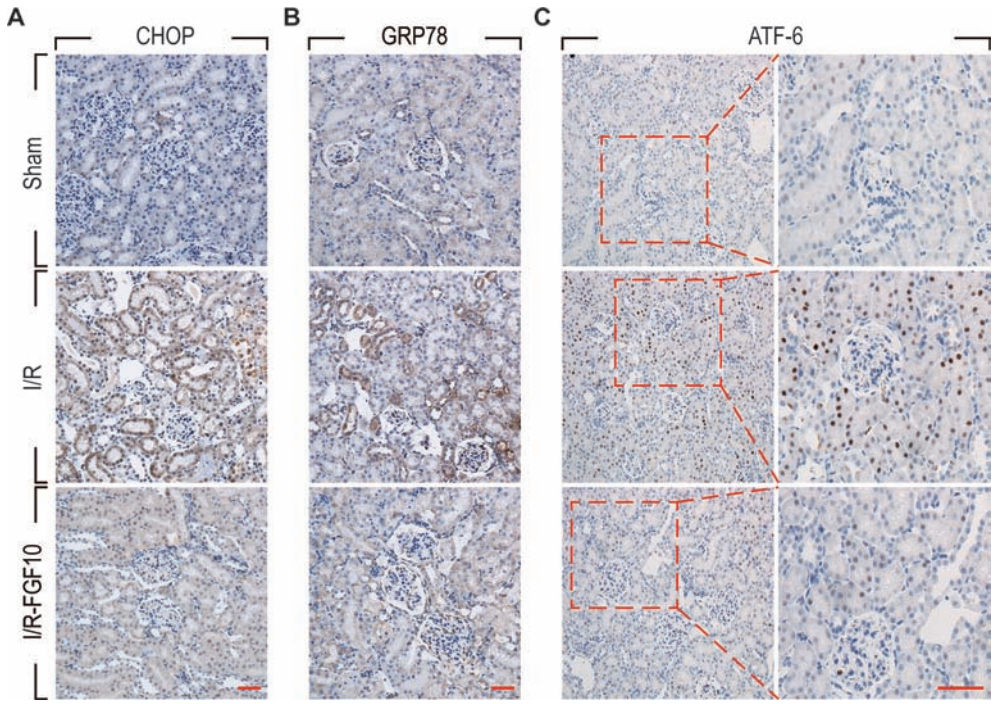

FIGURE 4 | Immunohistochemistry staining of ER stress relevant proteins in kidney tissues after reperfusion. **(A)** Immunohistochemistry staining for CHOP for renal tissues after 1 day of reperfusion. The expression of CHOP was significantly increased in the nucleus and cytoplasm of renal tubular epithelial cells after reperfusion, whereas FGF10 treatment reduced the expression of CHOP. **(B)** Immunohistochemistry staining for GRP78. FGF10 treatment reduced the expression of GRP78 in the cytoplasm of epithelial cells after reperfusion. **(C)** Immunohistochemistry staining for ATF-6. The expression of ATF-6 was significantly increased in the nucleus of renal tubular epithelial cells after reperfusion, whereas FGF10 treatment reduced the expression of ATF-6 compared to I/R alone. Panels are representative of five rats in each group. Scale bars represent 50 μm.

tubular epithelial cells after reperfusion, whereas FGF10 treatment reduced the expression of CHOP. FGF10 treatment reduced the expression of GRP78 in the cytoplasm of epithelial cells after reperfusion. The expression of ATF-6 was increased in the nucleus of renal tubular epithelial cells after reperfusion, FGF10 largely reduced the expression of ATF-6 compared to the I/R group. Results of immunohistochemistry staining confirmed that FGF10 could strikingly decreased the expression of ER stress relevant proteins induced by renal I/R injury. Western blotting was used to examine the expression of CHOP, GRP78, ATF-4, ATF6, PDI and XBP1, all of which are ER-stress effectors that, *via* regulation of the unfolded protein response, contribute to cellular homeostasis in kidney. As shown in **Figure 5A** and quantification analysis in **Figures 5B–G**, we observed elevated expression of these proteins in the kidney tissue of the I/R group, whereas pretreatment with FGF10 significantly down-regulated the expression of the proteins mentioned above. These results suggest that preadministration of FGF10 can effectively ameliorate I/R-induced maladaptive ER-stress response, which may contribute to mitigate tubular cell apoptosis. In addition, the apoptosis of renal tubular epithelial cells is the primary reason for AKI caused by I/R injury. We observed that cleaved Caspase-3, CHOP, GRP78, and ATF-6 are mainly expressed in the epithelial cells of the renal tubules (**Figures 3A** and **4**). Based on the results of immunohistochemistry staining, we could infer that FGF10 reduces apoptosis of renal tubular epithelial cells *via* inhibiting the excessive ER stress.

The Protective Effect of FGF10 Against Apoptosis Is Related to ERK1/2 Pathway

MAPK/ERK1/2 is a critical downstream pathway of FGF, which plays an important role in the regulation of variety of cellular processes including cell survival, proliferation, migration, and differentiation (Lunn et al., 2007). As mentioned above, FGF10 specifically binds to FGFR2b, which was distributed in the membrane of epithelial cells. To assess the effect of FGF10 on the activation of ERK1/2 pathway, we detected the phosphorylation of ERK1/2 in the kidney tissue of the Sham group, the I/R group, and the I/R–FGF10 group. As shown in **Figures 5A, H**, the phosphorylation of ERK1/2 was mildly increased in the kidney tissue of the I/R group compared to the Sham group. Preadministration of FGF10 led to a robust increase in the phosphorylation of ERK1/2 compared to the I/R group. The PI3K–Akt signal transduction pathway also plays an important role in the regulation of cell survival, proliferation, and migration (Wang et al., 2012). We also detected the phosphorylation of AKT in the kidney tissue of the Sham group, I/R group, and I/R–FGF10 group. As shown in **Figures 5A, I**, the phosphorylation of AKT was increased in the kidney tissue of the I/R group compared to the Sham group. However, there is no significant difference in the

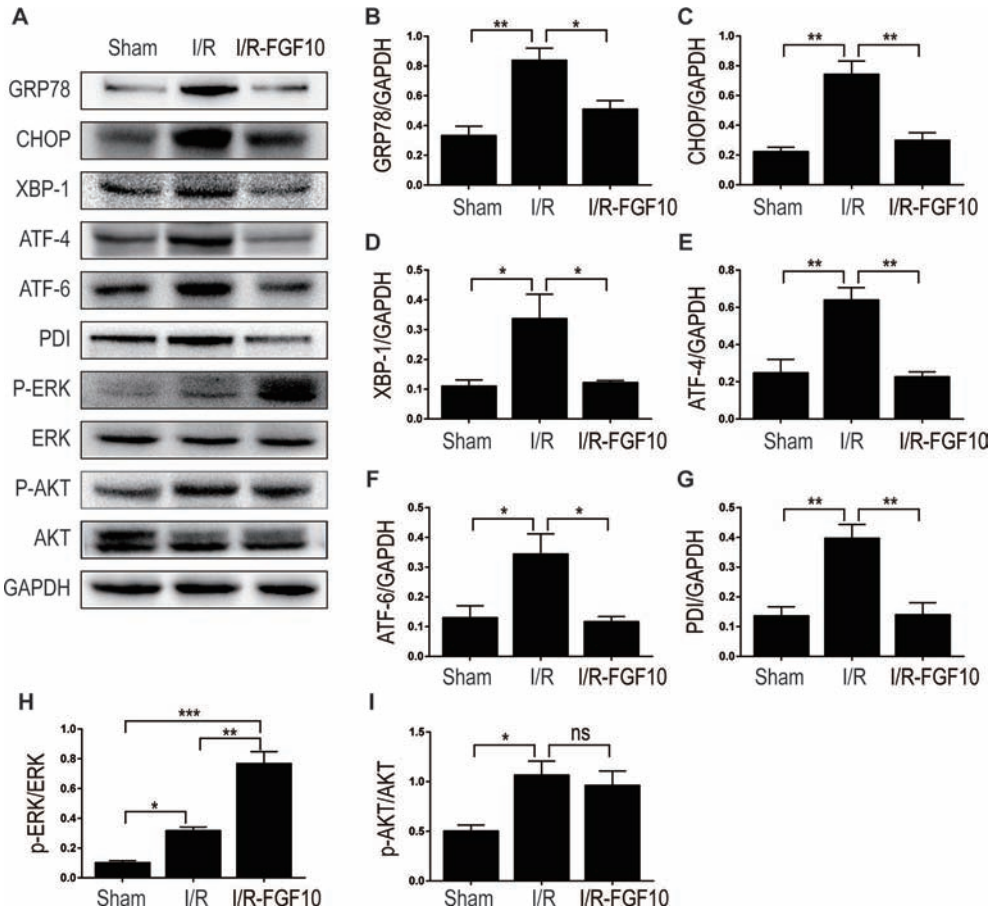

FIGURE 5 | The regulation effect of FGF10 on ER stress and ERK1/2 signaling pathway. **(A)** The expression levels of GRP-78, CHOP, XBP-1, ATF-4, ATF-6, PDI, ERK1/2, and phospho-ERK1/2 in kidney tissues of Sham group, I/R group and I/R-FGF10 group were determined by immunoblot analysis. FGF10 significantly increased the phosphorylation of ERK1/2. **(B–I)** The histograms show the normalized optical density analysis. Results are representative of five rats in each group. $^{*}P < 0.05$, $^{**}P < 0.01$, $^{***}P < 0.001$, *ns* represents no significant difference.

phosphorylation of AKT in the kidney tissue between the I/R group and I/R–FGF10 group. Those results may imply that FGF10 protects against renal I/R injury through activating the ERK1/2 signaling pathway, not the PI3K-Akt signaling pathway. To further clarify the relationship between the ERK1/2 signaling pathway and the protective effect of FGF10, we treated NRK-52E cells with TBHP, a commonly ROS inducer which is much stable compared with hydrogen peroxide (H_2O_2) solution. The apoptosis of NRK52E cells was detected by flow cytometric analysis with Annexin V-FITC-PI Apoptosis Detection Kit. As shown in **Figures 6A, B**, FGF10 treatment significantly reduced the apoptosis rate of NER-52E caused by TBHP. However, U0126, a selective inhibitor of MEK1/2 that blocks the phosphorylation of ERK1/2 (Shukla et al., 2007), largely abolished the protective effect of FGF10 on NRK-52E cells. To further confirm the role of ERK1/2 signaling pathway in the protective effect against TBHP-induced apoptosis, the expression of cleaved Caspase-3, cleaved Caspase-9, Bax, and Bcl2 was detected by immunoblots. Caspase-9 is an initiator caspase which could further process the activation of other caspases, including Caspase-3, to start the caspase cascade leading to apoptosis. Under the action of the apoptotic signals, the release of Cytochrome c from the mitochondria and activation of Apoptotic protease activating factor 1 (APAF1) cleave pro-caspase 9 into the active form (Li et al., 1997). Our results indicated that FGF10 pretreatment effectively antagonized TBHP-induced Caspase-3 and Caspase-9 cleavages. More importantly, the effect of FGF10 was completely reversed in the presence of MEK inhibitor U0126. Consistently, the drastically increased production of Bax caused by TBHP also appeared to be restored with the treatment of FGF10. However, U0126 exposure partially reversed the effect of FGF10 (**Figures 7A–D**).

As shown in **Figures 7A, E**, FGF10 treatment significantly activated ERK1/2 phosphorylation compared to the TBHP group, which is consistent with what we observed in the kidney tissue. As expected, preaddition of U0126, a highly specific inhibitor of MEK, largely abolished the effect of FGF10 on the phosphorylation of ERK1/2 in NRK-52E cells. These results strongly suggest that ERK1/2 activation is a crucial mechanism in FGF10-mediated protection against cell apoptosis in both I/R injured kidney and TBHP injured NRK-52E cells.

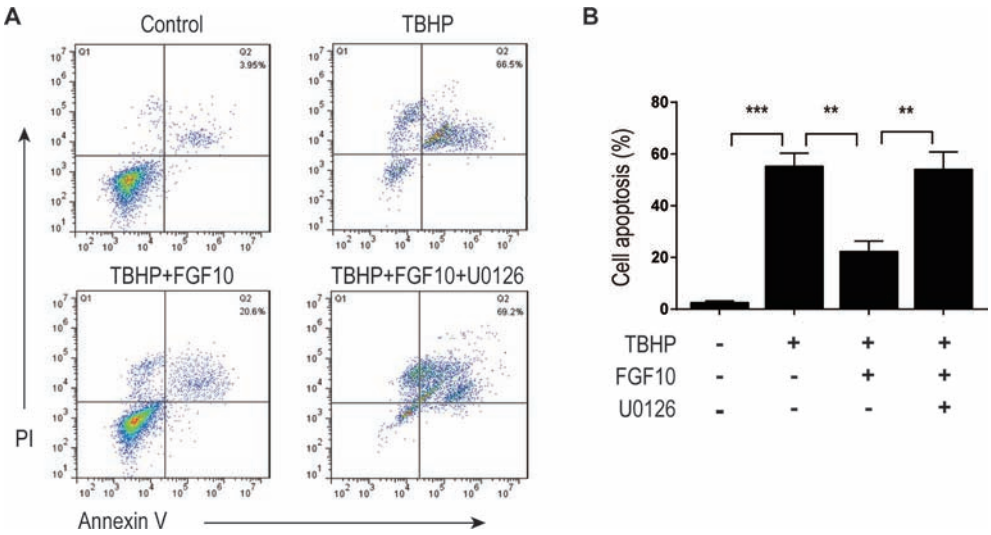

FIGURE 6 | FGF10 inhibits the apoptosis of NRK-52E induced by TBHP. **(A)** Apoptosis of NRK-52E was detected by flow cytometry with annexin V-FITC-/propidium iodide. The top-right panel indicates the apoptotic cells. **(B)** Bar chart represents the apoptosis rate of NRK-52E in each group with three separate experiments. $^{**}P < 0.01$, $^{***}P < 0.001$.

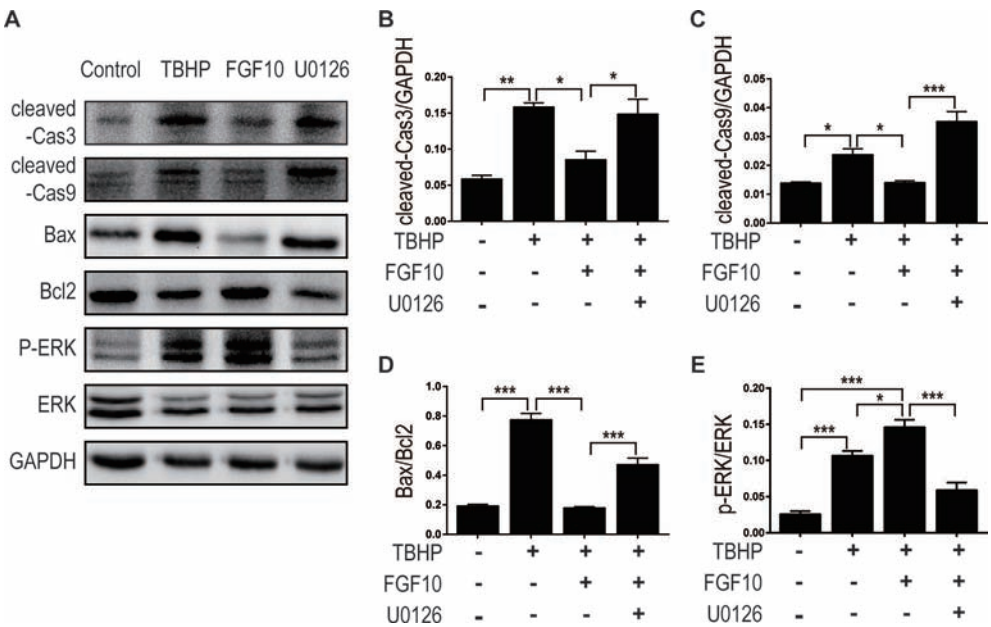

FIGURE 7 | FGF10 reduced the expression of proapoptotic proteins via activating ERK1/2 signaling pathway. **(A)** For protein analysis of *in vitro* samples, total proteins of NRK-52E were extracted using cell lysis buffer. NRK-52E was treated with different culture media and then the expression of cleaved Caspase-3, cleaved Caspase-9, Bax, Bcl-2, ERK1/2, and phosphor-ERK1/2 was detected by western blotting. **(B–E)** Histogram figures show the normalized optical density analysis. Results are representative of five rats in each group. $^{*}P < 0.05$, $^{**}P < 0.01$, $^{***}P < 0.001$.

The Effect of FGF10 on the Regulation of ER Stress Is Related to the Activation of ERK1/2 Pathway

To clarify the relationship between the protective effect of FGF10 and ER stress, we examined the expression of CHOP and GRP78 by immunofluorescence staining in NRK-52E cells respectively (**Figures 8A, B**). We observed that FGF10 effectively attenuated ER stress relevant proteins induced by TBHP, which was inhibited by U0126 to a large extent. The expression levels of CHOP and GRP78 were also examined by western blotting. As

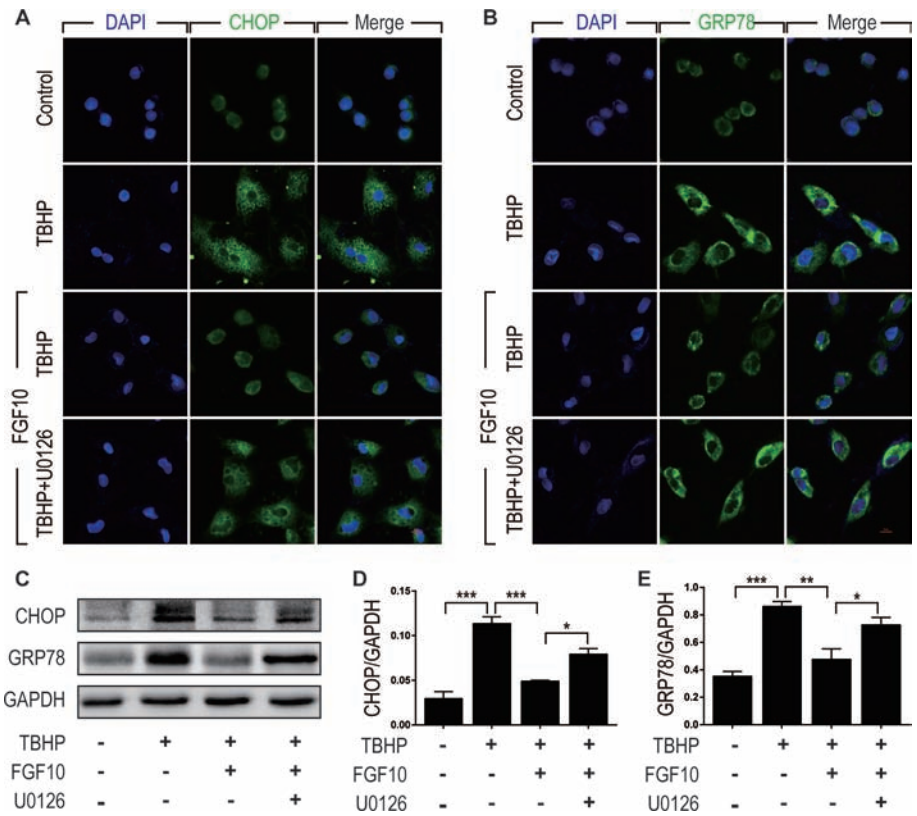

FIGURE 8 | FGF10 attenuates ER stress in NRK-52E cells. **(A, B)** Immunofluorescent staining for CHOP and GRP78 in NRK-52E. FGF10 significantly decreased the expression of CHOP and GRP78 in NRK-52E induced by TBHP, whereas U0126 largely eliminated the effect of FGF10. Panels are representative of five rats in each group. Scale bar represents 50 μm. **(C)** The expression of CHOP and GRP78 was detected by Western blotting. **(D, E)** Bar chart for quantification analysis for the expression of CHOP and GRP78. Results are representative of five rats in each group. GAPDH was used as a protein loading control. $^{*}P < 0.05$, $^{**}P < 0.01$, $^{***}P < 0.001$.

shown in **Figures 8C, D, E**, TBHP remarkably increased the expression of CHOP and GRP78 in NRK52E cells, indicating that oxidative stress triggered excessive ER stress in these cells. Similar to the results observed *in vivo*, FGF10 significantly reduced the expression of CHOP and GRP78 in NRK-52E cells treated with TBHP. The effect of FGF10 is partially abolished by U0126. Our results strongly suggested that activation of ERK1/2 signal pathway contributes to FGF10 mediated protection against maladaptive ER stress.

DISCUSSION

AKI, mainly caused by renal I/R injury, remains a vexing health problem. Despite the current clinical advances in prevention and treatment, the morbidity and mortality of AKI in hospitalized patients remain very high (Basile et al., 2012; Winterberg and Lu, 2012). As a crucial mesenchymal–epithelial signaling growth factor in embryonic development, tissue repair, and regeneration, the role of FGF10 has been investigated in several disease conditions such as cerebral ischemia injury, pulmonary fibrosis, and wound healing (Li et al., 2016; Chen et al., 2017; Chao et al., 2017; El Agha et al., 2017). However, whether FGF10 is capable of delivering a protective effect on AKI in rat model of I/R injury is still unclear.

Currently, many studies reported the relationship between ERK1/2, ER stress, and apoptosis (Sun et al., 2015; Yao et al., 2017). Generally, ERK1/2 are activated upon phosphorylation by MEK1/2 and are considered to promote cell survival (Darling and Cook, 2014). ERK1/2 signaling inhibits apoptosis *via* activating the expression of prosurvival proteins (BCL-2, MCL-1, and BCL-$_{XL}$) and repressing the expression of proapoptotic proteins (BAD, BIM, BMF, and PUMA). However, in some certain conditions such as starvation, ERK1/2 could also promote the expression of NOXA (phorbol-12-myristate-13-acetate-induced protein 1), a proapoptotic member of the BCL-2 family, to decide autophagy or apoptosis (Yao et al., 2017). ER stress could be triggered by a variety of extracellular stimuli and induces apoptosis. It has been reported that renal tubular cell apoptosis induced by I/R injury is associated with excessive ER stress. Excessive ER stress can activate apoptotic signaling pathways *via* CHOP, a master regulator of maladaptive

ER stress-induced apoptosis (Rutkowski et al., 2006). The interaction of ERK1/2 signaling pathway and ER stress has been reported in many studies (Zhang et al., 2009; Darling and Cook, 2014). The activation of the ERK1/2 signaling pathway exhibits an antiapoptotic role during ER stress through regulating the IRE1 (inositol requiring enzyme 1) axis of the UPR (Darling and Cook, 2014). FGF10 is a member of the FGF family with multifunctional effect in the regulation of development, wound healing, and tissue regeneration. It has been proved that FGF10 can ameliorate cerebral I/R injury and spinal cord injury *via* inhibiting NF-κB-dependent inflammation and activating the PI3K/Akt signaling pathway (Li et al., 2016; Chen et al., 2017; Dong et al., 2019). In our previous study, we demonstrated that FGF10 can protect the kidney against apoptosis *via* the regulation of inflammatory response and autophagy (Tan et al., 2018). In our present study, the administration of FGF10 can not only reduced the expression of proapoptotic proteins, but also effectively alleviated ER stress kidneys after I/R injury. Therefore, FGF10 exhibits reliable capability in the protection against AKI caused by I/R injury *via* inhibiting maladaptive ER stress.

ER stress and UPR, which could be provoked by glucose depletion and hypoxia after renal I/R injury, have previously shown to play a pivotal role in the enhancement of protein folding ability (Belaidi et al., 2013; Wang et al., 2015). However, excessive and prolonged ER stress and UPR can elicit glomerular and tubular cell damage in patients with AKI and CKD (Bhatt et al., 2008; Inagi, 2009; Xu et al., 2016). Our present results indicated that the expression of ER stress relevant proteins including CHOP, GRP78, XBP-1, ATF-4, ATF-6, and PDI was significantly increased after reperfusion. Importantly, treatment of recombination FGF10 can reduce ER stress relevant proteins and thus inhibited renal tubular cell apoptosis caused by I/R injury. The present study suggested that the renoprotective effect of FGF10 is associated with the regulation of ER stress.

Mitogen-activated protein kinases (MAPKs) are among the most commonly activated signaling pathways associated with various renal injuries (Tian et al., 2000). ERK, an important member of MAPK family, is mainly activated by mitogenic stimuli such as growth factor and hormones. The ERK1/2 signaling pathway is particularly important in the regulation of cell survival, migration, differentiation, and proliferation in a variety of circumstances (Sun et al., 2015; Yao et al., 2017). The role of ERK1/2 in the restoration of renal structure and function is still controversial (Feliers and Kasinath, 2011; Zhang and Cai, 2016; Li et al., 2018). To confirm the role of ERK1/2 in the protective effect of FGF10 on AKI caused by renal I/R injury, we examined the expression of phospho-ERK1/2 in the kidney tissue after reperfusion as shown in **Figure 5**. Our experiments' results confirmed that FGF10 treatment increased the phosphorylation of ERK1/2 in the kidney tissues after reperfusion. As the effect of FGF10 in reducing apoptosis and inhibiting ER stress has been verified in the present study, we speculate that the protective effect of FGF10 in down-regulation of apoptosis may be related to the activation of ERK1/2 signaling pathway.

To further clarify the role of ERK1/2 signaling pathway in the regulation of FGF10 on ER stress after reperfusion, we then examined the protective effect of FGF10 against apoptosis with NRK-52E induced by TBHP. TBHP is a widely used oxidative stress inducer which can increase intracellular ROS production. Our present study demonstrated that FGF10 treatment can strikingly inhibit the apoptosis of NER-52E induced by TBHP. U0126, a specific inhibitor of MKK, abrogated the antiapoptosis effect of FGF10 *via* blocking the phosphorylation of ERK1/2. Moreover, U0126 also reversed the down-regulation effect of FGF10 on ER stress related proteins including GRP78 and CHOP. These results suggest that ERK1/2 signaling pathway is probably the downstream signals induced by FGF10 in the restoration of renal I/R injury. U0126 could suppress the activation of ERK1/2 and abolish the role of FGF10 in the regulation of ER stress on injured NRK-52E induced by TBHP.

As a multifunctional growth factor, FGF10 has been reported to play crucial roles in development and disease. However, the protective mechanism of FGF10 on AKI has not yet been clearly elucidated. In the present study, we confirmed that renal tubular epithelial cell apoptosis induced by hypoxia injury is related to the excessive activation of ER stress. Convincing experimental evidence has been provided both *in vivo* and *in vitro* that exogenously administered FGF10 could attenuate renal tubular epithelial cell apoptosis *via* inhibiting excessive ER stress. Through *in vitro* experiments, we also demonstrated that the protective effect of FGF10 is, at least partly, mediated by MEK–ERK1/2 signaling pathway. In conclusion, results of our present study have implications for understanding the pathophysiology of AKI caused by renal I/R injury and indicate the therapeutic potential of FGF10 in clinical applications. Future research should clarify the exact protective mechanisms of FGF10 in tissue repair and provide novel insights in the field of regenerative medicine.

DATA AVAILABILITY STATEMENT

All datasets generated for this study are included in the article/supplementary material.

ETHICS STATEMENT

The animal study was reviewed and approved by the Animal Experimentation Ethics Committee of Wenzhou Medical University, Wenzhou, China.

AUTHOR CONTRIBUTIONS

XT, JX and J-SZ conceived and designed the experiments. XT, LY, and QT performed the animal operation. XT, LY, RY, and LX performed cell culture, apoptosis assay, FACS

analysis, immunoblot, immunohistochemistry, and immunofluorescent staining. XT and LY analyzed the experiments data and prepared the figures. XT and J-SZ wrote and revised the manuscript. J-SZ and JX funded the project.

ACKNOWLEDGMENTS

This study was supported by the National Natural Science Foundation of China (81500519, 81472601) and the Scientific Research Starting Foundation of Qingdao University (DC1900011202).

REFERENCES

Basile, D. P., Anderson, M. D., and Sutton, T. A. (2012). Pathophysiology of acute kidney injury. *Compr. Physiol.* 2 (2), 1303–1353. doi: 10.1002/cphy.c110041

Beenken, A., and Mohammadi, M. (2009). The FGF family: biology, pathophysiology and therapy. *Nat. Rev. Drug Discovery* 8 (3), 235–253. doi: 10.1038/nrd2792

Belaidi, E., Decorps, J., Augeul, L., Durand, A., and Ovize, M. (2013). Endoplasmic reticulum stress contributes to heart protection induced by cyclophilin D inhibition. *Basic Res. Cardiol.* 108 (4), 363. doi: 10.1007/s00395-013-0363-z

Bhatt, K., Feng, L. P., Pabla, N., Liu, K. B., Smith, S., and Dong, Z. (2008). Effects of targeted Bcl-2 expression in mitochondria or endoplasmic reticulum on renal tubular cell apoptosis. *Am. J. Physiol-Renal* 294 (3), F499–F507. doi: 10.1152/ajprenal.00415.2007

Bonventre, J. V., and Yang, L. (2011). Cellular pathophysiology of ischemic acute kidney injury. *J. Clin. Invest.* 121 (11), 4210–4221. doi: 10.1172/JCI45161

Cao, S. S., and Kaufman, R. J. (2012). Unfolded protein response. *Curr. Biol.* 22 (16), R622–R624. doi: 10.1016/j.cub.2012.07.004

Cao, S. S., and Kaufman, R. J. (2014). Endoplasmic reticulum stress and oxidative stress in cell fate decision and human disease. *Antioxid. Redox Signal* 21 (3), 396–413. doi: 10.1089/ars.2014.5851

Chao, C. M., Yahya, F., Moiseenko, A., Tiozzo, C., Shrestha, A., Ahmadvand, N., et al. (2017). Fgf10 deficiency is causative for lethality in a mouse model of bronchopulmonary dysplasia. *J. Pathol.* 241 (1), 91–103. doi: 10.1002/path.4834

Chen, J., Wang, Z., Zheng, Z., Chen, Y., Khor, S., Shi, K., et al. (2017). Neuron and microglia/macrophage-derived FGF10 activate neuronal FGFR2/PI3K/Akt signaling and inhibit microglia/macrophages TLR4/NF-kappaB-dependent neuroinflammation to improve functional recovery after spinal cord injury. *Cell Death Dis.* 8 (10), e3090. doi: 10.1038/cddis.2017.490

Chertow, G. M., Burdick, E., Honour, M., Bonventre, J. V., and Bates, D. W. (2005). Acute kidney injury, mortality, length of stay, and costs in hospitalized patients. *J. Am. Soc. Nephrol.* 16 (11), 3365–3370. doi: 10.1681/ASN.2004090740

Cho, K. W., Cai, J. L., Kim, H. Y., Hosoya, A., Ohshima, H., Choi, K. Y., et al. (2009). ERK Activation is Involved in Tooth Development via FGF10 Signaling. *J. Exp. Zool. Part B.* 312b (8), 901–911. doi: 10.1002/jez.b.21309

Darling, N. J., and Cook, S. J. (2014). The role of MAPK signalling pathways in the response to endoplasmic reticulum stress. *Biochim. Biophys. Acta* 1843 (10), 2150–2163. doi: 10.1016/j.bbamcr.2014.01.009

De Moerlooze, L., Spencer-Dene, B., Revest, J. M., Hajihosseini, M., Rosewell, I., and Dickson, C. (2000). An important role for the IIIb isoform of fibroblast growth factor receptor 2 (FGFR2) in mesenchymal-epithelial signalling during mouse organogenesis. *Development* 127 (3), 483–492.

Dong, L., Li, R., Li, D., Wang, B., Lu, Y., Li, P., et al. (2019). FGF10 enhances peripheral nerve regeneration via the preactivation of the PI3K/Akt signaling-mediated antioxidant response. *Front. Pharmacol.* 10, 1224. doi: 10.3389/fphar.2019.01224

El Agha, E., Al Alam, D., Carraro, G., MacKenzie, B., Goth, K., De Langhe, S. P., et al. (2012). Characterization of a novel fibroblast growth factor 10 (Fgf10) knock-in mouse line to target mesenchymal progenitors during embryonic development. *PloS One* 7 (6), e38452. doi: 10.1371/journal.pone.0038452

El Agha, E., Moiseenko, A., Kheirollahi, V., De Langhe, S., Crnkovic, S., Kwapiszewska, G., et al. (2017). Two-way conversion between lipogenic and myogenic fibroblastic phenotypes marks the progression and resolution of lung fibrosis. *Cell Stem Cell* 20 (4), 571. doi: 10.1016/j.stem.2017.03.011

Feliers, D., and Kasinath, B. S. (2011). Erk in kidney diseases. *J. Signal Transduct.* 2011, 768512. doi: 10.1155/2011/768512

Fernandes-Alnemri, T., Litwack, G., and Alnemri, E. S. (1994). CPP32, a novel human apoptotic protein with homology to Caenorhabditis elegans cell death protein Ced-3 and mammalian interleukin-1 beta-converting enzyme. *J. Biol. Chem.* 269 (49), 30761–30764.

Freytes, C. O., Ratanatharathorn, V., Taylor, C., Abboud, C., Chesser, N., Restrepo, A., et al. (2004). Phase I/II randomized trial evaluating the safety and clinical effects of repifermin administered to reduce mucositis in patients undergoing autologous hematopoietic stem cell transplantation. *Clin. Cancer Res.* 10 (24), 8318–8324. doi: 10.1158/1078-0432.CCR-04-1118

Havasi, A., and Borkan, S. C. (2011). Apoptosis and acute kidney injury. *Kidney Int.* 80 (1), 29–40. doi: 10.1038/ki.2011.120

Hetz, C. (2012). The unfolded protein response. controlling cell fate decisions under ER stress and beyond. *Nat. Rev. Mol. Cell Biol.* 13 (2), 89–102. doi: 10.1038/nrm3270

Hotamisligil, G. S. (2010). Endoplasmic reticulum stress and the inflammatory basis of metabolic disease. *Cell* 140 (6), 900–917. doi: 10.1016/j.cell.2010.02.034

Inagi, R. (2009). Endoplasmic reticulum stress in the kidney as a novel mediator of kidney injury. *Nephron Exp. Nephrol.* 112 (1), E1–E9. doi: 10.1159/000210573

Inoue, T., Maekawa, H., and Inagi, R. (2019). Organelle crosstalk in the kidney. *Kidney Int.* 95 (6), 1318–1325. doi: 10.1016/j.kint.2018.11.035

Ishani, A., Xue, J. L., Himmelfarb, J., Eggers, P. W., Kimmel, P. L., Molitoris, B. A., et al. (2009). Acute kidney injury increases risk of ESRD among elderly. *J. Am. Soc. Nephrol.* 20 (1), 223–228. doi: 10.1681/ASN.2007080837

Itoh, N., and Ohta, H. (2014). Fgf10: a paracrine-signaling molecule in development, disease, and regenerative medicine. *Curr. Mol. Med.* 14 (4), 504–509. doi: 10.2174/1566524014666140414204829

Itoh, N. (2015). FGF10: a multifunctional mesenchymal-epithelial signaling growth factor in development, health, and disease. *Cytokine Growth Factor Rev.* doi: 10.1016/j.cytogfr.2015.10.001

Li, P., Nijhawan, D., Budihardjo, I., Srinivasula, S. M., Ahmad, M., Alnemri, E. S., et al. (1997). Cytochrome c and dATP-dependent formation of Apaf-1/caspase-9 complex initiates an apoptotic protease cascade. *Cell* 91 (4), 479–489. doi: 10.1016/S0092-8674(00)80434-1

Li, Y. H., Fu, H. L., Tian, M. L., Wang, Y. Q., Chen, W., Cai, L. L., et al. (2016). Neuron-derived FGF10 ameliorates cerebral ischemia injury via inhibiting NF-kappaB-dependent neuroinflammation and activating PI3K/Akt survival signaling pathway in mice. *Sci. Rep.* 6, 19869. doi: 10.1038/srep19869

Li, Z., Xu, K., Zhang, N., Amador, G., Wang, Y., Zhao, S., et al. (2018). Overexpressed SIRT6 attenuates cisplatin-induced acute kidney injury by inhibiting ERK1/2 signaling. *Kidney Int.* 93 (4), 881–892. doi: 10.1016/j.kint.2017.10.021

Lunn, J. S., Fishwick, K. J., Halley, P. A., and Storey, K. G. (2007). A spatial and temporal map of FGF/Erk1/2 activity and response repertoires in the early chick embryo. *Dev. Biol.* 302 (2), 536–552. doi: 10.1016/j.ydbio.2006.10.014

Mehta, R. L., Kellum, J. A., Shah, S. V., Molitoris, B. A., Ronco, C., Warnock, D. G., et al. (2007). Acute Kidney Injury Network: report of an initiative to improve outcomes in acute kidney injury. *Crit. Care* 11 (2), R31. doi: 10.1186/cc5713

Michos, O., Cebrian, C., Hyink, D., Grieshammer, U., Williams, L., D'Agati, V., et al. (2010). Kidney development in the absence of Gdnf and Spry1 requires Fgf10. *PloS Genet.* 6 (1), e1000809. doi: 10.1371/journal.pgen.1000809

Ohuchi, H., Hori, Y., Yamasaki, M., Harada, H., Sekine, K., Kato, S., et al. (2000). FGF10 acts as a major ligand for FGF receptor 2 IIIb in mouse multi-organ development. *Biochem. Bioph Res. Co* 277 (3), 643–649. doi: 10.1006/bbrc.2000.3721

Paller, M. S., Hoidal, J. R., and Ferris, T. F. (1984). Oxygen free radicals in ischemic acute renal failure in the rat. *J. Clin. Invest.* 74 (4), 1156–1164. doi: 10.1172/JCI111524

Rochais, F., Sturny, R., Chao, C. M., Mesbah, K., Bennett, M., Mohun, T. J., et al. (2014). FGF10 promotes regional foetal cardiomyocyte proliferation and adult

cardiomyocyte cell-cycle re-entry. *Cardiovasc. Res.* 104 (3), 432–442. doi: 10.1093/cvr/cvu232

Rutkowski, D. T., Arnold, S. M., Miller, C. N., Wu, J., Li, J., Gunnison, K. M., et al. (2006). Adaptation to ER stress is mediated by differential stabilities of pro-survival and pro-apoptotic mRNAs and proteins. *PloS Biol.* 4 (11), 2024–2041. doi: 10.1371/journal.pbio.0040374

Salvesen, G. S. (2002). Caspases: opening the boxes and interpreting the arrows. *Cell Death Differ.* 9 (1), 3–5. doi: 10.1038/sj.cdd.4400963

Sandborn, W. J., Sands, B. E., Wolf, D. C., Valentine, J. F., Safdi, M., Katz, S., et al. (2003). Repifermin (keratinocyte growth factor-2) for the treatment of active ulcerative colitis: a randomized, double-blind, placebo-controlled, dose-escalation trial. *Aliment. Pharmacol. Ther.* 17 (11), 1355–1364. doi: 10.1046/j.1365-2036.2003.01589.x

Schuck, S., Prinz, W. A., Thorn, K. S., Voss, C., and Walter, P. (2009). Membrane expansion alleviates endoplasmic reticulum stress independently of the unfolded protein response. *J. Cell Biol.* 187 (4), 525–536. doi: 10.1083/jcb.200907074

Shukla, V., Coumoul, X., Wang, R. H., Kim, H. S., and Deng, C. X. (2007). RNA interference and inhibition of MEK-ERK signaling prevent abnormal skeletal phenotypes in a mouse model of craniosynostosis. *Nat. Genet.* 39 (9), 1145–1150. doi: 10.1038/ng2096

Sun, Y., Liu, W. Z., Liu, T., Feng, X., Yang, N., and Zhou, H. F. (2015). Signaling pathway of MAPK/ERK in cell proliferation, differentiation, migration, senescence and apoptosis. *J. Recept. Signal Transduct. Res.* 35 (6), 600–604. doi: 10.3109/10799893.2015.1030412

Tabas, I., and Ron, D. (2011). Integrating the mechanisms of apoptosis induced by endoplasmic reticulum stress. *Nat. Cell Biol.* 13 (3), 184–190. doi: 10.1038/ncb0311-184

Tan, X., Zhang, L., Jiang, Y., Yang, Y., Zhang, W., Li, Y., et al. (2013). Postconditioning ameliorates mitochondrial DNA damage and deletion after renal ischemic injury. *Nephrol. Dial. Transplant.* 28 (11), 2754–2765. doi: 10.1093/ndt/gft278

Tan, X. H., Zheng, X. M., Yu, L. X., He, J., Zhu, H. M., Ge, X. P., et al. (2017). Fibroblast growth factor 2 protects against renal ischaemia/reperfusion injury by attenuating mitochondrial damage and proinflammatory signalling. *J. Cell Mol. Med.* 21 (11), 2909–2925. doi: 10.1111/jcmm.13203

Tan, X., Zhu, H., Tao, Q., Guo, L., Jiang, T., Xu, L., et al. (2018). FGF10 protects against renal ischemia/reperfusion injury by regulating autophagy and inflammatory signaling. *Front. Genet.* 9, 556. doi: 10.3389/fgene.2018.00556

Thadhani, R., Pascual, M., and Bonventre, J. V. (1996). Acute renal failure. *N. Engl. J. Med.* 334 (22), 1448–1460. doi: 10.1056/NEJM199605303342207

Tian, W., Zhang, Z., and Cohen, D. M. (2000). MAPK signaling and the kidney. *Am. J. Physiol. Renal Physiol.* 279 (4), F593–F604. doi: 10.1152/ajprenal.2000.279.4.F593

Tsuda, H., Kawada, N., Kaimori, J., Kitamura, H., Moriyama, T., Rakugi, H., et al. (2012). Febuxostat suppressed renal ischemia-reperfusion injury via reduced oxidative stress. *Biochem. Bioph Res. Co* 427 (2), 266–272. doi: 10.1016/j.bbrc.2012.09.032

Uchino, S., Kellum, J. A., Bellomo, R., Doig, G. S., Morimatsu, H., Morgera, S., et al. (2005). Acute renal failure in critically ill patients: a multinational, multicenter study. *JAMA* 294 (7), 813–818. doi: 10.1001/jama.294.7.813

Walter, P., and Ron, D. (2011). The unfolded protein response: from stress pathway to homeostatic regulation. *Sci.* 334 (6059), 1081–1086. doi: 10.1126/science.1209038

Wang, X. F., Lin, G., Martins-Taylor, K., Zeng, H., and Xu, R. H. (2009). Inhibition of caspase-mediated anoikis is critical for basic fibroblast growth factor-sustained culture of human pluripotent stem cells. *J. Biol. Chem.* 284 (49), 34054–34064. doi: 10.1074/jbc.M109.052290

Wang, Z., Zhang, H., Xu, X., Shi, H., Yu, X., Wang, X., et al. (2012). bFGF inhibits ER stress induced by ischemic oxidative injury via activation of the PI3K/Akt and ERK1/2 pathways. *Toxicol. Lett.* 212 (2), 137–146. doi: 10.1016/j.toxlet.2012.05.006

Wang, Z. G., Wang, Y., Ye, J. M., Lu, X. H., Cheng, Y., Xiang, L. J., et al. (2015). bFGF attenuates endoplasmic reticulum stress and mitochondrial injury on myocardial ischaemia/reperfusion via activation of PI3K/Akt/ERK1/2 pathway. *J. Cell Mol. Med.* 19 (3), 595–607. doi: 10.1111/jcmm.12346

Winterberg, P. D., and Lu, C. Y. (2012). Acute kidney injury: the beginning of the end of the dark ages. *Am. J. Med. Sci.* 344 (4), 318–325. doi: 10.1097/MAJ.0b013e318228aef8

Xu, Y., Guo, M., Jiang, W., Dong, H., Han, Y. F., An, X. F., et al. (2016). Endoplasmic reticulum stress and its effects on renal tubular cells apoptosis in ischemic acute kidney injury. *Ren. Fail* 38 (5), 831–837. doi: 10.3109/0886022X.2016.1160724

Yao, Y., Lu, Q., Hu, Z., Yu, Y., and Chen, Q. (2017). Wang QK. a non-canonical pathway regulates ER stress signaling and blocks ER stress-induced apoptosis and heart failure. *Nat. Commun.* 8 (1), 133. doi: 10.1038/s41467-017-00171-w

Zhang, Z., and Cai, C. X. (2016). Kidney injury molecule-1 (KIM-1) mediates renal epithelial cell repair via ERK MAPK signaling pathway. *Mol. Cell Biochem.* 416 (1-2), 109–116. doi: 10.1007/s11010-016-2700-7

Zhang, X. Q., Ibrahimi, O. A., Olsen, S. K., Umemori, H., Mohammadi, M., and Ornitz, D. M. (2006). Receptor specificity of the fibroblast growth factor family - The complete mammalian FGF family. *J. Biol. Chem.* 281 (23), 15694–15700. doi: 10.1074/jbc.M601252200

Zhang, L. J., Chen, S., Wu, P., Hu, C. S., Thorne, R. F., Luo, C. M., et al. (2009). Inhibition of MEK blocks GRP78 up-regulation and enhances apoptosis induced by ER stress in gastric cancer cells. *Cancer Lett.* 274 (1), 40–46. doi: 10.1016/j.canlet.2008.08.030

Conflict of Interest: The authors declare that the research was conducted in the absence of any commercial or financial relationships that could be construed as a potential conflict of interest

frontiers in Pharmacology

ORIGINAL RESEARCH
published: 11 February 2020
doi: 10.3389/fphar.2020.00018

Fibroblast Growth Factor 22 Inhibits ER Stress-Induced Apoptosis and Improves Recovery of Spinal Cord Injury

Sipin Zhu[1†], Mengji Chen[1,2†], Min Chen[1,2†], Jiahui Ye[1,2†], Yibo Ying[1,2], Qiuji Wu[1,2], Haicheng Dou[1], Liyunian Bai[1,2], Fangmin Mao[1], Wenfei Ni[1*] and Kehe Yu[1*]*

[1] Department of Orthopaedics, The Second Affiliated Hospital and Yuying Children's Hospital of Wenzhou Medical University, Wenzhou, China, [2] Second Medical College of Wenzhou Medical University, Wenzhou, China

OPEN ACCESS

Edited by:
Zhouguang Wang,
Albert Einstein College of Medicine,
United States

Reviewed by:
Yingnyu Gao,
Marshall University,
United States
Xiao Xiao,
Merck,
United States

***Correspondence:**
Fangmin Mao
13868816296@163.com
Wenfei Ni
niwenfei@126.com
Kehe Yu
kehefish@163.com

[†]These authors have contributed equally to this work

Specialty section:
This article was submitted to Translational Pharmacology, a section of the journal Frontiers in Pharmacology

Received: 16 October 2019
Accepted: 07 January 2020
Published: 11 February 2020

Citation:
Zhu S, Chen M, Chen M, Ye J, , Ying Y, Wu Q, Dou H, Bai L, Mao F, Ni W and Yu K (2020) Fibroblast Growth Factor 22 Inhibits ER Stress-Induced Apoptosis and Improves Recovery of Spinal Cord Injury. Front. Pharmacol. 11:18. doi: 10.3389/fphar.2020.00018

Currently, inhibiting or reducing neuronal cell death is the main strategy to improve recovery of spinal cord injury (SCI). Therapies using nerve growth factors to treat SCI mainly focused on reducing the area damaged by postinjury degeneration to promote functional recovery. In this report, we investigated the mechanism of ER (endoplasmic reticulum) stress-induced apoptosis and the protective action of fibroblast growth factor 22 (FGF22) *in vivo*. Our results demonstrated that ER stress-induced apoptosis plays a significant role in injury of SCI model rats. FGF22 administration promoted recovery and increased neuron survival in the spinal cord lesions of model mice. The protective effect of FGF22 is related to decreased expression of CHOP (C/EBP-homologous protein), GRP78 (glucose-regulated protein 78), caspase-12, X-box binding protein 1 (XBP1), eukaryotic initiation factor 2α (Eif-2α) and Bad which are ER stress-induced apoptosis response proteins. Moreover, FGF22 administration also increased the number of neurons and the expression of growth-associated protein 43 (GAP43) which was related to axon regeneration. We also demonstrated that the protective effect of FGF22 effectively reduces neuronal apoptosis and promotes axonal regeneration. Our study first illustrated that the function of FGF22 is related to the inhibition of ER stress-induced cell death in SCI recovery *via* activation of downstream signals. This study also suggested a new tendency of FGF22 therapy development in central neural system injuries, which involved chronic ER stress-induced apoptosis.

Keywords: spinal cord injury, fibroblast growth factor 22, ER stress, apoptosis, nerve regeneration

INTRODUCTION

Spinal cord injury (SCI) is a destructive event that usually leads to significant functional impairment for the patient (Angeli et al., 2018). It triggers very limited regeneration in humans, leading to irreversible damage that can result in permanent motor dysfunction (Kumamaru et al., 2018; Sofroniew, 2018). SCI pathology can be divided into two stages: primary injury caused by direct disruption of the spinal cord, and secondary injury including neuronal apoptosis, autophagy,

vascular dysfunction, oxidative stress and inflammation, which lead to sustained and extensive tissue damage (Tohda and Kuboyama, 2011; Zhu et al., 2016; He et al., 2017a). SCI causes the injury loci to form a hypoxic microenvironment, which in turn causes neuronal death and dysfunction, ultimately limiting function recovery after SCI (Sabelstrom et al., 2013). Therefore, SCI treatment focuses on reducing neuronal death by inhibiting neuronal apoptosis.

The endoplasmic reticulum (ER) was initially identified as an intracellular organelle responsible for maintaining cellular homeostasis and resisting potential injury caused by misfolded proteins on the ER (Zhang et al., 2015; He et al., 2017b). During SCI, a large amount of protein misfolding caused by alteration of the microenvironment in the injured area leads to the unfolded protein response (UPR) (Hetz, 2012). The UPR activates three signal pathways that are regulated by activating transcription factor 6 (ATF6) and protein kinase RNA-like endoplasmic reticulum kinase (PERK), which increases the expression of apoptotic proteins and leads to neuronal death (Lee et al., 2014; Dou et al., 2018). Extensive neuronal death induced by apoptosis is the largest obstacle in recovery of spinal cord injury (Crowe et al., 1997).

The family of fibroblast growth factors and their receptors have been important regulators of presynaptic differentiation. FGF22 is a member of the FGF7 subfamily. It mainly activates FGF receptors FGFR1b and FGFR2b (Umemori et al., 2004). Studies have shown that FGF22 plays a significant part in SCI recovery as an endogenous regulator of synaptic plasticity and circuit remodeling in the adult nervous system (Jacobi et al., 2015). In this study, we injected different concentrations of FGF22 into the site of SCI in rats to observe the recovery of injured spinal cord. Here, we show that FGF22 can inhibit neuronal apoptosis induced by ER stress and promote SCI recovery.

MATERIALS AND METHODS

Cell Culture and Treatment

PC-12 cell lines obtained from the American Type Culture Collection (ATCC) were cultured in RPMI 1640 medium, which consisted of 10% fetal bovine serum (FBS), RPMI 1640 and 1% antibiotics. Cell incubation was performed in a humidified incubator at 37°C and 5% CO_2. All cells were randomly divided into four groups which included the 4-PBA (4-phenylbutyric acid) group, TG (thapsigargin) group, control group, treatment group with 5 μg/ml FGF22, treatment group with 10 μg/ml FGF22 and treatment group with 15 μg/ml FGF22.

In Vitro Scratch Motility Assay

A linear scratch was applied to cell monolayers with the help of a 200 μl pipette tip to create a cell-free area; then, cells were washed twice with PBS. Wound analysis and photography were performed by an inverted phase-contrast microscope and the wound area was calculated by ImageJ software.

Apoptosis Assay

The apoptotic rates of the PC-12 cells treated with TG, TG + 4-PBA, TG+5 μg/ml FGF22, TG + 10 μg/ml FGF22 and TG + 15 μg/ml FGF22 were measured by the PI/Annexin V-FITC kit (Invitrogen, Carlsbad, CA, USA) and then analyzed by FACS can flow cytometer (Becton Dickinson, Franklin Lakes, NJ, USA) as the manual description.

Western Blot Analysis

For protein analysis, PC12 cells were in RIPA buffer (25 mM Tris-HCl, 150 mM NaCl, 1% Nonidet P-40, 1% sodium deoxycholate, and 0.1% SDS) containing the protease and phosphatase inhibitor. Cracked. The above extracts were quantified using bicinchoninic acid (BCA) reagent (Thermo, Rockford, IL, USA). 50 μg of protein was placed on the 11.5% gel and then transferred to a PVDF membrane (Bio-Rad, Hercules, CA, USA). The membrane was blocked with 5% milk (Bio-Rad) in TBS containing 0.05% Tween 20 for 1 h and incubated with the following antibodies: CHOP (1: 300), GRP78 (1:300), caspase-12 (1:1000), and GAPDH (1:1000). The membrane was washed 3 times with TBS and treated with a horseradish peroxidase-conjugated secondary antibody for 1 hour at room temperature. The signals were visualized by the ChemiDoc ™ XRS+ imaging system (Bio-Rad), and the band density was quantified using the Multigauge Software (FUJIFILM Corporation, Tokyo, Japan) of the 2006 Scientific Laboratory. We analyzed the relative density of the bands using quantity one (version 4.5.2; Bio-Rad).

Animal Model of Spinal Cord Injury

Eighty adult female SD rats (weighing 220–250 g at the start of the experiment) were purchased from the Animal Center of Chinese Academy of Sciences, Shanghai, China. The Animal Care and Use Committee of Wenzhou Medical College ratified the experiments, and the experiments were carried out in accordance with the guidelines of the Care and Use of Laboratory Animals from the National Institutes of Health. Animals were randomly divided into four groups, which included the SCI group, sham group, treatment group with 5 μg/ml FGF22 and treatment group with 10 μg/ml FGF22. The animals were fixed with a skin incision along the midline of the back. The 8^{th}-to-10^{th} thoracic spinal vertebrae were exposed. The model of acute spinal cord injury was established by striking T9 segments of the spinal cord with a 10-g hammer and a 25-mm-height free fall. The sham group rats underwent the operation similarly without injury by collision. Animal care and handling involved bladder massage to induce urination twice daily, once in the morning and again in the evening, until cefazolin sodium reconstructed reflex bladder function (50 mg/kg, i.p.).

FGF22 Transplantation to Treat SCI

After building the SCI model, surgery was carried out immediately to microinject 5 μg/ml and 10 μg/ml of FGF22 into the rats of the two FGF22 treated groups. Through stereoscopic positioning instruments and microsyringes, FGF22 orthotopically arrived at the injured lesion. The sham group was

perfused with saline at the same site. All animals were returned to cages for recovery. We provided each group with the same moderate diet at fixed times.

Locomotion Recovery Assessment

To examine the locomotor function of rats after SCI, behavioral analyses were conducted by two well-trained investigators familiar with the score criteria but blinded to the experimental conditions.

Basso-Beattie-Bresnahan (BBB) is a scale with a total score of 22 points (scores 0–21) that logically and systematically follows functional recovery of hindlimbs from 0 points, reflecting complete paralysis of the lower limbs, to 21 points, reflecting normal locomotor function (Basso et al., 1995). The scale was formulated based on the natural progression of motor recovery in rats with thoracic spinal cord injury.

The inclined plane test was carried out by means of a testing apparatus (Rivlin and Tator, 1977). The maximum angle in which a rat's position could be maintained for 5 s without falling was recorded for each position, and then, the averages were taken to determine each rat's scores. Footprint analysis was performed by dipping the animal's hind paws in red dye and allowing them to crawl past a box of suitable size (1 m long and 7 cm wide) (de Medinaceli et al., 1982). Footprint scanning and digital image analysis were performed.

H&E Staining and Nissl Staining

The rats were re-anesthetized with 1% pentobarbital (40–50 mg/kg, i.p.). Thoracotomy was performed on the 60th day after injection. Rats were perfused with 0.9% NaCl, followed by 500 ml paraformaldehyde phosphate buffer solution injected into the heart to harden the tissue for complete removal. Spinal cord excision at the 8^{th}-to-10^{th} thoracic spinal vertebral level around the injury was performed. Spinal cords were fixed overnight in cold 4% paraformaldehyde and embedded with paraffin. For histopathological examination, transverse paraffin sections (10 μm thick) were subjected to hematoxylin and eosin (H&E) staining. For Nissl staining, sections were incubated in 1% cresyl violet. Two stained sections were examined and scanned under a light microscope.

Immunohistochemistry

Transverse paraffin sections were incubated in 80% carbinol and 3% H_2O_2 for 30 min, and then, the sections were transferred to blocking solution at room temperature for 1 h. Subsequently, the sections were incubated at 4°C overnight with the following primary antibodies: GRP78 (1:200), CHOP (1:200), caspase-12 (1:4000), XBP1 (1:400), Eif-2α (1:100) and Bad (1:200). After washing with PBS three times, sections were incubated with horseradish peroxidase-conjugated secondary antibodies at 37°C for 2h. We used 3,3-diaminobenzidine (DAB) to stop the reaction. Positive neuron numbers and optical densities of CHOP, GRP78, XBP1, Eif-2α, Bad and caspase-12 were counted in six randomly selected fields per sample. The results were imprinted using Nikon ECLPSE 80i (Nikon, Tokyo, Japan).

Video Images Locomotor Function

Forty-two adult female SD rats (weighting 220–250 g) are divided into six groups, sham group, SCI group, TG group, 4-PBA group, 5 μg/ml FGF22 group and 10 μg/ml FGF22 group. Using a camera (Leica), each group rats were photographed while walking through a 1-m-long glass runway with markers on the hindlimbs to estimate hip, knee, ankle, and foot position. The following parameters were used to evaluate locomotion: 1) weight support (height; hip height minus trunk width, equal to the torso gap on the ground), 2) leg extensor spasms (quantified as the time the foot is overstretched and dragged, relative to the foot cycle The duration is on the back surface), 3) the number of footsteps (the number of footsteps calculated relative to the number of forefoot steps) and 4) the posture of the foot (measurement of the foot offset behind the hip at the beginning of the ankle). The walking step rhythm is defined by the front leg (front leg steps/sec).

Immunofluorescence Staining

Sections were incubated with 10% normal bovine serum at 37°C for 1 h in PBS containing 0.1% Triton X-100 and then incubated with suitable primary antibodies overnight in the same buffer solution at 4°C. Nuclei were stained with DAPI (0.25 μg/ml) dye. To detect neurons and GAP43, we used anti-NeuN (1:500, Millipore) and anti-GAP43 (1:50) primary antibodies, respectively. After incubation with primary antibody, sections were triple washed with PBS at room temperature, followed by incubation with secondary antibody (1:500) at 37°C for 1 h. Then, sections were washed with PBS containing 0.1% Triton X-100 4×10 min and then washed with PBS 3×5 min. All images were captured under a Nikon ECLIPSE Ti microscope (Nikon, Tokyo, Japan).

Statistical Analysis

Statistically, data were expressed as the mean ± SEM. For two experimental groups, the Student's *t* test was used to determine statistical significance. Values of $P \leq 0.05$ were deemed significant. When there were more than two experimental groups, one-way analysis of variance (ANOVA) and Dunnett's *post hoc* test were used to statistically evaluate data, and $P \leq 0.05$ was considered statistically significant.

RESULTS

FGF22 by Inhibiting the Endoplasmic Reticulum Stress Increases the Migration and Repair Capability of PC-12 Cells

PC12 cells were derived from murine adrenal medullary pheochromocytoma, and were similar to normal nerve cells in terms of cell morphology, physiology, biochemistry and other functions (Shafer and Atchison, 1991). Wound healing assay results were shown for the control group, TG group, 4-PBA group, 5 μg/ml FGF22 group, 10 μg/ml FGF22 group and 15 μg/ml

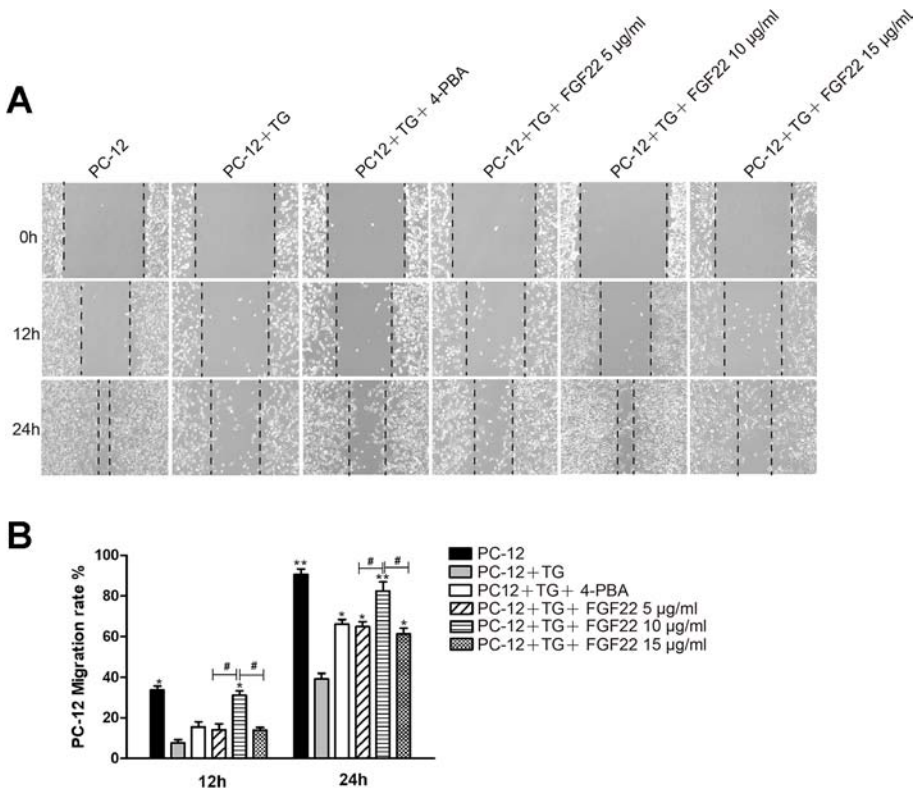

FIGURE 1 | FGF22 by inhibiting the endoplasmic reticulum stress promoted PC-12 cell migrate. **(A)** Images of wound healing in the control group, TG group, TG + 4-PBA group, TG + 5 μg/ml FGF22 group, TG + 10 μg/ml FGF22 group and TG + 15 μg/ml FGF22 group. These images were captured by an inverted phase-contrast microscope at 0, 12, and 24 h after the scratch. **(B)** The PC-12 migration rate that affected by the above factors for 12 h and 24 h. The data was acquired by using Image J 1.38 and were expressed as the mean values ± SEM, $n = 3$. "*"$p < 0.05$, "**" $p < 0.01$ vs PC-12+TG group and "#" represent $P < 0.05$ comparing the 5 μg/ml FGF22 group and the 15 μg/ml FGF22 group with the 10 μg/ml FGF22 group separately indicating statistical significance.

FGF22 group 12 h and 24 h after scratching (**Figure 1A**). Compared to the control group, the TG group displayed a larger cell-free area, and compared with the TG group, the 10 μg/ml FGF22 treatment group displayed an obviously reductive wound area and faster migration. Although the 4-PBA group, the 5 μg/ml FGF22 group and the 15 μg/ml FGF22 group had improved cell migration, the 10 μg/ml FGF22 treatment group was even more improved (**Figure 1B**). The effect of the 15 μg/ml FGF22 group was not as good as that of the 10 μg/ml FGF22 group, which may be due to the fact that FGF22 was the biological macromolecule. If the concentration was too high, the cells will dehydrate and the cell migration capacity will be reduced (Yurinskaya et al., 2005).

FGF22 Inhibit ER Stress-Induced Cell Apoptosis of PC-12 Cells

To further confirm the role of FGF22 in the ER stress induced apoptosis *in vitro*. The apoptosis model was replicated by ER stress specific activator TG was using to treat PC12 cells. Cell apoptosis rates were analyzed, and we found that FGF22 10 ug/ml significantly reduced TG-induced apoptosis rate in PC12 cells, compared with the TG, TG + 4-PBA, FGF22 5 μg/ml and FGF22 15 μg/ml groups (**Figures 2A, B**). Furthermore, the ER stress-related protein levels were detected by western blot. We observed that the levels of CHOP, GRP78, and cleaved caspase-12 protein significantly decreased in FGF22 10 ug/ml group than other groups ($P < 0.01$) (**Figures 2C–F**).

Maximizing Functional Recovery After SCI With a Higher Concentration of FGF22

FGF22 treatment reduced spinal cord injury and neuron death and improved motor recovery after SCI. The FGF22 injection groups showed significantly higher BBB scores than the SCI group after the operation, indicating that FGF22 promoted the recovery of nerve function. The results of the inclined plane test were similar. The 10 μg/ml FGF22 group showed the most complete anatomical appearance of SCI (**Figure 3A**). The mean BBB scores and angle of incline scores assessing locomotor skills over time were higher in the 10 μg/ml FGF22 group than in the other three groups (**Figures 3B, C**). Rats

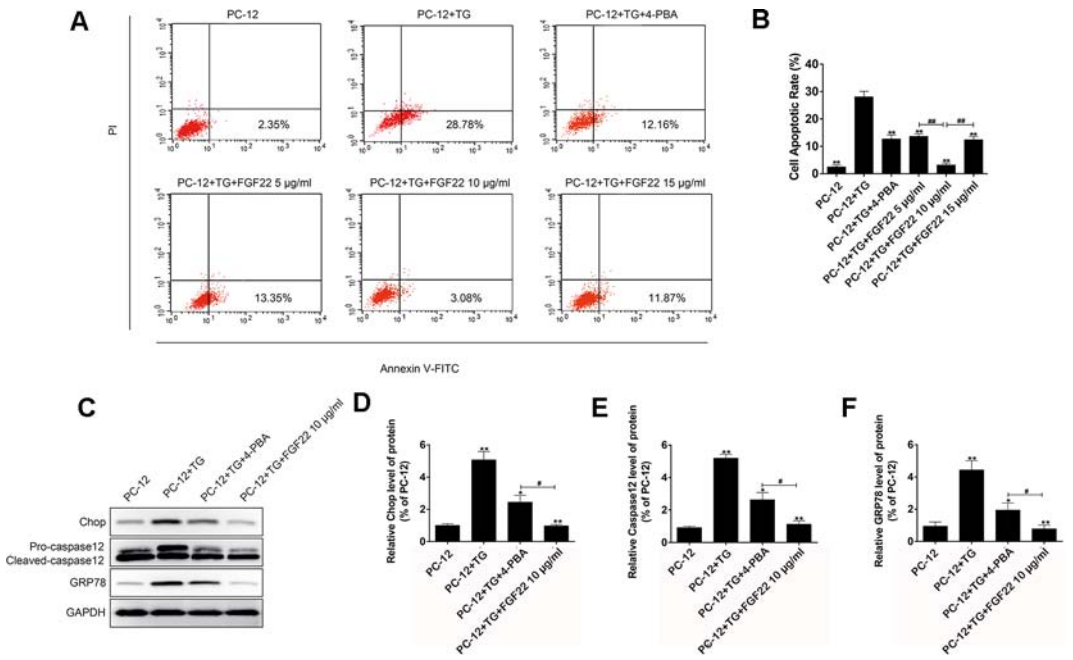

FIGURE 2 | FGF22 inhibit ER stress-induced cell apoptosis. **(A)** FACS can result from PI/annexin V-FITC staining for cell apoptosis analysis. **(B)** Statistical result of apoptosis rate in PC12 cells treated with TG, TG + 4-PBA, TG+5 μg/ml FGF22, TG + 10 μg/ml FGF22 and TG + 15 μg/ml FGF22. "**"$p < 0.01$ versus the TG treatment group and "##" $P < 0.01$ indicating statistically significant. **(C)** The protein expressions of GRP78, CHOP, and caspase-12 in the control group, TG group, TG + 4-PBA group, TG + 10 μg/ml FGF22 group were tested with western blotting. GAPDH was used as the loading control and for band density normalization. **(D–F)** The optical density analysis of GRP78, CHOP, and caspase-12 protein. "*"$P < 0.05$ and "**"$P < 0.01$ versus the SCI group, "#" $P < 0.05$ indicating statistically significant.

injected with 10 μg/ml FGF22 also showed a significant improvement in footprint analysis and at day 60 (**Figure 3D**).

FGF22 Increases Neuron Survival and Improves Tissue Density in SCI

Transverse and longitudinal H&E staining was performed on spinal cord samples in the sham group, SCI group, 5 μg/ml FGF22 group and 10 μg/ml FGF22 group after 60 days contusion (**Figures 4A, B**). Compared with the sham group, the SCI group showed progressive destruction of the dorsal white matter and central gray matter tissue. Compared with the SCI group, the 10 μg/ml FGF22 treatment group showed obvious protective impacts, such as less necrosis and karyopyknosis. Although the 5 μg/ml FGF22 group showed improvements in spinal cord sections, 10 μg/ml FGF22 treatment provided more amelioration (**Figures 4A, B**). These results further strengthen the neuroprotective efficacy of 10 μg/ml FGF22 for motor neurons in this SCI rat model.

FGF22 Treatment Inhibits ER Stress-Induced Apoptosis and Improves Recovery of SCI

To determine whether FGF22 promoted SCI recovery *via* inhibiting ER stress-induced apoptosis, we measured the expression of GRP78, caspase-12 and CHOP, which are related to ER stress, by immunofluorescence staining. As shown in **Figure 5**, caspase-12, GRP78 and CHOP expression were increased in SCI and remarkably inhibited by FGF22. Moreover, the 10 μg/ml FGF22 group showed fewer positive points than the 5 μg/ml FGF22 group. This indicates that, within a certain range, higher concentrations of FGF22 can better inhibit apoptosis and promote recovery of SCI (**Figures 5A–D**).

After SCI, the lateral intumescent spinal cord anterior horn displayed a decreased number of large and medium-sized neurons compared with the sham group, the survival rate decreased, and the cell outline was not clear, as seen by fuzzy Nissl staining. Nissl staining of crosscutting showed that the 10 μg/ml FGF22 group recovered well and the spinal cord anterior horn neurons of Nissl increased compared to the SCI group, providing further evidence that spinal cord function restoration and the treatment effect were more pronounced in the 10 μg/ml FGF22 group than in the 5 μg/ml FGF22 group (**Figures 5A, E**).

Regulation of Upstream and Downstream Signals Is Important for the Protection of FGF22

Eif-2α was an upstream factor of CHOP, which promoted JNK signaling and inhibited AKT signaling to promote apoptosis. XBP1 promoted apoptosis by activating JNK signaling (Li et al., 2019). Bad was the downstream factor of CHOP, CHOP-

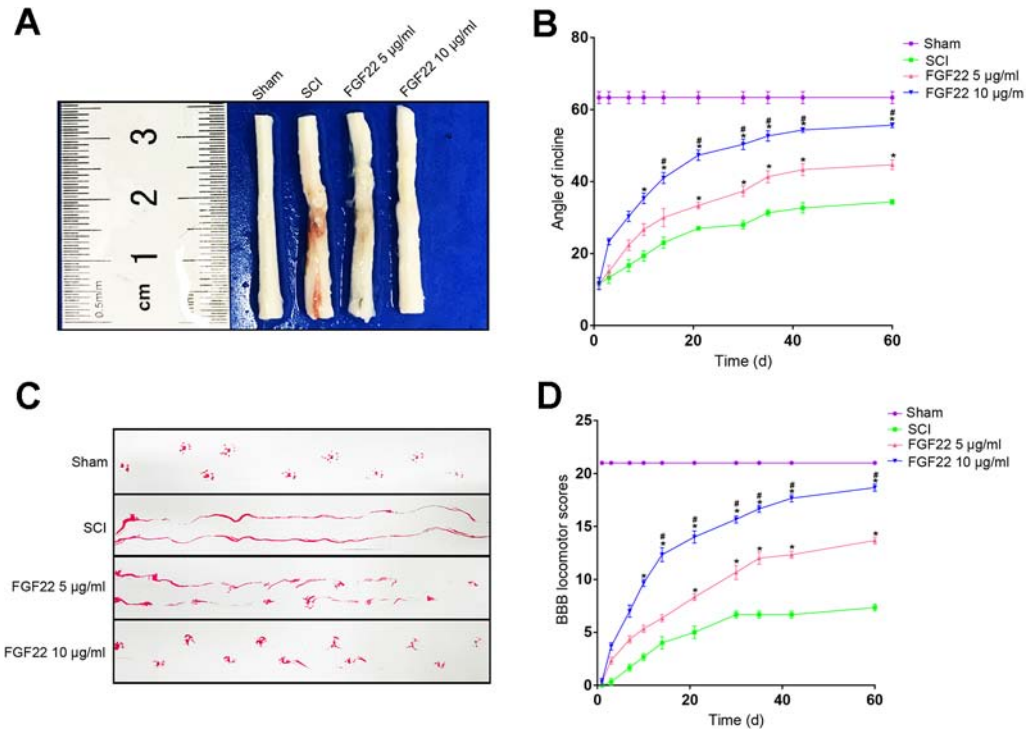

FIGURE 3 | FGF22 improved the motor function of rats with SCI. **(A)** Anatomical features of the sham group, SCI group, 5 μg/ml FGF22 group and 10 μg/ml FGF22 group in spinal cord injury, 60 days after SCI. **(B)** The BBB scores of the sham group, SCI group, 5 μg/ml FGF22 group and 10 μg/ml FGF22 group. The score of the sham group was 21 points, which indicates normal locomotion. "*" represents $P < 0.05$ versus the SCI group, "#" represents $P < 0.05$ versus the 5 μg/ml FGF22 group. Data are the mean values ± SEM, $n = 6$. **(C)** The inclined plane test scores of the different groups. "*" represents $P < 0.05$ versus the SCI group, "#" represents $P < 0.05$ versus the 5 μg/ml FGF22 group. Data are the mean values ± SEM, $n = 6$. **(D)** Footprint analyses of the different groups at 60 days.

ERO1α-caspase-dependent apoptosis signaling pathway activates mitochondrial-mediated apoptosis signaling pathway by up-regulating BAD and caspase-3 and down-regulating BCL-2/BAX ratio (Chen et al., 2019). To determine that the regulation of upstream and downstream signals was important for protecting FGF22, we measured the expression of Bad, XBP1, and Eif-2α associated with endoplasmic reticulum stress by immunohistochemical staining. As shown in **Figure 6**, the expression of Bad, XBP1 and Eif-2α increased in SCI and were significantly suppressed by FGF22. In addition, the 10 μg/ml FGF22 group had fewer positive spots than the 5 μg/ml FGF22 group. This indicates that within a certain range, 10 μg/ml FGF22 can better inhibited apoptosis and promoted the recovery of SCI (**Figures 6A–D**).

Recovery of Hindlimb Function in Rats Treated With FGF22 Inhibiting ER Stress-Induced Apoptosis

TG was an endoplasmic reticulum stress agonist and 4-PBA was an endoplasmic reticulum stress inhibitor (Rellmann et al., 2019). Adding these two groups as the comparison can showed that inhibition of endoplasmic reticulum stress can promoted the recovery of SCI. The FGF22 groups showed lower index of foot error and higher index of height and plantar steps which indicated preferable recoveries (**Figure 7A**). The 4-PBA group also showed better functional recovery, this illustrated that inhibiting ER stress promoted the recovery after SCI. It can also be obtained from video data that 10 μg/ml FGF22 group showed significantly recovery of hindlimb function of rats after SCI. It had least foot error, highest index of height and plantar steps than the other two groups (**Figures 7B–D**). Meanwhile, the TG treated group showed no obvious improvement. This suggested that ER stress has a negative effect on functional recovery after SCI. Inhibiting ER stress-induced apoptosis effectively promote the hindlimb function of SCI rats.

FGF22 Treatment Promotes Neuronal Survival and Nerve Regeneration

To determine the effect of FGF22 on apoptosis inhibition, NeuN was used to detect neuronal numbers. The neurons in the SCI group were largely lost, while the FGF22 treatment groups showed increases in the number of neurons, which proved that apoptosis was effectively inhibited. The higher concentration of FGF22 had more obvious protective effects on neurons. The experimental results showed an obvious enhancement of positive green fluorescence signal in the 10 μg/ml FGF22 administration group compared with the 5 μg/ml FGF22 group and SCI group (**Figures 8A, C**).

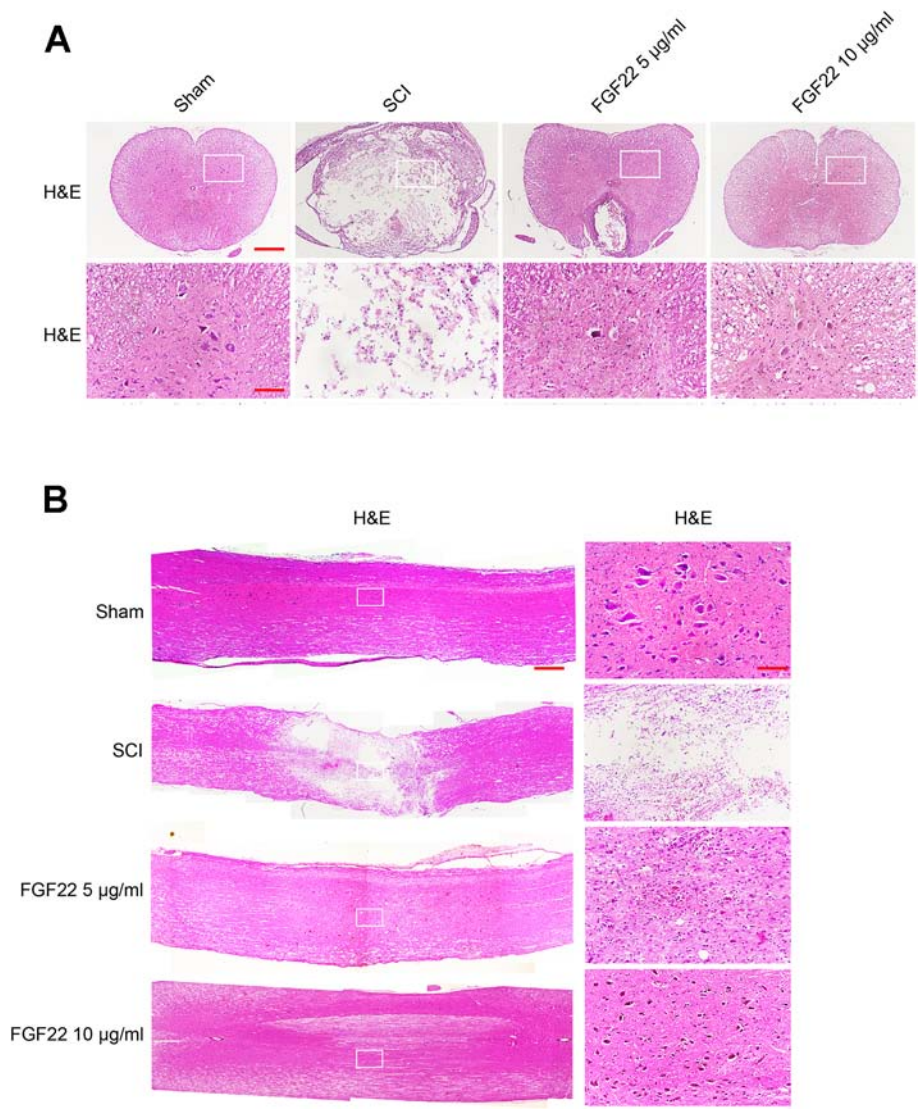

FIGURE 4 | FGF22 improved the recovery of SCI. **(A)** H&E staining (cross-section) results for the sham, SCI group, 5 μg/ml FGF22 group and 10 μg/ml FGF22 group, scale bar = 500 μm. A boxed region illustrates a representative region with high power images, scale bar = 100 μm. **(B)** H&E staining (longitudinal section) results for the sham, SCI group, 5 μg/ml FGF22 group and 10 μg/ml FGF22 group, scale bar = 500 μm. A boxed region illustrates a representative region with high power images, scale bar = 100 μm.

Moreover, we used GAP43 to detect the effect of FGF22 on axons. After SCI, axons break and are difficult to regenerate. The number of axons is significantly increased with the injection of FGF22. The experimental results showed an obvious enhancement of positive green fluorescence signal in the axons in the 10 μg/ml FGF22 administration group compared with the 5 μg/ml FGF22 group and SCI group (**Figures 8B, D**). This indicates that FGF22 can promote axonal regeneration after spinal cord injury, restore the nerve conduction pathway and promote functional recovery.

DISCUSSION

After SCI, the injury site forms a microenvironment of ischemia, hypoxia and inflammatory infiltration (Abbott et al., 2010). After the neurons are stimulated by the unbalanced microenvironment, protein folding errors, unfolded protein aggregation, and Ca^{2+} balance disorders occur in the ER (Soboloff and Berger, 2002; Montague et al., 2014). This state is called endoplasmic reticulum stress. ER stress can trigger a series of physiological changes, and the misfolded proteins accumulated in the endoplasmic reticulum are

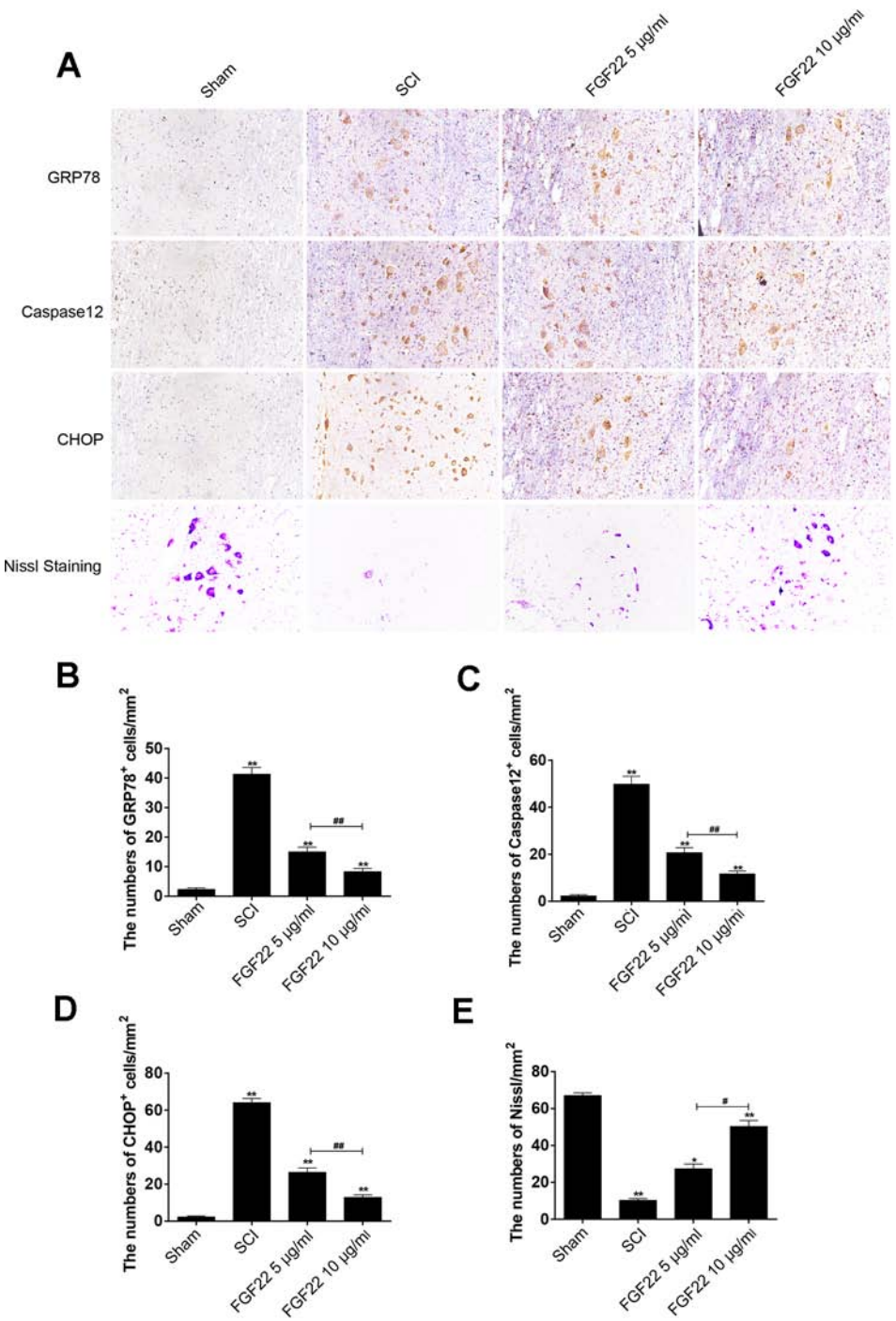

FIGURE 5 | FGF22 inhibited ER stress-induced apoptosis and improves the recovery of SCI. **(A)** Immunohistochemistry for GRP78, CHOP, and caspase-12 in the sham, SCI, 5 μg/ml FGF22 and 10 μg/ml FGF22 groups. **(B)** Nissl staining of crosscutting for the sham, SCI, 5 μg/ml FGF22 and 10 μg/ml FGF22 groups. **(C–E)** Analysis of positive cells in immunohistochemistry and Nissl staining of crosscutting. "*" and "**" represent $P < 0.05$ or $P < 0.01$ versus the sham group or SCI group, "#" and "##" represent $P < 0.05$ or $P < 0.01$ comparing the 10 μg/ml FGF22 group to the 5 μg/ml FGF22 group, indicating statistical significance. Data are the mean values ± SEM, $n = 6$.

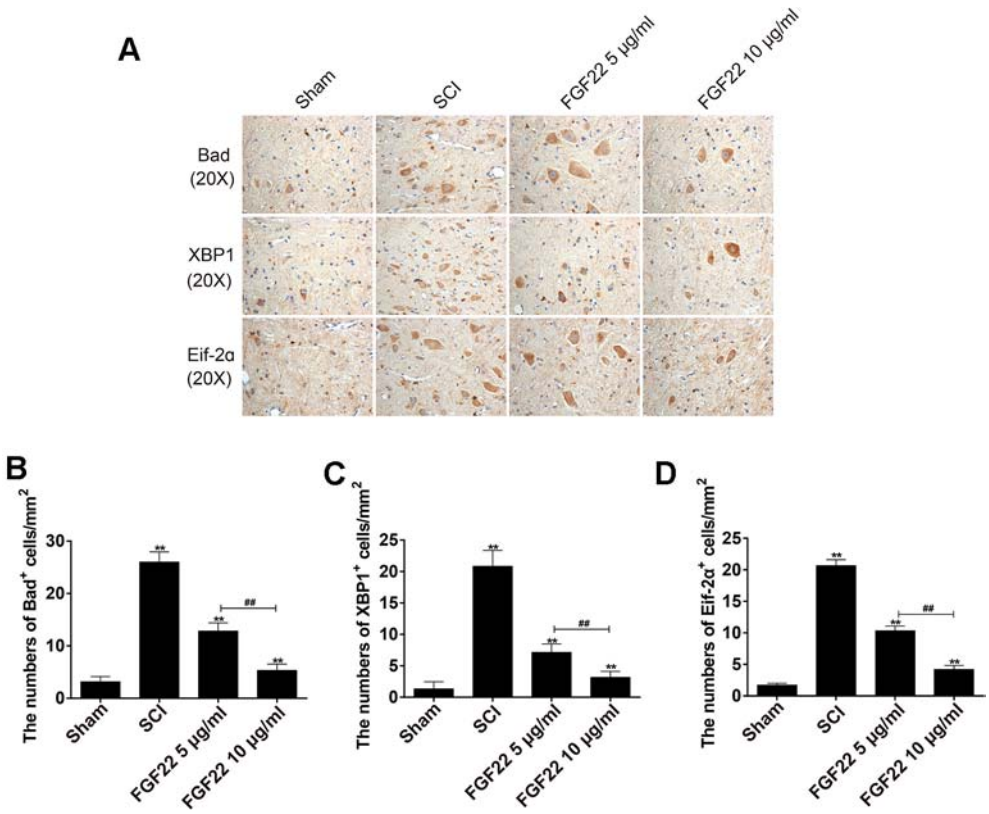

FIGURE 6 | Regulation of upstream and downstream signals is important for the protection of FGF22. **(A)** Immunohistochemistry for Bad, XBP1, and Eif-2α in the sham, SCI, 5 μg/ml FGF22 and 10 μg/ml FGF22 groups. **(B–D)** Analysis of positive cells in immunohistochemistry of crosscutting. "**" represent $P < 0.01$ versus the sham group or SCI group, "##" $P < 0.01$ indicating statistically significant. Data are the mean values ± SEM, $n = 6$.

processed, which is beneficial to the recovery of cell function (Lin et al., 2005). This process is called the unfolded protein response (UPR) and is a cytoprotective mechanism that restores ER homeostasis under cell pressure (Grootjans et al., 2016). However, if the UPR is beyond the control of protein folding and uncompensated, it will activate the apoptotic signaling pathway (Ohri et al., 2011). Unfolded proteins are stored in the ER and induce activation of PERK/ATF6 signaling pathways. The activation of this pathway results in upregulated expression of chaperones including GRP78, followed by activation of caspase-12 and other apoptotic proteins, such as CHOP, to induce cell apoptosis (Nakagawa et al., 2000; Li et al., 2016).

When ER stress occurs, ER oligomerization occurs, and phosphorylation leads to phosphorylation of Eif-2α, which forms the p-eIF2α pathway, inhibits and inhibits mRNA transcription, and reduces protein accumulation (Sozbilen et al., 2018). In addition to Eif-2α, XBP1 is also activated in the transcription of the ER chaperone gene (Wang et al., 2013). The following is the binding of the general transcription factor nuclear factor Y to the CCAAT part of the ERSE, which leads to the activation of ER chaperone gene transcription (Ubeda and Habener, 2000; Shifman et al., 2008).

Previous studies have indicated that SCI causes a large number of neuronal deaths, axonal rupture, and disruption of nerve conduction pathways (Zhou et al., 2017; Anderson et al., 2018). Among them, the loss of neurons has the most direct relationship with motor dysfunction (Liu et al., 2015). There is increasing evidence indicating that ER-stress-activated pathways may play a significant role in promoting cell death caused by apoptosis in CNS injury diseases (Byrnes et al., 2007; Ogawa et al., 2007). Therefore, a variety of mechanisms, such as disturbed ionic oxidative stress, homeostasis, ER stress, and inflammatory response, participate in the progression of the second pathological process of SCI (Rami and Kogel, 2008). Since neurons are difficult to regenerate, the best solution for neuronal loss is to protect neurons and reduce their apoptosis. Therefore, inhibiting this process to protect neurons from apoptosis might be an ideal therapeutic strategy for SCI.

Many therapeutic interventions utilizing growth factors, such as basic fibroblast growth factor (bFGF), nerve growth factor (NGF), and vascular endothelial growth factor (VEGF), have been confirmed to promote functional recovery after SCI (Rathbone et al., 1999; Zhu et al., 2016; Anderson et al., 2018). However, these factors are usually applied to promote

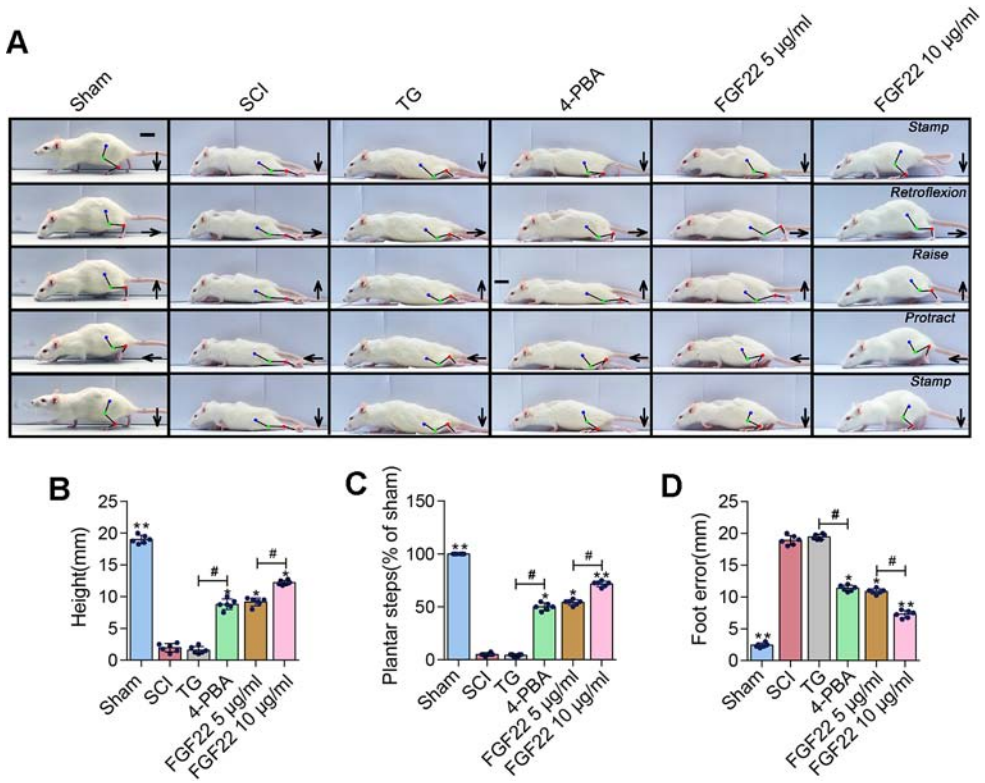

FIGURE 7 | FGF22 improved hindlimb function SCI rats *via* the inhibition of ER stress-induced apoptosis. **(A)** Video image sequence of rat walking posture of the sham group, SCI group, TG group, 4-PBA group, 5 μg/ml FGF22 group and 10 μg/ml FGF22 group in spinal cord injury, at 14 days after SCI. Lines and dots were used to mark the ankle, knee and hip joint, and foot movement was shown by arrows, scale bar = 500 μm. **(B)** Body height for each rat of the six groups. "*" and "**" represent $P < 0.05$ or $P < 0.01$ versus the SCI group, "#" represent $P < 0.05$. Data are the mean values ± SEM, $n = 6$. **(C)** Number of successful hind-limb steps for each rat of the six groups. "*" and "**" represent $P < 0.05$ or $P < 0.01$ versus the SCI group, "#" represent $P < 0.05$. Data are the mean values ± SEM, $n = 6$. **(D)** Foot-placement error for each rat of the six groups. "*" and "**" represent $P < 0.05$ or $P < 0.01$ versus the SCI group, "#" represent $P < 0.05$. Data are the mean values ± SEM, $n = 6$.

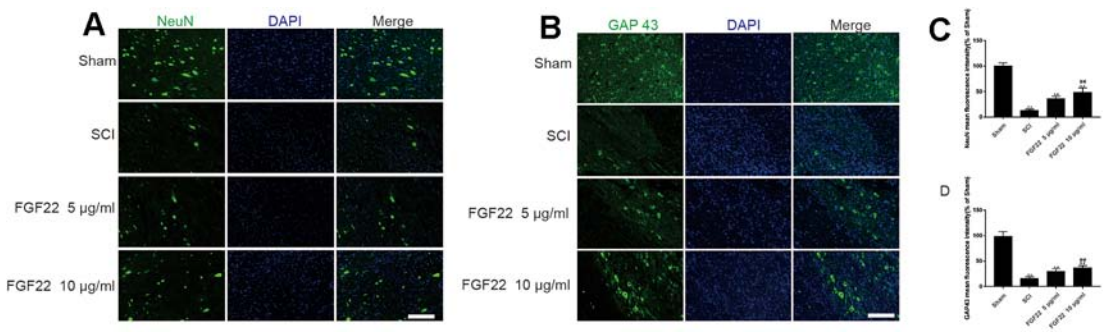

FIGURE 8 | FGF22 increased the level of NeuN and GAP43 in spinal cord lesions. **(A)** NeuN staining of the sham, SCI, 5 μg/ml FGF22, and 10 μg/ml FGF22 groups. The bright green dots in the right column are considered positively stained neurons, the nuclei are labeled by DAPI (blue). Magnification was ×20. **(B)** Immunofluorescence staining of GAP43 in spinal cord lesions; the nuclei are labeled by DAPI (blue). The bright green dots in the right column are considered positive staining for GAP43, magnification was ×20. **(C, D)** Analysis of positive cells in immunofluorescence staining. "**" represents $P < 0.01$ versus the sham group or SCI group, "##"represents $P < 0.01$ 10 μg/ml FGF22 than 5 μg/ml FGF22 group plays have statistical significance. Data are the mean values ± SEM, $n = 6$.

angiogenesis, neuronal proliferation and differentiation but are rarely used to inhibit neuronal apoptosis.

In this research, we demonstrated that ER stress-induced apoptosis participates in the response to SCI and the levels of proteins activated by apoptosis, including CHOP, GRP78, and caspase-12, were significantly increased by SCI. As intermediate signaling molecules of the ER stress pathway, these proteins mediate apoptosis through various pathways such as the IRE-1-CHOP pathway, ATF6-CHOP pathway, and PERK-elF2α-ATF4-CHOP pathway, which affect the expression and function of downstream proteins.

As an important promoter of circuit remodeling in the injured spinal cord, FGF22 treatment inhibited the expression of protein activated by ER stress and improved motor function and SCI recovery (Singh et al., 2012). Previous studies also showed that genetic destruction of the FGF22 signal not only reduces the number of new axons formed in the injured loci but also changes the molecular organization of the forming axons (Terauchi et al., 2010). Therefore, treatment of injured spinal cord with FGF22 can effectively promote axonal regeneration and functional recovery (Huang et al., 2017). The experimental results showed that apoptosis signaling molecules in the FGF22 treatment group were inhibited, which indicated that FGF22 can effectively inhibit endoplasmic reticulum stress, reduce neuronal apoptosis and play a crucial role in neuronal protection.

In conclusion, our research demonstrated that FGF22 plays a role in protecting neurons of SCI rats, promoting functional recovery after SCI by reducing apoptosis induced by ER stress and promoting axon regeneration [46]. To further prove that FGF22 indeed functions through the ER stress pathways to promote SCI recovery, we will use Chop knockout SD rats and further verify our experimental results.

DATA AVAILABILITY STATEMENT

All datasets generated for this study are included in the article/supplementary material.

ETHICS STATEMENT

The animal study was reviewed and approved by the Animal Care and Use Committee of Wenzhou Medical College.

AUTHOR CONTRIBUTIONS

SZ, MiC, MeC, and JY coordinated and carried out most of the experiments and data analysis and participated in drafting the manuscript. MeC to participate in the data. YY, QW, HD, and LB provided technical assistance, including drawing and tabulating. SZ, MiC, and JY carried out data analysis and revised the manuscript. FM, WN, and KY supervised the project and experimental design and provided financial support. SZ and MiC wrote the main part of the paper. All authors read and approved the final manuscript.

FUNDING

This work was partly supported by a research grant from the National Natural Science Foundation of China (81802235), Zhejiang Experimental Animal Science and Technology Project of China (2018C37112), Zhejiang Provincial Natural Science Foundation of China (LY17H060009, Y17H060051) and Wenzhou Basic Science Research Plan Project (Y20180033), which in part supported SZ as a visiting scholar at UWA. SZ made mutual collaborative visits for the purpose of this study.

REFERENCES

Abbott, N. J., Patabendige, A. A., Dolman, D. E., Yusof, S. R., and Begley, D. J. (2010). Structure and function of the blood–brain barrier. *Neurobiol. Dis.* 37, 13–25. doi: 10.1016/j.nbd.2009.07.030

Anderson, M. A., O'Shea, T. M., Burda, J. E., Ao, Y., Barlatey, S. L., Bernstein, A. M., et al. (2018). Required growth facilitators propel axon regeneration across complete spinal cord injury. *Nature* 561, 396–400. doi: 10.1038/s41586-018-0467-6

Angeli, C. A., Boakye, M., Morton, R. A., Vogt, J., Benton, K., Chen, Y., et al. (2018). Recovery of over-ground walking after chronic motor complete spinal cord injury. *N. Engl. J. Med.* 379, 1244–1250. doi: 10.1056/NEJMoa1803588

Basso, D. M., Beattie, M. S., and Bresnahan, J. C. (1995). A sensitive and reliable locomotor rating scale for open field testing in rats. *J. Neurotrauma* 12, 1–21. doi: 10.1089/neu.1995.12.1

Byrnes, K. R., Stoica, B. A., Fricke, S., Di Giovanni, S., and Faden, A. I. (2007). Cell cycle activation contributes to post-mitotic cell death and secondary damage after spinal cord injury. *Brain* 130, 2977–2992. doi: 10.1093/brain/awm179

Chen, F., Jin, J., Hu, J., Wang, Y., Ma, Z., and Zhang, J. (2019). Endoplasmic reticulum stress cooperates in silica nanoparticles-induced macrophage apoptosis *via* activation of CHOP-mediated apoptotic signaling pathway. *Int. J. Mol. Sci.* 20 (23), E5846. doi: 10.3390/ijms20235846

Crowe, M. J., Bresnahan, J. C., Shuman, S. L., Masters, J. N., and Beattie, M. S. (1997). Apoptosis and delayed degeneration after spinal cord injury in rats and monkeys. *Nat. Med.* 3, 73–76. doi: 10.1038/nm0197-73

de Medinaceli, L., Freed, W. J., and Wyatt, R. J. (1982). An index of the functional condition of rat sciatic nerve based on measurements made from walking tracks. *Exp. Neurol.* 77, 634–643. doi: 10.1016/0014-4886(82)90234-5

Dou, H. C., Chen, J. Y., Ran, T. F., and Jiang, W. M. (2018). *Panax quinquefolius* saponin inhibits endoplasmic reticulum stress-mediated apoptosis and neurite injury and improves functional recovery in a rat spinal cord injury model. *BioMed. Pharmacother.* 102, 212–220. doi: 10.1016/j.biopha.2018.03.074

Grootjans, J., Kaser, A., Kaufman, R. J., and Blumberg, R. S. (2016). The unfolded protein response in immunity and inflammation. *Nat. Rev. Immunol.* 16, 469–484. doi: 10.1038/nri.2016.62

He, J., Zhao, J., Peng, X., Shi, X., Zong, S., and Zeng, G. (2017a). Molecular mechanism of MiR-136-5p targeting NF-kappaB/A20 in the IL-17-mediated inflammatory response after spinal cord injury. *Cell Physiol. Biochem.* 44, 1224–1241. doi: 10.1159/000485452

He, Z., Zhou, Y., Huang, Y., Wang, Q., Zheng, B., Zhang, H., et al. (2017b). Dl-3-n-butylphthalide improves functional recovery in rats with spinal cord injury by inhibiting endoplasmic reticulum stress-induced apoptosis. *Am. J. Transl. Res.* 9, 1075, 1087.

Hetz, C. (2012). The unfolded protein response: controlling cell fate decisions under ER stress and beyond. *Nat. Rev. Mol. Cell Biol.* 13, 89–102. doi: 10.1038/nrm3270

Huang, J. Y., Lynn Miskus, M., and Lu, H. C. (2017). FGF-FGFR mediates the activity-dependent dendritogenesis of layer IV neurons during barrel formation. *J. Neurosci.* 37, 12094–12105. doi: 10.1523/JNEUROSCI.1174-17.2017

Jacobi, A., Loy, K., Schmalz, A. M., Hellsten, M., Umemori, H., Kerschensteiner, M., et al. (2015). FGF22 signaling regulates synapse formation during post-injury remodeling of the spinal cord. *EMBO J.* 34, 1231–1243. doi: 10.15252/embj.201490578

Kumamaru, H., Kadoya, K., Adler, A. F., Takashima, Y., Graham, L., Coppola, G., et al. (2018). Generation and post-injury integration of human spinal cord neural stem cells. *Nat. Methods* 15, 723–731. doi: 10.1038/s41592-018-0074-3

Lee, J. Y., Maeng, S., Kang, S. R., Choi, H. Y., Oh, T. H., Ju, B. G., et al. (2014). Valproic acid protects motor neuron death by inhibiting oxidative stress and endoplasmic reticulum stress-mediated cytochrome C release after spinal cord injury. *J. Neurotrauma* 31, 582–594. doi: 10.1089/neu.2013.3146

Li, Y. H., Tardif, G., Hum, D., Kapoor, M., Fahmi, H., Pelletier, J. P., et al. (2016). The unfolded protein response genes in human osteoarthritic chondrocytes: PERK emerges as a potential therapeutic target. *Arthritis Res. Ther.* 18, 172. doi: 10.1186/s13075-016-1070-6

Li, Y., Jiang, W., Niu, Q., Sun, Y., Meng, C., Tan, L., et al. (2019). eIF2alpha-CHOP-BCl-2/JNK and IRE1alpha-XBP1/JNK signaling promote apoptosis and inflammation and support the proliferation of Newcastle disease virus. *Cell Death Dis.* 10 (12), 891. doi: 10.1038/s41419-019-2128-6

Lin, W., Harding, H. P., Ron, D., and Popko, B. (2005). Endoplasmic reticulum stress modulates the response of myelinating oligodendrocytes to the immune cytokine interferon-gamma. *J. Cell Biol.* 169, 603–612. doi: 10.1083/jcb.200502086

Liu, S., Sarkar, C., Dinizo, M., Faden, A. I., Koh, E. Y., Lipinski, M. M., et al. (2015). Disrupted autophagy after spinal cord injury is associated with ER stress and neuronal cell death. *Cell Death Dis.* 6, e1582. doi: 10.1038/cddis.2014.527

Montague, K., Malik, B., Gray, A. L., La Spada, A. R., Hanna, M. G., Szabadkai, G., et al. (2014). Endoplasmic reticulum stress in spinal and bulbar muscular atrophy: a potential target for therapy. *Brain* 137, 1894–1906. doi: 10.1093/brain/awu114

Nakagawa, T., Zhu, H., Morishima, N., Li, E., Xu, J., Yankner, B. A., et al. (2000). Caspase-12 mediates endoplasmic-reticulum-specific apoptosis and cytotoxicity by amyloid-beta. *Nature* 403, 98–103. doi: 10.1038/47513

Ogawa, S., Kitao, Y., and Hori, O. (2007). Ischemia-induced neuronal cell death and stress response. *Antioxid Redox Signal* 9, 573–587. doi: 10.1089/ars.2006.1516

Ohri, S. S., Maddie, M. A., Zhao, Y., Qiu, M. S., Hetman, M., and Whittemore, S. R. (2011). Attenuating the endoplasmic reticulum stress response improves functional recovery after spinal cord injury. *Glia* 59, 1489–1502. doi: 10.1002/glia.21191

Rami, A., and Kogel, D. (2008). Apoptosis meets autophagy-like cell death in the ischemic penumbra: two sides of the same coin? *Autophagy* 4, 422–426. doi: 10.4161/auto.5778

Rathbone, M. P., Middlemiss, P. J., Gysbers, J. W., Andrew, C., Herman, M. A., Reed, J. K., et al. (1999). Trophic effects of purines in neurons and glial cells. *Prog. Neurobiol.* 59, 663–690. doi: 10.1016/S0301-0082(99)00017-9

Rellmann, Y., Gronau, I., Hansen, U., and Dreier, R. (2019). 4-Phenylbutyric acid reduces endoplasmic reticulum stress in chondrocytes that is caused by loss of the protein disulfide isomerase ERp57. *Oxid. Med. Cell Longev* 2019, 6404035. doi: 10.1155/2019/6404035

Rivlin, A. S., and Tator, C. H. (1977). Objective clinical assessment of motor function after experimental spinal cord injury in the rat. *J. Neurosurg.* 47, 577–581. doi: 10.3171/jns.1977.47.4.0577

Sabelstrom, H., Stenudd, M., Reu, P., Dias, D. O., Elfineh, M., Zdunek, S., et al. (2013). Resident neural stem cells restrict tissue damage and neuronal loss after spinal cord injury in mice. *Science* 342, 637–640. doi: 10.1126/science.1242576

Shafer, T. J., and Atchison, W. D. (1991). Transmitter, ion channel and receptor properties of pheochromocytoma (PC12) cells: a model for neurotoxicological studies. *Neurotoxicology* 12 (3), 473–492.

Shifman, M. I., Zhang, G., and Selzer, M. E. (2008). Delayed death of identified reticulospinal neurons after spinal cord injury in lampreys. *J. Comp. Neurol.* 510 (3), 269–282. doi: 10.1002/cne.21789

Singh, R., Su, J., Brooks, J., Terauchi, A., Umemori, H., and Fox, M. A. (2012). Fibroblast growth factor 22 contributes to the development of retinal nerve terminals in the dorsal lateral geniculate nucleus. *Front. Mol. Neurosci.* 4, 61. doi: 10.3389/fnmol.2011.00061

Soboloff, J., and Berger, S. A. (2002). Sustained ER Ca^{2+} depletion suppresses protein synthesis and induces activation-enhanced cell death in mast cells. *J. Biol. Chem.* 277, 13812–13820. doi: 10.1074/jbc.M112129200

Sofroniew, M. V. (2018). Dissecting spinal cord regeneration. *Nature* 557, 343–350. doi: 10.1038/s41586-018-0068-4

Sozbilen, M. C., Ozturk, M., Kaftan, G., Dagci, T., Ozyalcin, H., and Armagan, G. (2018). Neuroprotective effects of C-terminal domain of tetanus toxin on rat brain against motorneuron damages after experimental spinal cord injury. *Spine* 43 (6), E327–E333. doi: 10.1097/BRS.0000000000002357

Terauchi, A., Johnson-Venkatesh, E. M., Toth, A. B., Javed, D., Sutton, M. A., and Umemori, H. (2010). Distinct FGFs promote differentiation of excitatory and inhibitory synapses. *Nature* 465, 783–787. doi: 10.1038/nature09041

Tohda, C., and Kuboyama, T. (2011). Current and future therapeutic strategies for functional repair of spinal cord injury. *Pharmacol. Ther.* 132, 57–71. doi: 10.1016/j.pharmthera.2011.05.006

Ubeda, M., and Habener, J. F. (2000). CHOP gene expression in response to endoplasmic-reticular stress requires NFY interaction with different domains of a conserved DNA-binding element. *Nucleic Acids Res.* 28 (24), 4987–4997. doi: 10.1093/nar/28.24.4987

Umemori, H., Linhoff, M. W., Ornitz, D. M., and Sanes, J. R. (2004). FGF22 and its close relatives are presynaptic organizing molecules in the mammalian brain. *Cell* 118, 257–270. doi: 10.1016/j.cell.2004.06.025

Wang, F., Reece, E. A., and Yang, P. (2013). Superoxide dismutase 1 overexpression in mice abolishes maternal diabetes-induced endoplasmic reticulum stress in diabetic embryopathy. *Am. J. Obstet. Gynecol.* 209345 (4), e341–e347. doi: 10.1016/j.ajog.2013.06.037

Yurinskaya, V. E., Moshkov, A. V., Rozanov, Y. M., Shirokova, A. V., Vassilieva, I. O., Shumilina, E. V., et al. (2005). Thymocyte K^+, Na^+ and water balance during dexamethasone- and etoposide-induced apoptosis. *Cell Physiol. Biochem.* 16 (1–3), 15–22. doi: 10.1159/000087727

Zhang, H. Y., Wang, Z. G., Lu, X. H., Kong, X. X., Wu, F. Z., Lin, L., et al. (2015). Endoplasmic reticulum stress: relevance and therapeutics in central nervous system diseases. *Mol. Neurobiol.* 51, 1343–1352. doi: 10.1007/s12035-014-8813-7

Zhou, Y., Wu, Y., Liu, Y., He, Z., Zou, S., Wang, Q., et al. (2017). The cross-talk between autophagy and endoplasmic reticulum stress in blood–spinal cord barrier disruption after spinal cord injury. *Oncotarget* 8, 1688–1702. doi: 10.18632/oncotarget.13777

Zhu, S. P., Wang, Z. G., Zhao, Y. Z., Wu, J., Shi, H. X., Ye, L. B., et al. (2016). Gelatin nanostructured lipid carriers incorporating nerve growth factor inhibit endoplasmic reticulum stress-induced apoptosis and improve recovery in spinal cord injury. *Mol. Neurobiol.* 53, 4375–4386. doi: 10.1007/s12035-015-9372-2

Conflict of Interest: The authors declare that the research was conducted in the absence of any commercial or financial relationships that could be construed as a potential conflict of interest.

frontiers in Pharmacology

ORIGINAL RESEARCH
published: 21 February 2020
doi: 10.3389/fphar.2020.00066

The Protective Effect of Basic Fibroblast Growth Factor on Diabetic Nephropathy Through Remodeling Metabolic Phenotype and Suppressing Oxidative Stress in Mice

Tingting Wei[1,2], *Qi Shu*[1], *Jie Ning*[1], *Shuaijie Wang*[1], *Chen Li*[1], *Liangcai Zhao*[1], *Hong Zheng*[1*] and *Hongchang Gao*[1*]

[1] School of Pharmaceutical Sciences, Wenzhou Medical University, Wenzhou, China, [2] Laboratory Animal Centre, Wenzhou Medical University, Wenzhou, China

OPEN ACCESS

Edited by:
Jin-San Zhang,
Mayo Clinic, United States

Reviewed by:
Yi Tan,
University of Louisville Physicians, United States
Sandra Donnini,
University of Siena, Italy

***Correspondence:**
Hong Zheng
123zhenghong321@163.com
Hongchang Gao
gaohc27@wmu.edu.cn

Specialty section:
This article was submitted to Translational Pharmacology, a section of the journal Frontiers in Pharmacology

Received: 08 November 2019
Accepted: 22 January 2020
Published: 21 February 2020

Citation:
Wei T, Shu Q, Ning J, Wang S, Li C, Zhao L, Zheng H and Gao H (2020) The Protective Effect of Basic Fibroblast Growth Factor on Diabetic Nephropathy Through Remodeling Metabolic Phenotype and Suppressing Oxidative Stress in Mice. Front. Pharmacol. 11:66. doi: 10.3389/fphar.2020.00066

Diabetic nephropathy is a common complication in diabetes, but still lack of effective therapeutic strategies. This study aimed to investigate the therapeutic effect of basic fibroblast growth factor (bFGF) in *db/db* mice with diabetic nephropathy and explore its possible metabolic mechanisms using a nuclear magnetic resonance-based metabolomic approach. We found that bFGF treatment significantly alleviate urinary albumin to creatinine ratio and renal fibrosis in *db/db* mice, suggesting a potential renal protective effect. Metabolomics results reveal that bFGF remodeled metabolic phenotypes of the kidney and urine in *db/db* mice, mainly involving energy metabolism, methylamine metabolism, osmoregulation, and oxidative stress. Furthermore, the results show that bFGF-induced reductions of oxidative stress and apoptosis in *db/db* mice might be mediated by NOX-ROS-Nrf2 signaling. Therefore, our study suggests that the protective effect of bFGF on diabetic nephropathy could be mediated by remodeling metabolic phenotype and suppressing oxidative stress.

Keywords: bFGF, diabetes, metabolomics, nephropathy, taurine, oxidative stress

INTRODUCTION

Diabetic nephropathy (DN) is one of the most common microvascular complications of diabetes and has become the leading cause of end-stage renal failure and death of both type I and II diabetic patients (Yu and Bonventre, 2018; Wang et al., 2019). The progression of DN involve several stages, such as glomerular hypertrophy, proteinuria, glomerulosclerosis, interstitial fibrosis, and renal failure (Li et al., 2019). Several potential mechanisms underlying DN development have been reported, including oxidative stress (Barman et al., 2018), inflammation (Olatunji et al., 2018), advanced glycation end products, and polyol pathway (Pan et al., 2010). However, there is still a lack of effective treatments for DN, so elucidating the mechanisms and discovering new drugs of DN treatment are urgently required.

Basic fibroblast growth factor (bFGF), a member of the growth factor family, has been reported to reduce the functional and morphological damages in chronic kidney disease and induce the re-expression of nephrogenic/angiogenic factors (Villanueva et al., 2014). bFGF treatment can effectively reduce serum glucose and lipid levels in STZ-induced diabetic rats and prevent DN through inhibition of inflammation (Lin et al., 2016; Sheng et al., 2018). Additionally, Tan *et al*. reported that bFGF protects against renal ischemia reperfusion injury by attenuating mitochondrial damage and proinflammatory signaling (Tan et al., 2017). Of note, a recent review revealed that the FGF family possesses multifarious roles in metabolic homeostasis (Li, 2019). Yet, the metabolic mechanisms of bFGF on diabetic kidney diseases remain unclear.

Metabolomics is an omics approach that aims to analyze a comprehensive set of low-molecular weight metabolites in biological samples under pathophysiological conditions (Nagana Gowda and Raftery, 2017). It has been extensively applied for identifying potential biomarkers and exploring pathogenesis of diseases (Nicholson et al., 1999; Lu et al., 2013; Chen et al., 2014). Nuclear magnetic resonance (NMR) spectroscopy is a common analytical technique used in metabolomics studies owing to its advantages, such as simple sample preparation, rapid analysis, and high reproducibility. In our previous studies, we have reported several defective metabolic pathways in the kidney of diabetic mice and rats, such as TCA cycle, glycolysis, methylamine pathway, fatty acids β-oxidation, ketogenesis, and glycogenic amino acid pathway (Guan et al., 2013; Wei et al., 2015). Moreover, Zhao *et al.* have found that abnormal energy metabolism in the kidney of rats was associated with the pathogenic process of DN (Zhao et al., 2011).

In the present study, we analyzed metabolic profiles of the kidney and urine in type 2 diabetic *db/db* mice with DN after bFGF treatment by using a ^{1}H NMR-based metabolomic approach. The purposes of this study are (1) to examine the therapeutic effect of bFGF on DN, and (2) to explore its potential metabolic mechanisms.

MATERIALS AND METHODS

Animals

Eight-week-old male *db/db* (C57BLKS/J-lepr^{db}/lepr^{db}) mice and age-matched wild-type (wt) mice were purchased from the Model Animal Research Center of Nanjing University (Nanjing, China). Mice were housed in specific pathogen-free (SPF) colony under a fully controlled condition (room temperature, 22 ± 2°C; humidity, 50–60%; light/dark, 12 h/12 h) at the Laboratory Animal Center of Wenzhou Medical University (WMU, Wenzhou, China). All mice were given free access to standard rat chow and tap water. The present study was conducted on the basis of the Guide for the Care and Use of Laboratory Animals and approved by the Institutional Animal Care and Use Committee of WMU.

bFGF Treatment

All mice were acclimatized for 1 week and then randomly divided into bFGF-treated and control groups at 10 weeks of age. For bFGF group, *db/db* mice were intraperitoneally (i.p.) injected with bFGF at a dose of 0.5 mg/kg body weight every other day for 10 weeks (**Figure 1A**). The dose of bFGF treatment was selected according to the previous publication (Tan et al., 2017). Meanwhile, the wt mice and *db/db* mice in the control group received 0.9% saline using the same schedule.

Urine and Kidney Sample Collection

Urine samples were individually collected from mice before sacrifice in metabolic cages for 12 h. The urine samples were added with 0.1 ml of 1% sodium azide solution for avoiding bacterial contamination and then centrifuged at 3,000*g* at 4°C for 10 min. The supernatant was transferred into a new tube and stored at -80°C until analysis. Mice were sacrificed by cervical dislocation at 20 weeks of age, and their renal tissues were isolated, immediately snap-frozen in liquid nitrogen, and kept at -80°C until use.

Biochemical Analysis and Histopathological Examination

In this study, blood glucose level was measured using the Precision G Blood Glucose Testing System (Abbott Laboratories, Abbott Park, IL). Oral glucose tolerance test (OGTT) and insulin tolerance test (ITT) were performed on mice after 10 weeks of bFGF treatment (**Figure 1A**). After a 12 h fast, mice were orally administered with 50% glucose solution at a dose of 2 g/kg body weight. For ITT, mice were i.p. injected with insulin solution at a dose of 0.35 U/kg body weight after a 4 h fast. Blood glucose levels were measured from the tail vein at time 0, 30, 60, 90, 120, and 150 min. The levels of urea nitrogen (UN), uric acid (UA), urinary albumin to creatinine ratio (UACR) in the urine was determined using an automatic biochemistry analyzer (Mindray BS-300).

For pathologic examination, the kidney tissues were harvested, fixed overnight in 4% paraformaldehyde, and then embedded in paraffin. After deparaffinization and rehydration, the paraffin sections (5 mm) were stained with hematoxylin and eosin (HE) for routine histopathological observations. Periodic acid-Schiff (PAS) and Masson's trichrome staining were used to determine collagen deposition and fibrosis, respectively.

RNA Extraction, cDNA Synthesis, and Quantitative RT-PCR

Total RNA was extracted from renal tissues with Trizol reagent (Invitrogen, Carlsbad, CA). The purity of RNA was measured by a nanodrop spectrometry (Thermo Fisher Scientific, Beverly, MA) and expressed as the ratio of OD values at 260/280 nm. An OD 260/280 ratio greater than 1.80 represents high RNA purity. Then, RNA was used to synthesize the first-strand cDNAs by the Prime Script™ RT Reagent Kit (TaKaRa, Kusatsu, Japan). The quantification process was carried out in a 10 μl final

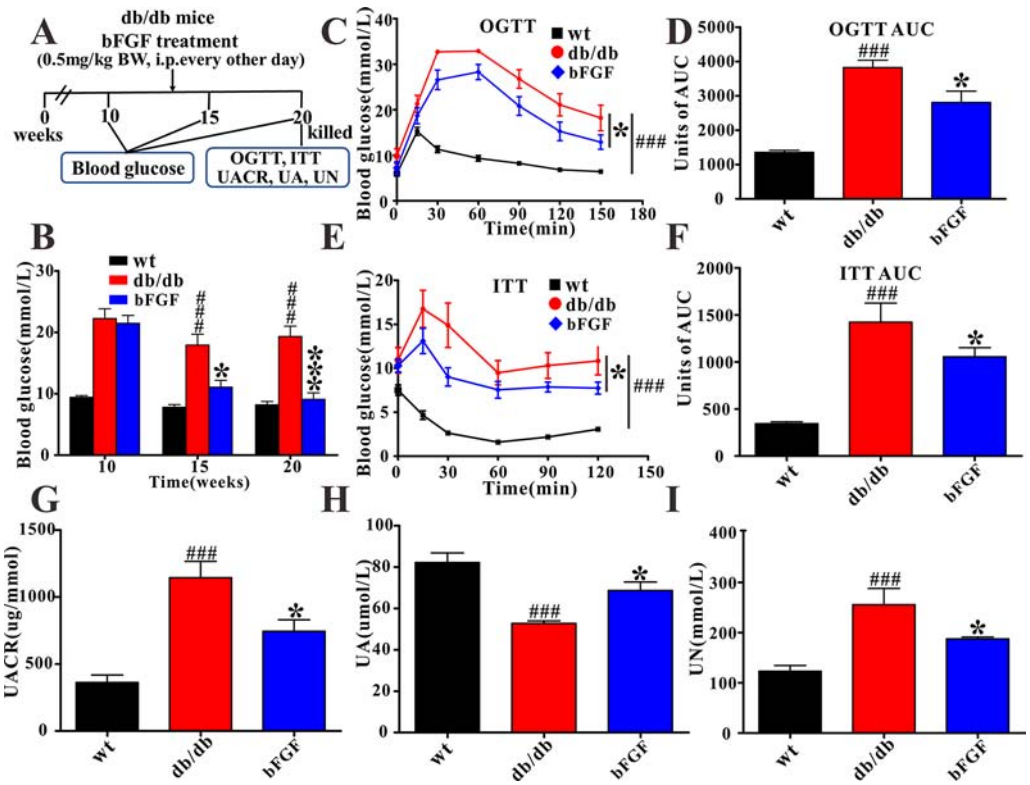

FIGURE 1 | The protective effect of bFGF on diabetic nephropathy in *db/db* mice. **(A)** bFGF treatment procedure for *db/db* mice. Arrows indicate when mice received i.p. injection of vehicle or bFGF (0.5 mg/kg BW) for10 weeks and then were killed at 20 weeks for study. **(B, C)** Oral glucose tolerance test in wild-type (wt), *db/db*, and bFGF-treated mice. **(D)** Random blood glucose level of wt, *db/db*, and bFGF-treated mice. **(E, F)** Insulin tolerance test in wt, *db/db*, and bFGF-treated mice. **(G, H, I)** The levels of urinary albumin to creatinine ratio, uric acid, and urea nitrogen in urine of wt, *db/db*, and bFGF-treated mice. Significant level: $^{###}P <$ 0.001 versus wildtype (wt) mice; $^{*}P < 0.05$ and $^{***}P < 0.001$ versus *db/db* mice.

reaction volume using a SYBR Green PCR Master Mix (Bio-Rad, CA, USA). In this study, GAPDH served as an endogenous control, and the primers were synthesized by Sunny Biotechnology (Sunny, Shanghai, China).

Western Blot Analysis

The renal tissues (30–40 mg) were lysed with RIPA buffer (25 mM Tris, pH 7.6, 150 mM NaCl, 1% NP-40, 1% sodium deoxycholate, and 0.1% SDS) supplemented with protease and phosphatase inhibitors (Thermo Fisher Scientific, MA). Total protein concentration was measured using the BCA protein assay kit (Bio-Rad, CA, USA). After normalization, equal amounts of proteins were separated by 10% SDS–PAGE and transferred to PVDF membranes (0.45 μm, Millipore, Germany). The membranes were blocked with 5% nonfat milk in TBST for 2 h and incubated overnight with primary antibodies at 4°C. After three washes with TBST, the membranes were incubated with secondary antibodies (Thermo Fisher Scientific, 1:10,000) at room temperature for 1 h. Finally, the blots were washed with TBST three times and incubated using the EasySee western Blot Kit (Transgen Biotech, China) to visualize the immunoreactive bands.

Sample Preparation and NMR Measurement

^{1}H NMR spectra were acquired at 25°C on a Bruker AVANCE III 600 MHz NMR spectrometer equipped with a triple resonance probe and a z-axis pulsed field gradient (Bruker BioSpin, Rheinstetten, Germany). Prior to NMR analysis, urine samples were thawed, and 200 μl aliquots of the samples were mixed with 50 μl D_2O containing sodium trimethylsilyl propionate-d_4 (TSP, 0.36 mg/ml) and 300 μl of phosphate buffer (0.2 M Na_2HPO_4/NaH_2PO_4, pH 7.4) to minimize pH variations (Xiao et al., 2009). The mixtures were centrifuged and then 500 μl of the supernatant was transferred to 5-mm NMR tubes for metabolomics analysis. One-dimensional NOESY pulse sequence with water signal pre-saturation was performed to acquire NMR spectra of urine samples. The main acquisition parameters were set as follows: spectral width = 12,000 Hz; data points = 256 K; relaxation delay = 4 s; acquisition time = 2.66 s per scan.

The frozen renal tissues were weighed into a centrifuge tube. Then, ice-cold methanol (4 ml/g) and distilled water (0.85 ml/g) was added into the tube, homogenized at 4°C after thawing and

mixed by vortex for 15 s. Subsequently, ice-cold chloroform (2 ml/g) and distilled water (2 ml/g) was added into the tube and mixed again for 15 s. The mixture were kept on ice for 15 min and centrifuged at 10,000*g* for 15 min at 4°C. The supernatant was extracted into a new tube and lyophilized for about 24 h. The lyophilized extract was reconstituted in 500 μl D_2O containing TSP and transferred to 5 mm NMR tubes for analysis. A one-dimensional ZGPR pulse sequence with water signal presaturation was used to acquire NMR data. In addition, the main acquisition parameters were set as follows: data points = 256 K; spectral width = 12,000 Hz; relaxation delay = 4 s; acquisition time = 2.66 s per scan.

Multivariate Data Analysis and Statistical Analysis

All NMR spectra were manually corrected for phase/baseline and referenced to TSP peak at 0 ppm using TopSpin 3.0 software (Bruker BioSpin, Rheinstetten, Germany). Then, the "icoshift" procedure was employed to align NMR spectra under the MATLAB environment (R2012a, The MathWorks Inc., Natick, MA, USA) (Savorani et al., 2010). The spectral region from 0.0 to 9.0 ppm excluding the residual water signals (4.65–5.05 ppm for kidney extract; 4.78–4.83 ppm for urine) were subdivided and integrated to binning data with a size of 0.01 ppm for further multivariate analysis.

To discriminate metabolic patterns between different groups, partial least squares-discriminant analysis (PLS-DA) was performed using Pareto-scaled NMR data in SIMCA 12.0 software (Umetrics, Umeå, Sweden). Leave one-out cross validation and permutation tests (200 cycles) were used to examine the performance of the model. PLS-DA loading plots were used to identify the important metabolites for the separation of groups. The significance of metabolites in PLS-DA was assessed using the absolute value of the correlation coefficient, $|r|$, and high $|r|$ value was considered important.

The differences in metabolite levels between two groups were analyzed using independent-samples *t*-tests with SPSS software (version 13.0; SPSS Inc., Chicago, IL, USA). Additionally, the differences in OGTT and ITT between two groups were assessed with repeated measure ANOVA in SPSS 13.0 software. A statistically significant difference was considered when P value <0.05.

RESULTS

The Protective Effect of bFGF on Diabetic Nephropathy in *db/db* Mice

In this study, as expected, *db/db* mice at 10 weeks of age exhibited a higher level of blood glucose than age-matched wild-type (wt) mice (**Figure 1B**). Of note, we found that blood glucose level was significantly reduced in *db/db* mice after 5 and 10 weeks of bFGF treatment, as shown in **Figure 1B**. Furthermore, OGTT demonstrated that administration of bFGF significantly improved blood glucose clearance in *db/db* mice (**Figures 1C, D**). As can be seen from insulin tolerance test, insulin sensitivity was also enhanced in *db/db* mice with bFGF treatment (**Figures 1E, F**). To evaluate renal function of mice, we measured UACR, which is a clinical marker of kidney damage and dysfunction (Teimoury et al., 2014). The result shows that the UACR level was significantly increased in *db/db* mice compared with age-matched wt mice (**Figure 1G**), whereas bFGF treatment significantly decreased its level in *db/db* mice. Additionally, uric acid and urea nitrogen are another two hallmarks of renal injury (Barutta et al., 2010). We found that the UA level was significantly reduced in *db/db* mice relative to age-matched wt mice (**Figure 1H**). However, interestingly, its level was significantly increased after bFGF treatment and reached to the normal level. In addition, *db/db* mice had a higher UN level than age-matched wt mice, but this increase can be recovered after bFGF treatment (**Figure 1I**).

Figure 2A shows that *db/db* mice displayed notable glomerular hypertrophy and mesangial matrix expansion as compared with age-matched wt mice, while these symptoms were markedly alleviated after bFGF treatment. In addition, Masson trichrome staining revealed a significant increase in renal fibrosis in *db/db* mice, but this change cannot be observed in *db/db* mice treated with bFGF. Consistent with our histological findings, the relative mRNA expression levels of profibrotic molecules transforming growth factor (TGF) β1 and type IV collagen were significantly increased in the kidney of *db/db* mice relative to age-matched wt mice; however, of note, these two indicators were recovered to the normal level after bFGF treatment (**Figure 2B**). Moreover, bFGF treatment induced parallel changes in the protein expression of these two profibrotic markers in renal tissues (**Figures 2C, D**). Taken together, these findings revealed that bFGF had a potential protective effect on diabetic nephropathy in *db/db* mice.

Changes of Metabolic Phenotypes in the Kidney and Urine in *db/db* Mice Treated With bFGF

Typical ^{1}H NMR spectra obtained from the kidney and urine samples of wt mice are illustrated in **Figures 3A, B**, respectively. In total, 43 metabolites were identified from NMR-based metabolome, mainly including energy metabolism-related metabolites (succinate, 2-oxoglutarate, citrate, creatine, creatinine, lactate, glucose, fumarate, ATP, AMP, and NAD+), amino acids (leucine, isoleucine, valine, alanine, glutamate, aspartate, taurine, glycine, tyrosine, and phenylalanine), methylamine metabolites (methylamine, dimethylamine, trimethylamine, choline, and TMAO), ketobodies (3-hydroxyisovalerate, 3-hydroxybutyrate, and 2-hydroxybutyrate), nucleotide metabolism-related metabolites (uracil, uridine, GTP, and allantion), short-chain fatty acids (formate, acetate, and propionate), and others (GPC, myo-inositol, inosine, niacinamide, 1-methylnicotinamide, hippurate, and 3-indoxylsulfate).

Furthermore, PLS-DA was used to examine changes in metabolic patterns among wt, *db/db*, and bFGF groups and identify key metabolites. The PLS-DA score plot showed a clear separation among these three groups (**Figure 4A**), which is validated by a permutation test (**Figure 4B**). According to its loading plot, a series of metabolites that contribute to this separation were identified, such as lactate, succinate, ATP,

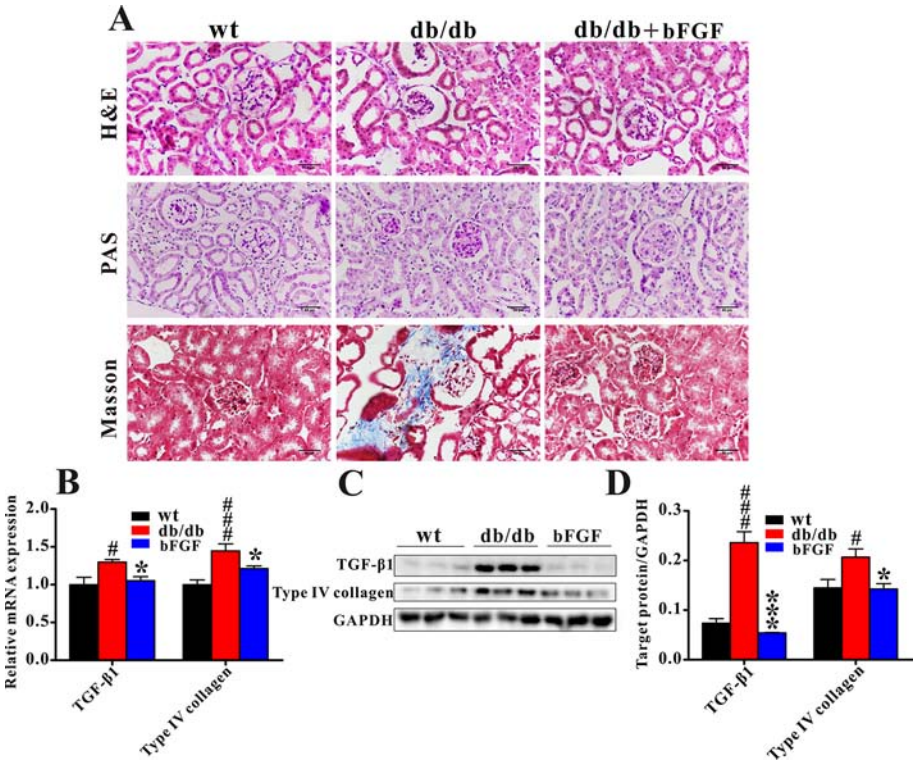

FIGURE 2 | bFGF recovered renal fibrosis in *db/db* mice. **(A)** Representative images of renal tissues stained with H&E and PAS (indicating glycogen) for evaluation of mesangial expansion, and Masson trichrome for type IV collagen. Bar = 50 μm. **(B)** The relative mRNA expression of TGF-β1 and type IV collagen in renal tissues of wild-type (wt), *db/db*, and bFGF-treated mice. **(C)** Western blot analysis of TGF-β1 and type IV collagen in renal tissues of wt, *db/db*, and bFGF-treated mice. **(C)** Intensities of TGF-β1 and type IV collagen normalized to GADPH. Significant level: $^{\#}P < 0.05$ and $^{\#\#\#}P < 0.001$ versus wt mice; $^{*}P < 0.05$ and $^{***}P < 0.001$ versus *db/db* mice.

AMP, glutamate, taurine, glycine, tyrosine, uracil, GTP, TMAO, inosine, and niacinamide, as shown in **Figure 4C**. However, of note, taurine showed the most significant contribution. In addition, PLS-DA score plot based on urine metabolome also showed a clear difference among these three groups (**Figure 5A**) which is validated by a permutation test (**Figure 5B**). The corresponding loading plot identified a series of important metabolites, including acetate, succinate, 2-oxoglutarate, citrate, creatine, creatinine, fumarate, hydroxybutyrate, DMA, propionate, allantion, hippurate, and 3-indoxylsulfate (**Figure 5C**).

Metabolic Changes in the Kidney and Urine of *db/db* Mice Treated With bFGF

Figure 6 shows the metabolic pathway changes in *db/db* mice after bFGF treatment. We found that the levels of creatinine, citrate, ATP, fumarate, TMAO, DMA, and myo-inositol were significantly increased in *db/db* mice compared with age-matched wt mice, but these increased trends were significantly reduced after bFGF treatment (**Figure 6**). Moreover, *db/db* mice had significantly lower creatine and taurine levels than age-matched wt mice, while bFGF treatment significantly increased their levels, as shown in **Figure 6**. Relative to age-matched wt mice, we also found that *db/db* mice had significantly decreased levels of alanine, uracil, acetate, glycine, methylamine, TMA, choline, and glutamate as well as increased levels of fumarate and AMP in the kidney, but no significant alterations were observed after bFGF treatment. Together, these metabolites mainly involved energy metabolism, amino acid metabolism, and methylamine metabolism.

bFGF Suppress Oxidative Stress in the Kidney of *db/db* Mice

To investigate whether bFGF can suppress oxidative stress, several relevant markers were detected in the kidney of *db/db* mice, as shown in **Figure 7**. As compared with age-matched wt mice, *db/db* mice had a significantly increased MDA level (**Figure 7A**) and a significantly decreased SOD level (**Figure 7B**). However, of note, these two markers were recovered to the normal level after bFGF treatment. In addition, the relative mRNA expression levels of antioxidant biomarkers, including nuclear factor erythroid-2 related factor 2 (Nrf2), NAD(P)H dehydrogenase quinone 1 (NQO1), and superoxide dismutase-2 (SOD2), were significantly down-regulated in the kidney of *db/db* mice, while the oxidative marker levels, such as NADPH oxidases 2 and 4 (NOX2 and NOX4), were significantly

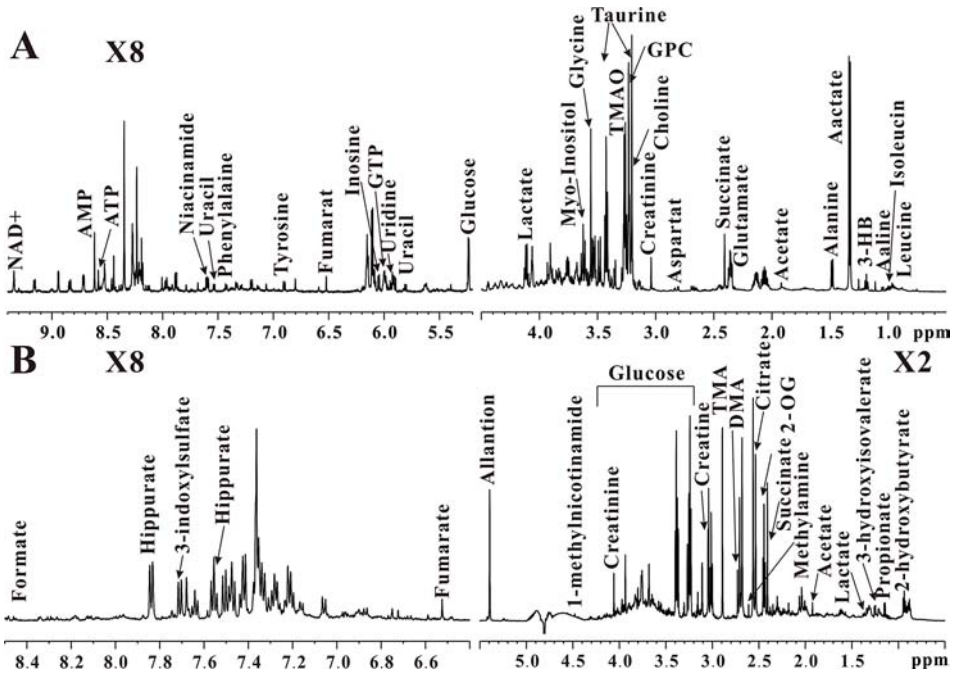

FIGURE 3 | Typical 600 MHz ^{1}H NMR spectra of kidney **(A)** and urine **(B)** in wild-type mice.

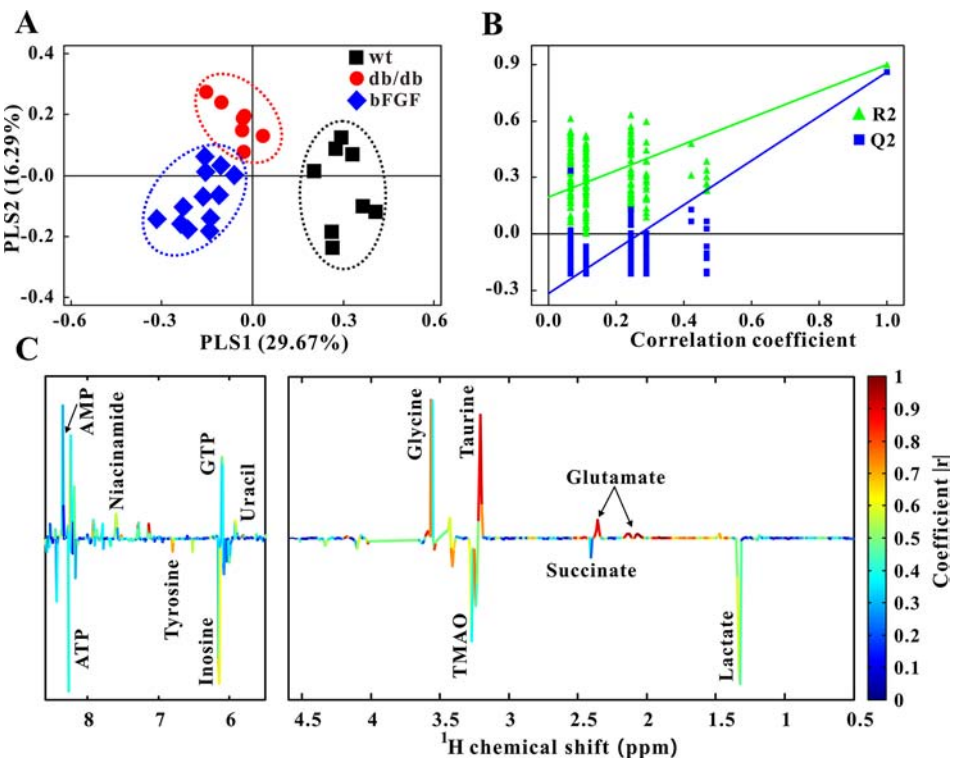

FIGURE 4 | Changes of metabolic phenotypes in kidney of *db/db* mice treated with bFGF. **(A)** PLS-DA score plot ($R^2X = 0.46$, $R^2Y = 0.747$, $Q^2 = 0.624$, $P < 0.001$). **(B)** Permutation test (200 cycles, $R^2 = 0.897$, $Q^2 = 0.858$). **(C)** Coefficient-coded loading plot.

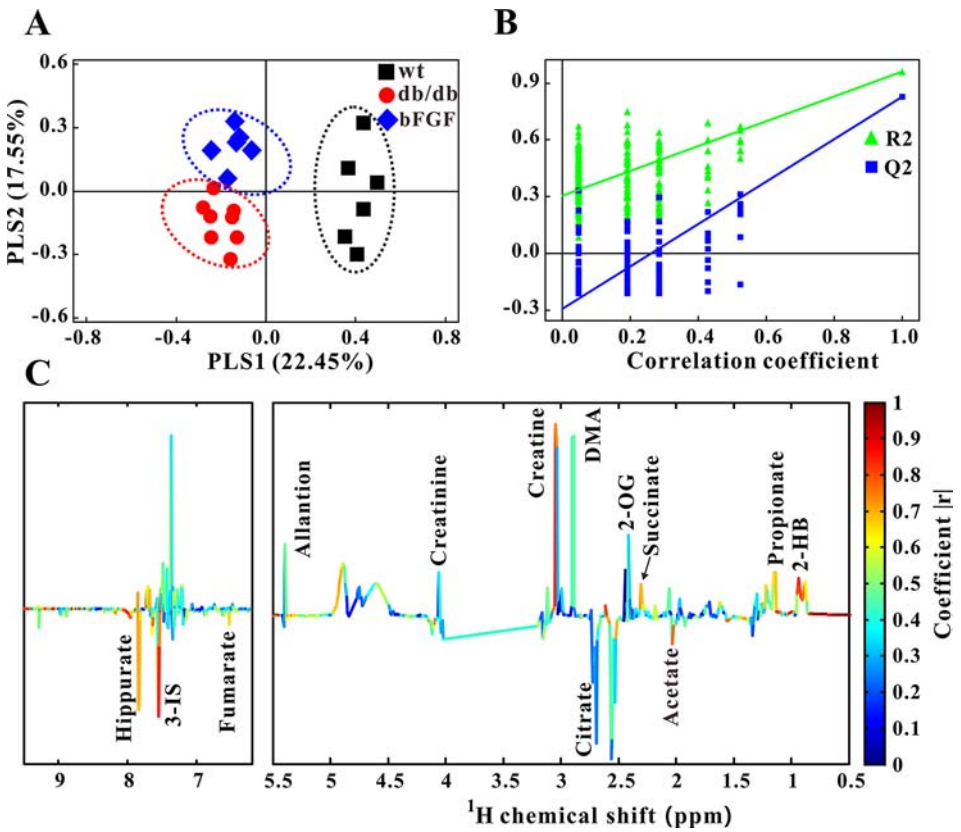

FIGURE 5 | Changes of metabolic phenotypes in urine of *db/db* mice treated with bFGF. **(A)** PLS-DA score plot ($R^2X = 0.4$, $R^2Y = 0.745$, $Q^2 = 0.491$, $P < 0.001$). **(B)** Permutation test (200 cycles, $R^2 = 0.961$, $Q^2 = 0.828$). **(C)** Coefficient-coded loading plot.

increased, as shown in **Figure 7C**. However, interestingly, these changes were recovered to the normal level after the treatment of bFGF. These results were further validated at the protein level using western blot analysis, where we found that bFGF treatment corrected the decreased levels of Nrf2, NQO1, and SOD2 as well as the increased levels of NOX2 and NOX4 in the kidney of *db/db* mice (**Figures 7D, E**). Additionally, we also observed that *db/db* mice had significantly increased levels of pro-apoptotic proteins (caspase-3, cleaved caspase-3, and Bax) and decreased level of apoptotic protein (Bcl-2) in the kidney relative to age-matched wt mice (**Figure 7F**). Of note, the recovery of these protein marker levels was obtained after bFGF treatment. Furthermore, we quantified the ratios of cleaved caspase-3/caspase-3 and Bax/Bcl-2, which have been commonly used to assess cell apoptosis. The results showed that these two ratios were significantly increased in the kidney of *db/db* mice relative to age-matched wt mice (**Figures 7G, H**), suggesting an enhanced cell apoptosis. Yet, bFGF treatment can significantly reduce renal cell apoptosis in *db/db* mice. **Figure 8** illustrates that the protective effect of bFGF on diabetic nephropathy may be mediated by correcting metabolic disorders and suppressing oxidative stress in *db/db* mice.

DISCUSSION

Diabetic nephropathy is a common diabetic complication and seriously affect human health worldwide (Yang, 2019), but so far no effective treatment strategies can be available. In the present study, our results reveal that bFGF could be a promising drug for the treatment of diabetic nephropathy, as indicated by reductions in urinary albumin to creatinine ratio and renal fibrosis. To explore its potential therapeutic mechanisms, we performed an NMR-based metabolomics study to analyze metabolic changes in the kidney and urine of *db/db* mice after bFGF treatment. The results show that bFGF treatment altered metabolic phenotypes in the kidney and urine of *db/db* mice, mainly involving energy metabolism, methylamine metabolism, osmoregulation, and oxidative stress.

Kidney is an organ with abundant mitochondria and high energy demand, followed by heart in the body (Forbes, 2016). Therefore, diabetic nephropathy is usually accompanied by abnormal energy metabolism (Zhong et al., 2012; Wei et al., 2015; Tanaka et al., 2018). In the present study, relative to age-matched wt mice, we found a disordered energy metabolism in *db/db* mice, as indicated by significantly increased levels of

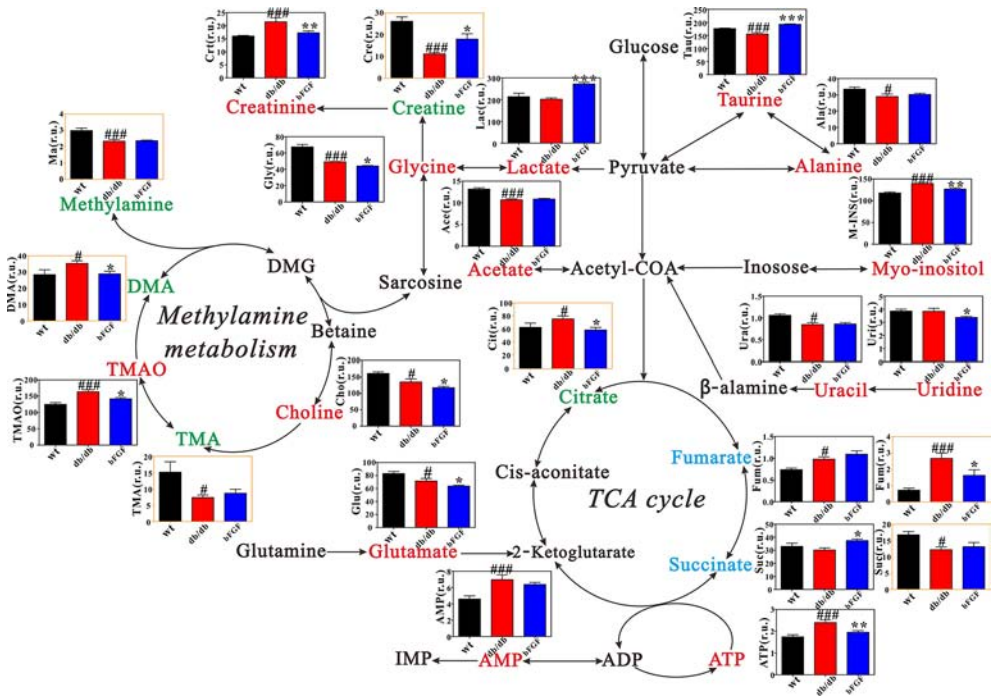

FIGURE 6 | Metabolic changes in kidney and urine of *db/db* mice treated with bFGF. Red and green texts indicate metabolites detected from kidney and urine samples, respectively. Blue text indicates metabolites detected from both kidney (black outline box) and urine (yellow outline box) samples. Metabolites: Tau, taurine; Ala, alanine; Crt, creatinine; Cre, creatine; Lac, lactate; Ace, acetate; M-INS, myo-inositol; Ura, uracil; Uri, uridine; Gly, glycine; Ma, methylamine; DMA, dimethylamine; TMA, trimethylamine; TMAO, Trimethylamine oxide; Cho, choline; Cit, citrate; Fum, fumarate; Suc, succinate; Glu, glutamate. r.u., relative unit. Significant level: $^{\#}P < 0.05$ and $^{\#\#\#}P < 0.001$ versus wt mice; $^{*}P < 0.05$, $^{**}P < 0.01$, and $^{***}P < 0.001$ versus *db/db* mice.

tricarboxylic acid (TCA) cycle intermediates, such as citrate, fumarate, ATP, and AMP. Interestingly, abnormal energy metabolism can be recovered by bFGF treatment. Mitochondrial damage was considered as the hallmark of kidney injury (Galvan et al., 2017), and the TCA intermediates were identified as the potential biomarkers for impairment of mitochondrial function in the kidney of diabetic animals (Zhao et al., 2011; Jiang et al., 2019). We thereby hypothesize that bFGF has a protective effect on renal mitochondrial function. Creatinine, as an indicator of renal function, is formed exclusively from creatine in the body, and creatine is a nitrogen-containing organic acid that provides energy for maintaining normal cellular physiology (Akira et al., 2012). In this study, we found a significantly higher metabolic rate from creatine to creatinine in *db/db* mice compared with age-matched wt mice, but notably this abnormal metabolism can be recovered in *db/db* mice after bFGF treatment. Taken together, our results reveal that the protective effect of bFGF on diabetic nephropathy in *db/db* mice may be associated with energy metabolism regulation. In addition, amino acid metabolism is necessary to protein synthesis for cell growth and also supports for energy metabolism. In this study, we found a significant reduction of amino acid metabolism in the kidney of *db/db* mice relative to age-matched wt mice, as indicated by decreases in alanine, glycine, and glutamate. Yet, their levels were not restored after the treatment of bFGF, which may imply that the protective effect of bFGF on diabetic nephropathy could be not achieved through amino acid metabolism.

Methylamine metabolites are produced from the degradation of dietary choline to TMA, TMAO, and DMA by the gut microflora (Messenger et al., 2013). In this study, *db/db* mice had significantly higher DMA and TMAO levels than age-matched wt mice, whereas their levels were significantly decreased by bFGF treatment, indicating a recovery of methylamine metabolism. TMAO has been reported to be closely associated with decreasing renal function (Mueller et al., 2015; Tang et al., 2015; Missailidis et al., 2016). Tang et al. also found that chronic dietary TMAO exposure directly resulted in progressive renal fibrosis and dysfunction in animal models. Thus, our results suggest that methylamine metabolism may contribute to the reno-protective effect of bFGF in *db/db* mice.

Myo-inositol as an osmolyte plays an important role in normal cellular physiology (Carlomagno et al., 2012). Previous studies have reported that myo-inositol could be an indicator for tubular dysfunction and renal cell stress under hyperglycemia, and has a key role in the etiology of diabetes mellitus, particularly for diabetic nephropathy (Prabhu et al., 2005; Kanwar et al., 2008). Gil et al. reported that in the level of urinary myo-inositol excretion indicated severity of chronic kidney disease (Gil et al.,

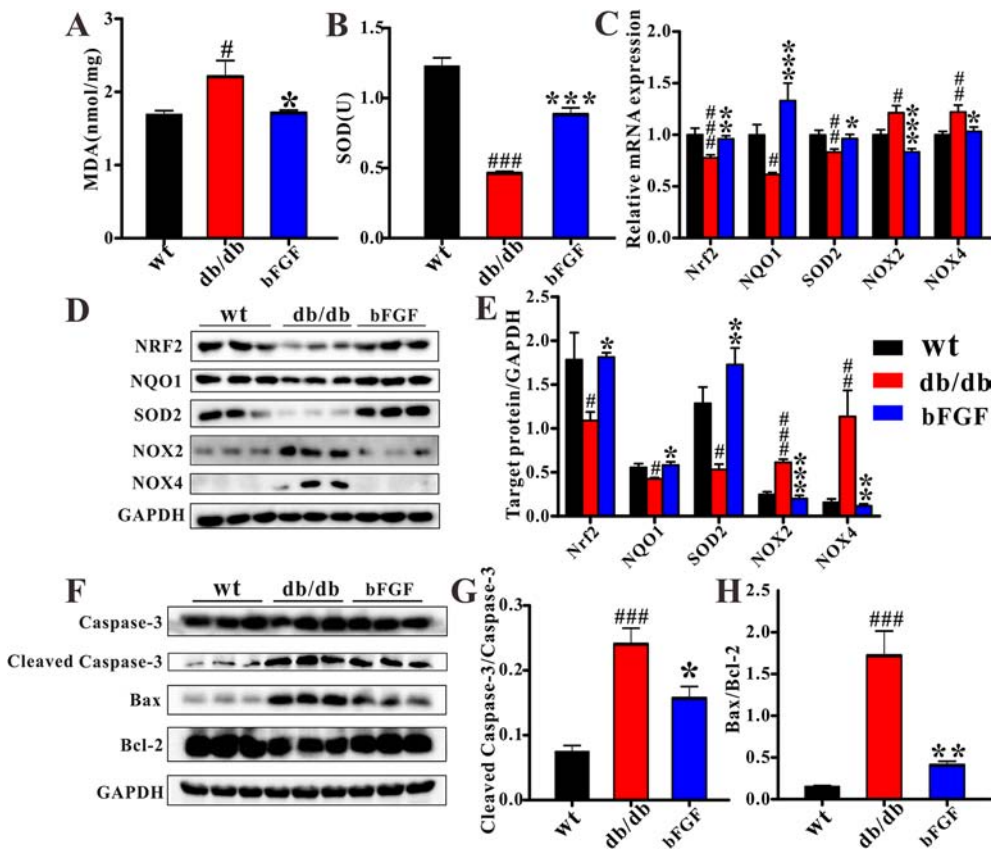

FIGURE 7 | bFGF suppressed oxidative stress and apoptosis in kidney of *db/db* mice. The levels of **(A)** MDA and **(B)** SOD in renal tissues of wild-type (wt), *db/db*, and bFGF-treated mice. **(C)** The relative mRNA expression of Nrf2, NQO1, SOD2, NOX2, and NOX4 in renal tissues of wt, *db/db*, and bFGF-treated mice. **(D)** Western blot analysis of Nrf2, NQO1, SOD2, NOX2, and NOX4 in renal tissues of wt, *db/db*, and bFGF-treated mice. **(E)** Intensities of Nrf2, NQO1, SOD2, NOX2, and NOX4 normalized to GADPH. **(F)** Western blot analysis of caspase-3, cleaved caspase-3, Bax, and Bcl-2 in renal tissues of wt, *db/db*, and bFGF-treated mice. **(G)** Intensities of cleaved caspase-3 normalized to caspase-3. **(H)** Intensities of Bax normalized to Bcl-2. Significant level: $^{\#}P < 0.05$, $^{\#\#}P < 0.01$, and $^{\#\#\#}P < 0.001$ versus wt mice; $^{*}P < 0.05$, $^{**}P < 0.01$, and $^{***}P < 0.001$ versus *db/db* mice.

2018). In the current study, we found a significantly increased myo-inositol level in the kidney of *db/db* mice relative to age-matched wt mice; however, this abnormal increase can be significantly reduced after bFGF treatment. This finding suggests that the protective effect of bFGF on diabetic nephropathy in *db/db* mice may be implicated in myo-inositol-mediated mechanisms such as osmoregulation.

It is worth noting that taurine was identified to have the greatest contribution to bFGF-induced metabolic changes. Taurine is one of abundant free amino acids in mammals' tissues and implicated in oxidative damage, endoplasmic reticulum stress, and apoptosis (Timbrell et al., 1995; Jong et al., 2017). Hence, taurine has been reported to protect against kidney injure (Adedara et al., 2017; Stacchiotti et al., 2018; Adedara et al., 2019). In the present study, *db/db* mice had a significantly lower level of renal taurine than age-matched wt mice, but its level was significantly increased after bFGF treatment. Our results also reveal that bFGF treatment corrected the decreased level of SOD, an antioxidant marker, and the increased level of MDA, a marker of lipid peroxidation, in the kidney of *db/db* mice. Additionally, significant reductions in apoptosis indicators were also detected in the kidney of *db/db* mice treated with bFGF. These findings suggest that the protective effect of bFGF on diabetic nephropathy may be also associated with taurine-mediated oxidative stress and apoptosis. Oxidative stress can increase ROS production and impair antioxidant capacity because of the generation of ROS exceeding the capacity of antioxidant defense system (Wilcox, 2005). Moreover, oxidative stress is believed to play an important role in cell apoptosis (Buttke and Sandstrom, 1994; Chandra et al., 2000) and also associated with diabetic complications (Ruiz et al., 2013; Yang et al., 2015). Nrf2 is a critical transcription factor to maintain redox homeostasis and regulates the expression of antioxidative stress genes including NQO1 and SODs (Dodson et al., 2019). It has been reported that hyperglycemia can induce oxidative stress and increase kidney injure *via* Nrf2 signaling (Wu et al., 2018). However, interestingly, our results show that bFGF treatment corrected the decreased levels of Nrf2, NQO1, and SOD2 in the kidney of *db/db* mice. In addition, NADPH oxidases (NOX2 and NOX4)

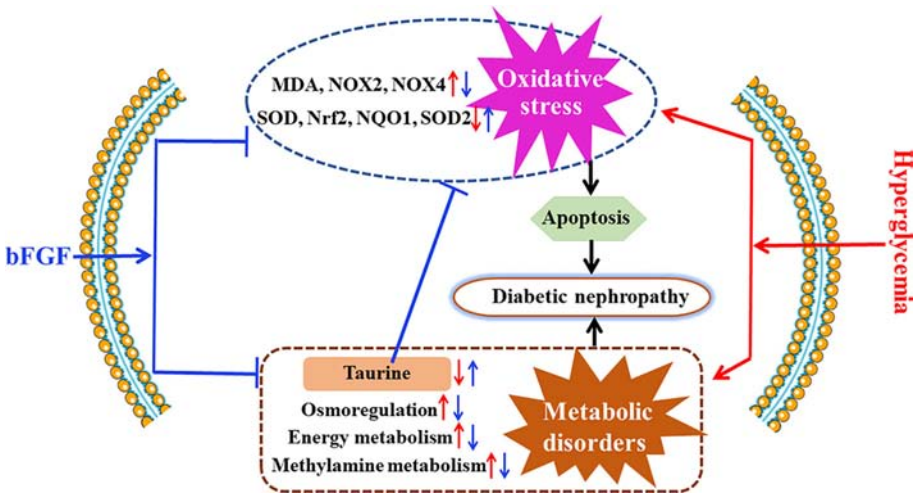

FIGURE 8 | Potential mechanisms for the protective effect of bFGF on diabetic nephropathy. bFGF treatment corrected metabolic disorders and suppressed oxidative stress in *db/db* mice with diabetic nephropathy. Red arrow indicates changes in diabetic nephropathy and blue arrow indicates changes after bFGF treatment.

are a family of enzymes that catalyze the generation of ROS, and have been linked with the development of kidney disease (Holterman et al., 2015). In this study, we found that the levels of NOX2 and NOX4 were significantly increased in the kidney of *db/db* mice relative to age-matched wt mice, but bFGF treatment recovered their levels to the normal level. Therefore, these findings reveal that bFGF may ameliorate oxidative stress and apoptosis during the development of diabetic nephropathy in *db/db* mice *via* NOX-ROS-Nrf2 signaling.

CONCLUSION

In this study, bFGF treatment can effectively reduce urinary albumin to creatinine ratio and renal fibrosis as well as remodel metabolic phenotype in *db/db* mice. Metabolomics analysis identified that taurine, as an antioxidative metabolite, had the greatest contribution to bFGF-induced metabolic changes. Additionally, we found that bFGF treatment alleviated oxidative stress and apoptosis in the kidney of *db/db* mice though NOX-ROS-Nrf2 signaling. However, several limitations or further works should be considered: (1) The biological activities of bFGF are mediated by FGF receptors, so changes in bFGF and its receptors need to be further analyzed in the kidney; (2) A multi-analytical platform is recommended to detect more detailed metabolic pathway changes; (3) A multi-omics analysis will advance a better understanding of the therapeutic effect of bFGF on diabetic nephropathy and its potential mechanisms. Further translational studies are encouraged to modify bFGF structure for excluding its potent mitogenic and angiogenic activities, and facilitate its clinical application for the treatment of diabetic nephropathy in humans.

DATA AVAILABILITY STATEMENT

All datasets generated for this study are included in the article/supplementary material.

ETHICS STATEMENT

The animal study was reviewed and approved by the Institutional Animal Care and Use Committee of Wenzhou Medical University.

AUTHOR CONTRIBUTIONS

HG and HZ contributed to experimental design. TW, JN, and SW contributed to animal experiments and metabolomics analysis. TW, QS, CL, and LZ contributed to molecular biology experiments and data analysis. HZ and TW contributed to result interpretation and writing. All authors have read, revised, and approved the final manuscript.

FUNDING

This work was supported by the National Natural Science Foundation of China (nos. 81600653, 21605115, and 21974096).

REFERENCES

Adedara, I. A., Ojuade, T. J. D., Olabiyi, B. F., Idris, U. F., Onibiyo, E. M., Ajeigbe, O. F., et al. (2017). Taurine ameliorates renal oxidative damage and thyroid dysfunction in rats chronically exposed to fluoride. *Biol. Trace Elem. Res.* 175 (2), 388–395. doi: 10.1007/s12011-016-0784-2

Adedara, I. A., Alake, S. E., Olajide, L. O., Adeyemo, M. O., Ajibade, T. O., and Farombi, E. O. (2019). Taurine ameliorates thyroid hypofunction and renal injury in L-NAME-induced hypertensive rats. *Drug Res. (Stuttg)* 69 (2), 83–92. doi: 10.1055/a-0643-4604

Akira, K., Masu, S., Imachi, M., Mitome, H., and Hashimoto, T. (2012). A metabonomic study of biochemical changes characteristic of genetically hypertensive rats based on (1)H NMR spectroscopic urinalysis. *Hypertens. Res.* 35 (4), 404–412. doi: 10.1038/hr.2011.182

Barman, S., Pradeep, S. R., and Srinivasan, K. (2018). Zinc supplementation alleviates the progression of diabetic nephropathy by inhibiting the overexpression of oxidative-stress-mediated molecular markers in streptozotocin-induced experimental rats. *J. Nutr. Biochem.* 54, 113–129. doi: 10.1016/j.jnutbio.2017.11.008

Barutta, F., Corbelli, A., Mastrocola, R., Gambino, R., Di Marzo, V., Pinach, S., et al. (2010). Cannabinoid receptor 1 blockade ameliorates albuminuria in experimental diabetic nephropathy. *Diabetes* 59 (4), 1046–1054. doi: 10.2337/db09-1336

Buttke, T. M., and Sandstrom, P. A. (1994). Oxidative stress as a mediator of apoptosis. *Immunol. Today* 15 (1), 7–10. doi: 10.1016/0167-5699(94)90018-3

Carlomagno, G., De Grazia, S., Unfer, V., and Manna, F. (2012). Myo-inositol in a new pharmaceutical form: a step forward to a broader clinical use. *Expert Opin. Drug Delivery* 9 (3), 267–271. doi: 10.1517/17425247.2012.662953

Chandra, J., Samali, A., and Orrenius, S. (2000). Triggering and modulation of apoptosis by oxidative stress. *Free Radic. Biol. Med.* 29 (3-4), 323–333. doi: 10.1016/s0891-5849(00)00302-6

Chen, W. L., Wang, J. H., Zhao, A. H., Xu, X., Wang, Y. H., Chen, T. L., et al. (2014). A distinct glucose metabolism signature of acute myeloid leukemia with prognostic value. *Blood* 124 (10), 1645–1654. doi: 10.1182/blood-2014-02-554204

Dodson, M., de la Vega, M. R., Cholanians, A. B., Schmidlin, C. J., Chapman, E., and Zhang, D. D. (2019). Modulating NRF2 in disease: timing is everything. *Annu. Rev. Pharmacol. Toxicol.* 59, 555–575. doi: 10.1146/annurev-pharmtox-010818-021856

Forbes, J. M. (2016). Mitochondria—power players in kidney function? *Trends Endocrinol. Metab.* 27 (7), 441–442. doi: 10.1016/j.tem.2016.05.002

Galvan, D. L., Green, N. H., and Danesh, F. R. (2017). The hallmarks of mitochondrial dysfunction in chronic kidney disease. *Kidney Int.* 92 (5), 1051–1057. doi: 10.1016/j.kint.2017.05.034

Gil, R. B., Ortiz, A., Sanchez-Nino, M. D., Markoska, K., Schepers, E., Vanholder, R., et al. (2018). Increased urinary osmolyte excretion indicates chronic kidney disease severity and progression rate. *Nephrol. Dial. Transplant.* 33 (12), 2156–2164. doi: 10.1093/ndt/gfy020

Guan, M., Xie, L., Diao, C., Wang, N., Hu, W., Zheng, Y., et al. (2013). Systemic perturbations of key metabolites in diabetic rats during the evolution of diabetes studied by urine metabonomics. *PLoS One* 8 (4), e60409. doi: 10.1371/journal.pone.0060409

Holterman, C. E., Read, N. C., and Kennedy, C. R. (2015). Nox and renal disease. *Clin. Sci. (Lond.)* 128 (8), 465–481. doi: 10.1042/CS20140361

Jiang, H., Shao, X., Jia, S., Qu, L., Weng, C., Shen, X., et al. (2019). The mitochondria-targeted metabolic tubular injury in diabetic kidney disease. *Cell. Physiol. Biochem.* 52 (2), 156–171. doi: 10.33594/000000011

Jong, C. J., Ito, T., Prentice, H., Wu, J. Y., and Schaffer, S. W. (2017). Role of mitochondria and endoplasmic reticulum in taurine-deficiency-mediated apoptosis. *Nutrients* 9 (8), 795. doi: 10.3390/nu9080795

Kanwar, Y. S., Wada, J., Sun, L., Xie, P., Wallner, E. I., Chen, S., et al. (2008). Diabetic nephropathy: mechanisms of renal disease progression. *Exp. Biol. Med. (Maywood)* 233 (1), 4–11. doi: 10.3181/0705-MR-134

Li, W., Sargsyan, D., Wu, R., Li, S., Wang, L., Cheng, D., et al. (2019). DNA methylome and transcriptome alterations in high glucose-induced diabetic nephropathy cellular model and identification of novel targets for treatment by tanshinone IIA. *Chem. Res. Toxicol.* doi: 10.1021/acs.chemrestox.9b00117

Li, X. (2019). The FGF metabolic axis. *Front. Med.* 13 (5), 511–530. doi: 10.1007/s11684-019-0711-y

Lin, X., Zhao, L., Tang, S., Zhou, Q., Lin, Q., Li, X., et al. (2016). Metabolic effects of basic fibroblast growth factor in streptozotocin-induced diabetic rats: a (1)H NMR-based metabolomics investigation. *Sci. Rep.* 6, 36474. doi: 10.1038/srep36474

Lu, J., Xie, G., Jia, W., and Jia, W. (2013). Metabolomics in human type 2 diabetes research. *Front. Med.* 7 (1), 4–13. doi: 10.1007/s11684-013-0248-4

Messenger, J., Clark, S., Massick, S., and Bechtel, M. (2013). A review of trimethylaminuria: (fish odor syndrome). *J. Clin. Aesthet. Dermatol.* 6 (11), 45–48.

Missailidis, C., Hallqvist, J., Qureshi, A. R., Barany, P., Heimburger, O., Lindholm, B., et al. (2016). Serum trimethylamine-N-oxide is strongly related to renal function and predicts outcome in chronic kidney disease. *PLoS One* 11 (1), e0141738. doi: 10.1371/journal.pone.0141738

Mueller, D. M., Allenspach, M., Othman, A., Saely, C. H., Muendlein, A., Vonbank, A., et al. (2015). Plasma levels of trimethylamine-N-oxide are confounded by impaired kidney function and poor metabolic control. *Atherosclerosis* 243 (2), 638–644. doi: 10.1016/j.atherosclerosis.2015.10.091

Nagana Gowda, G. A., and Raftery, D. (2017). Recent advances in NMR-based metabolomics. *Anal. Chem.* 89 (1), 490–510. doi: 10.1021/acs.analchem.6b04420

Nicholson, J. K., Lindon, J. C., and Holmes, E. (1999). 'Metabonomics': understanding the metabolic responses of living systems to pathophysiological stimuli *via* multivariate statistical analysis of biological NMR spectroscopic data. *Xenobiotica* 29 (11), 1181–1189. doi: 10.1080/004982599238047

Olatunji, O. J., Chen, H., and Zhou, Y. (2018). *Lycium chinense* leaves extract ameliorates diabetic nephropathy by suppressing hyperglycemia mediated renal oxidative stress and inflammation. *Biomed. Pharmacother.* 102, 1145–1151. doi: 10.1016/j.biopha.2018.03.037

Pan, H. Z., Zhang, L., Guo, M. Y., Sui, H., Li, H., Wu, W. H., et al. (2010). The oxidative stress status in diabetes mellitus and diabetic nephropathy. *Acta Diabetol.* 47 Suppl 1, 71–76. doi: 10.1007/s00592-009-0128-1

Prabhu, K. S., Arner, R. J., Vunta, H., and Reddy, C. C. (2005). Up-regulation of human myo-inositol oxygenase by hyperosmotic stress in renal proximal tubular epithelial cells. *J. Biol. Chem.* 280 (20), 19895–19901. doi: 10.1074/jbc.M502621200

Ruiz, S., Pergola, P. E., Zager, R. A., and Vaziri, N. D. (2013). Targeting the transcription factor Nrf2 to ameliorate oxidative stress and inflammation in chronic kidney disease. *Kidney Int.* 83 (6), 1029–1041. doi: 10.1038/ki.2012.439

Savorani, F., Tomasi, G., and Engelsen, S. B. (2010). icoshift: a versatile tool for the rapid alignment of 1D NMR spectra. *J. Magn. Reson.* 202 (2), 190–202. doi: 10.1016/j.jmr.2009.11.012

Sheng, W. S., Xu, H. L., Zheng, L., Zhuang, Y. D., Jiao, L. Z., Zhou, J. F., et al. (2018). Intrarenal delivery of bFGF-loaded liposome under guiding of ultrasound-targeted microbubble destruction prevent diabetic nephropathy through inhibition of inflammation. *Artif. Cells Nanomed Biotechnol.* 46 (sup2), 373–385. doi: 10.1080/21691401.2018.1457538

Stacchiotti, A., Favero, G., Lavazza, A., Monsalve, M., Rodella, L. F., and Rezzani, R. (2018). Taurine supplementation alleviates puromycin aminonucleoside damage by modulating endoplasmic reticulum stress and mitochondrial-related apoptosis in rat kidney. *Nutrients* 10 (6), 689. doi: 10.3390/nu10060689

Tan, X. H., Zheng, X. M., Yu, L. X., He, J., Zhu, H. M., Ge, X. P., et al. (2017). Fibroblast growth factor 2 protects against renal ischaemia/reperfusion injury by attenuating mitochondrial damage and proinflammatory signalling. *J. Cell. Mol. Med.* 21 (11), 2909–2925. doi: 10.1111/jcmm.13203

Tanaka, S., Sugiura, Y., Saito, H., Sugahara, M., Higashijima, Y., Yamaguchi, J., et al. (2018). Sodium-glucose cotransporter 2 inhibition normalizes glucose metabolism and suppresses oxidative stress in the kidneys of diabetic mice. *Kidney Int.* 94 (5), 912–925. doi: 10.1016/j.kint.2018.04.025

Tang, W. H., Wang, Z., Kennedy, D. J., Wu, Y., Buffa, J. A., Agatisa-Boyle, B., et al. (2015). Gut microbiota-dependent trimethylamine N-oxide (TMAO) pathway contributes to both development of renal insufficiency and mortality risk in chronic kidney disease. *Circ. Res.* 116 (3), 448–455. doi: 10.1161/CIRCRESAHA.116.305360

Teimoury, A., Iraj, B., Heidari-Beni, M., Amini, M., and Hosseiny, S. M. (2014). Why 24-h Urine albumin excretion rate method still is used for screening of diabetic nephropathy in Isfahan laboratories? *Int. J. Prev. Med.* 5 (3), 341–347.

Timbrell, J. A., Seabra, V., and Waterfield, C. J. (1995). The *in vivo* and *in vitro* protective properties of taurine. *Gen. Pharmacol.* 26 (3), 453–462. doi: 10.1016/0306-3623(94)00203-y

Villanueva, S., Contreras, F., Tapia, A., Carreno, J. E., Vergara, C., Ewertz, E., et al. (2014). Basic fibroblast growth factor reduces functional and structural damage

in chronic kidney disease. *Am. J. Physiol. Renal Physiol.* 306 (4), F430–F441. doi: 10.1152/ajprenal.00720.2012

Wang, G., Li, Q., Chen, D., Wu, B., Wu, Y., Tong, W., et al. (2019). Kidney-targeted rhein-loaded liponanoparticles for diabetic nephropathy therapy *via* size control and enhancement of renal cellular uptake. *Theranostics* 9 (21), 6191–6208. doi: 10.7150/thno.37538

Wei, T., Zhao, L., Jia, J., Xia, H., Du, Y., Lin, Q., et al. (2015). Metabonomic analysis of potential biomarkers and drug targets involved in diabetic nephropathy mice. *Sci. Rep.* 5, 11998. doi: 10.1038/srep11998

Wilcox, C. S. (2005). Oxidative stress and nitric oxide deficiency in the kidney: a critical link to hypertension? *Am. J. Physiol. Regul. Integr. Comp. Physiol.* 289 (4), R913–R935. doi: 10.1152/ajpregu.00250.2005

Wu, Y., Li, Y., Jiang, T., Yuan, Y., Li, R., Xu, Z., et al. (2018). Reduction of cellular stress is essential for fibroblast growth factor 1 treatment for diabetic nephropathy. *J. Cell. Mol. Med.* 22 (12), 6294–6303. doi: 10.1111/jcmm.13921

Xiao, C., Hao, F., Qin, X., Wang, Y., and Tang, H. (2009). An optimized buffer system for NMR-based urinary metabonomics with effective pH control, chemical shift consistency and dilution minimization. *Analyst* 134 (5), 916–925. doi: 10.1039/b818802e

Yang, P., Reece, E. A., Wang, F., and Gabbay-Benziv, R. (2015). Decoding the oxidative stress hypothesis in diabetic embryopathy through proapoptotic kinase signaling. *Am. J. Obstet. Gynecol.* 212 (5), 569–579. doi: 10.1016/j.ajog.2014.11.036

Yang, X. (2019). Design and optimization of crocetin loaded PLGA nanoparticles against diabetic nephropathy *via* suppression of inflammatory biomarkers: a formulation approach to preclinical study. *Drug Deliv.* 26 (1), 849–859. doi: 10.1080/10717544.2019.1642417

Yu, S. M., and Bonventre, J. V. (2018). Acute kidney injury and progression of diabetic kidney disease. *Adv. Chronic Kidney Dis.* 25 (2), 166–180. doi: 10.1053/j.ackd.2017.12.005

Zhao, L., Gao, H., Lian, F., Liu, X., Zhao, Y., and Lin, D. (2011). (1)H-NMR-based metabonomic analysis of metabolic profiling in diabetic nephropathy rats induced by streptozotocin. *Am. J. Physiol. Renal Physiol.* 300 (4), F947–F956. doi: 10.1152/ajprenal.00551.2010

Zhong, F., Liu, X., Zhou, Q., Hao, X., Lu, Y., Guo, S., et al. (2012). 1H NMR spectroscopy analysis of metabolites in the kidneys provides new insight into pathophysiological mechanisms: applications for treatment with *Cordyceps sinensis*. *Nephrol. Dial. Transplant.* 27 (2), 556–565. doi: 10.1093/ndt/gfr368

Conflict of Interest: The authors declare that the research was conducted in the absence of any commercial or financial relationships that could be construed as a potential conflict of interest.

frontiers in Pharmacology

REVIEW
published: 25 February 2020
doi: 10.3389/fphar.2020.00111

Progress in Research on the Role of FGF in the Formation and Treatment of Corneal Neovascularization

Mengji Chen, Licheng Bao, Mengying Zhao, Jiarong Cao and Haihua Zheng *

Department of Ophthalmology, The Second Affiliated Hospital and Yuying Children's Hospital of Wenzhou Medical University, Wenzhou, China

Corneal neovascularization (CNV) is a sight-threatening disease usually associated with inflammatory, infectious, degenerative, and traumatic disorders of the ocular surface. Fibroblast growth factor (FGF) family members play an important role in angiogenesis to induce corneal neovascularization, which significantly affects the differentiation, proliferation, metastasis, and chemotaxis of vascular endothelial cells. Both acidic fibroblast growth factor (aFGF) and basic fibroblast growth factor (bFGF) demonstrate positive staining in capillaries and induce corneal stromal cells. The anabolism of endothelial cells is induced by bFGF in corneal neovascularization. FGFs exert their effects *via* specific binding to cell surface-expressed specific receptors. We believe that both anti-FGF antibodies and anti-FGF receptor antibodies represent new directions for the treatment of CNV. Similar to anti-vascular endothelial growth factor antibodies, subconjunctival injection and eye drops can be considered effective forms of drug delivery.

Keywords: corneal neovascularization, fibroblast growth factor, development, treatment, drug delivery

OPEN ACCESS

Edited by:
Saverio Bellusci, University of Giessen, Germany

Reviewed by:
Elie El Agha, University of Giessen, Germany
Tingting Yuan, University of Alabama at Birmingham, United States

***Correspondence:**
Haihua Zheng
eyezhh@126.com

Specialty section:
This article was submitted to Translational Pharmacology, a section of the journal Frontiers in Pharmacology

Received: *23 October 2019*
Accepted: *28 January 2020*
Published: *25 February 2020*

Citation:
Chen M, Bao L, Zhao M, Cao J and Zheng H (2020) Progress in Research on the Role of FGF in the Formation and Treatment of Corneal Neovascularization. Front. Pharmacol. 11:111. doi: 10.3389/fphar.2020.00111

CORNEAL NEOVASCULARIZATION

The incidence rate of corneal neovascularization (CNV), a sight-threatening condition, is approximately 1.4 million patients per year (Bonini, 2016). It is usually associated with inflammatory, traumatic, or infectious disorders of the ocular surface. Corneal neovascularization can cause vision damage and even blindness, the rate of which is as high as 57.4% (Chang et al., 2001). The cornea needs to be transparent to allow the passage of light into the retina. When CNV occurs, abnormal blood vessels directly block light, indirectly diffract light as canals for inflammatory cells, and damage the structure of the cornea by depositing lipids and proteins into the corneal stroma. Various mechanisms of corneal neovascularization have been studied. A balance exists between angiogenic factors (such as fibroblast growth factor and vascular endothelial growth factor) and anti-angiogenic factors (such as angiostatin, endostatin, and pigment epithelium-derived factor) in the cornea (Senturk et al., 2016). An imbalance leads to CNV, which can be divided into superficial neovascularization and deep stromal neovascularization. In the normal cornea, heparan sulfate prevents the release of potent angiogenic cytokines, such as fibroblast growth factor (FGF) and vascular endothelial growth factor (VEGF). However, under stimulation, cytokines may be released, causing an imbalance (Gurung et al., 2018).

FGF

FGF

Fibroblast growth factor participates in cell proliferation, migration, and tissue repair in adults (Itoh and Ornitz, 2004). FGFs can stimulate many cell types, including endothelial cells and nerve cells. The FGF family comprises 22 members (FGF1-23, except FGF15 because mouse FGF15 is the orthologue of human and chick FGF19) (Beenken and Mohammadi, 2009). Many of these FGFs, particularly FGF-1 (acidic FGF) and FGF-2 (basic FGF), have been shown to influence angiogenesis in several tissues *in vivo* (**Table 1**) by acting on endothelial cells. Different factors affect FGFs in different tissues. FGFs are produced by endothelial cells and are stored in the extracellular matrix. They show a high affinity for heparin (Klagsbrun, 1990).

FGFs activate transmembrane tyrosine kinases and their coupled intracellular signalling pathways to stimulate biological activities and transduce external signals through the PI3K, MAPK, and phospholipase Cγ (PLCγ) pathways (Klagsbrun, 1990; Zhou et al., 2009; Francavilla et al., 2013; Huang et al., 2016). A dual-receptor system comprising a family of four receptor tyrosine kinases (FGFRs) and heparan sulfate proteoglycans (HSPGs) mediates the stimulation of cellular metabolism by FGFs. Thus, many of the FGFR isoforms bind several FGFs. HSPG receptors may provide additional specificity (Klagsbrun, 1990). ERK1/2, JNK1/2, and p38 alpha/beta are three main MAPK subgroups (Zhang et al., 2009). Phospholipase C can receive the signal from FGFRs and then activate PLCγ1 to induce cell proliferation and migration in vascular smooth muscle cells by cleaving the phospholipid phosphatidylinositol 4,5-bisphosphate into diacylglycerol and inositol 1,4,5-triphosphate (Michel, 1998). Studies have suggested that heparan may modulate the activity of FGFs (Ornitz, 2000). Additionally, studies have suggested that membrane-type 1 matrix metalloproteinase (MT1-MMP) plays an important role in modulating FGF-mediated signal pathways (Zhou et al., 2000). It controls FGF signalling by reducing the amount of FGF bound to the cell surface, increasing the proteolysis of FGFs and the downregulation of FGFR-1 and -4 (Tassone et al., 2015).

TABLE 1 | Fibroblast growth factors (FGFs) associated with angiogenesis.

FGFs	Pathway/influencing factor	Related tissue/disease
FGF-1	S156C-TIMP3 mutation	Choroid (Loren et al., 2009; de Oliveira Dias et al., 2011)
	P53	Inflammed tissue (Zhou et al., 2009)
	Erk and MMP-7	Colon cancer (Jin et al., 2016)
	S100A13	Endometriosis (Francavilla et al., 2013)
FGF-2	VEGF	Corneal, choroid, and retina (Senturk et al., 2016)
	NDY1/KDM2B-miR101-EZH2	Tumor tissue (Akpek et al., 2004)
	Interleukin-1β	Chondrocytes (Baradaran-Rafii et al., 2019)
	AKT/MMP-2	Human umbilical vein (Mimura et al., 2011)
FGF-3	Erk and MMP-7	Tumor tissue (Nor et al., 2001)
FGF-8	Co-expression of VEGF	Prostate cancer (Stevenson et al., 2012)
FGF-9	VEGF-A	Bone (Koolwijk et al., 1996)
FGF-18	Wnt/β-catenin	Hepatocellular carcinoma (Zheng et al., 2001)
FGF-21	Dynamin-2 and Rab5	Kidney (Kim et al., 2013)

FGFs in the Eye

mRNAs encoding basic FGF are produced by corneal epithelial cells, stromal fibroblasts, and corneal endothelial cells (Oladipupo et al., 2014). FGF-2 may have different functions in the three primary cell types of the cornea. Studies have shown that in corneal epithelial cells, FGF-2 stimulates the proliferation of corneal epithelial cells and increases the rate of epithelial wound healing through autocrine and paracrine effects (Kanayama et al., 2007). Rajesh et al. showed that FGF-2 promotes corneal stromal wound healing by increasing cellular proliferation (stimulated by TGF-beta *via* paracrine effects) (Moioli et al., 2006) and cellular motility (significant enhancement of stromal fibroblast motility by 100 ng/ml FGF-2 in animal experiments) (Rao et al., 1992). Cdc42 activation, Rho inactivation, and the phosphatidylinositol 3-kinase pathway in corneal endothelial cells (CECs) are essential for FGF-2-induced wound healing (Lee and Kay, 2006), and endothelial mesenchymal transformation can be mediated by FGFs in CECs. Additionally, FGFs can mediate the proliferation and regeneration of the lens (FGF-1 and FGF-2) (Zhu et al., 2012) and retinal cells (FGF-2, FGF-5, and FGF-9) through different signalling pathways (Gong et al., 2014). FGF-9, FGF-21, and FGF-23 are also expressed in choroidal endothelial cells and affect choroid plexus epithelial cell behaviour (Loren et al., 2009; de Oliveira Dias et al., 2011).

FGFs also play an important role in early mammalian eye development. The neuroepithelium of the optic vesicle separates into NR and RPE domains in a manner mediated by extrinsic factors that emanate from the surface ectoderm, for which fibroblast growth factors are prime candidates (Bassnett and Sikic, 2017).

FGFS AND RELATED CORNEAL DISEASES

Many FGFs affect angiogenesis, but FGF-2 is the most common isoform to be detected in the eye and to cause CNV in different eye diseases. One of these diseases is ocular chemical burn. We focused on alkali burns because of their severity. CNV can be caused by severe corneal alkali burn (Nominato et al., 2018), in which deep corneal stroma or full-thickness corneal injury is involved. In this situation, angiogenic factors play an important role in CNV. For example, experimental data have shown that on the second day after alkaline burn, b-FGF is obviously expressed in the corneal epithelium, substantia propria layer, and endothelium (Xiao et al., 2012). Additionally, studies have shown that the upregulation of related genes (microRNA-296) after alkali burn is positively correlated with the expression of related FGF isoforms (FGF-23). FGF-23 may influence corneal

inflammatory responses by participating in cytokine-cytokine receptor interaction pathways (Hayashi et al., 1996).

Keratitis is another important cause of corneal neovascularisation (Soiberman et al., 2017). In the initial stage of infection with herpes simplex virus type 1 (HSV-1), both virus and immune cells are present in the cornea. Meanwhile, various cytokines and growth factors (FGF-2 and Ang-2), which also permeate the cornea, lead to further inflammation. The origin of FGF-2 may not fibroblasts (keratocytes), epithelium, endothelium, blood endothelial cells, and lymphatic endothelial cells rather than leukocytes (Xu et al., 2019). In the late stage, immune cells and growth factors continue to be effective while the virus is removed from the cornea. Furthermore, FGF-2 mediates the expression of other cytokines (such as VEGF-A, IL-6, and Ang-2), which are crucial for HSV-1-induced corneal neovascularization (Klagsbrun, 1990).

Patients who undergo corneal transplantation can develop corneal neovascularization. Particularly, after high-risk keratoplasty, intense CNV outgrowth is a common phenomenon in the early postoperative period (Kelly et al., 2011). Corneal neovascularization can lead to an increased risk of graft rejection caused by an imbalance between angiogenic factors and anti-angiogenic factors. Additionally, FGF is an important angiogenic factor. Presently, no study has shown how FGFs cause CNV after corneal transplantation and which FGF isoform is involved, but this phenomenon warrants further research.

ROLE OF FGFS IN CNV FORMATION

Angiogenesis is the process by which new blood vessels grow by sprouting from established blood vessels (Carmeliet and Jain, 2011). In the cornea, these existing blood vessels can be part of the vascular plexus around the limbus of the anterior ciliary artery. Corneal angiogenesis occurs because of the release of proangiogenic factors, such as FGF-2, VEGF, and several other chemokines, from hypoxic or inflammatory cells. The binding of angiogenic factors to corresponding receptors on vascular endothelial cells leads to many events, including the following: (a) injury to endothelial cell junctions through the activation of non-receptor Src family kinases and increased expression of integrins; (b) the promotion of endothelial cell proliferation by mitogen-activated protein kinase and phosphoinositide 3' kinase; (c) the secretion of metalloproteinases (MMPs) by endothelial cells to promote basal membrane disruption and pericyte detachment; and (d) blood vessel destabilization caused by the release of angiopoietin 2 (ANG 2) from endothelial cell granules (**Figure 1**). Additionally, murine tissue inhibitor of metalloproteinase-4 (TIMP-4) expression in the cornea may play a role in regulating extracellular matrix remodelling associated with corneal wound healing and angiogenesis; however, the mechanism is unclear.

Vascular endothelial cells are stimulated directly by FGFs from angiogenic tissues. FGF-producing cells also release FGFs through autocrine or nuclear actions (**Figure 1**), and secondary angiogenic factors then act on the vasculature. The vascular endothelium can induce the secretion of secondary regulatory molecules in the same way, and such secretion can also be influenced by other angiogenic factors, such as VEGF. The specific role of FGFs depends on the environment in which they are located (Beenken and Mohammadi, 2009).

PROGRESS IN FGF RESEARCH FOR CNV TREATMENT

Current Effective Treatments for CNV

Presently, laser treatment, drug treatment, and surgical treatment are available to treat corneal neovascularization. Drugs used for treatment include glucocorticoids, immunosuppressive agents, and various vascular growth factor inhibitors. While the topical administration of steroidal anti-inflammatory drugs is the first-line treatment for corneal neovascularization, many side effects

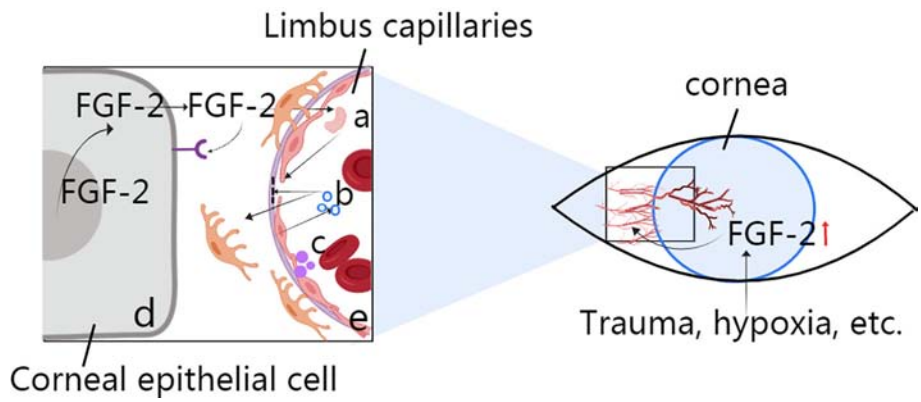

FIGURE 1 | Role of FGF-2 in corneal angiogenesis. **(A)** Activation for the destruction of endothelial cell junctions *via* MMP secretion. **(B)** Disruption of the basal membrane and pericytes *via* ANG2. **(C)** Secretion from vascular endothelial cells to induce blood vessel destabilization. **(D)** Corneal epithelial cell production through autocrine or nuclear actions during events such as trauma and hypoxia. **(E)** Limbus capillaries: activation of Src family kinases.

occur during long-term application (Mukwaya et al., 2019). Laser treatment is less effective for the dense mesh type of CNV. Corneal transplant surgery may also cause various complications, including HSV-1 infection of the cornea.

A novel therapy targeting angiogenic cytokines may have therapeutic potential for clinical use in the future, and it has been shown to inhibit corneal vascularization effectively in animal models (Klagsbrun, 1990). Repeated subconjunctival injections of Avastin® (the trade name of bevacizumab; 1.25 mg/0.05 ml) and topical cyclosporin-A drops appear to be safe and effective in treating aggressive corneal vascularization (Akpek et al., 2004; Stevenson et al., 2012). Subconjunctival bevacizumab injections were shown to be effective and safe in reducing corneal neovascularization within the first 4 months (Jacobs et al., 2009). Recent research has shown that bevacizumab can also be administered by corneal intrastromal injection for the inhibition of intrastromal vascularization after deep anterior lamellar keratoplasty (Sun et al., 2019). Additionally, there are few corneal epithelial side effects when bevacizumab eye drops are used to treat corneal neovascularization (Baradaran-Rafii et al., 2019). Anti-angiogenic effects and anti-fibrotic effects for the maintenance of corneal transparency have also been observed after the use of bevacizumab eye drops (25 mg/ml) for corneal burn (Koenig et al., 2012). However, only a few related studies using eye drops exist, and further verification is needed.

Comparison of Anti-FGF and Anti-VEGF

Anti-VEGF drugs include recombinant full-length VEGF monoclonal antibodies (Avastin), recombinants of VEGF subtype monoclonal antibody fragments (Lucentis), and RNA aptamers (Macugen). The mechanism of these drugs involves binding to VEGF and inhibiting the specific binding of VEGF to its receptor. Recent observations have shown that the soluble pattern recognition receptor long-pentraxin-3 binds FGF2 with high affinity and specificity and thus acts as an FGF2 antagonist (Presta et al., 2018). The novel RNA aptamer (a short single-stranded nucleic acid molecule) APT-F2, which is specific for human FGF2, was also recently discovered as an anti-FGF drug (Jin et al., 2016), but it has not been applied in anti-angiogenic studies. More types of anti-FGF drugs are yet to be discovered. The mechanism of anti-FGF drugs is similar to that of anti-VEGF drugs.

Studies have demonstrated that bFGF expression induces VEGF, MT1-MMP, and CD31 in the experimental mouse cornea (Nor et al., 2001; Mimura et al., 2011). Therefore, FGF treatment may be more comprehensive. Researchers believe that angiogenesis induced by basic fibroblast growth factor (bFGF) is immune to anti-VEGF/VEGFR (vascular endothelial growth factor/receptor) therapy (Koolwijk et al., 1996). Furthermore, patients may develop tolerance to anti-VEGF drugs. Experimental evidence suggests that FGF2-targeted drugs might provide cooperative effects with anti-VEGF monoclonal antibodies for the treatment of angiogenesis-related diseases. Another important advantage of anti-FGF drugs is that they may be beneficial for the recovery of vision. Researchers established a model of anti-FGF-2 antibody-treated mouse corneal neovascularization and then evaluated the corneal sensitivity and visual acuity of these mice to assess their functional vision. Time-course experiments revealed partial recovery of visual acuity in mice treated with an anti-FGF-2 antibody compared with control mice (Zheng et al., 2001). This finding supports anti-VEGF therapy for corneal neovascularization, but further experimental confirmation is needed.

FGF as a Drug Source and the Administration Route

Several anti-FGF2 monoclonal antibodies (mAbs) that can neutralize the activities of FGF2 *in vitro* and *in vivo* have been identified (Jin et al., 2016). However, to our knowledge, no anti-FGF2 mAb has entered clinical trials. Because of the similarity between VEGF and FGF antagonists, we can presume the likely effect of FGF antagonists in treating CNV based on the effects of anti-VEGF drugs.

A previous study demonstrated that the subconjunctival injection of anti-VEGF drugs (1.25 mg/0.05 ml bevacizumab) significantly reduces inflammation and fibroblast activity to inhibit corneal neovascularization in the cornea of a rat model of alkali burn. Rats in the test group were treated with a subconjunctival injection (Kim et al., 2013). Another researcher advocated combining subconjunctival (1.25 mg/0.05 ml) and intracorneal injection (1.25 mg/0.05 ml). They confirmed that combining subconjunctival and intracorneal injection did not damage corneal endothelial cells (Lichtinger et al., 2014). No clinical case featuring the administration of anti-FGF drugs through subconjunctival and intracorneal routes for the treatment of CNV exists, but we can refer to these modes of administration. Therefore, the drug concentration and side effects remain unclear, and further research is needed.

Recently, research on new eye drops has progressed. Considering the effects of anti-VEGF drugs, in the future, Avastin eye drops may be shown to exhibit the same anti-VEGF effects with fewer complications than intravitreal use (Kim et al., 2013). Bevacizumab eye drops seem to inhibit corneal neovascularization without inducing obvious corneal epithelial side effects. Bevacizumab eye drops are prepared by adding 0.9% physiological saline to the drug at a concentration of 5 mg/ml. The minimum storage temperature of the eye drops is –20°C (before opening), the maximum storage temperature is 4°C (after opening), and the maximum storage time is 14 days; after opening, they needs to be used within 1 day (Bock et al., 2008). Therefore, we believe that preparations of anti-FGF drugs as eye drops can be applied for the clinical treatment of corneal neovascularization. The effects of the FGF antagonist tecogalan sodium against corneal neovascularization were tested in animal experiments, and tecogalan sodium demonstrated dose-dependent antiangiogenic activity. The inhibitory effect of 100 ng terconazole sodium was weakly, and the effect of 250 ng was marked, indicating that corneal neovascularization induced by bFGF can be inhibited by the topical instillation of tecogalan sodium (Murata et al., 1995). However, no data regarding the

recommended dose of other anti-FGF drugs for the treatment of CNV are available. It is possible that we need to start with a low dose and simultaneously test the corneal toxicity of the drug.

SUMMARY

Corneal neovascularization is a pathological change in the cornea that blocks light, leads to inflammation and edema, and causes corneal scarring in severe cases. Ultimately, it leads to a serious decline in vision. When the balance between angiogenic and antiangiogenic factors shifts towards the former, corneal neovascularization occurs. FGF, particularly bFGF, plays a very important role in corneal neovascularization due to various factors. However, its exact role and mechanism require further research. Therefore, anti-FGF drugs can be used as new candidates for treating corneal neovascularization. Presently, steroidal anti-inflammatory drugs are the first-line therapy for corneal neovascularization. New types of drugs with fewer side effects need to be developed; anti-VEGF drugs are one of the candidates. Compared with anti-VEGF drugs, anti-FGF drugs have advantages. The discovery of additional FGF antagonists and the route of administration of anti-FGF drugs will become a new research direction. The authors believe that the subconjunctival and corneal stroma injection of anti-FGF drugs and anti-FGF eye drops will provide new strategies to treat corneal neovascularization.

AUTHOR CONTRIBUTIONS

MC and HZ participated in drafting the manuscript. LB, MZ, and JC provided technical assistance. MC and HZ revised the manuscript. HZ supervised the project and provided financial support. MC and HZ wrote the main part of the paper. All of the authors read and approved the final manuscript.

ACKNOWLEDGMENTS

This study was supported by all members of the Ophthalmology Department of the Second Affiliated Hospital of Wenzhou Medical University and by the Zhejiang Natural Science Foundation (LY18H120009). The authors also thank Professor Qianying Gao from the State Key Laboratory of Sun Yat-sen University.

REFERENCES

Akpek, E. K., Dart, J. K., Watson, S., Christen, W., Dursun, D., Yoo, S., et al. (2004). A randomized trial of topical cyclosporin 0.05% in topical steroid-resistant atopic keratoconjunctivitis. *Ophthalmology* 111 (3), 476–482. doi: 10.1016/j.ophtha.2003.05.035

Baradaran-Rafii, A., Ashnagar, A., Heidari Keshel, S., Jabbehdari, S., and Baradaran-Rafii, G. (2019). Regression of corneal neovascularization: adiponectin versus bevacizumab eye drops. *Eur. J. Ophthalmol*. doi: 10.1177/1120672119874947

Bassnett, S., and Sikic, H. (2017). The lens growth process. *Prog. Retin Eye Res.* 60, 181–200. doi: 10.1016/j.preteyeres.2017.04.001

Beenken, A., and Mohammadi, M. (2009). The FGF family: biology, pathophysiology and therapy. *Nat. Rev. Drug Discovery* 8 (3), 235–253. doi: 10.1038/nrd2792

Bock, F., Konig, Y., Kruse, F., Baier, M., and Cursiefen, C. (2008). Bevacizumab (Avastin) eye drops inhibit corneal neovascularization. *Graefes Arch. Clin. Exp. Ophthalmol.* 246 (2), 281–284. doi: 10.1007/s00417-007-0684-4

Bonini, S. (2016). Corneal neovascularization: clinical aspects and the role of the immune system. *Acta Ophthalmol.* 94 (S256). doi: 10.1111/j.1755-3768.2016.0241

Carmeliet, P., and Jain, R. K. (2011). Molecular mechanisms and clinical applications of angiogenesis. *Nature* 473 (7347), 298–307. doi: 10.1038/nature10144

Chang, J. H., Gabison, E. E., Kato, T., and Azar, D. T. (2001). Corneal neovascularization. *Curr. Opin. Ophthalmol.* 12 (4), 242. doi: 10.1097/00055735-200108000-00002

de Oliveira Dias, J. R., Rodrigues, E. B., Maia, M., Magalhaes, O. Jr., Penha, F. M., and Farah, M. E. (2011). Cytokines in neovascular age-related macular degeneration: fundamentals of targeted combination therapy. *Br. J. Ophthalmol.* 95 (12), 1631–1637. doi: 10.1136/bjo.2010.186361

Francavilla, C., Rigbolt, K. T., Emdal, K. B., Carraro, G., Vernet, E., Bekker-Jensen, D. B., et al. (2013). Functional proteomics defines the molecular switch underlying FGF receptor trafficking and cellular outputs. *Mol. Cell* 51 (6), 707–722. doi: 10.1016/j.molcel.2013.08.002

Gong, L., Ji, W. K., Hu, X. H., Hu, W. F., Tang, X. C., Huang, Z. X., et al. (2014). Sumoylation differentially regulates Sp1 to control cell differentiation. *Proc. Natl. Acad. Sci. U. S. A.* 111 (15), 5574–5579. doi: 10.1073/pnas.1315034111

Gurung, H. R., Carr, M. M., Bryant, K., Chucair-Elliott, A. J., and Carr, D. J. (2018). Fibroblast growth factor-2 drives and maintains progressive corneal neovascularization following HSV-1 infection. *Mucosal Immunol.* 11 (1), 172–185. doi: 10.1038/mi.2017.26

Hayashi, N., Nakayasu, K., and Okisaka, S. (1996). [Immunohistochemical localization of acidic and basic fibroblast growth factor through corneal neovascularization *in vivo* and *in vitro*]. *Nippon Ganka Gakkai Zasshi* 100 (8), 587–591.

Huang, Z., Marsiglia, W. M., Basu Roy, U., Rahimi, N., Ilghari, D., Wang, H., et al. (2016). Two FGF receptor kinase molecules act in concert to recruit and transphosphorylate phospholipase Cgamma. *Mol. Cell* 61 (1), 98–110. doi: 10.1016/j.molcel.2015.11.010

Itoh, N., and Ornitz, D. M. (2004). Evolution of the Fgf and Fgfr gene families. *Trends Genet.* 20 (11), 563–569. doi: 10.1016/j.tig.2004.08.007

Jacobs, D. S., Lim, M., Carrasquillo, K. G., and Rosenthal, P. (2009). Bevacizumab for corneal neovascularization. *Ophthalmology* 116 (3), 592–593. doi: 10.1016/j.ophtha.2008.10.011

Jin, L., Nonaka, Y., Miyakawa, S., Fujiwara, M., and Nakamura, Y. (2016). Dual therapeutic action of a neutralizing anti-FGF2 Aptamer in bone disease and bone cancer pain. *Mol. Ther.* 24 (11), 1974–1986. doi: 10.1038/mt.2016.158

Kanayama, S., Nishida, K., Yamato, M., Hayashi, R., Sugiyama, H., Soma, T., et al. (2007). Analysis of angiogenesis induced by cultured corneal and oral mucosal epithelial cell sheets *in vitro*. *Exp. Eye Res.* 85 (6), 772–781. doi: 10.1016/j.exer.2007.08.011

Kelly, T. L., Coster, D. J., and Williams, K. A. (2011). Repeat penetrating corneal transplantation in patients with keratoconus. *Ophthalmology* 118 (8), 1538–1542. doi: 10.1016/j.ophtha.2011.01.002

Kim, E. C., Ryu, H. W., Lee, H. J., and Kim, M. S. (2013). Bevacizumab eye drops delay corneal epithelial wound healing and increase the stromal response to epithelial injury in rats. *Clin. Exp. Ophthalmol.* 41 (7), 694–701. doi: 10.1111/ceo.12085

Klagsbrun, M. (1990). The affinity of fibroblast growth factors (FGFs) for heparin; FGF-heparan sulfate interactions in cells and extracellular matrix. *Curr. Opin. Cell Biol.* 2 (5), 857–863. doi: 10.1016/0955-0674(90)90084-r

Koenig, Y., Bock, F., Kruse, F. E., Stock, K., and Cursiefen, C. (2012). Angioregressive pretreatment of mature corneal blood vessels before keratoplasty: fine-needle vessel coagulation combined with anti-VEGFs. *Cornea* 31 (8), 887–892. doi: 10.1097/ICO.0b013e31823f8f7a

Koolwijk, P., van Erck, M. G., de Vree, W. J., Vermeer, M. A., Weich, H. A., Hanemaaijer, R., et al. (1996). Cooperative effect of TNFalpha, bFGF, and VEGF on the formation of tubular structures of human microvascular endothelial cells in a fibrin matrix. Role of urokinase activity. *J. Cell Biol.* 132 (6), 1177–1188. doi: 10.1083/jcb.132.6.1177

Lee, J. G., and Kay, E. P. (2006). FGF-2-induced wound healing in corneal endothelial cells requires Cdc42 activation and Rho inactivation through the phosphatidylinositol 3-kinase pathway. *Invest. Ophthalmol. Vis. Sci.* 47 (4), 1376–1386. doi: 10.1167/iovs.05-1223

Lichtinger, A., Yeung, S. N., Kim, P., Amiran, M. D., Elbaz, U., and Slomovic, A. R. (2014). Corneal endothelial safety following subconjunctival and intrastromal injection of bevacizumab for corneal neovascularization. *Int. Ophthalmol.* 34 (3), 597–601. doi: 10.1007/s10792-013-9807-6

Loren, C. E., Schrader, J. W., Ahlgren, U., and Gunhaga, L. (2009). FGF signals induce Caprin2 expression in the vertebrate lens. *Differentiation* 77 (4), 386–394. doi: 10.1016/j.diff.2008.11.003

Michel, J. B. (1998). [Role of endothelial nitric oxide in the regulation of the vasomotor system]. *Pathol. Biol. (Paris)* 46 (3), 181–189.

Mimura, T., Chang, J. H., Kim, T. I., Onguchi, T., Kojima, T., Sakimoto, T., et al. (2011). MT1-MMP cleavage of the antiangiogenic proteoglycan decorin: role in corneal angiogenesis. *Cornea* 30 Suppl 1, S45–S49. doi: 10.1097/ICO.0b013e31822816e0

Moioli, E. K., Hong, L., Guardado, J., Clark, P. A., and Mao, J. J. (2006). Sustained release of TGFbeta3 from PLGA microspheres and its effect on early osteogenic differentiation of human mesenchymal stem cells. *Tissue Eng.* 12 (3), 537–546. doi: 10.1089/ten.2006.12.537

Mukwaya, A., Jensen, L., Peebo, B., and Lagali, N. (2019). MicroRNAs in the cornea: role and implications for treatment of corneal neovascularization. *Ocul. Surf.* 17 (3), 400–411. doi: 10.1016/j.jtos.2019.04.002

Murata, T., Ishibashi, T., Yoshikawa, H., Khalil, A., and Inomata, H. (1995). Tecogalan sodium inhibits corneal neovascularization induced by basic fibroblast growth factor. *Ophthalmic Res.* 27 (6), 330–334. doi: 10.1159/000267744

Nominato, L. F., Dias, A. C., Dias, L. C., Fantucci, M. Z., Mendes da Silva, L. E. C., Murashima, A. A., et al. (2018). Prevention of corneal neovascularization by adenovirus encoding human vascular endothelial growth factor soluble receptor (s-VEGFR1) in lacrimal gland. *Invest. Ophthalmol. Vis. Sci.* 59 (15), 6036–6044. doi: 10.1167/iovs.17-22322

Nor, J. E., Christensen, J., Liu, J., Peters, M., Mooney, D. J., Strieter, R. M., et al. (2001). Up-Regulation of Bcl-2 in microvascular endothelial cells enhances intratumoral angiogenesis and accelerates tumor growth. *Cancer Res.* 61 (5), 2183–2188.

Oladipupo, S. S., Smith, C., Santeford, A., Park, C., Sene, A., Wiley, L. A., et al. (2014). Endothelial cell FGF signaling is required for injury response but not for vascular homeostasis. *Proc. Natl. Acad. Sci. U. S. A.* 111 (37), 13379–13384. doi: 10.1073/pnas.1324235111

Ornitz, D. M. (2000). FGFs, heparan sulfate and FGFRs: complex interactions essential for development. *Bioessays* 22 (2), 108–112. doi: 10.1002/(SICI)1521-1878(200002)22:2<108::AID-BIES2>3.0.CO;2-M

Presta, M., Foglio, E., Churruca Schuind, A., and Ronca, R. (2018). Long Pentraxin-3 modulates the angiogenic activity of fibroblast growth factor-2. *Front. Immunol.* 9, 2327. doi: 10.3389/fimmu.2018.02327

Rao, R. C., Varani, J., and Soong, H. K. (1992). FGF promotes corneal stromal fibroblast motility. *J. Ocul. Pharmacol.* 8 (1), 77–81. doi: 10.1089/jop.1992.8.77

Senturk, B., Cubuk, M. O., Ozmen, M. C., Aydin, B., Guler, M. O., and Tekinay, A. B. (2016). Inhibition of VEGF mediated corneal neovascularization by anti-angiogenic peptide nanofibers. *Biomaterials* 107, 124–132. doi: 10.1016/j.biomaterials.2016.08.045

Soiberman, U., Kambhampati, S. P., Wu, T., Mishra, M. K., Oh, Y., Sharma, R., et al. (2017). Subconjunctival injectable dendrimer-dexamethasone gel for the treatment of corneal inflammation. *Biomaterials* 125, 38–53. doi: 10.1016/j.biomaterials.2017.02.016

Stevenson, W., Cheng, S. F., Dastjerdi, M. H., Ferrari, G., and Dana, R. (2012). Corneal neovascularization and the utility of topical VEGF inhibition: ranibizumab (Lucentis) vs bevacizumab (Avastin). *Ocul. Surf.* 10 (2), 67–83. doi: 10.1016/j.jtos.2012.01.005

Sun, J. G., Jiang, Q., Zhang, X. P., Shan, K., Liu, B. H., Zhao, C., et al. (2019). Mesoporous silica nanoparticles as a delivery system for improving antiangiogenic therapy. *Int. J. Nanomed.* 14, 1489–1501. doi: 10.2147/IJN.S195504

Tassone, E., Valacca, C., and Mignatti, P. (2015). Membrane-type 1 matrix metalloproteinase downregulates fibroblast growth factor-2 binding to the cell surface and intracellular signaling. *J. Cell Physiol.* 230 (2), 366–377. doi: 10.1002/jcp.24717

Xiao, O., Xie, Z. L., Lin, B. W., Yin, X. F., Pi, R. B., and Zhou, S. Y. (2012). Minocycline inhibits alkali burn-induced corneal neovascularization in mice. *PLoS One* 7 (7), e41858. doi: 10.1371/journal.pone.0041858

Xu, H. L., Tong, M. Q., Wang, L. F., Chen, R., Li, X. Z., Sohawon, Y., et al. (2019). Thiolated gamma-polyglutamic acid as a bioadhesive hydrogel-forming material: evaluation of gelation, bioadhesive properties and sustained release of KGF in the repair of injured corneas. *Biomater. Sci.* 7 (6), 2582–2599. doi: 10.1039/c9bm00341j

Zhang, Y., Hao, C. G., Hu, L. Q., Dong, J., Wei, P., Xu, D., et al. (2009). Recombinant DNA vaccine against inhibition of neurite outgrowth promotes functional recovery associated with endogenous NGF expression in spinal cord hemisected adult rats. *Neurochem. Res.* 34 (9), 1635–1641. doi: 10.1007/s11064-009-9951-6

Zheng, M., Deshpande, S., Lee, S., Ferrara, N., and Rouse, B. T. (2001). Contribution of vascular endothelial growth factor in the neovascularization process during the pathogenesis of herpetic stromal keratitis. *J. Virol.* 75 (20), 9828–9835. doi: 10.1128/JVI.75.20.9828-9835.2001

Zhou, Z., Apte, S. S., Soininen, R., Cao, R., Baaklini, G. Y., Rauser, R. W., et al. (2000). Impaired endochondral ossification and angiogenesis in mice deficient in membrane-type matrix metalloproteinase I. *Proc. Natl. Acad. Sci. U. S. A.* 97 (8), 4052–4057. doi: 10.1073/pnas.060037197

Zhou, W., Feng, X., Wu, Y., Benge, J., Zhang, Z., and Chen, Z. (2009). FGF-receptor substrate 2 functions as a molecular sensor integrating external regulatory signals into the FGF pathway. *Cell Res.* 19 (10), 1165–1177. doi: 10.1038/cr.2009.95

Zhu, Y. T., Chen, H. C., Chen, S. Y., and Tseng, S. C. (2012). Nuclear p120 catenin unlocks mitotic block of contact-inhibited human corneal endothelial monolayers without disrupting adherent junctions. *J. Cell Sci.* 125 (Pt 15), 3636–3648. doi: 10.1242/jcs.103267

Conflict of Interest: The authors declare that the research was conducted in the absence of any commercial or financial relationships that could be construed as a potential conflict of interest.

frontiers in Pharmacology

ORIGINAL RESEARCH
published: 28 February 2020
doi: 10.3389/fphar.2020.00154

FGF21 Attenuated LPS-Induced Depressive-Like Behavior *via* Inhibiting the Inflammatory Pathway

Xue Wang[1,2†], Liyun Zhu[1†], Jian Hu[1], Ruili Guo[1], Shasha Ye[1], Fei Liu[1], Dongxue Wang[1], Yeli Zhao[1,2], Aiping Hu[1], Xiaojie Wang[1,2], Kaiming Guo[1] and Li Lin[1,2*]*

[1] School of Pharmaceutical Sciences, Wenzhou Medical University, Wenzhou, China, [2] Engineering Laboratory of Zhejiang Province for Pharmaceutical Development of Growth Factors, Biomedical Collaborative Innovation Center of Wenzhou, Wenzhou, China

OPEN ACCESS

Edited by:
Jin-San Zhang,
Mayo Clinic, United States

Reviewed by:
Ying Peng,
Chinese Academy of Medical Sciences and Peking Union Medical College, China
Yun Seon Song,
Sookmyung Women's University, South Korea

****Correspondence:***
Kaiming Guo
gkm6662@163.com
Li Lin
linliwz@163.com

[†]These authors have contributed equally to this work

Specialty section:
This article was submitted to Translational Pharmacology, a section of the journal Frontiers in Pharmacology

Received: *23 October 2019*
Accepted: *05 February 2020*
Published: *28 February 2020*

Citation:
Wang X, Zhu L, Hu J, Guo R, Ye S, Liu F, Wang D, Zhao Y, Hu A, Wang X, Guo K and Lin L (2020) FGF21 Attenuated LPS-Induced Depressive-Like Behavior via Inhibiting the Inflammatory Pathway. Front. Pharmacol. 11:154. doi: 10.3389/fphar.2020.00154

Major depressive disorder is a serious neuropsychiatric disorder with high rates of recurrence and mortality. Many studies have supported that inflammatory processes play a central role in the etiology of depression. Fibroblast growth factor 21 (FGF21), a member of the fibroblast growth factors (FGFs) family, regulates a variety of pharmacological activities, including energy metabolism, glucose and lipid metabolism, and insulin sensitivity. In addition, recent studies showed that the administration of FGF21, a regulator of metabolic function, had therapeutic effects on mood stabilizers, indicating that FGF21 could be a common regulator of the mood response. However, few studies have highlighted the antidepressant effects of FGF21 on lipopolysaccharide (LPS)-induced mice, and the anti-inflammatory mechanism of FGF21 in depression has not yet been elucidated. The purpose of the current study was to determine the antidepressant effects of recombinant human FGF21 (rhFGF21). The effects of rhFGF21 on depression-like behaviors and the inflammatory signaling pathway were investigated in both an LPS-induced mouse model and primary microglia *in vitro*. The current study demonstrated that LPS induced depressive-like behaviors, upregulated proinflammatory cytokines, and activated microglia in the mouse hippocampus and activated the inflammatory response in primary microglia, while pretreatment with rhFGF21 markedly improved depression-like behavior deficits, as shown by an increase in the total distance traveled and number of standing numbers in the open field test (OFT) and a decrease in the duration of immobility in the tail suspension test (TST) and forced swimming test (FST). Furthermore, rhFGF21 obviously suppressed expression levels of the proinflammatory cytokines interleukin-1β (IL-1β), tumor necrosis factor-α (TNF-α), and interleukin-6 (IL-6) and inhibited microglial activation and the nuclear factor-κB (NF-κB) signing pathway. Moreover, coadministration of rhFGF21 with the fibroblast growth factor receptor 1 (FGFR1) inhibitor PD173074 significantly reversed these protective effects, indicating that the antidepressant effects of rhFGF21 occur through FGFR1 activation. Taken together, the results of the current study demonstrated for the first time that exogenous rhFGF21 ameliorated LPS-induced depressive-like behavior by inhibiting microglial

expression of proinflammatory cytokines through NF-κB suppression. This new discovery suggests rhFGF21 as a new therapeutic candidate for depression treatment.

Keywords: major depressive disorder, depressive-like behavior, FGF21, inflammation, NF-κB signaling pathway

INTRODUCTION

Major depression disorder (MDD), a mood disorder characterized by the symptoms of a persistent feeling of sadness, loss of interest, and worthlessness, affects approximately 300 million people worldwide (Zhang et al., 2019). A total of 0.8 million patients with depression commit suicide annually (Lee et al., 2019). There are some clinical antidepressants on the market, such as norepinephrine reuptake inhibitors, selective serotonin reuptake inhibitors, and monoamine oxidase inhibitors; however, only one-third of patients respond to these therapeutics (Li, 2019), which are often associated with numerous side effects and a high risk of relapse after drug withdrawal, such as the 61.8% relapse rate in the case of fluoxetine (Andrews et al., 2012; Lee et al., 2019). Therefore, further study to develop novel effective antidepressants is urgently needed.

Several hypotheses to explain the pathology of depression, including glutamatergic excitotoxicity, monoamine system impairment, hypothalamic-pituitary-adrenal axis dysfunction, neuroinflammation, and neural plasticity and neurogenesis disruption, have emerged (Taniguti et al., 2019). Among these hypotheses, inflammatory processes have been suggested to be involved in the etiology of depression in many studies (Domingues et al., 2018). Increasing amounts of preclinical and clinical research have shown that proinflammatory cytokines might contribute to depression. The proinflammatory cytokines tumor necrosis factor-α (TNF-α) and interleukin-6 (IL-6) play critical roles in the process of inflammation and can induce depressive disorders (Wright et al., 2005; Guo et al., 2019). The levels of IL-6 and TNF-α were reported to be increased in the blood and cerebrospinal fluid of MDD patients (Syed et al., 2018). Escherichia coli lipopolysaccharide (LPS), a commonly used proinflammatory endotoxin, can trigger microglial activation and induce immune activation and behavioral changes that are similar to the clinical symptoms of human depression (Adzic et al., 2015; Taniguti et al., 2019). Therefore, mice were administered LPS to serve as a model of central nervous system (CNS) inflammation and induce depression-like behaviors. Nuclear factor-κB (NF-κB), a major transcription factor, is involved in the activation of an exceptionally large number of genes in response to inflammation. Once stimulated by LPS, NF-κB translocates to the nucleus and regulates the expression of inflammatory cytokines such as TNF-α, interleukin-1β (IL-1β), and IL-6 (Lin et al., 2007; Domingues et al., 2018; Muhammad et al., 2019).

Fibroblast growth factor 21 (FGF21), a member of the fibroblast growth factor (FGF) family, is mainly expressed in the liver and functions as a hormone. After its secretion, FGF21 regulates a variety of pharmacological activities; whole-body energy metabolism, especially glucose and lipid metabolism; and insulin sensitivity (Xu et al., 2009; Gaich et al., 2013; Pan et al., 2018; Li, 2019). In addition, recent studies showed that the administration of FGF21, a regulator of metabolic function, had a therapeutic effect on mood stabilizers (Chang et al., 2018). In bipolar disorder (BD) patients, the FGF21 level was significantly enhanced after valproate treatment; however, there was no significant difference between the FGF21 levels of healthy control and BD patients, indicating that FGF21 may be a common regulator of the mood response (Chang et al., 2018). Moreover, a previous study reported a significant negative association between cerebrospinal fluid FGF21 levels and Beck Depression Inventory (BDI) scores in male Chinese subjects, but not in female (Liu et al., 2017). These results further demonstrate that FGF21 plays a role in mood regulation; however, the mechanism by which FGF21 mediates mood disorders is not clear.

In the current study, the effects of recombinant human FGF21 (rhFGF21) on the depression-like behaviors of LPS-induced mice models were evaluated. The NF-κB signaling pathway is involved in inflammatory events. Once stimulated by LPS, NF-κB is phosphorylated and activated, and phosphorylated NF-κB translocates into the nucleus and binds a consensus sequence in targeted genes to regulate the expression of inflammatory cytokines such as TNF-α, IL-6, and IL-1β (Yang M. et al., 2018). Therefore, we speculated that the anti-depressive effect of rhFGF21 is mediated by NF-κB signaling pathway regulation. To confirm this hypothesis, we evaluated the expression levels of inflammatory cytokines in the hippocampus of an LPS-induced depression-like model and in primary microglia. Additionally, the NF-κB signaling pathway was analyzed to further explore the possible underlying mechanism of the antidepressant effects of rhFGF21.

MATERIALS AND METHODS

Reagents and Antibodies

rhFGF21 was supported from Key Laboratory of Biopharmaceutical, School of Pharmaceuticals Sciences, Wenzhou Medical University, that is produced and purified from Escherichia according to the reference (Wang et al., 2010). FGFR1 inhibitor PD173074 was purchased from Selleckchem (Houston, TX, USA). LPS was obtained from Sigma (Sigma-Aldrich, St Louis, MO). The following primary antibodies applied were purchased from Abcam (Cambridge, MA, USA): anti-FGFR1 (No. ab824), anti-p-FGFR1 (No. ab59194), and anti-β-actin (No. ab8227); anti-NF-κB (No. 8242) and anti-p-NF-κB (No. 3033s) were purchased from Cell Signalling Technology (Danvers, MA, USA); anti-BDNF (No. BS9896M) and anti-Iba1 (No. 019-19741) were purchased from

Bioworld technology (Louis Park, MN, USA) and FUJIFILM Wako Pure Chemical Corporation (Osaka, Japan), respectively. The secondary antibodies used in this study were goat anti-rabbit IgG H&L (HRP) (No. ab6721) and Alexa Fluor ®488-conjugated donkey anti-rabbit (No. ab150073) purchased from Abcam (Cambridge, MA, USA).

Animals

The experiments were conducted in male C57BL/6N mice (20–25 g), which were purchased from the Animal Center of the Chinese Academy of Sciences (Beijing, China). The animal use and care protocol conformed to the Guide for the Care and Use of Laboratory Animals from the National Institutes of Health and was approved by the Animal Care and Use Committee of Wenzhou Medical University.

Drug Administration and Animal Experimental Procedures

The experimental design and protocol used for the animal experiment in this study are illustrated in **Figure 1A**. The mice were divided into three groups randomly; (1) the control vehicle (normal saline, NP) administered group; (2) the LPS + NP treated group; (3) the LPS + rhFGF21 treated group. Mice were pretreated intraperitoneally (i.p.) with vehicle or rhFGF21 (0.75, 1.5, and 3 mg/kg) twice daily for three consecutive days. These doses were chosen because it has previously been shown that rhFGF21 with the dose of 1.5 mg/kg dramatically attenuated locomotor function deficits in mice (Jiang et al., 2018). One hour after the last rhFGF21 administration on day 3, the mice were treated i.p. with LPS (0.83 mg/kg) dissolved in sterile saline. The concentration of LPS was based on the results of previous studies (Tomaz et al., 2014; Taniguti et al., 2019; Wang et al., 2019a; Wang et al., 2019b). The animals were subjected to following behavioral tests 24 h after LPS. Then, the animals were deeply anesthetized with isoflurane and euthanized by decapitation. The hippocampal tissue was rapidly removed and stored at -80°C until assays. NF-κB, iNOS, and brain-derived neurotrophic factor (BDNF) protein levels were assessed by western blot analysis (n = 5). Levels of the proinflammation factors IL1-β, TNF-α, and IL-6 were determined by RT-PCR (n = 5). To detect Iba1, NF-κB, and FGFR1 by immunofluorescence localization (n = 4), mice were deeply anesthetized and subjected to cardiac perfusion with saline followed by perfusion with 4% paraformaldehyde (PFA). Their brains were rapidly removed

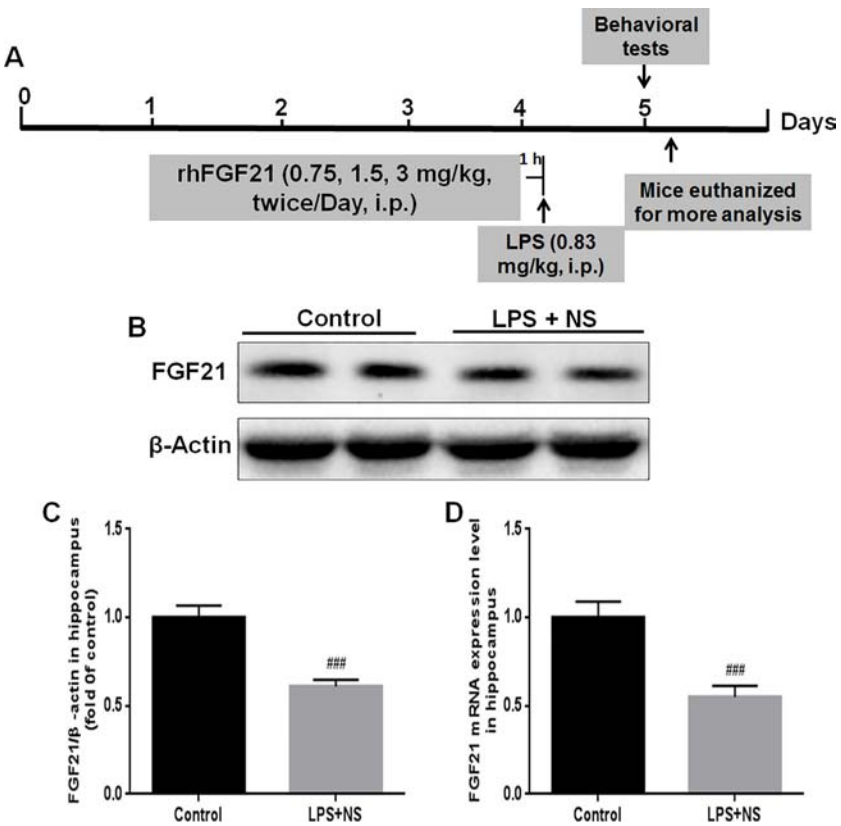

FIGURE 1 | Endogenous FGF21 expression level in the hippocampus of LPS-induced mice was reduced. **(A)** Schematic illustration of animal experimental procedures showing the duration of the lipopolysaccharide (LPS) and/or exogenous rhFGF21 administration in adult mice and analysis. **(B)** Representative bands of endogenous FGF21 expression detected by western blot. **(C)** Densitometric analysis for the protein expression of FGF21. **(D)** Endogenous FGF21 mRNA expression level in the hippocampus of LPS-induced mice. Data are means ± SEM (n = 5). $^{###}p < 0.001$ compared to control group.

and post-fixed in 4% PFA overnight for further immunofluorescence analysis (**Figure 1A**).

Behavioral Assay

Depression behavior was monitored by increased duration of immobility in the forced swim test (FST) and decreased sucrose preference; meanwhile, sickness behavior was measured by body weight loss, reduced food intake, and locomotor activity. It has been reported that LPS-induced depression-like behaviors can be dissociated from sickness from 24 h after LPS administration (Walker et al., 2013; Walker et al., 2019). The sickness responses and behavior (piloerection, ptosis and lethargy) was usually measured during peak period of sickness at 6 h after LPS administration (Silverman et al., 2013; Walker et al., 2019). In our behavioral experiment, we forced on examining the effects of rhFGF21 on depression-like behavior measured at 24 h after LPS, which include FST and locomotor activity monitored by tail suspension test (TST) and open field test (OFT) (n = 9) (Yu et al., 2019).

The TST, a behavioral test used to evaluate depressive-like behavior in animals, was conducted as previously described (Steru et al., 1985; Lee et al., 2019) with slight modifications. The TST was carried out in a soundproof box (40 × 20 × 60 cm) with cameras on the side and bottom of the box. Briefly, a string was fixed to each mouse with tape 1 cm from the tip of its tail. The mice were 20 cm above the ground, and the test was carried out for 6 min. The immobility time was recorded during 5 min of a 6-min observation period.

The FST is a common behavior test used to evaluate depression-like behavior. The immobility time after each mice ceased struggling and remained floating motionless in the water was recorded. A decrease in the duration of immobility is indicative of an antidepressant-like effect (Porsolt et al., 1977). In this test, mice were individually placed into a cylinder (25 cm in height, 10 cm in diameter) containing water at a depth of 19 cm of water at 25 ± 1°C. After a habituation period (2 min), the total amount of time each animal remained immobile during a 6-min session was scored as the immobility time, as described previously (Taniguti et al., 2019).

The OFT, a method used to evaluate the autonomous behavior, inquiry behavior, and tension of experimental animals in new environments, was carried out according to a previous study with few modifications (Ieraci and Herrera, 2006). In brief, mice were individually placed in the center of a black wooden box (50 × 50 × 50 cm) that served as the open field. Locomotion behavior indicated by the number of standing number was recorded for 5 min using a camera and analyzed using an open field experimental video analysis system (Smart 3.0, Panlab SMART video tracking system, Barcelona, Spain). The arena floor was cleaned with a 10% ethanol solution between trials.

Primary Rat Microglia Culture

Primary rat microglia cultures were prepared from the cerebral cortices of 1–2-day-old neonatal Sprague-Dawley rat pups with mild trypsinization as previously described with minor modifications (Lin et al., 2017). Briefly, after removing the meninges of the brain, the cortical cortices were dissected and cut into small, 2-mm pieces, and tissues were digested with 0.25% trypsin for 30 min at 37°C. The tissues were suspended in DMEM/F12 containing 10% FBS and 1% penicillin-streptomycin and mechanically triturated with a plastic P1000 pipette tip. Then, the mixed cells were passed through a 70-μm nylon mesh cell strainer and plated on 6-well plates or cell culture dishes. After three days, the medium was completely replaced and changed every three days with fresh medium. After approximately 14 days, the mixed cells achieved 90% confluency, and microglia were isolated from mixed glial cultures *via* mild trypsinization according to our previous study (Lin et al., 2017). Mixed glial cultures were incubated with a trypsin solution containing 0.25% trypsin-EDTA for 30 min to detach a layer of cells. Primary microglial cells remained attached to the bottom of the plate and were used for further study.

Western Blot Analysis

Total protein from brain hippocampal tissue and primary microglia was extracted using protein extraction reagents containing 1% protease and phosphatase inhibitors. Nuclear and cytoplasmic protein was purified using a Nuclear and Cytoplasmic Protein Extraction Kit (Beyotime Biotechnology, Shanghai, China). The protein content of the samples was measured by a BCA Protein Assay Kit (Beyotime Biotechnology, Shanghai, China). An equivalent amount of protein (30 μg) was separated on an SDS-PAGE gel and then transferred onto a Polyvinylidene Fluoride (PVDF) membrane. After being blocked with 5% non-fat milk in Tris-buffered saline (TBS) containing 1% Tween for 2 h at room temperature, the membranes were further incubated with primary antibodies overnight at 4°C (a 1:400 dilution of anti-FGFR1, and 1:1,000 dilution of anti-p-FGFR1, anti NF-κB, anti-p-NF-κB, anti-BDNF, and β-Actin). After three washes with TBST, the membranes were incubated with a 1:10,000 dilution of goat anti-rabbit IgG secondary antibody for 1 h at room temperature. Finally, the immunoreactive protein bands were developed and visualized with an enhanced chemiluminescence (ECL) kit (Biological Industries, Kibbutz Beit-Haemek, Israel), and the band densities were quantified using Image Lab 5.0 software (Bio-Rad, CA, USA).

Immunofluorescence Analysis

Immunofluorescence analysis was performed to determine the localization of Iba1 in the mice brain hippocampal tissue. In brief, the whole brain was post-fixed by 4% PFA for 12 h, embedded in paraffin, and cut into section (5 μm thick), followed by mounted on slides. Sections were deparaffinized and rehydrated. Then tissue was incubated with 3% H_2O_2 for 15 min, followed blocked nonspecific binding in 5% bovine serum albumin (BSA) for 30 min at 37°C. Then sections were treated with primary antibodies anti-Iba1 (1:1,000), NF-κB (1:1,000), FGFR1 (1:1,000) overnight at 4°C, followed by incubation with AlexaFluor 488 donkey anti-rabbit secondary antibody (1:1,000) at 37°C for 1 h. Then, the nuclei were stained with DAPI for 7 min. The immunostained sections were observed and imaged using a Nikon ECLPSE 80i fluorescence microscope (Nikon, Tokyo, Japan). Three indexes of microglia activation (number, soma size, and process length) were measured according to the previous study (Tang et al., 2018). The density of Iba1 positive

cells were automatically analyzed by Image-Pro plus 6.0 software (Bethesda MD, USA) at ×10 magnification in a defined area. The area of microglia soma and the microglia process length were measured at ×20 magnification by Image-Pro plus 6.0 software. For each group, at least six representstive images were taken from four mice.

RNA Extraction and RT-PCR

Quantitative real-time PCR with SYBR Green dye was applied to measure whether rhFGF21 affected the mRNA expression level of pro-inflammation cytokines including IL-1β, TNF-α, and IL-6. Total RNA was extracted from mice brain hippocampal tissue and primary microglia by the RNeasy Mini Kit (Qiagen, Hilden, Germany) according to the manufacturer's instructions. The residual genomic DNA was removed by RQ1 RNase-Free DNase (Promega, Fitchburg, WI, USA), and 1 μg of the total RNA from each sample was applied for complementary DNA (cDNA) synthesis using the PrimeScriptTM RT Reagent Kit (TaKaRa, Kusatsu, Japan). Real-time qRT-PCR was performed in 96-well plates using a quantitative PCR system (CFX ConnectTM Real-Time System, Bio-Rad, CA, USA). Each reaction mixture consisted of 10 μl of the SYBR Green PCR Master Mix Kit (Applied Biosystems, Carlsbad, CA, USA), 2 μl of the forward and reverse primers (5 pmol each), 25 ng of the cDNA, and diethylpyrocarbonate water for a final volume of 20 μl. The oligonucleotide PCR primer pairs are listed in **Table 1**, purchased from Sangon Biotech (Shanghai, China). The cycling program was an initial hold at 95°C for 5 min, followed by 40 cycles of denaturation at 95°C for 30 s, annealing at 62°C for 30 s, and extension at 72°C for 30 s. The mRNA expression levels of the target genes were normalized to the mRNA expression level of the housekeeping gene β-actin, and analyzed by the $2^{-\Delta\Delta CT}$ method. The results are expressed as the means ± SEMs of duplicate samples from three independent experiments.

Statistical Analysis

All data are presented as mean ± SEM from at least three independent experiments. Statistical analyses were performed using GraphPad Prism 7 (GraphPad software Inc., San Diego, CA, USA). Statistical significance between groups was determined by one-way analysis of variance (ANOVA) followed by Turkey's test using. $P < 0.05$ was considered statistically significant.

TABLE 1 | Primers' sequences used for real-time PCR analysis.

Gene	Sequence 5'-3'	Amplification length (bp)
FGF21	CGACTGCTGCTGGCTGTCTTC GGCTTCAGTGTCTTGGTCGTCATC	135
IL-1β	AAGCCTCGTGCTGTCGGACC TGAGGCCCAAGGCCACAGGT	140
TNF-α	CAAGGGACAAGGCTGCCCCG GCAGGGGCTCTTGACGGCAG	109
IL-6	AGAAGGAGTGGCTAAGGACCAA AACGCACTAGGTTTGCCGAGTA	101
β-actin	CACTGCAAACGGGGAAATGG TGAGATGGACTGTCGGATGG	198

RESULTS

Endogenous FGF21 Was Reduced in the Hippocampus of the LPS-Induced Mouse Brain

FGF21 plays an important role in mood regulation, and its levels were significantly increased in BD patients after treatment with the antidepressant drug valproate (Chang et al., 2018). Therefore, we detected the endogenous expression levels of both FGF21 protein and FGF21 mRNA. LPS treatment significantly decreased the endogenous FGF21 protein (**Figures 1B, C**) and mRNA (**Figure 1D**) expression levels compared to those in saline-treated mice (control group).

Exogenous rhFGF21 Administration Alleviated Depressive-Like Behavior Induced by LPS

To evaluate the effects of rhFGF21 on depressive-like behavior induced by LPS, the OFT, FST, and TST were performed. Mice were pretreated with saline or rhFGF21 (0.75, 1.5, and 3 mg/kg, i.p.) for three days, followed by LPS administration (0.83 mg/kg, i.p.). In the OFT, a general measure of curiosity and detective behavior, the total distance traveled, line crossings, and number of standing events are used to assess locomotor activity. LPS significantly suppressed the total distance traveled and number of standing events compared with those in the control group (**Figures 2A, B**). Pretreatment with different concentrations of rhFGF21 significantly improved the decreased total distance traveled (**Figure 2A**) and number of standing events caused by LPS treatment (**Figure 2B**). In the FST, a putative indicator of behavioral despair, LPS administration markedly increased the mouse immobility time compared with that of the control group, and rhFGF21 treatment significantly decreased the increased immobility time induced by LPS (**Figure 2C**). In the TST, a classic method to assess mood, the time taken until the mouse remained immobile was measured. LPS significantly increased the immobility time during suspension, indicating that LPS induced depression-like behaviors. rhFGF21 administration significantly reduced immobility compared with that in the LPS-treated group (**Figure 2D**). As shown by behavioral analyses, pretreatment with rhFGF21 at doses of 0.75, 1.5, and 3 mg/kg significantly alleviated LPS-induced depression behavioral deficits; however, 1.5 and 3 mg/kg rhFGF21 had a greater effect than 0.75 mg/kg rhFGF21. Therefore, rhFGF21 at a dose of 1.5 mg/kg was applied in further studies. Moreover, rhFGF21 without LPS administration did not change the total distance traveled, or number of standing events in the OFT or the immobility time of the mice in the FST and TST (**Figures 3A–D**). These results demonstrate that rhFGF21 improved depression-like behaviors induced by LPS and was effective only in disease conditions.

Exogenous rhFGF21 Administration Reduced LPS-Induced Microglial Activation

Microglia, the innate immune cells in the brain, responds to inflammation (Lenz and Nelson, 2018). In depressed patients who

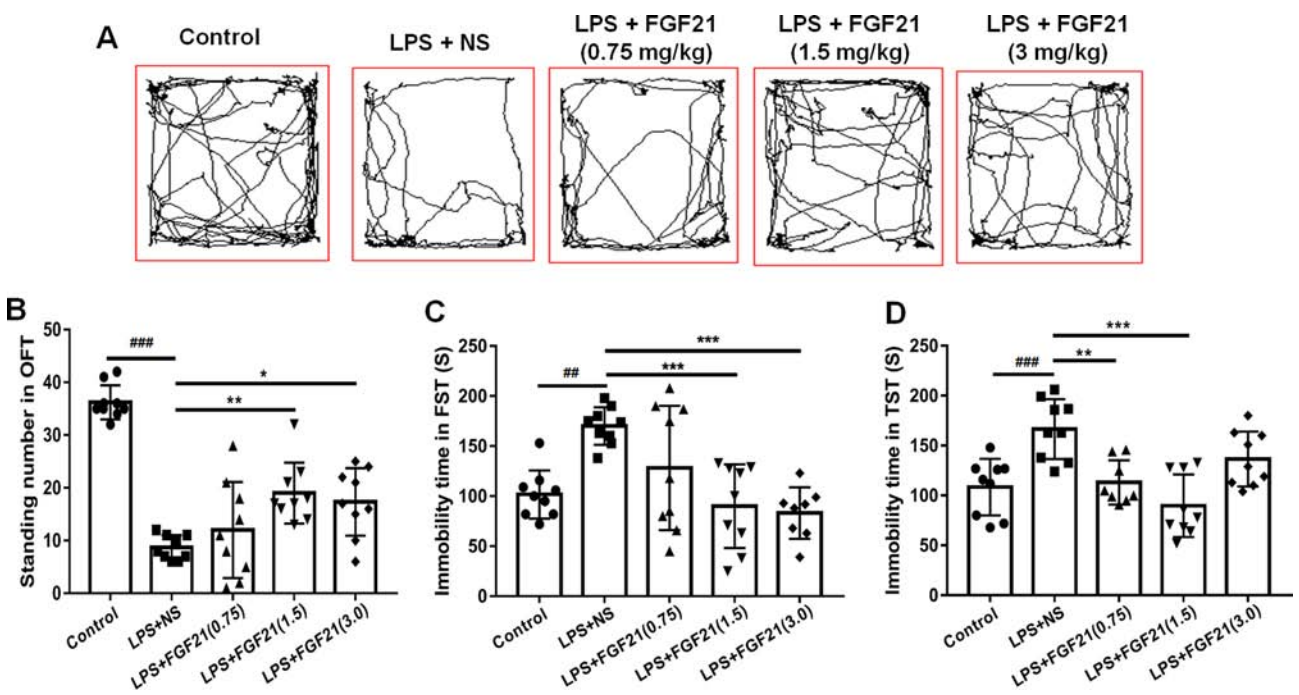

FIGURE 2 | Exogenous rhFGF21 (0.75, 1.5, and 3 mg/kg) administration alleviated depression-like behaviors in LPS-induced mice. **(A)** Total distance traveled and line crossing in the open filed. **(B)** Standing number in the open filed. **(C)** Immobile time during the FST. **(D)** Immobile time during the TST. Data are means ± SEM (n = 9). *p < 0.05, **p < 0.01, ***p < 0.001, ###p < 0.001, ##p < 0.01.

committed suicide, microglial activation was observed, indicating that microglia play an important role in neuroinflammation in the brain during the pathogenesis of depression (Brites and Fernandes, 2015). The transfer of microglia from a ramified status to an activated status is marked by reduced process length and swollen soma (Kettenmann et al., 2011; Tang et al., 2018). To further investigate the antidepressant effect of rhFGF21 on the inflammatory response, microglial activation in the mouse hippocampus was assessed by immunofluorescence labeling to determine the number, soma area, and process length of microglia. Iba1 immunofluorescence assessment demonstrated that LPS exposure significantly enhanced the number of microglia (**Figures 4A, B, D**) and activated microglia, as indicated by an increased soma area (**Figures 4A, B, E**) and shorter ramified processes (**Figures 4A, B, F**) compared with the control group. Interestingly, after pretreatment with rhFGF21 for 3 days, LPS-induced changes in microglial numbers and morphologies in the hippocampus were significantly reversed (**Figure 4**).

Exogenous rhFGF21 Administration Reduced the Production of Proinflammatory Cytokines Induced by LPS Through Inhibiting NF-κB Signaling Pathway

Microglial activation can induce the expression of inflammatory cytokines. Therefore, the expression levels of the critical proinflammatory cytokines IL-1β, TNF-α, and IL-6 were measured by RT-PCR, and iNOs expression was measured by western blotting. LPS exposure significantly triggered the mRNA expression of cytokines in the hippocampus, as indicated by the enhanced release of TNF-α, IL-1β, and IL-6. Conversely, rhFGF21 administration markedly reversed LPS-induced changes in the expression levels of these inflammatory cytokines (**Figures 5A–C**). As shown by western blot analysis, LPS administration significantly increased the production of iNOS, and pretreatment with rhFGF21 considerably reversed this increase (**Figures 5D, E**).

The expression of inflammatory factors in LPS-triggered activated glial cells is regulated by NF-κB signaling pathways (Chen G. et al., 2018; Muhammad et al., 2019). LPS activated the NF-κB signaling pathway, as reflected by the increased nuclear level of NF-κB protein. To investigate whether rhFGF21 can decrease proinflammatory cytokine expression through inhibiting the NF-κB signaling pathway, cytoplasmic and nuclear proteins were extracted, and NF-κB was measured by western blotting with β-actin and H3 used as cytoplasmic and nuclear housekeeping proteins, respectively. There were no significant differences in NF-κB expression levels in the cytoplasm of cells in the LPS and rhFGF21 pretreatment groups (**Figures 5D, F**). However, LPS treatment markedly increased nuclear NF-κB, and this increase was markedly reversed by pretreatment with rhFGF21 for 3 days (**Figures 5D, G**).

Exogenous rhFGF21 Could Function Through FGFR1 Activation

FGFR1 is widely expressed throughout the nervous system and contributes to hippocampal nerve growth and long-term potentiation (Deng et al., 2019). To investigate whether the

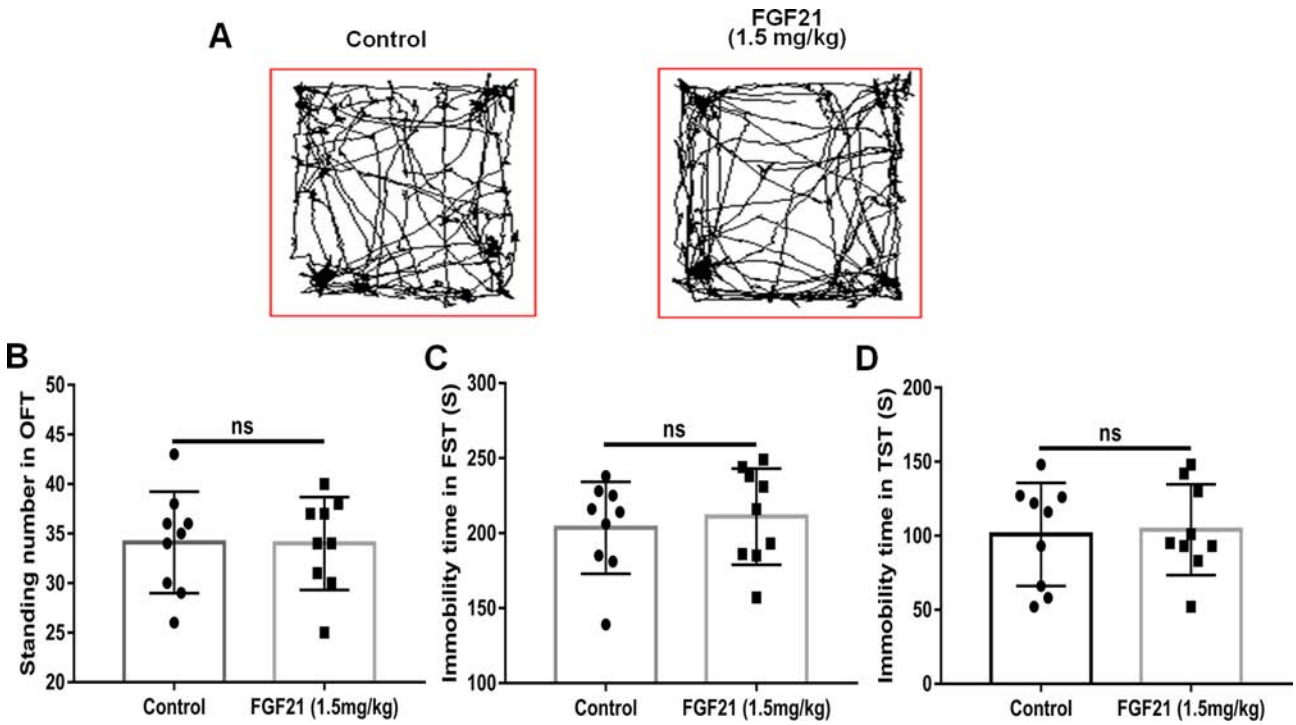

FIGURE 3 | Exogenous rhFGF21 administration (1.5 mg/kg) did not change the behavior of normal mice. **(A)** Total distance traveled and line crossing in the open filed. **(B)** Immobile time during the FST. **(C)** Standing number in the open filed. **(D)** Immobile time during the TST. Data are means ± SEM (n = 9). ns, no significant difference.

effect of rhFGF21 on depression is mediated through the FGFR1 signaling pathway, we detected the expression levels of FGFR1 and p-FGFR1 by western blotting. LPS administration markedly reduced FGFR1 and p-FGFR1 levels in the hippocampus compared with those in the control group, and rhFGF21 treatment significantly rescued this decrease in hippocampal FGFR1 and p-FGFR1 (**Figures 6A–C**).

BDNF is a major representative of the brain neurotrophic factors, which are involved in cognition control. Cognitive dysfunction in depressive patients is due to decreased levels of BDNF (Domingues et al., 2018), and BDNF has been suggested to influence the response to antidepressant treatment (Hennings et al., 2019). Therefore, the effect of rhFGF21 on BDNF expression was measured. LPS treatment significantly reduced BDNF expression compared with that in the control group. Interestingly, rhFGF21 prevented the decrease in BDNF levels in the mouse hippocampus induced by LPS administration (**Figures 6A, D**).

Exogenous rhFGF21 Administration Inhibited Inflammatory Cytokines Expression Through NF-κB Inhibition Mediated by FGFR1 Activation in Cultured Primary Microglia

To further evaluate the effects of rhFGF21 on the inflammatory response of microglia and the underlying possible mechanism of action of these effects, primary microglia were extracted and isolated from the cerebral cortices of 1–2-day-old neonatal Sprague-Dawley rat pups. Meanwhile, since FGF21 usually functions by activating its receptor, to further investigate the function of FGFR1, its receptor, the FGFR1-specific inhibitor PD173074 (10 nM) was applied. Levels of the inflammatory cytokines IL-1β, TNF-α, and IL-6 were assessed by RT-PCR. The mRNA levels of IL-1β, TNF-α, and IL-6 were higher in the primary microglia of the LPS-treated group compared with the control group, while rhFGF21 treatment significantly reduced IL-1β, TNF-α, and IL-6 upregulation induced by LPS. Additionally, PD173074 significantly reversed the rhFGF21 treatment-induced downregulation of TNF-α, IL-1β, and IL-6 mRNA (**Figures 7A–C**), indicating that rhFGF21 suppresses inflammatory cytokine expression through activating FGFR1 in microglia.

NF-κB signaling pathway activation is involved and critical to the development of depression as it triggers the production of proinflammatory mediators (Su et al., 2017). To further explore the anti-depressive effects mediated by the anti-inflammatory mechanism of rhFGF21 in microglia, the protein levels of p-NF-κB and NF-κB in cultured primary microglia were analyzed by western blotting. The levels of p-NF-κB/NF-κB were significantly higher in the LPS-treated group than in the control group, and rhFGF21 could suppress NF-κB activation stimulated by LPS administration, while cotreatment with the FGFR1 inhibitor PD173074 and rhFGF21 significantly reversed the inhibitory effects of rhFGF21 on NF-κB (**Figures 7D, E**). Consistent with the western blot data, LPS significantly

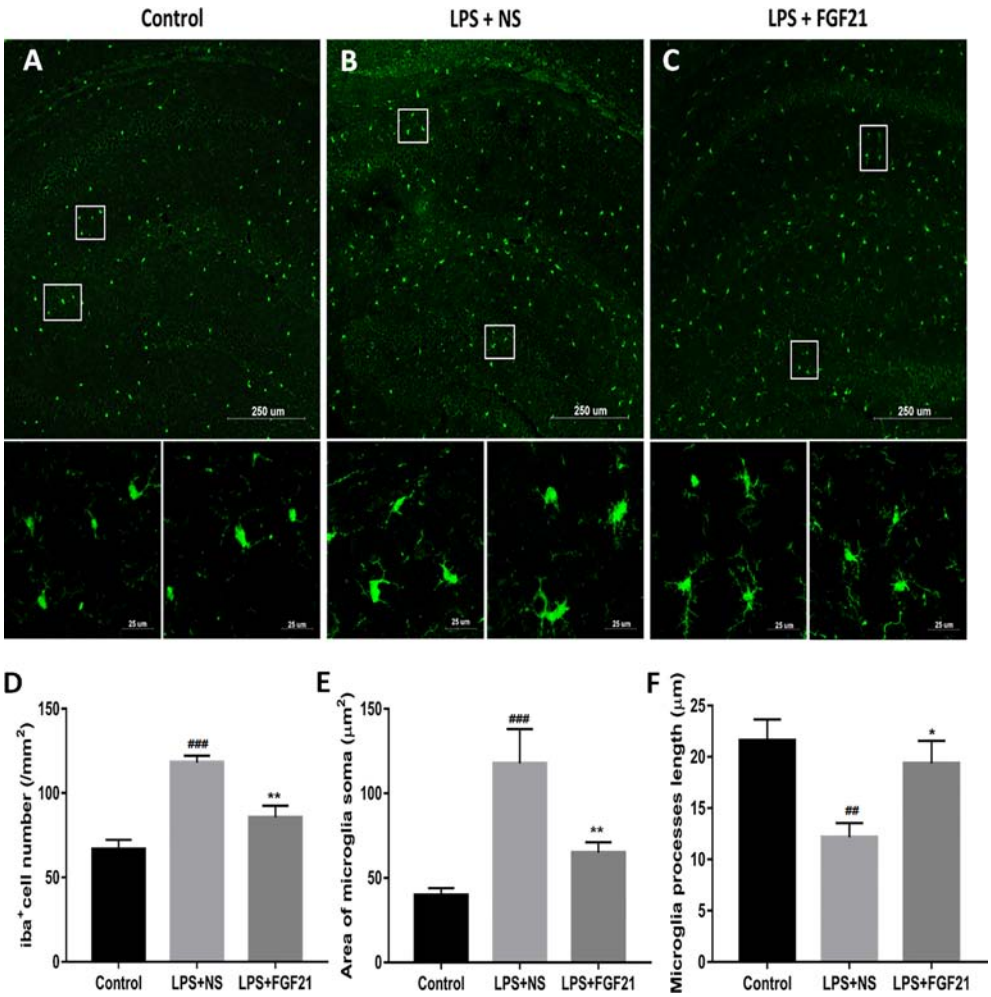

FIGURE 4 | Exogenous rhFGF21 administration reduced microglial activation in LPS-induced mice hippocampus. **(A)** Representative images of microglia in control group. **(B)** Representative images of microglial activation in LPS-induced group. **(C)** Representative images of microglial activation in rhFGF21 pretreated LPS-induced group. **(D)** Quantification of microglial cell number per square millimeter. **(E)** Quantification of microglial area soma. **(F)** Quantification of microglial process length. Data are means ± SEM (n = 4, 3–4 tissue sections per animal). $^{\#\#}p < 0.01$, $^{\#\#\#}p < 0.001$ compared to control group, $^{*}p < 0.05$, $^{**}p < 0.01$ compared to LPS-induced group.

stimulated NF-κB activation and translocated into nucleus. Exogenous rhFGF21 treatment obviously suppressed this translocation. Whereas PD173074 co-administration significantly reversed the effects of rhFGF21 on NF-κB (**Figure 7G**). Besides, the effect of rhFGF21 on BDNF expression was also analyzed. Consistent with the results in the animal study, LPS administration significantly reduced the level of BDNF compared with that in the control group; however, rhFGF21 markedly upregulated BDNF expression, and as expected, the FGFR1 inhibitor PD173074 significantly reversed this upregulation of BDNF (**Figures 7D, F**). To further confirm whether rhFGF21 functions through its receptor FGFR1, the immunofluorescence staining of FGFR1 was also performed. Consistent with the result in the animal model, LPS markedly suppressed FGFR1 activation, rhFGF21 rescued FGFR1 activation. Nevertheless, this was reversed by PD173074 coadministration (**Figure 8**). In summary, these results indicate that rhFGF21 inhibits proinflammatory cytokine expression through NF-κB inhibition mediated by FGFR1 activation.

DISCUSSION

Studies have demonstrated the association of four FGFs, FGF2, FGF9, FGF21, and FGF22, with depression, and the correlation between these FGFs and depression has been well reviewed by Deng et al. (2019). FGF2 is a neurotrophic factor widely expressed in the CNS. Administration of a combination of the antidepressants olanzapine and fluoxetine upregulated FGF2

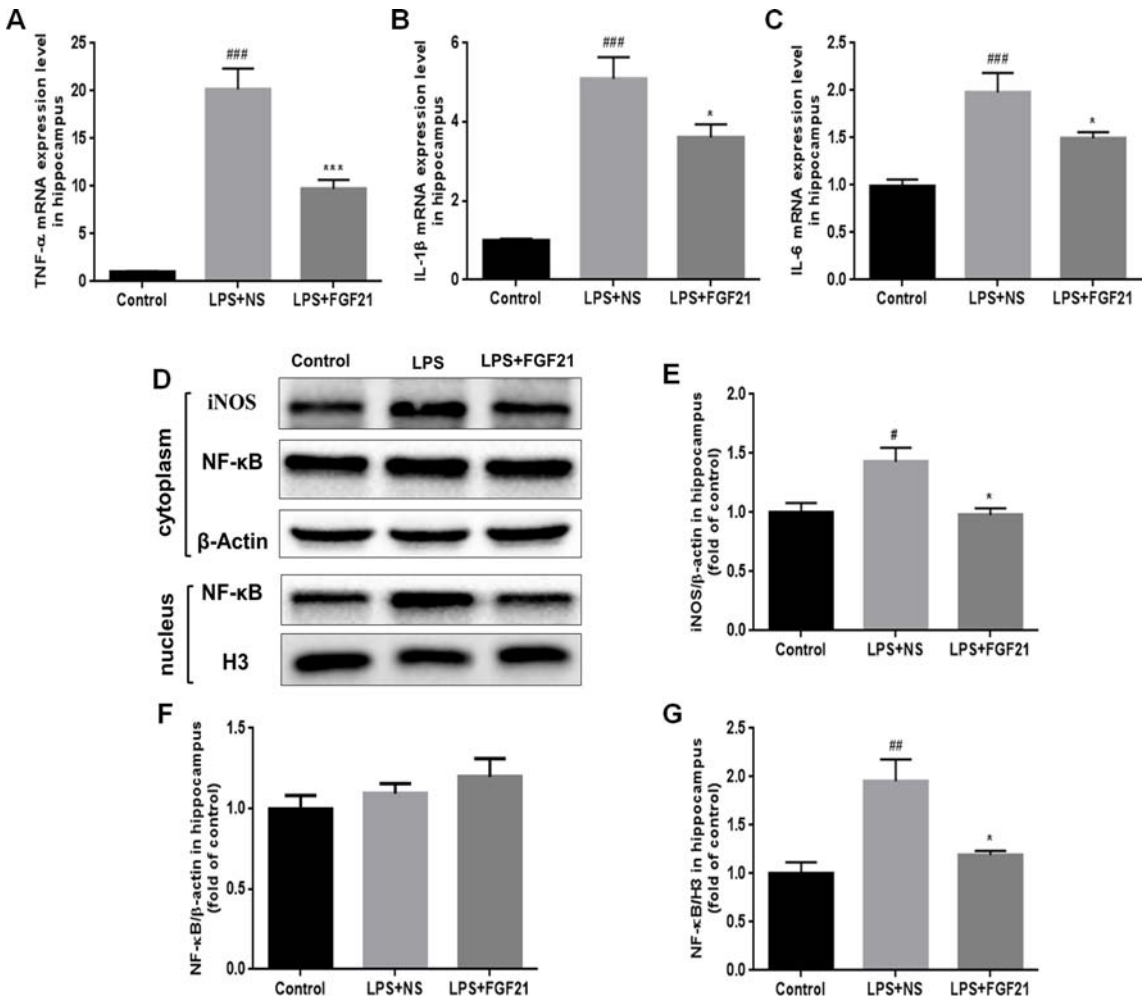

FIGURE 5 | Exogenous rhFGF21 administration reduced levels of proinflammatory cytokines TNF-α, IL-1β and IL-6 induced by LPS through inhibiting NF-κB signaling pathway in the mouse hippocampus. **(A)** rhFGF21 decreased LPS-enhanced hippocampal pro-inflammatory cytokine TNF-α. **(B)** rhFGF21 decreased LPS-enhanced hippocampal pro-inflammatory cytokine IL-1β. **(C)** rhFGF21 decreased LPS-enhanced hippocampal pro-inflammatory cytokine IL-6. **(D)** Representative images of pro-inflammatory cytokine iNOS and NF-κB expression in cytoplasm and nucleus detected by western blot. **(E)** Densitometric analysis for the protein expression of iNOS in cytoplasm. **(F)** Densitometric analysis for the protein expression of NF-κB in cytoplasm. **(G)** Densitometric analysis for the protein expression of NF-κB in nucleus. Data are means ± SEM (n=5). $^{\#}P < 0.05$, $^{\#\#}P < 0.01$, $^{\#\#\#}P < 0.001$ compared to control group; $^{*}P < 0.05$, $^{***}P < 0.001$ compared to LPS-induced group.

levels (Maragnoli et al., 2004). Furthermore, FGF2 alleviated depression-like behaviors in rats (Turner et al., 2008). Chronic FGF-2 infusion blocked deficits in the sucrose preference test (SPT) and FST caused by chronic unpredictable stress (Elsayed et al., 2012). FGF9 is expressed mainly by neurons in the brain (Garcès et al., 2000). Exogenous FGF9 administration was found to increase depression-like behaviors, and exogenous FGF9 knockdown in the dentate gyrus improved anxiety-like behavior in rats (Aurbach et al., 2015). The effect of FGF9 was found to be opposite that of FGF2, which may be due to the inverse relationship between FGF9 expression and FGF2 expression, and FGF2 and FGF9 may act as physiological antagonists to mediate emotionality and vulnerability in mood disorders (Aurbach et al., 2015). FGF22 is expressed mainly in the skin and brain, and the deletion of endogenous FGF22 induced depression-like behavior, as shown by the FST, TST, and SPT (Williams et al., 2016). Recent studies have reported that FGF21 possesses various pharmacological activities including its antioxidant activity, suppression of apoptosis induced by endoplasmic reticulum stress (Liang et al., 2017), and anti-inflammatory activity (Wang Q. et al., 2018; Zhang et al., 2019). FGF21 weakly binds heparin and can pass through the blood-brain barrier by simple diffusion (Hsuchou et al., 2007). rhFGF21 has been demonstrated to have potent therapeutic activity in various neurological disorders, such as Parkinson's disease (Makela et al., 2014), Alzheimer's disease (Amiri et al., 2018; Chen et al., 2019), and ischemic stroke (Jiang et al., 2018; Yang X. et al., 2018). In the current study,

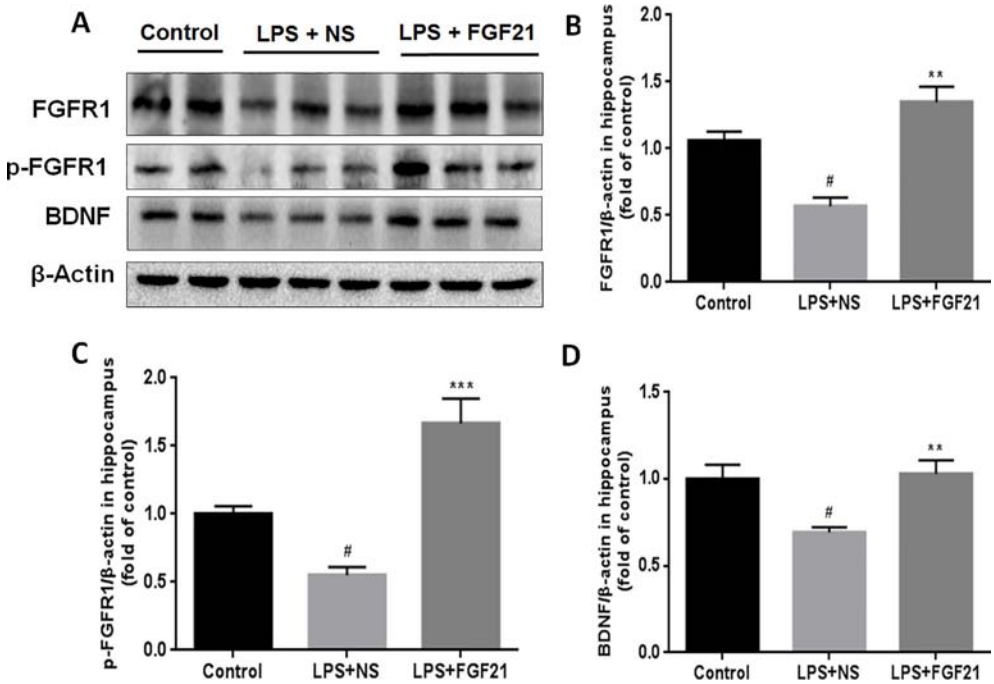

FIGURE 6 | Exogenous rhFGF21 supplement functioned through FGFR1 activation and enhanced BDNF deficiency induced by LPS. **(A)** Representative images of FGFR1, p-FGFR1, and BDNF expression in the mouse hippocampus detected by western blot. **(B)** Densitometric analysis for the protein expression of FGFR1. **(C)** Densitometric analysis for the protein expression of p-FGFR1. **(D)** Densitometric analysis for the protein expression of BDNF. Data are means ± SEM (n=5). $^{\#}P < 0.05$ compared to control group; $^{**}P < 0.01$, $^{***}P < 0.001$ compared to LPS-induced group.

pretreatment with rhFGF21 at doses of 1.5 and 3.0 mg/kg significantly prevented the increase in immobility time induced by LPS administration in the FST and TST, indicating the antidepressant-like effect of this large molecule. Notably, the administration of rhFGF21 alone did not significantly alter behavior compared with the control group, demonstrating that rhFGF21 is effective under only disease conditions.

The central or peripheral administration of LPS, an endotoxin, results in depression in animal models. Therefore, LPS treatment is a validated approach to establish a depression model, and LPS-induced depression-like animal models are commonly used to assess the anti-depressive effects of molecules. Various studies have demonstrated LPS-induced behavioral impairments including increased immobile time in the FST and TST (Brites and Fernandes, 2015), which is consistent with the results of our study. Pretreatment with 1.5 mg/kg rhFGF21 for three days markedly prevented and ameliorated LPS-induced depression-like behaviors (the increased total distance traveled and number of line crossings revealed by the OFT and decreased immobility time revealed by FST and TST), indicating the potential antidepressant effects of rhFGF21.

An increasing number of studies have suggested that inflammation plays a crucial role in the process of MDD (Rush et al., 2016; Yang M. et al., 2018). The activation of microglia, a kind of macrophage in the brain, can trigger the expression of proinflammatory cytokines involved in the pathological development of neuroinflammation- and degeneration-related diseases. The hippocampus is a brain region with a high density of microglia. Some studies have shown that microglia is activated in neuroinflammation, contributing to the development of depression (Wang Q. et al., 2018). LPS administration induced depression-like behaviors, triggered microglial activation in the hippocampus, and upregulated proinflammatory cytokine expression (Brites and Fernandes, 2015). Activated microglia are the major source of proinflammatory cytokines, such as TNF-α, IL-1β, and IL-6, in the CNS (Yang M. et al., 2018). Preclinical and clinical studies have proposed that proinflammatory cytokines are associated with the pathogenesis of depression (Karson et al., 2013) and that an increase in pro-inflammatory cytokines contributes to depressive-like behaviors (Raison et al., 2006; Guo et al., 2019). In addition, various studies demonstrated increased serum levels of TNF-α, IL-1β, and IL-6 in patients with depression (Song et al., 2009; Brites and Fernandes, 2015). In the current study, rhFGF21 could inhibit the activation of microglia and reduce the expression levels of the proinflammatory cytokines TNF-α, IL-1β, and IL-6 in the hippocampus of a depressive-like mouse model induced by LPS administration and in primary microglia stimulated by LPS.

The NF-κB signaling pathway plays a critical role in the inflammatory response. Under normal conditions, NF-κB is

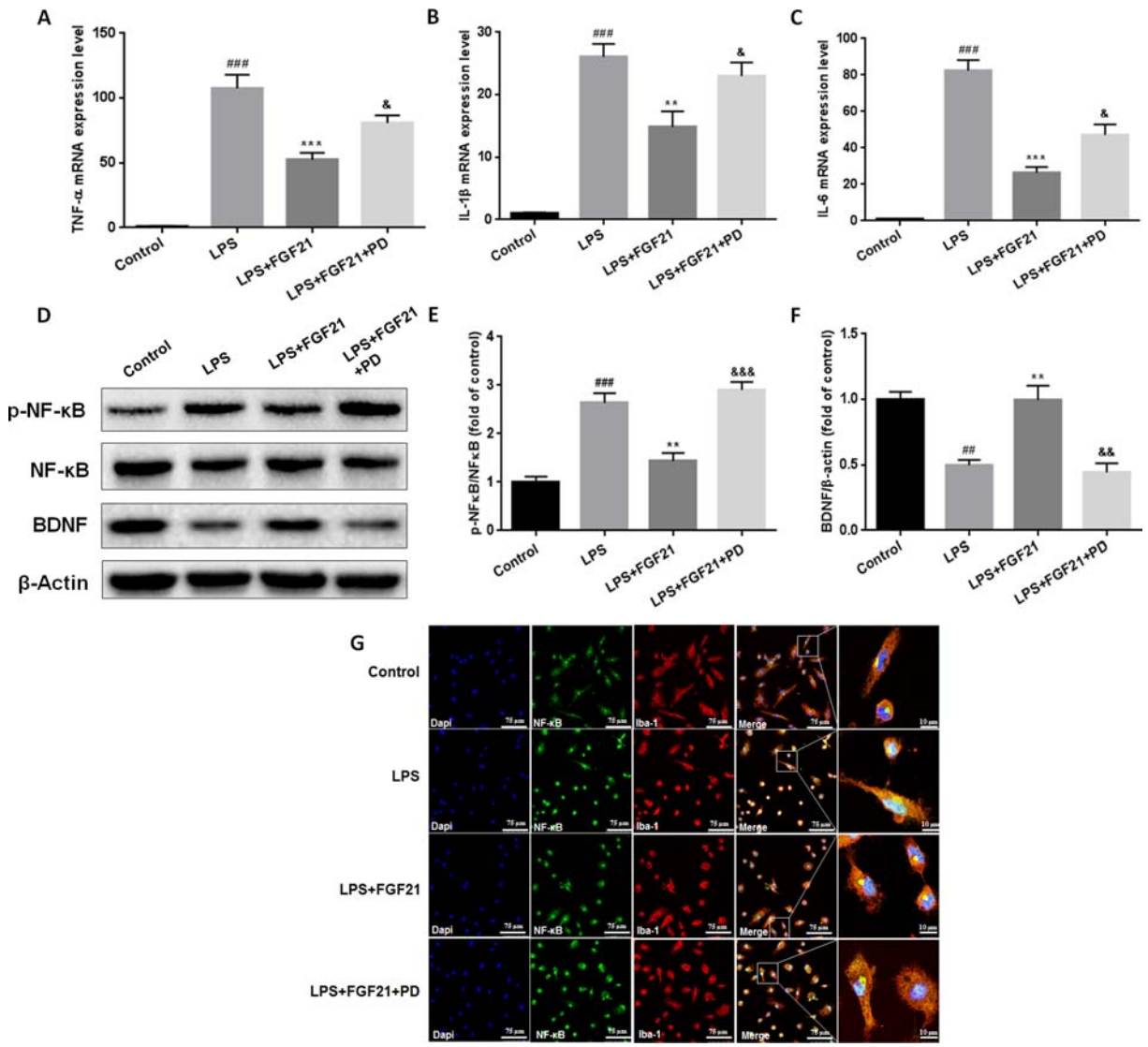

FIGURE 7 | Exogenous rhFGF21 supplement suppressed pro-inflammation cytokines expression by activating FGFR1 through inhibiting phosphorylation of NF-κB, and ameliorated BDNF deficiency induced by LPS in primary microglia cells. **(A)** rhFGF21 administration suppressed pro-inflammation cytokines TNF-α mRNA level. **(B)** rhFGF21 administration suppressed pro-inflammation cytokines IL-1β mRNA level. **(C)** rhFGF21 administration suppressed IL-6 mRNA level. **(D)** Representative bands of NF-κB, p-NF-κB, and BDNF expression detected by western blot. **(E)** Densitometric analysis for the protein expression of p-NF-κB/NF-κB. **(F)** Densitometric analysis for the protein expression of BDNF. Data are means ± SEM (n = 5). $^{\#\#}P < 0.01$, $^{\#\#\#}P < 0.001$ compared to control group. $^{**}P < 0.01$, $^{***}P < 0.001$ compared to LPS treated group. $^{\&}P < 0.05$, $^{\&\&}P < 0.01$, $^{\&\&\&}P < 0.001$ compared to LPS and rhFGF21 co-treated group.

bound to the inhibitor IκB, and exists in an inactive state in the cellular cytoplasm. However, once activated by an activator, such as LPS, NF-κB is phosphorylated to p-NF-κB, which is then released and translocated into the nucleus, where it promotes the expression of inflammatory cytokines (Luo et al., 2014; Yang M. et al., 2018). In the current study, we examined nuclear and cytoplasmic levels of NF-κB in the hippocampus of an LPS-induced depression mouse model and determined the expression levels of NF-κB and p-NF-κB in LPS-induced primary microglia to assess the effects of rhFGF21 on the NF-κB signaling pathway. rhFGF21 could reduce the increase in the ratio of p-NF-κB/NF-κB induced by LPS and decrease the enhanced level of nuclear NF-κB induced by LPS, indicating that rhFGF21 could inhibit NF-κB activation and translocation into the nucleus. These results indicated that rhFGF1 may exert an anti-inflammatory effect by mediating the NF-κB signaling pathway and that rhFGF1 is a novel antidepressant candidate.

FGF21 activity requires its binding to a receptor complex that consists of FGFR1 and the coreceptor β-Klotho (Min et al., 2018). Previous studies have demonstrated that FGF21/FGFR1 signaling plays a major role in increasing basal glucose uptake (Hsu et al., 2019), inducing macrophages through the Ox-LDL-

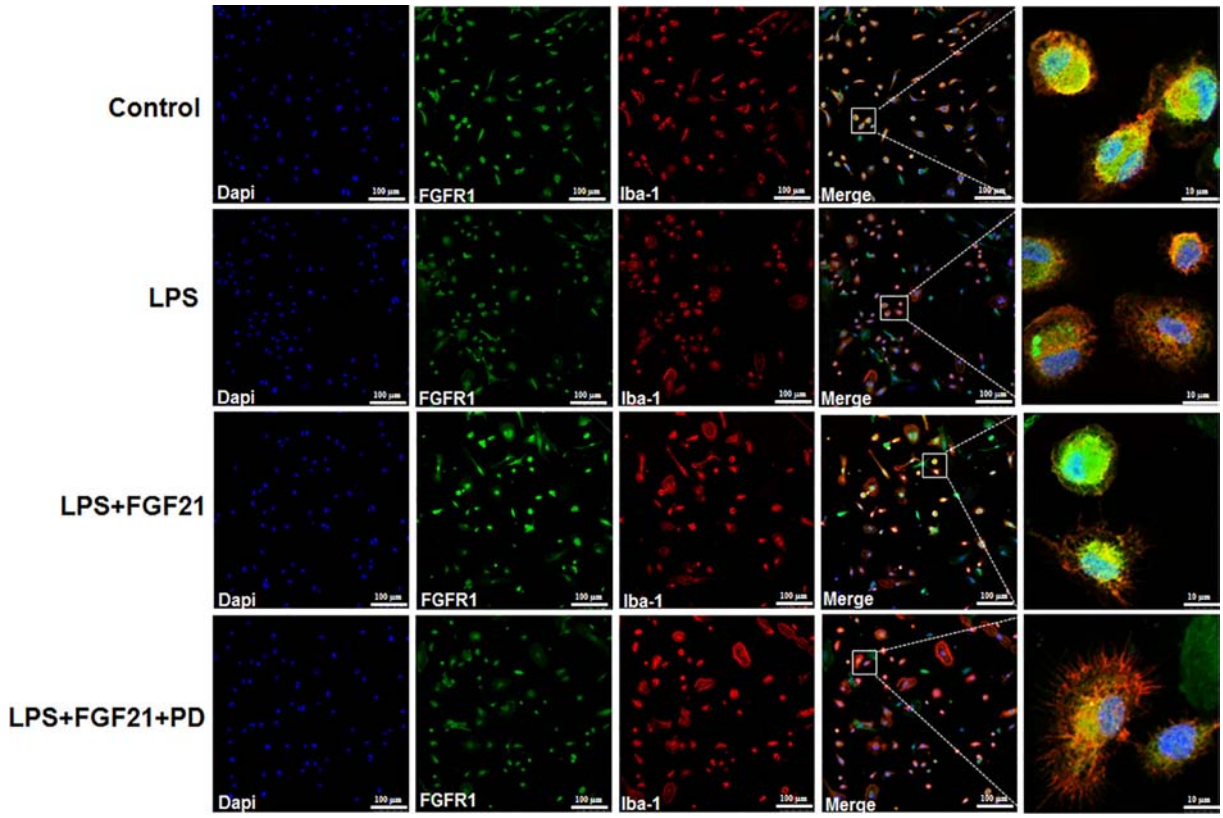

FIGURE 8 | Exogenous rhFGF21 rescued LPS-induced downregulated FGFR1 activity detected by immunofluorescence staining.

induced inflammatory response (Wang N. et al., 2018), attenuating neuronal apoptosis in the penumbra of rats after permanent middle cerebral artery occlusion (MCAO) (Zheng et al., 2019), and protecting the blood-brain barrier by increasing tight junction and adhesion junction proteins after traumatic brain injury (Chen J. et al., 2018). In the current study, to further investigate the functions of rhFGF21 in suppressing the NF-κB pathway to inhibit microglial activation and proinflammatory cytokine expression mediated through FGFR1 activation, the FGFR1 inhibitor PD173074 and rhFGF21 were used to treat primary microglia stimulated with LPS. rhFGF21 activated FGFR1, which suppressed proinflammatory cytokine expression and reduced the ratio of p-NF-κB/NF-κB expression stimulated by LPS in primary microglia. In contrast, PD173074 blocked these inhibitory effects of rhFGF21, indicating that rhFGF21 suppresses the NF-κB pathway to inhibit microglial activation and proinflammatory cytokine expression mediated through FGFR1 activation. Proinflammatory cytokines can reduce the expression of BDNF, and neurotrophic factors are critical in the pathogenesis of depression and brain neuroplasticity (Lee and Kim, 2010). Several reports demonstrated that LPS administration induced inflammatory cytokine expression and reduced BDNF and other neurotrophin expression, which could cause cognitive dysfunction. BDNF levels are much higher in the hippocampus than in other brain structures due to the great biological importance of the hippocampus in memory maintenance and its involvement with emotions. In addition, our study demonstrated that rhFGF21 could prevent LPS-induced BDNF downregulation by increasing BDNF expression in the mouse hippocampus and in primary microglia, which was reversed by its combination treatment with PD173074.

CONCLUSION

In conclusion, the current study provides evidence that rhFGF21 treatment improves LPS-induced depression-like behaviors and decreases proinflammatory cytokine expression. In addition, the current study demonstrates that rhFGF21 can act as an antidepressant upon hippocampal microglial stimulation through inhibiting activation of the NF-κB signaling pathway by activating FGFR1. Accordingly, the present study indicates that rhFGF21 could be a potent candidate drug for antidepressant therapy. However, the underlying mechanism by which rhFGF21

affects activated microglia and inflammatory factors requires further study.

DATA AVAILABILITY STATEMENT

The raw data supporting the conclusions of this article will be made available by the authors, without undue reservation, to any qualified researcher.

ETHICS STATEMENT

All animal use and care protocol conformed to the Guide for the Care and Use of Laboratory Animals from the National Institutes of Health and was approved by the Animal Care and Use Committee of Wenzhou Medical University.

AUTHOR CONTRIBUTIONS

XW and LL designed the experiment and wrote the manuscript. LZ, JH, RG, and SY performed the animal experiments and analyzed the data. FL, DW, and KG performed the cells experiments and analyzed the data. YZ, AH, and XW supervised the study and contributed to the design of the study. All the authors read and approved the final version of the manuscript.

FUNDING

This work was supported by the National Natural Science Foundation of China (No. 81771284, 81971180), Natural Science Foundation of Zhejiang Province (LQ19H090012) and Wenzhou Municipal Science and Technology Bureau Project (Y20160078).

REFERENCES

Adzic, M., Djordjevic, J., Mitic, M., Brkic, Z., Lukic, I., and Radojcic, M. (2015). The contribution of hypothalamic neuroendocrine, neuroplastic and neuroinflammatory processes to lipopolysaccharide-induced depressive-like behaviour in female and male rats: involvement of glucocorticoid receptor and C/EBP-beta. *Behav. Brain Res.* 291, 130–139. doi: 10.1016/j.bbr.2015.05.029

Amiri, M., Braidy, N., and Aminzadeh, M. (2018). Protective effects of fibroblast growth factor 21 against amyloid-beta-induced toxicity in SH-SY5Y cells. *Neurotox. Res.* 34, 574–583. doi: 10.1007/s12640-018-9914-2

Andrews, P. W., Thomson, J. A.Jr., Amstadter, A., and Neale, M. C. (2012). Primum non nocere: an evolutionary analysis of whether antidepressants do more harm than good. *Front. Psychol.* 3, 117. doi: 10.3389/fpsyg.2012.00117

Aurbach, E. L., Inui, E. G., Turner, C. A., Hagenauer, M. H., Prater, K. E., Li, J. Z., et al. (2015). Fibroblast growth factor 9 is a novel modulator of negative affect. *Proc. Natl. Acad. Sci. U.S.A.* 112, 11953–11958. doi: 10.1073/pnas.1510456112

Brites, D., and Fernandes, A. (2015). Neuroinflammation and depression: microglia activation, extracellular microvesicles and microRNA dysregulation. *Front. Cell Neurosci.* 9, 476. doi: 10.3389/fncel.2015.00476

Chang, H. H., Chen, P. S., Cheng, Y. W., Wang, T. Y., Yang, Y. K., and Lu, R. B. (2018). FGF21 is associated with metabolic effects and treatment response in depressed bipolar ii disorder patients treated with valproate. *Int. J. Neuropsychopharmacol.* 21, 319–324. doi: 10.1093/ijnp/pyx093

Chen, G., Liu, J., Jiang, L., Ran, X., He, D., Li, Y., et al. (2018). Peiminine protects dopaminergic neurons from inflammation-induced cell death by inhibiting the ERK1/2 and NF-kappaB signalling pathways. *Int. J. Mol. Sci.* 19, E821. doi: 10.3390/ijms19030821

Chen, J., Hu, J., Liu, H., Xiong, Y., Zou, Y., Huang, W., et al. (2018). FGF21 Protects the blood-brain barrier by upregulating PPARγ *via* FGFR1/β-klotho after traumatic brain injury. *J. Neurotrauma.* 35, 2091–2103. doi: 10.1089/neu.2017.5271

Chen, S., Chen, S. T., Sun, Y., Xu, Z., Wang, Y., Yao, S. Y., et al. (2019). Fibroblast growth factor 21 ameliorates neurodegeneration in rat and cellular models of Alzheimer's disease. *Redox Biol.* 22, 101133. doi: 10.1016/j.redox.2019.101133

Deng, Z., Deng, S., Zhang, M. R., and Tang, M. M. (2019). Fibroblast growth factors in depression. *Front. Pharmacol.* 10, 60. doi: 10.3389/fphar.2019.00060

Domingues, M., Casaril, A. M., Birmann, P. T., Lourenço, D. A., Vieira, B., Begnini, K., et al. (2018). Selanylimidazopyridine prevents lipopolysaccharide-induced depressive-like behavior in mice by targeting neurotrophins and inflammatory/oxidative mediators. *Front. Neurosci.* 12, 486. doi: 10.3389/fnins.2018.00486

Elsayed, M., Banasr, M., Duric, V., Fournier, N. M., Licznerski, P., and Duman, R. S. (2012). Antidepressant effects of fibroblast growth factor-2 in behavioral and cellular models of depression. *Biol. Psychiatry* 72, 258–265. doi: 10.1016/j.biopsych.2012.03.003

Gaich, G., Chien, J. Y., Fu, H., Glass, L. C., Deeg, M. A., Holland, W. L., et al. (2013). The effects of LY2405319, an FGF21 analog, in obese human subjects with type 2 diabetes. *Cell Metab.* 18, 333–340. doi: 10.1016/j.cmet.2013.08.005

Garcès, A., Nishimune, H., Philippe, J. M., Pettmann, B., and deLapeyrière, O. (2000). FGF9: a motoneuron survival factor expressed by medial thoracic and sacral motoneurons. *J. Neurosci. Res.* 60, 1–9. doi: 10.1002/(SICI)1097-4547(20000401)60:1<1::AID-JNR1>3.0.CO;2-P

Guo, L. T., Wang, S. Q., Su, J., Xu, L. X., Ji, Z. Y., Zhang, R. Y., et al. (2019). Baicalin ameliorates neuroinflammationinduced depressive-like behavior through inhibition of toll-like receptor 4 expression *via* the PI3K/AKT/FoxO1 pathway. *J. Neuroinflammation* 16, 95. doi: 10.1186/s12974-019-1474-8

Hennings, J. M., Kohli, M. A., Uhr, M., Holsboer, F., Ising, M., and Lucae, S. (2019). Polymorphisms in the BDNF and BDNFOS genes are associated with hypothalamus-pituitary axis regulation in major depression. *Prog. Neuropsychopharmacol. Biol. Psychiatry* 95, 109686. doi: 10.1016/j.pnpbp.2019.109686

Hsu, J. W., Yeh, S. C., Tsai, F. Y., Chen, H. W., and Tsou, T. C. (2019). Fibroblast growth factor 21 secretion enhances glucose uptake in mono(2-ethylhexyl) phthalate-treated adipocytes. *Toxicol. Vitro.* 59, 246–254. doi: 10.1016/j.tiv.2019.04.021

Hsuchou, H., Pan, W., and Kastin, A. J. (2007). The fasting polypeptide FGF21 can enter brain from blood. *Peptides* 28, 2382–2386. doi: 10.1016/j.peptides.2007.10.007

Ieraci, A., and Herrera, D. G. (2006). Nicotinamide protects against ethanolinduced apoptotic neurodegeneration in the developing mouse brain. *PloS Med.* 3, e101. doi: 10.1371/journal.pmed.0030101

Jiang, Y., Liu, N., Wang, Q., Yu, Z., Lin, L., Yuan, J., et al. (2018). Endocrine regulator rFGF21 (Recombinant Human Fibroblast Growth Factor 21) improves neurological outcomes following focal ischemic stroke of type 2 diabetes mellitus male mice. *Stroke* 49, 3039–3049. doi: 10.1161/STROKEAHA.118.022119

Karson, A., Demirtaş, T., Bayramgürler, D., Balci, F., and Utkan, T. (2013). Chronic administration of infliximab (TNF-α inhibitor) decreases depression and anxiety-like behaviour in rat model of chronic mild stress. *Basic Clin. Pharmacol. Toxicol.* 112, 335–340. doi: 10.1111/bcpt.12037

Kettenmann, H., Hanisch, U. K., Noda, M., and Verkhratsky, A. (2011). Physiology of microglia. *Physiol. Rev.* 91, 461–553. doi: 10.1152/physrev.00011.2010

Lee, B. H., and Kim, Y. K. (2010). The roles of BDNF in the pathophysiology of major depression and in antidepressant treatment. *Psychiatry Investig.* 7, 231–235. doi: 10.4306/pi.2010.7.4.231

Lee, J. S., Kim, W. Y., Jeon, Y. J., Lee, S. B., Lee, D. S., and Son, C. G. (2019). Antidepressant-like activity of myelophil attenuation of microglial-mediated neuroinflammation in mice undergoing unpredictable chronic mild stress. *Front. Pharmacol.* 10. doi: 10.3389/fphar.2019.00683

Lenz, K. M., and Nelson, L. H. (2018). Microglia and beyond: innate immune cells as regulators of brain development and behavioral function. *Front. Immunol.* 9, 698. doi: 10.3389/fimmu.2018.00698

Li, X. (2019). The FGF metabolic axis. *Front. Med.* 13, 511–530. doi: 10.1007/s11684-019-0711-y

Liang, P., Zhong, L., Gong, L., Wang, J., Zhu, Y., Liu, W., et al. (2017). Fibroblast growth factor 21 protects rat cardiomyocytes from endoplasmic reticulum stress by promoting the fibroblast growth factor receptor 1-extracellular signalregulated kinase 1/2 signaling pathway. *Int. J. Mol. Med.* 40, 1477–1485. doi: 10.3892/ijmm.2017.3140

Lin, W. N., Luo, S. F., Lee, C. W., Wang, C. C., Wang, J. S., and Yang, C. M. (2007). Involvement of MAPKs and NF-κB in LPS-induced VCAM-1 expression in human tracheal smooth muscle cells. *Cell Signal.* 19, 1258–1267. doi: 10.1016/j.cellsig.2007.01.009

Lin, L., Desai, R., Wang, X., Lo, E. H., and Xing, C. (2017). Characteristics of primary rat microglia isolated from mixed cultures using two different methods. *J. Neuroinflammation* 14, 101. doi: 10.1186/s12974-017-0877-7

Liu, Y., Wang, M., Tan, X., Wang, X., Yang, X., Xiao, J., et al. (2017). Negative correlation between cerebrospinal fluid FGF21 levels and BDI scores in male Chinese subjects. *Psychiatry Res.* 252, 111–113. doi: 10.1016/j.psychres.2017.01.075

Luo, J. G., Zhao, X. L., Xu, W. C., Zhao, X. J., Wang, J. N., Lin, X. W., et al. (2014). Activation of spinal NF-κB/p65 contributes to peripheral inflammation and hyperalgesia in rat adjuvant-induced arthritis. *Arthritis Rheumatol.* 66, 896–906. doi: 10.1002/art.38328

Makela, J., Tselykh, T. V., Maiorana, F., Eriksson, O., Do, H. T., Mudo, G., et al. (2014). Fibroblast growth factor-21 enhances mitochondrial functions and increases the activity of PGC-1alpha in human dopaminergic neurons *via* Sirtuin-1. *Springerplus* 3, 2. doi: 10.1186/2193-1801-3-2

Maragnoli, M. E., Fumagalli, F., Gennarelli, M., Racagni, G., and Riva, M. A. (2004). Fluoxetine and olanzapine have synergistic effects in the modulation of fibroblast growth factor 2 expression within the rat brain. *Biol. Psychiatry* 55, 1095–1102. doi: 10.1016/j.biopsych.2004.02.003

Min, X., Weiszmann, J., Johnstone, S., Wang, W., Yu, X., Romanow, W., et al. (2018). Agonistic β-Klotho antibody mimics fibroblast growth factor 21 (FGF21) functions. *J. Biol. Chem.* 293, 14678–14688. doi: 10.1074/jbc.RA118.004343

Muhammad, T., Ikram, M., Ullah, R., Rehman, S. U., and Kim, M. O. (2019). Hesperetin, a citrus flavonoid, attenuates LPS-induced neuroinflammation, apoptosis and memory impairments by modulating TLR4/NF-κB signaling. *Nutrients* 11, E648. doi: 10.3390/nu11030648

Pan, X., Shao, Y., Wu, F., Wang, Y., Xiong, R., Zheng, J., et al. (2018). FGF21 prevents angiotensin II-induced hypertension and vascular dysfunction by activation of ACE2/Angiotensin-(1-7) axis in mice. *Cell. Metab.* 27, 1323–1337.e5. doi: 10.1016/j.cmet.2018.04.002

Porsolt, R. D., Bertin, A., and Jalfre, M. (1977). Behavioral despair in mice: a primary screening test for antidepressants. *Arch. Int. Pharmacodyn. Ther.* 229, 327–336.

Raison, C. L., Capuron, L., and Miller, A. H. (2006). Cytokines sing the blues: inflammation and the pathogenesis of depression. *Trends Immunol.* 27, 24–31. doi: 10.1016/j.it.2005.11.006

Rush, G., O'Donovan, A., Nagle, L., Conway, C., McCrohan, A. M., O'Farrelly, C., et al. (2016). Alteration of immune markers in a group of melancholic depressed patients and their response to electroconvulsive therapy. *J. Affect. Disord.* 205, 60–68. doi: 10.1016/j.jad.2016.06.035

Silverman, M. N., Mukhopadhyay, P., Belyavskaya, E., Tonelli, L. H., Revenis, B. D., Doran, J. H., et al. (2013). Glucocorticoid receptor dimerization is required for proper recovery of LPS-induced inflammation, sickness behavior and metabolism in mice. *Mol. Psychiatry* 18, 1006–1017. doi: 10.1038/mp.2012.131

Song, C., Halbreich, U., Han, C., Leonard, B. E., and Luo, H. (2009). Imbalance between pro- and anti-inflammatory cytokines and between Th1 and Th2 cytokines in depressed patients: the effect of electroacupuncture or fluoxetine treatment. *Pharmacopsychiatry* 42, 182–188. doi: 10.1055/s-0029-1202263

Steru, L., Chermat, R., Thierry, B., and Simon, P. (1985). The tail suspension test: a new method for screening antidepressants in mice. *Psychopharmacol. (Berl)* 85, 367–370. doi: 10.1007/BF00428203

Su, W. J., Zhang, Y., Chen, Y., Gong, H., Lian, Y. J., Peng, W., et al. (2017). NLRP3 gene knockout blocks NF-κB and MAPK signaling pathway in CUMSinduced depression mouse model. *Behav. Brain Res.* 322 (Pt A), 1–8. doi: 10.1016/j.bbr.2017.01.018

Syed, S. A., Beurel, E., Loewenstein, D. A., Lowell, J. A., Craighead, W. E., Dunlop, B. W., et al. (2018). Defective inflammatory pathways in never-treated depressed patients are associated with poor treatment response. *Neuron* 99, 914–924.e3. doi: 10.1016/j.neuron.2018.08.001

Tang, M. M., Lin, W. J., Pan, Y. Q., and Li, Y. C. (2018). Fibroblast growth factor 2 modulates hippocampal microglia activation in a neuroinflammation induced model of depression. *Front. Cell Neurosci.* 12, 255. doi: 10.3389/fncel.2018.00255

Taniguti, E. H., Ferreira, Y. S., Stupp, I. J. V., Fraga-Junior, E. B., Doneda, D. L., Lopes, L., et al. (2019). Atorvastatin prevents lipopolysaccharide-induced depressive-like behaviour in mice. *Brain Res. Bull.* 146, 279–286. doi: 10.1016/j.brainresbull.2019.01.018

Tomaz, V. S., Cordeiro, R. C., Costa, A. M., de Lucena, D. F., Nobre Júnior, H. V., de Sousa, F. C., et al. (2014). Antidepressant-like effect of nitric oxide synthase inhibitors and sildenafil against lipopolysaccharide-induced depressive-like behavior in mice. *Neuroscience* 268, 236–246. doi: 10.1016/j.neuroscience.2014.03.025

Turner, C. A., Gula, E. L., Taylor, L. P., Watson, S. J., and Akil, H. (2008). Antidepressant-like effects of intracerebroventricular FGF2 in rats. *Brain Res.* 1224, 63–68. doi: 10.1016/j.brainres.2008.05.088

Walker, A. K., Budac, D. P., Bisulco, S., Lee, A. W., Smith, R. A., Beenders, ,. B., et al. (2013). NMDA receptor blockade by ketamine abrogates lipopolysaccharide-induced depressive-like behavior in C57BL/6J mice. *Neuropsychopharmacology* 38, 1609–1616. doi: 10.1038/npp.2013.71

Walker, A. K., Wing, E. E., Banks, W. A., and Dantzer, R. (2019). Leucine competes with kynurenine for blood-to-brain transport and prevents lipopolysaccharide-induced depression-like behavior in mice. *Mol. Psychiatry* 24, 1523–1532. doi: 10.1038/s41380-018-0076-7

Wang, H., Xiao, Y., Fu, L., Zhao, H., Zhang, Y., Wan, X., et al. (2010). High-level expression and purification of soluble recombinant FGF21 protein by SUMO fusion in Escherichia coli. *BMC Biotechnol.* 10, 14. doi: 10.1186/1472-6750-10-14

Wang, Q., Yuan, J., Yu, Z., Lin, L., Jiang, Y., Cao, Z., et al. (2018). FGF21 attenuates high-fat diet-induced cognitive impairment *via* metabolic regulation and anti-inflammation of obese mice. *Mol. Neurobiol.* 55, 4702–4717. doi: 10.1007/s12035-017-0663-7

Wang, N., Li, J. Y., Li, S., Guo, X. C., Wu, T., Wang, W. F., et al. (2018). Fibroblast growth factor 21 regulates foam cells formation and inflammatory response in Ox-LDL-induced THP-1 macrophages. *Biomed. Pharmacother.* 108, 1825–1834. doi: 10.1016/j.biopha.2018.09.143

Wang, Y., Ni, J., Gao, C., Xie, L., Zhai, L., Cui, G., et al. (2019a). Mitochondrial transplantation attenuates lipopolysaccharide-induced depression-like behaviors. *Prog. Neuropsychopharmacol. Biol. Psychiatry* 93, 240–249. doi: 10.1016/j.pnpbp.2019.04.010

Wang, Y., Ni, J., Zhai, L., Gao, C., Xie, L., Zhao, L., et al. (2019b). Inhibition of activated astrocyte ameliorates lipopolysaccharide- induced depressive-like behaviors. *J. Affect. Disord.* 242, 52–59. doi: 10.1016/j.jad.2018.08.015

Williams, A. J., Yee, P., Smith, M. C., Murphy, G. G., and Umemori, H. (2016). Deletion of fibroblast growth factor 22 (FGF22) causes a depression-like phenotype in adult mice. *Behav. Brain Res.* 307, 11–17. doi: 10.1016/j.bbr.2016.03.047

Wright, C. E., Strike, P. C., Brydon, L., and Steptoe, A. (2005). Acute inflammation and negative mood: mediation by cytokine activation. *Brain Behav. Immun.* 19, 345–350. doi: 10.1016/j.bbi.2004.10.003

Xu, J., Lloyd, D. J., Hale, C., Stanislaus, S., Chen, M., Sivits, G., et al. (2009). Fibroblast growth factor 21 reverses hepatic steatosis, increases energy expenditure, and improves insulin sensitivity in diet-induced obese mice. *Diabetes* 58, 250–259. doi: 10.2337/db08-0392

Yang, M., Dang, R., Xu, P., Guo, Y., Han, W., Liao, D., et al. (2018). Dl-3-n-Butylphthalide improves lipopolysaccharide-induced depressive-like behavior in rats: involvement of Nrf2 and NF-kappaB pathways. *Psychopharmacol. (Berl).* 235, 2573–2585. doi: 10.1007/s00213-018-4949-x

Yang, X., Hui, Q., Yu, B., Huang, Z., Zhou, P., Wang, P., et al. (2018). Design and evaluation of lyophilized fibroblast growth factor 21 and its protection against ischemia cerebral injury. *Bioconjug. Chem.* 29, 287–295. doi: 10.1021/acs.bioconjchem.7b00588

Yu, X. B., Zhang, H. N., Dai, Y., Zhou, Z. Y., Xu, R. A., Hu, L. F., et al. (2019). Simvastatin prevents and ameliorates depressive behaviors *via* neuroinflammatory regulation in mice. *J. Affect. Disord.* 245, 939–949. doi: 10.1016/j.jad.2018.11.086

Zhang, Y., Bi, X., Adebiyi, O., Wang, J., Mooshekhian, A., Cohen, J., et al. (2019). Venlafaxine improves the cognitive impairment and depression-like behaviors in a cuprizone mouse model by alleviating demyelination and neuroinflammation in the brain. *Front. Pharmacol.* 10, 332. doi: 10.3389/fphar.2019.00332

Zheng, W., Matei, N., Pang, J., Luo, X., Song, Z., Tang, J., et al. (2019). Delayed recanalization at 3 days after permanent MCAO attenuates neuronal apoptosis through FGF21/FGFR1/PI3K/Caspase-3 pathway in rats. *Exp. Neurol.* 320, 113007. doi: 10.1016/j.expneurol.2019.113007

Conflict of Interest: The authors declare that the research was conducted in the absence of any commercial or financial relationships that could be construed as a potential conflict of interest.

The handling editor is currently organizing a Research Topic with one of the authors LL, and confirms the absence of any other collaboration.

frontiers in Pharmacology

ORIGINAL RESEARCH
published: 02 March 2020
doi: 10.3389/fphar.2020.00120

Temporospatial Expression of Fgfr1 and 2 During Lung Development, Homeostasis, and Regeneration

Tingting Yuan[1†], Kylie Klinkhammer[1†], Handeng Lyu[1,2], Shan Gao[1], Jie Yuan[1], Seantel Hopkins[1], Jin-San Zhang[2] and Stijn P. De Langhe[1*]*

[1] Department of Medicine, Division of Pulmonary, Allergy & Critical Care Medicine, University of Alabama at Birmingham, Birmingham, AL, United States, [2] School of Pharmaceutical Sciences, Wenzhou Medical University, Wenzhou, China

OPEN ACCESS

Edited by:
Ramaswamy Krishnan, Harvard Medical School, United States

Reviewed by:
Reinoud Gosens, University of Groningen, Netherlands
Erzsébet Bartolák-Suki, Boston University, United States

***Correspondence:**
Tingting Yuan
tyuan@uabmc.edu
Stijn P. De Langhe
sdelanghe@uabmc.edu

[†]These authors have contributed equally to this work

Specialty section:
This article was submitted to Translational Pharmacology, a section of the journal Frontiers in Pharmacology

Received: 13 November 2019
Accepted: 28 January 2020
Published: 02 March 2020

Citation:
Yuan T, Klinkhammer K, Lyu H, Gao S, Yuan J, Hopkins S, Zhang J-S and De Langhe SP (2020) Temporospatial Expression of Fgfr1 and 2 During Lung Development, Homeostasis, and Regeneration. Front. Pharmacol. 11:120. doi: 10.3389/fphar.2020.00120

Fgfr1 (Fibroblast growth factor receptor 1) and Fgfr2 are dynamically expressed during lung development, homeostasis, and regeneration. Our current analysis indicates that Fgfr2 is expressed in distal epithelial progenitors AT2, AT1, club, and basal cells but not in ciliated or neuroendocrine cells during lung development and homeostasis. However, after injury, Fgfr2 becomes upregulated in neuroendocrine cells and distal club cells. Epithelial Fgfr1 expression is minimal throughout lung development, homeostasis, and regeneration. We further find both Fgfr1 and Fgfr2 strongly expressed in cartilage progenitors and airway smooth muscle cells during lung development, whereas Fgfr1 but not Fgfr2 was expressed in lipofibroblasts and vascular smooth muscle cells. In the adult lung, Fgfr1 and Fgfr2 were mostly downregulated in smooth muscle cells but became upregulated after injury. Fgfr1 remained expressed in mesenchymal alveolar niche cells or lipofibroblasts with lower levels of expression in their descendant (alveolar) myofibroblasts during alveologenesis.

Keywords: lung, Fgf, homeostasis, development, regeneration

INTRODUCTION

Fgfr1 and Fgfr2, two of the four fibroblast growth factor receptors, play important roles during lung development and regeneration, often mediating reciprocal signaling between the epithelium and mesenchyme *via* their ligand Fgfs (Jaskoll et al., 2005; MacKenzie et al., 2015; Balasooriya et al., 2017; Yuan et al., 2019). Our recent studies showed that Fgf10-Fgfr2b signaling is critical for generating basal cells and to drive alveolar epithelial regeneration after bleomycin injury in the lung (Yuan et al., 2019). Both Fgfr1 and Fgfr2 are also considered as potential targets for lung cancer therapy (Weiss et al., 2010; Theelen et al., 2016). However, most studies have focused on Fgfr1 or Fgfr2 signaling pathways. The temporospatial expression pattern of both Fgfr1 and Fgfr2 has not been carefully assessed.

In this study, using two mouse models featuring nuclear expression of cerulean under control of the *Fgfr1* promoter and nuclear expression of mCherry under control the *Fgfr2* promoter, we sought to explore the temporospatial expression pattern of these two receptors at the single cell level, during lung development, homeostasis and response to naphthalene or bleomycin injury. Since Fgf signaling regulates the expression of its receptor, this expression profile will not only provide a spatiotemporal map of which cells respond to Fgfr1 or Fgfr2 signaling at a given point in time, but

also to what extent. Note that both Fgfr1 and Fgfr2 have two isoforms, b and c, which are respectively thought to be expressed in the epithelium vs mesenchyme; however, our reporter line cannot distinguish between these two isoforms.

Fgfr1 and Fgfr2 Expression During Embryonic Lung Development

We find that during early lung development, around E13.5, Fgfr1 is moderately expressed in both the epithelium (Sox9, Sox2) and mesenchyme (Acta2, Adrp) (**Figures 1A, D** and **2D, G**) and is upregulated in Sox9$^+$ cartilage progenitors (**Figure 2A**). At E15.5, Fgfr1 is expressed at low levels in the epithelium and remains expressed in developing lipofibroblasts (**Figures 1B** and **2H**), vascular smooth muscle cells, and cartilage progenitors (**Figures 2B, E, H**). By E18.5, Fgfr1 expression becomes relatively restricted to ADRP$^+$ lipofibroblasts aka mesenchymal AT2 niche cells (MANC) (**Figure 2I**), vascular smooth muscle cells (**Figure 2F**) and tracheal cartilage (**Figure 2C**), with low expression levels in the conducting airway (**Figures 1C, F**).

Interestingly, we found Fgfr2 expression to be homogenously expressed in the lung epithelium at E13.5 (**Figures 1A, D**) as well as in airway smooth muscle cells (**Figure 2D**), and Sox9$^+$ cartilage progenitors (**Figure 2A**). At E15.5, Fgfr2 is expressed in the epithelium with higher levels proximally vs distally (**Figures 1B, E, G**), airway smooth muscle cells (**Figure 2E**), and cartilage progenitors (**Figure 2B**). A downregulation of

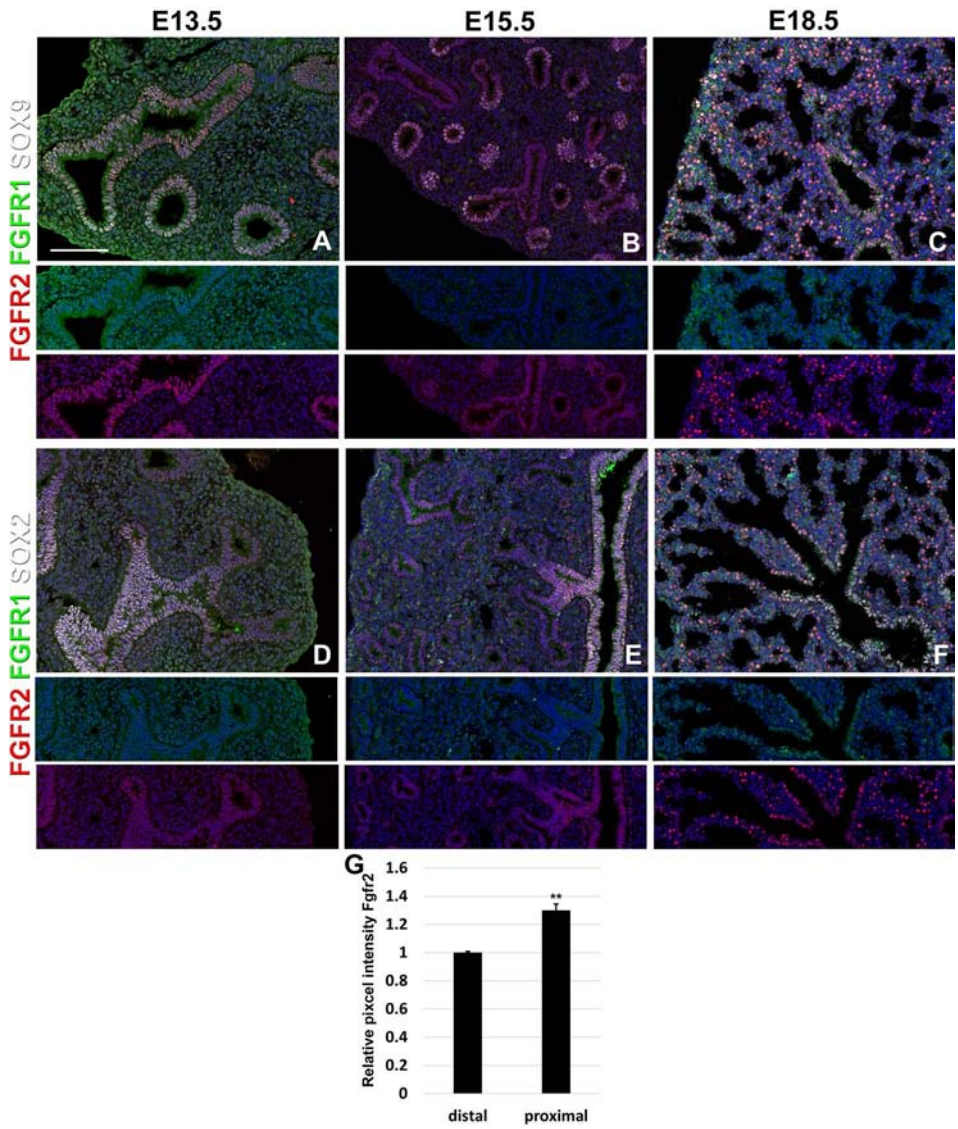

FIGURE 1 | Epithelial Fgfr1 and Fgfr2 expression during embryonic lung development. **(A–F)** Immunostaining on E13.5, E15.5, and E18.5 *Fgfr1-Cerulean;Fgfr2-mCherry* lungs for GFP (Fgfr1-Cerulean, green), RFP (Fgfr2-mCherry, red), Sox9 (white), or Sox2 (white). Lower panels for each individual image show GFP (green) and RFP (red) channels only without the far red channels. **(G)** Quantification of relative average pixel intensity for Fgfr2 in distal vs proximal epithelium at E15.5. Data are mean ± s.e.m. **P < 0.01, as determined by a two-tailed t-test; n = 6 biological replicates for each experimental group. Scale bars, 100 μm.

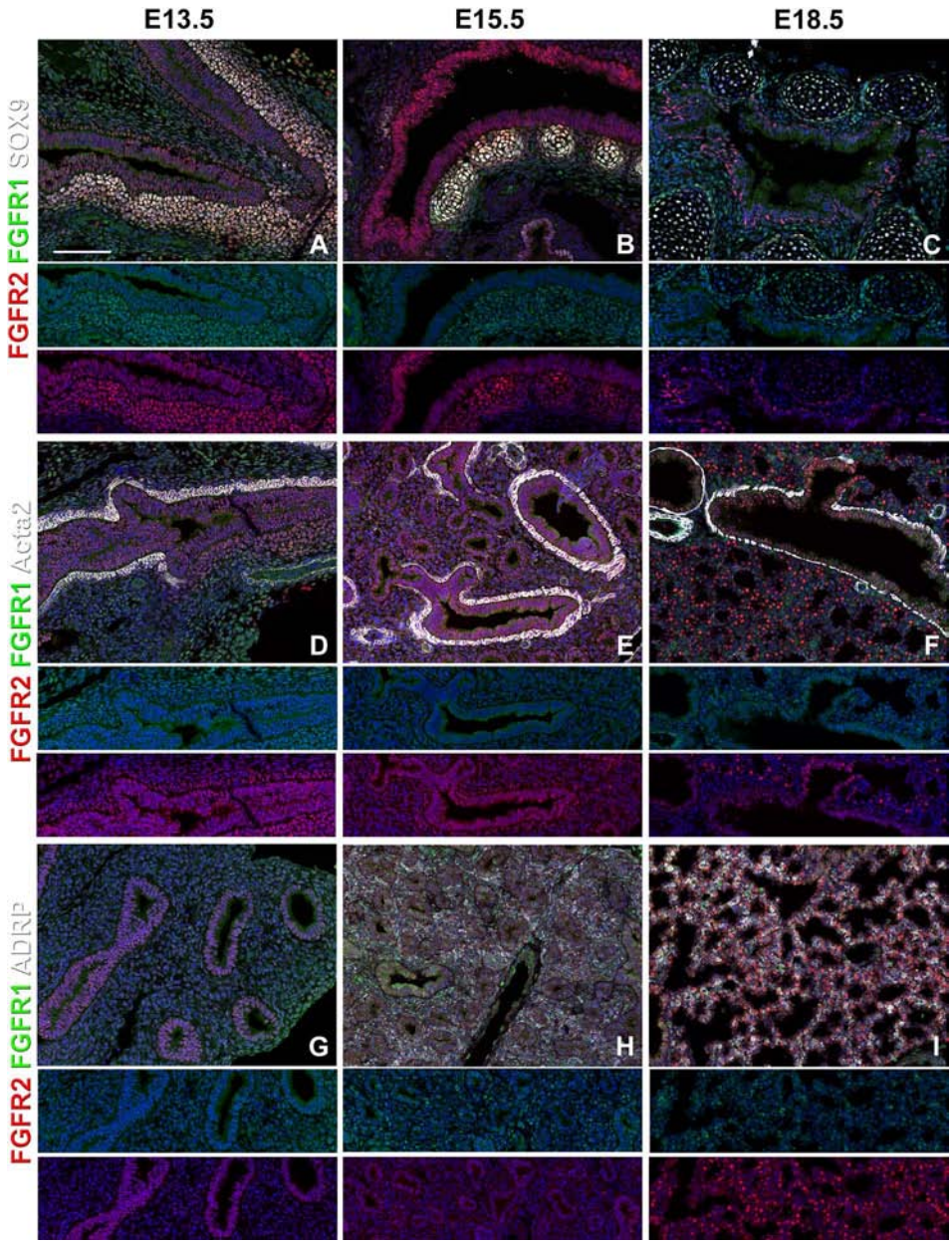

FIGURE 2 | Mesenchymal Fgfr1 and Fgfr2 expression during embryonic lung development. **(A–C)** Immunostaining on E13.5, E15.5, and E18.5 *Fgfr1-Cerulean; Fgfr2-mCherry* proximal lungs for GFP (Fgfr1-Cerulean, green), RFP (Fgfr2-mCherry, red), Sox9 (white); **(D–I)** Immunostaining on E13.5, E15.5, and E18.5 *Fgfr1-Cerulean;Fgfr2-mCherry* lungs for GFP (Fgfr1-Cerulean, green), RFP (Fgfr2-mCherry, red), Acta2 (white), or ADRP (white). Lower panels for each individual image show GFP (green) and RFP (red) channels only without the far red channel. Scale bars, 100 μm, n ≥ 6.

Fgfr2 signaling distally around E15.5 is required for the lung to transition from a branching program into an alveolar differentiation program; as we have previously demonstrated that overexpression of *Fgf10* starting from E15.5 onwards prevents this transition by inducing distal epithelial Fgfr2 signaling (Volckaert et al., 2013b; Volckaert et al., 2019). Upregulation of Fgfr2 in the proximal epithelium at this stage also coincides with the differentiation of the basal cell lineage (Volckaert et al., 2013b; Balasooriya et al., 2017; Volckaert et al., 2017; Volckaert et al., 2019).

At E18.5 we find Fgfr2 to be highly expressed in the developing AT2 cells (**Figures 3B, G**), basal cells (**Figures 3C, G**), distal airway clubs at the BADJ (**Figures 1F** and **3G**) and in cartilage cells (**Figure 2C**), with lower levels of expression in AT1 (**Figures 3A, G**) and proximal club cells (**Figures 3D, G**) and surrounding airway smooth muscle cells (**Figure 2F**). Furthermore, we find that at

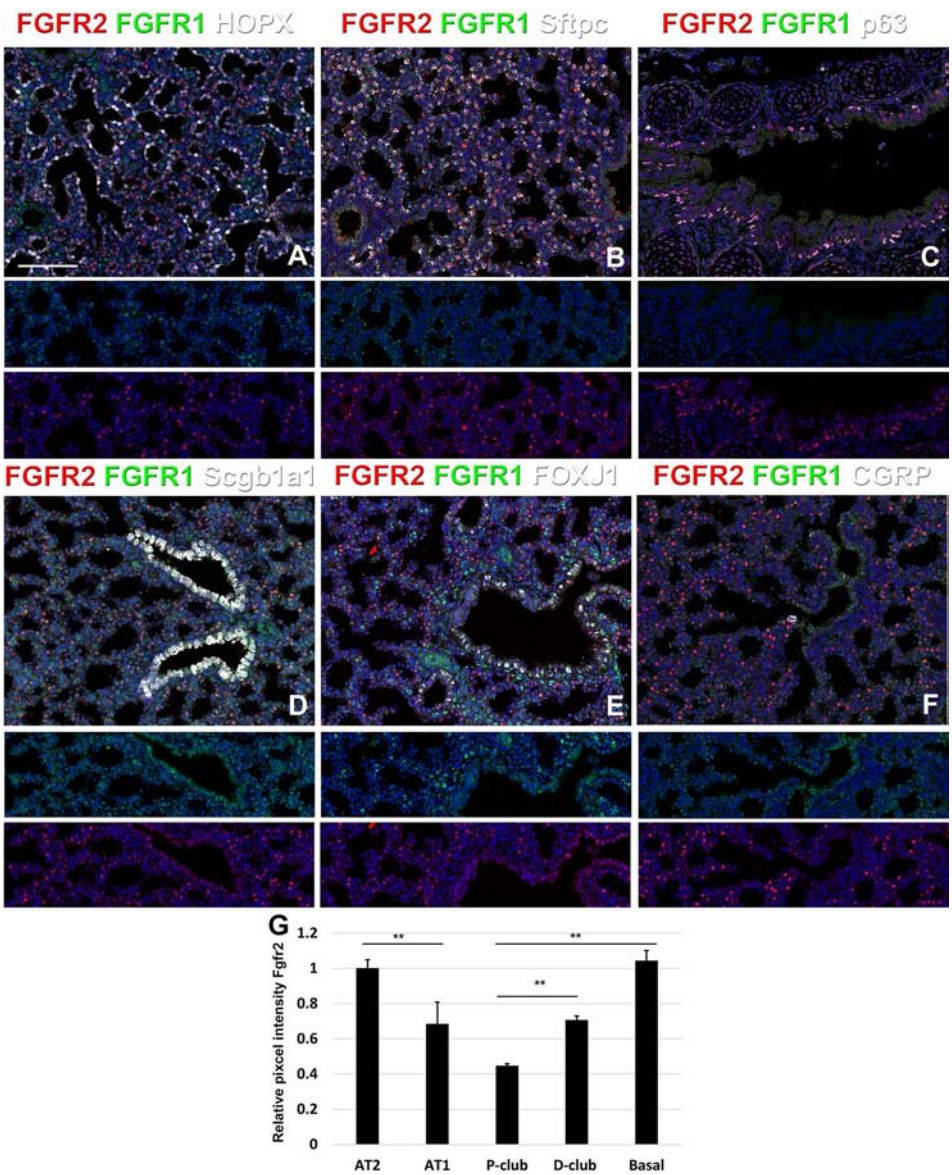

FIGURE 3 | Fgfr1 and Fgfr2 expression during late embryonic lung development in specific epithelial lineages. **(A–E)** Immunostaining on E18.5 *Fgfr1-Cerulean;Fgfr2-mCherry* lungs for GFP (Fgfr1-Cerulean), RFP (Fgfr2-mCherry, red), Hopx (white), Sftpc (white), p63 (white), Scgb1a1 (white), Foxj1 (white), or CGRP (white). **(G)** Quantification of relative average pixel intensity for Fgfr2 in alveolar type 2 (AT2) cells, AT1 cells, proximal and distal club cells and tracheal basal cells at E18.5. Data are mean ± s.e.m. **P < 0.01, as determined by a two-tailed t-test; n = 6 biological replicates for each experimental group. Scale bars, 100 μm.

E18.5, there is no Fgfr2 expression in Foxj1$^+$ ciliated cells or CGRP$^+$ neuroendocrine cells (**Figures 3E, F**). These observations are consistent with our previous reports that overexpression of *Fgf10* during late lung development blocks the differentiation of AT1 and ciliated cells in favor of AT2 and club or basal cells, respectively (Volckaert et al., 2013b; Volckaert et al., 2019).

Fgfr1 and Fgfr2 Expression During Postnatal Lung Development

During postnatal lung development, we found strong Fgfr2 expression in AT2 cells and strong Fgfr1 signaling in adjacent mesenchymal alveolar niche cells or lipofibroblasts (**Figures 4A–D, U–Y**). Interestingly, Fgfr2 expression was still present in AT1 cells but at lower level than in AT2 cells (**Figures 4E–H, Y**), which is consistent with an important role for Fgfr2 signaling in AT2 stem cell maintenance (Yuan et al., 2019). We further found Fgfr2 expression in club cells (**Figures 4M–P**), but not in ciliated cells (**Figures 4I–L**). Expression of Fgfr1 and 2 was low in airway and vascular smooth muscle cells (**Figures 4Q–T**). However, alveolar myofibroblasts exhibited modest Fgfr1 expression at P7 and P14 (**Figures 4Q, R, Y**), which is consistent with a lineage relationship with lipofibroblasts (Al Alam et al., 2015; El Agha et al., 2017; Li et al., 2018).

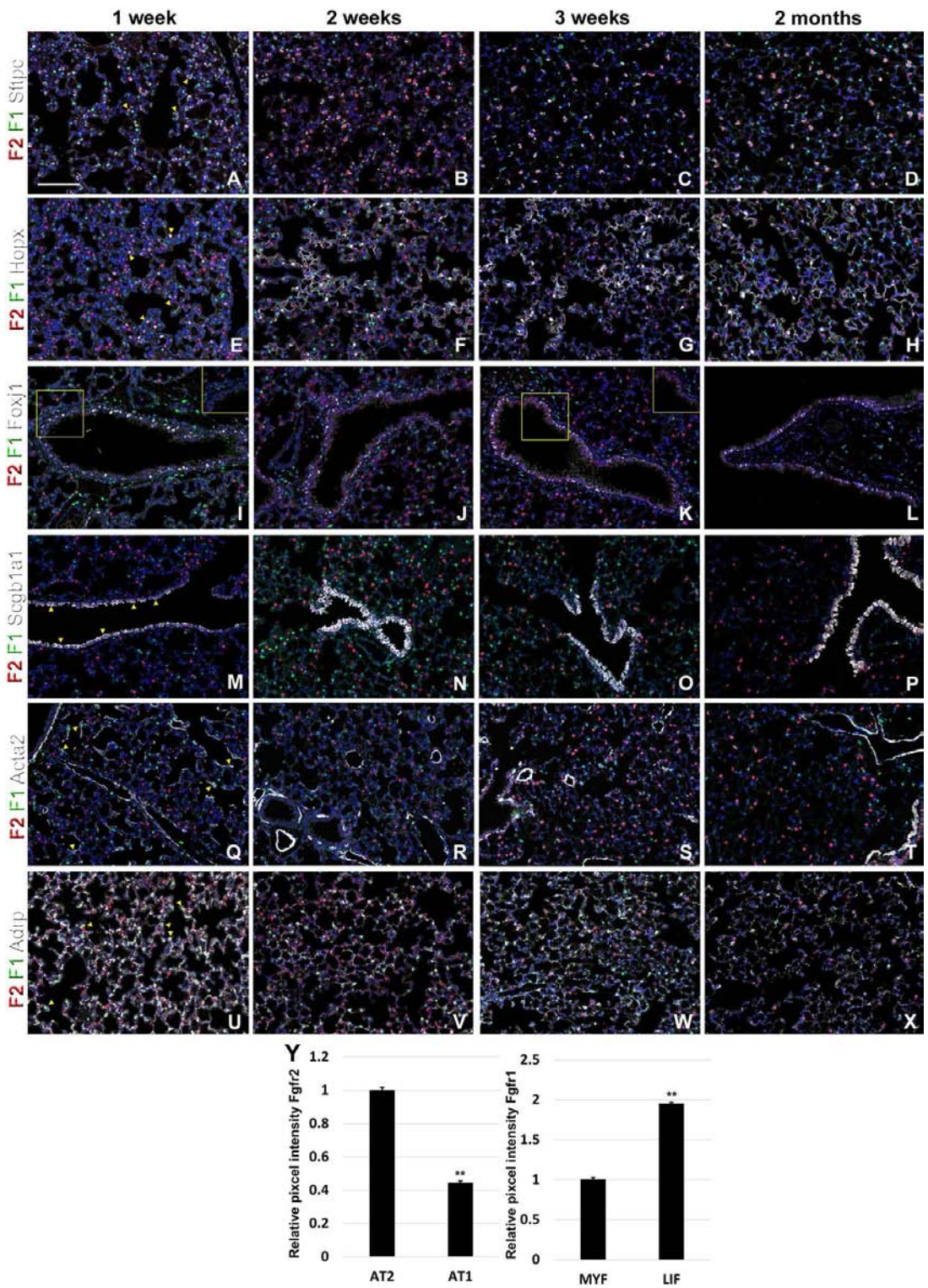

FIGURE 4 | Fgfr1 and Fgfr2 expression during postnatal lung development. **(A–X)** Immunostaining on P7, P14, P21, and 2 month old *Fgfr1-Cerulean;Fgfr2-mCherry* lungs for GFP (Fgfr1-Cerulean, green), RFP (Fgfr2-mCherry, red), Sftpc (white), Hopx (white), Fox1 (white), Scgb1a1 (white), Acta2 (white), or ADRP (white) (arrowheads indicate double labeled cells whereas frames show only GFP and RFP). **(Y)** Quantification of relative average pixel intensity for Fgfr2 in alveolar type 2 (AT2) vs AT1 cells at 2 months of age or Fgfr1 in alveolar myofibroblasts vs lipofibroblasts at P7. Data are mean ± s.e.m. $^{**}P < 0.01$, as determined by a two-tailed t-test; $n \geq 3$ biological replicates for each experimental group. Scale bars, 100 μm.

Dynamic Fgfr1 and Fgfr2 Expression After Naphthalene or Bleomycin Injury

Next, to investigate the dynamic changes in both Fgfr1 and Fgfr2 expression after lung injury, we performed naphthalene and bleomycin injuries on adult mice at 8 weeks of age and traced the expression changes during lung regeneration. As expected, we found that Fgfr2 expression was pretty much gone in the airway at 3 and 7 days after naphthalene injury, consistent with a loss of club cells the main Fgfr2 expression cell type in the adult conducting airway (**Figures 5A–C**, **E–G** and **S1**) (Volckaert et al., 2011). However, upon the return of club cells, Fgfr2 expression was gradually restored by 14 days after naphthalene injury (**Figures 5D**, **H**). We further found a modest increase in both Fgfr1 and Fgfr2 signaling in the airway smooth muscle cells upon naphthalene injury, consistent with an activation of this stem cell niche upon injury (**Figures 5I–L**) (Volckaert et al., 2011; Volckaert et al., 2013a; Lee et al., 2017). Remarkably, we found Fgfr2 upregulated in neuroendocrine bodies upon naphthalene injury, consistent with a role for Fgf10 signaling in regeneration of the airway epithelium by this distinct stem cell population (**Figures 5M–Q**) (Volckaert et al., 2011).

Lastly, we monitored the expression of Fgfr1 and Fgfr2 upon bleomycin injury. We found Fgfr2 to be higher in the distal airway club cells compared to proximal airway club cells at 3 and 6 weeks after bleomycin injury (**Figures 6A–C, P**). These findings are consistent with our previous report on the role of Fgf10-Fgfr2 signaling in alveolar epithelial regeneration by bronchial epithelial stem cells (Yuan et al., 2019). We found similarly high expression of Fgfr2 in regeneration AT2 cells upon bleomycin injury (**Figures 6D–F, P** and **S2**) and in proximal neo-basal cells but significantly lower expression of Fgfr2 in more distal neo-basal cells (**Figures 6G–I, P**), consistent with our previous finding that Fgfr2 is required for the development of neo-basal cells upon bleomycin injury and that increased Fgf10 signaling can drive these cells along the AT2 cell lineage whereas reduced Fgfr2 signaling leads to their differentiation into AT1 cells (Yuan et al., 2019). Interestingly, we found Fgfr1 expression

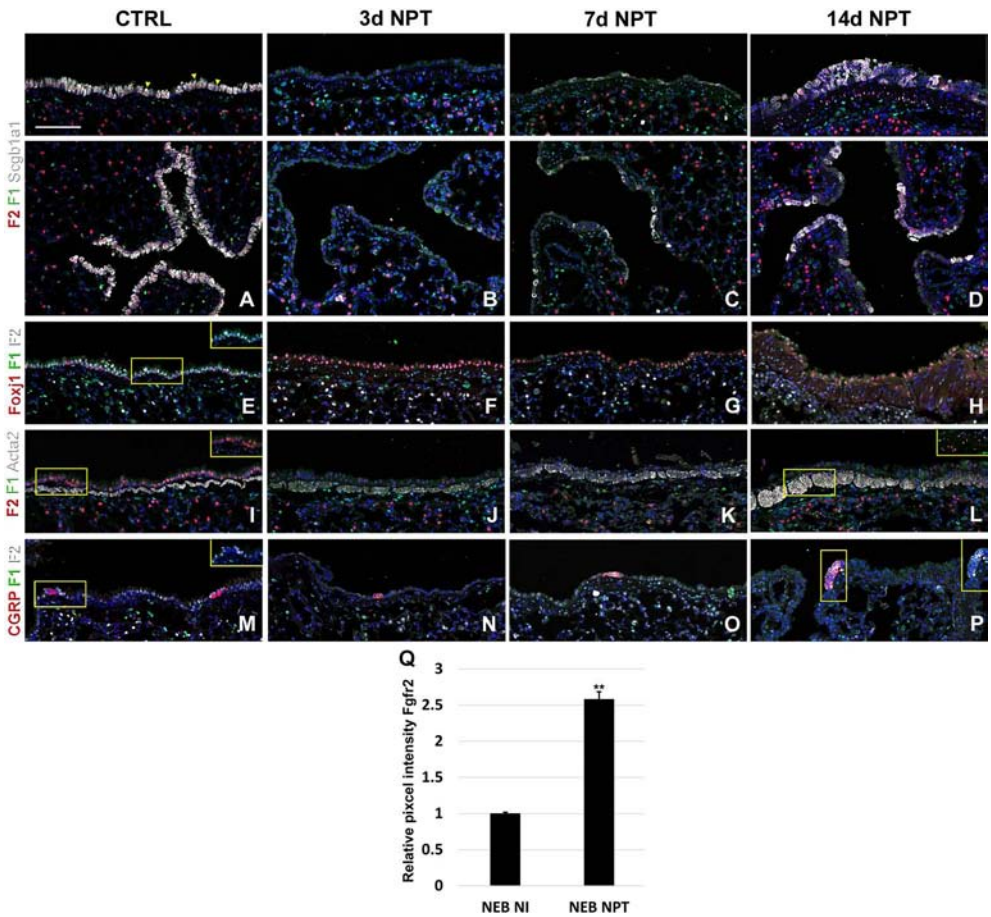

FIGURE 5 | Fgfr1 and Fgfr2 expression in the adult lung after naphthalene injury. **(A–P)** Immunostaining on ctrl and naphthalene injured adult *Fgfr1-Cerulean;Fgfr2-mCherry* lungs for GFP (Fgfr1-Cerulean, green), RFP (Fgfr2-mCherry, red), Scgb1a1 (white), Foxj1 (white), Acta2 (white), or CGRP (white) (arrowheads indicate double labeled cells whereas frames show only GFP and RFP). **(Q)** Quantification of relative average pixel intensity for Fgfr2 in NEBs after naphthalene injury. Data are mean ± s.e.m. **P < 0.01, as determined by a two-tailed t-test; n ≥ 5 biological replicates for each experimental group. Scale bars, 100 μm.

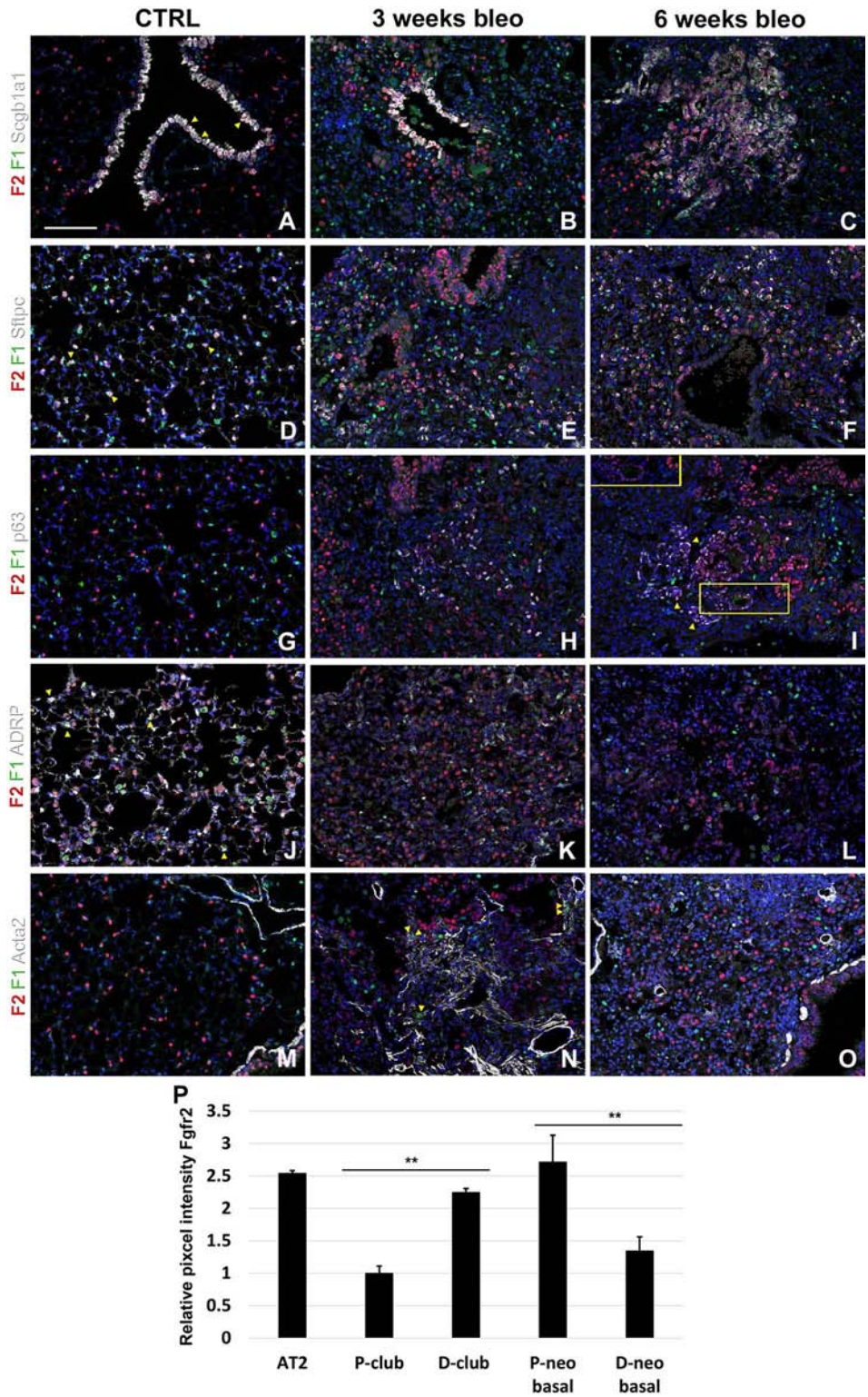

FIGURE 6 | Fgfr1 and Fgfr2 expression in the adult lung after bleomycin injury. **(A–X)** Immunostaining on ctrl and naphthalene injured adult *Fgfr1-Cerulean;Fgfr2-mCherry* lungs for GFP (Fgfr1-Cerulean, green), RFP (Fgfr2-mCherry, red), Scgb1a1 (white), Sftpc (white), p63 (white), ADRP (white), or Acta2 (white) (arrowheads indicate double labeled cells whereas frames show only GFP and RFP). **(P)** Quantification of relative average pixel intensity for Fgfr2 in alveolar type 2 (AT2) cells and proximal and distal club vs neo-basal cells after bleomycin injury. Data are mean ± s.e.m. $^{**}P < 0.01$, as determined by a two-tailed t-test; $n \geq 10$ biological replicates for each experimental group. Scale bars, 100 μm.

in myofibroblasts upon bleomycin injury (**Figures 6J–O**) consistent with them being derived from lipofibroblasts (El Agha et al., 2017; Yuan et al., 2019).

DISCUSSION

We found that during early lung development, Fgfr1 and Fgfr2 show different expression patterns. Fgfr1 is more dominantly expressed in mesenchymal cells; whereas, Fgfr2 is preferentially expressed in epithelial cell lineages (**Figures 1–3**). This trend continuous during the postnatal stage, with strong Fgfr2 expression in AT2 and basal cells, lower expression in club cells, and strong Fgfr1 expression in mesenchymal alveolar niche lipofibroblast cells and vascular smooth muscle cells (**Figure 4**). In the developing lung, Fgf10, expressed and released by the distal mesenchyme, binds and activates Fgfr2 on distal tip epithelial progenitors epithelium to keep them in a progenitor-like state by inducing Sox9 (Volckaert et al., 2013b; Volckaert et al., 2019). In this study, we detected that at E15.5, Fgfr2 expression becomes downregulated in the $Sox9^+$ distal epithelium (**Figures 1B, G**) and upregulated more proximally, indicating that downregulation of Fgfr2 signaling distally is required for the lung to transition from a branching program into an alveolar differentiation program.

After naphthalene injury, Fgf10 signaling is reactivated in the parabronchial smooth muscle cells (PSMCs), and Fgfr2 is upregulated in neuroendocrine bodies, suggesting that Fgf10 signaling may activate this reserve stem cell population upon injury (**Figures 5M–P**), consistent with previous findings (Volckaert et al., 2011; Volckaert et al., 2013a; Lee et al., 2017).

We recently discovered that Fgf10-Fgfr2b signaling is critical for the neo-basal cell generation and alveolar epithelial regeneration after bleomycin injury (Yuan et al., 2019). From this study, we find similarly high levels of Fgfr2 in distal airway club cells, AT2 cells, and proximal-neo basal cells supporting our previous findings. Intriguingly, lineage tracing data from our previous study indicate that the majority of neo-basal cells, which appear near BADJs after injury, are generated through the dedifferentiation of club cells and function as a transitional epithelial cell lineage to assist in alveolar epithelial regeneration (Yuan et al., 2019). The dynamic reduction in Fgfr2 expression in a subset of $p63^+$ basal cells (**Figures 6H, I, P**) implies their direct differentiation into AT1 cells, whereas increasing Fgfr2 expression might help boost basal cell to AT2 cell reprogramming (Yuan et al., 2019). The differentiation of lipofibroblasts (LIFs) into myofibroblast (MYFs) is a classical feature during bleomycin injury (Yuan et al., 2018). Fgf10, as one of the most important fibroblast growth factors during lung development binds with high affinity to Fgfr2b but has a lower affinity to Fgfr1b. During homeostasis, in adult lungs, Fgf10 is expressed in the mesenchymal niches between the cartilage rings where normally basal cells reside in the trachea and in the lipofibroblast or mesenchymal alveolar niche cells adjacent to AT2 cells in the alveoli. Whole lung *Fgf10* expression goes up after bleomycin injury due to the amplification of myofibroblasts yet on a per cell basis Fgf10 expression is reduced in myofibroblasts compared to the lipofibroblasts they are derived from (Yuan et al., 2019). It is possible that Fgf10 expressing mesenchymal alveolar niche lipofibroblasts express Fgfr1b and therefore, respond to Fgf10 signaling in an autocrine fashion. Future experiments will need to be designed to assess this (Al Alam et al., 2015).

MATERIALS AND METHODS

Contact for Reagent and Resource Sharing

Further information and requests for resources and reagents should be directed to and will be fulfilled by the Lead contact, SL (sdelanghe@uabmc.edu).

Experimental Model Details

All mice were bred and maintained in a pathogen-free environment with free access to food and water. Both male and female mice were used for all experiments. *Fgfr1*^{Cerulean} (JAX 030708), *Fgfr2*^{mCherry} (JAX 030710) (Molotkov et al., 2017) mice were obtained from Jackson laboratories and crossbred to homozygosity. For bleomycin injury, adult 8 week old mice were intratracheally instilled with 50 µl bleomycin (1U/kg body weight for females, and 0.8U/kg body weight for males) as previously described (Yuan et al., 2019). For naphthalene injury, adult 8 week old mice were intraperitoneally injected with naphthalene dissolved in corn oil (325 mg/kg body weight for males and 300 mg/kg body weight for females) as previously described (Volckaert et al., 2011). All experiments were approved by the University of Alabama at Birmingham Institutional animal care and use committee.

Immunohistochemistry and Fluorescence

All staining was done on paraffin sections of formalin-fixed lungs or tracheas. Immunofluorescent staining was performed with the following primary antibodies: goat anti-Scgb1a1 (1:200; clone T-18; sc-9772; Santa Cruz Biotechnology Inc.), rabbit anti-Scgb1a1 (1:500; WRAB-CCSP; Seven Hills Bioreagents), mouse anti-α-Actin (1:500; clone 1A4; sc-32251; Santa Cruz Biotechnology Inc.), chicken anti-GFP (1:250; GFP-1020; Aves Labs Inc.), rabbit anti-Keratin 5 (1:200; clone EP1601Y; MA5-14473; Thermo Fisher Scientific), chicken anti-Keratin 5 (1:500; clone Poly9059; 905904; BioLegend); rabbit anti-p63 (ΔN) (1:500; clone poly6190, 619002; BioLegend), 3862S; mouse anti-p63 (1:50; clone 4A4; CM163B; Biocare Medical), rabbit anti-RFP (1:200; 600-401-379; Rockland Immunochemicals Inc), mouse anti-RFP (1:200; sc-390909; Santa Cruz Biotechnology Inc.), rabbit anti-Sftpc (1:200; WRAB-9337; Seven hills bioreagents), mouse anti-Hop (1:100; Clone E-1; sc-398703; Santa Cruz Biotechnology Inc.), guinea pig anti-ADRP (Adipophilin) (1:200; 20R-AP002; Fitzgerald Industries), rabbit anti-Sox2 (1:1,000; WRAB-1236; Seven hills bioreagents), goat anti-Sox9 (1:500; AF3075; R&D systems), rabbit anti-CGRP (1:5,000; C8198; Sigma) and Mouse anti-Foxj1 (1:500, 14-9965-82, Invitrogen).

After deparaffinization, slides were rehydrated through a series of decreasing ethanol concentrations and antigens unmasked by either microwaving in citrate-based antigen unmasking solution (Vector Labs, H-3000) or by incubating sections with proteinase K (7.5 μg/ml) (Invitrogen, 25530-049) for 7 min at 37°C. Tissue sections were then washed in TBS with 0.1% Tween-20 and blocked with 3% bovine serum albumin (BSA), 0.4% Triton X-100 in Tris buffered saline (TBS) for 30 min at room temperature followed by overnight incubation of primary antibodies diluted in 3% BSA, 0.1% Triton X-100 in TBS. The next day, slides were washed in TBS with 0.1% Tween-20 and incubated with secondary antibodies diluted in 3% BSA, 0.1% Triton X-100 in TBS for 3h at room temperature. All fluorescent staining was performed with appropriate secondary antibodies from Jackson Immunoresearch, except for mouse anti-Hop (1:500; A-21125; Thermo Fisher Scientific). Slides were mounted using Vectashield with (Vector Labs, H-1200) or without DAPI (Vector Labs, H-1000) depending on immunostaining.

Microscopy and Imaging

Tissue was imaged using a micrometer slide calibrated Zeiss LSM800 Laser scanning confocal microscope using ZEN imaging software. Images were processed and analyzed using Zen blue and Adobe Photoshop software. Average immunostaining intensity was quantified after segmentation and thresholding for pixel intensity.

DATA AVAILABILITY STATEMENT

All datasets generated for this study are included in the article/ **Supplementary Material**.

ETHICS STATEMENT

All experiments were approved by the University of Alabama at Birmingham Institutional Animal Care and Use Committee.

AUTHOR CONTRIBUTIONS

TY designed and performed experiments, analyzed data, and wrote and edited the manuscript. KK performed experiments, analyzed data, and edited the manuscript. HL, JY, SG, and SH performed experiments. JZ edited the manuscript. SDL conceived and led the project, performed experiments, analyzed data, and wrote and edited the manuscript.

FUNDING

This study was supported by NIH R01 HL126732, HL132156, and HL146160 awards to SDL; and Cystic Fibrosis Foundation (CFF) YUAN19F0 awards to TY.

SUPPLEMENTARY MATERIAL

The Supplementary Material for this article can be found online at: https://www.frontiersin.org/articles/10.3389/fphar.2020.00120/full#supplementary-material

FIGURE S1 | Fgfr1, Fgfr2 and Scgb1a1 expression after naphthalene injury. Immunostaining on ctrl and naphthalene injured adult *Fgfr1-Cerulean;Fgfr2-mCherry* lungs for GFP (Fgfr1-Cerulean, green), RFP (Fgfr2-mCherry, red), Scgb1a1 (white).

FIGURE S2 | Fgfr1, Fgfr2 and Sftpc expression after bleomycin injury. Immunostaining on ctrl and bleomycin injured adult *Fgfr1-Cerulean;Fgfr2-mCherry* lungs for GFP (Fgfr1-Cerulean, green), RFP (Fgfr2-mCherry, red), Sftpc (white).

REFERENCES

Al Alam, D., El Agha, E., Sakurai, R., Kheirollahi, V., Moiseenko, A., Danopoulos, S., et al. (2015). Evidence for the involvement of fibroblast growth factor 10 in lipofibroblast formation during embryonic lung development. *Development* 142 (23), 4139–4150. doi: 10.1242/dev.109173

Balasooriya, G. I., Goschorska, M., Piddini, E., and Rawlins, E. L. (2017). FGFR2 is required for airway basal cell self-renewal and terminal differentiation. *Development* 144 (9), 1600–1606. doi: 10.1242/dev.135681

El Agha, E., Moiseenko, A., Kheirollahi, V., De Langhe, S., Crnkovic, S., Kwapiszewska, G., et al. (2017). Two-way conversion between lipogenic and myogenic fibroblastic phenotypes marks the progression and resolution of lung fibrosis. *Cell Stem Cell* 20261-273 (2), e263. doi: 10.1016/j.stem.2016.10.004

Jaskoll, T., Abichaker, G., Witcher, D., Sala, F. G., Bellusci, S., Hajihosseini, M. K., et al. (2005). FGF10/FGFR2b signaling plays essential roles during *in vivo* embryonic submandibular salivary gland morphogenesis. *BMC Dev. Biol.* 5, 11. doi: 10.1186/1471-213X-5-11

Lee, J. H., Tammela, T., Hofree, M., Choi, J., Marjanovic, N. D., Han, S., et al. (2017). Anatomically and functionally distinct lung mesenchymal populations marked by Lgr5 and Lgr6. *Cell* 1701149-1163 (6), e1112. doi: 10.1016/j.cell.2017.07.028

Li, R., Bernau, K., Sandbo, N., Gu, J., Preissl, S., and Sun, X. (2018). Pdgfra marks a cellular lineage with distinct contributions to myofibroblasts in lung maturation and injury response. *Elife* 7. doi: 10.7554/eLife.3686536865[pii]

MacKenzie, B., Korfei, M., Henneke, I., Sibinska, Z., Tian, X., Hezel, S., et al. (2015). Increased FGF1-FGFRc expression in idiopathic pulmonary fibrosis. *Respir. Res.* 16, 83. doi: 10.1186/s12931-015-0242-2

Molotkov, A., Mazot, P., Brewer, J. R., Cinalli, R. M., and Soriano, P. (2017). Distinct requirements for FGFR1 and FGFR2 in primitive endoderm development and exit from pluripotency. *Dev. Cell* 41511-526 (5), e514. doi: 10.1016/j.devcel.2017.05.004

Theelen, W. S., Mittempergher, L., Willems, S. M., Bosma, A. J., Peters, D. D., van der Noort, V., et al. (2016). FGFR1, 2 and 3 protein overexpression and molecular aberrations of FGFR3 in early stage non-small cell lung cancer. *J. Pathol. Clin. Res.* 2 (4), 223–233. doi: 10.1002/cjp2.51

Volckaert, T., Dill, E., Campbell, A., Tiozzo, C., Majka, S., Bellusci, S., et al. (2011). Parabronchial smooth muscle constitutes an airway epithelial stem cell niche in the mouse lung after injury. *J. Clin. Invest.* 121 (11), 4409–4419. doi: 10.1172/JCI58097

Volckaert, T., Campbell, A., and De Langhe, S. (2013a). c-Myc Regulates Proliferation and Fgf10 expression in airway smooth muscle after airway epithelial injury in mouse. *PloS One* 8 (8), e71426. doi: 10.1371/journal.pone.0071426PONE-D-13-13952[pii]

Volckaert, T., Campbell, A., Dill, E., Li, C., Minoo, P., and De Langhe, S. (2013b). Localized Fgf10 expression is not required for lung branching morphogenesis but prevents differentiation of epithelial progenitors. *Development* 140 (18), 3731–3742. doi: 10.1242/dev.096560

Volckaert, T., Yuan, T., Chao, C. M., Bell, H., Sitaula, A., Szimmtenings, L., et al. (2017). Fgf10-hippo epithelial-mesenchymal crosstalk maintains and recruits lung basal stem cells. *Dev. Cell* 4348-59 (1), e45. doi: 10.1016/j.devcel.2017.09.003

Volckaert, T., Yuan, T., Yuan, J., Boateng, E., Hopkins, S., Zhang, J. S., et al. (2019). Hippo signaling promotes lung epithelial lineage commitment by curbing Fgf10 and beta-catenin signaling. *Development* 146 (2). doi: 10.1242/dev.166454

Weiss, J., Sos, M. L., Seidel, D., Peifer, M., Zander, T., Heuckmann, J. M., et al. (2010). Frequent and focal FGFR1 amplification associates with therapeutically tractable FGFR1 dependency in squamous cell lung cancer. *Sci. Transl. Med.* 2 (62), 62ra93. doi: 10.1126/scitranslmed.3001451

Yuan, T., Volckaert, T., Chanda, D., Thannickal, V. J., and De Langhe, S. P. (2018). Fgf10 signaling in lung development, homeostasis, disease, and repair after injury. *Front. Genet.* 9, 418. doi: 10.3389/fgene.2018.00418

Yuan, T., Volckaert, T., Redente, E. F., Hopkins, S., Klinkhammer, K., Wasnick, R., et al. (2019). FGF10-FGFR2B signaling generates basal cells and drives alveolar epithelial regeneration by bronchial epithelial stem cells after lung injury. *Stem Cell Rep.* 12 (5), 1041–1055. doi: 10.1016/j.stemcr.2019.04.003

Conflict of Interest: The authors declare that the research was conducted in the absence of any commercial or financial relationships that could be construed as a potential conflict of interest.

frontiers in Pharmacology

ORIGINAL RESEARCH
published: 03 March 2020
doi: 10.3389/fphar.2020.00059

Non-Mitogenic Fibroblast Growth Factor 1 Enhanced Angiogenesis Following Ischemic Stroke by Regulating the Sphingosine-1-Phosphate 1 Pathway

Yuchi Zou[1†], Jian Hu[2†], Wenting Huang[3], Shasha Ye[2], Fanyi Han[2], Jingting Du[2], Mingjie Shao[3], Ruili Guo[2], Jingjing Lin[2], Yeli Zhao[2,4], Ye Xiong[1] and Xue Wang[1,2*]*

[1] The Frist Affiliated Hospital of Wenzhou Medical University, Wenzhou, China, [2] School of Pharmaceutical Sciences, Wenzhou Medical University, Wenzhou, China, [3] School of the First Clinical Medical Science, Wenzhou Medical University, Wenzhou, China, [4] Engineering Laboratory of Zhejiang Province for Pharmaceutical Development of Growth Factors, Biomedical Collaborative Innovation Center of Wenzhou, Wenzhou, China

OPEN ACCESS

Edited by:
Li Lin,
Wenzhou Medical University, China

Reviewed by:
Yu-Jie Fu,
Northeast Forestry University, China
Changhong Xing,
UT Southwestern Medical Center, United States
Ning Liu,
Tulane University, United States

***Correspondence:**
Ye Xiong
xiongye2310@163.com
Xue Wang
xinyuw001@163.com

[†]These authors have contributed equally to this work

Specialty section:
This article was submitted to Translational Pharmacology, a section of the journal Frontiers in Pharmacology

Received: 13 November 2019
Accepted: 22 January 2020
Published: 03 March 2020

Citation:
Zou Y, Hu J, Huang W, Ye S, Han F, Du J, Shao M, Guo R, Lin J, Zhao Y, Xiong Y and Wang X (2020) Non-Mitogenic Fibroblast Growth Factor 1 Enhanced Angiogenesis Following Ischemic Stroke by Regulating the Sphingosine-1-Phosphate 1 Pathway. Front. Pharmacol. 11:59. doi: 10.3389/fphar.2020.00059

Ischemic strokes account for about 80% of all strokes and are associated with a high risk of mortality. Angiogenesis of brain microvascular endothelial cells may contribute to functional restoration following ischemia. Fibroblast growth factor 1 (FGF1), a member of FGF superfamily, involved in embryonic development, angiogenesis, wound healing, and neuron survival. However, the mitogenic activity of FGF1 is known to contribute to several human pathologies, thereby questioning the safety of its clinical applications. Here, we explored the effects and mechanism of action of non-mitogenic FGF1 (nmFGF1) on angiogenesis in mice after ischemia stroke and an oxygen-glucose deprivation (OGD)-induced human brain microvascular endothelial cells (HBMECs) injury model. We found that intranasal administration nmFGF1 significantly promoted angiogenesis in mice after stroke, and significantly increased the formation of matrigel tube and promoted scratch migration in a dose-dependent manner in OGD-induced HBMECs *in vitro*. However, the co-administration of an FGF receptor 1 (FGFR1)-specific inhibitor PD173074 significantly reversed the effects of nmFGF1 *in vitro*, suggesting that nmFGF1 functions *via* FGFR1 activation. Moreover, nmFGF1 activated sphingosine-1-phosphate receptor 1 (S1PR1, S1P1) in mice after stroke *in vivo*. S1P1 protein antagonist VPC23019 and agonist FTY720 were used to confirm that nmFGF1 promotes angiogenesis *in vitro* partially through the S1P1 pathway. OGD induced downregulation of S1P1 expression. The S1P1 antagonist VPC23019 blocked the stimulatory effects of nmFGF1, whereas the S1P1 agonist FTY720 exerted effects comparable with those of nmFGF1. Furthermore, PD173074 reversed the effect of nmFGF1 on upregulating S1P1 signaling. In conclusion, nmFGF1 enhanced angiogenesis in mice following stroke and OGD-induced HBMECs through S1P1 pathway regulation mediated *via* FGFR1 activation.

This new discovery suggests the potential therapeutic role of nmFGF1 for the treatment of ischemic strokes.

Keywords: ischemic stroke, nmFGF1, angiogenesis, migration, S1P1 pathway

INTRODUCTION

Neurological disorders are the leading cause of disability-adjusted life-years (DALYs) worldwide and the second leading cause of deaths following cardiovascular diseases. Stroke, a global health problem, was the largest contributor to global neurological DALYs in 2016, and ischemic stroke is known to account for about 80% of all stroke cases (Markus, 2011; GBD 2016 Neurology Collaborators, 2019). However, current therapeutic approaches for ischemia stroke include intravenous thrombolysis, surgical thrombectomy, and neuroprotection (Wang et al., 2019). Recombinant plasminogen activator (rtPA), as the only approved thrombolytic agent for the acute ischemic stroke treatment, can only be administrated up to 6 hours after stroke onset, and may enhance the risk of hemorrhagic transformation. Therefore, development of an effective therapeutic strategy for stroke is urgent.

Neurorestorative progression in stroke is characterized with neurogenesis, angiogenesis, and synaptic plasticity, and is beneficial for functional recovery after stroke (Gopurappilly et al., 2011; Chen et al., 2019a). Angiogenesis, the formation of new capillaries from the pre-existing blood vessels, is observed in the penumbra of brain infarct region in animal model following stroke and in the brain of patients with stroke (Ruan et al., 2015). In the early stages of ischemia, capillaries proliferate, and damaged cells release a various factors to enhance angiogenesis, thus resulting in the formation of new blood vessels and increase of cerebral blood perfusion (Arenillas et al., 2007; Wang et al., 2019), which considered as a defense system that restores nutrient and oxygen supplies to the ischemic brain tissue (Tomanek and Schatteman, 2000; Chen et al., 2019a; Kanazawa et al., 2019). However, endogenous ischemic tissue stimulated angiogenesis may not adequately compensate for the acute impaired circulation (Nariai et al., 1994; Wang et al., 2019). Therefore, angiogenesis promotion exogenously is a promising treatment strategy for ischemic stroke, thereby, facilitating survival of brain tissue following ischemia stroke.

Sphingosine-1-phosphate (S1P), a bioactive lysophospholipid, and its receptors (S1PR1-5) highly expressed in various system including vascular, immune, nervous, and reproductive systems (Hla, 2004; Sartawi et al., 2017). S1P receptor 1 (S1PR1, S1P1) signaling is essential in endothelial cells (ECs) and regulates sprouting angiogenesis. S1PR1 is induced in angiogenic ECs and plays an important role in vascular development (Liu et al., 2000; Jung et al., 2012). On the contrary, blocking S1P signaling *via* S1PR1 inhibition may provide a new direction for antiangiogenic therapy to treat tumors (Liu et al., 2019; Rostami et al., 2019). It has been previously demonstrated that S1P1 activation could alleviate brain injuries in experimental ischemia stroke models such as transient middle cerebral artery occlusion (MCAO) (Hasegawa et al., 2010) and neonatal hypoxia-ischemia (Zhou et al., 2010). S1PR1 modulators involved in S1P1 signaling pathway improve microvascular circulation after thrombosis and exert beneficial roles in cerebral ischemia (Li et al., 2019). The above evidences indicated S1P1 activation could be considered as a good candidate target for ischemia stroke treatment.

Fibroblast growth factor 1 (FGF1) is a member of the FGF family and regulates various cellular processes such as angiogenesis, cell migration, cell differentiation, wound healing, and tube formation *via* binding to FGF receptors and heparin sulfate proteoglycans (Cheng et al., 2011; Wu et al., 2017; Kerr et al., 2019). However, the mitogenic activity of FGF1 is known to contribute to metastasis and tumorigenesis (Cronauer et al., 2003; Li et al., 2007). In the present study, the effects of non-mitogenic FGF1 (nmFGF1) derived from the deletion of the N terminal residues 1–27 of the full length wild-type FGF1 were investigated in an oxygen-glucose deprivation (OGD)-induced human brain microvascular endothelial cell (HBMECs) injury model and an ischemia and reperfusion-injured MCAO mouse model. Previous studies have demonstrated that FGF1 could induce neurogenesis and angiogenesis in rats after ischemic stroke (Cheng et al., 2011) and rescue hippocampal neurons from apoptotic death induced by ischemia (Cuevas et al., 1998). However, the mechanism underlying the action of FGF1 on angiogenesis is yet unclear. Here, we investigated whether exogenous nmFGF1 administration could promote angiogenesis through the S1P1 signaling pathway.

MATERIALS AND METHODS

Reagents and Antibodies

NmFGF1 was produced in *Escherichia coli* and purified to be endotoxin free as previously described (Wu et al., 2005). The FGFR1-specific inhibitor PD173074 was purchased from Abcam (Cambridge, MA, USA). S1P1 antagonist VPC23019 was purchased from Cayman Chemical (Ann Arbor, MI). The primary antibodies applied in this study including anti-FGFR1 (No. ab824), anti-p-FGFR1 (No. ab59194), anti-S1P1 (No. ab11424), anti-CD31 (No. ab28364), and anti-β-Actin (No. ab8227) were purchased from Abcam (Cambridge, MA, USA), and anti-FGF1 (No. BM5544) was obtained from Bosterbio (Pleasanton, CA, USA). The secondary antibody used were goat anti-rabbit IgG H&L (HRP) (No. ab6721), and Alexa Fluor ®488-conjugated donkey anti-rabbit (No. ab150073) which were also purchased from Abcam (Cambridge, MA, USA). 3-(4,5-dimethylthiazol-2-yl)-2,5-diphenyl-tetrazolium bromide (MTT) and S1P1 agonist FTY720 were purchased from Sigma-Aldrich (St. Louis, MO, USA). EBM-2 medium was purchased from Lonza (Hopkinton, MA, USA). Matrigel

matrix was obtained from Corning Inc (Tewksbury, MA, USA). All other chemicals were of analytical-reagent grade.

Animals Grouping and Drug Administration

The experiments were conducted with male C57BL/6N mice (20–25 g), which were purchased from the Animal Center of the Chinese Academy of Sciences (Beijing, China). The animal use and care protocol conformed to the Guide for the Care and Use of Laboratory Animals from the National Institutes of Health and was approved by the Animal Care and Use Committee of Wenzhou Medical University.

After MCAO, the mice were randomly divided into two groups, mice subjected to MCAO treated with saline (MCAO + vehicle group) and nmFGF1 treatment MCAO-induced mice (MCAO + nmFGF1 group). For MCAO + nmFGF1 group, nmFGF1 was intranasally administrated at a dose of 0.75 mg/kg, followed by MCAO surgery. NmFGF was intranasally administrated once daily for 10 consecutive days, then the brain of animals were prepared for further immunofluorescence analysis (**Figure 1A**).

Transient Focal Cerebral Ischemia and Reperfusion Model Preparation

A transient focal cerebral ischemia mouse model was generated by MCAO followed by reperfusion, as previously reported (Zhang et al., 2017) with minor modifications. Briefly, the mice were anesthetized by isoflurane, and a surgical incision was made in the midline neck. The common carotid artery (CCA), external carotid artery (ECA), and internal carotid artery (ICA) were carefully separated and ligated. An appropriate nylon monofilament for MCAO (Guangzhou Jialin Co., Ltd, Guangzhou, China) coated with 1% poly-L-lysine was inserted from the right ECA to ICA and gently advanced to the origin of the middle cerebral artery (MCA) until some resistance occurred after the movement of the nylon monofilament. The nylon monofilament was gently removed after 1 hour of occlusion to allow reperfusion. During surgery, the regional cerebral blood flow (CBF) was measured by Laser-Doppler flowmetry (Perimed, Jarfalla, Sweden) based on the previous study (Jiang et al., 2016; Wang et al., 2018). And the mice that did not show a significant CBF reduction of at least 75% of baseline levels after MCA occlusion, or that died after ischemia stimulation or reperfusion excluded from further experimental study.

Immunofluorescence Analysis

To evaluate cell proliferation, 5-ethynyl-2-deoxyuridine (EdU) labeling was performed using BeyoClickTM EdU-488 kit (C0071S, Beyotime, Shanghai, China) according to the manufacturer's protocol. From day 6 to day 10, all groups of mice were treated with EdU [50 mg/kg intraperitoneal (i.p.) injection in saline] once daily for 4 consecutive days. After 4 hours, the mice were transcardially perfused with ice-cold phosphate-buffered saline (PBS; 0.1 M), followed by 4%

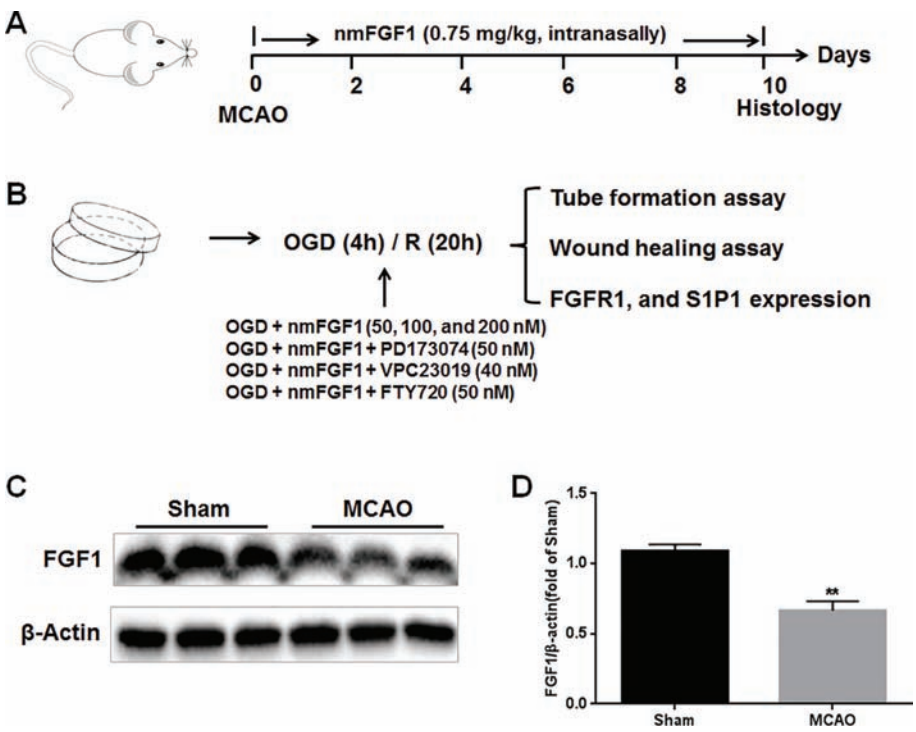

FIGURE 1 | Illustration of experimental procedure. **(A)** Schematic illustration of animal experimental timeline showing the duration exogenous non-mitogenic fibroblast growth factor 1 (nmFGF1) administration after middle cerebral artery occlusion (MCAO) in adult mice and analysis. **(B)** Schematic illustration of cell experimental procedure after oxygen-glucose deprivation (OGD)/R and analysis. **(C)** Representative bands of endogenous FGF1 expression detected by western blot. **(D)** Densitometric analysis for the protein expression of FGF1. Data are expressed as means ± SEM (n = 5). **p < 0.01.

paraformaldehyde (dissolved in PBS). The brains were quickly excised for immunofluorescence staining. EdU staining was assessed with immunofluorescence.

Immunofluorescence staining was used to detect microvessel density. The whole brain tissue was post-fixed with 4% paraformaldehyde for 12 hours, embedded in paraffin, and cut into sections (5 μm thickness), followed by mounting on slides. The sections were treated with a primary antibody against CD31 (1:500 dilution) overnight at 4°C and then washed thrice with PBST at an interval of 5 minutes, followed by incubated with Alexa Fluor 488 or Alexa Fluor 647 donkey anti-rabbit/goat secondary antibodies (1:1000) for 1 hour at room temperature. Nuclear staining was performed with 4′,6-diamidino-2-phenylindole (DAPI) for 5 minutes. The stained sections were stored at 4°C. The immunostained sections were observed and imaged using a Nikon ECLPSE 80i fluorescence microscope (Nikon, Tokyo, Japan). Image-Pro plus 6.0 software (Bethesda MD, USA) was applied to analyze the images as previously described (Jiang et al., 2016). In brief, the density of the new blood vessel (EdU^+ cells), blood vessel ($CD31^+$ cells), or $S1P1^+$ cells were automatically counted from three microscopic field randomly chosen from the peri-infarct regions in each three section from four animals of each group.

HBMECs Culture and Treatment

HBMECs were purchased from Cell Systems Corporation (ACBRI376, Kirkland, WA, USA) and cultured in complete growth EBM-2 Medium with 10% FBS and penicillin/streptomycin (100 U/ml) in an atmosphere containing 5% CO_2 at 37°C. To assess the effects of nmFGF1 on OGD-induced HBMECs and the possible underlying mechanisms, the cells were divided into the following groups: control group, OGD treatment group, OGD+nmFGF1-treated group, and OGD+nmFGF1 +PD173074-treated group, OGD+nmFGF1+VPC23019-treated group, or OGD+nmFGF1+FTY720-treated group.

Control group is the HBMECs monolayers culture without OGD/R treatment. For the OGD/R treatment, the protocol was performed as described previously (Lin et al., 2018; Chen et al., 2019b). In brief, HBMECs cultured EBM-2 media were replaced with glucose free DMEM media, and then the cells cultured dish or plates were put in a specialized, humidified chamber (Heidolph, incubator 1000, Brinkmann Instruments, Westbury, NY) at 37°C, which contained an anaerobic gas mixture (90% N_2, 5% H_2, and 5% CO_2), for 20 minutes to ensure anaerobic conditions, and for a further 4 hours incubation. Reperfusion was started by removing the culture dish or plates from the anaerobic chamber, and replacing the OGD medium with EBM-2 complete medium. Then the cells were allowed to reoxygenate in a regular incubator for 20 hours before further analysis. For nmFGF1-treated group, the cells were exposure to nmFGF1 containing medium with final concentration of 50, 100, and 200 nM during OGD/R. For OGD+ nmFGF1+PD173074-treated group, OGD+nmFGF1+VPC23019-treated group, or OGD +nmFGF1+FTY720-treated group, the cells were co-treated with nmFGF1 and PD173074 (50 nM), VPC23019 (40 nM), and FTY720 (50 nM) during OGD/R, respectively. Then these cells were applied for tube formation and wound healing assay. To explore the underlying mechanism of action, the FGFR1 and S1P1 expression level was assessed by western blot (**Figure 1B**).

Cell Viability Assay

MTT assay was performed to determine cell viability as described previously (Huang et al., 2019). Briefly, HBMECs (1×10^4 cells/well) were seeded in 96-well plates in complete growth EBM-2 medium and cultured overnight. After treatment, the medium was replaced with fresh medium containing 0.5 mg/ml MTT. After 3-hour incubation at 37°C, the medium was removed, followed by the formazan crystals dissolved in dimethyl sulfoxide. The absorbance was measured at 570 nm by a microplate reader with a reference setting of 630 nm.

Tube Formation Assay

Tube formation is a classical *in vitro* model to assess the angiogenesis (Lu et al., 2019). To assess the effect of nmFGF1 on the angiogenic capacity of OGD-treated HBMECs, the tube formation assay was performed as described previously (Huang et al., 2019). In brief, Matrigel matrix was thawed at 4°C and added into each wells of a 48-well plate, and the plate was incubated 30 minutes to allow Matrigel solidification. The treated cells were seeded in the above Matrigel-coated plate (6×10^4 per well) triplicate, and incubated in a 37°C incubator for 16 hours, after which the number of tubes in two random fields from each well was counted under a bright field microscope.

Wound Healing Assay

Wound healing assay used to evaluate cell migration across a scratch gap *in vitro*, is also a classical *in vitro* model of angiogenesis (Lu et al., 2019). After OGD/R treatment, the smooth scratches was made perpendicular to the well plate by a 10 μl pipette tip, and the width of each scratch wound should be as close to identical as possible. Afterward, the treated cells were cultured in medium with 1% FBS for further 16 hour incubation. Bright field images of migration were taken and compared with images of the cells before scratching. The relative migration distance was quantified by ImageJ software. The value of gap closure was calculated by the following equation: % of gap closure = $(W_0-W_n)/W_0\times\%$, where W_0 is the gap width at 0 hour, and W_n is the gap width at 16 hours. Data were acquired from three independent experiments with each condition performed in triplicate.

Western Blot Analysis

Ipsilateral hemisphere after MCAO with 1 hour reperfusion and HBMECs were lysed and proteins were extracted with RIPA lysis buffer (R0278, Sigma-Aldrich, St. Louis, MO, USA)) with 1% protease and phosphatase inhibitor cocktail (P1261, Solarbio, Beijing, China) at 4°C. The supernatant was collected after cell lysate centrifuge, and the protein concentration was measured by a Bradford Protein Assay Kit. An equivalent amount of protein (80 μg) was separated on 12% SDS-PAGE and transferred to PVDF membranes. The membranes were blocked with 5% nonfat milk at room temperature for 1 hour and were then blocked with primary antibodies, including those targeting FGFR1 (1:500), p-FGFR1 (1:500), S1P1 (1:1000), FGF1 (1:1000), and β-

actin (1:1000), and then incubated with goat anti-rabbit IgG secondary antibody (1:10000). Finally, the immunolabeling was detected by an enhanced chemiluminescence (ECL; GE Healthcare) detection system according to the manufacturer's instruction. The intensity of the bands was quantified using Image Lab 3.0 software (Bio-Rad, Hercules, CA, USA).

Statistical Analysis

The results are expressed as mean ± SEM. Three or more replicates were performed for each experiment. Statistical differences among data from multiple groups were analyzed by one-way ANOVA followed by Tukey's posttest using GraphPad Prism 7 (GraphPad Software, San Diego, CA, USA). $P < 0.05$ was considered statistically significant.

RESULTS

nmFGF1 Promoted Angiogenesis in Ischemic Boundary Following Ischemia and Reperfusion

To evaluate the effects of exogenous FGF1 on angiogenesis after ischemia stroke, we firstly assessed the changes of endogenous FGF1 expression after MCAO by western blot analysis. As the result shown, the expression level of endogenous FGF1 was significantly reduced after MCAO with 1 hour reperfusion. (**Figures 1C, D**).

EdU was intraperitoneally injected to mark proliferating cells, while CD31 was used as a marker of vessels. EdU- and CD31-immunoreactive cells are defined as markers of angiogenesis. To assess the effect of nmFGF1 on angiogenesis, the number of EdU-positive cells and vessel-associated EdU-positive cells was detected in peri-infarct corpus callosum at 10 days after reperfusion (**Figure 2A**). The number of EdU-positive cells (**Figures 2B, C**) and vessel-associated EdU-positive cells (**Figures 2B, D**) was significantly higher in nmFGF1 administration group than in MCAO + vehicle group. Vascular density was evaluated with CD31 immunofluorescence analysis. Quantitative analysis of CD31 labeling revealed that the number of vessels in the boundary region of ischemia at 10 days after reperfusion was significant higher in the mice treated with nmFGF1 than in those from MCAO + vehicle group (**Figures 2E, F**).

nmFGF1 Promoted Angiogenesis *via* S1P1 Pathway Regulation

S1P signaling *via* the cell surface receptor S1P1 is involved in several physiological processes, including angiogenesis, cell survival, and cell proliferation (Reinhard et al., 2017; Xie et al., 2017). nmFGF1 may enhance angiogenesis following stroke *via* S1P1 activation; hence, we evaluated the effect of nmFGF1 on S1P1 expression in peri-infarct corpus callosum at 10 days after reperfusion (**Figure 3A**). In comparison with the vehicle-treated MCAO-induced mice, the intranasal administration of nmFGF1-treated MCAO-induced mice showed a significant

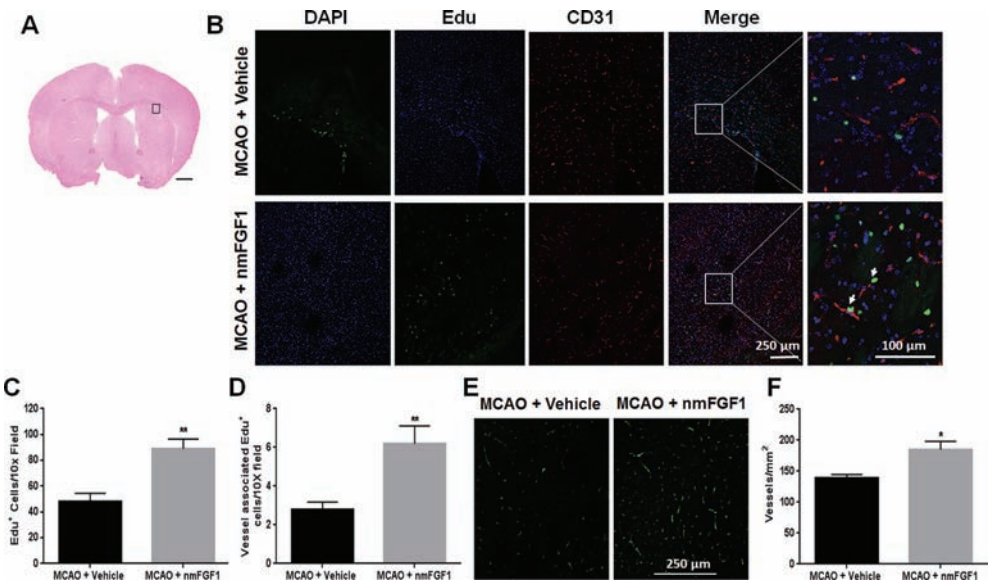

FIGURE 2 | Non-mitogenic fibroblast growth factor 1 (nmFGF1) promoted angiogenesis in ischemic boundary following ischemia stroke. **(A)** A representative image of hematoxylin-eosin (HE) staining in a coronal brain section at 10 days after middle cerebral artery occlusion (MCAO). Box illustrates the peri-infarct areas from the corpus callosum where images in B were taken. **(B)** Representative immunofluorescence images of DAPI and EdU staining along with the staining for the vascular endothelium marker CD31 at 10 days after stroke. **(C)** Quantitative analysis of EdU- labeled cells in ischemic boundary following stroke. **(D)** Quantitative analysis of $EdU^+/CD31^+$ co-labeled cells in ischemic boundary following stroke. **(E)** Representative fluorescence image for vascular density analysis following staining with CD31 at 10 days after stroke. **(F)** Quantitative analysis of vascular density by CD31 labeling. Data are expressed as means ± SEM (n = 5). *p < 0.05 and **p < 0.01 as compared with the MCAO + vehicle group.

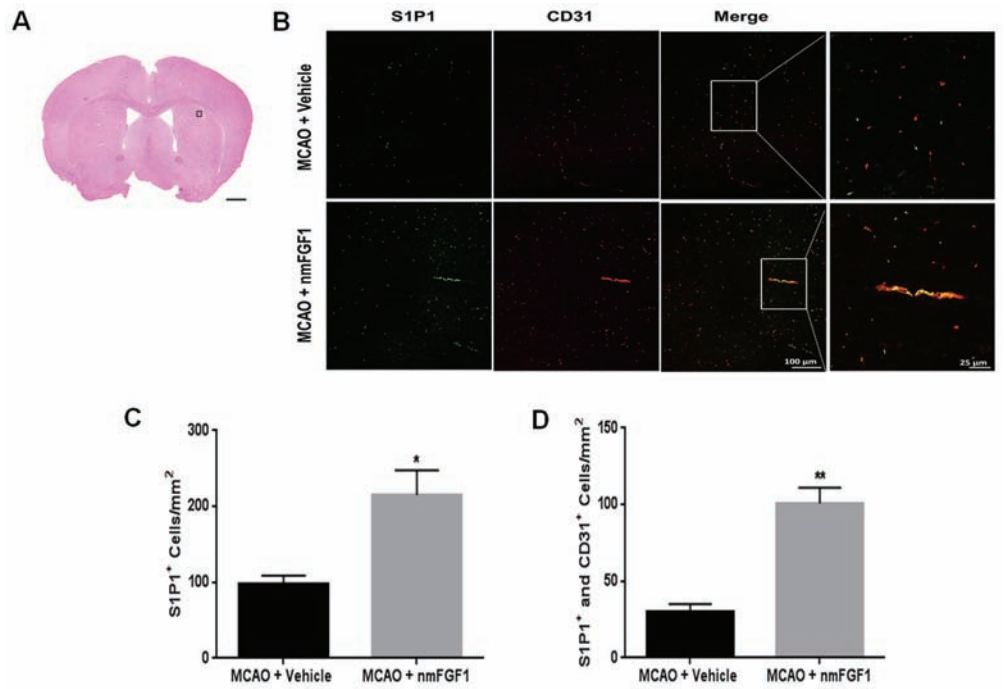

FIGURE 3 | Non-mitogenic fibroblast growth factor 1 (nmFGF1) enhanced angiogenesis in ischemic boundary following ischemia stroke by S1P1 signaling pathway. **(A)** A representative image of HE staining in a coronal brain section at 10 days after middle cerebral artery occlusion (MCAO). Box illustrates the peri-infarct areas from the corpus callosum where images in B were taken. **(B)** Representative immunofluorescence images showing the co-localization of S1P1 and CD31 at 10 days after stroke. **(C)** Quantitative analysis of S1P1-positive cells in ischemic boundary following stroke. **(D)** Quantitative analysis of co-localization of S1P1 and CD31 at 10 days after stroke. Date are means ± SEM (n = 5). *p < 0.05, and **p < 0.01 as compared to the middle cerebral artery occlusion (MCAO) + vehicle group.

regulatory effect on the expression of S1P1 after 10 days (**Figures 3B, C**). The number of S1P1- and CD31-positive vascular ECs was markedly higher in these mice than in the vehicle-treated mice (**Figures 3B, D**). These results indicate nmFGF1 promoted angiogenesis through the activation of the S1P1 signaling pathway following stroke.

nmFGF1 Enhanced Tube Formation and Wound Healing of HBMECs After OGD

To confirm our hypothesis that nmFGF1 promotes angiogenesis after stoke, OGD/R-induced HBMECs were used. We tested whether nmFGF1 imparts protection against OGD/R-induced cytotoxicity by assessing the viability of HBMECs with the MTT assay. To induce OGD/R, HBMECs were subjected to OGD for 4 hours, followed by 20 hours of reoxygenation treatment. In nmFGF1 treatment group, HBMECs were exposed to nmFGF1 at 50, 100, and 200 nM concentrations during OGD/R. The effect of nmFGF1 (100 nm) on cell proliferation and tube formation under normal oxygen conditions was also assessed. As a result, we found that 100 nM nmFGF1 had no effect on cell proliferation under normal oxygen conditions, and OGD/R exhibited no significant effects on cell viability. nmFGF1 at 50, 100, and 200 nM concentrations did not markedly change the viability of cells under OGD conditions (**Figure 4A**), indicating that the protective effect of nmFGF1 on cell angiogenesis after OGD/R was not mediated through an increase in cell viability.

To elucidate the effect of nmFGF1 on angiogenesis after OGD, tube formation assay was performed. The results demonstrate that nmFGF1 at a dose of 100 nm significantly increased the number of tubes and tubular structures as compared with the control group comprising cells cultured under normal conditions (complete medium). However, OGD-induced HBMECs showed lower angiogenic capacity than the control cells. Interestingly, nmFGF1 at 100, and 200 nM could markedly rescue the angiogenesis of HBMECs after OGD, while low dose (50 nM) nmFGF1 treatment failed to impart obvious protection (**Figure 4B**). Quantitative analysis revealed that nmFGF1 (100 and 200 nM) significantly increased the tube formation ability of HBMECs with similar angiogenesis efficacy (**Figure 4C**).

EC migration is another classical method for vascular angiogenesis assessment. The effects of nmFGF1 at different concentrations (50, 100, and 200 nM) on cell migration were analyzed by the scratch wound healing assay. As a result, nmFGF1 at a dose of 100 nm could significantly increase EC migration as compared with the control treatment. While OGD condition induced migration defects, nmFGF1 (100 and 200 nM) treatment could obviously facilitate wound healing. Quantitative analysis revealed that 100 and 200 nM nmFGF1 exerted similar effects; however, 50 nM nmFGF1 had no significant effects on cell migration (**Figures 4D, E**). Based on the above results, 100 nM nmFGF1 was used in the subsequent experiment to study the underlying mechanism of action.

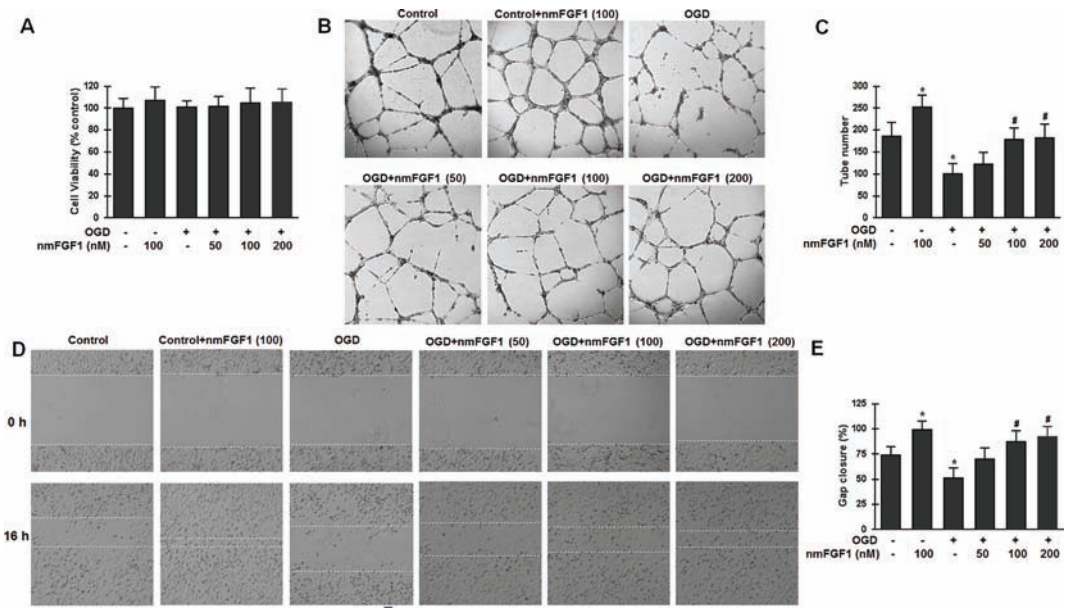

FIGURE 4 | Non-mitogenic fibroblast growth factor 1 (nmFGF1) enhanced angiogenesis and wound healing in oxygen-glucose deprivation (OGD)-exposed HBMECs without affecting viability. **(A)** OGD and three concentrations of nmFGF1 (50, 100, and 200 nm) had no effect on cell viability. **(B)** Representative images to study the effect of OGD exposure and nmFGF1 treatment on tube formation ability of cells. **(C)** Quantification of the effects of nmFGF1 on the number of capillary-like tubes in OGD-treated cells. **(D)** Representative images to study the effect of nmFGF1 on wound healing in OGD-stimulated cells. **(E)** Quantification of the effects of nmFGF1 on wound closure in OGD-treated cells. Date are expressed as means ± SEM (n = 6). *p < 0.05 as compared to the control group, #p < 0.05 as compared to the OGD-treated group.

nmFGF1 Induced Angiogenesis in HBMECs After OGD *via* Activation of FGFR1 Signaling

FGFs and their receptors (FGFRs) are critical in many biological processes, including angiogenesis, wound healing, and tissue regeneration (Sun et al., 2017; Xue et al., 2018). To investigate whether FGFR1 signaling is involved in angiogenesis mediated by nmFGF1 in HBMECs after OGD, cells were treated with the combination of FGFR1 inhibitor PD173074 (10 nM) and nmFGF1, and the activation of FGFR1 was detected by measuring the phosphorylation of FGFR1 (p-FGFR1) using western blotting. As a result, we found that the ratio of p-FGFR1/FGFR1 was not changed after OGD treatment; however, nmFGF1 significantly upregulated the ratio of p-FGFR1/FGFR1. As expected, PD173074 prevented the increase in the ratio of p-FGFR1/FGFR1 (**Figures 5A, B**).

We also assessed angiogenesis and migration ability and found that PD173070 administration alone had no effects on the tube formation ability of HBMECs under normal culture conditions. On the other hand, 100 nM nmFGF1 treatment significantly improved the tube formation ability of OGD-induced cells, while cotreatment with nmFGF1 and PD173074 significantly suppressed this proangiogenic effect. PD173074 alone had no effect on angiogenesis of OGD-induced cells (**Figures 5C, D**). Consistent with the effect of nmFGF1 on HBMECs tube formation ability, treatment with 100 nM nmFGF1 significantly promoted HBMECs migration, which was significantly suppressed in the presence of PD173074; however, PD173074 alone had no effect on cell migration (**Figures 5E, F**). These results suggest that the protective effects of nmFGF1 on tube formation and wound healing of OCD-induced HBMECs could be dependent on FGFR1 signaling activation.

nmFGF1 Induced Angiogenesis in HBMECs After OGD/R by Upregulating S1P1 Expression

To confirm whether S1P1 is necessary to mediate the angiogenesis effects of nmFGF1 on HBMECs, the cells were treated with the S1P1-specific inhibitor VPC23019 (40 nM) and agonist FTY720 (50 nM) in the presence of nmFGF1 during OGD/R (Lin et al., 2018), and tube formation and scratch wound healing assays were performed. The results show that VPC23019 and FTY720 administration alone had no effect on the tube number in control cells. While VPC23019 treatment alone failed to affect the tube formation ability of HBMECs subjected to OGD/R, the treatment with FTY720 markedly enhanced the number of tubes. VPC23019 significantly inhibited the tube formation ability of nmFGF1 in HBMECs during OGD/R, and FTY720 in combination with nmFGF1 increased the number of tubes (**Figures 6A, B**).

We examined the wound healing ability of cells after treatment with VPC23019 and FTY720. While nmFGF1 significantly promoted the migration of OGD/R-induced cells in the scratch wound healing assay, VPC23019 obviously

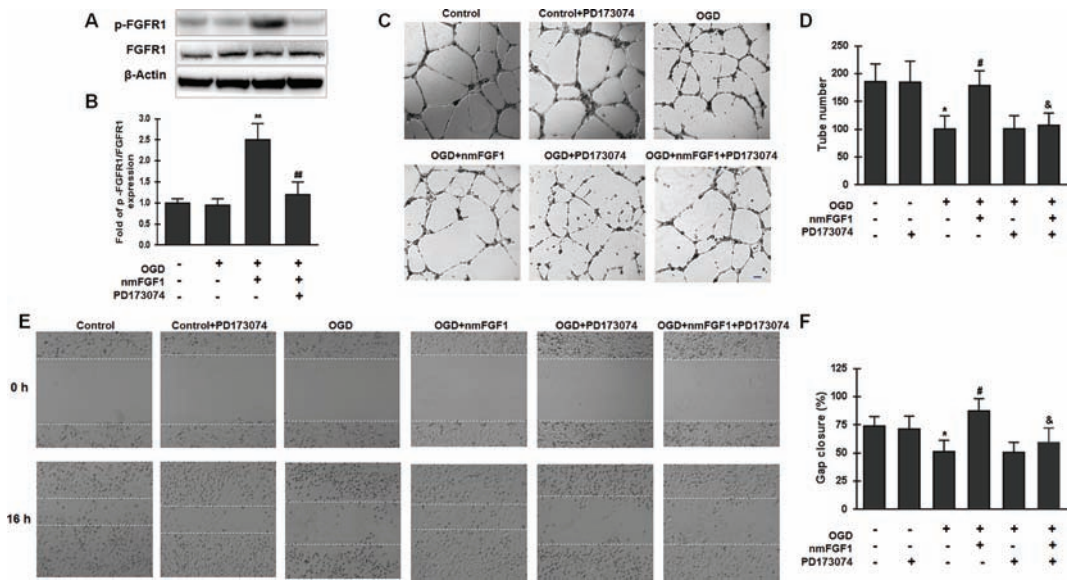

FIGURE 5 | Non-mitogenic fibroblast growth factor 1 (nmFGF1) promoted angiogenesis through FGFR1 activation. **(A)** Representative image of western blot analysis for FGFR1 and p-FGFR1 expression. **(B)** Quantification of relative protein levels of p-FGFR1 and FGFR1. **(C)** Representative images for the analysis of the effects of cotreatment with the FGFR1 inhibitor PD173074 and nmFGF1 (100 nM) on tube formation ability of oxygen-glucose deprivation (OGD)-treated HBMECs. **(D)** Quantification of the effects of nmFGF1 and PD173074 cotreatment on the number of capillary-like tubes in OGD-treated cells. **(E)** Representative images showing the effects of PD173074 and nmFGF1 (100 nM) co-administration on wounding healing in OGD-stimulated cells. **(F)** Quantification of the effects of PD173074 and nmFGF1 (100 nM) co-administration on gap closure in OGD-treated cells. Date are means ± SEM (n = 6). *$p < 0.05$ compared to control group, $^{\#}p < 0.05$ as compared to the OGD-treated group, $^{\&}p < 0.05$ as compared to the nmFGF1 treated group.

reversed this effect. S1P1 agonist FTY720 alone or in combination with nmFGF1 significantly increased the migration ability of cells. VPC23019 alone had no significant effects on the migration of HBMECs in both normal conditions and OGD/R environment (**Figures 7A, B**). These results suggest that nmFGF1 could rescue the OGD/R-induced S1P1 downregulation to enhance the tube formation and migration abilities of HBMECs under OGD/R conditions.

nmFGF1 Rescued the OGD/R-Induced Downregulation of S1P1 Mediated by FGFR1 Activation

S1P signaling through its cell surface receptor S1P1 is involved in several physiological processes, including angiogenesis, cell survival, and cell proliferation (Reinhard et al., 2017; Xie et al., 2017). We investigated whether nmFGF1 affects S1P1 expression. HBMECs were subjected to OGD for 4 hours and reoxygenation for 4 hours, and were simultaneously treated with nmFGF1. The protein expression of S1P1 was measured with western blotting. As a result, we found that S1P1 protein level was significantly suppressed by OGD/R. However, nmFGF1 administration obviously rescued S1P1 expression (**Figures 8A, B**). Moreover, FGFR1-specific inhibitor PD173074 markedly reversed the nmFGF1-mediated increase in S1P1 expression level (**Figures 8A, B**). This result suggests that nmFGF1 upregulates S1P1 expression through FGFR1 activation.

DISCUSSION

Angiogenesis is the formation of new microvessels from the pre-existing vessels (Ruan et al., 2015; Hatakeyama et al., 2020). Stroke is the primary cause of disability, owing to the limited ability to restore the damaged brain tissue (Nih et al., 2018; Rust et al., 2019). After ischemia stroke injury, inflammatory response coupled with limited angiogenesis and neuronal growth leads to functional deficits. A model of cerebral ischemia-reperfusion was established to investigate the pathophysiology of stroke. MCAO model is widely used for the induction of focal cerebral ischemia (Cotrina et al., 2017). OGD serves as an experimental approach to replicate ischemic stroke (Chen et al., 2019a). Angiogenesis is essential for brain tissue repair following ischemia stroke, as it may increase blood flow containing oxygen and metabolic nutrients to reach the affected brain regions (Hatakeyama et al., 2020). Several studies have focused on angiogenic therapy development for the recovery of injured brain following ischemia. In the current study, we explored the effects of nmFGF1 on angiogenesis in an MCAO ischemia mouse model and OGD-induced HBMECs *in vitro*. We found that nmFGF1 improved the angiogenesis in cerebral ischemia mice at day 10 after MCAO. We also demonstrate that nmFGF1 promoted angiogenesis and wound healing in OGD-induced HBMECs. In addition, we show for the first time that the angiogenesis effects of nmFGF1 were abolished by FGFR1- and S1P1-specific inhibitor, indicating that these effects were mediated through the activation of S1P1 signaling pathway and FGFR1.

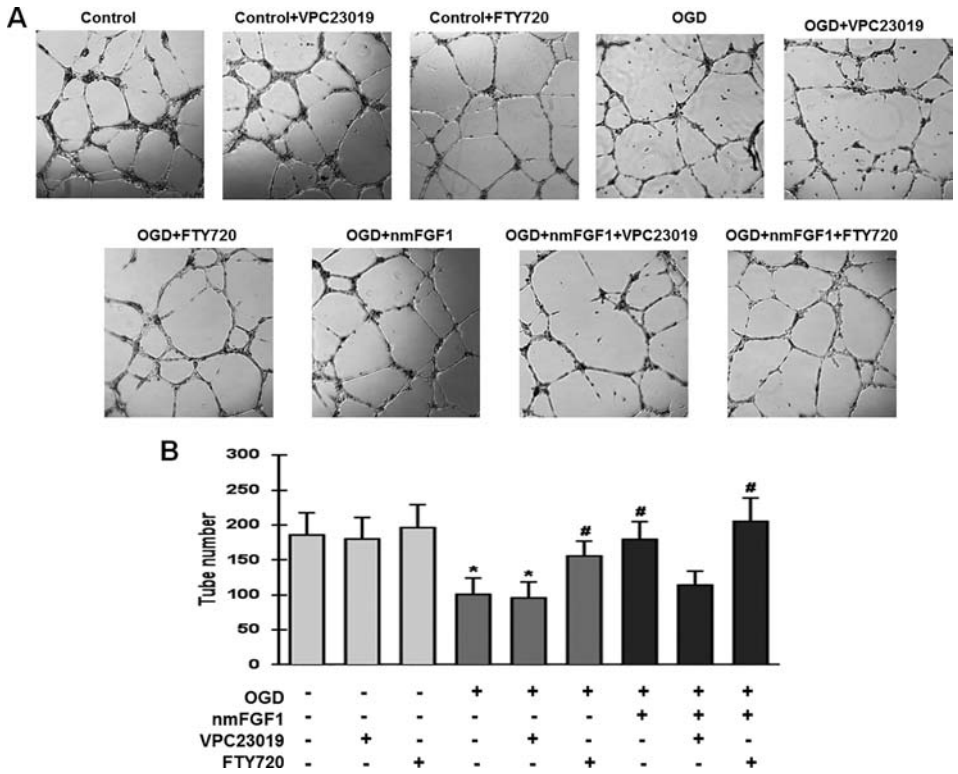

FIGURE 6 | Non-mitogenic fibroblast growth factor 1 (nmFGF1) promoted angiogenesis of oxygen-glucose deprivation (OGD)-exposed HBMECs *via* S1P signaling pathway. **(A)** Representative images showing the tube formation ability of OGD-exposed cells treated with the S1PR1 inhibitor VPC23019 (40 nM) and agonist FTY720 (50 nM) in the presence or absence of nmFGF1. **(B)** Quantification of the effects of the S1P1 inhibitor VPC23019 (40 nM) and agonist FTY720 (50 nM) in the presence or absence of nmFGF1 on tube formation ability. Date are means ± SEM (n = 6). *$p < 0.05$ as compared to the control group, $^{\#}p < 0.05$ as compared to the OGD-treated group.

FGF1 is unable to freely cross the brain upon systemic administration because of its filtration by the blood-brain barrier (BBB). However, intranasal administration may facilitate its direct entry into the central nervous system without exerting any adverse effects (Cheng et al., 2011). Previous studies have shown that the intranasal administration of FGF1 could enhance angiogenesis after stroke (Cheng et al., 2011). However, the mitogenic activity of FGF1 may contribute to several pathologies or metastasis and tumorigenesis (Cronauer et al., 2003; Li et al., 2007). For the safe application of FGF1, we applied nmFGF1 to mice after stroke and HBMECs after OGD/R. As expected, nmFGF1 treatment could enhance angiogenesis after ischemia injury in mice and promote angiogenesis and wound healing in OGD/R-induced HBMECs.

Although several studies have reported the protective effects of FGF1 on angiogenesis, the underlying mechanism of action on angiogenesis is unclear. FGFR1 is expressed in the brain (Wang et al., 2017; Huang et al., 2019), and its activation may protect the BBB in OGD/R-induced HBMECs (Lin et al., 2018). Cotreatment with the FGFR1 inhibitor PD173074 reversed the positive effects of nmFGF1 on migration and angiogenesis, indicating that FGFR1 activation induced migration and angiogenesis of HBMECs stimulated with OGD/R. In addition, S1P and its five receptors (S1PR1-5) are widely expressed in several systems, including the vascular, nervous, and reproductive system (Sartawi et al., 2017). S1P signaling pathway has been implicated in angiogenesis and is required for vascular stabilization. Dysfunction in the S1P-S1PR signaling pathway induces various vascular defects (Fischl et al., 2019; Obinata and Hla, 2019). The temporal profile of changes of the S1P1 expression in the early phase after transient MCAO was documented by Hasegawa et al. (2013), that the expression of S1P1 was significantly decreased in the infarct cortex but preserved in the peri-infarct cortex at 24 hours after MCAO. It has been reported that S1P1 expression on ECs of leptomeningeal arteries and capillaries upregulated early after permanent MCAO, peaking at 6 hours, whereas a significant increase in the expression of S1P1 in neurons was observed from 24 hours later (Iwasawa et al., 2018). S1PR modulators exerted protective effects in preclinical and clinical studies following ischemic stroke. In addition, these agents may improve microvascular circulation in cerebral ischemia (Lin et al., 2018). It has been reported that S1P1 agonist LAS1238 significantly reduced infarct volume of mice model after ischemia/reperfusion, indicating S1P1 is potential target for ischemic stroke treatment (Brait et al., 2016). Besides, a

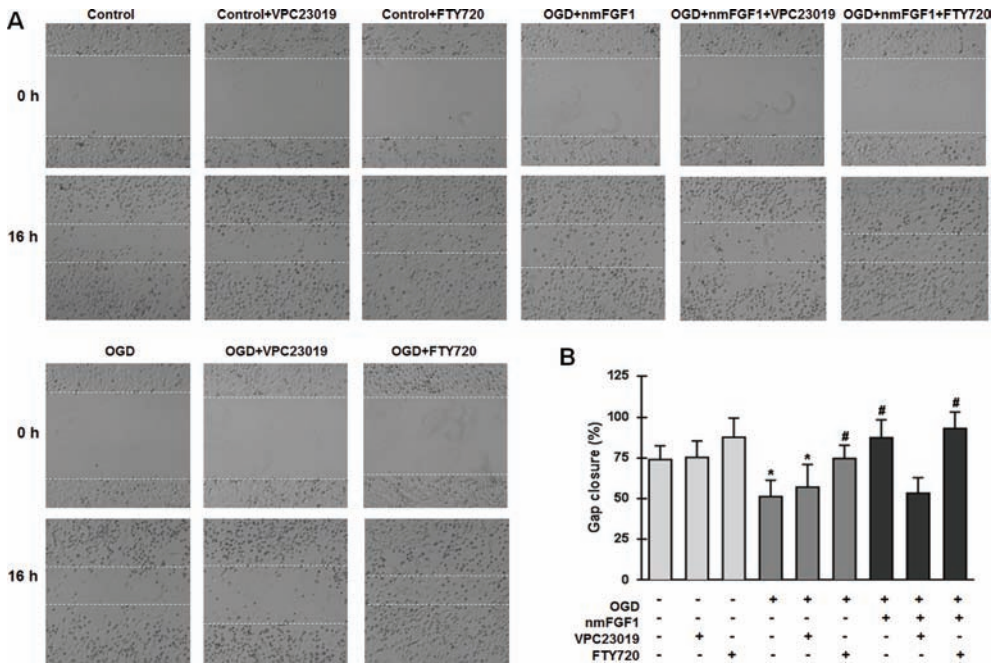

FIGURE 7 | Non-mitogenic fibroblast growth factor 1 (nmFGF1) promoted wound repair in oxygen-glucose deprivation (OGD)-exposed HBMECs *via* S1P signaling pathway. **(A)** Representative images showing the migration of OGD-exposed cells treated with the S1P1 inhibitor VPC23019 (40 nM) and agonist FTY720 (50 nM) in the presence or absence of nmFGF1. **(B)** Quantification of the effects of the S1P1 inhibitor VPC23019 (40 nM) and agonist FTY720 (50 nM) in the presence or absence of nmFGF1 on wound healing. Date are means ± SEM (n = 6). *p < 0.05 compared to control group, #p < 0.05 as compared to the OGD-treated group.

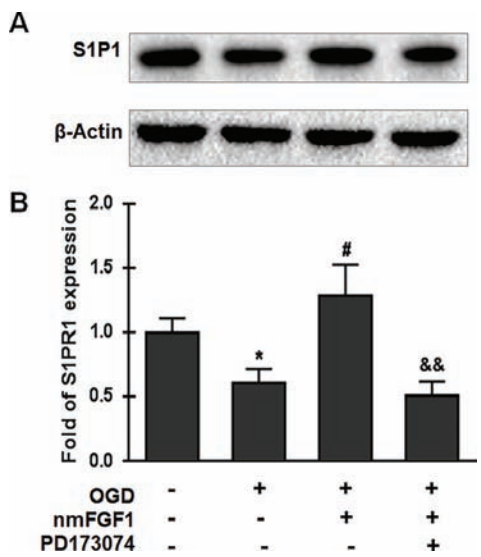

FIGURE 8 | Non-mitogenic fibroblast growth factor 1 (nmFGF1) rescued oxygen-glucose deprivation (OGD)/R-induced downregulation of S1P1 expression by FGFR1 activation. **(A)** Representative western blots for S1P1 expression. **(B)** Quantification of the relative expression level of S1P1. Date are expressed as the means ± SEM (n = 4). *p < 0.05 as compared to the control group, #p < 0.05 as compared to the OGD-treated group, &&p < 0.01 as compared to the nmFGF1-treated group.

previous study reported that the activation of S1P signaling could protect the BBB after exposure of HBMECs to OGD/R (Lin et al., 2018). However, the effects of nmFGF1 on S1P signaling pathway are unknown. In our current study, we confirmed nmFGF1 significantly increased S1P1 expression in the ECs indicated by colocation of CD31 and S1P1 by immunofluorescence assay after 10 days following MCAO, that was consisted with previous study (Iwasawa et al., 2018). We treated OGD/R-induced HBMECs with S1P1 antagonist VPC23019 and S1PR1 agonist FTY720 in combination with nmFGF1. VPC23019 treatment alone had no effect on tube formation, while FTY720 markedly enhanced the number of tubes. In the presence of VPC23019, the tube formation ability of HBMECs induced by nmFGF1 was significantly inhibited during OGD/R, and FTY720 in combination with nmFGF1 increased the tube number. nmFGF1 exhibited similar angiogenesis ability with S1PR1 agonist FTY720, that was consisted with previous study (Shang et al., 2020). Although we did not perform the experiment to observe the effects of nmFGF1 on neuroprotection after stroke, combined with the previous study that FGF1 enhanced neurogenesis after stroke (Cheng et al., 2011), we can speculate one potential mechanism of nmFGF1 neuroprotection was that enhanced angiogenesis might be partially due to improvements in the microenvironment of vessel growth. As the data shown, PD173074 also inhibited the positive effects of nmFGF1 on S1P1 signaling. Taken together, nmFGF1 can promote angiogenesis through S1P signaling pathway mediated by FGFR1 activation.

CONCLUSION

Our study provides the first evidence that intranasal nmFGF1 administration enhanced angiogenesis *via* S1P1 signaling pathway following stroke and highlights the need to better understand the mechanism underlying nmFGF1 function in ischemia protection. Taken together, these results suggest that nmFGF1 could be considered as potential angiogenic agent for ischemic stroke treatment.

DATA AVAILABILITY STATEMENT

The datasets generated for this study are available on request to the corresponding authors.

ETHICS STATEMENT

All animal use and care protocols conformed to the Guide for the Care and Use of Laboratory Animals from the National Institutes of Health and were approved by the Animal Care and Use Committee of Wenzhou Medical University.

AUTHOR CONTRIBUTIONS

XW and YX designed the experiment and wrote the manuscript. YuZ, JH, WH, and SY performed the animal experiments. FH, JD, RG, and MS performed the cells experiments. JL and YeZ analyzed the data. All the authors read and approved the final version of the manuscript.

FUNDING

This work was supported by Wenzhou Municipal Science and Technology Bureau Project (Y20170224 and Y20170686), Natural Science Foundation of Zhejiang Province (LQ19H090012), and Medical and Health Science and Technology Program of Zhejiang Province (2018KY505).

REFERENCES

Arenillas, J. F., Sobrino, T., Castillo, J., and Da´valos, A. (2007). The role of angiogenesis in damage and recovery from ischemic stroke. *Curr. Treat Options Cardiovasc. Med.* 9, 205–212. doi: 10.1007/s11936-007-0014-5

Brait, V. H., Tarrasón, G., Gavaldà, A., Godessart, N., and Planas, A. M. (2016). Selective sphingosine 1-phosphate receptor 1 agonist is protective against ischemia/reperfusion in Mice. *Stroke* 47, 3053–3056. doi: 10.1161/STROKEAHA.116.015371

Chen, J., Zhang, X., Liu, X., Zhang, C., Shang, W., Xue, J., et al. (2019a). Ginsenoside Rg1 promotes cerebral angiogenesis *via the* PI3K/Akt/mTOR signaling pathway in ischemic mice. *Eur. J. Pharmacol.* 856, 172418. doi: 10.1016/j.ejphar.2019.172418

Chen, J., Sun, L., Ding, G. B., Chen, L., Jiang, L., Wang, J., et al. (2019b). Oxygen-glucose deprivation/reoxygenation induces human brain microvascular endothelial cell hyperpermeability *via* VE-cadherin internalization: roles of RhoA/ROCK2. *J. Mol. Neurosci.* 69 (1), 49–59. doi: 10.1007/s12031-019-01326-8

Cheng, X., Wang, Z., Yang, J., Ma, M., Lu, T., Xu, G., et al. (2011). Acidic fibroblast growth factor delivered intranasally induces neurogenesis and angiogenesis in rats after ischemic stroke. *Neurol. Res.* 33 (7), 675–680. doi: 10.1179/1743132810Y.0000000004

Cotrina, M. L., Lou, N., Tome-Garcia, J., Goldman, J., and Nedergaard, M. (2017). Direct comparison of microglial dynamics and inflammatory profile in photothrombotic and arterial occlusion evoked stroke. *Neuroscience.* 343, 483–494. 2016.12.012. doi: 10.1016/j.neuroscience.2016.12.012

Cronauer, M. V., Schulz, W. A., Seifert, H. H., Ackermann, R., and Burchardt, M. (2003). Fibroblast growth factors and their receptors in urological cancers: basic research and clinical implications. *Eur. Urol.* 43 (3), 309–319. doi: 10.1016/S0302-2838(03)00005-8

Cuevas, P., Carceller, F., Reimers, D., Saenz de Tejada, I., and Giménez-Gallego, G. (1998). Acidic fibroblast growth factor rescues gerbil hippocampal neurons from ischemic apoptotic death. *Neurol. Res.* 20 (3), 271–274. doi: 10.1080/01616412.1998.11740518

Fischl, A. S., Wang, X., Falcon, B. L., Almonte-Baldonado, R., Bodenmiller, D., Evans, G., et al. (2019). Inhibition of sphingosine phosphate receptor 1 signaling enhances the efficacy of VEGF receptor inhibition. *Mol. Cancer Ther.* 18 (4), 856–867. doi: 10.1158/1535-7163.MCT-18-0548

GBD 2016 Neurology Collaborators. (2019). Global, regional, and national burden of neurological disorders 1990-2016: a systematic analysis for the Global Burden of Disease Study 2016. *Lancet Neurol.* 18 (5), 459–480. doi: 10.1016/S1474-4422(18)30499-X

Gopurappilly, R., Pal, R., Mamidi, M. K., Dey, S., Bhonde, R., and Das, A. K. (2011). Stem cells in stroke repair: current success and future prospects. *CNS Neurol. Disord. Drug Targets.* 10 (6), 741–756. doi: 10.2174/187152711797247894

Hasegawa, Y., Suzuki, H., Sozen, T., Rolland, W., and Zhang, J. H. (2010). Activation of sphingosine 1-phosphate receptor-1 by FTY720 is neuroprotective after ischemic stroke in rats. *Stroke* 41, 368–374. doi: 10.1161/STROKEAHA.109.568899

Hasegawa, Y., Suzuki, H., Altay, O., Rolland, W., and Zhang, J. H. (2013). Role of the sphingosine metabolism pathway on neurons against experimental cerebral ischemia in rats. *Transl. Stroke Res.* 4, 524–532. doi: 10.1007/s12975-013-0260-7

Hatakeyama, M., Ninomiya, I., and Kanazawa, M. (2020). Angiogenesis and neuronal remodeling after ischemic stroke. *Neural Regener. Res.* 15 (1), 16–19. doi: 10.4103/1673-5374.264442

Hla, T. (2004). Physiological and pathological actions of sphingosine 1-phosphate. *Semin. Cell Dev. Biol.* 15 (5), 513–520. doi: 10.1016/j.semcdb.2004.05.002

Huang, W., Shao, M., Liu, H., Chen, J., Hu, J., Zhu, L., et al. (2019). Fibroblast growth factor 21 enhances angiogenesis and wound healing of human brain microvascular endothelial cells by activating PPARγ. *J. Pharmacol. Sci.* 140 (2), 120–127. doi: 10.1016/j.jphs.2019.03.010

Iwasawa, E., Ishibashi, S., Suzuki, M., Li, F., Ichijo, M., Miki, K., et al. (2018). Sphingosine-1-phosphate receptor 1 activation enhances leptomeningeal collateral development and improves outcome after stroke in mice. *J. Stroke Cerebrovasc. Dis.* 27, 1237–1251. doi: 10.1016/j.jstrokecerebrovasdis.2017.11.040

Jiang, X., Pu, H., Hu, X., Wei, Z., Hong, D., Zhang, W., et al. (2016). A post-stroke therapeutic regimen with omega-3 polyunsaturated fatty acids that promotes white matter integrity and beneficial microglial responses after cerebral ischemia. *Transl. Stroke Res.* 7, 548–561. doi: 10.1007/s12975-016-0502-6

Jung, B., Obinata., H., Galvani., S., Mendelson, K., Ding, B. S., Skoura, A., et al. (2012). Flow-regulated endothelial S1P receptor-1 signaling sustains vascular development. *Dev. Cell.* 23 (3), 600–610. doi: 10.1016/j.devcel.2012.07.015

Kanazawa, M., Takahashi, T., Ishikawa, M., Onodera, O., Shimohata, T., and Del Zoppo, G. J. (2019). Angiogenesis in the ischemic core: a potential treatment target? *J. Cereb. Blood Flow. Metab.* 39 (5), 753–769. doi: 10.1177/0271678X19834158

Kerr, R., Agrawal, S., Maity, S., Koppolu, B., Jayanthi, S., Suresh Kumar, G., et al. (2019). Design of a thrombin resistant human acidic fibroblast growth factor (hFGF1) variant that exhibits enhanced cell proliferation activity. *Biochem. Biophys. Res. Commun.* 518 (2), 191–196. doi: 10.1016/j.bbrc.2019.08.029

Li, H. H., Fu, X. B., Sun, T. Z., Cai, C. L., Zhou, G., Chen, W., et al. (2007). Non-mitogenic acidic fibroblast growth factor reduces intestinal dysfunction induced by ischemia and reperfusion injury in rats. *J. Gastroenterol. Hepatol.* 22 (3), 363–370. doi: 10.1111/j.1440-1746.2006.04457.x

Li, H., Zhou, X., Li, Y., Ma, X., Gonzales, R. J., Qiu, S., et al. (2019). The selective sphingosine 1-phosphate receptor 1 modulator RP101075 improves microvascular circulation after cerebrovascular thrombosis. *FASEB J.* 33 (10), 10935–10941. doi: 10.1096/fj.201900282R

Lin, L., Wang, Q., Qian, K., Cao, Z., Xiao, J., Wang, X., et al. (2018). bFGF protects against oxygen glucose deprivation/reoxygenation-induced endothelial monolayer permeability *via* S1PR1-dependent mechanisms. *Mol. Neurobiol.* 55 (4), 3131–3142. doi: 10.1007/s12035-017-0544-0

Liu, Y., Wada, R., Yamashita, T., Mi, Y., Deng, C. X., Hobson, J. P., et al. (2000). Edg-1, the G protein-coupled receptor for sphingosine-1-phosphate, is essential for vascular maturation. *J. Clin. Invest.* 106 (8), 951–961. doi: 10.1172/JCI10905

Liu, S., Ni, C., Zhang, D., Sun, H., Dong, X., Che, N., et al. (2019). S1PR1 regulates the switch of two angiogenic modes by VE-cadherin phosphorylation in breast cancer. *Cell Death Dis.* 10 (3), 200. doi: 10.1038/s41419-019-1411-x

Lu, W. J., Liang, H. B., Li, Y. F., Tu, X. Q., He, J. R., Ding, K. Q., et al. (2019). MicroRNA-210-3p targets RGMA to enhance the angiogenic functions of endothelial progenitor cells under hypoxic conditions. *Front. Cell Neurosci.* 13, 223. doi: 10.3389/fncel.2019.00223

Markus, H. S. (2011). Stroke genetics. *Hum. Mol. Genet.* 20, R124–R131. doi: 10.1093/hmg/ddr345

Nariai, T., Suzuki, R., Matsushima, Y., Ichimura, K., Hirakawa, K., Ishii, K., et al. (1994). Surgicallyinduced angiogenesis to compensate for hemodynamic cerebral ischemia. *Strokes* 25, 1014–1021. doi: 10.1161/01.STR.25.5.1014

Nih, L. R., Gojgini, S., Carmichael, S. T., and Segura, T. (2018). Dual-function injectable angiogenic biomaterial for the repair of brain tissue following stroke. *Nat. Mater.* 17 (7), 642–651. doi: 10.1038/s41563-018-0083-8

Obinata, H., and Hla, T. (2019). Sphingosine 1-phosphate and inflammation. *Int. Immunol.* 31 (9), 617–625. doi: 10.1093/intimm/dxz037

Reinhard, N. R., Mastop, M., Yin, T., Wu, Y., Bosma, E. K., Gadella, T. W. J., et al. (2017). The balance between Gα-Cdc42/Rac and Gα/-RhoA pathways determines endothelial barrier regulation by sphingosine-1-phosphate. *Mol. Biol. Cell.* 28 (23), 3371–3382. doi: 10.1091/mbc.e17-03-0136

Rostami, N., Nikkhoo, A., Ajjoolabady, A., Azizi, G., Hojjat-Farsangi, M., Ghalamfarsa, G., et al. (2019). S1PR1 as a novel promising therapeutic target in cancer therapy. *Mol. Diagn. Ther.* 23 (4), 467–487. doi: 10.1007/s40291-019-00401-5

Ruan, L., Wang, B., ZhuGe, Q., and Jin, K. (2015). Coupling of neurogenesis and angiogenesis afer ischemic stroke. *Brain Res.* 1623, 166–173. doi: 10.1016/j.brainres.2015.02.042

Rust, R., Grönnert, L., Gantner, C., Enzler, A., Mulders, G., Weber, R. Z., et al. (2019). Nogo-A targeted therapy promotes vascular repair and functional recovery following stroke. *Proc. Natl. Acad. Sci. U.S.A.* 116 (28), 14270–14279. doi: 10.1073/pnas.1905309116

Sartawi, Z., Schipani, E., Ryan, K. B., and Waeber, C. (2017). Sphingosine 1-phosphate (S1P) signalling: role in bone biology and potential therapeutic target for bone repair. *Pharmacol. Res.* 125 (Pt B), 232–245. doi: 10.1016/j.phrs.2017.08.013

Shang, K., He, J., Zou, J., Qin, C., Lin, L., Zhou, L. Q., et al. (2020). Fingolimod promotes angiogenesis and attenuates ischemic brain damage *via* modulating microglial polarization. *Brain Res.* 1726, 146509. doi: 10.1016/j.brainres.2019.146509

Sun, H. J., Cai, W. W., Gong, L. L., Wang, X., Zhu, X. X., Wan, M. Y., et al. (2017). FGF-2-mediated FGFR1 signaling in human microvascular endothelial cells is activated by vaccarin to promote angiogenesis. *Biomed. Pharmacother.* 95, 144–152. doi: 10.1016/j.biopha.2017.08.059

Tomanek, R. J., and Schatteman, G. C. (2000). Angiogenesis: new insights and therapeutic potential. *Anat. Rec.* 261 (3), 126–135. doi: 10.1002/1097-0185(20000615)261:3<126::AID-AR7>3.0.CO;2-4

Wang, J., Fu, X., Zhang, D., Yu, L., Li, N., Lu, Z., et al. (2017). ChAT-positive neurons participate in subventricular zone neurogenesis after middle cerebral artery occlusion in mice. *Behav. Brain Res.* 316, 145–151. doi: 10.1016/j.bbr.2016.09.007

Wang, H. J., Wei, J. Y., Liu, D. X., Zhuang, S. F., Li, Y., Liu, H., et al. (2018). Endothelial Atg7 deficiency ameliorates acute cerebral injury induced by ischemia/reperfusion. *Front. Neurol.* 9, 998. doi: 10.3389/fneur.2018.00998

Wang, M. L., Zhang, L. X., Wei, J. J., Li, L. L., Zhong, W. Z., Lin, X. J., et al. (2019). Granulocyte colony-stimulating factor and stromal cell-derived factor-1 combination therapy: a more effective treatment for cerebral ischemic stroke. *Int. J. Stroke.* 30, 1747493019879666. doi: 10.1177/1747493019879666

Wu, X., Su, Z., Li, X., Zheng, Q., Huang, Y., and Yuan, H. (2005). High-level expression and purification of a nonmitogenic form of human acidic fibroblast growth factor in Escherichia coli. *Protein Expr. Purif.* 42 (1), 7–11. doi: 10.1016/j.pep.2004.07.021

Wu, F., Chen, Z., Tang, C., Zhang, J., Cheng, L., Zuo, H., et al. (2017). Acid fibroblast growth factor preserves blood-brain barrier integrity by activating the PI3K-Akt-Rac1 pathway and inhibiting RhoA following traumatic brain injury. *Am. J. Transl. Res.* 9 (3), 910–925.

Xie, Z., Liu, H., and Geng, M. (2017). Targeting sphingosine-1-phosphate signaling for cancer therapy. *Sci. China Life Sci.* 60 (6), 585–600. doi: 10.1007/s11427-017-9046-6

Xue, W. J., Li, M. T., Chen, L., Sun, L. P., and Li, Y. Y. (2018). Recent developments and advances of FGFR as a potential target in cancer. *Future Med. Chem.* 10 (17), 2109–2126. doi: 10.4155/fmc-2018-0103

Zhang, X., Zheng, W., Wang, T., Ren, P., Wang, F., Ma, X., et al. (2017). Danshen-chuanxiong-honghua ameliorates cerebral impairment and improves spatial cognitive deficits after transient focal ischemia and identification of active compounds. *Front. Pharmacol.* 8, 452. doi: 10.3389/fphar.2017.00452

Zhou, Y., Lekic, T., Fathali, N., Ostrowski, R. P., Martin, R. D., Tang, J., et al. (2010). Isoflurane posttreatment reduces neonatal hypoxic-ischemic brain injury in rats by the sphingosine-1-phosphate/phosphatidylinositol-3-kinase/Akt pathway. *Stroke* 41, 1521–1527. doi: 10.1161/STROKEAHA.110.583757

Conflict of Interest: The authors declare that the research was conducted in the absence of any commercial or financial relationships that could be construed as a potential conflict of interest.

The handling editor declared a shared affiliation, though no other collaboration, with the authors at time of review.

frontiers in Pharmacology

ORIGINAL RESEARCH
published: 03 March 2020
doi: 10.3389/fphar.2020.00052

Fibroblast Growth Factor 1 Ameliorates Diabetes-Induced Liver Injury by Reducing Cellular Stress and Restoring Autophagy

Zeping Xu[1†], Yanqing Wu[2†], Fan Wang[3,4†], Xiaofeng Li[1], Ping Wang[1], Yuying Li[1], Junnan Wu[1], Yiyang Li[1], Ting Jiang[1], Xindian Pan[5], Xie Zhang[6], Longteng Xie[7], Jian Xiao[1] and Yanlong Liu[1,8*]*

[1] School of Pharmaceutical Sciences, Wenzhou Medical University, Wenzhou, China, [2] Institute of Life Sciences, Wenzhou University, Wenzhou, China, [3] The Second Affiliated Hospital, Xinjiang Medical University, Urumqi, China, [4] Beijing Hui-Long-Guan Hospital, Peking University, Beijing, China, [5] School of Medicine, Hangzhou Normal University, Hangzhou, China, [6] Department of Pharmacy, Ningbo Medical Treatment Center, Li Huili Hospital, Ningbo, China, [7] Department of Infection Diseases, Ningbo Fourth Hospital, Xiangshan, China, [8] Center for Health Assessment, Wenzhou Medical University, Wenzhou, China

OPEN ACCESS

Edited by:
Saverio Bellusci,
University of Giessen, Germany

Reviewed by:
Hao Wang,
RMIT University, Australia
Huatao Chen,
Northwest A&F University, China
Cho-Ming Chao,
German Center for Lung Research, Germany

***Correspondence:**
Jian Xiao
xfxj2000@126.com
Yanlong Liu
benjaminlyl@wmu.edu.cn

[†]These authors have contributed equally to this work

Specialty section:
This article was submitted to Translational Pharmacology, a section of the journal Frontiers in Pharmacology

Received: *20 August 2019*
Accepted: *16 January 2020*
Published: *03 March 2020*

Citation:
Xu Z, Wu Y, Wang F, Li X, Wang P, Li Y, Wu J, Li Y, Jiang T, Pan X, Zhang X, Xie L, Xiao J and Liu Y (2020) Fibroblast Growth Factor 1 Ameliorates Diabetes-Induced Liver Injury by Reducing Cellular Stress and Restoring Autophagy. Front. Pharmacol. 11:52. doi: 10.3389/fphar.2020.00052

Background: Type 2 diabetes (T2D) is a metabolic dysfunction disease that causes several complications. Liver injury is one of these that severely affects patients with diabetes. Fibroblast growth factor 1 (FGF1) has glucose-lowering activity and plays a role in modulation of several liver injuries. Nevertheless, the effects and potential mechanisms of FGF1 against diabetes-induced liver injury are unknown.

Methods: To further investigate the effect of FGF1 on diabetic liver injury, we divided db/db mice into two groups and intraperitoneally (i.p.) injected either with FGF1 at 0.5 mg/kg body weight or saline every other day for 4 weeks. Then body weights were measured. Serum and liver tissues were collected for biochemical and molecular analyses.

Results: FGF1 significantly reduced blood glucose and ameliorated diabetes-induced liver steatosis, fibrosis, and apoptosis. FGF1 also restored defective hepatic autophagy in db/db mice. Mechanistic investigations showed that diabetes markedly induced oxidative stress and endoplasmic reticulum stress and that FGF1 treatment significantly attenuated these effects.

Conclusions: FGF1-associated glucose level reduction and amelioration of cellular stress are potential protective effects of FGF1 against diabetes-induced liver injury.

Keywords: fibroblast growth factor 1, diabetes, liver injury, oxidative stress, endoplasmic reticulum stress

INTRODUCTION

Type 2 diabetes (T2D) is a complex metabolic disease characterized by insulin resistance and pancreatic cell failure (Kasuga, 2006). Hyperglycemia resulting in glucotoxicity is the primary pathophysiological trigger of diabetes-induced complications (Wu et al., 2015a; Wu et al., 2016). Liver injury occurs commonly in patients with diabetes (Gezginci-Oktayoglu et al., 2009). Liver

damage caused by diabetes is characterized by abnormal liver enzyme levels, steatosis, fibrosis, and cirrhosis. Diabetes-induced liver damage produces several pathological changes in the morphology and microstructure of hepatic tissues and functions, including vacuolization and lipid accumulation, resulting in significant damage (Wu et al., 2015a). There are many mechanisms mediating liver damage caused by diabetes, including hyperglycemia, oxidative stress, endoplasmic reticulum stress, and advanced glycation end-products (JaeMyoung et al., 2014). Therefore, it is important to detail these pathophysiological mechanisms and to explore effective therapeutic strategies to meliorate diabetes-induced liver injury.

Fibroblast growth factor 1 (FGF1) releases from cells through a nonclassical secretory pathway, acting on cells in various tissues, including liver and vasculature, where it exerts classic mitogenic activity (Jiang et al., 2016). FGF1 has an unique ability to lower blood glucose, and pharmacologically-relevant FGF1 (0.5 mg/kg) leads to impressive changes in several measurements, including blood glucose, nearly normalizing after 35 days in T2D mice models with impaired insulin sensitivity (JaeMyoung et al., 2014). Administration of exogenous FGF1 stimulates glucose uptake in an insulin-dependent fashion and suppressed the hepatic production of glucose to achieve whole-body insulin sensitization in a mouse model of T2D (JaeMyoung et al., 2014). As an insulin sensitizer, FGF1 mediates homeostatic control of glycemia by acting on several pathways (Li, 2019). The glucose-lowering activity of FGF1 is dissociated from its mitogenic activity and is mediated predominantly *via* FGF receptor 1 signaling (JaeMyoung et al., 2014).

FGF1 also reverses hepatic lipid steatosis by improving lipid catabolism (Liu W. et al., 2016). Chronic treatment with rFGF1 led to reduced hepatic steatosis and augmented liver glycogen content (JaeMyoung et al., 2014). A recent study showed that FGF1 meliorated acetaminophen (APAP)-induced hepatotoxicity in mice through suppression of inflammation, apoptosis, and oxidative and endoplasmic reticulum stress (Wang et al., 2019). These findings suggest that FGF1 may have hepato-protective properties beyond its anti-steatotic and anti-inflammatory properties. Based on these studies, we aimed to investigate the effects and molecular mechanisms of FGF1 in diabetic-induced liver injury.

MATERIALS AND METHODS

Animal Experiments

Twelve-week-old male db/db mice and their nondiabetic db/m littermates were purchased from the Model Animal Research Center of Nanjing University (Nanjing, China). Animals were maintained under 12:12 h light:dark cycle conditions. The db/db mice were divided into two groups and were intraperitoneally (i.p.) injected either with FGF1 (Guang et al., 2018) (0.5 mg/kg body weight, n = 8) or physiologic saline (n = 8) every other day for 4 weeks (Wu et al., 2018). After 4 weeks, body weights were measured. Then serum and liver tissues samples of these mice were collected for biochemical and molecular analyses.

Biochemical Analysis

Blood glucose levels were monitored from tail blood samples using a blood glucose meter (Glucometer, SANNUO, China). Serum levels of alanine aminotransferase (ALT), triglyceride (TG), liver glutathione peroxidase (GSH-PX), and liver 4-hydroxynonenal (4-HNE) protein adducts were measured according to the manufacturer's instructions (Jian Cheng Biotechnology Co., Ltd. of Nanjing, China). Total antioxidant capacity (T-AOC), malondialdehyde (MDA), and superoxide dismutase (SOD) activity were also measured with various assay kits (Beyotime Biotechnology Corporation, Shanghai, China). Plasma glycosylated hemoglobin (GHbA1c) levels were measured using the Mouse Glycated Hemoglobin A1c (GHbA1c) ELISA Kit (Enzyme-linked Biotechnology Co., Ltd. Shanghai, China).

Liver Triglyceride Assay

Hepatic triglyceride (TG) levels were determined as described previously (Liu Y. et al., 2016), using the TG reagent (Thermo Fisher Scientific, Middletown, VA).

Pathology and Immunohistochemical Staining on Liver Tissue

Hematoxylin and eosin (H&E) staining and Masson's trichrome (MT) staining (Solarbio Science & Technology, Beijing, China G1340) were employed to evaluate the characteristics of liver tissues in histological changes and fibrosis. Immunohistochemical staining was used to further verify the deposition of collagen I (collagen I, 1:500; Abcam, Cambridge, UK) in fibrotic liver. The procedure was performed as described previously (Hao et al., 2009).

Terminal Deoxynucleotidyl Transferase Deoxyuridine Triphosphate Nick End Labeling Assay

Liver sections of 5 μm were stained for terminal deoxynucleotidyl transferase deoxyuridine triphosphate nick end labeling (TUNEL) according to the manufacturer's instruction using the ApopTag Peroxidase In Situ Apoptosis Detection Kit (Chemicon, CA, USA).

Western Blotting Analysis

Liver tissues were homogenized and determined as described previously (Wang et al., 2019). The blots were incubated with primary antibodies: cleaved caspase-3, Bax, Bcl-2, ATF6, GRP78, Nrf2, SOD2, collagen IA1, ATG5, p62 and LC3 (Abcam, USA), HO-1 (Santa Cruz Biotechnology, CA, USA), CHOP, P-IRE1α, P-eIF2α, P-PERK, PERK, FGFR1, P-AMPK and AMPK (Cell Signaling Technology, Danvers, MA, US), and α-SMA, TGF-β, and GAPDH (Proteintech, China) followed by incubation with their corresponding secondary antibodies: anti-rabbit and anti-mouse (Proteintech, China).

Statistical Analysis

All data were expressed as mean ± standard error of the mean (SEM). Statistical differences were determined using one-way ANOVA (for comparison of two experimental conditions).

Statistical significance was considered at P values < 0.05. Statistical calculations were done using GraphPad Prism 6 (GraphPad Software, Inc., San Diego, USA).

RESULTS

FGF1 Treatment Reduced Blood Glucose and Ameliorated Hepatic Steatosis

A previous study showed that a single injection of FGF1 was sufficient to restore blood glucose levels to the normal range for more than 2 days in both db/db and DIO mouse models (JaeMyoung et al., 2014). In agreement with that study, our results showed that FGF1 treatment markedly reduced blood glucose levels in db/db mice (**Figure 1B**). HbA1c levels in db/db mice were markedly higher than those of db/m mice. No significant differences were found between db/db mice with FGF1 treatment and db/db mice with respect to HbA1c levels (**Figure 1C**). In addition, db/db mice had distinctly elevated plasma alanine aminotransaminase (ALT) levels, a liver injury marker, at 16 weeks of age compared with the db/m mice, an effect that was distinctly reduced by FGF1 treatment (**Figure 1D**). Body weights of db/db mice were significantly greater than those of db/m mice, an effect that was markedly decreased with FGF1 treatment (**Figure 1E**). Compared with db/m mice, liver weights of db/db mice were markedly higher, an effect reversed by FGF1 treatment (**Figure 1F**). Although no significant difference was found between db/m mice and db/db mice with respect to the ratio of liver/body weight, the liver/body weight ratio in db/db mice was reduced by FGF1 treatment (**Figure 1G**). Pathological hepatic lipid accumulation is a characteristic of diabetes liver injury. As previously reported, accumulated fat interferes with insulin signaling pathways and consequently reduces the glucose content taken up from the bloodstream, an effect that is tightly connected to hepatic injury and steatosis in T2DM (Marchesini et al., 2001). In the present study, db/db mice had elevated plasma TG levels, a common feature of dyslipidemia accompanying with type 2 diabetes; this effect was diminished by FGF1 treatment (**Figure 1H**). Histological analyses revealed significant lipid accumulation in liver cells from db/db mice as shown by H&E staining. This effect was significantly attenuated by FGF1 treatment (**Figure 1A**).

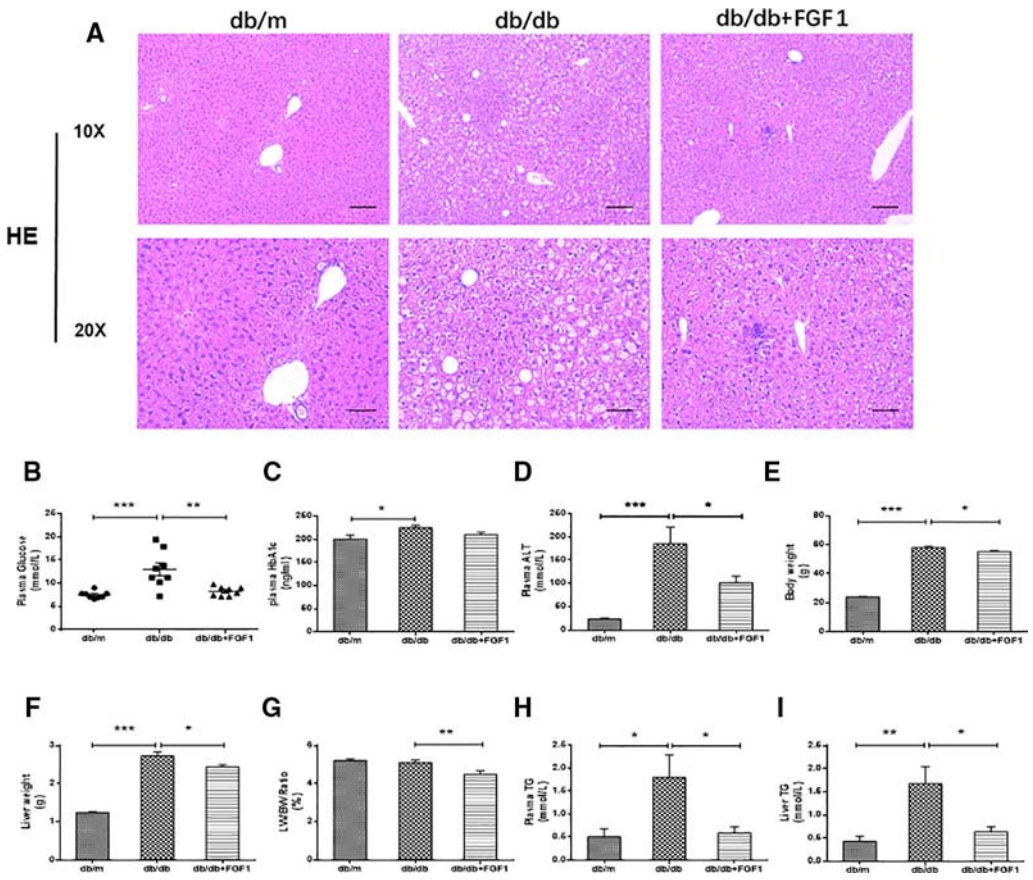

FIGURE 1 | FGF1 ameliorated blood glucose and hepatic steatosis. **(A)** Hematoxylin and eosin (H&E) staining of livers from db/m, db/db, and db/db + FGF1 mice (10 x:scale bars = 100 μm 20 x:scale bars = 50 μm). **(B)** Plasma glucose levels. **(C)** Plasma HbA1C levels. **(D)** Plasma alanine aminotransaminase (ALT) levels. **(E)** Body weights. **(F)** Liver weights. **(G)** Liver weight/body weight ratios. **(H)** Plasma triglyceride (TG) levels. **(I)** Liver TG levels. All data are presented as mean ± SEM, n = 8. *P < 0.05 **P < 0.01 ***P < 0.001 *vs*. the db/m group and db/db + FGF1 group.

The db/db mice had elevated liver TG levels, and FGF1 treatment ameliorated these increases (**Figure 1I**). Taken together, our results suggest that db/db mice had fatty livers, and FGF1 treatment reduced blood glucose and attenuated diabetes-induced hepatic steatosis.

FGF1 Treatment Ameliorated Diabetes-Induced Liver Fibrosis by Reducing Deposition of Collagen

The expression of collagen is used as an index of liver injury. We graded the degree of hepatic fibrosis using Masson staining and collagen I immunohistochemical staining (**Figures 2A, B**). The areas of collagen fibers deposition were more significantly expressed in the central vein and surrounding sinus gaps in db/db mice than those in db/m control mice (**Figures 2C**). Consistent with the immunohistochemical results, western blotting results showed that protein levels of collagen IA1 in livers from db/db mice were significantly greater, but that were much lower in the FGF1 treatment group (**Figures 2D, E**). Furthermore, protein levels of α-SMA and TGF-β were substantially greater in db/db mice livers (**Figures 2D, F, G**). All these changes in db/db mice were reversed by FGF1 treatment, suggesting that FGF1 inhibited diabetes-induced liver fibrosis by abolishing collagen accumulation in the liver.

FGF1 Treatment Ameliorated Diabetes-Induced Hepatic Apoptosis

To determine the mechanisms by which FGF1 protects against diabetes-induced liver damage, we examined apoptosis pathways. Compared with liver cells in db/m mice, we found that liver cells of db/db mice were severely damaged, characterized by irregular shapes and chaotic arrangement of cells. Numbers of TUNEL-positive staining cells were substantially greater in liver cells from db/db mice than those in db/m liver cells, an effect that was inhibited by FGF1 treatment (**Figures 3A, B**). Apoptosis indicators were also measured (**Figures 3C–F**). Expression levels of cleaved caspase-3 and Bax were much higher in db/db mice than those in db/m mice (**Figures 3C, E, F**). By contrast, compared with the db/m mice, Bcl2, an anti-apoptotic protein (Yu et al., 2019), was expressed at lower level in db/db mice livers (**Figures 3C, D**). All these changes were reversed by FGF1 treatment. Taken together, these observations suggest that FGF1 ameliorated diabetes-induced hepatic apoptosis in db/db mice.

FGF1 Treatment Restored Defective Hepatic Autophagy in Diabetic Mice

Previous studies showed that diabetes impaired hepatic autophagy and that obesity caused markedly decreased

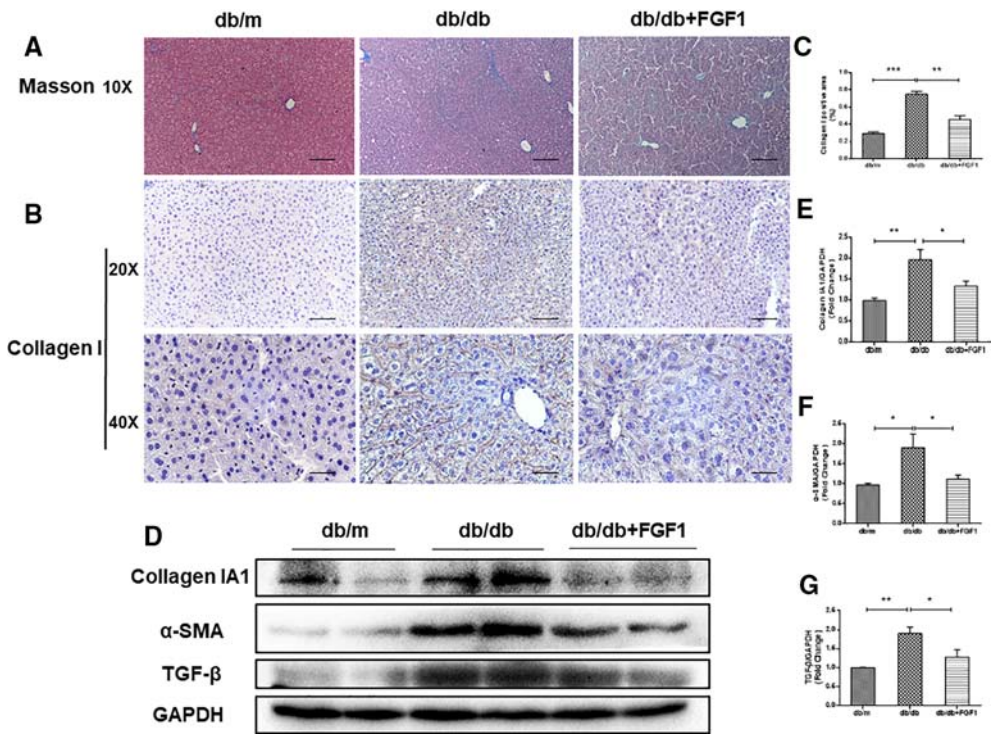

FIGURE 2 | FGF1 treatment ameliorated diabetes-induced liver fibrosis by reducing deposition of collagen. **(A)** Masson staining of liver from db/m, db/db, and db/db + FGF1 mice (10 x:scale bars = 100 μm). **(B, C)** Immunohistochemical staining of collagen I and collagen I positive area of liver from db/m, db/db and db/db + FGF1 mice (20 x:scale bars = 50 μm 40 x:scale bars = 25 μm). **(D)** Protein expression of collagen I, α-SMA, and TGF-β in livers from db/m, db/db, and db/db + FGF1 mice. **(E–G)** Intensities of collagen I, α-SMA, and TGF-β normalized to GAPDH. All data are presented as mean ± SEM, n = 8. *P < 0.05 **P < 0.01 ***P < 0.001 *vs*. the db/m group and db/db + FGF1 group.

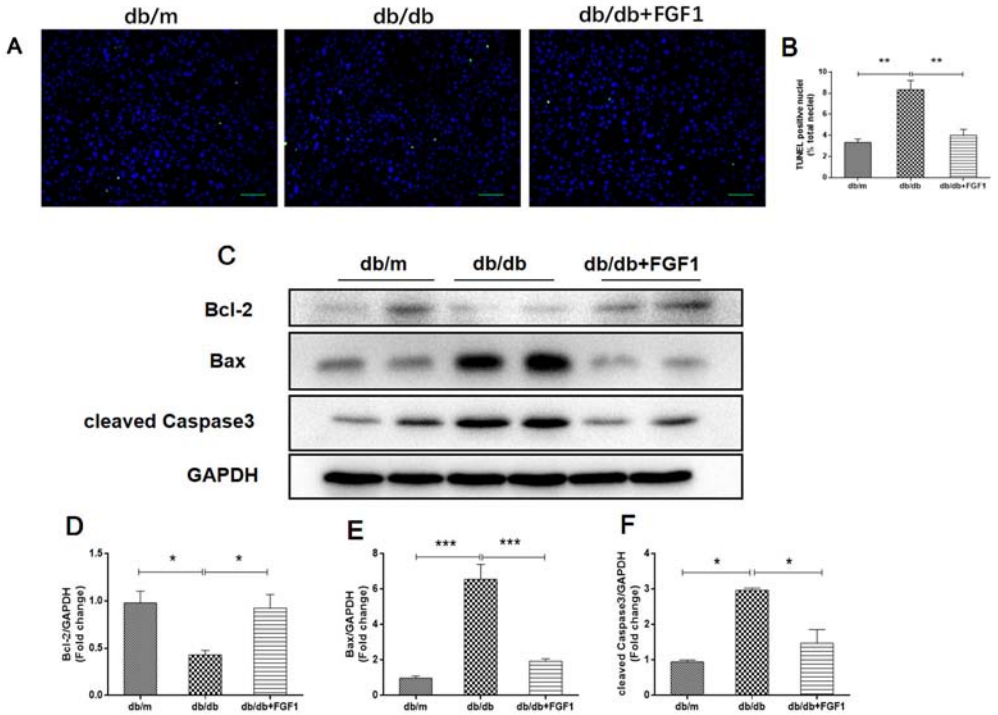

FIGURE 3 | FGF1 ameliorated diabetes-induced hepatic apoptosis in liver. **(A, B)** TUNEL-positive nuclear staining of liver from db/m, db/db and db/db + FGF1 mice (scale bars = 100 μm). **(C)** Protein expression of cleaved caspase-3, Bax, and Bcl2 of liver from db/m, db/db, and db/db + FGF1 mice. **(D–F)** Intensities of cleaved caspase-3, Bax, and Bcl2 normalized to GAPDH. All data are presented as mean ± SEM, n = 8. *P < 0.05 **P < 0.01 ***P < 0.001 *vs*. the db/m group and db/db + FGF1 group.

autophagy in livers of both genetic and dietary mice models; this effect was demonstrated by decreased expression levels of LC3 and Atg5 (Yang et al., 2010). By contrast, p62 is involved in aggresome formation and is degraded through autophagy (Iwadate et al., 2014), with higher levels in ob/ob mice livers than in lean controls (Yang et al., 2010). To study the regulation of autophagy in the present diabetes model, we first examined expression patterns of molecular indicators of autophagy. In line with previous studies, we found that diabetes was characterized by lower expression of autophagy indicators in db/db mice livers, demonstrated by lower expression levels of LC3 and ATG5 proteins (**Figures 4A, C, D**). Levels of p62 protein level were substantially higher in db/db mice livers than that in db/m mice (**Figures 4A, B**). As expected, these changes were reversed by FGF1 treatment, suggesting that FGF1 treatment restored defective hepatic autophagy in db/db mice.

FGF1 Treatment Blocked Diabetes-Induced Oxidative Stress in Liver

Oxidative stress is a molecular mechanism that characterizes diabetes complications (Yang et al., 2015). Fatty acids in the liver induce free radical formation, causing lipid peroxidation and inducing release of proinflammatory cytokines. The release of malondialdehyde and 4-hydroxynonenal correspondingly causes cell death, protein cross-linkage, and stellate cells activation, leading to collagen synthesis and fibrosis (Xiao et al., 2017). Oxidative stress is also a critical factor in the progression of nonalcoholic fatty liver disease associated with diabetes (Mohamed et al., 2016). In the present study, we determined whether FGF1 treatment reversed diabetes-induced oxidative stress by measuring glutathione levels and oxidative stress markers (**Figure 5**). Plasma malondialdehyde (MDA) levels were significantly greater in db/db mice livers than those in of db/m mice livers (**Figure 5A**), an effect that was reduced by FGF1 treatment. As expected, liver glutathione peroxidase (GSH-PX) levels were lower in db/db mice livers than those in db/m mice livers, an effect that was increased by FGF1 treatment (**Figure 5B**). There were no significant differences in plasma MDA levels and liver GSH-PX levels between db/db mice and db/db + FGF1 mice. 4-hydroxynonenal (4-HNE)-protein adducts and protein carbonyl content were measured to assess lipid peroxidation and protein oxidation levels, respectively (Valle et al., 2012). Consistently higher levels of carbonyl and 4-HNE adducts were observed in db/db mice, an effect that was decreased by FGF1 treatment (**Figure 5C**). Although no significant differences were found between db/m mice and db/db mice with respect to liver 4-HNE levels and plasma T-AOC levels, FGF1 treatment significantly increased liver 4-HNE levels and plasma T-AOC levels in db/db mice (**Figures 5C, D**). HO-1 is the rate limiting enzyme in heme degradation, being the first step, catalyzing degradation of pro-oxidant heme to carbon monoxide,

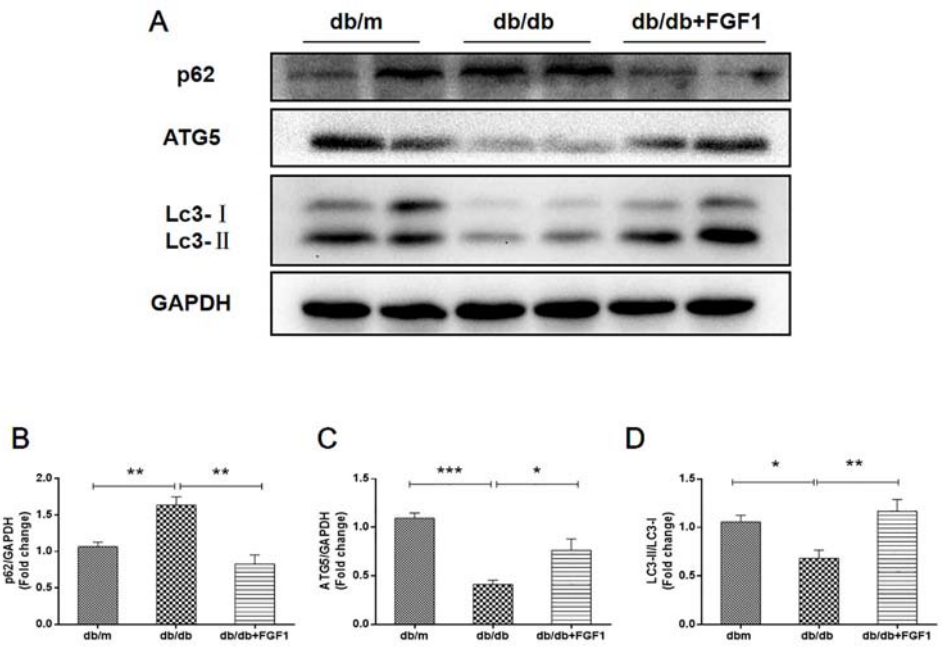

FIGURE 4 | FGF1 restored hepatic autophagy in db/db mice. **(A)** Protein expression of p62, ATG5 and LC3 in livers from db/m, db/db and db/db + FGF1 mice. **(B, C)** Intensities of p62 and ATG5 normalized to GAPDH. **(D)** LC3II/LC3I. All data are presented as mean ± SEM, n = 8. *P < 0.05 **P < 0.01 ***P < 0.001 *vs*. the db/m group and db/db + FGF1 group.

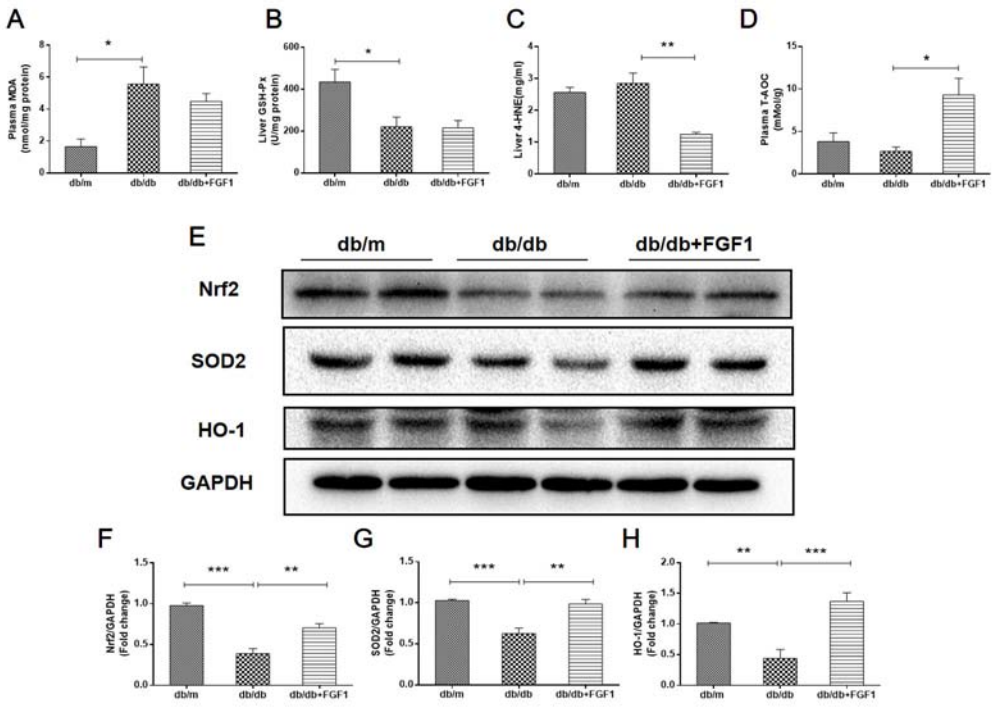

FIGURE 5 | FGF1 blocked diabetes-induced liver oxidative stress. **(A)** Plasma malondialdehyde (MDA) levels. **(B)** Liver glutathione peroxidase (GSH-PX) levels. **(C)** liver 4-hydroxynonenal (4-HNE) levels. **(D)** Plasma total antioxidant capacity (T-AOC) levels. **(E)** Protein expression of Nrf2, HO-1, and SOD2 in livers from db/m, db/db, and db/db + FGF1 mice. **(F–H)** Intensities of Nrf2, HO-1, and SOD2 normalized to GAPDH. All data are presented as mean ± SEM, n = 8. *P < 0.05 **P < 0.01 ***P < 0.001 *vs*. the db/m group and db/db + FGF1 group.

biliverdin, and ferrous iron (Abraham and Kappas, 2008). HO-1 gene expression is regulated by the transcriptional activator Nrf2 (Jiying et al., 2004; Igarashi and Sun, 2006). In the present study, FGF1 treatment caused significant increases in expression levels of Nrf2 in db/db mice, which ameliorated diabetes-induced oxidative stress in liver tissue (**Figures 5E, F**). Furthermore, expression levels of HO-1 in db/db mice liver were also lower than those of db/m mice, an effect that was diminished by FGF1 treatment (**Figures 5E, G**). SOD2 protein expression levels in liver were also significantly lower in db/db mice than those in db/m mice, an effect that was markedly ameliorated in FGF1-treated db/db mice (**Figures 5E, H**). Taken together, these data suggest that FGF1 treatment markedly reversed diabetes-induced hepatic oxidative stress in db/db mice.

In addition, we also examined FGFR1-AMP-activated protein kinase (AMPK) signaling pathway. Western blotting results show that FGFR1 expression level in db/db + FGF1 liver was markedly higher than that in db/db liver, indicating that FGFR1 signaling was activated by FGF1 treatment (**Supplement Figures 1A, B**). AMPK, a serine kinase, has been reported to enhance cellular antioxidant capacity through inducing activation of Nrf2 and HO-1 (Lee et al., 2019). In the present study, as shown in **Supplement Figures 1A, C**, hepatic P-AMPK levels were significantly lower in db/db mice compared with the db/m mice. As expected, these changes were reversed by FGF1 treatment. Taken together, these data suggest that FGF1 treatment markedly reversed diabetes-induced hepatic oxidative stress by regulating FGFR1-AMPK pathway.

FGF1 Treatment Suppressed Diabetes-Induced Endoplasmic Reticulum Stress in Liver

Diabetes-induced liver injury causes changes in microstructure and morphology of liver tissues, leading to changes of hydrophilic and hydrophobic domains in endoplasmic reticulum, an effect that was closely associated with changes of cellular endoplasmic reticulum (ER) polarity. These data suggest that differences in ER polarity can suggest degree of diabetes-induced liver injury (Xiao et al., 2017). Proteins enter the ER as unfolded polypeptide chains, also called the unfolded protein response (UPR) (Ron and Walter, 2007). Elevation in the phosphorylation of eIF2α and PERK (P-eIF2α and P-PERK) is indicative marker of ER stress in diabetes mice. Furthermore, P-IRE1α, an early and crucial indicator of ER stress, plays an important role in mediating the UPR response under ER stress (Wang et al., 2013). To measure FGF1 treatment mediated inhibition of diabetes-induced ER stress in liver, we measured expression levels of ER stress protein markers. Hepatic protein levels of glucose-regulated protein 78 (GRP78), activating transcription factor 6 (ATF6), and C/EBP-homologous protein (CHOP) were significantly greater in db/db mice and these changes were reversed by FGF1 treatment (**Figures 6A–D**).

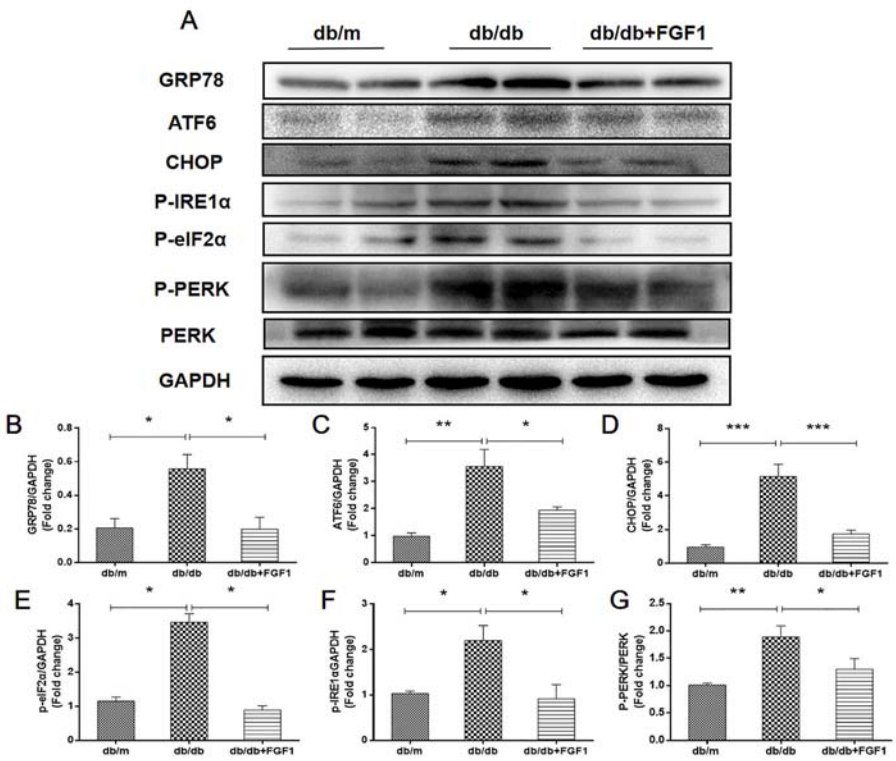

FIGURE 6 | FGF1 suppressed diabetes-induced liver endoplasmic reticulum stress. **(A)** Protein expression of GRP78, ATF6, CHOP, P-eIF2α, P-IRE1α, and P-PERK in liver from db/m, db/db, and db/db + FGF1 mice. **(B–F)** Intensities of GRP78, ATF6, CHOP, P-eIF2α, and P-IRE1α normalized to GAPDH. **(G)** Intensity of P-PERK normalized to PERK. All data are presented as mean ± SEM, n = 8. *P < 0.05 **P < 0.01 ***P < 0.001 *vs*. the db/m group and db/db + FGF1 group.

Notably, we identified dramatically higher P-IRE1α, P-eIF2α, and P-PERK protein expression levels in livers of db/db mice than in those of db/m mice, an effect that was inhibited by FGF1 treatment (**Figures 6A, E–G**). Taken together, these data suggest that FGF1 treatment significantly suppressed diabetes-induced ER stress.

DISCUSSION

In the present study, we demonstrated the glucose-lowing effect of FGF1 in db/db mice and its effects on the progression of liver injury in T2DM. These observations were associated with reduced plasma ALT, liver, and plasma TG levels, and decreased ER stress and oxidative stress as well as hepatic apoptosis. Furthermore, hepatic autophagy was corrected by FGF1 treatment.

The db/db mouse model is characterized by leptin receptor deficiency, and displays hyperinsulinemia, hyperglycemia, and glucosuria phenotypes (Razzoli et al., 2015). Previous studies have shown that FGF1 has therapeutic potential for insulin resistance and type 2 diabetes. A single injection of 0.5 mg/kg rFGF1 corrected hyperglycemia in ob/ob mice. This effect of FGF1 is dose-dependent, and even at the maximal dose (2.0 mg/kg) it does not produce hypoglycemia. Moreover, FGF1 has no effect on blood glucose or insulin levels in normoglycemic chow-fed mice. Furthermore, chronic rFGF1 treatment in mice with diet-induced obesity (DIO) also caused pronounced and sustained lowering of blood glucose levels and increased insulin sensitization (JaeMyoung et al., 2014). The glucose-lowering effects of FGF1 are mediated predominantly *via* FGF receptor 1 signaling. Injection of agonistic anti-FGF receptor 1 antibodies into obese diabetic mice induced acute and sustained amelioration of hyperglycemia, accompanied by significant improvement in hyperlipidemia, hyperinsulinemia, and hepatosteatosis (Wu et al., 2015b). In the present study, treatment of FGF1 for 4 weeks significantly reduced glucose levels in the circulation. Our results further confirmed the therapeutic potential of FGF1 for insulin resistance and type 2 diabetes.

Previous studies have shown that recombinant FGF1 (rFGF1) effectively improved hepatic damage and inflammation in ob/ob mice and choline-deficient mice, two etiologically-different models of NAFLD. Studies have reported that rFGF1 reduced steatosis in the periportal zone first, and subsequently improved hepatic lipid catabolism (Liu Y. et al., 2016). Consistent with these findings, we confirmed that FGF1 administration ameliorated diabetes-induced liver damage. We showed that FGF1 treatment reduced plasma ALT levels, ameliorated liver lipid accumulation as well as hepatic apoptosis and liver fibrosis and corrected hepatic autophagy. Furthermore, we demonstrated that FGF1 treatment blocked diabetes-associated collagen accumulation. All these findings are consistent with previous observations demonstrating the hepatic-protective effects of FGF1 in various animal models. Mechanistic studies demonstrated that induction of cellular stress in diabetic liver was inhibited by FGF1 treatment, suggesting that reduction of cellular stress was a potential molecular mechanism in course of FGF1 treatment for diabetes-induced liver injury.

Previous studies reported that FGF1 inhibited oxidative stress and consequently blocked diabetes-induced cardiomyopathy (Wu et al., 2016). Elevated oxidative stress is a major causal factor in diabetes-associated complications (Wu et al., 2011). Liver tissues from diabetic rats also showed significantly increased levels of reactive oxygen species (ROS), and dramatically lower levels of GSH, catalase, and superoxide dismutase (SOD) (Borderud et al., 2014). In the resting state, Nrf2 is in a non-free and non-active state of continuous degradation. When stimulated by electrophiles or ROS, Keap1 is uncoupled from Nrf2, allowing Nrf2 to transfer to the nucleus, and the Maf protein in the gene. Binding to the heterodimer recognizes and binds ARE, initiates transcription of the downstream protective protein genes, and enhances cell's ability to resist oxidative stress (McMahon et al., 2006). Nrf2 signaling may compensatorily increase the response to acute stress (Stewart et al., 2003), modulating expression of several oxidative damage genes, including HO-1 and SOD2 that are protective in diverse models of liver diseases (Ge et al., 2015; Peng et al., 2018). In our study, diabetes markedly resulted in down-regulation of Nrf2, HO-1 and SOD2, an effect that was reversed by FGF1 treatment. Furthermore, FGF1 treatment regulated FGFR1-AMPK signaling pathway. The above-mentioned data suggest that FGF1 treatment ameliorated hyperglycemia and subsequently oxidative stress during diabetes-induced liver injury *via* regulation of the FGFR1-AMPK-Nrf2/HO-1 signaling pathway.

A previous report showed that ER stress induced the production of reactive oxygen species (ROS) (Peng et al., 2018), thereby leading to oxidative stress (Hyung-Ryong et al., 2009). ER stress occurs when misfolded proteins accumulate in the ER lumen, and this is referred to as the unfolded protein response (UPR) (Hyung-Ryong et al., 2009). The UPR is made up of three main branches, controlled by ER membrane proteins: activating transcription factor (ATF), inositol-requiring enzyme (IRE), and protein kinase-like ER kinase (PERK), all of which are suppressed by binding to GRP78 (Hummasti and Hotamisligil, 2010). Elevated ER chaperone proteins are biological indicators of ER stress. In mammalian cells, 2 kinases, the inositol-requiring enzyme-1α (IRE1α) and PERK are responsible for activation of UPR. In diabetes, ER stress is caused by increased secretory demands to compensate for insulin resistance and is further aggravated by a fatty acid-induced ER dysfunction in β-cells (Saltiel and Kahn, 2001). Under these conditions, IRE1α activation induces messenger RNA (mRNA) splicing of transcription factors, whereas PERK activation inhibits protein translation and increases the expression of proapoptotic C/EBP-homologous protein (CHOP) *via* phosphorylation of eukaryotic initiation factor 2α (eIF2α) (Zinszner et al., 1998). In accordance with these data, we found that expression levels of ER stress markers, including CHOP, GRP78, and ATF6, were elevated in db/db mice. Protein expression levels of P-IRE1α, P-eIF2α, and P-PERK were much higher in livers of db/db mice than in those

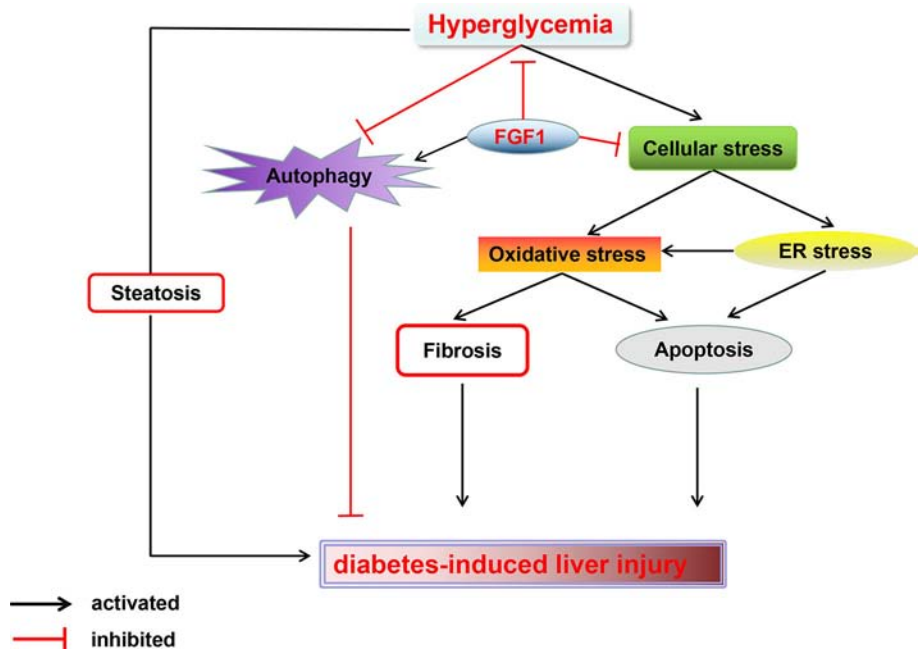

FIGURE 7 | A Schematic showing the effects of FGF1 treatment on diabetic-induced liver injury. As reported that FGF1 can restore blood glucose levels to the normal range in reference 7. FGF1 treatment blocked hyperglycemia-induced cellular stress (oxidative stress and ER stress) and restored autophagy in liver, which ameliorates hepatic steatosis and fibrosis, consequently ameliorates diabetes-induced liver injury.

of db/m mice, an effect reversed by FGF1 treatment. Taken together, these data suggest that FGF1 exerted effects on diabetes-induced liver injury by suppressing diabetes-induced ER stress.

According to previous studies, overload of misfolded and/or aggregated proteins in ER lumen leads to ER dysfunction, resulting in ER stress and apoptosis (Varadarajan et al., 2012). Apoptosis is a primary characteristic of the pathogenesis of liver disease. In accordance with results of previous studies, we found that diabetes boosted apoptosis-related proteins expression levels including Bax and cleaved caspase3, and decreased Bcl2 protein expression level, all of which were reversed by FGF1 treatment. Hepatic apoptosis is regulated by autophagic activity. In addition, cross-talk between autophagy and apoptosis have been manifested by regulatory genes sharing common pathways. These regulatory genes include ATG5 and Bcl2 (Kewei, 2015). Previous studies showed that reduction in expression of autophagy-related protein ATG5, and ATG protein is an essential mediator of the autophagic process, resulting in defective insulin responsiveness. In the current study, we demonstrated that FGF1 increased defective hepatic autophagy in db/db mice *via* regulation of autophagy related proteins, including LC3II, ATG5 and p62 (**Figure 4**).

In summary, our findings expand the notion that FGF1 controlled hyperglycemia and normalized blood glucose levels in db/db mice. Treatment with FGF1 for 4 weeks significantly reduced blood glucose levels. These observations were associated with reduced diabetic liver damage. The protective effect of FGF1 on diabetes-induced injury was demonstrated by significantly lower plasma ALT activity levels, TG levels, and hepatic lipid accumulation as well as suppressed cellular stress, reduced diabetes-induced hepatic apoptosis, and restored defective hepatic autophagy. We confirmed that inhibition of cellular stress and restoring autophagy are the potential molecular mechanisms of FGF1 inhibition of diabetes-induced liver injury (**Figure 7**). One limitation is that we did not record food intake; this will be measured in a future study to fully understand the role of FGF1 in reducing glucose effect and ameliorating diabetes-induced liver injury.

DATA AVAILABILITY STATEMENT

The raw data supporting the conclusions of this article will be made available by the authors, without undue reservation, to any qualified researcher.

ETHICS STATEMENT

The animal study was reviewed and approved by the Laboratory Animal Ethics Committee of Wenzhou Medical University & the Laboratory Animal Centre of Wenzhou Medical University.

AUTHOR CONTRIBUTIONS

YAL and JX conceived and designed the research. ZX performed the experiments and wrote the paper. YW gave important and thoughtful advices and performed the experiments. FW performed the statistical analysis and supplied a lot of technology and served as a fund assistant. XL, PW, YUL, JW, YIL, TJ, XP, XZ, and LX provided assistance with the experiments. All authors discussed the drafting of the manuscript.

FUNDING

This work was partly supported by the National Natural Science Foundation of China (81300311), the Opening Project of Zhejiang Provincial Top Key Discipline of Pharmaceutical Sciences, the Technology Support Project of Xinjiang (2017E0267), the Xinjiang Tianshan Youth Project for Outstanding Young Scientists (2017Q007), Natural Science Foundation of Xinjiang Province (2018D01C228), Zhejiang public welfare technology research project (LGF19H030008), Ningbo Huimin project (2016C51004), and Ningbo Natural Science Funding (2018A610376), Project of Medical Technology of Zhejiang Province (2020KY908), and Natural Science Foundation of Xinjiang Uyghur Autonomous Region (2018D01C228).

ACKNOWLEDGMENTS

We thank Prof. Xiaokun Li for his advice on experimental design.

SUPPLEMENTARY MATERIAL

The Supplementary Material for this article can be found online at: https://www.frontiersin.org/articles/10.3389/fphar.2020.00052/full#supplementary-material

SUPPLEMENT FIGURE 1 | FGFR1-AMPK signaling pathway was activated. **(A)** Protein expression of FGFR1, P-AMPK and AMPK in liver from db/m, db/db and db/db + FGF1 mice. **(B)** Intensities of FGFR1 normalized to GAPDH. **(C)** Intensity of P-AMPK normalized to AMPK. All data are presented as mean ± SEM, n = 8. *P < 0.05 **P < 0.01 ***P < 0.001 *vs*. the db/m group and db/db + FGF1 group.

REFERENCES

Abraham, N. G., and Kappas, A. (2008). Pharmacological and clinical aspects of heme oxygenase. *Pharmacol. Rev.* 60 (1), 79–127. doi: 10.1124/pr.107.07104

Borderud, S. P., Li, Y., Burkhalter, J. E., Sheffer, C. E., and Ostroff, J. S. (2014). Electronic cigarette use among patients with cancer: characteristics of electronic cigarette users and their smoking cessation outcomes. *Cancer* 120 (22), 3527–3535. doi: 10.1002/cncr.28811

Guang, L., LinTao, S., Zilu, C., Yuanyuan, Q., Junjun, X., Longwei, Z., et al. (2018). Fibroblast growth factor 1 ameliorates diabetic nephropathy by an anti-inflammatory mechanism. *Kidney Int.* 93 (1), 95–109. doi: 10.1016/j.kint.2017.05.013

Ge, M., Yao, W., Wang, Y., Yuan, D., Chi, X., Luo, G., et al. (2015). Propofol alleviates liver oxidative stress via activating Nrf2 pathway. *J. Surg. Res.* 196 (2), 373–381. doi: 10.1016/j.jss.2015.03.016

Gezginci-Oktayoglu, S., Basaraner, H., Yanardag, R., and Bolkent, S. (2009). The effects of combined treatment of antioxidants on the liver injury in STZ diabetic rats. *Dig. Dis. Sci.* 54 (3), 538–546. doi: 10.1007/s10620-008-0381-0

Hao, L. S., Zhang, X. L., An, J. Y., Karlin, J., Tian, X. P., Dun, Z. N., et al. (2009). PTEN expression is down-regulated in liver tissues of rats with hepatic fibrosis induced by biliary stenosis. *APMIS* 117 (9), 681–691. doi: 10.1111/j.1600-0463.2009.02515.x

Hyung-Ryong, K., Geum-Hwa, L., Eun Yi, C., Soo-Wan, C., Taeho, A., and Han-Jung, C. (2009). Bax inhibitor 1 regulates ER-stress-induced ROS accumulation through the regulation of cytochrome P450 2E1. *J. Cell Sci.* 122 (null), 1126–1133. doi: 10.1242/jcs.038430

Hummasti, S., and Hotamisligil, G. S. (2010). Endoplasmic reticulum stress and inflammation in obesity and diabetes. *Circ. Res.* 107 (5), 579–591. doi: 10.1161/CIRCRESAHA.110.225698

Igarashi, K., and Sun, J. (2006). The heme-Bach1 pathway in the regulation of oxidative stress response and erythroid differentiation. *Antioxid.s Redox Signaling* 8 (null), 107–118. doi: 10.1089/ars.2006.8.107

Iwadate, R., Inoue, J., Tsuda, H., Takano, M., Furuya, K., Hirasawa, A., et al. (2014). High expression of SQSTM1/p62 protein is associated with poor prognosis in epithelial ovarian cancer. *Acta Histochem. Cytochem.* 47 (6), 295–301. doi: 10.1267/ahc.14048

Jiying, S., Marjorie, B., Yukari, Z., Satoshi, T., Mark, G., and Kazuhiko, I. (2004). Heme regulates the dynamic exchange of Bach1 and NF-E2-related factors in the Maf transcription factor network. *Proc. Natl. Acad. Sci. U. S. A.* 101 (6), 1461–1466. doi: 10.1073/pnas.0308083100

Jiang, W., Jingjing, Z., Chaochao, H., Zecong, X., Jingjing, Y., Yi, L., et al. (2016). Comparative study of heparin-poloxamer hydrogel modified bFGF and aFGF for *in vivo* wound healing efficiency. *ACS Appl. Mater. Interfaces* 8 (29), 18710–18721. doi: 10.1021/acsami.6b06047

JaeMyoung, S., JohanW, J., Maryam, A., Regina, G., Denise, L., Olivia, O., et al. (2014). Endocrinization of FGF1 produces a neomorphic and potent insulin sensitizer. *Nature* 513 (7518), 436–439. doi: 10.1038/nature13540

Kewei, W. (2015). Autophagy and apoptosis in liver injury. *Cell Cycle (Georgetown Tex.)* 14 (11), 1631–1642. doi: 10.1080/15384101.2015.1038685

Kasuga, M. (2006). Insulin resistance and pancreatic beta cell failure. *J. Clin. Invest.* 116 (7), 1756–1760. doi: 10.1172/JCI29189

Lee, E. H., Baek, S. Y., Park, J. Y., and Kim, Y. W. (2019). Rifampicin activates AMPK and alleviates oxidative stress in the liver as mediated with Nrf2 signaling. *Chem. Biol. Interact.* 315, 108889. doi: 10.1016/j.cbi.2019.108889

Li, X. (2019). The FGF metabolic axis. *Front. Med.* 13 (5), 511–530. doi: 10.1007/s11684-019-0711-y

Liu, W., Struik, D., Nies, V. J., Jurdzinski, A., Harkema, L., de Bruin, A., et al. (2016). Effective treatment of steatosis and steatohepatitis by fibroblast growth factor 1 in mouse models of nonalcoholic fatty liver disease. *Proc. Natl. Acad. Sci. U. S. A* 113 (8), 2288–2293. doi: 10.1073/pnas.1525093113

Liu, Y., Zhao, C., Xiao, J., Liu, L., Zhang, M., Wang, C., et al. (2016). Fibroblast growth factor 21 deficiency exacerbates chronic alcohol-induced hepatic steatosis and injury. *Sci. Rep.* 6, 31026. doi: 10.1038/srep31026

Marchesini, G., Brizi, M., Bianchi, G., Tomassetti, S., Bugianesi, E., Lenzi, M., et al. (2001). Nonalcoholic fatty liver disease: a feature of the metabolic syndrome. *Diabetes* 50 (8), 1844–1850. doi: 10.2337/diabetes.50.8.1844

McMahon, M., Thomas, N., Itoh, K., Yamamoto, M., and Hayes, J. D. (2006). Dimerization of substrate adaptors can facilitate cullin-mediated ubiquitylation of proteins by a "tethering" mechanism: a two-site interaction model for the Nrf2-Keap1 complex. *J. Biol. Chem.* 281 (34), 24756–24768. doi: 10.1074/jbc.M601119200

Mohamed, J., Nazratun Nafizah, A. H., Zariyantey, A. H., and Budin, S. B. (2016). Mechanisms of diabetes-induced liver damage: the role of oxidative stress and inflammation. *Sultan Qaboos Univ. Med. J.* 16 (2), e132–e141. doi: 10.18295/squmj.2016.16.02.002

Peng, X., Dai, C., Liu, Q., Li, J., and Qiu, J. (2018). Curcumin attenuates on carbon tetrachloride-induced acute liver injury in mice via modulation of the Nrf2/

HO-1 and TGF-beta1/Smad3 pathway. *Molecules* 23 (1), 8–9. doi: 10.3390/molecules23010215

Razzoli, M., McCallum, J., Gurney, A., Engeland, W. C., and Bartolomucci, A. (2015). Chronic stress aggravates glucose intolerance in leptin receptor-deficient (db/db) mice. *Genes Nutr.* 10 (3), 458. doi: 10.1007/s12263-015-0458-2

Ron, D., and Walter, P. (2007). Signal integration in the endoplasmic reticulum unfolded protein response. *Nat. Rev. Mol. Cell Biol.* 8 (7), 519–529. doi: 10.1038/nrm2199

Saltiel, A. R., and Kahn, C. R. (2001). Insulin signalling and the regulation of glucose and lipid metabolism. *Nature* 414 (6865), 799–806. doi: 10.1038/414799a

Stewart, D., Killeen, E., Naquin, R., Alam, S., and Alam, J. (2003). Degradation of transcription factor Nrf2 via the ubiquitin-proteasome pathway and stabilization by cadmium. *J. Biol. Chem.* 278 (4), 2396–2402. doi: 10.1074/jbc.M209195200

Valle, A., Catalan, V., Rodriguez, A., Rotellar, F., Valenti, V., Silva, C., et al. (2012). Identification of liver proteins altered by type 2 diabetes mellitus in obese subjects. *Liver Int.* 32 (6), 951–961. doi: 10.1111/j.1478-3231.2012.02765.x

Varadarajan, S., Bampton, E. T. W., Smalley, J. L., Tanaka, S. K., Caves, R. E., Butterworth, M., et al. (2012). A novel cellular stress response characterised by a rapid reorganisation of membranes of the endoplasmic reticulum. *Cell Death Differentiation* 19 (12), 1896–1907. doi: 10.1038/cdd.2012.108

Wang, F., Reece, E. A., and Yang, P. (2013). Superoxide dismutase 1 overexpression in mice abolishes maternal diabetes-induced endoplasmic reticulum stress in diabetic embryopathy. *Am. J. Obstet. Gynecol.* 209 (4), 345 e341–347. doi: 10.1016/j.ajog.2013.06.037

Wang, X., Zhang, X., Wang, F., Pang, L., Xu, Z., Li, X., et al. (2019). FGF1 protects against APAP-induced hepatotoxicity via suppression of oxidative and endoplasmic reticulum stress. *Clin. Res. Hepatol. Gastroenterol.* 43 (6), 1–7. doi: 10.1016/j.clinre.2019.03.006

Wu, A. L., Kolumam, G., Stawicki, S., Chen, Y., Li, J., Zavala-Solorio, J., et al. (2011). Amelioration of type 2 diabetes by antibody-mediated activation of fibroblast growth factor receptor 1. *Sci. Transl. Med.* 3 (113), 113ra126. doi: 10.1126/scitranslmed.3002669

Wu, Y., Wang, F., Fu, M., Wang, C., Quon, M. J., and Yang, P. (2015a). Cellular stress, excessive apoptosis, and the effect of metformin in a mouse model of Type 2 diabetic embryopathy. *Diabetes* 64 (7), 2526–2536. doi: 10.2337/db14-1683

Wu, Y., Wang, F., Reece, E. A., and Yang, P. (2015b). Curcumin ameliorates high glucose-induced neural tube defects by suppressing cellular stress and apoptosis. *Am. J. Obstet. Gynecol.* 212 (6), 802 e801–808. doi: 10.1016/j.ajog.2015.01.017

Wu, Y., Reece, E. A., Zhong, J., Dong, D., Shen, W. B., Harman, C. R., et al. (2016). Type 2 diabetes mellitus induces congenital heart defects in murine embryos by increasing oxidative stress, endoplasmic reticulum stress, and apoptosis. *Am. J. Obstet. Gynecol.* 215 (3), 366 e361–366 e310. doi: 10.1016/j.ajog.2016.03.036

Wu, Y., Li, Y., Jiang, T., Yuan, Y., Li, R., Xu, Z., et al. (2018). Reduction of cellular stress is essential for Fibroblast growth factor 1 treatment for diabetic nephropathy. *J. Cell Mol. Med.* 22 (12), 6294–6303. doi: 10.1111/jcmm.13921

Xiao, H., Wu, C., Li, P., Gao, W., Zhang, W., Zhang, W., et al. (2017). Ratiometric photoacoustic imaging of endoplasmic reticulum polarity in injured liver tissues of diabetic mice. *Chem. Sci.* 8 (10), 7025–7030. doi: 10.1039/C7SC02330H

Yang, L., Li, P., Fu, S., Calay, E. S., and Hotamisligil, G. S. (2010). Defective hepatic autophagy in obesity promotes ER stress and causes insulin resistance. *Cell Metab.* 11 (6), 467–478. doi: 10.1016/j.cmet.2010.04.005

Yang, P., Reece, E. A., Wang, F., and Gabbay-Benziv, R. (2015). Decoding the oxidative stress hypothesis in diabetic embryopathy through proapoptotic kinase signaling. *Am. J. Obstet. Gynecol.* 212 (5), 569–579. doi: 10.1016/j.ajog.2014.11.036

Yu, L., Zheng, J., Li, J., Wang, Y., Lu, X., and Fan, X. (2019). Integrating serum exosomal microRNA and liver microRNA profiles disclose the function role of autophagy and mechanisms of Fructus Meliae Toosendan-induced hepatotoxicity in mice. *BioMed. Pharmacother.* 123, 109709. doi: 10.1016/j.biopha.2019.109709

Zinszner, H., Kuroda, M., Wang, X., Batchvarova, N., Lightfoot, R. T., Remotti, H., et al. (1998). CHOP is implicated in programmed cell death in response to impaired function of the endoplasmic reticulum. *Genes Dev.* 12 (7), 982–995. doi: 10.1101/gad.12.7.982

Conflict of Interest: The authors declare that the research was conducted in the absence of any commercial or financial relationships that could be construed as a potential conflict of interest.

frontiers in Pharmacology

MINI REVIEW
published: 10 March 2020
doi: 10.3389/fphar.2020.00250

The Role of Fibroblast Growth Factor 10 Signaling in Duodenal Atresia

*Matthew L. M. Jones[1,2,3], Gulcan Sarila[1], Pierre Chapuis[2], John M. Hutson[1,4,5], Sebastian K. King[1,2,3,4] and Warwick J. Teague[1,2,3,4]**

[1] F. Douglas Stephens Surgical Research Laboratory, Murdoch Children's Research Institute, Melbourne, VIC, Australia, [2] Discipline of Surgery, Sydney Medical School, The University of Sydney, Sydney, NSW, Australia, [3] Department of Paediatric Surgery, The Royal Children's Hospital, Melbourne, VIC, Australia, [4] Department of Paediatrics, The University of Melbourne, Melbourne, VIC, Australia, [5] Department of Urology, The Royal Children's Hospital Melbourne, Melbourne, VIC, Australia

Introduction: Duodenal atresia (DA) is a congenital bowel obstruction requiring major surgery in the first week of life. Three morphological phenotypes are described, reflecting increasing degrees of obstruction and discontinuity of the duodenum. The cause of DA is not known. Tandler's original "solid cord" hypothesis conflicts with recent biological evidence, and is unable to account for differing DA types. In humans, a genetic etiology is supported by the association between Trisomy 21 and DA, and reports of familial inheritance patterns. Interruption of FGF10/FGFR2b signaling is the best demonstrated genetic link to DA in mice, with 35–75% of homozygous knockout embryos developing DA.

Purpose: This review examines the current evidence surrounding the etiology of DA. We focus on research regarding FGF10/FGFR2b signaling and its role in duodenal and other intestinal atresia. Further, we outline planned future research in this area, that we consider necessary to validate and better understand this murine model in order to successfully translate this research into clinical practice.

Conclusion: Determining the etiology of DA in humans is a clinical and scientific imperative. *Fgf10/Fgfr2b* murine models represent current science's best key to unlocking this mystery. However, further research is required to understand the complex role of FGF10/FGFR2b signaling in DA development. Such complexity is expected, given the lethality of their associated defects makes ubiquitous interruption of either *Fgf10* or *Fgfr2b* genes an unlikely cause of DA in humans. Rather, local or tissue-specific mutation in *Fgf10*, *Fgfr2b*, or their downstream targets, is the hypothesized basis of DA etiology.

Keywords: duodenal obstruction, congenital intestinal atresia, fibroblast growth factor 10, fibroblast growth factor receptor 2b, morphogenesis

OPEN ACCESS

Edited by:
Saverio Bellusci, University of Giessen, Germany

Reviewed by:
Stefano Rivetti, University of Giessen, Germany
Denise Al Alam, University of Southern California, United States

***Correspondence:**
Warwick J. Teague
warwick.teague@rch.org.au

Specialty section:
This article was submitted to Translational Pharmacology, a section of the journal Frontiers in Pharmacology

Received: *22 November 2019*
Accepted: *24 February 2020*
Published: *10 March 2020*

Citation:
Jones MLM, Sarila G, Chapuis P, Hutson JM, King SK and Teague WJ (2020) The Role of Fibroblast Growth Factor 10 Signaling in Duodenal Atresia. Front. Pharmacol. 11:250. doi: 10.3389/fphar.2020.00250

INTRODUCTION

Duodenal atresia (DA) is a congenital foregut malformation affecting 1 in 5,000–10,000 live births (Escobar et al., 2004). Three morphological types of DA are described, reflecting increasing degrees of obstruction and discontinuity; type 1: bowel continuity but luminal obstruction or stenosis, type 2: bowel discontinuity with a connecting "bridge" of tissue, and, type 3: bowel discontinuity

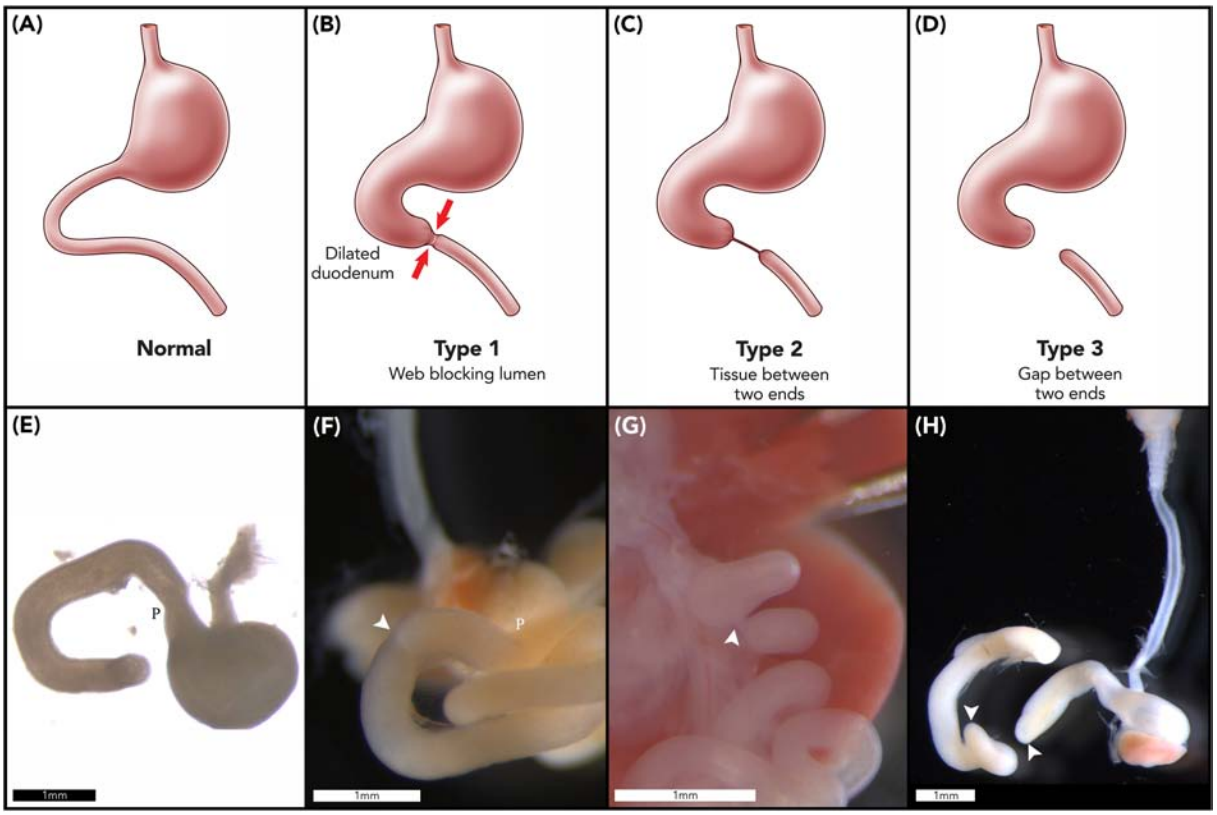

FIGURE 1 | Duodenal atresia phenotype characterization. Normal gastric, pyloric, and duodenal morphology demonstrated pictorially **(A)** and as seen in wildtype murine embryos **(E)**. Type 1 DA is characterized by bowel continuity with luminal obstruction or stenosis **(B)**. Type 2 DA demonstrates bowel discontinuity with a connecting "bridge" of tissue **(C)**. Type 3 DA shows bowel discontinuity with complete separation **(D)**. Our CRISPR-derived *Fgf10* knockout embryos provided examples of type 1 DA **(F)**; type 2 DA **(G)**; and type 3 DA **(H)** including demonstration of an intact esophagus, in the presence of tracheal atresia **(H)**. Annotations denote scale bars, and location of the pylorus, P. Arrows indicate location of an atresia. Figures **(E–H)** reused from Teague et al. (2018), held under the CC-BY 4.0 license.

with complete separation (Skandalakis and Gray, 1994; **Figures 1A–D**). Duodenal atresia was first described in humans by Calder (1733), but it was not until the early twentieth century that Vidal and Ernst performed the first reported successful surgical repair (Vidal, 1905; Ernst, 1916). Nowadays, DA is routinely surgically repaired in the first week of life, with re-establishment of duodenal continuity and minimal postoperative morbidity or mortality (Zani et al., 2017).

The cause of DA is not known. In 1900, Julius Tandler published a hypothesis on the origins of DA, based on his studies of normal duodenal development (Tandler, 1900). Tandler meticulously dissected 11 human embryos and theorized, on the basis of his macroscopic observations, that normal duodenal development includes a "solid cord" phase due to exuberant endodermal growth. As such, he proposed that failure of this "solid cord" to re-canalize may result in DA in humans. Even then, Tandler cautioned readers, stating: "It is clear to me that the opinion represented here does not exceed the status of a new hypothesis, and it is not meant to exceed this." (Nichol et al., 2011). Notwithstanding, Tandler's "solid cord" hypothesis is generally accepted worldwide by the majority of pediatric surgeons. This is despite conflicting developmental biology findings (Cheng and Tam, 1998; Botham et al., 2012), and failure of Tandler's theory to account for the morphological variations of DA (Merrot et al., 2006).

As will be discussed in detail in this review, murine studies have shown that interruption of the *Fgf10-Fgfr2b* signaling axis may result in DA in 35–75% of knockout mice (Fairbanks et al., 2004b; Kanard et al., 2005; Botham et al., 2012; Reeder et al., 2012b; Teague et al., 2018). This also supports a genetic etiology for DA in humans, however, no specific genetic cause has been demonstrated to date. In humans, the association between DA and Trisomy 21 is well recognized, with DA occurring in 20% of cases (Khan et al., 2017). Yet, animal models of Trisomy 21 fail to demonstrate DA or other associated gastrointestinal malformations (Delabar et al., 2006). Again in humans, an autosomal recessive inheritance pattern for familial cases has been proposed, albeit based on a limited number of isolated and historical case reports (Fonkalsrud et al., 1969; Berant and Kahana, 1970; Best et al., 1989; Gross et al., 1996; Lambrecht and Kluth, 1998). Finally, whilst associations between DA and specific chromosomal anomalies have been reported (Mora et al., 2014; Zamfir et al., 2016), none relate to Chromosome 21, or to Chromosome 5 which houses the *FGF10* gene in humans.

FGF SIGNALING IN GASTROINTESTINAL DEVELOPMENT

The mammalian fibroblast growth factors (FGF) family contains 22 genes, 18 of which have been shown to bind and activate tyrosine kinase FGF receptors (FGFR), using either heparin-like molecules or klotho cofactors receptor binding (Ornitz and Itoh, 2015). These 18 FGFs have been grouped into six sub-families based on biochemical function, sequence homology and evolutionary traits (Ornitz and Itoh, 2001). The FGF7 sub-family is comprised of FGF3, FGF7, FGF10, and FGF22, and preferentially binds and activates FGFR2b (the IIIb splice variant of the FGFR2 receptor). This receptor is expressed in the epithelial layer and can be activated by FGF7 and FGF10 ligands (Ibrahimi et al., 2001). These ligands show no binding activity with the mesenchyme-expressed FGFR2c variant (Igarashi et al., 1998; Zhang et al., 2006). Conversely, FGF8 ligand preferentially binds and activates FGFR2c, with no binding activity toward FGFR2b (Macarthur et al., 1995; Ornitz et al., 1996).

The activation of FGFR2b by FGF10 is associated with mesenchymal/epithelial interactions which instruct branching and budding morphogenesis. This is a key signaling pathway for normal development of the gastrointestinal tract [e.g., stomach (Spencer-Dene et al., 2006), duodenum (Kanard et al., 2005), and large intestine (Burns et al., 2004)] and its derivatives [e.g., lung (Park et al., 1998)]. Indeed, gastrointestinal development involves multiple signaling pathways and their associated transcription factors, including FGF10-FGFR2b, which are summarized in **Figure 2A** and reviewed elsewhere (Kim and Shivdasani, 2016; Danopoulos et al., 2017).

FGF10-FGFR2b binding is implicated in the activation of multiple intracellular signaling pathways, including the ERK1/2, MAP kinase (MAPK) pathway, to induce downstream activation of proliferation and cell survival genes (Luo et al., 2008; Yang et al., 2011; **Figure 2B**). TBX4/TBX5 may induce *Fgf10* expression to promote region-specific stimulation of the mesenchymal proliferation at the initial sites of foregut growth. This growth depends on the regulation of the HOX and TBX genes, which are mediated by retinoic acid (RA) (Wang et al., 2006). Potentially, RA acts on TBX genes, such as TBX4 and TBX5, as a co-factor to activate FGF10 transcription and, as a result, mediates the FGF10-FGF8 positive feedback loop which is required for outgrowth (Nishimoto et al., 2015). Embryos that are RA-deficient fail to outgrow due to defective FGF10 signaling, resulting in a lack of FGF-target genes in the epithelium. Interestingly, the development of the foregut may be partly restored in the defective embryos by introducing RA supplementation early on in development (between E7.5 and E8.5), suggesting that RA regulation is upstream of FGF10 (**Figure 2B**; Wang et al., 2006).

Within the cecum and proximal colon FGF9 binds to the mesenchyme-expressed FGFR2c receptor to direct cecal mesenchyme expansion via the expression of PITX2. In conjunction with this, FGF10 acts to trigger the budding of the epithelium into the cecal mesenchyme, again through mediation of PITX2 expression. Thus, the interaction between FGF10 and PITX2 is critical for the maintenance and the proliferation of the epithelial progenitor cells of the colon (**Figure 2B**). During embryonic development, FGF10 is also expressed in the mesenchyme of the distal colon, where it binds and activates FGFR1b and FGFR2b to promote proliferation, differentiation and survival of the epithelium. This activation maintains progenitor cells within the embryonic small intestine by targeting E26 transformation-specific (ETS)-Family genes such as ETV4, ETV5, and CCND1 through the MAPK pathway (Nyeng et al., 2011; **Figure 2B**).

The homozygous deletion of the *Fgf10* or *Fgfr2b* gene results in mice with multiple organ defects, including lung, limb and mammary glands (with failure to form buds 1, 2, 3, and 5). The resultant mice are non-viable after birth due to lung agenesis (De Moerlooze et al., 2000; Mailleux et al., 2002).

Fgf10/Fgfr2b SIGNALING IN DUODENAL ATRESIA

Fairbanks et al. (2004b) were the first to identify a link between the *Fgf10/Fgfr2b* signaling pathway and intestinal atresia in mice. Using *Fgfr2b* knockout mice, they observed DA in 35% of null embryos when examined at gestational stage E18.5. These authors reported examples of both type 1 DA (57%) and type 3 DA (43%), but no type 2 DA (Fairbanks et al., 2004b). The same group then turned their attention to interruption of the ligand instead of receptor, knocking out *Fgf10* (Kanard et al., 2005). Interestingly, *Fgf10* knockout embryos were found to have a similar penetrance of DA (38%) compared to *Fgfr2b* knockouts, but with notably different relative frequency of DA types; type 1 DA (8%), type 3 DA (92%), and still no type 2 DA (Kanard et al., 2005). Further emphasizing the importance of the *Fgf10/Fgfr2b* pathway in intestinal development, deletion of either *Fgf10* or *Fgfr2b* also resulted in a more distally located intestinal atresia, i.e., colonic atresia (Fairbanks et al., 2004a). In contrast with the incomplete penetrance of DA, colonic atresia was present in 100% of *Fgf10* and *Fgfr2b* knockout mice embryos (Fairbanks et al., 2004a).

Importantly, the morphology of the duodenum is normal in *Fgf10* hypomorphic mice, with no examples of DA in this setting of *Fgf10* under-expression (Teague et al., 2018). Thus, even reduced Fgf10 signaling is sufficient for morphologically normal duodenal development. Similarly, Sala et al. (2006) found normal colonic development in *Fgf10* hypomorphic mice, whereas complete loss of *Fgf10* gene function resulted in colonic atresia. In the colon, *Fgf10* expression was shown to be expressed first distally before extending proximally, and was found to be critical for the maintenance and proliferation of the epithelial progenitor cells in the colon. Furthermore, crypt formation seen within the proximal colon in the absence of *Fgf10* suggested other signaling pathways were active in the development of this region, reinforcing the early anatomical and functional regionalization of the GI tract early during development. Another important finding of Sala et al. (2006) was that atresia occured without and associated loss of mesenchyme. This finding makes vascular compromise an unlikely mechanism for colonic atresia in Fgf10

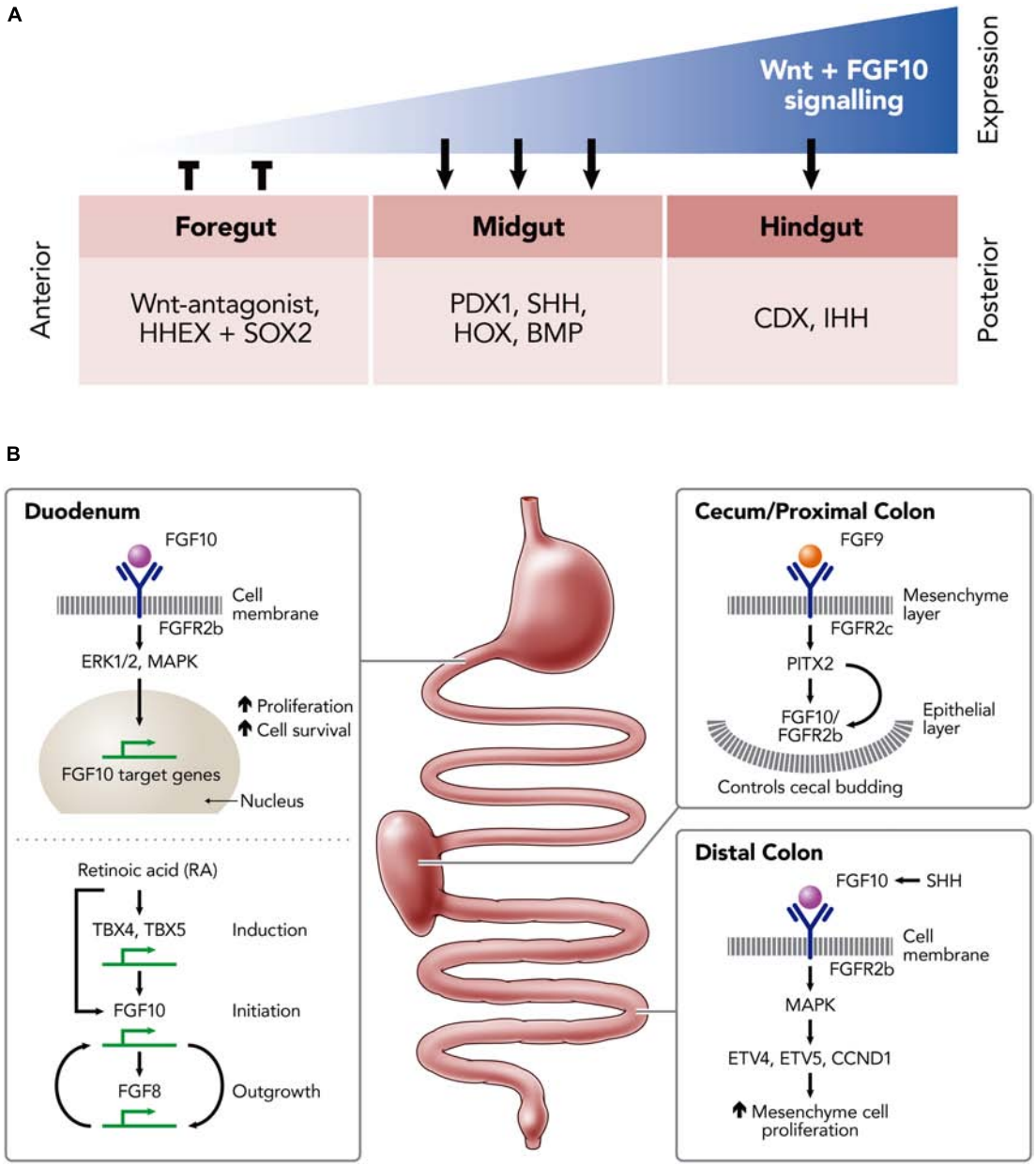

FIGURE 2 | Schematic illustrations of the role of FGF10 in the developing and developed murine intestine. **(A)** The expression-dependent changes of key transcription factors in the foregut, midgut and hindgut mediated by differing levels of FGF10 and Wnt-signaling expression; hematopoietically expressed homeobox protein (HHEX), SRY (sex determining region Y)-box 2 (SOX2) in the foregut; pancreatic and duodenal homeobox 1 (PDX1), Sonic Hedgehog (SHH), homeobox genes (HOX), Bone morphogenetic proteins (BMP) in the midgut; Caudal-Type Homeobox Protein (CDX), Indian hedgehog (IHH) in the hindgut. **(B)** Key FGF10-pathways involved the development of the duodenum, cecum/proximal colon and distal colon; Fibroblast growth factor (FGF) 8, 9, and 10; Tyrosine kinase fibroblast growth factor receptors (FGFR) 2b, 2c; extracellular signal-regulated kinases (ERK1/2); mitogen-activated protein kinase (MAPK); Thromboxanes B4 (TXB4); Thromboxanes B5 (TBX5); ETS translocation variant 4 (ETV4); ETS translocation variant 5 (ETV5); Cyclin D1 (CCND1); Sonic Hedgehog (SHH).

knockouts, as a vascular event would be expected to cause loss of both mesenchyme and epithelium.

The impact of Fgf10 over-expression has also been investigated in both *ex vivo* and *in vivo* models. Torashima et al. (2016) showed that the addition of *Fgf10* to tissue-engineered small intestine (TESI) resulted in increased size and weight of the sample, and increased villi height and crypt depth. In this setting, epithelial differentiation was not inhibited by over-expression of *Fgf10*, a finding attributed to the lack of normal feedback inhibitory mechanisms in the *ex vivo* TESI samples. Nyeng et al. (2011) studied *in vivo* over-expression of *Fgf10* within the developing duodenum. In these embryos, *Fgf10* over-expression caused attenuation of cell differentiation and expansion of the progenitor niche along with upregulation of

FGFR signaling targets known to exert feedback inhibition on the FGF pathway (e.g., Sprouty2, Etv4, and Etv5) (Minowada et al., 1999; Nyeng et al., 2011). Conversely, complete loss of *Fgf10* led to the premature differentiation of all enteric cell lineages in the duodenum (Nyeng et al., 2011). These findings support the inference that *Fgf10* is necessary to prevent premature differentiation of enteric cell lineages, and so maintain the epithelial progenitor cell population during development. In extension of this conclusion, these authors hypothesized that premature differentiation and resultant depletion of the progenitor cell population is responsible for the epithelial deficiencies of DA in *Fgf10* knockout mice (Nyeng et al., 2011).

An alternative to the premature differentiation hypothesis, is that proposed by Botham et al. (2012). These investigators concluded that exaggerated endodermal apoptosis, rather than terminal differentiation of progenitor cells was the root cause for DA in *Fgfr2b* knockout mice. Apoptosis was seen in the endoderm at E10.5, disappearance of the endoderm in the atretic region by E11.5, followed by involution of the mesoderm in the absence of further apoptosis at E13.5. This timeline corresponded with first recognition of DA in these *Fgfr2b* knockout mice, also at E13.5. Comparisons were also made between the duodenum of *Fgfr2b* knockout mice and otherwise normal, human embryo samples. In mice, loss of endoderm is complete at an earlier stage of development (E11.5, Carnegie Stage 16). In humans, however, "epithelial crowding" with corresponding apparent loss of duodenal lumen is not seen until Carnegie Stage 17 with "recanalization" only at Carnegie Stage 18. Thus, there is a temporal dislocation between luminal occlusion in atretic murine and normal human duodenal development (Matsumoto et al., 2002; Botham et al., 2012). The timeline for murine DA is supported by the findings of Nichol et al. (2012), who showed murine duodenal narrowing evident from E11.5 and DA from E13.5.

Yet another hypothesis is that of Merei (2004), who proposed that intestinal atresia may be the result of aberrant notochord signaling. Reeder et al. (2012a) used *Fgfr2b* knockout mice, reporting 42% penetrance of DA and 100% penetrance of colonic atresia. These investigators refuted the role of aberrant notochord signaling as the basis for murine DA, showing neither disruption of sonic hedgehog (*Shh*) expression nor notochordal discontinuity in *Fgfr2b* knockouts. Furthermore, organ culture of explanted wildtype murine gut in the presence of supra-physiological concentrations of *Shh* failed to induce atresia in either the duodenum or colon.

One striking feature of the DA reported in the aforementioned, seminal studies is the morphological types of DA reported in *Fgf10* and *Fgfr2b* knockout mice (Fairbanks et al., 2004b; Kanard et al., 2005; Botham et al., 2012; Reeder et al., 2012b). In humans, the distribution of DA types shows similar proportions of type 1 and type 3 DA, and few cases of type 2 DA; e.g., 54% type 1, 4% type 2, and 42% type 3 DA (Khan et al., 2017). In contrast to this, when collated together, 93% of all murine DA cases reported in these studies were examples of type 3 DA, i.e., the most severe type of DA with complete discontinuity of the duodenum (**Figure 1D**; Fairbanks et al., 2004b; Kanard et al., 2005; Botham et al., 2012; Reeder et al., 2012b). Also, none of these studies reported any examples of type 2 DA in mice.

Of relevance to DA type and the severity of malformation is the work by Reeder et al. (2012b). Reeder et al. (2012b) investigated a role for retinaldehyde dehydrogenase 2 (*Raldh2*), a gene which encodes the enzyme responsible for the final step of vitamin A conversion to RA. *Raldh2* is critical for normal posterior foregut development (Wang et al., 2006), and is under-expressed in the duodenum of *Fgfr2b* knockout mice (Botham et al., 2012). Therefore, Reeder et al. combined heterozygous *Raldh2* deletion with homozygous deletion of *Fgfr2b* with the hypothesis of generating a more severe DA phenotype than with homozygous deletion of *Fgfr2b* alone. Contrary to this hypothesis, addition of *Raldh2* haploinsufficiency resulted in a reduced rather than increased penetrance of atresia (21 vs 45%), and a shift toward less severe atresia types: *Fgfr2IIIb*−/−; *Raldh2*± (80% type 1 DA, 20% type 2 DA, and no type 3) versus *Fgfr2IIIb*-/-; *Raldh2*+/+ (7% type 1 DA, 0% type 2 DA, and 93% type 3 DA). These authors suggested that signaling downstream of *Fgf10/Fgfr2b*, i.e., *Raldh2*, was responsible for the phenotypic variations in DA type morphology.

We have recently reported a more human-like distribution of DA types, including type 2 DA, in two strains of CRISPR-derived *Fgf10* knockout mouse (Teague et al., 2018). Of note, these newly reported strains; tm1 (B6-Fgf10<c.[464_470dup;506_645del]APNMu>); and tm2 (B6-Fgf10<c.495_507delAPNMu>) (Eppig et al., 2006) each demonstrate all three DA types (**Figures 1F–H**), and a significantly higher penetrance of DA than previous animal models [74% (Teague et al., 2018) versus 35–45% (Fairbanks et al., 2004b; Kanard et al., 2005; Botham et al., 2012; Reeder et al., 2012b). The basis for such differences in type-distribution and penetrance when compared with previously reported *Fgf10* knockout mouse strains remains unclear. The various strains are of consistent background, namely C57/Bl6 (Fairbanks et al., 2004b; Kanard et al., 2005), and whilst the genetics differ, each represents a nonsense mutation (Eppig et al., 2006). We hypothesize that signaling molecules and pathways downstream of *Fgf10-Fgfr2b* are moderating the morphology and penetrance of the DA phenotype in these various strains.

Our hypothesis is supported by the findings of Al Alam et al. (2012). While an FGF9/Pitx2/FGF10 signaling axis has been proposed within the lung (De Langhe et al., 2008), Al Alam et al. demonstrated that the same signaling axis is active in developing gut (Al Alam et al., 2012). Using tissue specific *Fgf9* and *Pitx2* conditional knockout they demonstrated that, within the cecum, FGF9 controls mesenchymal *Pitx2* expression and, in turn, *Fgf10* expression. They also found that *Pitx2* induced the expression of *Fgf10*, even in the absence of *Fgf9*, suggesting that *Pitx2* is downstream of *Fgf9*. In further attempts to define pathways upstream of *Fgf10* involved in atresia, Reeder et al. investigated the role that *Shh* plays with *Fgfr2b* (Reeder et al., 2014). Using a Matrigel culture system and focusing on the colon of *Fgfr2b* knockout mice, they found a downregulation of *Shh* at E11.5 throughout the entire colon, and then loss of *Foxf1* expression 12 h later in the mid-to-distal colon prior to its

involution. They also found that the exogenous addition of *Shh* to the *Fgfr2b* deficient colon failed to prevent the formation of atresia, suggesting that the loss of *Shh* is not a critical event in atresia formation.

FORTH-COMING RESEARCH INTO DUODENAL ATRESIA ETIOLOGY

Based on the currently available literature regarding *Fgf10-Fgfr2b* signaling in duodenal atresia, we hypothesize that the etiology of DA in humans is genetically driven, and that the causative genetic changes are downstream of *Fgf10-Fgfr2b*. This downstream locus may account for both the incomplete penetrance of DA in the murine model, and the different morphological types (i.e., severity) of DA. It may also explain why human DA patients lack the non-survivable associations of *Fgf10* deletion such as pulmonary agenesis. Therefore, we plan to test this hypothesis by further investigating the up- and down-regulation of genes and pathways in atretic and morphologically normal duodenum. Coordinated RNA sequencing, validation, and protein interaction analyses are planned, focusing on the duodenum of CRISPR-derived *Fgf10* knockout mice with and without duodenal atresia, as well as additional wildtype controls. We consider that all three of these mice populations are necessary to discern candidate genes and pathways responsible for DA within the murine model. Also, given the complete penetrance of colonic atresia in the setting of *Fgf10-Fgfr2b* signaling interruption, we plan additional experiments to delineate the up- and down-regulation of genes and pathways in atretic and morphologically normal colon. We consider the results of colonic analyses may aid discernment of the genetic changes which hold true relevance for atresia formation, amongst the high volume of genetic changes we expect to observe in this model. Furthermore, we plan to test the aforementioned dose-dependence hypothesis, by scrutinizing gene expression differences between the three morphological types of DA in our CRISPR-derived *Fgf10* knockout mice.

In order to determine the translational relevance of the genetic analysis within our murine DA model, we plan to study the genetic profile of a thought-provoking subset of human DA patients with known associated anomalies akin to Fgf10-Fgfr2b signaling-related defects, e.g., craniofacial, limb, and lung anomalies. We consider this human DA subset to be at particular "risk" of demonstrating an underlying genetic basis for their DA related to the FGF10-FGFR2b signaling pathway. For this analysis, we will screen our institutional DA patient database for case with potential *Fgf10-Fgfr2b* signaling-related defects, and perform detailed clinical genetic phenotyping and exon sequencing of phenotypically homogenous patient groups. During the subsequent bioinformatic and genetic analyses, we will pay particular attention those genes and pathways evidenced to be associated with DA in our murine model.

Ultimate translation of these further studies will be to determine the cause of DA in humans, which will have immediate and therapeutic application in the clinical context of antenatal counseling. Also, these may provide the bases for future hypothesis-driven clinical targets and trials to ameliorate or prevent the development of DA in humans.

SUMMARY

Interruption of FGF10-FGFR2b signaling is the best demonstrated genetic link to DA in mice. This corresponds in importance, and hypothesis-formulating relevance, to the association between DA and Trisomy 21 in humans. *FGF10* haploinsufficiency and *FGF10* mutations have been linked to human disease, principally to craniofacial syndromes (Entesarian et al., 2005; Milunsky et al., 2006; Rohmann et al., 2006), chronic respiratory disease (Klar et al., 2011), but no human gastrointestinal tract atresia cases to date (Tatekawa et al., 2007). In contrast to this narrative of haploinsufficiency, homozygous *Fgf10* invalidation appears necessary for DA in our animal models (Teague et al., 2018), albeit accompanied by non-survivable anomalies such as lung agenesis. Therefore, we hypothesize that DA is caused by conditional tissue-specific deletion in *Fgf10*, *Fgfr2b* or their downstream targets (e.g., spatially limited to the duodenum or foregut). Constitutional deletion of this nature is less likely to explain DA in humans for reasons of non-survivable anomalies as detailed previously.

We consider determining the etiology of DA in humans to be a clinical and scientific imperative. Therefore, further study is required to understand the exact role of FGF10-FGFR2b signaling in this. Murine models of DA based on interruption of this signaling will be key to unlocking the mystery of DA in humans. Parallel genetic studies of human DA patients will enable translation of model-derived lessons from bench to bedside.

AUTHOR CONTRIBUTIONS

MJ conceived the project, conducted the review of literature, analyzed the evidence, and wrote and finalized the manuscript. GS provided specific scientific input into the analysis of evidence, and assisted in writing and finalizing the manuscript. PC mentored MJ and assisted in finalization of the manuscript. JH mentored MJ, and assisted in the analysis of evidence and finalization of the manuscript. SK mentored MJ, and assisted in the review of literature, analysis of evidence, and finalization of the manuscript. WT mentored MJ, conceived the project, and assisted in the review of literature, analysis of evidence, and writing and finalization of the manuscript.

FUNDING

Our laboratory's past and future work included in this review is supported by a Royal Australasian College of Surgeons (RACS) Foundation in Surgery Small Project Grant, a Colorectal Surgical Society of Australia and New Zealand (CSSANZ) Foundation Research Grant, and an Australian New Zealand Association

of Paediatric Surgeons (ANZAPS) Douglas Stephens Research Grant. MJ is supported in his higher degree research through the John Brooke Moore Scholarship at the University of Sydney. In addition, WT and SK are both generously supported by The Royal Children's Hospital Foundation, Melbourne.

ACKNOWLEDGMENTS

The authors would like to acknowledge Mr. Bill Reid, The Royal Children's Hospital Creative Studio, for his assistance in the art production of the figures for this review.

REFERENCES

Al Alam, D., Sala, F. G., Baptista, S., Galzote, R., Danopoulos, S., Tiozzo, C., et al. (2012). FGF9-Pitx2-FGF10 signaling controls cecal formation in mice. *Dev. Biol.* 369, 340–348. doi: 10.1016/j.ydbio.2012.07.008

Berant, M., and Kahana, D. (1970). Familial duodenal atresia. *Arch. Dis. Child.* 45, 281–282. doi: 10.1136/adc.45.240.281

Best, L. G., Wiseman, N. E., and Chudley, A. E. (1989). Familial duodenal atresia: a report of two families and review. *Am. J. Med. Genet.* 34, 442–444. doi: 10.1002/ajmg.1320340322

Botham, R. A., Franco, M., Reeder, A. L., Lopukhin, A., Shiota, K., Yamada, S., et al. (2012). Formation of duodenal atresias in fibroblast growth factor receptor 2IIIb-/- mouse embryos occurs in the absence of an endodermal plug. *J. Pediatr. Surg.* 47, 1369–1379. doi: 10.1016/j.jpedsurg.2012.02.001

Burns, R. C., Fairbanks, T. J., Sala, F., De Langhe, S., Mailleux, A., Thiery, J. P., et al. (2004). Requirement for fibroblast growth factor 10 or fibroblast growth factor receptor 2-IIIb signaling for cecal development in mouse. *Dev. Biol.* 265, 61–74. doi: 10.1016/j.ydbio.2003.09.021

Calder, E. (1733). Two examples of children born with preternatural conformation of the guts. *Med. Essays* 1:203.

Cheng, W., and Tam, P. K. (1998). Murine duodenum does not go through a "solid core" stage in its embryological development. *Eur. J. Pediatr. Surg.* 8, 212–215. doi: 10.1055/s-2008-1071156

Danopoulos, S., Schlieve, C. R., Grikscheit, T. C., and Al Alam, D. (2017). Fibroblast growth factors in the gastrointestinal tract: twists and turns. *Dev. Dyn.* 246, 344–352. doi: 10.1002/dvdy.24491

De Langhe, S. P., Carraro, G., Tefft, D., Li, C., Xu, X., Chai, Y., et al. (2008). Formation and differentiation of multiple mesenchymal lineages during lung development is regulated by beta-catenin signaling. *PLoS One* 3:e1516. doi: 10.1371/journal.pone.0001516

De Moerlooze, L., Spencer-Dene, B., Revest, J. M., Hajihosseini, M., Rosewell, I., and Dickson, C. (2000). An important role for the IIIb isoform of fibroblast growth factor receptor 2 (FGFR2) in mesenchymal-epithelial signalling during mouse organogenesis. *Development* 127, 483–492.

Delabar, J. M., Aflalo-Rattenbac, R., and Créau, N. (2006). Developmental defects in trisomy 21, and mouse models. *Sci. World J.* 6, 1945–1964. doi: 10.1100/tsw.2006.322

Entesarian, M., Matsson, H., Klar, J., Bergendal, B., Olson, L., Arakaki, R., et al. (2005). Mutations in the gene encoding fibroblast growth factor 10 are associated with aplasia of lacrimal and salivary glands. *Nat. Genet.* 37, 125–127.

Eppig, J. J., Fox, J., Barthold, S., Davvison, M., Newcomber, C., Quimby, F., et al. (2006). Mouse strain and genetic nomenclature: an abbreviated guide. *Mouse Biomed. Res.* 1, 79–98. doi: 10.1016/b978-012369454-6/50017-0

Ernst, N. P. (1916). A case of congenital atresia of the duodenum treated successfully by operation. *Br. Med. J.* 1, 644–645. doi: 10.1136/bmj.1.2888.644

Escobar, M. A., Ladd, A. P., Grosfeld, J. L., West, K. W., Rescorla, F. J., Scherer, L. R., et al. (2004). Duodenal atresia and stenosis: long-term follow-up over 30 years. *J. Pediatr. Surg.* 39, 867–871. discussion 867–871, doi: 10.1016/j.jpedsurg.2004.02.025

Fairbanks, T. J., Kanard, R., Del Moral, P. M., Sala, F. G., De Langhe, S., Warburton, D., et al. (2004b). Fibroblast growth factor receptor 2 IIIb invalidation–a potential cause of familial duodenal atresia. *J. Pediatr. Surg.* 39, 872–874. doi: 10.1016/j.jpedsurg.2004.02.026

Fairbanks, T. J., Kanard, R. C., De Langhe, S. P., Sala, F. G., Del Moral, P. M., Warburton, D., et al. (2004a). A genetic mechanism for cecal atresia: the role of the Fgf10 signaling pathway. *J. Surg. Res.* 120, 201–209. doi: 10.1016/j.jss.2003.12.017

Fonkalsrud, E. W., Delorimier, A. A., and Hays, D. M. (1969). Congenital atresia and stenosis of the duodenum. A review compiled from the members of the Surgical Section of the American Academy of Pediatrics. *Pediatrics* 43, 79–83.

Gross, E., Armon, Y., Abu-Dalu, K., Gale, R., and Schiller, M. (1996). Familial combined duodenal and jejunal atresia. *J. Pediatr. Surg.* 31:1573. doi: 10.1016/s0022-3468(96)90182-7

Ibrahimi, O. A., Eliseenkova, A. V., Plotnikov, A. N., Yu, K., Ornitz, D. M., and Mohammadi, M. (2001). Structural basis for fibroblast growth factor receptor 2 activation in Apert syndrome. *Proc. Natl. Acad. Sci. U.S.A.* 98, 7182–7187. doi: 10.1073/pnas.121183798

Igarashi, M., Finch, P. W., and Aaronson, S. A. (1998). Characterization of recombinant human fibroblast growth factor (FGF)-10 reveals functional similarities with keratinocyte growth factor (FGF-7). *J. Biol. Chem.* 273, 13230–13235. doi: 10.1074/jbc.273.21.13230

Kanard, R. C., Fairbanks, T. J., De Langhe, S. P., Sala, F. G., Del Moral, P. M., Lopez, C. A., et al. (2005). Fibroblast growth factor-10 serves a regulatory role in duodenal development. *J. Pediatr. Surg.* 40, 313–316. doi: 10.1016/j.jpedsurg.2004.10.057

Khan, A., Tanny, S. T., Perkins, E. J., Hunt, R. W., Hutson, J. M., King, S. K., et al. (2017). Is selective echocardiography in duodenal atresia the future standard of care? *J. Pediatr. Surg.* 52, 1952–1955. doi: 10.1016/j.jpedsurg.2017.08.046

Kim, T. H., and Shivdasani, R. A. (2016). Stomach development, stem cells and disease. *Development* 143, 554–565. doi: 10.1242/dev.124891

Klar, J., Blomstrand, P., Brunmark, C., Badhai, J., Hakansson, H. F., Brange, C. S., et al. (2011). Fibroblast growth factor 10 haploinsufficiency causes chronic obstructive pulmonary disease. *J. Med. Genet.* 48, 705–709. doi: 10.1136/jmedgenet-2011-100166

Lambrecht, W., and Kluth, D. (1998). Hereditary multiple atresias of the gastrointestinal tract: report of a case and review of the literature. *J. Pediatr. Surg.* 33, 794–797. doi: 10.1016/s0022-3468(98)90225-1

Luo, B., Cheung, H. W., Subramanian, A., Sharifnia, T., Okamoto, M., Yang, X., et al. (2008). Highly parallel identification of essential genes in cancer cells. *Proc. Natl. Acad. Sci. U.S.A.* 105, 20380–20385. doi: 10.1073/pnas.0810485105

Macarthur, C. A., Lawshe, A., Xu, J., Santos-Ocampo, S., Heikinheimo, M., Chellaiah, A. T., et al. (1995). FGF-8 isoforms activate receptor splice forms that are expressed in mesenchymal regions of mouse development. *Development* 121, 3603–3613.

Mailleux, A. A., Spencer-Dene, B., Dillon, C., Ndiaye, D., Savona-Baron, C., Itoh, N., et al. (2002). Role of FGF10/FGFR2b signaling during mammary gland development in the mouse embryo. *Development* 129, 53–60.

Matsumoto, A., Hashimoto, K., Yoshioka, T., and Otani, H. (2002). Occlusion and subsequent re-canalization in early duodenal development of human embryos: integrated organogenesis and histogenesis through a possible epithelial-mesenchymal interaction. *Anat Embryol.* 205, 53–65. doi: 10.1007/s00429-001-0226-5

Merei, J. M. (2004). Notochord-gut failure of detachment and intestinal atresia. *Pediatr. Surg. Int.* 20, 439–443.

Merrot, T., Anastasescu, R., Pankevych, T., Tercier, S., Garcia, S., Alessandrini, P., et al. (2006). Duodenal duplications. Clinical characteristics, embryological hypotheses, histological findings, treatment. . *Eur. J. Pediatr. Surg.* 16, 18–23. doi: 10.1055/s-2006-923798

Milunsky, J. M., Zhao, G., Maher, T. A., Colby, R., and Everman, D. B. (2006). LADD syndrome is caused by FGF10 mutations. *Clin. Genet.* 69, 349–354. doi: 10.1111/j.1399-0004.2006.00597.x

Minowada, G., Jarvis, L. A., Chi, C. L., Neubuser, A., Sun, X., Hacohen, N., et al. (1999). Vertebrate Sprouty genes are induced by FGF signaling and can cause chondrodysplasia when overexpressed. *Development* 126, 4465–4475.

Mora, M. C., Volk, J., Cuevas-Ocampo, A. K., Wong, K. E., Rockwell, G., Tirabassi, M. V., et al. (2014). Martinez-Frias syndrome: evidence of linkage to RFX6

mutation. *J. Pediatr. Surg. Case Rep.* 2, 492–494. doi: 10.1016/j.epsc.2014.10.003

Nichol, P. F., Reeder, A., and Botham, R. (2011). Humans, mice, and mechanisms of intestinal atresias: a window into understanding early intestinal development. *J. Gastrointest. Surg.* 15, 694–700. doi: 10.1007/s11605-010-1400-y

Nichol, P. F., Tyrrell, J. D., and Saijoh, Y. (2012). Retinaldehyde dehydrogenase 2 is down-regulated during duodenal atresia formation in Fgfr2IIIb-/- mice. *J. Surg. Res.* 175, 82–87. doi: 10.1016/j.jss.2011.02.040

Nishimoto, S., Wilde, S. M., Wood, S., and Logan, M. P. (2015). RA Acts in a Coherent Feed-Forward Mechanism with Tbx5 to Control Limb Bud Induction and Initiation. *Cell Rep.* 12, 879–891. doi: 10.1016/j.celrep.2015.06.068

Nyeng, P., Bjerke, M. A., Norgaard, G. A., Qu, X., Kobberup, S., and Jensen, J. (2011). Fibroblast growth factor 10 represses premature cell differentiation during establishment of the intestinal progenitor niche. *Dev. Biol.* 349, 20–34. doi: 10.1016/j.ydbio.2010.09.010

Ornitz, D. M., and Itoh, N. (2015). the fibroblast growth factor signaling pathway. *Wiley Interdiscip. Rev. Dev. Biol.* 4, 215–266. doi: 10.1002/wdev.176

Ornitz, D. M., Xu, J., Colvin, J. S., Mcewen, D. G., Macarthur, C. A., Coulier, F., et al. (1996). Receptor specificity of the fibroblast growth factor family. *J. Biol. Chem.* 271, 15292–15297.

Ornitz, D. M., and Itoh, N. (2001). Fibroblast growth factors. *Genome Biol.* 2, reviews3005.1. doi: 10.1186/gb-2001-2-3-reviews3005

Park, W. Y., Miranda, B., Lebeche, D., Hashimoto, G., and Cardoso, W. V. (1998). FGF-10 is a chemotactic factor for distal epithelial buds during lung development. *Dev. Biol.* 201, 125–134. doi: 10.1006/dbio.1998.8994

Reeder, A. L., Botham, R. A., Franco, M., Zaremba, K. M., and Nichol, P. F. (2012a). Formation of intestinal atresias in the Fgfr2IIIb-/- mice is not associated with defects in notochord development or alterations in Shh expression. *J. Surg. Res.* 177, 139–145. doi: 10.1016/j.jss.2012.04.024

Reeder, A. L., Botham, R. A., Zaremba, K. M., and Nichol, P. F. (2012b). Haploinsufficiency of retinaldehyde dehydrogenase 2 decreases the severity and incidence of duodenal atresia in the fibroblast growth factor receptor 2IIIb-/- mouse model. *Surgery* 152, 768–775. doi: 10.1016/j.surg.2012.07.022 discussion 775–776.,

Reeder, A. L., Zaremba, K. M., Liebl, R. M., Kowalkowski, A., and Nichol, P. F. (2014). Exogenous Sonic hedgehog protein does not rescue cultured intestine from atresia formation. *J. Surg. Res.* 187, 14–18. doi: 10.1016/j.jss.2013.11.1114

Rohmann, E., Brunner, H. G., Kayserili, H., Uyguner, O., Nurnberg, G., Lew, E. D., et al. (2006). Mutations in different components of FGF signaling in LADD syndrome. *Nat. Genet.* 38, 414–417. doi: 10.1038/ng1757

Sala, F. G., Curtis, J. L., Veltmaat, J. M., Del Moral, P. M., Le, L. T., Fairbanks, T. J., et al. (2006). Fibroblast growth factor 10 is required for survival and proliferation but not differentiation of intestinal epithelial progenitor cells during murine colon development. *Dev. Biol.* 299, 373–385. doi: 10.1016/j.ydbio.2006.08.001

Skandalakis, J. E., and Gray, S. W. (1994). *Embryology for Surgeons: the Embryological Basis for the Treatment of Congenital Anomalies*. Baltimore: Williams & Wilkins.

Spencer-Dene, B., Sala, F. G., Bellusci, S., Gschmeissner, S., Stamp, G., and Dickson, C. (2006). Stomach development is dependent on fibroblast growth factor 10/fibroblast growth factor receptor 2b-mediated signaling. *Gastroenterology* 130, 1233–1244. doi: 10.1053/j.gastro.2006.02.018

Tandler, J. (1900). Zur Entwicklingsgeschichte des menschlichen duodenums im frühen embryonalstadium. *Morphol. Jahrb.* 29, 187–216.

Tatekawa, Y., Kanehiro, H., and Nakajima, Y. (2007). Duodenal atresia associated with "apple peel" small bowel without deletion of fibroblast growth factor-10 or fibroblast growth factor receptor 2IIIb: report of a case. *Surg. Today* 37, 430–433. doi: 10.1007/s00595-006-3415-2

Teague, W. J., Jones, M. L. M., Hawkey, L., Smyth, I. M., Catubig, A., King, S. K., et al. (2018). FGF10 and the mystery of duodenal atresia in humans. *Front. Genet.* 9:530. doi: 10.3389/fgene.2018.00530

Torashima, Y., Levin, D. E., Barthel, E. R., Speer, A. L., Sala, F. G., Hou, X., et al. (2016). Fgf10 overexpression enhances the formation of tissue-engineered small intestine. *J. Tissue Eng. Regen. Med.* 10, 132–139. doi: 10.1002/term.1720

Vidal, E. (1905). *18e Congrès de Chirurgie*. Paris: Procès verbaux mémoires et discussion, Ass Fr Chir.

Wang, Z., Dolle, P., Cardoso, W. V., and Niederreither, K. (2006). Retinoic acid regulates morphogenesis and patterning of posterior foregut derivatives. *Dev. Biol.* 297, 433–445. doi: 10.1016/j.ydbio.2006.05.019

Yang, Q. E., Giassetti, M. I., and Ealy, A. D. (2011). Fibroblast growth factors activate mitogen-activated protein kinase pathways to promote migration in ovine trophoblast cells. *Reproduction* 141, 707–714. doi: 10.1530/REP-10-0541

Zamfir, C., Dassonville, M., Rodesch, G., and Steyaert, H. (2016). A rare malformation: double duodenal atresia associated with malrotation in a patient with "Cri du Chat" syndrome. *J. Pediatr. Surg. Case Rep.* 12, 3–5. doi: 10.1016/j.epsc.2016.06.003

Zani, A., Yeh, J. B., King, S. K., Chiu, P. P., and Wales, P. W. (2017). Duodeno-duodenostomy or duodeno-jejunostomy for duodenal atresia: is one repair better than the other? *Pediat.r Surg. Int.* 33, 245–248. doi: 10.1007/s00383-016-4016-9

Zhang, X., Ibrahimi, O. A., Olsen, S. K., Umemori, H., Mohammadi, M., and Ornitz, D. M. (2006). Receptor specificity of the fibroblast growth factor family. The complete mammalian FGF family. *J. Biol. Chem.* 281, 15694–15700. doi: 10.1074/jbc.m601252200

Conflict of Interest: The authors declare that the research was conducted in the absence of any commercial or financial relationships that could be construed as a potential conflict of interest.

frontiers in Pharmacology

ORIGINAL RESEARCH
published: 10 March 2020
doi: 10.3389/fphar.2020.00241

SIRT1 Mediates Effects of FGF21 to Ameliorate Cisplatin-Induced Acute Kidney Injury

Qiongzhen Chen[1†], Junfeng Ma[2†], Xiaoning Yang[2], Qinyao Li[2], Zhuofeng Lin[2,3] and Fanghua Gong[2,3*]*

[1] College of Life and Environmental Science, Wenzhou University, Wenzhou, China, [2] School of Pharmacy, Wenzhou Medical University, Wenzhou, China, [3] Engineering Laboratory of Zhejiang Province for Pharmaceutical Development of Growth Factors, Biomedical Collaborative Innovation Center of Wenzhou, Wenzhou, China

Acute kidney injury (AKI) is a common complication in cancer patients. Kidney function is closely related to patients' quality of life and tumor prognosis. Cisplatin is a highly effective anti-tumor drug. However, the use of cisplatin is limited by its nephrotoxicity. It has been reported that FGF21 has a renal-protective function, but the mechanisms by which it does so remain unclear. In this study, we show that the expression of FGF21 is significantly upregulated in both *in vitro* and *in vivo* cisplatin-induced AKI models. Administration of recombinant FGF21 to cisplatin-induced AKI mice resulted in significantly decreased blood urea nitrogen (BUN) and serum creatinine levels, as well as significantly reduced protein levels of kidney injury molecule-1 (TIM-1), C-caspase 3, and Bax. H&E-stained kidney sections from cisplatin-induced AKI mice treated with recombinant FGF21 showed a relatively normal renal tissue structure, a reduced number of necrotic sites and vacuolar changes, and decreased casts, suggesting alleviated renal tubular injury. Experiments with an AKI cell model (cisplatin-treated HK-2 cells) yielded similar results as the mouse model; recombinant FGF21 significantly downregulated protein expression levels of TIM-1, C-caspase 3, and Bax. Furthermore, administration of recombinant FGF21 to cisplatin-treated AKI models significantly increased SIRT1 expression, and the beneficial effects of FGF21 on kidney injury were reversed by *SIRT1* knockdown. Collectively, our results suggest that SIRT1 mediates the protective effect of FGF21 on cisplatin-induced kidney injury.

Keywords: acute kidney injury, renal tubular injury, fibroblast growth factor 21, sirtuin1, cisplatin

OPEN ACCESS

Edited by:
Zhouguang Wang,
Albert Einstein College of Medicine, United States

Reviewed by:
Chen Li,
Charité Medical University of Berlin, Germany
Yingnyu Gao,
Marshall University, United States

****Correspondence:***
Zhuofeng Lin
zhuofenglin@wzmc.edu.cn
Fanghua Gong
gongwenheng@163.com

[†]These authors have contributed equally to this work

Specialty section:
This article was submitted to Translational Pharmacology, a section of the journal Frontiers in Pharmacology

Received: *18 October 2019*
Accepted: *21 February 2020*
Published: *10 March 2020*

Citation:
Chen Q, Ma J, Yang X, Li Q, Lin Z and Gong F (2020) SIRT1 Mediates Effects of FGF21 to Ameliorate Cisplatin-Induced Acute Kidney Injury. Front. Pharmacol. 11:241. doi: 10.3389/fphar.2020.00241

INTRODUCTION

Acute kidney injury (AKI) is a clinical syndrome characterized by an abrupt decline in kidney function, a decrease in glomerular filtration rate, and the accumulation of nitrogenous waste in the kidney (Vanmassenhove et al., 2017). Many factors contribute to the induction of AKI, including drugs, hypovolemia, sepsis, and surgical injury (Motwani et al., 2018). Hence, AKI is widely distributed among clinical departments (Basile et al., 2016). In hospitalized patients, AKI incidence has reached 5–7% and is still rising, with a mortality rate of 40%. AKI is also important risk factor for the development of chronic kidney disease (Coca et al., 2012; Oh et al., 2017).

Abbreviations: AKI, acute kidney injury; CIS, cisplatin; kidney injury molecule-1, TIM-1; SIRT1, sirtuin1; FGF21, fibroblast growth factor 21; CKD, chronic kidney disease; NC, negative control; BUN, blood urea nitrogen; C-caspase 3, cleaved caspase-3.

Cisplatin (CDDP, cis-Diaminodichloroplatinum) is used as a chemotherapeutic drug for the treatment of many different types of cancer. However, about one-third of the tumor patients develop AKI several days after cisplatin treatment. Therefore, the clinical application of cisplatin is frequently limited by its adverse effects (Fernández-Martínez et al., 2016; Kim et al., 2017; Hori et al., 2017; Oh et al., 2017; Li Z. et al., 2018).

Fibroblast growth factor 21 (FGF21) is mainly expressed in the liver, adipose tissue, and pancreatic islet, and is also expressed in muscle and kidney tissues (Nishimura et al., 2000; So and Leung, 2016; Li, 2019). Due to a lack of the typical heparin-binding domain found in the other family members, FGF21 enters the blood circulation through the endocrine system (Fisher and Maratos-Flier, 2016). FGF21 activity depends on its binding to β-Klotho protein and FGF receptors (FGFRs) and the formation of a stable FGF21/β-Klotho/FGFR complex, which regulates the biological effects of downstream signaling molecules (Kuro, 2019). Previous studies showed that serum levels of FGF21 are significantly increased in both AKI and CKD, and FGF21 concentration is correlated with the severity of kidney injury (Li F. et al., 2018; Suassuna et al., 2019). However, numerous studies have demonstrated that FGF21 functions in alleviating inflammation and in the regulation of oxidative stress and autophagy-induced apoptosis (Lu et al., 2019; Suassuna et al., 2019). Recent works also showed that FGF21 significantly reduces urinary albumin levels in type II diabetic mice and alleviates kidney injury (So and Leung, 2016; Zhao et al., 2017).

Sirtuins are NAD-dependent deacetylases that function in multiple biological processes, such as proliferation, DNA repair, mitochondrial energy homeostasis, and anti-oxidation. Mammals contain seven sirtuins (SIRT1–7), located in different subcellular compartments. SIRT1 is one of the most widely studied sirtuins in kidney. It inhibits cell apoptosis, inflammation, and fibrosis by targeting the deacetylation of p53, FoxO1, and NF-κB, and hence functions in protecting cells (Kim and Lee, 2015; Phillipson-Weiner et al., 2016; Wang et al., 2017, 2019; Zhang et al., 2017; Morigi et al., 2018; Sun et al., 2018; Abdolvahabi et al., 2019).

In this study, we found that recombinant human FGF21 (rhFGF21) exerted significant beneficial effects on tubular epithelial cells and alleviated the decline in renal function in cisplatin-induced AKI. In addition, we found that SIRT1 expression was significantly upregulated in renal tubular epithelial cells and renal tissues during the process of cisplatin-induced kidney injury. rhFGF21 treatment further increased the expression of SIRT1, resulting in decreased apoptosis in cells and improved kidney function.

MATERIALS AND METHODS

Cell Culture

Human renal proximal tubule cells (HK-2) were kindly provided by the Stem Cell Bank at Chinese Academy of Sciences. Cells were cultured in DMEM/F-12 media supplemented with 10% fetal bovine serum (FBS, Gibco, United States), 100 U/ml penicilin, and 100 μg/ml streptomycin. HK-2 cells were transfected with lentivirus siRNA against *SIRT1* (LV-SIRT1-RNAi) (Genechem, Shanghai, China) and Control-RNAi (Genechem, Shanghai, China) for 72 h according to the manufacturer's instructions. HK-2 cells were pretreated with/without rhFGF21 (5 nM; provided by Key Laboratory of Biotechnology Pharmaceutical Engineering, Wenzhou Medical University) for 1 h, and cultured in the presence of cisplatin (20 μM, Sigma-Aldrich, United States). Cells were collected at different time points (12, 18, and 24 h).

Mice and AKI Model

Healthy C57BL/6 male mice (∼25 g, 8 wk of age, purchased from Shanghai Slac Laboratory Animal Co., Ltd.) were kept at the barrier facility of the Laboratory Animal Centre of Wenzhou Medical University. All animals were kept for 1 week before the experiments started. All animal procedures were carried out in accordance with the principles of the Basel Declaration and Recommendations. Two experiments were conducted. The first experiment consisted of three different groups representing three different time points (24, 48, and 72 h). The experimental mice were randomly divided into three subgroups at each time point, i.e., the control group (NC), cisplatin model group (CIS), and treatment group (FGF21 + CIS) ($n = 5$ in each subgroup). Based on the procedure described by Li F. et al. (2018), we used a high dose (30 mg/kg) of cisplatin in a single intraperitoneal injection to establish the AKI mouse model. The control group was injected with the same volume of normal saline. As for the FGF21 + CIS group, rhFGF21 was dissolved in PBS and stored at 4°C, and mice were pretreated with rhFGF21 at 0.5 mg/kg intraperitoneally 1 h prior to cisplatin injection. rhFGF21 was administered every 24 h based on the *in vivo* elimination rate of rhFGF21 after cisplatin injection, and the same volume of physiological saline was injected into other groups. Mice were euthanized at different time points (24, 48, and 72 h) after cisplatin injection. In the second experiment, we randomly divided the experimental mice into four groups ($n = 5$ per group), i.e., the control group (Ctrl-RNAi), the model group (Ctrl-RNAi + CIS), the treatment group (Ctrl-RNAi + rhFGF21 + CIS), and the SIRT1 knockdown group (LV-SIRT1-RNAi + rhFGF21 + CIS). LV-SIRT1-RNAi or Ctrl-RNAi (1.6×10^9 TU/kg) (Zheng et al., 2017) was administered by tail vein injection 72 h before cisplatin treatment, followed by the same procedure as in the first the experiment. Mice were euthanized 72 h after cisplatin injection. Blood and kidney tissues were collected and used for biochemical and histopathological examinations. Serum creatinine levels were measured using a Creatinine Assay Kit (Sarcosine Oxidase method); blood urea nitrogen (BUN) levels were measured by a Urea Nitrogen Kit (Urease method). The kits were obtained from the Nanjing Institute of Bioengineering (Nanjing, China).

Immunoblotting

Analysis was performed to measure the protein levels in kidney tissue and HK-2 cells. Protein in total cell lysates was extracted and quantified by BCA Protein Assay. Protein was separated by SDS-PAGE and transferred to a PVDF membrane (Bio-Rad, Hercules). After blocking the membrane in a TBST solution containing 10% (w/v) non-fat milk for 1.5 h at room temperature, different proteins were probed with corresponding antibodies

overnight at 4°C. The following antibodies were used: anti-FGF21 (1:1000, Abcam), anti-SIRT1 (1:1000, Abcam), anti-TIM-1 (1:20,000, Abcam), anti-Bax (1:10,000, Abcam), anti-cleaved caspase-3 (1:1000, Abcam), anti-β-Klotho (1:1000, Abcam), anti-β-actin (1:1000, Cell Signaling Technology), and anti-GAPDH (1:1000, Cell Signaling Technology). Subsequently, membranes were washed three times with TBST and then incubated with horseradish peroxidase (HRP)-conjugated secondary antibody for 1 h at room temperature. Protein signals were detected using a Tanon 5200 Chemiluminescence Imaging system (Tanon-5200) and bands were quantified using ImageJ software.

Histology and Immunohistochemistry

Prior to histological analysis, kidney tissues were fixed in 4% paraformaldehyde for over 24 h, embedded in paraffin, cut into 5 μm sections, stained with hematoxylin and eosin (H&E), sealed with neutral resin, and observed under an optical microscope. Tissue damage and necrosis were assessed by microscopy (×400) in 10–20 randomly selected fields of view. Tissue damage was scored by the percentages of renal tubular injury, cell debris, brush border loss, and cast formation (0, no damage; 1, less than 25% damage; 2, 25–50% damage; 3, 50–75% damage; 4, more than 75% damage).

For immunohistochemistry analysis, 5 μm kidney tissue sections were incubated with anti-FGF21 (Abcam; Cambridge, United Kingdom) and anti-SIRT1 (Abcam; Cambridge, United Kingdom), followed by the secondary antibody (ZSGB-Bio, Beijing, China) and DAB. For each mouse, 10–20 randomly selected fields of view were scanned under an upright microscope. The percentages of positive staining regions of FGF21 or SIRT1 were quantified using Image-Pro 6.0.

Immunofluorescent Staining

For immunofluorescent staining analysis, cells were fixed with 4% paraformaldehyde and incubated with Triton X-100 (1%) for 15 min. The cells were incubated with anti-FGF21 and anti-SIRT1 overnight at 4°C, incubated with fluorescent-probe-conjugated goat anti-rabbit at room temperature for 1 h, stained with DAPI (Abcam, Cambridge, United Kingdom), and mounted. Images were captured using a laser confocal microscope (Nikon, Ti-E and A1 plus) and quantitatively analyzed using Image-Pro 6.0.

Apoptosis Assay

Five-micrometer-thick tissue sections were used for TUNEL staining with the apoptosis detection kit (Boster Biological Technology Co., Ltd., Wuhan, China). Briefly, the slides were deparaffinized, rehydrated, and treated with proteinase K (20 mg/ml) for 15 min at room temperature. The slide was preliminarily incubated with labeling buffer (digoxigenin-dUTP) at room temperature for 2 h. Then blocking solution incubated 30 min at room temperature, and added the reaction mixture containing anti-digoxigenin antibody and Fluorescein-Streptavidin (FITC, green), incubated at 37°C for 30 min. DAPI was used for nuclear counterstaining.

The HK-2 cells (1×10^6 cells/well) were seeded on six-well chamber slides. After different treatments, the slides were detected with the apoptosis detection kit (CY3, red). DAPI was used for nuclear counterstaining. TUNEL-positive cells were imaged under a laser confocal microscope (Nikon, Ti-E and A1 plus).

Statistical Analysis

Data analysis was performed using GraphPad Prism 6.0 software. All data are expressed as mean ± SEM of three independent experiments; the Student's *t*-test or one-way ANOVA was used for statistical comparisons of different groups. The Pearson test was performed to determine the linear correlation of two variables. $P < 0.05$ indicated a significant statistical difference.

RESULTS

Cisplatin Induces HK-2 Cell Apoptosis *in vitro* and AKI *in vivo*

HK-2 cells were treated with cisplatin for 12, 18, and 24 h. The expression of the apoptosis-related proteins C-caspase 3 and Bax increased in a time-dependent manner (**Figures 1A–C**). TUNEL analysis showed nucleus aggregation and significantly increased numbers of apoptotic cells in HK-2 cells after 24 h as compared with control cells ($P < 0.001$, **Figures 1D,E** and **Supplementary Figure S1**).

As for *in vivo* experiments in mice, we found that both BUN levels and serum creatinine levels began to rise 24 h after cisplatin treatment, reaching a maximum at 72 h. Both serum creatinine and BUN concentrations at 72 h were about 4.5-fold greater than in the control group, indicating that kidney function was significantly impaired ($P < 0.001$, **Figures 1F,G**). Analysis of kidney tissue showed that the protein levels of the AKI markers TIM-1, C-caspase 3, and Bax increased significantly in a time-dependent manner (**Figures 1H–K**). Renal pathological changes were evaluated 72 h after cisplatin administration using H&E staining of mouse kidney paraffin sections. The control group displayed an intact tubular structure, the renal tubules were shaped regularly and arranged neatly, glomerular space was normal without obvious damage, the tubular epithelial cells were arranged in high density, nuclei were round and large, nucleoli were clear and distributed evenly, and no obvious apoptosis and necrosis were found. On the contrary, cisplatin administration resulted in renal tubular damage, necrosis, a large amount of cell debris, vacuolar changes, multiple sites of casts, increased glomerular space, and tissue damage; the average renal tubular injury score was ∼3.5 (**Figures 1L,M**).

Collectively, these findings indicate that cisplatin causes HK-2 cell apoptosis *in vitro*, and induces AKI *in vivo*, with an impaired tubular structure and a reduced glomerular filtration rate.

Cisplatin Induces a Significant Upregulation of FGF21 in Renal Tubular Cells *in vitro* and *in vivo*

Because FGF21 plays an important role in energy metabolism and cellular stress response, we examined the expression of FGF21 in HK-2 cells after cisplatin treatment. FGF21 expression was significantly upregulated after 12 h; the highest FGF21 levels were

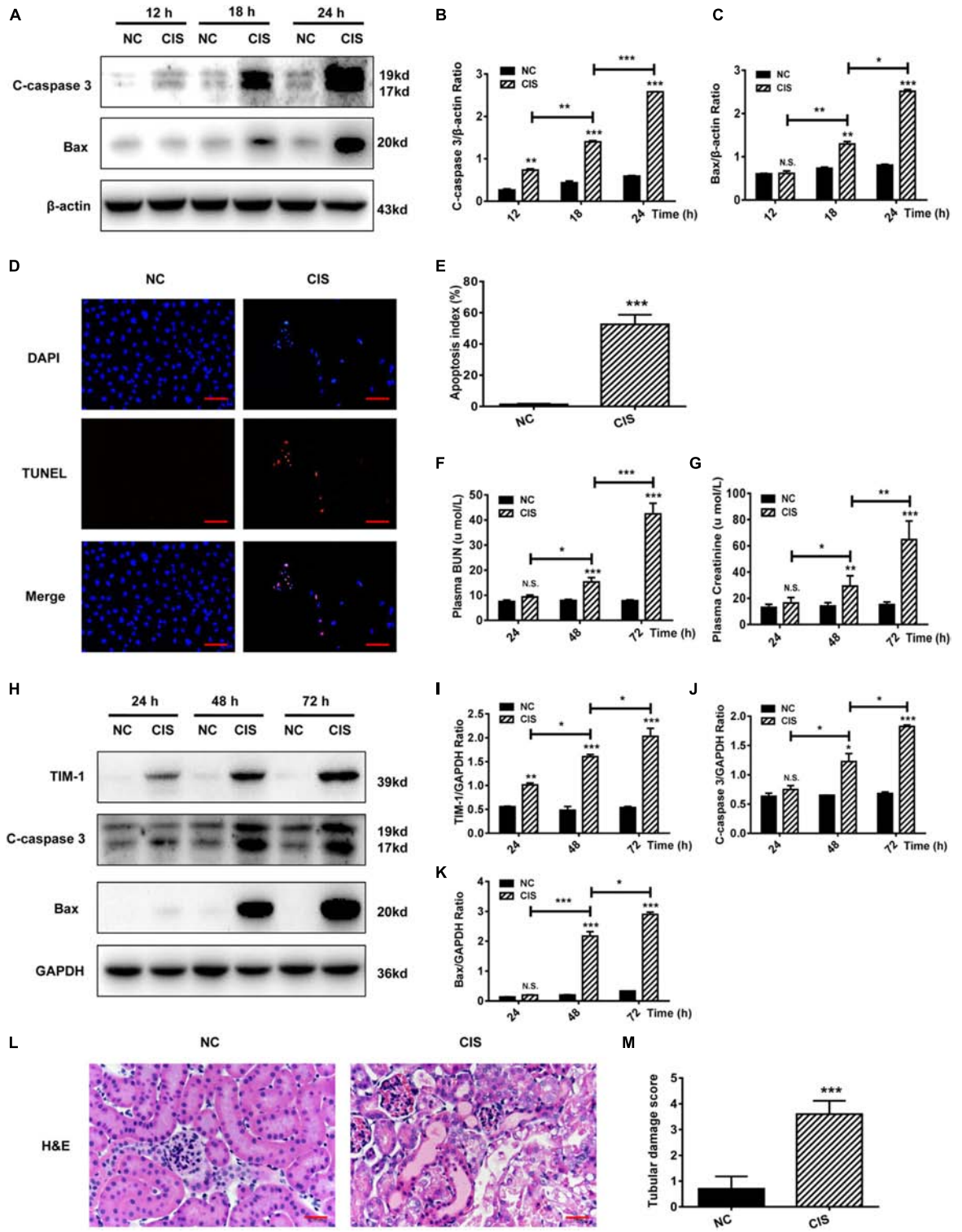

FIGURE 1 | Cisplatin induces tubular cell damage in in vitro and in vivo AKI models. **(A–C)** Representative immunoblotting analysis of C-caspase 3 and Bax in HK-2 cells. Protein levels of C-caspase 3 and Bax were quantified by densitometry, with β-actin as protein loading control. **(D,E)** TUNEL staining in HK-2 cells (scale bar: 100 μm; DAPI: blue, TUNEL: red), and quantitative analysis of TUNEL staining. **(F)** Changes in mouse BUN levels. **(G)** Changes in mouse serum creatinine levels. **(H–K)** Representative immunoblotting analysis of TIM-1, C-caspase 3, and Bax in mouse renal tissue. Expression levels of TIM-1, C-caspase 3, and Bax were quantified by densitometry, with GAPDH as protein loading control. **(L)** H&E staining of mouse renal tissue (scale bar: 100 μm). **(M)** Histopathological scores of H&E staining of mouse kidney tissue. $^{***}P < 0.001$, $^{**}P < 0.01$, $^{*}P < 0.05$.

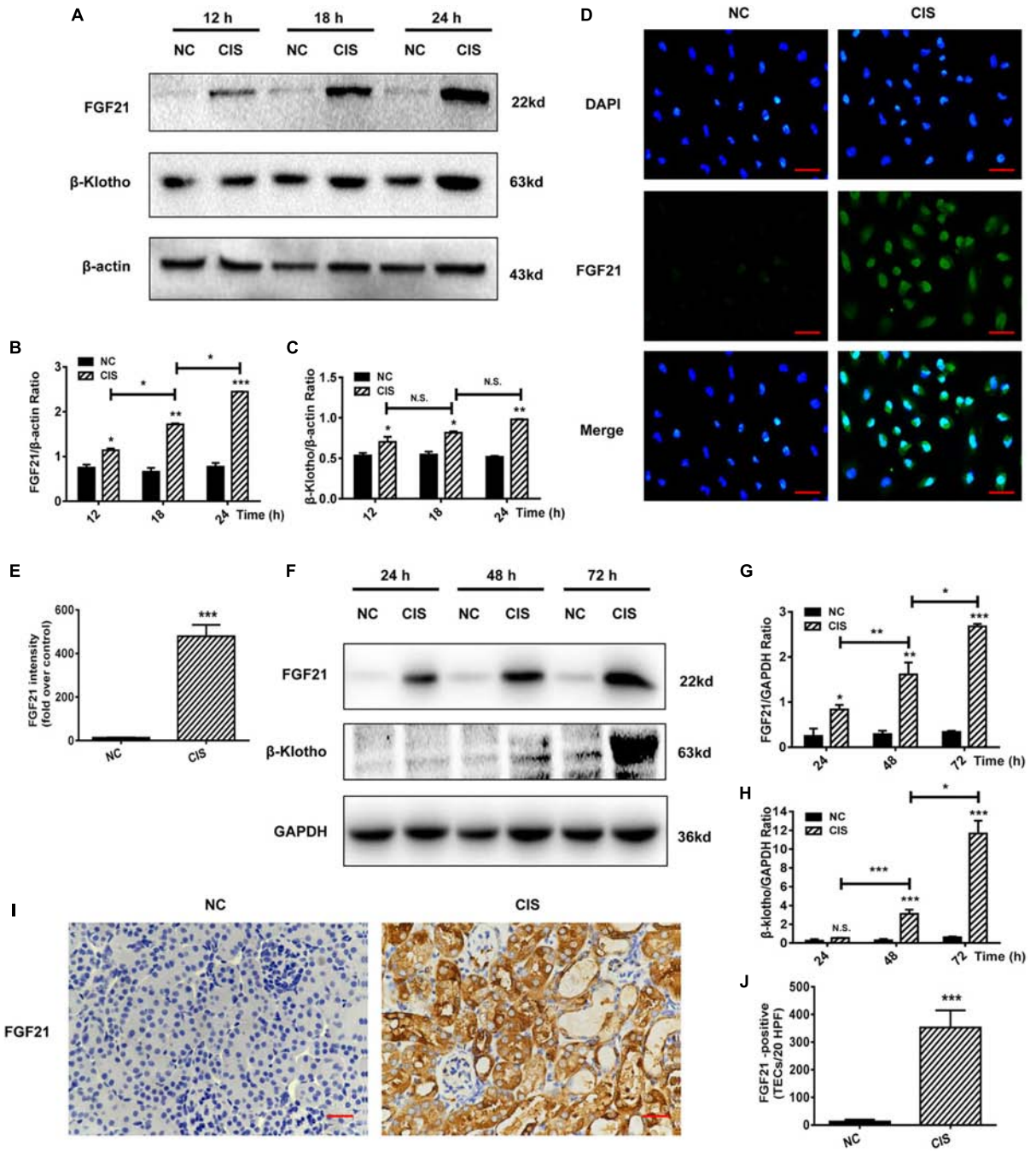

FIGURE 2 | FGF21 is upregulated in *in vivo* and *in vitro* models of renal injury. **(A–C)** Representative immunoblotting analysis of FGF21 and β-Klotho in HK-2 cells. Protein levels of FGF21 and β-Klotho were quantified by densitometry, with β-actin as protein loading control. **(D,E)** Immunofluorescence intensity of FGF21 in HK-2 cells (scale, 100 μm; DAPI: blue, FGF21: green). **(F–H)** Representative immunoblotting analysis of FGF21 and β-Klotho in mouse renal tissue. Expression levels of FGF21 and β-Klotho were quantified by densitometry, with GAPDH as protein loading control. **(I)** Immunohistochemistry staining of FGF21 in mouse renal tissue (scale bar: 100 μm). **(J)** Quantitative immunohistochemistry analysis of FGF21. $^{***}P < 0.001$, $^{**}P < 0.01$, $^{*}P < 0.05$.

observed at 24 h ($P < 0.001$, **Figures 2A,B**). Expression levels of the FGF21 receptor β-Klotho also increased (**Figures 2A,C**). Immunofluorescence staining revealed a significant increase in intracellular protein levels of FGF21 after 24 h of cisplatin treatment ($P < 0.001$, **Figures 2D,E**).

Levels of FGF21 and FGF21 receptor β-Klotho in the AKI mouse model were measured at different time points after cisplatin administration (24, 48, and 72 h). Consistent with the cell culture experiments, *in vivo* FGF21 expression increased in a time-dependent manner,

and β-Klotho was significantly upregulated 72 h after cisplatin administration ($P < 0.001$, **Figures 2F–H**). Immunohistochemistry results showed that 72 h after cisplatin administration, the levels of FGF21 were significantly increased in the area of renal tubular injury, especially in the areas with severe tissue damage or necrosis ($P < 0.001$, **Figures 2I,J**).

Collectively, our results indicate that cisplatin induces the upregulation of FGF21 expression in renal tubular cells *in vitro* and *in vivo*.

rhFGF21 Significantly Attenuates Cisplatin-Induced Acute Injury of Renal Tubular Cells *in vitro* and *in vivo*

HK-2 cells were pretreated *in vitro* with rhFGF21 for 1 h before cisplatin treatment. We found that rhFGF21 downregulated the expression of C-caspase 3 and Bax differently at different time points (12, 18, and 24 h) compared with cisplatin-treated cells (**Figures 3A–C**). Moreover, TUNEL staining results indicate that the apoptosis rate of cisplatin-treated HK-2 cells was >50%. In comparison, rhFGF21 pretreatment reduced the percentage of apoptotic cells to less than 20% (**Figures 3D,E**).

Similarly, we studied the protective effects of rhFGF21 on renal tissues in the mouse AKI model. Our results indicate that at 24 h after rhFGF21 administration, there was no significant difference in BUN and serum creatinine levels among the three groups. At 48 h and later, the administration of rhFGF21 significantly decreased the BUN and serum creatinine levels (**Figures 4A,B**). In addition, immunoblot analysis demonstrated that mice treated with both cisplatin and rhFGF21 had significantly lower levels of TIM-1, C-caspase 3, and Bax than those treated with cisplatin alone (**Figures 4C–F**). Renal pathological changes were evaluated 72 h after cisplatin administration by H&E staining of mouse kidney paraffin sections. Microscopic evaluation of the control group showed that the tubular structure was unchanged, tubular epithelial cells were arranged in high density, and no obvious tissue damage was observed. In contrast, intraperitoneal injection of cisplatin resulted in impaired tubular structure, accompanied by increases in glomerular space and casts, a large amount of cell debris, and vacuolar changes, and the average renal tubular injury score was ∼3. rhFGF21 treatment reversed cisplatin-induced renal injury.

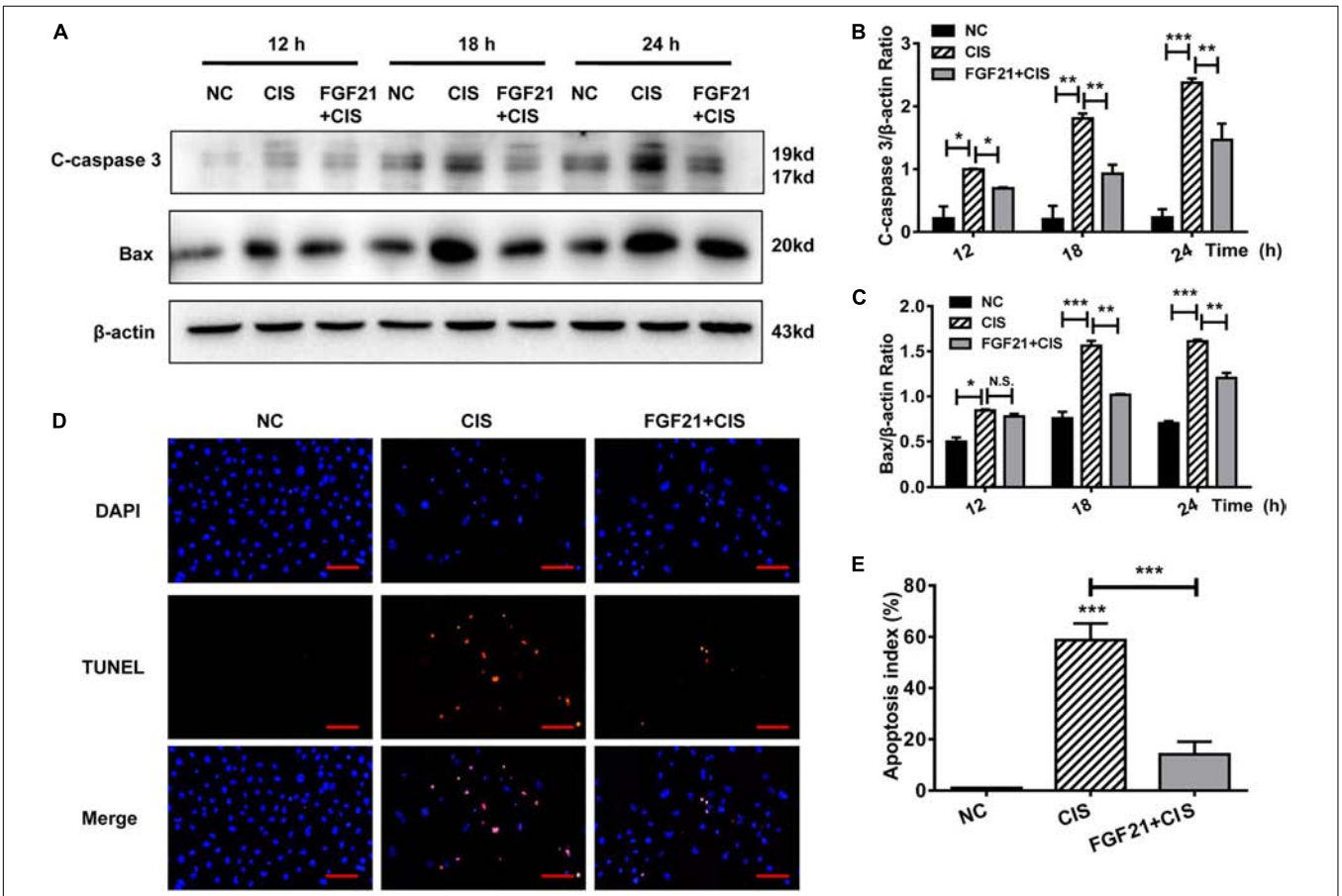

FIGURE 3 | rhFGF21 significantly alleviates HK-2 cell damage. **(A–C)** Representative immunoblotting analysis of C-caspase 3 and Bax in HK-2 cells. Protein levels of C-caspase 3 and Bax were quantified by densitometry, with β-actin as protein loading control. **(D,E)** TUNEL staining in HK-2 cells (scale bar: 100 μm; DAPI: blue, TUNEL: red), and quantitative analysis of TUNEL staining. ***$P < 0.001$, **$P < 0.01$, *$P < 0.05$.

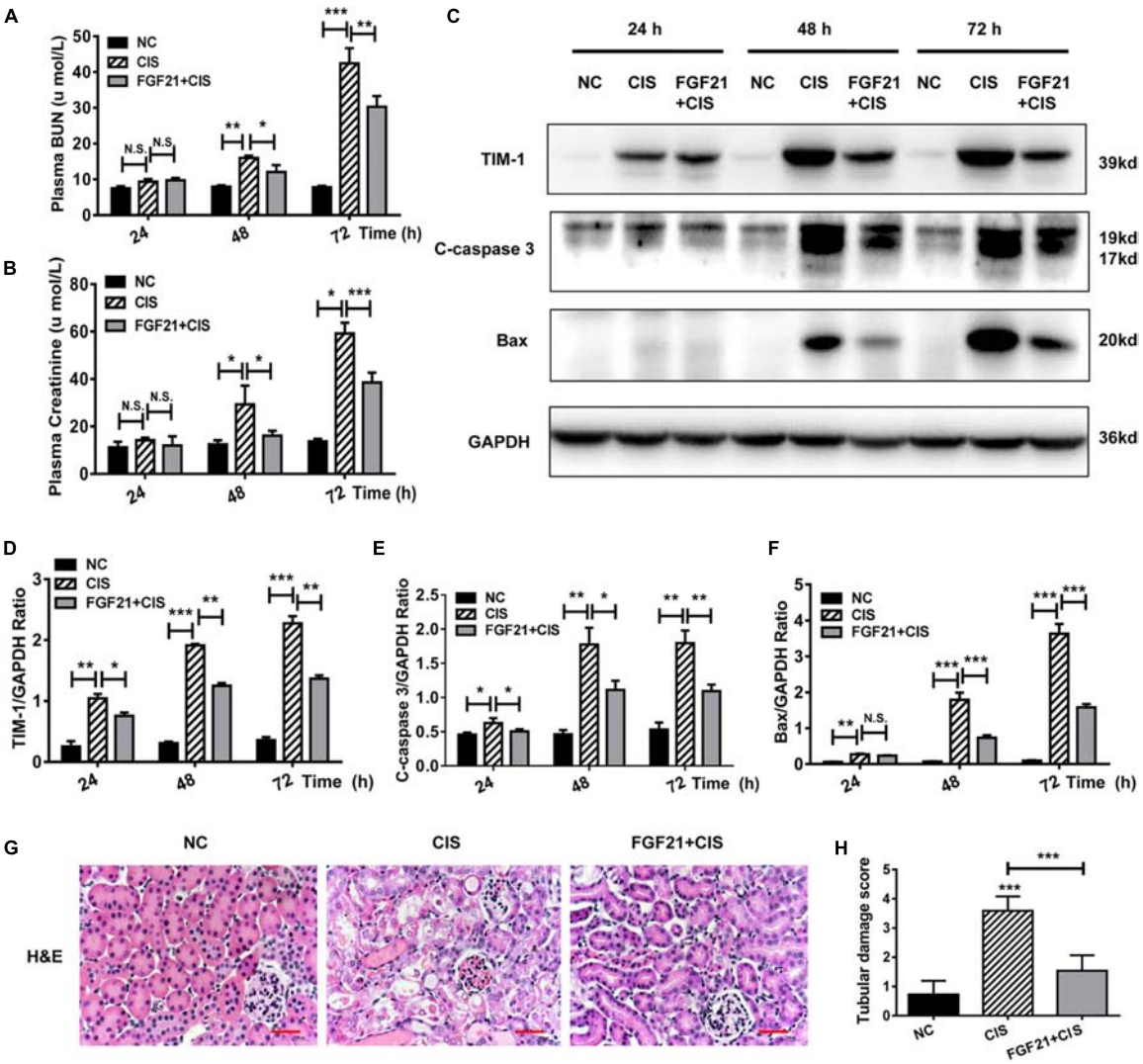

FIGURE 4 | rhFGF21 significantly reduces tubular cell damage in AKI mouse model. **(A)** Changes in mouse BUN levels. **(B)** Changes in mouse serum creatinine levels. **(C–F)** Representative immunoblotting analysis of TIM-1, C-caspase 3, and Bax in mouse renal tissue. Expression levels of TIM-1, C-caspase 3, and Bax were quantified by densitometry, with GAPDH as protein loading control. **(G)** H&E staining of mouse renal tissue (scale bar: 100 μm). **(H)** Histopathological scores of H&E staining of mouse kidney tissue. ***$P < 0.001$, **$P < 0.01$, *$P < 0.05$.

Although tissue damage was more severe than in the control group, rhFGF21 treatment resulted in a relatively normal tissue structure, fewer necrotic sites and vacuolar changes, and fewer casts as compared with cisplatin-treated mice. The average tissue damage score was reduced to ∼1 by rhFGF21 (**Figures 4G,H**).

These experimental results demonstrate that rhFGF21 plays a cytoprotective or prosurvival role during cisplatin treatment in HK-2 cells and mouse AKI.

rhFGF21 Upregulates SIRT1 Expression in Renal Tubular Cells *in vivo* and *in vitro*

SIRT1 is a key player in cisplatin-induced AKI and nephrotoxicity (Kim et al., 2019; Zhang et al., 2019). In cisplatin-treated HK-2 cells, SIRT1 protein levels were upregulated, similarly to FGF21 (**Figures 5A,B**). In cisplatin-treated HK-2 cells, SIRT1 expression was increased, and rhFGF21 further promoted SIRT1 expression (**Figures 5C,D** and **Supplementary Figures S2A–D**). Quantification of immunofluorescence signals confirmed that rhFGF21 promotes the expression of SIRT1 (**Figures 5E,F**).

In the AKI mouse model, SIRT1 expression was not significantly increased at 24 h, but it was increased at 48 h and later (**Figures 5G,H**). Consistent with our *in vitro* study, we found that rhFGF21 treatment upregulated SIRT1 expression in AKI mice at different time points ($P < 0.05$ at 24 h, **Figures 5I,J**). Our immunohistochemistry results indicate that cisplatin induced expression of SIRT1 72 h after cisplatin injection, and rhFGF21 further promoted renal SIRT1 expression (**Figures 5K,L**).

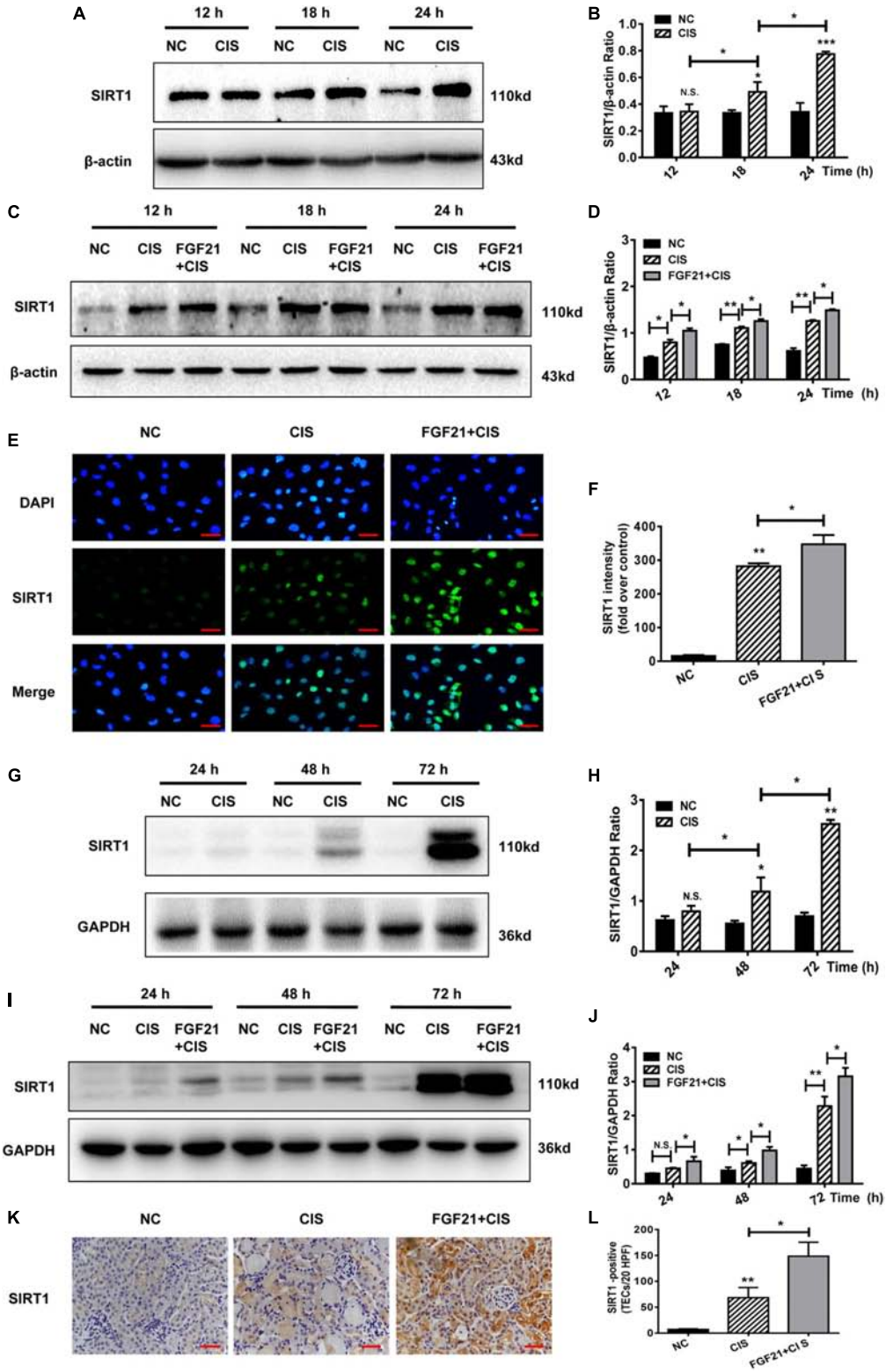

FIGURE 5 | rhFGF21 upregulated SIRT1 expression in renal injury models. **(A–D)** Representative immunoblotting analysis of SIRT1 in HK-2 cells. Protein levels of SIRT1 were quantified by densitometry, with β-actin as protein loading control. **(E,F)** Immunofluorescence intensity of SIRT1 in HK-2 cells (scale, 100 μm; DAPI: blue, SIRT1: green). **(G–J)** Representative immunoblotting analysis of SIRT1 in mouse renal tissue. Expression level of SIRT1 was quantified by densitometry, with GAPDH as protein loading control. **(K)** Immunohistochemistry staining of SIRT1 in mouse renal tissue (scale bar: 100 μm). **(L)** Quantitative immunohistochemistry analysis of SIRT1. ***$P < 0.001$, **$P < 0.01$, *$P < 0.05$.

Collectively, these results indicate that rhFGF21 can upregulate SIRT1 expression in injured renal tubular cells in a timely manner. Hence, the underlying mechanisms by which rhFGF21 attenuates cisplatin-induced AKI may involve SIRT1.

SIRT1 Mediates FGF21-Induced Attenuation of Cisplatin-Induced HK-2 Cell Apoptosis and Mouse AKI

SIRT1 plays an important role in the repair of organ and cell damage. Our previous experiments showed that cisplatin induces the expression of SIRT1 in HK-2 cells and mouse kidney tissue. Moreover, rhFGF21 further upregulates the expression of SIRT1 and improves cisplatin-induced AKI. To determine whether rhFGF21 prevents cisplatin-induced AKI by activating SIRT1, we examined the function of rhFGF21 in HK-2 cells after *SIRT1* knockdown. Results indicate that SIRT1 expression was effectively downregulated after LV-SIRT1-RNAi transfection in HK-2 cells. SIRT1 protein levels in HK-2 cells were reduced by approximately 80% after LV-SIRT1-RNAi transfection compared with Ctrl-RNAi (**Figures 6A,B**).

Next, we knocked down *SIRT1* in HK-2 cells; we found that *SIRT1* knockdown significantly reversed the beneficial effect of rhFGF21 on cisplatin-induced apoptosis (**Figures 6C,D**). Compared with the rhFGF21 + cisplatin group, *SIRT1* knockdown cells treated with rhFGF21 + cisplatin showed significantly higher expression levels of C-caspase 3 and Bax (**Figures 6C,E,F**). In cells treated with rhFGF21 + cisplatin, TUNEL analysis showed a significant increase in the percentage of apoptotic cells after *SIRT1* knockdown (**Figures 6G,H**). These results indicate that the beneficial effects of rhFGF21 on cell damage are significantly decreased in *SIRT1*-knockdown HK-2 cells.

Similar results were obtained in our *in vivo* experiments. SIRT1 expression in C57BL/6 mice was effectively knocked down after LV-SIRT1-RNAi transfection (**Figures 7A,B**). In mice treated with rhFGF21 + cisplatin, BUN and serum creatinine levels were significantly increased (**Figures 7C,D**). When SIRT1 expression was inhibited (**Figures 7E,F,J,K**), BUN and serum creatinine levels were higher than in rhFGF21 + cisplatin mice (**Figures 7C,D**). Immunoblot analysis showed that SIRT1 knockdown increased TIM-1, C-caspase 3, and Bax levels in mouse kidney compared with rhFGF21 + cisplatin mice (**Figures 7E,G–I**). H&E staining showed that rhFGF21 could not effectively ameliorate kidney damage after SIRT1 knockdown, and kidney tissue exhibited tubular structure disorder, a large amount of cell debris, vacuolar changes, increased casts and glomerular space, and aggravated tissue damage (**Figures 7L,M**). Furthermore, TUNEL analysis was performed using cisplatin-treated mice after SIRT1 knockdown. We found that the percentage of apoptotic cells in renal tissue was higher than 50%, even after rhFGF21 treatment (**Figures 7N,O**).

In conclusion, these results indicate that *SIRT1* knockdown reduces the protective effects of rhFGF21 on cisplatin-induced AKI both *in vitro* and *in vivo*.

DISCUSSION

In this study, we discovered that cisplatin induces acute tubular cell injury *in vitro* and *in vivo*. Cisplatin also increases FGF21 and SIRT1 protein levels in kidney. Our results indicate that rhFGF21 administration attenuates cisplatin-induced nephrotoxicity. We further explored the involvement of FGF21/SIRT1 in renal protection.

Two phenomena cause cisplatin-induced AKI, i.e., cisplatin accumulation in tubular cells and renal tubular cell injury (Fernández-Martínez et al., 2016; Oh et al., 2017). Tumor patients are prone to AKI during cisplatin treatment. Their clinical manifestations include a decrease in glomerular filtration rate, an increase in BUN and serum creatinine levels, and electrolyte disorders (Arany and Safirstein, 2003). Our results indicate that both BUN levels and serum creatinine levels began to rise 24 h after cisplatin treatment, reaching a maximum at 72 h in mice. Currently, levels of serum creatinine, BUN, cystatin-C, TIM-1, and NGAL are routinely measured to investigate cisplatin-induced AKI models (Holditch et al., 2019). Our studies also indicate the protein levels of the AKI markers TIM-1, C-caspase 3, and Bax increased significantly in a time-dependent manner.

Previous studies have shown that FGF21 regulates glucose and lipid metabolism to maintain energy balance and metabolic homeostasis. It is mainly expressed in the liver, adipose tissue, and pancreatic islet under physiological conditions (So and Leung, 2016). It has been shown that the serum FGF21 concentration is significantly increased in patients with diabetic nephropathy, chronic kidney disease, and long-term dialysis (Shahbazi et al., 2015; Li Y.Z. et al., 2018). This is possibly related to the decline in kidney function. Studies also showed that FGF21 has beneficial effects on tissue damage caused by metabolic abnormalities and responses to various cellular and metabolic stresses. It was significantly upregulated as an effective catabolic factor in order to antagonize metabolism and energy imbalance (Gómez-Sámano et al., 2017; Luo et al., 2017). In addition, it has been indicated that upregulation of serum FGF21 levels may delay the progression of diabetic nephropathy and chronic kidney disease (Li F. et al., 2018; Suassuna et al., 2019). Many studies have previously shown that loss of FGF21 causes pathologic damage in multiple animal models, including decreased productivity of pancreatic beta cells and insulin sensitivity (Lee et al., 2018; Wanders et al., 2017), promotion of the development of fatty liver in mice followed by aggravation of liver fibrosis (Singhal et al., 2018), and even aggravation of cisplatin-induced AKI (Holditch et al., 2019). Similarly, overexpression of FGF21 or administration of exogenous FGF21 regulates metabolism, controls the stress response, and attenuates organ damage (So and Leung, 2016; Kang et al., 2018; Lu et al., 2019; Suassuna et al., 2019). Our results are consistent with previous reports. Cisplatin induces a significant upregulation of FGF21 in renal tubular cells *in vitro* and *in vivo*. Administration of rhFGF21 *in vitro* and *in vivo* reduced cisplatin-induced tubular cell death, significantly decreased BUN and serum creatinine levels, and downregulated the expression of TIM-1, C-caspase 3, and Bax in kidney tissue. We further have confirmed that increased FGF21 expression during AKI can protect the kidneys.

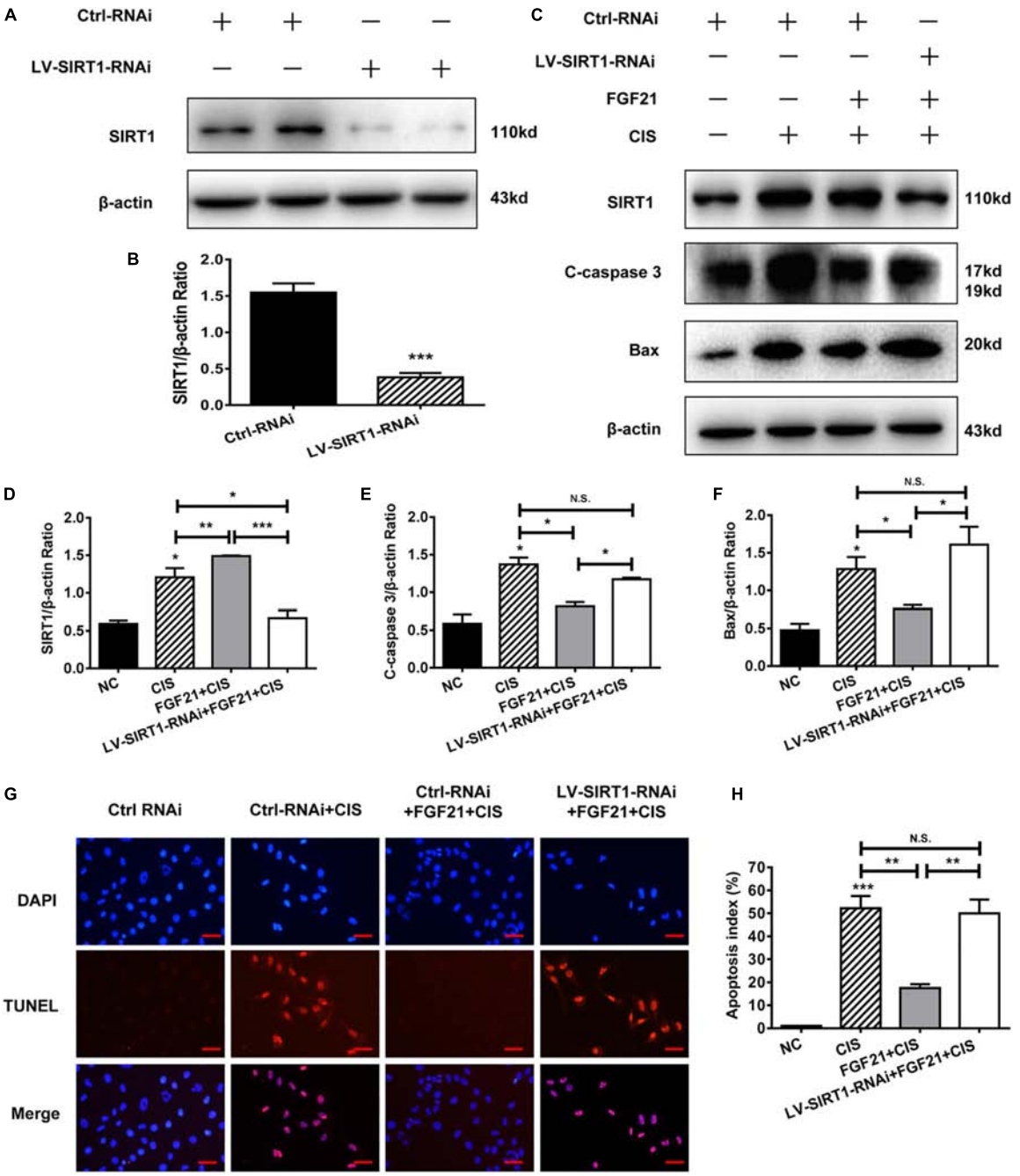

FIGURE 6 | SIRT1 mediates the beneficial effects of FGF21 on cisplatin-induced HK-2 cell damage. **(A,B)** Representative immunoblotting analysis of SIRT1 after LV-SIRT1-RNAi transfection in HK-2 cells. Protein levels of SIRT1 were quantified by densitometry, with β-actin as protein loading control. **(C–F)** Representative immunoblotting analysis of SIRT, C-caspase 3, and Bax after LV-SIRT1-RNAi transfection in HK-2 cells. Protein levels of SIRT1, C-caspase 3, and Bax were quantified by densitometry, with β-actin as protein loading control. **(G,H)** TUNEL staining in HK-2 cells (scale bar: 100 μm; DAPI: blue, TUNEL: red), and quantitative analysis of TUNEL staining. ***$P < 0.001$, **$P < 0.01$, *$P < 0.05$.

A previous study demonstrated that FGF21 may protect kidney tubular cells by suppressing P53 (Li F. et al., 2018). Here, we investigated the role of SIRT1 from a new perspective. SIRT1 is a key molecule involved in kidney injury (Kim et al., 2019; Zhang et al., 2019). Our study provides both *in vitro* and *in vivo* evidence to show that SIRT1 expression is upregulated in damaged tubular cells during cisplatin-induced AKI. Previous studies have demonstrated the beneficial effects of SIRT1 in many organs, including the liver (Zhu et al., 2014; Abd Elwahab et al., 2017), heart (Li et al., 2019), bone (Hou et al., 2019), and

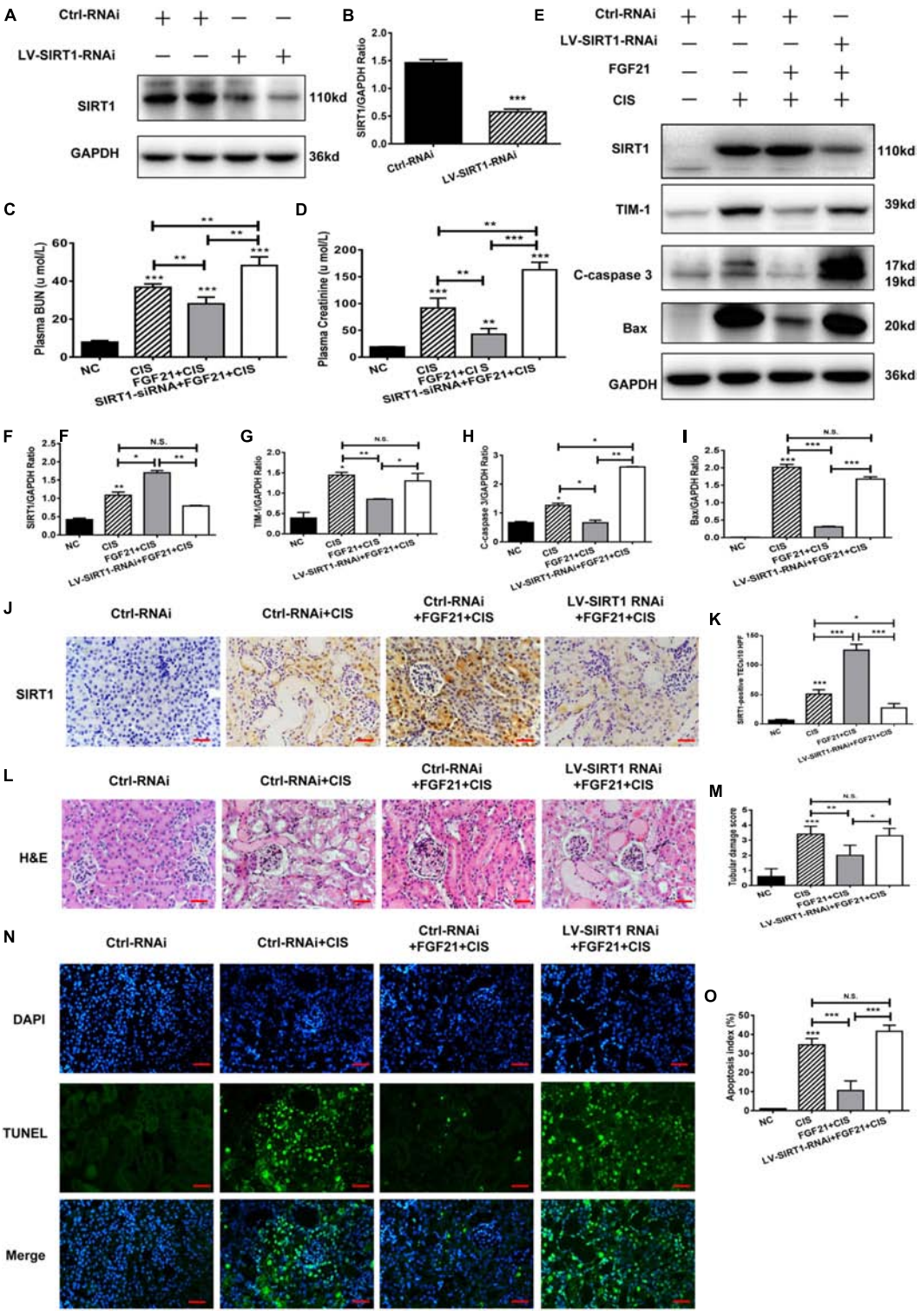

FIGURE 7 | SIRT1 mediates the beneficial effects of FGF21 on cisplatin-induced mouse AKI. **(A,B)** Representative immunoblotting analysis of SIRT1 in *SIRT1* knockdown mice. Protein levels of SIRT1 were quantified by densitometry, with β-actin as protein loading control. **(C)** Changes in mouse BUN levels. **(D)** Changes in mouse serum creatinine levels. **(E–I)** Representative immunoblotting analysis of SIRT1, TIM-1, C-caspase 3, and Bax. Protein levels of SIRT1, TIM-1, C-caspase 3, and Bax were quantified by densitometry, with GAPDH as loading control. **(J)** Immunohistochemistry staining of SIRT1 in mouse renal tissue (scale bar: 100 μm). **(K)** Quantitative immunohistochemistry analysis of SIRT1. **(L)** H&E staining of mouse renal tissue (scale bar: 100 μm). **(M)** Histopathological score of H&E staining of renal tissue. **(N,O)** TUNEL staining of renal tissue (scale bar: 100 μm; DAPI: blue, TUNEL: green), and quantitative analysis of TUNEL staining. ***$P < 0.001$, **$P < 0.01$, *$P < 0.05$.

kidney (Kim et al., 2019). In the ischemia-reperfusion AKI model, SIRT1 targets the deoxyacetylation of p53, FoxO1, and NF-κB to regulate the stress response, inflammation, cell senescence, and apoptosis (Grabowska et al., 2017; Zhang et al., 2017; Abdolvahabi et al., 2019; Wang et al., 2019). In addition, SIRT1-mediated inhibition of tubular cell apoptosis has been shown to be the primary mechanism of renal protection (Liao et al., 2019; Ryu et al., 2019; Zhang et al., 2019). Our data also suggest that such a mechanism is important during cisplatin-induced AKI.

Recently, pharmacologic studies have suggested that FGF21 improves cardiac function and alleviates Ang II-induced cardiac hypertrophy in a SIRT1-dependent manner (Li et al., 2019). Similarly, studies have reported that the anti-senescence effect of FGF21 on human umbilical vascular endothelial cells (HUVECs) is SIRT1-dependent (Yan et al., 2017). These findings imply that SIRT1 may contribute to the beneficial effects of FGF21. However, further experiments are needed to verify this hypothesis in cisplatin-induced AKI. In the present study, we demonstrate that rhFGF21 induces the expression of SIRT1, further attenuates renal tubular cell injury, and inhibits apoptosis. Moreover, the renal protective effects of rhFGF21 are decreased upon SIRT1 knockdown, suggesting that SIRT1 mediates the beneficial effects of FGF21 on cisplatin-induced AKI.

In summary, our results demonstrate that FGF21 ameliorates cisplatin-induced nephrotoxicity through SIRT1, preventing kidney failure and tubular cell damage.

DATA AVAILABILITY STATEMENT

The datasets generated for this study are available on request to the corresponding author.

ETHICS STATEMENT

All animal experimentation was carried out in accordance with the principles of the Basel Declaration and recommendations of the Laboratory Animal Guidelines for Ethical Review of Animal Welfare, Laboratory Animal Ethics Committee of Wenzhou Medical University. The protocol was approved by the Laboratory Animal Centre of Wenzhou Medical University.

AUTHOR CONTRIBUTIONS

QC, JM, XY, and QL performed experiments. FG and ZL coordinated the study and oversaw all experiments. FG wrote the manuscript. All authors discussed the results and commented on the manuscript.

FUNDING

This research was supported by the Zhejiang Provincial Natural Science Foundation of China under grant LY17H160048 and National Key R&D Program of China (2017YFA0506000).

SUPPLEMENTARY MATERIAL

The Supplementary Material for this article can be found online at: https://www.frontiersin.org/articles/10.3389/fphar.2020.00241/full#supplementary-material

FIGURE S1 | TUNEL staining in HK-2 cells at different time points. HK-2 cells were treated with cisplatin for 12 h, 18 h, and 24 h. TUNEL staining in HK-2 cells (scale bar: 100 μm; DAPI: blue, TUNEL: red).

FIGURE S2 | rhFGF21 upregulated SIRT1 expression in HK-2 cells. **(A–D)** Representative immunoblotting analysis of SIRT1 in HK-2 cells. Protein levels of SIRT1 were quantified by densitometry, with β-actin as protein loading control. $^{***}P < 0.001$, $^{**}P < 0.01$, $^{*}P < 0.05$.

REFERENCES

Abd Elwahab, A. H., Ramadan, B. K., Schaalan, M. F., and Tolba, A. M. (2017). A novel role of SIRT1/ FGF-21 in taurine protection against cafeteria diet-induced steatohepatitis in rats. *Cell Physiol. Biochem.* 43, 644–659. doi: 10.1159/000480649

Abdolvahabi, Z., Nourbakhsh, M., Hosseinkhani, S., Hesari, Z., Alipour, M., Jafarzadeh, M., et al. (2019). MicroRNA-590-3P suppresses cell survival and triggers breast cancer cell apoptosis via targeting sirtuin-1 and deacetylation of p53. *J. Cell. Biochem.* 120, 9356–9368. doi: 10.1002/jcb.28211

Arany, I., and Safirstein, R. L. (2003). Cisplatin nephrotoxicity. *Semin. Nephrol.* 23, 460–464. doi: 10.1016/S0270-9295(03)00089-5

Basile, D. P., Bonventre, J. V., Mehta, R., Nangaku, M., Unwin, R., Rosner, M. H., et al. (2016). Progression after AKI: understanding maladaptive repair processes to predict and identify therapeutic treatments. *J. Am. Soc, Nephrol.* 27, 687–697. doi: 10.1681/asn.2015030309

Coca, S. G., Singanamala, S., and Parikh, C. R. (2012). Chronic kidney disease after acute kidney injury: a systematic review and meta-analysis. *Kidney Int.* 81, 442–448. doi: 10.1038/ki.2011.379

Fernández-Martínez, A. B., Benito Martinez, S., and Lucio Cazana, F. J. (2016). Intracellular prostaglandin E2 mediates cisplatin-induced proximal tubular cell death. *Biochim. Biophys. Acta* 1863, 293–302. doi: 10.1016/j.bbamcr.2015.11.035

Fisher, F. M., and Maratos-Flier, E. (2016). Understanding the physiology of FGF21. *Annu. Rev. Physiol* 78, 223–241. doi: 10.1146/annurev-physiol-021115-105339

Gómez-Sámano, M. Á, Grajales-Gómez, M., Zuarth-Vázquez, J. M., Navarro-Flores, M. F., Martínez-Saavedra, M., Juárez-León, ÓA., et al. (2017). Fibroblast growth factor 21 and its novel association with oxidative stress. *Redox Biol.* 11, 335–341. doi: 10.1016/j.redox.2016.12.024

Grabowska, W., Sikora, E., and Bielak-Zmijewska, A. (2017). Sirtuins, a promising target in slowing down the ageing process. *Biogerontology* 18, 447–476. doi: 10.1007/s10522-017-9685-9

Holditch, S. J., Brown, C. N., Lombardi, A. M., Nguyen, K. N., and Edelstein, C. L. (2019). Recent advances in models, mechanisms, biomarkers, and interventions in cisplatin-induced acute kidney injury. *Int. J. Mol. Sci.* 20:3011. doi: 10.3390/ijms20123011

Hori, Y., Aoki, N., Kuwahara, S., Hosojima, M., Kaseda, R., Goto, S., et al. (2017). Megalin blockade with cilastatin suppresses drug-induced nephrotoxicity. *J. Am. Soc. Nephrol.* 28, 1783–1791. doi: 10.1681/asn.2016060606

Hou, W., Ye, C., Chen, M., Li, W., Gao, X., He, R., et al. (2019). Bergenin activates SIRT1 as a novel therapeutic agent for osteogenesis of bone mesenchymal stem cells. *Front. Pharmacol.* 10:618. doi: 10.3389/fphar.2019.00618

Kang, H., Seo, E., Park, J. M., Han, N. Y., Lee, H., and Jun, H. S. (2018). Effects of FGF21-secreting adipose-derived stem cells in thioacetamide-induced hepatic fibrosis. *J. Cell Mol. Med.* 22, 5165–5169. doi: 10.1111/jcmm.13795

Kim, K. H., and Lee, M.-S. (2015). FGF21 as a mediator of adaptive responses to stress and metabolic benefits of anti-diabetic drugs. *J. Endocrinol.* 226, R1–16. doi: 10.1530/joe-15-0160

Kim, M., Jung, J. Y., Choi, S., Lee, H., Morales, L. D., Koh, J. T., et al. (2017). GFRA1 promotes cisplatin-induced chemoresistance in osteosarcoma by inducing autophagy. *Autophagy* 13, 149–168. doi: 10.1080/15548627.2016.1239676

Kim, J. Y., Jo, J., Kim, K., An, H. J., Gwon, M. G., Gu, H., et al. (2019). Pharmacological activation of Sirt1 ameliorates cisplatin-induced acute kidney injury by suppressing apoptosis, oxidative stress, and inflammation in mice. *Antioxidants* 8:322 doi: 10.3390/antiox8080322

Kuro, O. M. (2019). The Klotho proteins in health and disease. *Nat. Rev. Nephrol.* 15, 27–44. doi: 10.1038/s41581-018-0078-3

Lee, Y. S., Lee, C., Choung, J. S., Jung, H. S., and Jun, H. S. (2018). Glucagon-like peptide 1 Increases Beta-Cell Regeneration By Promoting Alpha- To Beta-Cell Transdifferentiation. *Diabetes* 67, 2601–2614. doi: 10.2337/db18-0155

Li, F., Liu, Z., Tang, C., Cai, J., and Dong, Z. (2018). FGF21 is induced in cisplatin nephrotoxicity to protect against kidney tubular cell injury. *Faseb. J.* 32, 3423–3433. doi: 10.1096/fj.201701316R

Li, Y. Z., Ren, S., Yan, X. T., Li, H. P., Li, W., Zheng, B., et al. (2018). Improvement of Cisplatin-induced renal dysfunction by Schisandra chinensis stems via anti-inflammation and anti-apoptosis effects. *J. Ethnopharmacol.* 217, 228–237. doi: 10.1016/j.jep.2018.01.033

Li, Z., Xu, K., Zhang, N., Amador, G., Wang, Y., Zhao, S., et al. (2018). Overexpressed SIRT6 attenuates cisplatin-induced acute kidney injury by inhibiting ERK1/2 signaling. *Kidney Int.* 93, 881–892. doi: 10.1016/j.kint.2017.10.021

Li, S., Zhu, Z., Xue, M., Yi, X., Liang, J., Niu, C., et al. (2019). Fibroblast growth factor 21 protects the heart from angiotensin II-induced cardiac hypertrophy and dysfunction via SIRT1. *Biochim. Biophys. Acta Mol. Basis Dis.* 1865, 1241–1252. doi: 10.1016/j.bbadis.2019.01.019

Li, X. (2019). The FGF metabolic axis. *Front. Med.* 13:511–530. doi: 10.1007/s11684-019-0711-y

Liao, Z., Zhang, J., Wang, J., Yan, T., Xu, F., Wu, B., et al. (2019). The anti-nephritic activity of a polysaccharide from okra (Abelmoschus esculentus (L.) Moench) via modulation of *AMPK-Sirt*1-PGC-1alpha signaling axis mediated anti-oxidative in type 2 diabetes model mice. *Int. J. Biol. Macromol.* 140, 568–576. doi: 10.1016/j.ijbiomac.2019.08.149

Lu, Y., Li, R., Zhu, J., Wu, Y., Li, D., Dong, L., et al. (2019). Fibroblast growth factor 21 facilitates peripheral nerve regeneration through suppressing oxidative damage and autophagic cell death. *J. Cell Mol. Med.* 23, 497–511. doi: 10.1111/jcmm.13952

Luo, Y., Ye, S., Chen, X., Gong, F., Lu, W., and Li, X. (2017). Rush to the fire: FGF21 extinguishes metabolic stress, metaflammation and tissue damage. *Cytokine Growth Factor Rev.* 38, 59–65. doi: 10.1016/j.cytogfr.2017.08.001

Morigi, M., Perico, L., and Benigni, A. (2018). Sirtuins in renal health and disease. *J. Am. Soc. Nephrol.* 29, 1799–1809. doi: 10.1681/asn.2017111218

Motwani, S. S., McMahon, G. M., Humphreys, B. D., Partridge, A. H., Waikar, S. S., and Curhan, G. C. (2018). Development and validation of a risk prediction model for acute kidney injury after the first course of cisplatin. *J. Clin. Oncol.* 36, 682–688. doi: 10.1200/jco.2017.75.7161

Nishimura, T., Nakatake, Y., Konishi, M., and Itoh, N. (2000). Identification of a novel FGF, FGF-21, preferentially expressed in the liver. *Biochim. Biophys. Acta* 1492, 203–206. doi: 10.1016/s0167-4781(00)00067-1

Oh, C. J., Ha, C. M., Choi, Y. K., Park, S., Choe, M. S., Jeoung, N. H., et al. (2017). Pyruvate dehydrogenase kinase 4 deficiency attenuates cisplatin-induced acute kidney injury. *Kidney Int.* 91, 880–895. doi: 10.1016/j.kint.2016.10.011

Phillipson-Weiner, L., Mirek, E. T., Wang, Y., McAuliffe, W. G., Wek, R. C., and Anthony, T. G. (2016). General control nonderepressible 2 deletion predisposes to asparaginase-associated pancreatitis in mice. *Am. J. Physiol. Gastrointest. Liver Physiol.* 310, G1061–G1070. doi: 10.1152/ajpgi.00052.2016

Ryu, D. R., Yu, M. R., Kong, K. H., Kim, H., Kwon, S. H., Jeon, J. S., et al. (2019). Sirt1-hypoxia-inducible factor-1alpha interaction is a key mediator of tubulointerstitial damage in the aged kidney. *Aging Cell* 18:e12904. doi: 10.1111/acel.12904

Shahbazi, F., Sadighi, S., Dashti-Khavidaki, S., Shahi, F., Mirzania, M., Abdollahi, A., et al. (2015). Effect of silymarin administration on cisplatin nephrotoxicity: report from A pilot, randomized, double-blinded, placebo-controlled clinical trial. *Phytother. Res.* 29, 1046–1053. doi: 10.1002/ptr.5345

Singhal, G., Kumar, G., Chan, S., Fisher, F. M., Ma, Y., Vardeh, H. G., et al. (2018). Deficiency of fibroblast growth factor 21 (FGF21) promotes hepatocellular carcinoma (HCC) in mice on a long term obesogenic diet. *Mol. Metab.* 13, 56–66. doi: 10.1016/j.molmet.2018.03.002

So, W. Y., and Leung, P. S. (2016). Fibroblast growth factor 21 as an emerging therapeutic target for type 2 diabetes mellitus. *Med. Res. Rev.* 36, 672–704. doi: 10.1002/med.21390

Suassuna, P. G. A., de Paula, R. B., Sanders-Pinheiro, H., Moe, O. W., and Hu, M. C. (2019). Fibroblast growth factor 21 in chronic kidney disease. *J. Nephrol.* 32, 365–377. doi: 10.1007/s40620-018-0550-y

Sun, Y., Xia, M., Yan, H., Han, Y., Zhang, F., Hu, Z., et al. (2018). Berberine attenuates hepatic steatosis and enhances energy expenditure in mice by inducing autophagy and fibroblast growth factor 21. *Br. J. Pharmacol.* 175, 374–387. doi: 10.1111/bph.14079

Vanmassenhove, J., Kielstein, J., Jörres, A., and Biesen, W. V. (2017). Management of patients at risk of acute kidney injury. *Lancet* 389, 2139–2151. doi: 10.1016/s0140-6736(17)31329-6

Wanders, D., Forney, L. A., Stone, K. P., Burk, D. H., Pierse, A., and Gettys, T. W. (2017). FGF21 mediates the thermogenic and insulin-sensitizing effects of dietary methionine restriction but not its effects on hepatic lipid metabolism. *Diabetes* 66, 858–867. doi: 10.2337/db16-1212

Wang, S., Wang, Y., Zhang, Z., Liu, Q., and Gu, J. (2017). Cardioprotective effects of fibroblast growth factor 21 against doxorubicin-induced toxicity via the SIRT1/LKB1/AMPK pathway. *Cell Death Dis.* 8:e3018. doi: 10.1038/cddis.2017.410

Wang, Y., Huo, J., Zhang, D., Hu, G., and Zhang, Y. (2019). Chemerin/ChemR23 axis triggers an inflammatory response in keratinocytes through ROS-sirt1-NF-kappaB signaling. *J. Cell Biochem.* 120, 6459–6470. doi: 10.1002/jcb.27936

Yan, J., Wang, J., Huang, H., Huang, Y., Mi, T., Zhang, C., et al. (2017). Fibroblast growth factor 21 delayed endothelial replicative senescence and protected cells from H2O2-induced premature senescence through SIRT1. *Am. J. Transl. Res.* 9, 4492–4501.

Zhang, J., Bi, R., Meng, Q., Wang, C., Huo, X., Liu, Z., et al. (2019). Catalpol alleviates adriamycin-induced nephropathy by activating the SIRT1 signalling pathway in vivo and in vitro. *Br. J. Pharmacol.* 176, 4558–4573. doi: 10.1111/bph.14822

Zhang, M., Zhang, Q., Hu, Y., Xu, L., Jiang, Y., Zhang, C., et al. (2017). miR-181a increases FoxO1 acetylation and promotes granulosa cell apoptosis via SIRT1 downregulation. *Cell Death Dis.* 8:e3088. doi: 10.1038/cddis.2017.467

Zhao, L., Wang, H., Xie, J., Chen, Z., Li, X., and Niu, J. (2017). Potent long-acting rhFGF21 analog for treatment of diabetic nephropathy in db/db and DIO mice. *BMC Biotechnol.* 17:58. doi: 10.1186/s12896-017-0368-z

Zheng, X., Xu, F., Liang, H., Cao, H., Cai, M., Xu, W., et al. (2017). SIRT1/HSF1/HSP pathway is essential for exenatide-alleviated, lipid-induced hepatic endoplasmic reticulum stress. *Hepatology* 66, 809–824. doi: 10.1002/hep.29238

Zhu, S., Ma, L., Wu, Y., Ye, X., Zhang, T., Zhang, Q., et al. (2014). FGF21 treatment ameliorates alcoholic fatty liver through activation of AMPK-SIRT1 pathway. *Acta Biochim. Biophys. Sin.*46, 1041–1048. doi: 10.1093/abbs/gmu097

Conflict of Interest: The authors declare that the research was conducted in the absence of any commercial or financial relationships that could be construed as a potential conflict of interest.

frontiers in Pharmacology

MINI REVIEW
published: 08 April 2020
doi: 10.3389/fphar.2020.00426

Fibroblast Growth Factors in the Management of Acute Kidney Injury Following Ischemia-Reperfusion

Lian-Cheng Deng[1†], *Tahereh Alinejad*[1†], *Saverio Bellusci*[1,2*] *and Jin-San Zhang*[1,2*]

[1] Center for Precision Medicine, The First Affiliated Hospital of Wenzhou Medical University, Wenzhou, China, [2] Institute of Life Sciences, Wenzhou University, Wenzhou, China

Ischemia-reperfusion injury (IRI), which is triggered by a transient reduction or cessation of blood flow followed by reperfusion, is a significant cause of acute kidney injury (AKI). IRI can lead to acute cell death, tissue injury, and even permanent organ dysfunction. In the clinic, IRI contributes to a higher morbidity and mortality and is associated with an unfavorable prognosis in AKI patients. Unfortunately, effective clinical drugs to protect patients against the imminent risk of renal IRI or treat already existing AKI are still lacking. Fibroblast growth factors (FGFs) are important regulators of key biological and pathological processes, such as embryonic development, metabolic homeostasis and tumorigenesis through the regulation of cell differentiation, migration, proliferation and survival. Accumulating evidence suggests that altered expression of endogenous FGFs is associated with IRI and could be instrumental in mediating the repair process. Therefore, FGFs have been proposed as potential biomarkers in the clinic. More importantly, exogenous FGF ligands have been reported to protect against renal IRI and display promising features for therapy. In this review, we summarize the evidence and mechanisms of AKI following IRI with a focus on the therapeutic capacity of several members of the FGF family to treat AKI after IRI.

Keywords: fibroblast growth factors, ischemia-reperfusion injury, acute kidney injury, protection, therapy

OPEN ACCESS

Edited by:
Zhouguang Wang,
Albert Einstein College of Medicine,
United States

Reviewed by:
Sandra Donnini,
University of Siena, Italy
Michele Samaja,
University of Milan, Italy

***Correspondence:**
Saverio Bellusci
saverio.bellusci@innere.med.uni-giessen.de
Jin-San Zhang
Zhang_JinSan@wmu.edu.cn

[†]*These authors have contributed equally to this work*

Specialty section:
This article was submitted to Translational Pharmacology, a section of the journal Frontiers in Pharmacology

Received: *05 November 2019*
Accepted: *19 March 2020*
Published: *08 April 2020*

Citation:
Deng L-C, Alinejad T, Bellusci S and Zhang J-S (2020) Fibroblast Growth Factors in the Management of Acute Kidney Injury Following Ischemia-Reperfusion. Front. Pharmacol. 11:426. doi: 10.3389/fphar.2020.00426

INTRODUCTION

Acute kidney injury (AKI) is a syndrome and significant cause of death among hospitalized patients. AKI is characterized by a rapid decline in renal function and predisposes the transition of AKI patients to chronic kidney disease (CKD) and end-stage renal disease (ESRD) (Chawla et al., 2014). Ischemia-reperfusion injury (IRI) is the primary cause of AKI worldwide related to different clinical

Abbreviations: AKI, acute kidney injury; AKT, protein kinase B; CKD, chronic kidney disease; CSA-AKI, cardiac surgery-associated AKI; DAMP, damage-associated molecular pattern; ERK, extracellular signal-regulated kinase; ER, endoplasmic reticulum; ESRD, end-stage renal disease; FGF, fibroblast growth factor; FGFR, fibroblast growth factor receptor; FRS-2, fibroblast growth factor receptor substrate 2; HMGB1, high mobility group protein 1; HSPG, heparin sulphate proteoglycan, ICK, intracellular kinase domain; IL-1β, Interleukin-1 beta; IL-6, Interleukin-6; IR, ischemia reperfusion; IRI, ischemia reperfusion injury; MAPK, mitogen-activated protein kinase; NF-κB, nuclear factor kappa-B; PI3K, phosphatidylinositol-4,5-bisphosphate 3-kinase; PLCγ: phospholipase C gamma; ROS, reactive oxygen species; TGF-β: transforming growth factor beta; TLR2; toll-like receptor 2; TLR4, toll-like receptor 4; TM, trans-membrane domain; TNF-α, tumor necrosis factor alpha; UPR, unfolded protein response.

circumstances such as shock, low cardiac output, and organ transplantation (Park et al., 2017; Ronco et al., 2019). Under these conditions, the reestablishment of blood flow after transient obstruction of circulation leads to renal injury. A multinational, multicenter study on critically affected patients confirmed the prevalence of AKI (5.7% of the patients included in the study) and association with a high mortality rate (Uchino et al., 2005). Another independent study shows an even higher percentage of patients admitted to hospital with such a complication, 10–15% of all hospitalisations (Al-Jaghbeer et al., 2018), the number is as high as 50% in patients in the intensive care unit (ICU) 50% (Hoste et al., 2015).

The disease mechanisms underlying the etiology and pathogenesis of AKI are complex and include mitochondrial dysfunction, reactive oxygen species (ROS), endoplasmic reticulum stress (ERS), autophagy, inflammation, apoptosis, and necrosis (Verma and Molitoris, 2015; Duann et al., 2016; **Figure 1A**). Even though renal IRI is known to be the predominant cause of morbidity and mortality, no effective treatment is currently available. Therefore, much attention has been dedicated to seeking novel therapeutic strategies for AKI. Intense research efforts using animal models have shed light on the pathophysiology of AKI. It has been reported that the expression of Fibroblast growth factors (FGFs) and their receptors (FGFRs) are increased in the context of AKI (Wai et al., 2013; Tan et al., 2017). Furthermore, AKI is more severe upon FGFR deficiency or blockade of its signalling (Villanueva et al., 2008; Xu and Dai, 2017). Some studies demonstrated that renal function recovered after administering various medications, including growth factors and cell transplantation (Ichimura et al., 1996; Patel et al., 2012). These results show that FGFs and their receptors are important for AKI.

In the context of IRI, several growth factors have been reported to exhibit protective effects as well as therapeutic potential as they not only prevent the damages from occurring, but also improve functional recovery after the damages are done (**Figure 1A**, **Table 1**). New functions of FGFs have recently emerged. Evidence for FGF1, FGF2, FGF7, and FGF10 to trigger mitogenic and antiapoptosis activities correlates with their ability to enhance the survival and outgrowth of various kidney cell types, such as collective cells, tubule cells, and glomerular cells. Progress has also been made in understanding the roles and associated mechanisms of FGFs in AKI (**Figure 1B**).

Here, we will summarize the available data on the roles and known mechanisms of FGFs in the pathogenesis, prevention, and repair of AKI with a focus on IRI. The discussion will first provide a succinct overview of FGF/FGFR signalling specificity and function, followed by a detailed summary of the published work on the roles of FGFs/FGFRs in the AKI, impact of endogeneous and recombinant FGFs as prevention and therapeutic measures for the IRI, pathophysiological processes and conclude with a highlight for future research to better understand underlying mechanism and FGFs in AKI disease and provide viable strategies to prevent IRI or avert progression to CKD.

A SUCCINCT OVERVIEW OF FGF LIGANDS AND THEIR RECEPTORS

In mammalians, the FGF system consists of 18 ligands signalling through their specific FGFRs (Goetz and Mohammadi, 2013; Ornitz and Itoh, 2015, **Figure 2A**). The molecular weight of vertebrate FGFs ranges from 17 to 34 kDa and the proteins consist of a central core of 140 amino acids and 12 antiparallel β chains. The sequence similarity among different members is between 30% and 60%. FGFs are structurally related and functionally relevant, they elicit a redundant but also distinct repertoire of biological activities. FGFs are further divided into several subfamilies based on their sequence identity, receptor binding specificity and biological activities. These are the FGF1 subfamily, including FGF1 and FGF2; FGF4 subfamily, which includes FGF4, FGF5, and FGF6, the FGF7 subfamily made of FGF3, FGF7, FGF10, and FGF22, the FGF8 subfamily, which consists of FGF8, FGF17, and FGF18, as well as the FGF9 subfamily, which is made of FGF9, FGF16, and FGF20 (Ornitz and Itoh, 2015, **Table 2**). Finally, the FGF19 subfamily includes FGF19, FGF21, and FGF23 (Li, 2019). Heparin sulphate proteoglycan (HSPG) binding domains and N-terminal signalling peptides for secretion are common features shared by FGFs.

In most cases, FGFs are secreted into the extracellular space *via* the classical secretory pathway. FGFs have been described to act both in an autocrine and paracrine fashion. They signal through their specific trans-membrane receptors consisting of five members, FGFR1-5. FGFRs bind their ligands with high affinity and various degrees of specificity (**Figure 2A**). All FGFRs has a single pass trans-membrane domain (TM) and two intracellular kinase domains (ICKs) except for the atypical FGFR5, which has no enzymatic activity (Trueb, 2011). The extracellular segments of FGFRs are composed of three Ig-like domains (IgGI-IgGIII), and between the first and second Ig-like domains is the acid-box domain that determines ligand-specificity. The ICKs harbor the catalytic activity of receptors as well as autophosphorylation sites, which interact with intracellular substrates (**Table 2**).

THE ROLE OF FGFS IN AKI

Many FGF ligands and their associated receptors are found to be highly expressed during kidney development. Genetic ablation and transgenic overexpression in mouse models, as well as exposure to exogenous FGF ligands, have established the critical regulatory roles of multiple FGF ligands in kidney development, particularly those that signal through FGFR1 and FGFR2 (Walker et al., 2016; **Figure 1B**). Some of the developmentally important FGFs/FGFRs expressed early during kidney development get re-expressed or activated in the regeneration phase after IRI (Villanueva et al., 2006; Tan et al., 2017). Currently, most of the FGFs reported to participate in AKI pathogenesis or reveal protective/therapeutic potentials are derived from FGF1, FGF7, and FGF19 subfamilies (**Figures 1A, B**), which we will be discussing in more detail.

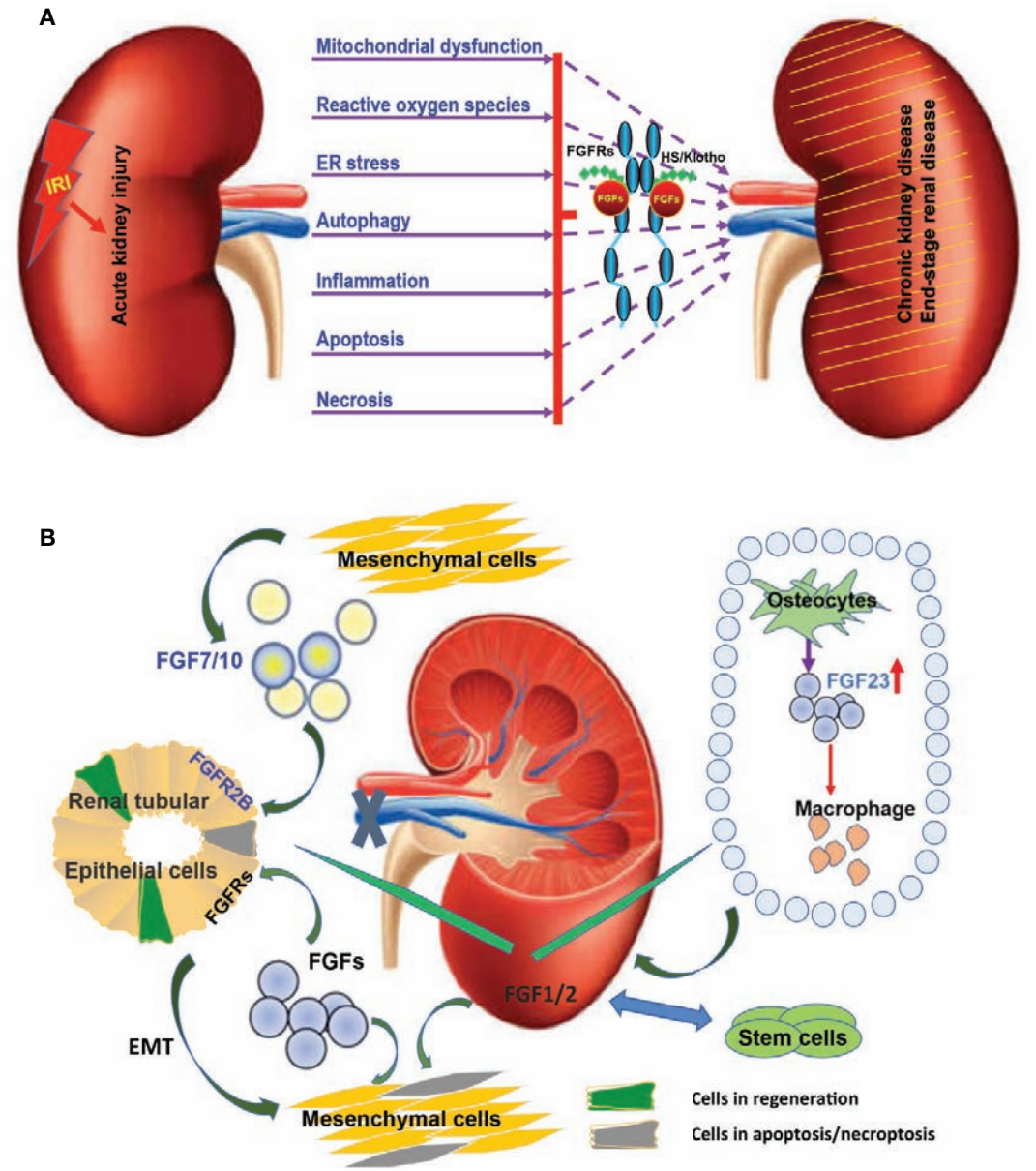

FIGURE 1 | Multiple FGFs are involved in the etiology and pathogenesis of AKI after IRI. **(A)** Diagram summarizing key biological processes underlying the etiology and pathogenesis of AKI. The interactions of these complex disease mechanisms can lead to CKD and ESRD. FGFRs can be activated by endogenous FGFs and co-ligands following IRI. Exogenous recombinant FGFs such as FGF2 and FGF10 can protect again IRI and inhibit the transition of AKI to CKD and ESRD *via* regulating this complex pathogenesis and repair process. **(B)** The expression of several FGFs including FGF1/2/7/10 is induced upon IRI and is capable of promoting tubular epithelial cell proliferation through a paracrine effect. Furthermore, FGF1/2 mediated activation of FGFRs can inhibit the apoptosis of tubular epithelial cells and promote the transformation of tubular epithelium to mesenchymal cells. Exogenous stem cells can ease IRI by producing FGF1/2. Increased FGF1/2 can further support the survival of stem cells. FGF23 is produced by osteoblasts in bone in response to local and systemic factors and targets the kidney to create multiple endocrine networks. FGF23 also impacts macrophage infiltration through adjusting the immune system after IRI.

MULTIFACETED ROLES OF FGF1/2 IN AKI

FGF1 (or Acidic FGF) and FGF2 (or basic FGF) are the prototypic members of the FGF family that have a similar broad range of biological activities. Both are *in vitro* mitogens for most of the ectodermal- and mesodermal-derived cell lines. Numerous studies have shown that intravenous administration of exogenous FGF1 or FGF2 can improve the physiological functions of different organs after IRI.

TABLE 1 | Fibroblast growth factors (FGFs) directly involved in regulating acute kidney injury (AKI).

FGF Subfamily	FGF ligand	Mode of action	Pathophysiological function
FGF1	**FGF1**	Autocrine and paracrine	Inhibition of neutrophil infiltration (Cuevas et al., 1999); Antiapoptosis and regeneration (Fu et al., 2004; Weng et al., 2004)
	FGF2	Paracrine	Attenuating mitochondrial damage and proinflammatory response (Tan et al., 2017) reduce renal damage and participate in the regeneration (Villanueva et al., 2006)
FGF7	**FGF7**	Paracrine	Promote bladder progenitor proliferation (Vinsonneau et al., 2010)
	FGF10	Paracrine	Antiapoptosis and inflammatory response; suppressing excessive autophagy and ER stress (Tan et al., 2018; Tan et al., 2020)
FGF19	**FGF23**	Endocrine	Biomarkers for injury and prognosis; amplify myofbroblast activation; potential target of therapy (Leaf et al., 2017; Smith et al., 2017b; Leaf et al., 2018; Volovelsky et al., 2018; Christov et al., 2019, and references within)

FGF1 is an autocrine/paracrine regulator known to act on cells from various organs and tissues, including liver, vasculature, and skin. FGF1 exerts significant beneficial effects in different organs after IRI (Fu et al., 1995; Cuevas et al., 2000; Chen et al., 2005; Wang et al., 2010). The skeletal muscle damage protection provided by FGF1 may arise from its ability to regulate extra-cellular and intra-cellular calcium ions concentrations (Fu et al., 1995). FGF1 can promote small intestine epithelial cell proliferation in IRI in rats and its activity is associated with the activation of ERK1/2. Intravenously administered FGF1 could also alleviate IRI-induced apoptosis in rat intestinal tissues (Weng et al., 2004). In other studies, FGF1 was reported to activate PI3K/AKT-mediated suppression of oxidative stress and inflammation, especially for diabetic nephropathy (Pena et al., 2017). FGF1 can protect hepatic and renal functions after intestinal IRI (Weng et al., 2004). Fu et al. showed that the protective effects of FGFs might originate from the non-mitogenic effects of FGFs at the early stage and the mitogenic effects at the late stage of tissue repair (Fu et al., 2004). Cuevas et al. demonstrated a role for FGF1 after acute kidney damage following IRI by inhibiting neutrophil infiltration (Cuevas et al., 1999).

FGF2 is another vital protein for ureteric bud formation, and also necessary for the induction of mesenchymal cells aggregation. The mesenchymal aggregates cannot give rise to epithelial cells in the absence of FGF2. In the adult mice, FGF2 exerted a protective function against IRI in several organs such as the retina, brain, spinal cord, heart, and intestine. FGF2 also has a beneficial role in renal IRI. The primary mechanism is *via* the activation of the PI3K/AKT and ERK1/2 pathways. The expression of FGF2 is not observed in the adult kidney during homeostasis, but a strong induction is observed in the regeneration phase of AKI. FGF2 reduces the expression of renal damage markers such as ED-1 and α-smooth muscle actin and participates in the regeneration process after ischemic acute renal failure (Villanueva et al., 2006). Xu et al. revealed the same results upon the ablation of the receptor FGFR2 in fibroblasts (Xu and Dai, 2017). Such genetic manipulation ameliorates kidney fibrosis after IRI in mice. On the other hand, inhibition of FGFR2 sensitize kidney damage and suppresses nephrogenic protein expression (Villanueva et al., 2008). Another study demonstrated that FGF2 protects against renal IRI by attenuating mitochondrial damage and proinflammatory signals (Tan et al., 2017). Functional studies

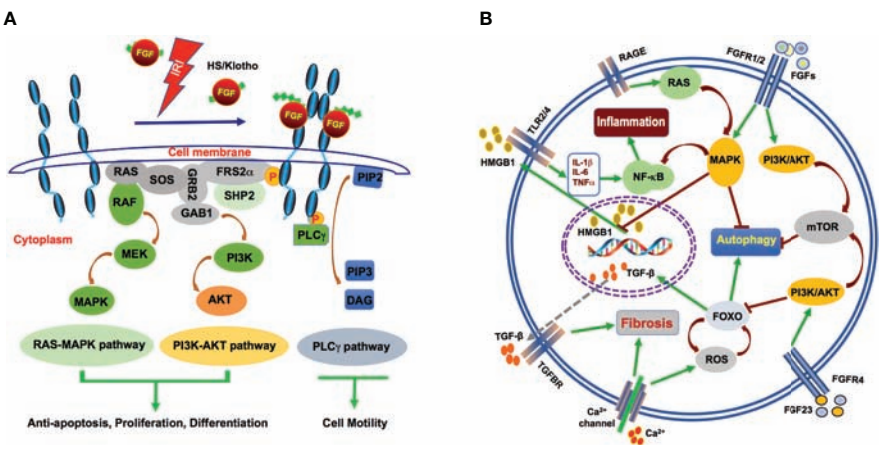

FIGURE 2 | Mechanism of FGFs signalling during AKI after IRI. **(A)** FGFs interact with FGFRs with HS (and klotho for FGF23) as cofactor after IRI. The interactions induce activation of the RAS-MAPK, PI3K-AKT, and PLCγ pathways. These pathways mediate antiapoptosis, differentiation, proliferation, and cell motility. **(B)** HMGB1, a nuclear transcription factor protein is released upon IR injury. Circulating HMGB1 can interact with TLRs to promote inflammatory cytokine secretion. Increased IL-1β, IL-6 and TNF-α in turn, activate NF-κB and further enhance inflammation. FGF2 may inhibit inflammation through robust protection of renal tubular cells from IR-induced apoptosis and subsequent release of HMGB1. FGF2 and FGF10 may inhibit autophagy *via* activation of PI3K/AKT and MAPK signalling. On the other hand, the endocrine FGF23 binds FGFR4 to activate the calcium channel and contribute to renal fibrosis. A large amount of calcium ion influx results in ROS activation, which also leads to increase in TGF-β expression and its down stream signalling to promote fibrosis.

TABLE 2 | Overview of Mammalian FGF subfamilies, receptor specificity and physiological functions.

The FGF Subfamilies	Ligands Human/mouse	Cofactor	Receptor Specificity	Major physiological function
FGF1 subfamily	FGF1/Fgf1	Heparin or heparin sulfate	All FGFRs	Adipose tissue homeostasis
	FGF2/Fgf2		FGFR1b,1c,2b,2c,3c,4	Wound healing and angiogenesis
FGF4 subfamily	FGF4/Fgf4		FGFR1c,2c,3c,4	Limb bud and heart development
	FGF5/Fgf5		FGFR1c,2c,3c	Hair follicle growth and development
	FGF6/Fgf6		FGFR1c,2c,3c,4	Muscle development and regeneration
FGF7 subfamily	FGF3/Fgf3		FGFR1b,2b	Inner ear and skeleton development
	FGF7/Fgf7		FGFR2b	Branching morphogenesis
	FGF10/Fgf10		FGFR1b,2b	Lung branching morphogenesis; inner ear, hair follicle, and limb development
	FGF22/Fgf22		FGFR1b,2b	Synaptogenesis
FGF8 subfamily	FGF8/Fgf8		FGFR1c,2c,3c,4	Brain, eye, ear, limb bud, kidney, and heart development
	FGF17/Fgf17		FGFR1c,2c,3c,4	Cerebellum and frontal cortex development
	FGF18/Fgf18		FGFR3c,4	Lung alveolar, bone, CNS, skeletal, and palate development
FGF9 subfamily	FGF9/Fgf9		FGFR1c,2c,3b,3c,4	Inner ear, gonad, and kidney development
	FGF16/Fgf16		FGFR1c,2c,3b,3c,4	Heart development
	FGF20/Fgf20		FGFR1c,2b,2c,3b,3c,4	Kidney, hair, teeth, cochlea, and central nervous development
FGF15/19 subfamily	FGF19/Fgf15		FGFR1c,2c,3c,4	Bile acid metabolism, gall bladder filling, lipid, and energy metabolism
	FGF21/Fgf21	β-Klotho	FGFR1c,3c,	Lipid, glucose, and energy metabolism, macronutrient preference, starvation response, insulin sensitivity
	FGF23/Fgf23	α-Klotho	FGFR1c,3c,4	Phosphate, calcium, sodium, and vitamin D homeostasis

have shown that FGF2 promotes proliferation on a variety of renal cell types, especially interstitial fibroblasts. FGF2 facilitates the epithelial to mesenchymal transition of tubular epithelial cells and contributes in the initial stage to an increase in the stroma population. The expression of FGF2 is increased in the process of stem cell treatment of AKI (Patel et al., 2012). We propose that both endogenous and exogenous FGF2 react to the transplanted stem cells after injury. The mechanism of stem cell therapy is not only the replacement of dead cells but more importantly, the role it plays through the secretion of growth factor as well as antiinflammatory molecules.

EXOGENOUS FGF10 PROTECTS AGAINST IRI

FGF7 and FGF10 were initially isolated as a keratinocyte growth factor 1 and 2, respectively. Both are expressed in the kidney, but unlike other FGFs, which are paracrine factors that are expressed exclusively in the mesenchyme. They interact primarily with the "b" isoforms of FGFR2 (FGFR2b), which is an alternatively spliced RNA isoform containing a unique domain (called IIIb) in the third IgG-like loop (Zhang et al., 2006). FGF7 and FGF10 have been documented to play an essential role in the development, growth, differentiation, and homeostasis of the muscosal lining of the urinary tract (Qiao et al., 1999; Walker et al., 2016).

Both FGF7 and FGF10 bind FGFR2b, but exert largely distinct physiological functions. FGF7 is implicated in both the induction of basal urothelial cell proliferation and the expansion of transitional epithelium. It is an efficient growth and differentiation factor during development and wound healing. FGF7 also has a significant effect on the kidney. Compared to wild type littermates, Fgf7 knockout mice display smaller kidneys with fewer ureteric buds and nephrons. Earlier reports showed that the expression of both FGF-7 and FGFR2b is induced and segregated between interstitial and epithelial cells in response to chemically-induced proximal tubular damage. The activation of this mesenchymal to epithelial paracrine signaling is implicated in the regulation of tubular repair process (Ichimura et al., 1996). Additionally, renal IRI is found to promote FGFR2 phosphorylation together with the selective upregulation of FGF7 and FGF2. Recombinant FGF7 administration can induce FGFR2 expression and promote bladder progenitor proliferation (Vinsonneau et al., 2010; **Figure 1B**), but no study on FGF7 and renal IRI has been published.

FGF10 is a multifunctional growth factor playing crucial roles in the development of multiple organs and tissues, including the kidney (Itoh, 2016). In contrast to the Fgf7-null mice, which do not display significant developmental abnormalities, the inactivation of Fgf10 in mice causes broad developmental defects including limb bud induction, lung as well as kidney agenesis (Ohuchi et al., 2000). Similar to FGF7, FGF10 also signals *via* interaction with its high-affinity receptor FGFR2b. Deletion of Fgf10 in mice led to kidney dysgenesis characterized by fewer collecting ducts and nephrons. Overexpression of a soluble dominant-negative FGFR2b isoform in transgenic mice revealed more striking defects, including renal aplasia or severe dysplasia (Celli et al., 1998). Intra-tracheal administration of FGF10 in rats with IR (Ischemia-Reperfusion) induced lung injury significantly diminished lung edema, the release of inflammatory cytokines, immune infiltration, and protein exudation. Activation of PI3K pathway has been reported to

underlie FGF10-mediated protection against I/R-induced endothelial cell apoptosis and barrier dysfunction (Fang et al., 2014). More recent studies provided further evidence that exogenous recombinant FGF10 mediates protection against renal IRI through suppression of excessive autophagy and ER stress (Tan et al., 2018; Tan et al., 2020), which will be further discussed later.

FGF23 AS BIOMARKERS OF AKI AND CKD

FGF23 belongs to the FGF19 subfamily of endocrine FGFs which play important roles in interorgan crosstalk that governs a broad spectrum of metabolic homeostasis (Degirolamo et al., 2016; Li, 2019). Although there are a number of reports on the protective effect of FGF21 on the myocardial IRI, there has yet to be any published research directly addressing the role of either FGF19 or FGF21 in renal IRI. FGF23 is mainly produced by osteocytes and possibly osteoblasts. Significantly, it is dramatically increased in CKD and ESRD, and has been proposed as a biomarker for adverse outcomes in patients with CKD and ESRD (Isakova, 2012; Christov et al., 2019 **Figure 1B**). Similar to FGF19 and FGF21, FGF23 binding to FGFRs and the subsequent activation of FGF signal transduction requires a co-receptor, Klotho (Kurosu et al., 2006). The structure of FGF23 ternary complex together with α-klotho extracellular domain and the FGFR1c ligand-binding domain has recently been solved (Smith et al., 2014; Chen et al., 2018). FGF23 controls renal phosphate reabsorption, modulates the production of parathyroid hormone (PTH) and 1,25-(OH)2-vitamin D. It also participates in mineral homeostasis. FGF23 acts on the kidney to increase renal phosphate excretion and to decrease 1,25-dihydroxy vitamin D (1,25D) production (Li et al., 2019; Musgrove and Wolf, 2020).

FGF23 levels rose acutely in patients who underwent cardiac surgery and developed AKI, even before a significant increase in serum creatinine (Christov et al., 2013). In the current era of heightened awareness of the dire need for early diagnosis of AKI, FGF23 has been touted as a potential marker of the complex AKI syndrome (Leaf et al., 2017; Leaf et al., 2018). Shaker et al. reported that the change of plasma FGF23 concentrations at 24 hours after cardiac bypass surgery was associated with the severity of renal injury, whose sensitivity was 100%, and specificity was 97.1% suggesting that FGF23 could have a role as an early biomarker of AKI and predicts adverse outcomes among patients with established AKI (Shaker et al., 2018; Volovelsky et al., 2018). A recent prospective investigation in a large cohort of patients with CKD stages have identified elevated serum levels of interleukin-6, C-reactive protein, and FGF23 as independent risk factors for mortality in CKD (Munoz Mendoza et al., 2017). Circulating levels of FGF23 are increased in human AKI and CKD of various settings, and correlate to poor survival in patients across infants, children, and adults (David et al., 2017; Czaya and Faul, 2019). Therefore, serum FGF23 level is proposed to be an even more significant parameter than creatinine to assess the severity of the AKI (Christov et al., 2019).

Other studies demonstrate that tubule-derived FGF23 might amplify myofibroblast activation in AKI (Smith et al., 2017b). FGF23 is found to augment profibrotic signalling cascades in injury-primed renal fibroblasts *via* activation of FGFR4 and upregulation of the calcium transporter, a transient receptor potential cation channel. This function was independent of α-Klotho. Restoration of α-Klotho, as upstream regulators, can regulate the off-target effects of FGF23 (Smith et al., 2017a). Both FGF23 and α-Klotho have been proposed as prognostic biomarkers of AKI and also targets of therapeutic intervention for CKD or CVD after AKI. The effects of different FGF family members in the context of AKI is summarized (**Table 1**).

FGFRS INVOLVED IN AKI

The FGF ligands signal through four receptors (FGFR1-4) and an atypical, kinase inactive FGFR5 or FGFRlL (Ornitz and Itoh, 2015). Some of FGFs/FGFRs are important during normal kidney development and also during postnatal repair. FGFs stimulate kidney cell fate determination, migration, and differentiation during organogenesis (Bates, 2011; Trueb et al., 2013) and regulate the proliferation, mobilization, and regeneration during repair after injury (Strutz, 2009; Gallegos et al., 2019).

FGFRs elicit different functions in mammalian development and diseases. Conditional knockout of Fgfr1 in ureteric bud and metanephric mesenchyme did not lead to any kidney development defects (Revest et al., 2001; Poladia et al., 2006). Ablation of Fgfr2 led to the formation of a smaller kidney with fewer nephrons (Sims-Lucas et al., 2011). The combined inactivation of Fgfr2 and Fgfr1 knockout in mice led to severe kidney aplasia (Sims-Lucas et al., 2011). General knockout of Fgfr3 and Fgfr4 did not affect early kidney development (Colvin et al., 1996; Weinstein et al., 1998). It has been previously reported that a given FGF ligand can bind multiple receptors and that conversely, the same receptor can bind different ligands, therefore allowing a very complex set of biological activities downstream of FGF/FGFR activation (Li, 2019). FGFR1, for example, can bind to most of FGFs except FGF7 and FGF18. FGFR2b, on the other hand, binds only FGF1 and the members of the FGF7 subfamily. Due to potential redundancy in FGFRs, their role in acute kidney injury is still unclear. However, exogenous FGF ligands, through the activation of the FGFR signalling pathway, are protective against renal damage. During IR-induced acute renal injury, increased expression of FGF activates FGFR phosphorylation and recruitment of FRS-2 and PLC-γ. The classical downstream PI3K/AKT and MAPK signalling pathways are subsequently activated to control cell proliferation, differentiation and apoptosis as well as cell migration and other processes. This leads to decreased renal injury caused by IRI (**Figure 2A**).

Although IRI mainly affects renal tubular cells, IR-induced pathogenic process and its repair involve interactions between interstitial cells, infiltrated inflammatory cells and epithelial cells. Interestingly, a recent study using a mouse model with fibroblast-specific ablation of Fgfr2 gene indicated that FGFR2 expression in fibroblast may contribute to kidney fibrosis after IRI through

promoting renal fibroblast activation and proliferation (Xu and Dai, 2017).

IMPACT OF FGFS ON PATHOPHYSIOLOGY OF IRI

IRI represents a frequent underlying cause for both ischemic heart disease and AKI. Compared to the numerous publications on a broad spectrum and relatively extensive research on FGFs in ischemic heart injury, only a limited number of reports are available on FGFs (mainly FGF2, FGF10, and FGF23) in renal IRI and AKI. Additionally, most of FGF23-related studies focus on its role as a key metabolic regulator and an injury or prognosis biomarker. Consequently, FGF23 is a proinjury factor rather than a protective or therapeutic agent for AKI. Therefore, our following discussions will only focus on FGF2 and FGF10, both of which exhibit potent protection against IRI and therapeutic potential *via* impacting several key pathophysiological mechanisms.

FGF2 PROTECTS AGAINST IR-INDUCED TUBULAR CELLS DEATH

Acute cell death of proximal renal tubules and inflammatory response of both innate and adoptive nature are hallmark features of IRI. Apoptosis plays an important role in the IR-induced pathogenesis and is a validated parameter to evaluate the cellular damage induced by ischemia. The protective role of FGF2 against IRI is well documented for ischemic myocardial infarction. Studies in genetically engineered mouse models established the antiapoptotic effect of endogenous FGF2 toward ischemic cardiac injury. FGF2 also exerts a positive impact on the repair process that may involve its activation of both MAPK and PKC pathways (House et al., 2003; House et al., 2005; House et al., 2007). Furthermore, under cardiac IRI conditions mimicking clinical acute myocardial infarction, endogenous FGF2 is considered an essential acute cardioprotective factor and a longer term proangiogenic factor (House et al., 2015). The protective effect of FGF2 against IRI and in promoting repair was also appreciated in renal IRI (Villanueva et al., 2008; Tan et al., 2017). Interestingly, FGF2 is found to be expressed early during kidney development, and gets re-expressed upon IRI and participates in the recovery process by promoting the expression of morphogen proteins to accelerate the repair process in the kidneys (Villanueva et al., 2006). Additionally, treatment with antisense oligoes targeting FGFR2 led to a significant increase in tubular TUNEL positive cells and expression of damage markers in an AKI model, whereas the expression of morphogenic proteins and cellular mitosis was inhibited (Villanueva et al., 2008). Our study demonstrated that exogenous recombinant FGF2 also exhibited robust protection against IRI and significantly improved animal survival in a rat IRI model (Tan et al., 2017).

Under hypoxic conditions, FGF2 may alleviate oxidative stress and IR-induced mitochondrial DNA damage and proapoptotic alteration of Bcl2/Bax expression and caspase-3 activation. The remarkable protective effect of FGF2 owns, at least in part, to its ability to preserve the integrity of the mitochondrial ATP-sensitive potassium channel (Tan et al., 2017). It is worth noting that, besides the major FGF2 protein isoform (18 kD, low molecular weight), there exist at least 4 other isoforms of higher molecular weight, which are reported to exert different or even opposite effects on apoptosis (Kardami et al., 2007; Liao et al., 2010; Manning et al., 2013) *via* different mechanisms. Besides apoptosis, other types of cell death such as necrosis, necroptosis, pyroptosis, ferroptosis, have been also been implicated to underlie the tubular cell damage, the potential role of FGFs on these additional pathways and the their interplay remain to be characterized (Xu and Han, 2016; Han and Lee, 2019; Hu et al., 2019). On the other hand, renal recovery from AKI requires the replacement of injured cells by new ones that can restore tubular epithelial integrity. In this regard, FGF2 may also facilitate the repair process of IRI, as post-IRI administration of FGF2 also exhibited effective protection of IRI and improved animal survival (Tan et al., 2017). The results collectively indicate that FGF2 has promising clinical potential for the prevention and treatment of IR-related AKI.

FGF10 INHIBITS EXCESSIVE AUTOPHAGY AND ER STRESS

Autophagy is an evolutionarily conserved pathway that leads to lysosomal degradation of cytoplasmic substrates, such as damaged organelles and cytoplasmic proteins. The autophagic response is triggered under various stress conditions including nutrient starvation, hypoxia, and growth-factor deprivation, as well as ER stress and oxidant injury, most of which are involved in the pathogenesis of AKI. Knockout of Atg5 or Atg7 in proximal tubule led to accumulation of deformed mitochondria, ubiquitin-positive inclusion bodies increased apoptosis and worsened renal dysfunction upon IRI suggesting a role of autophagy to the normal homeostasis of the kidney and renoprotective effect in IR injury (Jiang et al., 2010). However, some studies also report that autophagic response exacerbates renal IRI (Kaushal and Shah 2016; Tan et al., 2018). Therefore, it is likely that autophagy may exhibit both protective and detrimental properties in renal IRI, depending on the duration, the phase, and even the extent of the IRI.

FGF can inhibit autophagy through the mTOR pathway and block differentiation during organogenesis (Zhang et al., 2012; Cinque et al., 2015). Different FGFs may have distinct activities to regulate autophagy. FGF21 protects cardiomyocytes by promoting autophagic flux with hypoxia/reoxygenation injury (Ren et al., 2019). On the other hand, FGF2 and FGF10 can alleviate IRI by suppressing excessive autophagy *via* PI3K/AKT and MAPK signaling in the kidney and other organs (Wang et al., 2015; Sun et al., 2018; Tan et al., 2018, **Figure 2B**). Based on the analysis of renal tissues for their LC3, Beclin-1 and SQSTM1 expression and localization, FGF10 treatment was found to significantly suppress autophagic phenotype, which was highly activated during IRI, whereas co-treatment of FGF10 with

Rapamycin partially reversed such renoprotective effect, suggesting the involvement of mTOR pathway in the process. This study established that exogenously administered recombinant FGF10 is protective against IR-induced functional and tissue damage to the kidney, at least partially through mitigating excessive autophagy.

Recent studies further showed that IRI is accompanied with excessive activation of ER stress, which is involved in hypoxia injury-induced apoptosis of renal tubular epithelial cells. ER, a specialized organelle for protein synthesis, folding and trafficking, is highly sensitive to the intracellular microenvironment changes. Hypoxia and oxidative stress are intrinsic to IRI, which disturb ER functions and lead to impaired protein folding (Walter and Ron, 2011; Cao and Kaufman, 2014). Excessive accumulation of unfolded proteins activates Unfolded Protein Response (UPR), a cellular stress response mechanism to improve the protein folding efficiency while reducing mRNA translation along with protein expression (Schuck et al., 2009). Although ER stress plays an important role in cell growth and differentiation, excessive activation of ER stress and UPR can activate apoptotic signaling (Tabas and Ron, 2011; Hetz, 2012), which is mainly mediated by C/EBP homologous proteins (CHOP), a master regulator of maladaptive ER stress-induced apoptosis. FGF10 effectively alleviated IRI evoked expression of ER stress-related proteins in the kidney including CHOP, GRP78, XBP-1, and ATF-4 and ATF-6, which may contribute to inhibit IR-induced activation of proapoptotic caspase-3 and Bax expression. Results from IRI model *in vivo* and *in vitro* cell culture experiments together indicate that FGF10 attenuates renal tubular epithelial cell death *via* inhibiting excessive ER stress, which is, at least in part, mediated by MEK-ERK1/2 signaling pathway (Tan et al., 2020). Therefore, FGF10 contributes to restore the balance between the adaptive pathway and the apoptotic pathway of UPR by inhibiting excessive ER stress.

ROLE OF FGFS ON INFLAMMATION

The inflammatory response is an integral component in the initiation and exacerbation of AKI. Although a crucial element of the repair process, excessive activation of inflammatory signals and cytokine secretion may impose further damage to renal parenchyma cells. FGFs may exhibit different impacts on the inflammatory process of IRI. Contrary to the protective effects of FGF2 and FGF10 against IRI/AKI, FGF23 appears to be a deleterious factor.

Under normal physiology, FGF23 is mainly produced in bone by osteoblasts/osteocytes in response to local and systemic factors and targets the kidney to create multiple endocrine networks (Bergwitz and Juppner, 2010). Although some studies suggest that FGF23 interacts with the immune system, it is not clear whether FGF23 directly regulates immune cell functions or indirectly impacts immune responses through FGF23 regulation of 1,25-dihydroxyvitamin-D. FGF23 is increased in CKD. Macrophages do not regularly express FGF23 or α-Klotho, but in acute inflammation, FGF23 stimulates proinflammatory responses in M1 macrophages and blocks the transition to M2 macrophages (**Figure 1B**). In addition, FGF23 is proposed to activate FGFR2 in polymorphonuclear leukocyte to directly decrease their recruitment. Given the link of increased serum FGF23 to various tissue injuries, as well as evidence that the sources of FGF23 and control of its production in AKI and CKD differ from those in the physiologic conditions, mediators of inflammation contributing to elevated FGF23 have recently been proposed as potential drug targets, in addition to repurposing existing strategies to target FGF23 (Musgrove and Wolf, 2020).

High mobility group box 1 protein (HMGB1) is a highly conserved nuclear protein that functions as an architectural chromatin-binding factor and regulator of gene transcription. HMGB1 assumes diverse roles as an immuno-modulator in the form of a cytokine molecule or as nuclear chromatin and transcription regulator. HMGB1 can be activated and gets released from damaged parenchymal cells as a sterile inflammatory molecule and a major damage-associated molecular pattern (DAMP). Translocation of HMGB1 from the nucleus to the cytoplasm and subsequent release to the extracellular milieu is reported to promote inflammatory response *via* the activation of TLRs (Yang et al., 2010). HMGB1-TLRs pathway has long been recognized as an essential and early mediator in renal IRI and an attractive target of AKI and other disease therapies (Li et al., 2011; Zhang et al., 2016; Vijayakumar et al., 2019).

Recent efforts to explore the potential protective effect of exogenous FGFs on renal IRI illustrated that, besides promoting proliferation and inhibiting apoptosis, both FGF2 and FGF10 effectively inhibited IRI-induced release of HMGB1 from the nucleus to the extracellular domain, which is associated with a marked decrease in the expression of inflammatory cytokines such as TNF-α, IL-1β, and IL-6 following IRI (Tan et al., 2017; Tan et al., 2018, **Figure 2B**). This novel function of FGFs on the inflammatory cascade may be related to the inhibition of HMGB1-mediated TLR2 and/or TLR4 signaling (Leemans et al., 2009; Wu et al., 2010; Chen et al., 2017). It has been reported that FGF10 ameliorates cerebral ischemia injury *via* inhibiting NF-κB-dependent neuroinflammation and activating PI3K/AKT survival signalling pathway (Li et al., 2016). Whether the inhibition of HMGB1 and associated inflammatory cytokine release by FGFs is due to their protective effect against renal damage and therefore less DAMP release, or through some other mechanism(s) remains to be further elucidated.

CONCLUSION AND PROSPECT

Extensive research in the past years have established FGFs as vital regulators in tissue repair and regeneration, as well as in metabolic homeostasis. Along with advances in our understanding of FGF biology and their regulation of various pathophysiologic processes comes the inspiration of harnessing their power for potential disease therapies.

In this review, we summarized the available data on the FGFs that have shown promising features related to IRI either as a

preventative/therapeutic agent or a biomarker. We highlighted some functional and biological aspects that constitute the promising features of FGFs, particularly FGF2 and FGF10, in averting IR-induced tubular cell death and inhibition of overt inflammatory response, which may all contribute to their net beneficial effect on reducing the IRI and promoting recovery.

Admittedly, the exploration of FGFs as preventative or therapeutic agents in the management of clinical IRI is still in its rudimentary stages. Most of the published work has been conducted in pre-clinical settings. These widely used animal models, including the bilateral IR that is considered to best resemble clinical AKI, still have certain limitations in fully mimicking human AKI, which can be caused by numerous and complicated clinical conditions. Additionally, the underlying pathophysiology of IRI and how FGFs impact key biological and pathophysiological processes, such as apoptosis, autophagy, ERS, and oxidative stress, remains poorly understood. Future research should encourage more clinical-based and patient-oriented studies. Moreover, the utilization of advanced genetic animal models will also be instrumental in elucidating the disease mechanisms. This will allow for the labeling and tracing of specific cell populations to gain deeper insights about the effects of FGF. Collectively, these approaches, combined with proteomic and genomic technologies, will better delineate FGF signalling targets and support the therapeutic potential of FGFs toward AKI.

AUTHOR CONTRIBUTIONS

J-SZ and L-CD conceived the study. L-CD, TA, SB, and J-SZ drafted and revised the manuscript.

REFERENCES

Al-Jaghbeer, M., Dealmeida, D., Bilderback, A., Ambrosino, R., and Kellum, J. A. (2018). Clinical Decision Support for In-Hospital AKI. *J. Am. Soc. Nephrol.* 29 (2), 654–660. doi: 10.1681/asn.2017070765

Bates, C. M. (2011). Role of fibroblast growth factor receptor signaling in kidney development. *Am. J. Physiol. Renal Physiol.* 301 (2), F245–F251. doi: 10.1152/ajprenal.00186.2011

Bergwitz, C., and Juppner, H. (2010). Regulation of phosphate homeostasis by PTH, vitamin D, and FGF23. *Annu. Rev. Med.* 61, 91–104. doi: 10.1146/annurev.med.051308.111339

Cao, S. S., and Kaufman, R. J. (2014). Endoplasmic reticulum stress and oxidative stress in cell fate decision and human disease. *Antioxid Redox Signal* 21 (3), 396–413. doi: 10.1089/ars.2014.5851

Celli, G., LaRochelle, W. J., Mackem, S., Sharp, R., and Merlino, G. (1998). Soluble dominant-negative receptor uncovers essential roles for fibroblast growth factors in multi-organ induction and patterning. *EMBO J.* 17 (6), 1642–1655. doi: 10.1093/emboj/17.6.1642

Chawla, L. S., Eggers, P. W., Star, R. A., and Kimmel, P. L. (2014). Acute kidney injury and chronic kidney disease as interconnected syndromes. *N Engl. J. Med.* 371 (1), 58–66. doi: 10.1056/NEJMra1214243

Chen, W., Fu, X. B., Ge, S. L., Sun, T. Z., Zhou, G., Han, B., et al. (2005). Intravenous acid fibroblast growth factor protects intestinal mucosal cells against ischemia-reperfusion injury via regulating Bcl-2/Bax expression. *World J. Gastroenterol.* 11 (22), 3419–3425. doi: 10.3748/wjg.v11.i22.3419

Chen, C. B., Liu, L. S., Zhou, J., Wang, X. P., Han, M., Jiao, X. Y., et al. (2017). Up-Regulation of HMGB1 Exacerbates Renal Ischemia-Reperfusion Injury by Stimulating Inflammatory and Immune Responses through the TLR4 Signaling Pathway in Mice. *Cell Physiol. Biochem.* 41 (6), 2447–2460. doi: 10.1159/000475914

Chen, G., Liu, Y., Goetz, R., Fu, L., Jayaraman, S., Hu, M. C., et al. (2018). alpha-Klotho is a non-enzymatic molecular scaffold for FGF23 hormone signalling. *Nature* 553 (7689), 461–466. doi: 10.1038/nature25451

Christov, M., Waikar, S. S., Pereira, R. C., Havasi, A., Leaf, D. E., Goltzman, D., et al. (2013). Plasma FGF23 levels increase rapidly after acute kidney injury. *Kidney Int.* 84 (4), 776–785. doi: 10.1038/ki.2013.150

Christov, M., Neyra, J. A., Gupta, S., and Leaf, D. E. (2019). Fibroblast Growth Factor 23 and Klotho in AKI. *Semin. Nephrol.* 39 (1), 57–75. doi: 10.1016/j.semnephrol.2018.10.005

Cinque, L., Forrester, A., Bartolomeo, R., Svelto, M., Venditti, R., Montefusco, S., et al. (2015). FGF signalling regulates bone growth through autophagy. *Nature* 528 (7581), 272–275. doi: 10.1038/nature16063

Colvin, J. S., Bohne, B. A., Harding, G. W., McEwen, D. G., and Ornitz, D. M. (1996). Skeletal overgrowth and deafness in mice lacking fibroblast growth factor receptor 3. *Nat. Genet.* 12 (4), 390–397. doi: 10.1038/ng0496-390

Cuevas, P., Martinez-Coso, V., Fu, X., Orte, L., Reimers, D., Gimenez-Gallego, G., et al. (1999). Fibroblast growth factor protects the kidney against ischemia-reperfusion injury. *Eur. J. Med. Res.* 4 (10), 403–410.

Cuevas, P., Carceller, F., Martinez-Coso, V., Asin-Cardiel, E., and Gimenez-Gallego, G. (2000). Fibroblast growth factor cardioprotection against ischemia-reperfusion injury may involve K+ ATP channels. *Eur. J. Med. Res.* 5 (4), 145–149.

Czaya, B., and Faul, C. (2019). FGF23 and inflammation-a vicious coalition in CKD. *Kidney Int.* 96 (4), 813–815. doi: 10.1016/j.kint.2019.05.018

David, V., Francis, C., and Babitt, J. L. (2017). Ironing out the cross talk between FGF23 and inflammation. *Am. J. Physiol. Renal Physiol.* 312 (1), F1–f8. doi: 10.1152/ajprenal.00359.2016

Degirolamo, C., Sabba, C., and Moschetta, A. (2016). Therapeutic potential of the endocrine fibroblast growth factors FGF19, FGF21 and FGF23. *Nat. Rev. Drug Discovery* 15 (1), 51–69. doi: 10.1038/nrd.2015.9

Duann, P., Lianos, E. A., Ma, J., and Lin, P. H. (2016). Autophagy, Innate Immunity and Tissue Repair in Acute Kidney Injury. *Int. J. Mol. Sci.* 17 (5). doi: 10.3390/ijms17050662

Fang, X., Wang, L., Shi, L., Chen, C., Wang, Q., Bai, C., et al. (2014). Protective effects of keratinocyte growth factor-2 on ischemia-reperfusion-induced lung injury in rats. *Am. J. Respir. Cell Mol. Biol.* 50 (6), 1156–1165. doi: 10.1165/rcmb.2013-0268OC

Fu, X., Cuevas, P., Gimenez-Gallego, G., Sheng, Z., and Tian, H. (1995). Acidic fibroblast growth factor reduces rat skeletal muscle damage caused by ischemia and reperfusion. *Chin Med. J. (Engl)* 108 (3), 209–214.

Fu, X. B., Li, X. K., Wang, T., Cheng, B., and Sheng, Z. Y. (2004). Enhanced anti-apoptosis and gut epithelium protection function of acidic fibroblast growth factor after cancelling of its mitogenic activity. *World J. Gastroenterol.* 10 (24), 3590–3596. doi: 10.3748/wjg.v10.i24.3590

Gallegos, T. F., Kamei, C. N., Rohly, M., and Drummond, I. A. (2019). Fibroblast growth factor signaling mediates progenitor cell aggregation and nephron regeneration in the adult zebrafish kidney. *Dev. Biol.* 454 (1), 44–51. doi: 10.1016/j.ydbio.2019.06.011

Goetz, R., and Mohammadi, M. (2013). Exploring mechanisms of FGF signalling through the lens of structural biology. *Nat. Rev. Mol. Cell Biol.* 14 (3), 166–180. doi: 10.1038/nrm3528

Han, S. J., and Lee, H. T. (2019). Mechanisms and therapeutic targets of ischemic acute kidney injury. *Kidney Res. Clin. Pract.* 38 (4), 427–440. doi: 10.23876/j.krcp.19.062

Hetz, C. (2012). The unfolded protein response: controlling cell fate decisions under ER stress and beyond. *Nat. Rev. Mol. Cell Biol.* 13 (2), 89–102. doi: 10.1038/nrm3270

Hoste, E. A., Bagshaw, S. M., Bellomo, R., Cely, C. M., Colman, R., Cruz, D. N., et al. (2015). Epidemiology of acute kidney injury in critically ill patients: the multinational AKI-EPI study. *Intensive Care Med.* 41 (8), 1411–1423. doi: 10.1007/s00134-015-3934-7

House, S. L., Bolte, C., Zhou, M., Doetschman, T., Klevitsky, R., Newman, G., et al. (2003). Cardiac-specific overexpression of fibroblast growth factor-2 protects against

myocardial dysfunction and infarction in a murine model of low-flow ischemia. *Circulation* 108 (25), 3140–3148. doi: 10.1161/01.Cir.0000105723.91637.1c

House, S. L., Branch, K., Newman, G., Doetschman, T., and Schultz Jel, J. (2005). Cardioprotection induced by cardiac-specific overexpression of fibroblast growth factor-2 is mediated by the MAPK cascade. *Am. J. Physiol. Heart Circ. Physiol.* 289 (5), H2167–H2175. doi: 10.1152/ajpheart.00392.2005

House, S. L., Melhorn, S. J., Newman, G., Doetschman, T., and Schultz Jel, J. (2007). The protein kinase C pathway mediates cardioprotection induced by cardiac-specific overexpression of fibroblast growth factor-2. *Am. J. Physiol. Heart Circ. Physiol.* 293 (1), H354–H365. doi: 10.1152/ajpheart.00804.2006

House, S. L., Wang, J., Castro, A. M., Weinheimer, C., Kovacs, A., and Ornitz, D. M. (2015). Fibroblast growth factor 2 is an essential cardioprotective factor in a closed-chest model of cardiac ischemia-reperfusion injury. *Physiol. Rep.* 3 (1). doi: 10.14814/phy2.12278

Hu, Z., Zhang, H., Yang, S. K., Wu, X., He, D., Cao, K., et al. (2019). Emerging Role of Ferroptosis in Acute Kidney Injury. *Oxid. Med. Cell Longev* 2019, 8010614. doi: 10.1155/2019/8010614

Ichimura, T., Finch, P. W., Zhang, G., Kan, M., and Stevens, J. L. (1996). Induction of FGF-7 after kidney damage: a possible paracrine mechanism for tubule repair. *Am. J. Physiol.* 271 (5 Pt 2), F967–F976. doi: 10.1152/ajprenal.1996.271.5.F967

Isakova, T. (2012). Fibroblast growth factor 23 and adverse clinical outcomes in chronic kidney disease. *Curr. Opin. Nephrol. Hypertens.* 21 (3), 334–340. doi: 10.1097/MNH.0b013e328351a391

Itoh, N. (2016). FGF10: A multifunctional mesenchymal-epithelial signaling growth factor in development, health, and disease. *Cytokine Growth Factor Rev.* 28, 63–69. doi: 10.1016/j.cytogfr.2015.10.001

Jiang, M., Liu, K., Luo, J., and Dong, Z. (2010). Autophagy is a renoprotective mechanism during in vitro hypoxia and in vivo ischemia-reperfusion injury. *Am. J. Pathol.* 176 (3), 1181–1192. doi: 10.2353/ajpath.2010.090594

Kardami, E., Detillieux, K., Ma, X., Jiang, Z., Santiago, J. J., Jimenez, S. K., et al. (2007). Fibroblast growth factor-2 and cardioprotection. *Heart Fail Rev.* 12 (3-4), 267–277. doi: 10.1007/s10741-007-9027-0

Kaushal, G. P., and Shah, S. V. (2016). Autophagy in acute kidney injury. *Kidney Int.* 89 (4), 779–791. doi: 10.1016/j.kint.2015.11.021

Kurosu, H., Ogawa, Y., Miyoshi, M., Yamamoto, M., Nandi, A., Rosenblatt, K. P., et al. (2006). Regulation of fibroblast growth factor-23 signaling by klotho. *J. Biol. Chem.* 281 (10), 6120–6123. doi: 10.1074/jbc.C500457200

Leaf, D. E., Jacob, K. A., Srivastava, A., Chen, M. E., Christov, M., Juppner, H., et al. (2017). Fibroblast Growth Factor 23 Levels A ssociate with AKI and Death in Critical Illness. *J. Am. Soc. Nephrol.* 28 (6), 1877–1885. doi: 10.1681/asn.2016080836

Leaf, D. E., Siew, E. D., Eisenga, M. F., Singh, K., Mc Causland, F. R., Srivastava, A., et al. (2018). Fibroblast Growth Factor 23 Associates with Death in Critically Ill Patients. *Clin. J. Am. Soc. Nephrol.* 13 (4), 531–541. doi: 10.2215/cjn.10810917

Leemans, J. C., Butter, L. M., Pulskens, W. P., Teske, G. J., Claessen, N., van der Poll, T., et al. (2009). The role of Toll-like receptor 2 in inflammation and fibrosis during progressive renal injury. *PloS One* 4 (5), e5704. doi: 10.1371/journal.pone.0005704

Li, J., Gong, Q., Zhong, S., Wang, L., Guo, H., Xiang, Y., et al. (2011). Neutralization of the extracellular HMGB1 released by ischaemic damaged renal cells protects against renal ischaemia-reperfusion injury. *Nephrol. Dial Transplant.* 26 (2), 469–478. doi: 10.1093/ndt/gfq466

Li, Y. H., Fu, H. L., Tian, M. L., Wang, Y. Q., Chen, W., Cai, L. L., et al. (2016). Neuron-derived FGF10 ameliorates cerebral ischemia injury via inhibiting NF-kappaB-dependent neuroinflammation and activating PI3K/Akt survival signaling pathway in mice. *Sci. Rep.* 6, 19869. doi: 10.1038/srep19869

Li, Y., Yin, P., Guo, Z., Lv, H., Deng, Y., Chen, M., et al. (2019). Bone-Derived Extracellular Vesicles: Novel Players of Interorgan Crosstalk. *Front. Endocrinol. (Lausanne)* 10, 846. doi: 10.3389/fendo.2019.00846

Li, X. (2019). The FGF metabolic axis. *Front. Med.* 13 (5), 511–530. doi: 10.1007/s11684-019-0711-y

Liao, S., Bodmer, J. R., Azhar, M., Newman, G., Coffin, J. D., Doetschman, T., et al. (2010). The influence of FGF2 high molecular weight (HMW) isoforms in the development of cardiac ischemia-reperfusion injury. *J. Mol. Cell Cardiol.* 48 (6), 1245–1254. doi: 10.1016/j.yjmcc.2010.01.014

Manning, J. R., Perkins, S. O., Sinclair, E. A., Gao, X., Zhang, Y., Newman, G., et al. (2013). Low molecular weight fibroblast growth factor-2 signals via protein kinase C and myofibrillar proteins to protect against postischemic cardiac dysfunction. *Am. J. Physiol. Heart Circ. Physiol.* 304 (10), H1382–H1396. doi: 10.1152/ajpheart.00613.2012

Munoz Mendoza, J., Isakova, T., Cai, X., Bayes, L. Y., Faul, C., Scialla, J. J., et al. (2017). Inflammation and elevated levels of fibroblast growth factor 23 are independent risk factors for death in chronic kidney disease. *Kidney Int.* 91 (3), 711–719. doi: 10.1016/j.kint.2016.10.021

Musgrove, J., and Wolf, M. (2020). Regulation and Effects of FGF23 in Chronic Kidney Disease. *Annu. Rev. Physiol.* 82, 365–390. doi: 10.1146/annurev-physiol-021119-034650

Ohuchi, H., Hori, Y., Yamasaki, M., Harada, H., Sekine, K., Kato, S., et al. (2000). FGF10 acts as a major ligand for FGF receptor 2 IIIb in mouse multi-organ development. *Biochem. Biophys. Res. Commun.* 277 (3), 643–649. doi: 10.1006/bbrc.2000.3721

Ornitz, D. M., and Itoh, N. (2015). The Fibroblast Growth Factor signaling pathway. *Wiley Interdiscip. Rev. Dev. Biol.* 4 (3), 215–266. doi: 10.1002/wdev.176

Park, S. K., Hur, M., and Kim, W. H. (2017). Acute kidney injury after pediatric liver transplantation. *J. Anesth* 31 (6), 923–924. doi: 10.1007/s00540-017-2412-5

Patel, J., Pancholi, N., Gudehithlu, K. P., Sethupathi, P., Hart, P. D., Dunea, G., et al. (2012). Stem cells from foreign body granulation tissue accelerate recovery from acute kidney injury. *Nephrol. Dial Transplant.* 27 (5), 1780–1786. doi: 10.1093/ndt/gfr585

Pena, A. M., Chen, S., Feng, B., Cai, L., Li, X., Liang, G., et al. (2017). Prevention of Diabetic Nephropathy by Modified Acidic Fibroblast Growth Factor. *Nephron* 137 (3), 221–236. doi: 10.1159/000478745

Poladia, D. P., Kish, K., Kutay, B., Hains, D., Kegg, H., Zhao, H., et al. (2006). Role of fibroblast growth factor receptors 1 and 2 in the metanephric mesenchyme. *Dev. Biol.* 291 (2), 325–339. doi: 10.1016/j.ydbio.2005.12.034

Qiao, J., Uzzo, R., Obara-Ishihara, T., Degenstein, L., Fuchs, E., and Herzlinger, D. (1999). FGF-7 modulates ureteric bud growth and nephron number in the developing kidney. *Development* 126 (3), 547–554.

Ren, Z., Xiao, W., Zeng, Y., Liu, M.H., Li, G.H., Tang, Z.H., et al (2019). Fibroblast growth factor-21 alleviates hypoxia/reoxygenation injury in H9c2 cardiomyocytes by promoting autophagic flux. *Int. J. Mol. Med.* 43 (3), 1321–1330. doi: 10.3892/ijmm.2019.4071

Revest, J. M., Spencer-Dene, B., Kerr, K., De Moerlooze, L., Rosewell, I., and Dickson, C. (2001). Fibroblast growth factor receptor 2-IIIb acts upstream of Shh and Fgf4 and is required for limb bud maintenance but not for the induction of Fgf8, Fgf10, Msx1, or Bmp4. *Dev. Biol.* 231 (1), 47–62. doi: 10.1006/dbio.2000.0144

Ronco, C., Bellomo, R., and Kellum, J. A. (2019). Acute kidney injury. *Lancet* 394 (10212), 1949–1964. doi: 10.1016/s0140-6736(19)32563-2

Schuck, S., Prinz, W. A., Thorn, K. S., Voss, C., and Walter, P. (2009). Membrane expansion alleviates endoplasmic reticulum stress independently of the unfolded protein response. *J. Cell Biol.* 187 (4), 525–536. doi: 10.1083/jcb.200907074

Shaker, A. M., El Mohamed, E., Samir, H. H., Elnokeety, M. M., Sayed, H. A., and Ramzy, T. A. (2018). Fibroblast growth factor-23 as a predictor biomarker of acute kidney injury after cardiac surgery. *Saudi J. Kidney Dis. Transpl* 29 (3), 531–539. doi: 10.4103/1319-2442.235180

Sims-Lucas, S., Cusack, B., Baust, J., Eswarakumar, V. P., Masatoshi, H., Takeuchi, A., et al. (2011). Fgfr1 and the IIIc isoform of Fgfr2 play critical roles in the metanephric mesenchyme mediating early inductive events in kidney development. *Dev. Dyn* 240 (1), 240–249. doi: 10.1002/dvdy.22501

Smith, E. R., McMahon, L. P., and Holt, S. G. (2014). Fibroblast growth factor 23. *Ann. Clin. Biochem.* 51 (Pt 2), 203–227. doi: 10.1177/0004563213510708

Smith, E. R., Holt, S. G., and Hewitson, T. D. (2017a). FGF23 activates injury-primed renal fibroblasts via FGFR4-dependent signalling and enhancement of TGF-beta autoinduction. *Int. J. Biochem. Cell Biol.* 92, 63–78. doi: 10.1016/j.biocel.2017.09.009

Smith, E. R., Tan, S. J., Holt, S. G., and Hewitson, T. D. (2017b). FGF23 is synthesised locally by renal tubules and activates injury-primed fibroblasts. *Sci. Rep.* 7 (1), 3345. doi: 10.1038/s41598-017-02709-w

Strutz, F. (2009). The role of FGF-2 in renal fibrogenesis. *Front. Biosci (Schol Ed)* 1, 125–131. doi: 10.2741/s12

Sun, D., Wang, W., Wang, X., Wang, Y., Xu, X., Ping, F., et al. (2018). bFGF plays a neuroprotective role by suppressing excessive autophagy and apoptosis after transient global cerebral ischemia in rats. *Cell Death Dis.* 9 (2), 172. doi: 10.1038/s41419-017-0229-7

Tabas, I., and Ron, D. (2011). Integrating the mechanisms of apoptosis induced by endoplasmic reticulum stress. *Nat. Cell Biol.* 13 (3), 184–190. doi: 10.1038/ncb0311-184

Tan, X. H., Zheng, X. M., Yu, L. X., He, J., Zhu, H. M., Ge, X. P., et al. (2017). Fibroblast growth factor 2 protects against renal ischaemia/reperfusion injury by attenuating mitochondrial damage and proinflammatory signalling. *J. Cell Mol. Med.* 21 (11), 2909–2925. doi: 10.1111/jcmm.13203

Tan, X., Zhu, H., Tao, Q., Guo, L., Jiang, T., Xu, L., et al. (2018). FGF10 Protects Against Renal Ischemia/Reperfusion Injury by Regulating Autophagy and Inflammatory Signaling. *Front. Genet.* 9, 556. doi: 10.3389/fgene.2018.00556

Tan, X., Yu, L., Yang, R., Tao, Q., Xiang, L., Xiao, J., et al. (2020). Fibroblast Growth Factor 10 Attenuates Renal Damage by Regulating Endoplasmic Reticulum Stress After Ischemia-Reperfusion Injury. *Front. Pharmacol.* 11, 39. doi: 10.3389/fphar.2020.00039

Trueb, B., Amann, R., and Gerber, S. D. (2013). Role of FGFRL1 and other FGF signaling proteins in early kidney development. *Cell Mol. Life Sci.* 70 (14), 2505–2518. doi: 10.1007/s00018-012-1189-9

Trueb, B. (2011). Biology of FGFRL1, the fifth fibroblast growth factor receptor. *Cell Mol. Life Sci.* 68 (6), 951–964. doi: 10.1007/s00018-010-0576-3

Uchino, S., Kellum, J. A., Bellomo, R., Doig, G. S., Morimatsu, H., Morgera, S., et al. (2005). Acute renal failure in critically ill patients: a multinational, multicenter study. *Jama* 294 (7), 813–818. doi: 10.1001/jama.294.7.813

Verma, S. K., and Molitoris, B. A. (2015). Renal endothelial injury and microvascular dysfunction in acute kidney injury. *Semin. Nephrol.* 35 (1), 96–107. doi: 10.1016/j.semnephrol.2015.01.010

Vijayakumar, E. C., Bhatt, L. K., and Prabhavalkar, K. S. (2019). High Mobility Group Box-1 (HMGB1): A Potential Target in Therapeutics. *Curr. Drug Targets* 20 (14), 1474–1485. doi: 10.2174/1389450120666190618125100

Villanueva, S., Cespedes, C., Gonzalez, A., and Vio, C. P. (2006). bFGF induces an earlier expression of nephrogenic proteins after ischemic acute renal failure. *Am. J. Physiol. Regul. Integr. Comp. Physiol.* 291 (6), R1677–R1687. doi: 10.1152/ajpregu.00023.2006

Villanueva, S., Cespedes, C., Gonzalez, A. A., Roessler, E., and Vio, C. P. (2008). Inhibition of bFGF-receptor type 2 increases kidney damage and suppresses nephrogenic protein expression after ischemic acute renal failure. *Am. J. Physiol. Regul. Integr. Comp. Physiol.* 294 (3), R819–R828. doi: 10.1152/ajpregu.00273.2007

Vinsonneau, C., Girshovich, A., M'Rad M, B., Perez, J., Mesnard, L., Vandermersch, S., et al. (2010). Intrarenal urothelium proliferation: an unexpected early event following ischemic injury. *Am. J. Physiol. Renal Physiol.* 299 (3), F479–F486. doi: 10.1152/ajprenal.00585.2009

Volovelsky, O., Gist, K. M., Terrell, T. C., Bennett, M. R., Cooper, D. S., Alten, J. A., et al. (2018). Early postoperative measurement of fibroblast growth factor 23 predicts severe acute kidney injury in infants after cardiac surgery. *Clin. Nephrol.* 90 (3), 165–171. doi: 10.5414/CN109359

Wai, K., Soler-Garcia, A. A., Perazzo, S., Mattison, P., and Ray, P. E. (2013). A pilot study of urinary fibroblast growth factor-2 and epithelial growth factor as potential biomarkers of acute kidney injury in critically ill children. *Pediatr. Nephrol.* 28 (11), 2189–2198. doi: 10.1007/s00467-013-2543-3

Walker, K. A., Sims-Lucas, S., and Bates, C. M. (2016). Fibroblast growth factor receptor signaling in kidney and lower urinary tract development. *Pediatr. Nephrol.* 31 (6), 885–895. doi: 10.1007/s00467-015-3151-1

Walter, P., and Ron, D. (2011). The unfolded protein response: from stress pathway to homeostatic regulation. *Science* 334 (6059), 1081–1086. doi: 10.1126/science.1209038

Wang, Y., Lin, H., Lin, S., Qu, J., Xiao, J., Huang, Y., et al. (2010). Cell-penetrating peptide TAT-mediated delivery of acidic FGF to retina and protection against ischemia-reperfusion injury in rats. *J. Cell Mol. Med.* 14 (7), 1998–2005. doi: 10.1111/j.1582-4934.2009.00786.x

Wang, Z. G., Wang, Y., Huang, Y., Lu, Q., Zheng, L., Hu, D., et al. (2015). bFGF regulates autophagy and ubiquitinated protein accumulation induced by myocardial ischemia/reperfusion via the activation of the PI3K/Akt/mTOR pathway. *Sci. Rep.* 5, 9287. doi: 10.1038/srep09287

Weinstein, M., Xu, X., Ohyama, K., and Deng, C. X. (1998). FGFR-3 and FGFR-4 function cooperatively to direct alveogenesis in the murine lung. *Development* 125 (18), 3615–3623.

Weng, L. X., Fu, X. B., Li, X. X., Sun, T. Z., Zheng, S. Y., and Chen, W. (2004). [Effects of acidi fibroblast growth factor on hepatic and renal functions after intestinal ischemia/reperfusion injury]. *Zhongguo Wei Zhong Bing Ji Jiu Yi Xue* 16 (1), 19–21.

Wu, H., Ma, J., Wang, P., Corpuz, T. M., Panchapakesan, U., Wyburn, K. R., et al. (2010). HMGB1 contributes to kidney ischemia reperfusion injury. *J. Am. Soc. Nephrol.* 21 (11), 1878–1890. doi: 10.1681/asn.2009101048

Xu, Z., and Dai, C. (2017). Ablation of FGFR2 in Fibroblasts Ameliorates Kidney Fibrosis after Ischemia/Reperfusion Injury in Mice. *Kidney Dis. (Basel)* 3 (4), 160–170. doi: 10.1159/000484604

Xu, Y., and Han, J. (2016). The Necrosome in Acute Kidney Injury. *Semin. Nephrol.* 36 (3), 199–207. doi: 10.1016/j.semnephrol.2016.03.007

Yang, H., Hreggvidsdottir, H. S., Palmblad, K., Wang, H., Ochani, M., Li, J., et al. (2010). A critical cysteine is required for HMGB1 binding to Toll-like receptor 4 and activation of macrophage cytokine release. *Proc. Natl. Acad. Sci. U S A* 107 (26), 11942–11947. doi: 10.1073/pnas.1003893107

Zhang, X., Ibrahimi, O. A., Olsen, S. K., Umemori, H., Mohammadi, M., and Ornitz, D. M. (2006). Receptor specificity of the fibroblast growth factor family. *complete Mamm. FGF family. J. Biol. Chem.* 281 (23), 15694–15700. doi: 10.1074/jbc.M601252200

Zhang, J., Liu, J., Liu, L., McKeehan, W. L., and Wang, F. (2012). The fibroblast growth factor signaling axis controls cardiac stem cell differentiation through regulating autophagy. *Autophagy* 8 (4), 690–691. doi: 10.4161/auto.19290

Zhang, J., Xia, J., Zhang, Y., Xiao, F., Wang, J., Gao, H., et al. (2016). HMGB1-TLR4 signaling participates in renal ischemia reperfusion injury and could be attenuated by dexamethasone-mediated inhibition of the ERK/NF-kappaB pathway. *Am. J. Transl. Res.* 8 (10), 4054–4067.

Conflict of Interest: The authors declare that the research was conducted in the absence of any commercial or financial relationships that could be construed as a potential conflict of interest.

The handling editor is currently organizing a Research Topic with several of the authors SB, J-SZ, and confirms the absence of any other collaboration.

Advantages of publishing in Frontiers

OPEN ACCESS
Articles are free to read for greatest visibility and readership

FAST PUBLICATION
Around 90 days from submission to decision

HIGH QUALITY PEER-REVIEW
Rigorous, collaborative, and constructive peer-review

TRANSPARENT PEER-REVIEW
Editors and reviewers acknowledged by name on published articles

Frontiers
Avenue du Tribunal-Fédéral 34
1005 Lausanne | Switzerland

Visit us: www.frontiersin.org
Contact us: info@frontiersin.org | +41 21 510 17 00

REPRODUCIBILITY OF RESEARCH
Support open data and methods to enhance research reproducibility

DIGITAL PUBLISHING
Articles designed for optimal readership across devices

FOLLOW US
@frontiersin

IMPACT METRICS
Advanced article metrics track visibility across digital media

EXTENSIVE PROMOTION
Marketing and promotion of impactful research

LOOP RESEARCH NETWORK
Our network increases your article's readership